

# Space Qualified 5MHz Crystal Oscillators with maximum Stability between 1 and 10 Seconds

von der Fakultät 1 – MINT – Mathematik, Informatik, Physik,  
Elektro- und Informationstechnik der Brandenburgischen Technischen  
Universität Cottbus-Senftenberg genehmigte Dissertation zur  
Erlangung des akademischen Grades eines „Dr.-Ing.“

von

Dipl.-Ing. Wolfgang Griebel

aus Landsberg am Lech, Deutschland, geboren am 12.6.1961 in  
Salzburg/Österreich

Vorsitzender: Prof. Dr.-Ing. Dirk Killat

Gutachter: Prof. Dr.-Ing. habil Ulrich L. Rohde

Prof. Dr.-Ing. Matthias Rudolph

Prof. Dr. Ignaz Eisele

Tag der mündlichen Prüfung: 15. April 2021

## Table of Contents

1	Introduction .....	12
1.1	Why This Thesis? .....	12
1.2	Acknowledgements .....	13
2	History and Background.....	2-1
2.1	An Overview over Current 5MHz USO Parts for Space and Terrestrial Applications .....	2-2
2.2	The Evolution of Phase Noise Measurement Systems .....	2-5
2.3	Performance Levels .....	2-7
3	Principles of Oscillator Design.....	3-1
3.1	Basic Principles of Oscillation .....	3-1
3.1.1	A Little Excursion to a Nonlinear Oscillator Using a General Dynamics Approach ...	3-2
3.2	Phase Noise Basics and Important Properties .....	3-8
3.3	A Phasor Approach to Noise and Phase Noise.....	3-10
3.3.1	Why is Phase Noise an Important Problem? .....	3-11
3.3.2	Phase Noise in the Signal Processing Chain .....	3-13
3.4	Physical Effects in Oscillators.....	3-16
3.4.1	Existing Approaches to Explain and Design USO Clapp Oscillators .....	3-16
3.4.2	Small Signal and Simple Nonlinear Approaches, Bessel Function Bias Shift .....	3-17
3.4.3	Sanity Checks by Observing Waveforms - Surprises.....	3-18
3.4.4	Improvements to the Completeness of Transistor Models .....	3-19
3.4.5	Systematic Measurements of Oscillator Conditions.....	3-20
3.4.6	Simulations, Models, Parameters .....	3-24
3.4.7	The Influence of Early Voltage on Oscillators.....	3-25
3.5	Saturation and its Effect of Oscillator Performance.....	3-30
3.5.1	Simulation Results for Saturation.....	3-37
3.5.2	Saturation and Noise.....	3-41
3.5.3	Outlook regarding Saturation Effects .....	3-42
3.6	Base Emitter Breakdown and its Effect of Oscillator Performance .....	3-42
3.6.1	Squegging Related to BE Breakdown, Semi-Isolated Topologies .....	3-44
3.6.2	Harmonic Balance Simulator Results.....	3-46
3.6.3	What about RF Transistors? .....	3-47
3.6.4	Outlook for BE Breakdown.....	3-47
3.7	Phase Plots.....	3-47
3.8	Next Steps.....	3-50
3.9	LC Oscillators.....	3-52
3.9.1	Oscillator Topologies .....	3-53
3.9.2	Colpitts/Clapp Varieties, Input Impedance .....	3-53

3.9.3	Optimization.....	3-54
3.9.4	Semi-Isolated Colpitts/Clapp.....	3-55
3.9.5	Emitter-Tapped Colpitts/Clapp .....	3-57
3.9.6	Resonator-Decoupled Colpitts/Clapp.....	3-58
3.9.7	Phase Noise .....	3-60
3.9.8	LC Oscillators, A Pragmatic Design Method.....	3-64
	Next Steps.....	3-65
3.10	Crystal Oscillators .....	3-67
3.10.1	The Behavior of Precision Crystal Oscillators .....	3-67
3.10.2	What Kind of Solutions to Expect from a Complex Oscillator Circuit? .....	3-70
3.10.3	An Example Clapp Oscillator with a Multiresonator Model.....	3-73
3.10.4	Other Possible Multiresonator Clapp Oscillator Solutions.....	3-78
3.10.5	Limitations.....	3-78
3.10.6	Mathematic Approaches to the Problem of Multiresonator Oscillators .....	3-78
3.10.7	Design Steps for a High Stability / Low Power Oscillator .....	3-79
3.10.8	Consequences .....	3-81
3.10.9	Design Ideas .....	3-82
3.10.10	B Mode Trapping .....	3-82
4	Oscillator Components .....	4-1
4.1	Quartz Properties .....	4-1
4.2	Transistor Properties.....	4-1
4.3	Crystal Properties .....	4-1
4.3.1	Electric Properties of Packaged Crystals, Equivalent Circuits.....	4-2
4.3.2	Nonlinear Effects.....	4-4
4.3.3	Drive Level Dependency (DLD) .....	4-4
4.3.4	Frequency Pulling.....	4-7
4.3.5	Dips, Mode Coupling .....	4-9
4.3.6	Memory Effects .....	4-10
4.3.7	Crystal Ageing.....	4-11
4.3.8	Crystal Noise .....	4-12
4.3.9	Environmental Effects .....	4-14
4.3.10	Crystal in Oscillator Circuits .....	4-16
4.3.11	Crystal Q Limitations .....	4-17
5	Oscillator Measurement Techniques .....	5-1
5.1	How to Probe an Oscillator Without Unacceptable Loading or Detuning .....	5-1
5.2	Measuring Base Current.....	5-7
5.3	Noise Caused by Base Emitter Breakdown.....	5-11
5.4	What Does “loaded Q” Mean? .....	5-12

5.5	Phase Noise Measurement Techniques at 5MHz .....	5-17
5.5.1	The Discovery of Phase Noise .....	5-17
5.5.2	Measuring Phase Noise – Spectrum Analysis .....	5-18
5.5.3	Measuring Phase Noise – The Phase Shifter Method.....	5-18
5.5.4	Measuring Phase Noise – The Mixer Method.....	5-19
5.5.5	Measuring Phase Noise – Modern Correlator Analyzers .....	5-19
5.5.6	Measuring Phase Noise – Measuring Extreme Performance USOs .....	5-20
5.5.7	Measuring Phase Noise – The Direct Method using a Precision Counter.....	5-21
6	Simulation Problems and Strategies.....	6-1
6.1	A stripped-down Circuit to test Simulators .....	6-1
6.1.1	Simulators and Q Values .....	6-2
6.2	Oscillator Abstractions.....	6-2
6.2.1	Stiffness and Startup Values.....	6-7
6.3	Integration Methods, Precision.....	6-9
6.4	Further Research.....	6-12
6.5	The Simulation Program.....	6-12
6.6	A Simulated High Q Clapp Oscillator.....	6-14
6.6.1	A stripped-down Circuit to test Simulators .....	6-14
6.6.2	A Simplified Model for Simulation.....	6-15
6.6.3	Results .....	6-17
6.6.4	The Next Step - Limiting Mechanisms.....	6-19
6.6.5	Modeling of the Transistor including Saturation.....	6-22
7	Thermal and Environmental Aspects .....	7-1
7.1	Temperature Regulator.....	7-1
7.2	Influence of Mechanical Vibrations .....	7-3
7.3	Black Magic .....	7-5
7.3.1	Crystals.....	7-5
7.3.2	Transistors .....	7-6
7.3.3	Passive Components.....	7-7
7.3.4	Radiation .....	7-7
7.4	Measurement Problems Without a Clear Cause .....	7-7
8	A Prototype USO Design .....	8-1
8.1	The Oscillator Core of The Prototype USO .....	8-2
8.1.1	Amplitude Regulation .....	8-3
8.1.2	The Heater Regulator .....	8-11
8.1.3	Phase Noise and Allen Deviation .....	8-20
8.1.4	The Complete Setup .....	8-23
8.1.5	A Full Simulation of the Amplitude Regulator .....	8-24



8.2	A Tracking Crystal Filter.....	8-28
8.2.1	Overall Architecture .....	8-28
8.2.2	Designing the Filter Stage .....	8-29
8.2.3	Crystal Properties .....	8-30
8.2.4	Regulation .....	8-31
8.2.5	Results .....	8-32
9	Suggestions for Further Research.....	9-1
9.1	Refine and Improve the In-Oscillator Measurement Capabilities to Higher Frequencies....	9-1
9.2	Extend the Usability of Simulation Programs to Circuits with Extremely High Q Components.....	9-1
9.3	Take the Performance of USOs to New Frontiers.....	9-2
9.4	Develop a Time Domain Simulator that Incorporates Realistic Noise.....	9-2
9.5	Create a Theoretical Foundation to Determine the Character of the Solutions of the Equations Governing Ultra Stable Oscillators. ....	9-3
10	Appendix A: An In-Depth Analysis of the HP10811OCXO .....	10-1
10.1	HP10811 Oscillator Building Blocks .....	10-2
10.2	The Oscillator Part.....	10-3
10.3	The Buffer/AGC/Stabilizer Part.....	10-5
10.4	The Output Buffer .....	10-7
10.5	Heater Architecture .....	10-8
10.6	Phase Noise Performance .....	10-8
11	Appendix B: Quartz Crystal Physics.....	11-1
11.1	The Piezoelectric Effect .....	11-1
11.2	Equations for a Piezoelectric Resonating Body .....	11-3
11.3	Modes .....	11-3
11.4	Quartz Cuts.....	11-4
11.5	Thickness Shear Mode .....	11-6
11.6	Active Regions .....	11-6
11.6.1	Fundamental Frequency, Overtones, Spurs.....	11-7
11.6.2	Temperature Dependency, Compensation.....	11-8
11.6.3	Crystal Defects .....	11-9
12	Appendix C: Crystal Measurements.....	12-1
12.1	Measurement Set-up.....	12-1
12.2	Results .....	12-2
13	Appendix D: Measuring Crystal Properties .....	13-1
13.1	Instruments for Measuring Premium Crystals.....	13-1
13.2	Standardized Measurement Procedures for Crystals .....	13-1
13.2.1	Crystal Noise Measurements .....	13-6
13.2.2	General Caveats when Measuring Premium Crystals .....	13-10

14	Appendix E: The Measurement of Transistor DC Parameters .....	14-1
14.1	The Measurement Setup .....	14-1
14.2	USO Transistor Candidates .....	14-2
14.3	2N2222A Measurement Results .....	14-3
14.4	2N2857 Measurement Results .....	14-6
14.5	Base Emitter Breakdown .....	14-9
15	Appendix F: The Measurement of Transistor AC Parameters .....	15-1
15.1	Introduction .....	15-1
15.2	The Measurement Setup .....	15-1
15.3	Temperature Effects .....	15-2
16	Appendix G: Transistor Noise Measurements .....	16-1
16.1	The Direct Method Measurement Setup .....	16-1
16.2	The Oscillator Method .....	16-6
16.3	Noise and Saturation .....	16-7
17	Appendix H: Chaos and Noise .....	17-1
17.1	Background Theory .....	17-1
17.2	A Simple Example for Noise and Chaos .....	17-2
18	Appendix I: Manufacturer SPICE Models for the 2N2222A .....	18-1
19	Appendix J: A Modeling Approach to BE Breakdown Noise .....	19-1
19.1	Difficulties .....	19-1
19.2	BE Breakdown Operation .....	19-1
19.3	Summary of Breakdown Physics, Modeling Approaches .....	19-3
19.4	An Experimental Sanity Check for the Breakdown Noise Current .....	19-4
19.5	A Fitted Model for the Measured 2N2222A Clapp Oscillator .....	19-9
19.6	Summary .....	19-14
20	Appendix K: Thermal Design .....	20-1
20.1	Oven Designs .....	20-1
20.2	Oven Physics .....	20-1
21	Appendix L: Space Qualified Transistors .....	21-1
21.1	Background .....	21-1
21.2	Transistor Choices .....	21-1
21.3	Transistors Suitable for High Stability Space Qualified Oscillators at 5MHz .....	21-2
21.4	Transistors Selected for the Circuits to be Analyzed and Developed .....	21-3
21.5	SPICE Models for the Transistors Found on the Web .....	21-4
22	Appendix M: Vibrations .....	22-1
22.1	The Acceleration Sensor .....	22-5
22.2	The Acceleration Sensor Postprocessing Amplifier .....	22-7
22.3	Damping .....	22-8

22.4	Modeling the Vibration Setup .....	22-9
22.5	Determining Physical Parameters.....	22-11
22.6	Vibration Measurements of Commercial OCXOs.....	22-15
22.7	Random Vibrations.....	22-18
22.8	Crystal Frequency Dependence on Orientation.....	22-23
22.9	OCXO Types, Measurement Procedure for Vibration Measurements.....	22-24
23	Symbols and Abbreviations.....	23-1

## Zusammenfassung

Um zu verstehen welche Effekte im Oszillator signifikant sind wurden Meßköpfe konstruiert, die den Oszillator kapazitiv und resistiv nur vernachlässigbar belasten und ihn damit weder verstimmen noch dämpfen. Es konnte nachgewiesen werden, daß sich die beobachteten Wellenformen sehr gut mit einer Zeitbereichssimulation decken, aber nur dann wenn auch alle relevanten physikalischen Effekte im Transistor (Bessel-Verschiebung, siehe „Physical Effects“, Early-Effekt, Sättigung und BE-Durchbruch) mitberücksichtigt wurden. Eine spezielle Testumgebung für LC und Quarzoszillatoren gestattete die Extraktion aller Spannungen, der Ausgangsleistung, des Phasenrauschens und zum Nachweis des BE-Durchbruchs auch des Basisstroms. Simulationen im Frequenzbereich waren aus mehreren Gründen (z.B. fehlende Effekte im Transistormodell) nicht in der Lage, alle Betriebszustände korrekt abzubilden.

Die Simulationsprobleme mit Oszillatoren extremer Güte konnten auf unzureichende numerische Genauigkeit der Standard (IEEE) Gleitpunktarithmetik zurückgeführt werden. Wie eigene Simulationsprogramme mit höherer Genauigkeit demonstrieren konnten, sind diese high-Q Oszillatoren sehr wohl simulierbar, aber eben nicht mit Standardprogrammen.

Um realistische Transistorparameter zu erhalten wurde eine Umgebung zur Parameterextraktion geschaffen, die statt der (pessimistischen) Datenblattwerte reale Parameter eines speziellen Transistorexemplars lieferte, die dann in realistische Modelle eingebracht werden konnten.

Um die gewonnenen Erkenntnisse zu demonstrieren, wurde ein Prototyp gebaut, der in einigen Daten die Werte kommerzieller Produkte übertrifft.

Die wichtigsten Ergebnisse der Dissertation waren:

1. Ein einfacher Clapp-Oszillator ist physikalisch und mathematisch äußerst komplex, wenn man alle physikalisch relevanten Effekte berücksichtigt.
2. Die Vorhersagen von Theorien mit stark vereinfachter physikalischer Grundlage (keine Sättigung, BE-Durchbruch, ...) sind extrem unzuverlässig.
3. Die dem Oszillator zugrundeliegenden Gleichungen haben theoretisch wie praktisch chaotische Lösungen, die für ein erfolgreiches Design ausgeschlossen werden müssen.
4. Bei 5MHz waren Zeitbereichssimulatoren wesentlich genauer und nützlicher als HB (Harmonic Balance) Ansätze. Der Grund dafür liegt in der Genauigkeit der HB-Modelle sowie in der extrem hohen Zahl erforderlicher Harmonischer.
5. Eine experimentelle Bestätigung von Simulationsergebnissen ist entscheidend für das korrekte Verständnis eines Oszillators. Alle Wellenformen müssen korrekt sein, um ein Modell zu verifizieren, nicht nur eine leicht anpassbare Phasenrauschkurve.
6. Die häufig verwendete Leeson-Formel hat eine nur sehr eingeschränkte Aussagekraft. Die darin enthaltenen Parameter sind nicht messbar, sondern Periodenmittel (Rauschzahl, Güte, Flickerparameter, ...). Im Prinzip ist der Leeson-Ansatz nur für ein a posteriori-Fitting geeignet.
7. Die formelbasierte, intuitive und einfache Designmethodik zum Entwurf von Oszillatoren kann nur einen Ausgangspunkt für ein Design liefern und prognostiziert gerade bei höheren Leistungen falsche Ergebnisse. Ein optimiertes Design kann nur durch Parametervariation und Kennfeldmessungen erzielt und dann auch verifiziert werden. Faustregeln (z.B. „Sättigung unbedingt vermeiden“) sind oft falsch.

Um die Wellenformen innerhalb eines Oszillators nachzumessen wurde eine „Oszillator-Workbench“ konstruiert, mit der sich alle relevanten Spannungen innerhalb des Oszillators ohne störende Beeinflussung abgreifen und darstellen lassen. Mit dieser Workbench konnten die wichtigen Effekte für jeden Arbeitspunkt bestimmt und in Relation zur Signalqualität am Oszillatorausgang gebracht werden.

Um die gewonnenen Erkenntnisse zu verifizieren wurde ein Oszillatorprototyp gebaut. Anstatt herkömmlicher Amplitudenregler wurde eine logarithmische Regelung konstruiert, die die Quarzleistung minimiert und auf 0.1dB konstant hält. Die Ergebnisse bezüglich Phasenrauschen (-120dBc/1Hz and -162dBc/>10 kHz) übertreffen kommerzielle, weltraumtaugliche Oszillatoren.

Wird ein niedrigeres trägerfernes Phasenrauschen benötigt kann ein nachgeschaltetes Filter eingesetzt werden. Statt der in der Industrie üblichen AT-Quarz Filter wurde ein wesentlich schmalbandigeres SC-Quarz Filter konstruiert, das durch eine phasengesteuerte Temperaturführung genau auf die Oszillatorfrequenz gezogen und dort stabilisiert wird. Die Alterung durch die Quarzbelastung, die bei höheren Leistungen auftritt wird durch diese Regelung kompensiert. Die Verbesserung des trägerfernen Phasenrauschens betrug 15dB.

## Summary

As a start I tried to build some rather conventional 5MHz test oscillators with the new crystals, and I immediately ran into problems that I did not foresee:

1. The new super-Q crystals had a very strong, highly drive level dependent (DLD) B Mode (a parasitic resonance close to the nominal frequency) and created spurious oscillations.
2. Simulation programs failed to simulate the oscillator waveforms correctly, if the Q of the crystals was too high. It only worked as the Q was reduced to about 10000.
3. The waveforms (tapped with classic low-capacitance scope probes) looked totally different compared to the predictions of the simulation programs, especially at higher amplitudes.
4. The predicted output power was up to 10dB off compared to the values measured with spectrum analyzer or scope.
5. Simulation results did not consider the limit of the Base-Emitter (BE) voltage, so the simulation results were simply wrong. A paper was written on the subject, published in the IETE journal of research [4].
6. In some high-power oscillators, phase noise increased with power instead of dropping as proposed by the theory (i.e., the Leeson formula, discussed later).
7. The performance of dedicated RF transistors was found to be worse than 250 MHz range fr transistors like the classic 2N2222A.

At first, I was puzzled about the results, but as my measurements were correct the common understanding how these crystal oscillators work was flawed.

In order to bring some light into the situation I was able to construct specialized probes that did not present much loading at 5MHz. All voltages at all circuit nodes were now accessible, and by current probes even the base current could be measured. The key lesson learned from this was that the waveforms are completely plausible with a *realistic transistor model* including all relevant physics, but not at all compatible with the simplified approach of classic oscillator theory. With a transistor model augmented by a BE (base emitter) breakdown part a very good agreement between time domain simulation and observed waveforms became possible, for all bias conditions I tried and also at high output power levels.

Regarding the simulation problems of circuits containing ultrahigh Q resonators, I was able to track down the failures to start up an oscillator to a numeric precision problem. The discretized equations are so ill-conditioned that the double precision IEEE floating point arithmetic is not able to properly describe the evolvment of an oscillation from zero (cold start, all voltages at 0V). The existing, but numerically extremely small solution components that would lead the current state to leave the origin are swamped out by arithmetic operations where the number of significant digits is not enough to cover the small amplitude increase. There is no easy solution; the numeric precision of commercially available simulation programs is fixed at IEEE double (64Bit). So, I had to write my own, specialized

ODE solvers using Python and C where I could prove that the extreme Q oscillators start up with sufficient precision, using a different, low order integration method.

Using time domain modeling, the measurement/simulation discrepancy in output power could be reduced to a dB and less.

To make sanity checks, and also because manufacturer's datasheets and simulation models were often very inaccurate and incomplete, I built a series of device extraction instruments. Instead of worse-case values, I needed realistic BE breakdown voltage values, gains, saturation parameters and others. After including these in the simulation process, it was possible to define design limits where the transistor would be working outside its specs. For the BE breakdown, I could also show the long-term deterioration of device parameters and the increase in phase noise, explaining why the noise does not decrease with power if a BE breakdown sets in.

Noise measurements of several space qualified transistors revealed that old, diffused LF transistors provided a better flicker noise contribution than more modern RF parts. This effect was crucial for close-to-carrier low phase noise, so LF transistors were preferred. Very modern transistors like HBT or SiGe are completely unsuitable at 5 MHz because of their high flicker noise corner frequency.

Contradicting established theory [2], saturation as such does not always deteriorate phase noise. In an experiment where an oscillator was operated over a grid of different bias conditions the lowest phase noise points were located where moderate saturation was present. A suggestion why this happened was given, but could not be proven without device engineering.

Classical theory [3, p65ff], based on a single-effect limiting mechanism (Bessel bias shift), delivers extremely unstable output power levels. I found this out using time domain simulated load lines for low and high-power oscillators. This explains – a bit a posteriori – why all reverse engineered USOs have an active amplitude regulator circuit instead of letting the oscillator core set its amplitude by bias shifting. A new log-detector based amplitude regulator was proposed, with a target accuracy of 0.2dB.

The classic theory treats oscillators as simple, single resonator circuits. For SC cut crystals, this is fundamentally wrong, and the equation systems governing the circuit using Kirchhoff's voltage and current rules (KCL and KVL) become a lot more complicated and have chaotic solutions. The whole repertoire of dynamic, high stored energy, high nonlinearity systems is actually contained in these equations, as simulations and measurements have shown. Squegging, mode-hopping, frequency-doubling, banded and non-banded chaos can be observed in time domain simulation and from prototypes. Frequency domain simulators are generally unable to model oscillator startup or true chaos, but I could demonstrate some of these effects by simulators and a "chaotic" prototype oscillator.

A workbench to extract oscillator waveforms using ultra low capacitance probes was built and implemented in a computer driven test frame running an oscillator through a grid of base and collector bias conditions and recording all waveforms, supply voltages and currents, phase noise, power output, and the output spectrum. This would be the approach for finding the best oscillator operating point and components by parameter optimization.

To demonstrate some of the points above a prototype USO was build. This prototype contains a Dewar flask with an oscillator core, a heater regulator, a precision amplitude regulator and an ultra-low noise voltage stabilizer for the whole setup. Using new crystals, a phase noise of better then -120dBc/1Hz and -162dBc/>10 kHz (10dBm output power) was achieved, with a low crystal power that could be regulated down to 1μW, settable by an external control. This oscillator outperformed a commercial

space oscillator. A phase noise and Allen deviation comparison is shown below (see USO prototype chapter, see footnote <sup>1</sup>):

RAKON is currently the leading high performance and space qualified company, followed by Wenzel (USA) and Morion (Russia).

Specification	PN@1Hz spec.	PN@1Hz typ.	PN@10kHz spec.	PN@10Khz typ.
RAKON RK410	-110	-120	-145	-146
USO Prototype	-120.21	-122 (best)	-160	-162 (best).

Relative long-term stability was in the range of 50E-12 per day, comparable to recent commercial USOs and also to vintage equipment.

A post-oscillator tracking filter was constructed again using an SC cut filter crystal with a very low bandwidth. The tracking is provided automatically by heating the filter crystal until a zero-phase condition across the crystal is reached (a temperature locked loop, so to say). Far-off phase noise could be improved by another 20dB, while the attenuation close to the carrier caused a phase noise increase of ca. 7dB at 1Hz, with a crossover at 10Hz. Crystal power was up to 2mW (after a cross-check with the manufacturer), and aging is of no concern due to the active temperature regulation and the wide tuning range compared with the nominal frequency, so this filter can be used to improve the noise floor.

A test setup was constructed to evaluate the vibration performance of oscillators. Based on an arbitrary signal generator, a power amplifier, a mechanical vibrator device and a vibration sensor I made a vibration workbench for commercial and self-built oscillators. Key results were that vibrations are a major threat to top USO performance. Sensitivity depends on (undocumented) internal resonances, but what can be said is that shocks are much worse than a sinusoidal acceleration or noise, even at low amplitudes.

The key lessons I learned by working on this fascinating topic were:

1. Never underestimate the complexity of seemingly simple nonlinear circuits like a Clapp oscillator.
2. Pencil and paper math is only useful if the relevant physics is included. If not, it could be strongly misleading by predicting results that are physically impossible.
3. All governing differential equations of a USO Clapp SC oscillator can have chaotic solutions. Chaos must be meticulously excluded by simulation and experiment, including parameter variation.
4. At 5MHz, time domain simulators have proven much more useful than frequency domain simulators. They can predict chaos, the waveforms match better with the experiments, models can be changed more easily, and startup can be covered as well. The big problems, however, are long simulation times and difficulties with very high Q resonators. Time domain simulators, however, do not provide phase noise results.
5. It was found that harmonic balance simulations delivered significantly less accurate predictions regarding waveforms and output power (when compared to measured or time domain simulated results). The reasons were that a usually large number of harmonics is needed to accurately model fast rise time phenomena, and that the models contained in the software did not include breakdown or deep saturation effects properly.
6. Experimental confirmation of simulated/calculated results is crucial. Any useful theory must be able to *explain all current and voltage waveforms* correctly and in line with the

---

<sup>1</sup> We were able to improve the 1Hz value to -128.73dBc using filtering refinements. A paper about this is forthcoming.

measurements, plus phase noise output. Retrofitting parameters (like in the Leeson formula) does **not** provide physical insight, even if the fitting parameters carry the name of physical quantities.

7. The intuitive simplicity and elegance of the first available design procedures cannot not be preserved if a usable level of accuracy is needed. All future cookbooks for designing/improving oscillators must rely on a solid physical foundation (covering all relevant nonlinear effects) and, due to sheer complexity, on numerical instead of algebraic computations. The optimization process involves a mixture of parameterized simulations and parameter space searches.
8. The math currently available (as far as I am aware of) is not usable for the simulation of nonlinear, chaotic, extremely high-Q, multi-resonator equations including nonlinear noise sources with a non-white (e.g., flicker) spectrum. What we see is a system of extremely stiff, chaotic, stochastic differential equations with no promising computer solution strategy. This, in my opinion, is a worthwhile problem for further research.
9. I was able to build oscillator prototypes that had better performance than commercial space parts (see engineering results).



## 1 Introduction

The master clocks of deep space exploration vehicles have always been an extremely crucial component of all space missions, from the Apollo series, to the extreme depths of the Voyager mission, the Cassini mission to the rings of Saturn, and many more.

The most critical success factors are extreme long-term stability / low aging and low phase noise. Stability is so important not because of spaceship to earth communication, but because of navigation and telemetry where the allowable deviations from a correct course are extremely small and space distances must be measured with a relative precision of  $10^{-9}$  and less. Distance measurements in space are made by measuring the time between radio signals, and these travel with the speed of light (approximately  $3 \cdot 10^8$  m/s), so a measurement error of 1 ns means 30 cm of distance error (one way). When used in a very long baseline interferometry (VLBI) arrangement, the error in the triangulated object distance is many times this amount.

Given the severe consequences of a mission failure the deep space ultra-stable oscillators (USOs) have always been built using the best available technology available. For the American space program this technology was provided by the Jet Propulsion Laboratory (JPL).

Most publications about oscillators refer to frequencies above 100 MHz, mostly VCO's. As circuit simulation at these frequencies is more often done with Harmonic Balance Simulators a SPICE re-simulation is a good thing to validate the waveforms. If the typical number of harmonics set in the HB program is set to a small value in order to save computing time there will be a significant difference compared to SPICE results. To minimize the influence of parasitic effects and yet to have high frequency behavior a prototype LC oscillator at 5 MHz was chosen. While the final 5 MHz oscillator will have a very high Q crystal the use of an LC oscillator as a test vehicle gives better insights. High voltage tolerant probes not loading and/or detuning the circuit were developed accordingly (more details to follow). It turned out that this sequence showed some of the CAD software problems to be discussed and logical remedies were found. None of these important details were found in the literature. An article [4] in the IETE Journal of Research covers some findings made by the analysis regarding the effects of base emitter breakdown.

I believe my major contributions were to find and overcome those problems, to design a crystal oscillator that operates reliably down to 2  $\mu$ W of crystal dissipation and to use a constant temperature stabilization circuit for a high-Q crystal filter which also can compensate the effect of aging by tracking and regulating filter phase. This filter can further improve the Signal to Noise (S/N) ratio of the oscillator signal.

Also, better crystal resonators were invented, and the mathematical theory for the crystal oscillators to predict phase noise correctly is now available. Finally, high precision phase noise analyzer became available, like the R&S FSWP signal analyzer.

### 1.1 Why This Thesis?

When looking at the circuits of oscillators actually used in real missions, we mostly see a standard Clapp oscillator with a surprisingly small number of components. After an idea from Rohde [1] the output signal is decoupled directly through the resonator, adding a very selective output filter. The oscillator seen from the "outside" appears as a black box emitting a very clean signal.

Prof. Rohde also had asked me some time ago if I could build a better oscillator at 5 MHz based on a new crystal generation. After I had built a successful prototype Prof. Rohde asked me if I would be interested in turning this into a PhD project on highly stable oscillators with less than  $50 \cdot 10^{-12}$  frequency change relative to 5 MHz between 1 and 20 sec.

At the time, I assumed I was working with a very well understood circuitry. Practically unlimited publications on the topic were available, but these publications were not detailed enough to explain how to achieve this performance and fundamental research became necessary.

The sequence of the chapters here may appear unorthodox and opposite to the normal pathway of explaining circuits first and then dive into components and details. In the classic literature focusing on linear or quasilinear approaches, this works fine, but in the case of extreme Q multiresonator circuits like we have here it does not at all, as was found out the hard way. The basic paradigm needs to be adapted: the oscillators here are inherently nonlinear, potentially chaotic, depending on a lot more physical effects than in classic theory and they needed to be treated as such to obtain a reasonable agreement of theory and experiment. So, the basics come first, and real oscillators follow.

## 1.2 Acknowledgements

The present work would not have been possible without key people who helped me through the whole, somewhat surprising, always interesting but nevertheless very challenging process. So, I want to thank

Firstly, Prof. Dr.-Ing. Habil. Ulrich L. Rohde for providing excellent expertise at the same time for being patient with me finding all kinds of interesting problems along the way instead of solutions on the direct path. He encouraged me very much and many times to question established theories and to work my way thoroughly through all the new facts and form them into a consistent and practically verifiable proposition how things inside an oscillator really work.

Prof. Dr.-Ing. Matthias Rudolph from the BTU thanks for a lot of good advice of how to work oneself into the scientific way to work and for constructive critique on my problem-solving suggestions.

Prof. Dr. rer. nat. Ignaz Eisele thanks for alighting discussions on device physics issues where his valuable insider information could provide information about semiconductor fabrication processes, noise properties and physical effects that could not be obtained from manufacturers and the available literature.

Dipl.Phys. Dipl.Ing Bernd Neubig, CEO of AXTAL measured the crystal parameters of the special crystals on his analyzer and IEC444-conformant crystal test environment. With standard equipment it would not have been possible to measure resonances and Q factors precisely enough. He also helped me with answers to my questions about physical crystal properties and manufacturing processes.

Luke Mueller, BSEE, CEO of Croven Crystals provided me with USO-grade sample crystals to build the prototypes. Without those, my oscillator performance would not have been possible. He also provided very detailed information about his crystals.

Dipl.Ing. Markus Müller from the Dresden Technical University helped me adapting the measurement and model-creation technology of wafer-based measurements for packaged devices.

Andreas Bergmann supplied me with vintage transistors to support the theory that older devices have better flicker noise performance.

Richard Kaußler provided me with high quality chip photographs of decapped transistors, along with BE breakdown electroluminescence snapshots.

Dipl.Ing. Alexander Roth from Rohde & Schwarz Munich helped me to understand the very powerful but complex FSWP phase noise analyzer and providing interesting test oscillators to verify my thoughts and to be used for test objects in vibration tests.

I thank my family for understanding and supporting my new challenge even if it was coming with a lot less spare time for family activities, especially my parents, they educated me to be curious and persistent.

## References

- [1] Ulrich L. Rohde, “Crystal Oscillator Provides Low Noise,” *Electronic Design*, vol. 21, Oct. 1975.
- [2] Michael M. Driscoll, “Low Noise Oscillator Design and Performance,” presented at the 2002 IEEE Frequency Control Symposium, New Orleans, LA, USA, Jun. 2002.
- [3] Ulrich L. Rohde, “A New and Efficient Method of Designing Low Noise Microwave Oscillators,” TU Berlin, Berlin, 2004.
- [4] Wolfgang Griebel, Matthias Rudolph & Ulrich L. Rohde (2020) Added Noise in Oscillators Caused by the Transistor Base Emitter Breakdown Phenomenon, IETE Journal of Research, DOI: [10.1080/03772063.2020.1847702](https://doi.org/10.1080/03772063.2020.1847702)

## 2 History and Background

This chapter deals with the history of space qualified oscillators, the components used, and the uses of USOs (Ultra Stable Oscillators) for communication and telemetry. An industry standard oscillator is analyzed in detail, and a short market survey shows the performance limits achievable today.

The first crystal oscillator to work in a space environment was the tube-based 20MHz and 40MHz beacon operating on board of the Sputnik satellite in 1957. It was a Colpitts design with a push-pull output stage feeding two whip antennas. The Sputnik oscillator had no oven for frequency stabilization, not a problem for a beacon transmitter (circuit documented in [1]) at the time.



*Figure 1 - The World's First Satellite - The Sputnik (1957)  
Picture from AntenTop Journal [1]*

Only a few years later, in 1962, the USA had launched several satellites for navigational purposes and the issue of frequency accuracy immediately became extremely important. Navigational satellites circling around the earth suffer from large temperature differences between sunlight and shade, so an OCXO design became mandatory. A double Dewar design (proposed by the JPL in 1963, [2]) was used to obtain aging rates of  $1.3 \times 10^{-9}$  per day.

The United States pursued a very ambitious space program to set their foot on the moon (in 1969) before the Soviet Union. Precision telemetry was key to success if you wanted to navigate precisely over extremely long distances. The signal roundtrip times to the moon (384400km away) are in the range of ca. 2.5 seconds. Similar times apply to other communication between satellites or satellites to ground. This means that the Allan variance of the oscillators used should have their lowest Allan deviation values from 100ms to 10s to make runtime (i.e., distance) measurements as precise as possible. Some documentation of the Apollo program is available [3], although the schematics of their USOs are still confidential.

A big step forwards towards lower phase noise and better aging was the invention of doubly rotated crystal cuts like the SC (stress compensated) cut. These crystals achieved Q values in excess of 2.5 million compared to the 100.000 of conventional AT cut parts and were since used for all newer space missions. Other benefits of the SC cut were increased radiation tolerance, less vibration sensitivity, less DLD (Drive Level Dependency) effect, lower thermal hysteresis and retrace, and some more.

At present, USOs seem to share some common characteristics, regardless of the manufacturer:

1. All use SC cut crystals
2. The best performing units run at 5MHz, the second-best ones at 10MHz.
3. The crystals are always run-in 3<sup>rd</sup> overtone mode, never at the fundamental frequency
4. Clapp topologies are preferred (as far as designs are published)
5. Only vacuumized crystals are used (either in glass or cold weld)
6. All USOs run in double ovens (as far as designs are published)
7. The top USOs use Dewar flasks
8. Top USOs have anti-vibration provisions.

## 2.1 An Overview over Current 5MHz USO Parts for Space and Terrestrial Applications

USOs have a history dating back several decades. In the 70ies and 80ies they became packaged industrial products that supported a wide range of instruments like spectrum analyzers, VNAs, signal generators and synthesizers, counters, radars, transmitters, telemetry equipment and the like. Except for the very beginning, the skills to make USOs were considered highly proprietary and detailed descriptions like schematics or component values are usually trade secrets and never published. By reverse engineering undertaken by several researches some statements can nevertheless be made about the performance and evolution of USOs over the last 20 years and the frontiers reached today.

The frequency of 5MHz is uncommon today, even if the best performance can still be achieved at this frequency (due to the Vig curve, see [4]). 5MHz is a good compromise between crystal thickness, (in 3<sup>rd</sup> overtone mode), size, power, aging, tolerances and the maximum Q that can be achieved. For all modern parts, the phase noise and Allen deviation data for 5MHz is better than for the much more common frequency of 10MHz.

The following USO products for 5MHz were found in a market analysis conducted in Aug. 2020:

**USO Comparison for 5MHz Crystal Oscillators**

Manufacturer	Type	Space	Frequency [MHz]	Output Power [dBm]	ADEV/1s	ADEV/10s	PN/1Hz	PN/10Hz	PN/100Hz	PN/1kHz	PN/10kHz	PN/100kHz	Aging/day	Aging/Year
Morion	MV83M	N	5	0	5,00E-13	N/A	-115	-135	-150	-155	-158	N/A	3,00E-10	3,00E-08
Merion	MV89	N	5	7	2,00E-12	N/A	-105	-130	-145	-150	-155	N/A	1,00E-10	5,00E-09
Merion	MV180	N	5	7	2,00E-12	N/A	-105	-130	-145	-150	-155	N/A	1,00E-10	1,00E-08
Merion	MV207	N	5	2,5	2,00E-12	N/A	-100	-130	-153	-158	-160	N/A	N/A	2,00E-08
Merion	MV267	N	5	7	5,00E-13	N/A	-118	-148	-155	-160	-161	N/A	N/A	1,00E-08
Rakon	HSO14	N	5	8	1,00E-13	8,00E-14	-130	-150	-157	-160	-160	N/A	5,00E-11	1,00E-08
Rakon	RK410	Y	5	5	5,00E-13	N/A	-120	-135	-140	-146	-146	N/A	N/A	1,00E-08
Microsemi	9500B	Y	5	7	3,00E-13	3,00E-13	-120	-145	-155	-157	-160	-160	5,00E-11	1,00E-08
CMAC	Experimental	Y	5		1,00E-13	1,00E-13	-131	-147	-156	-156	-156	N/A	1,00E-10	N/A
Vectron	OXI74	N	10	8	2,00E-12	2,00E-12	-105	-135	-157	-167	-172	-173	5,00E-10	3,00E-08
Wenzel	500-19933	Y	10	13	N/A	N/A	-100	-130	-150	-155	-155	N/A	5,00E-10	N/A
Wenzel	500-27991	Y	10	12	3,00E-12	3,00E-12	-108	-138	-155	-161	-162	N/A	2,00E-10	2,00E-08

Figure 2 - Table of The Best 5MHz Oscillators Commercially Available

Exceptionally good values are marked in green.

The following remarks apply:

1. Only models where a 5MHz frequency was available were selected
2. Only stock models were chosen - no parts made to order
3. When several grades were available, the best one was chosen
4. Values apply after warmup and burn-in (up to 90 days)
5. Oscillator data obtained by web snapshots made on 2020-08-15.
6. Vibration, shock, radiation effects are not considered
7. Daily aging values estimated with datasheet formula where no direct value was available
8. The CMAC Data is from a 2003 paper. Improved version announced with BVA4
9. Vectron/Wenzel: No 5MHz Datasheet available, but 5MHz data should be better than 10MHz

Datasheets were obtained for all parts on the list. As said, no detailed information about circuits, components, thermal design, and packaging is available from the manufacturers. For some parts, other researches have reverse-engineered the parts and documented interesting information on the web. We will discuss these designs as far as available information permits. As a caveat, the parts could look different now due to product evolution.

## Conclusions

The 2020 performance limits of non-space USOs are defined by the HSO14, and for space units we have the RK410 and the 9500B. The key facts are:

1. The 1s Allen deviation optimum is  $1 \cdot 10^{-13}$  for ground USOs and  $3 \cdot 10^{-13}$  for space USOs.
2. For phase noise at 1Hz offset we have -130dBc for ground and -120dBc for space USOs.
3. Daily aging is  $5 \cdot 10^{-11}$  for both.
4. The best noise floor we can expect is -160dBc at 10kHz offset for both.

It should be noted that:

1. All premium parts for ground and space do not use standard crystals. HSO14 and RK410 uses a BVA4/QAS, probably also true for the 9600B.
2. These crystals have a Q close to the theoretical maximum, and we may expect that they are also selected for minimum flicker noise.
3. Reverse engineering suggests that *all* oscillator components are selected. Very low tolerance resistors, glass encapsulated components, selected semiconductors and military range IC components are used, no surprise for a mission critical space component where every single part of the oscillator must comply to rigid MIL-norm quality assurance processes.
4. The measurement of the close to carrier noise levels of -130dBc or less asks for nonstandard measurement techniques involving a cryogenic sapphire reference with an Allen deviation of less than  $1^{-14}$  at 1s. Another important prerequisite is a lab environment with perfect thermal, electrical, magnetic, and mechanical shielding. Phase noise testing is discussed in a separate chapter.
5. Replicating the top performance offered by the best commercial oscillators today with standard components is probably not possible.

If we make an educated guess about the most critical component of the oscillator, we end up with the crystal itself. Here is why:

1. The topology of all reverse-engineered premium performance USOs is a Clapp with decoupling the power through the resonator. It is probably safe to assume that all top performers today use the same topology.
2. If we use high-quality capacitors (NP0 ceramic or Styroflex), resistors (low tolerance low noise metal film) and inductors there is no big advantage from high quality commercial to space components. The influence on noise can be assumed to be negligible.

3. The transistor used in the oscillator core has a critical influence on flicker noise. Low frequency transistors are used in all premium USOs that have been reverse engineered, so we may assume that the top performers today do the same. A carefully selected LF transistor like the 2N2222A, or the BC107B, or a similar part is probably the best choice, so, unfortunately, there is not a lot to be gained here.
4. What is left is the crystal. Standard non-swept SC crystals have a Q of ca. 2.2 million, a BVA/QAS can reach 2.58 million. The Q has a square influence on phase noise, so we can lower noise by 1.38dB. The amount of flicker noise is the next important factor. The filter bandwidth at 5MHz and Q of 2.5 million is 2Hz, so just at the 1Hz carrier offset where we want a phase noise minimum the filter effect is no longer helpful and the bare noise of all noise sources in the core will add up. As the other noise sources have been optimized, crystal flicker noise is the only free variable left. The BVAs and successors (QAS) are the best solutions available today.

Caveats:

None of the top performers discloses information about schematics, thermal and mechanical design, or component values and types. All what we know comes from sparse datasheets and the reverse engineering of similar or predecessor parts.

## 2.2 The Evolution of Phase Noise Measurement Systems

The first phase noise test systems capable of measuring close to carrier phase noise by using FFT (Fast Fourier Transform) techniques came from HP was called the HP3048A [4] and filled a whole room with a computer-controlled setup containing signal generators, spectrum and FFT analyzers, switches and other auxiliary equipment. At 1Hz, measurement limits were around -120dBc for a 10MHz oscillator with a few dBm output.

The next generation of phase noise measurement test equipment integrated all the components in a single instrument and increased performance drastically. Examples of this second-generation equipment are the HP5052B and the R&S FSUP models.

As more computing power became available better (and faster) signal processing algorithms were possible inside the instruments. The newest generation of phase noise analyzers grew slightly in size, but now has the possibility to do all IF in digital, including a correlation option lowering the noise floor by another 10dB (100 correlations). The current instruments are touchscreen enabled Windows machines.



In 2017 the present top instrument was introduced by R&S, the FSWP [5] phase noise analyzer ranging from 1MHz to 26.5GHz, using hardware correlators capable of running a 10Hz to 1MHz analysis with 100 correlations for a 5MHz oscillator in about 3 minutes:



Figure 3 - Rohde & Schwarz FSWP Phase Noise and Signal Analyzer  
Photo from Rohde&Schwarz Website

Frequency range starts at 1MHz and goes up to 50GHz (internal). This instrument is not just a phase noise analyzer, but can also provide spectral, noise, channel, pulsed and vector measurements depending on options. All high-precision measurements in this thesis were done on the FSWP.

When it comes to extreme performance levels (like RAKON HSO14 and successors) even the FSWP reaches its limits. In fact, no general-purpose phase noise analyzer on the market can make reliable measurements of oscillators of the  $10^{-14}$  class (1 second Allen deviation). Specialized mixing, digitizing and correlation hardware, multiple, even cryogenic reference oscillators, extremely shielded and environmentally controlled lab environments can push the limits to  $-145\text{dBc}/\text{Hz}$ . Techniques like this are discussed in the “Phase Noise Measurement Techniques Section” but are out of reach of most electronics labs, how well equipped they may be.

### 2.3 Performance Levels

Current master oscillators have further improved performance over the older models. While the daily aging rate has not gone down by much (Apollo had 1.3ppb, we are now at 100ppt), the Allen deviation has. If we look at an R&S Unit from the beginning of the 70ies (XSD), the stability looks like this:

Measuring time	Scatter ( $\Delta f/f$ )
1 msec	$< 1 \times 10^{-9}$
10 msec	$< 1.5 \times 10^{-10}$
100 msec	$< 2 \times 10^{-11}$
1 sec	$< 3.5 \times 10^{-12}$
10 sec	$< 4.5 \times 10^{-12}$
Test setup acc. to Fig. 1	

Figure 4- R&S 1971 XSD Crystal Standard Frequency Stability Chart  
Picture from the XSD Service Manual

Today, the best space units are now at or below  $7 \times 10^{-13}$  in the range between 100ms and 10s. For ground-based units the performance is even better (e.g., RAKON HSO14, with  $5 \times 10^{-11}$  aging per day, and an Allen variance of  $8 \times 10^{-14}$  at 1s, [6]). These units need a perfect lab environment and are not space qualified, however.

It is a legitimate question why one does not resort to atomic standards like Rubidium or Caesium for even higher stability. The reason is that long-term stability is exceptional, but phase noise is not, as can be seen in the picture below, taken from an HP5061 Caesium frequency standard:

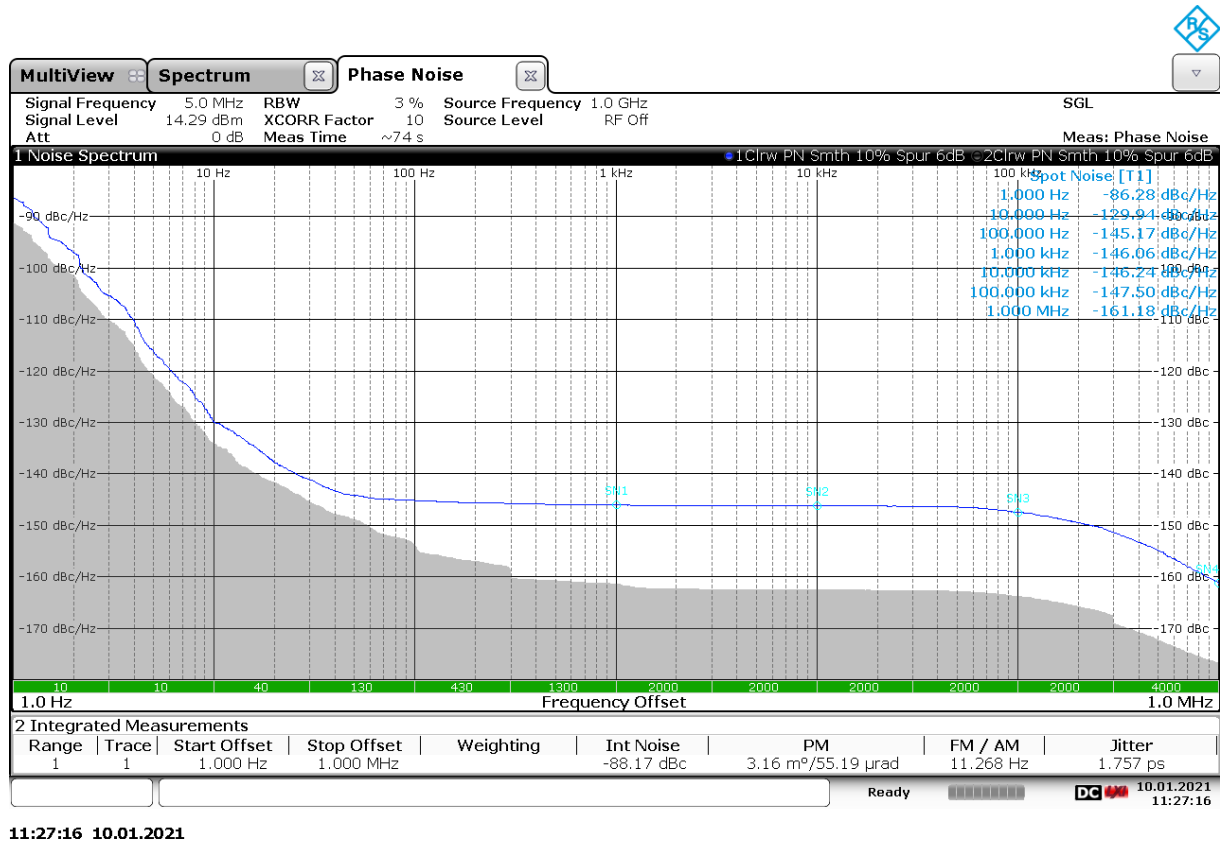


Figure 5 - Phase Noise of an HP5061C Caesium Atomic Frequency Standard, Picture Courtesy of Prof. Ulrich L. Rohde

This, combined with the added weight, size, complexity, power consumption and limited lifetime makes Quartz crystal based USOs preferable in many space missions.

The HP10811 oscillator is a classic that no PhD thesis on USOs even today should ignore. In my opinion, this was a benchmark design successful for twenty years. It was used to power generations of professional HP RF equipment like spectrum analyzers, VNAs, counters, ... Unlike modern parts, the HP10811A is fully documented, including schematics, service manuals, parts lists, and several articles explaining how the circuit works. The circuit of the HP10811A implements a design from Rohde where the crystal is simultaneously used as a resonator and a filter, improving signal quality (discussed in detail later). The architecture of the HP10811A (oscillator core, buffer, amplitude regulator, output stage and temperature regulator) can be found in almost all USOs made today.

A full description of the HP10811A can be found in appendix A.

The HP oscillator is a Colpitts oscillator in which the inductor is replaced by a series crystal, therefore called a Clapp oscillator, as shown in the circuit below:

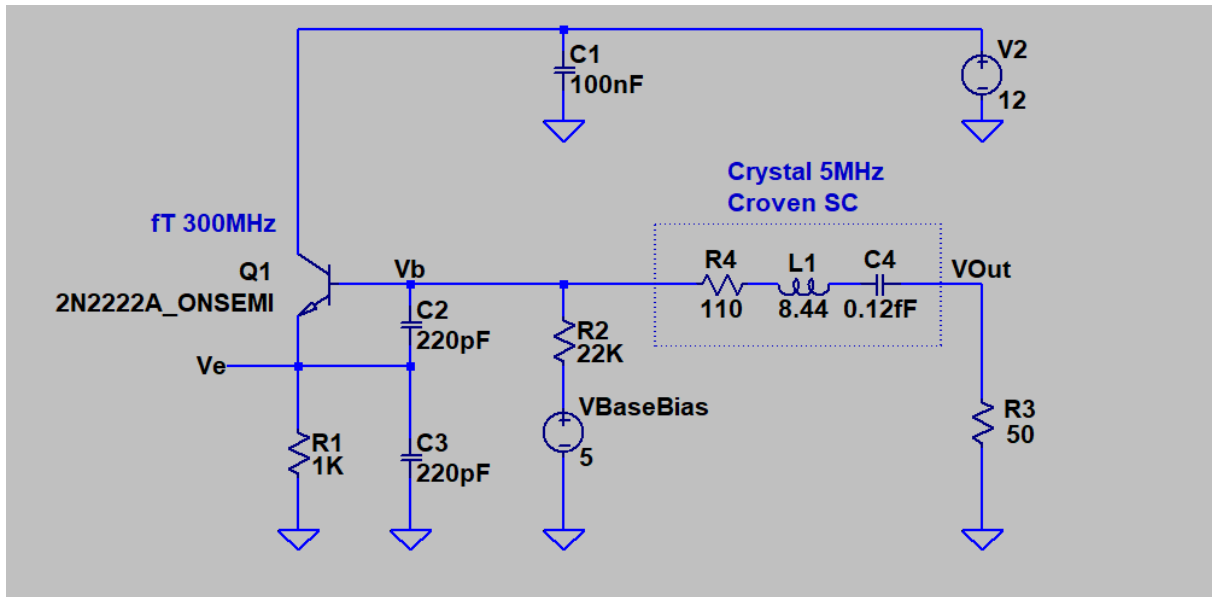


Figure 6 – Sample 5 MHz Clapp Oscillator with Crystal Resonator

This is the type of oscillator this dissertation is based on.

## References

- [1] Unknown Author, “Sputnik Transmitter,” *Antentop (Russian)*, vol. 21, no. 1/2017, p. 2, 2017.
- [2] J. B. Oakes, W. J. Billerbeck, K. F. Read, “Design of an Ultra Stable Oscillator for Satellites,” in *APL Technical Digest*, 1963.
- [3] Granata, R. L. and (NASA Goddard Space Flight Center Greenbelt, MD, United States), “Proceedings of the Apollo unified S-band technical conference,” Jan. 1965, [Online]. Available: <https://ntrs.nasa.gov/citations/19750003182>.
- [4] Hewlett Packard Co., *3048A Phase Noise Measurement System Reference Manual*. 1989.
- [5] R&S, “R&S FSWP Phase Noise Analyzer Specifications.” Accessed: Nov. 17, 2020. [Online]. Available: [https://scdn.rohde-schwarz.com/ur/pws/dl\\_downloads/dl\\_common\\_library/dl\\_brochures\\_and\\_datasheets/pdf\\_1/FSWP\\_d-at-sw\\_en\\_3607-2090-22\\_v0900.pdf](https://scdn.rohde-schwarz.com/ur/pws/dl_downloads/dl_common_library/dl_brochures_and_datasheets/pdf_1/FSWP_d-at-sw_en_3607-2090-22_v0900.pdf).
- [6] RAKON Corp., “RAKON HSO14 Ground USO Specifications.” Accessed: Nov. 16, 2020. [Online]. Available: <https://www.google.com/search?client=firefox-b-d&q=RAKON+HSO14>.

## 3 Principles of Oscillator Design

The following chapters deal with several aspects of general and USO oscillators. Please refer to the following appendices about some additional information regarding oscillator design:

**Appendix H, Chaos and Noise** discusses the effects of noise in a chaotic system. Using the simple logistics equation as a template, it can be shown that noise, to some extent, cover up or even suppress chaotic behavior.

**Appendix I, Manufacturer Spice Models** shows a collection of SPICE models for a single transistor type, the 2N2222A (A common part available in a space qualified version). Even important parameters can vary considerably, making some device parameter extraction inevitable.

### 3.1 Basic Principles of Oscillation

Before we go into more details about the history of oscillators, circuits, components, performance and so on, we should give a definition what should be understood as an oscillator circuit.

A fairly general definition would be that an oscillator is a circuit that uses some DC input to create a (hopefully periodic) output signal.

Several principal ideas have been invented to describe and analyze oscillator circuits. One of the most primitive models is a lossy resonator combined with a negative resistance replenishing the losses (used, e.g., in the papers of Lee and Hajimiri, [1, p.19]).

The next common approach was that of an amplifier/feedback network. Barkhausen [2] and Nyquist [3] formulated conditions that allowed to compute the frequency of oscillations (i.e., frequencies where the output of amplifier routed through the feedback network would satisfy a total gain of 1 and a phase which is zero or a multiple of  $360^\circ$ ). This theory uses the practical properties of analytic functions and has been a standard method of design for decades. Both approaches are so called LTI (linear time independent) theories.

The approaches using the negative resistance or the Barkhausen/Nyquist criteria deliberately overlook a central mechanism of any real-world oscillator – a limiting mechanism. Without this, we cannot compute an output amplitude from neither the negative resistance nor the feedback loop model.

A limiting mechanism, is by nature, a nonlinear mechanism. At small amplitudes, it is ineffective, at larger amplitudes it reduces gain more and more until a stable output amplitude is reached. Clear enough, the idea that an oscillator still only works with sinusoidal voltages and currents needs to be dropped, making the negative resistance and the feedback loop model problematic.

Many arguments have been produced to still adhere to the very practical methods of the linear network theory, most of them arguing that the nonlinear effects are so small that they can be treated by a sort of “small disturbance” approach. This can explain some benevolent circuits, but it completely fails with circuit having stronger nonlinearities or saturation effects.

Rohde [4] was the first to create an oscillator theory that did no longer rely on an LTI approach. Using a decomposition of the collector current into harmonics whose amplitudes are given by modified Bessel functions depending on the ratio of the AC base voltage swing over the temperature voltage, he derived a method to design oscillators that, for the first time, had a physically plausible, built-in limiting effect.

It turned out that other limiting effects like saturation, the Early effect and BE breakdown also were important and often stronger than the Bessel function limiting effect. This will be discussed in detail later in this thesis.

It is important to understand that adding physical effects to a model improves accuracy and predictability, but all this comes at a prize – The clarity, simplicity and elegance of the simpler approaches is completely lost, the complexity almost explodes and numeric methods and simulations are the only methods left. Simple, linear equations in LTI are now systems of nonlinear differential equations in the time domain with (if noise is included) stochastic components for a realistic case.

### 3.1.1 A Little Excursion to a Nonlinear Oscillator Using a General Dynamics Approach

Just to demonstrate the completely different approach taken by the theory of general nonlinear dynamics, let us create a very simple nonlinear oscillator with an LCR series resonator as above, but now with a nonlinear negative resistance as the active element instead of the transistor.

We could therefore use a simple (cubic) nonlinear term to incorporate nonlinear damping into our model. From an AC perspective, the circuit now looks like this:

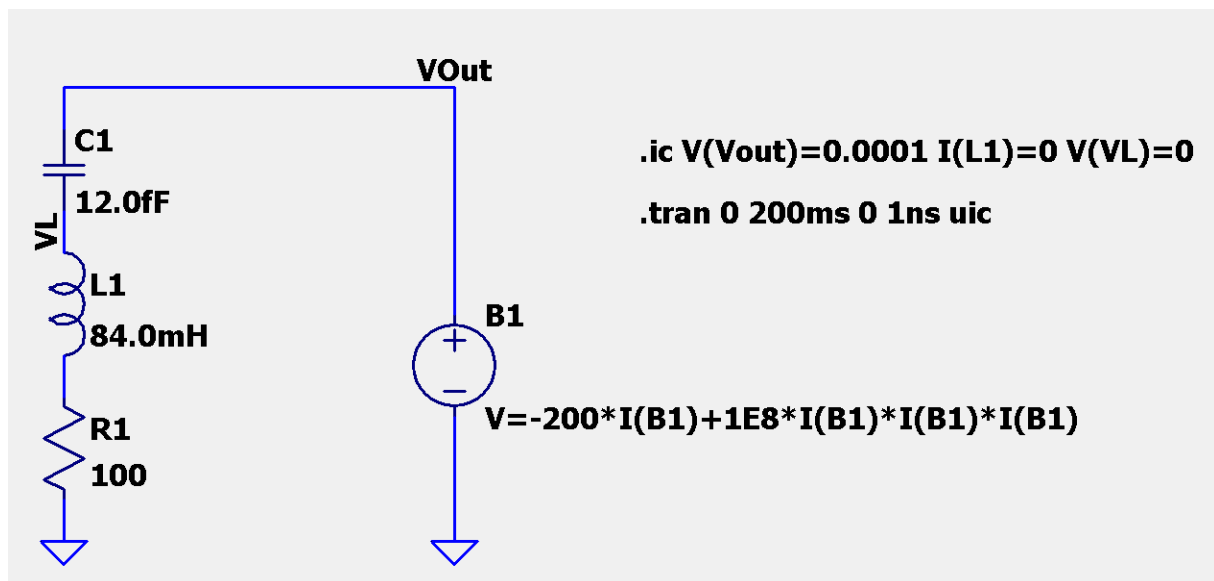


Figure 7 - Simple Nonlinear Oscillator Schematics

The “behavioral” voltage source incorporates the negative resistance and the cubic damping factor, the rest is a resonator with a Q of about 25.000. When we treat this analytically using the KVL, we get an equation like

$$RI + LI' + \frac{1}{C} \int_0^t Idt + \alpha I + \gamma I^3 = 0$$

where R, L and C are the resonator parameters and  $\alpha$  and  $\gamma$  are the parameters of the nonlinear resistance. Differentiating over time, normalizing, and reordering gives a Van der Pol type equation [5]:

$$I'' + I'(a + bI^2) + \omega_0^2 I = 0$$

where

$$a = (R + \alpha)/L, b = 3\gamma/L \text{ and } \omega_0^2 = 1/(LC).$$

As all sufficiently interesting nonlinear circuits van der Pol equations have no closed form solutions.

Any useful *oscillator* design must be *unstable* and capable to start itself from a powerless, steady state (e.g.,  $I=0$ , and  $I'=0$ ). Heuristically, we can assume that the current is so small at startup so that the square term can be neglected. The equation then becomes a linear harmonic oscillator:

$$I'' + aI' + \omega_0^2 I = 0$$

and the conditions for an increasing amplitude over time is that the total damping is negative, meaning that  $a$  is smaller than 0 and subsequently

$$a < -R$$

must be fulfilled. Then we get a solution over time of the form:

$$I(t) = e^{-\delta t} \{ I_{t=0} \cos(\omega_d t) + (I_{t=0} \delta + I'_{t=0} \sin(\omega_d t) / \omega_d) \}$$

Where

$$\delta = a/2 \text{ and } \omega_d^2 = \omega_0^2 - \delta^2$$

If we assume a cold start so that

$$I_{t=0} = 0 \text{ and } I'_{t=0} = 0$$

the consequence is that the current  $I$  will always be zero, too, not what we like. We seem to need an external stimulus, even if the damping is negative. For a more profound analysis we can use the theory of dynamic systems to assess the fixed point (there is only one in this case) of the van der Pol equation and its stability. To do this, we convert the second order differential equation into a set of two differential equations by substituting a variable  $X = I'$ . We then get (by substituting into the original equation and solving for  $X'$ ):

$$\begin{pmatrix} I' \\ X' \end{pmatrix} = F(I, X) = \begin{pmatrix} f_i(I, X) \\ f_x(I, X) \end{pmatrix} = \begin{pmatrix} X \\ -X(a + bI^2) - \omega_0^2 I \end{pmatrix}$$

which is a just a reformulation as a system of two first-order differential equations where we can compute the derivatives  $I'$  and  $X'$  at a given point from the coordinates  $I$  and  $X$ , using the vector function  $F$ . If we ask for local properties, we need to take the total derivative (the Jacobian matrix) of our equation system, by  $I$  and  $X$ , like

$$J = \begin{pmatrix} \frac{df_i(I, X)}{dI} & \frac{df_i(I, X)}{dX} \\ \frac{df_x(I, X)}{dI} & \frac{df_x(I, X)}{dX} \end{pmatrix} = \begin{pmatrix} 0 & 1 \\ -2XbI - \omega_0^2 & -(a + bI^2) \end{pmatrix}$$

The Jacobian acts as a “tangent” to our matrix function at a given point and can be used to approximate the vector function in the vicinity of the point we have computed the Jacobian for.

The Eigenvalues of this matrix determine the local behavior around a given point. Several possibilities exist:

1. All Eigenvalues have a real part smaller than 0. This corresponds to a stable point where a neighboring point to our given starting point move closer to the given point over time (a “sink”).
2. If one Eigenvalue is 0, we have a “saddle point” some points around move in, and some out. The other Eigenvalue determines the direction.
3. If both Eigenvalues have a real part  $> 0$ , we have a “source” where points would move away from the starting point.
4. Imaginary Eigenvalue components indicate a rotation of a neighboring point around the point  $(I, X)$ . Together with the sign of their real parts we get inbound or outbound spirals.

If we compute the equation for the Eigenvalues of  $J$  we obtain

$$\text{Det}(J - \lambda E) = \begin{vmatrix} -\lambda & 1 \\ -2XbI - \omega_0^2 & -(a + bI^2) - \lambda \end{vmatrix} = 0$$

Solving this for  $\lambda$  results in

$$\lambda = -\frac{(a + bI^2)}{2} \pm \sqrt{\frac{(a + bI^2)^2}{4} - 2XbI - \omega_0^2}$$

For the starting fixed point with  $X = 0$  and  $I = 0$  we have:

$$\lambda = -\frac{a}{2} \pm \sqrt{\frac{a^2}{4} - \omega_0^2}$$

If we go back to the definition for our SC cut model crystal with 5MHz from the circuit diagram above, we obtain a  $\lambda$  that has a small positive real part (remember  $a$  is negative, and  $O(1)$ ) but the expression under the root is a huge negative number, giving a result which is almost completely imaginary. So, the point  $(0,0)$  is an unstable fixed point, yes, but the movement of neighboring points is a spiral with an extremely small slope, again explaining the long startup times. The derivation above confirms the common rule of thumb formula for an oscillator startup which is

$$\tau = \frac{Q}{2\omega_0} \text{ with } Q = \omega_0 L / (R + \alpha)$$

Another result (not derived here) is that the oscillations have a stable limit cycle as an attractor, plus that the simple case here has no chaotic attractors (by virtue of the Poincaré–Bendixson theorem [6]. This theorem is **not** valid for more complex nonlinear equations or more variables).

For a further mathematical treatment and simulation effort, it makes sense to transform the equation into a form with less parameters. If we start from

$$I'' + I'(R + \alpha + 3\gamma I^2)/L + I/LC = 0$$

The first step is to introduce a normalized time

$$T = \frac{t}{\sqrt{LC}} \text{ so we have } \frac{dI}{dt} = \frac{dI}{dT} \frac{1}{\sqrt{LC}} \text{ and } \frac{d^2I}{dt^2} = \frac{d^2I}{dT^2} \frac{1}{LC}$$

And our equation now reads:

$$\frac{d^2I}{dT^2} \frac{1}{LC} + \frac{\frac{dI}{dT} \frac{1}{\sqrt{LC}} (R + \alpha + 3\gamma I^2)}{L} + \frac{I}{LC} = 0$$

Cleaning up gives:

$$\frac{d^2I}{dT^2} + \frac{dI}{dT} \sqrt{\frac{C}{L}} (R + \alpha + 3\gamma I^2) + I = 0$$

We could get rid of some more parameters by setting

$$x = I \sqrt{\frac{-3\gamma}{R + \alpha}} \text{ remembering } \alpha \text{ is negative and larger than } R$$

Substituting this and rewriting results we get



$$\frac{d^2x}{dT^2} \sqrt{\frac{R + \alpha}{-3\gamma}} + \frac{dx}{dT} \sqrt{\frac{C}{L}} \sqrt{\frac{R + \alpha}{-3\gamma}} \left( R + \alpha + 3\gamma \frac{R + \alpha}{-3\gamma} x^2 \right) + x \sqrt{\frac{R + \alpha}{-3\gamma}} = 0$$

And finally

$$\frac{d^2x}{dT^2} + \frac{dx}{dT} \sqrt{\frac{C}{L}} (R + \alpha)(1 - x^2) + x = 0$$

If we now set

$$\varepsilon = -(R + \alpha) \sqrt{\frac{C}{L}} = \frac{-(R + \alpha)}{\omega_0 L} = \frac{1}{Q_U} \text{ where } Q_U \text{ stands for undamped } Q$$

and revert to the prime notation, now for T, we get:

$$x'' - \varepsilon(1 - x^2)x' + x = 0$$

which is the van der Pol differential equation [5] in classic notation known for over a century and extensively treated in the literature. In fact, this is bad news because, depending on  $\varepsilon$ , this differential equation is notorious for bringing simulators to their limit.

The range of  $\varepsilon$  for the oscillator types we are trying out therefore is in the order of  $10^{-1}$  (LC tank) to  $10^{-6}$  (SC cut crystal).

So, as a conclusion for now, we have derived that the Clapp circuit used in USOs can be approximately modelled by a van der Pol type nonlinear oscillator, at least when looking at the startup process.

The oscillations obtained depend strongly on  $\varepsilon$ . A strongly nonlinear case with  $\varepsilon = 5$  is shown below:

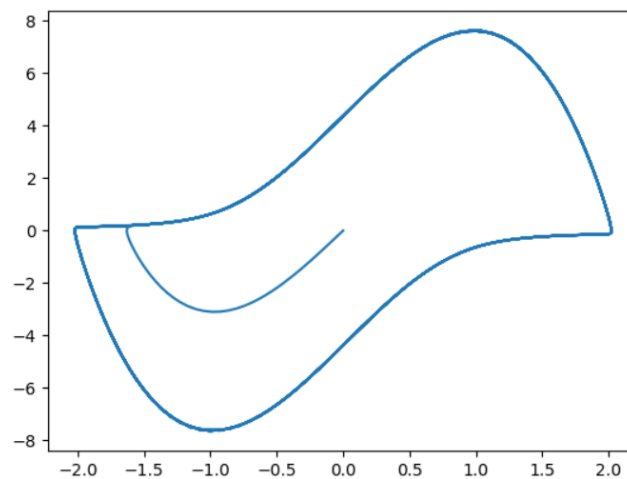


Figure 8 - Large  $\varepsilon$  Limit Cycle

A **large**  $\varepsilon$  causes an immediate startup (just the single branch coming from the origin), and the resulting periodic limit cycle has sharp corners designating abrupt changes in value.

The time plot shown below confirms this:

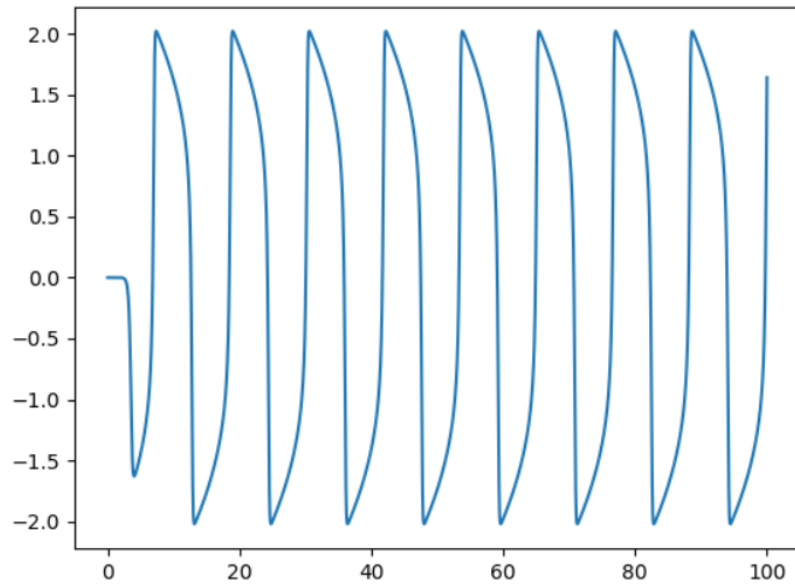


Figure 9 - Large  $\varepsilon$  Waveform

Very **small** values ( $\varepsilon < 0.1$ ) result in very different picture (with  $\varepsilon = 0.1$ ):

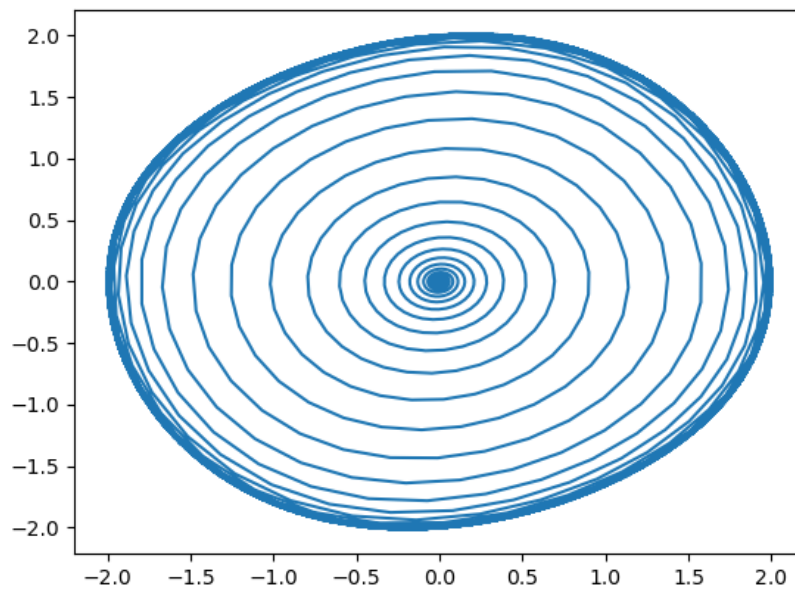


Figure 10 - - Small  $\varepsilon$  Startup

The startup now takes much longer. The final limit cycle resembles an ellipsoid, with no sharp edges present anymore.

The waveform looks almost sinusoidal:

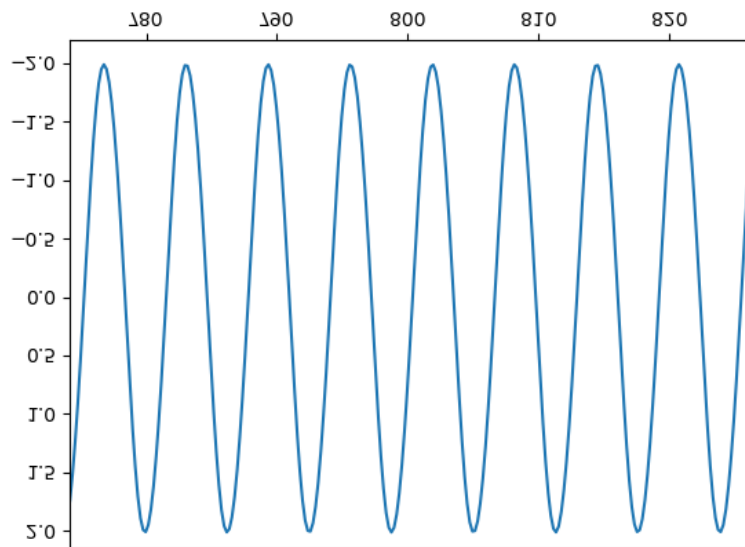


Figure 11 -- Small  $\varepsilon$  Waveform

When going back to the derivation of the Van der Pol equation above  $\varepsilon$  is inversely proportional to the undamped  $Q$ . For an ultra-high- $Q$  oscillator, like an SC cut crystal with a  $Q$  of 2.5 Million,  $Q$  is in the range of  $10^6$  and this implies that several hundred thousand cycles will be needed to start an oscillator from zero. This brings classic simulators to their limits but can be successfully treated by specialized approaches (hardcoded ODE solvers, higher precision math libraries, ...) to be discussed later.

As a conclusion to the general dynamics intermezzo, the nonlinear general dynamics approach does not need to make invalid simplifications about the physics, but due to exploding mathematical complexity there are no pencil-and-paper derivable results even for the simplest circuits. Careful and appropriate numerics and simulations are the only choices.

On the other hand, plots in the phase space can be highly informative about the physical effects taking place in a realistic oscillator model. This will be shown in real-world examples.

An important point when progressing from the simple van der Pol equation to more complex models including realistic transistors is that the solutions can now exhibit *all kinds of periodic, quasi-periodic and chaotic behavior*. This is not just a theoretical possibility. Especially Colpitts/Clapp oscillators are prone to chaos, as several researchers have shown. Avoiding this is a critically important goal when building USOs. Satisfactory explanations of chaos cannot be obtained by linearized oscillator models.

## References

- [1] A. Hajimiri and T. H. Lee, *The Design of Low Noise Oscillators*. Boston: Kluwer Academic Publishers, 1999.
- [2] Heinrich Barkhausen, *Elektronen-Röhren*, 4. Auflage., vol. 3. Band Rückkopplung. S.Hirzel, Leipzig, 1931.
- [3] Harry Nyquist, “Regeneration Theory,” *Bell Systems Technical Journal*, no. 1/1932, Jan. 1932.
- [4] Ulrich L. Rohde, “Crystal Oscillator Provides Low Noise,” *Electronic Design*, vol. 21, Oct. 1975.
- [5] B. van der Pol, “On oscillation hysteresis in a triode generator with two degrees of freedom,” *Philos. Mag.*, vol. 6, no. 1922.
- [6] I. Bendixson, “Sur les courbes définies par des équations différentielles,” *Acta Math.*, vol. 24, no. 0, pp. 1–88, 1901, doi: [10.1007/BF02403068](https://doi.org/10.1007/BF02403068).

### 3.2 Phase Noise Basics and Important Properties

If we start from the approach used by the discoverer of phase noise [1], David Leeson, he used a feedback oscillator model to understand the principles. His block diagram looked like this:

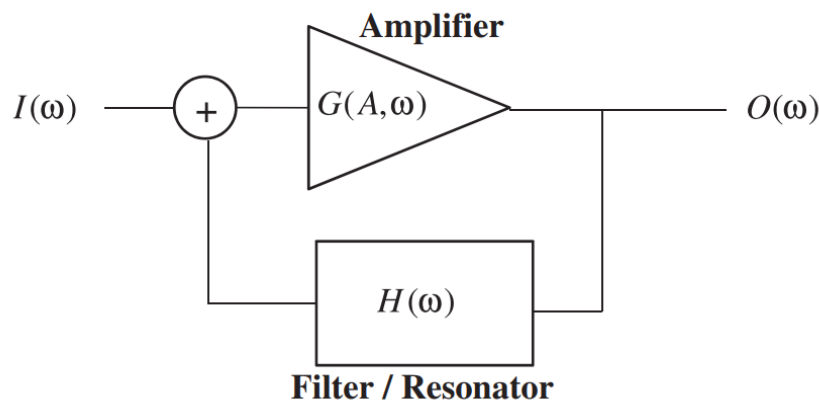


Figure 12 - Leeson Block Diagram used to Compute Phase Noise

$G(A, \omega)$  stands for the transfer function of the amplifier,  $H(\omega)$  describes the feedback path, and  $I(\omega)$  and  $O(\omega)$  stand for the input and output signals, respectively. If we assume that the circuit contains noisy elements, their noise will be both amplified and filtered by the resonator, but it will appear at the output, together with the nominal output frequency. The spectrum of the output signal depends of the spectral distribution of the noise, modified by resonator filtering and amplifier nonlinearities, but in general it will no longer appear as a single tone, but a distributed spectrum with a finite width depending on the spectrum and intensity of the noise sources. After a series of assumptions and computation steps Leeson arrived at his famous formula (valid for white noise sources only):

$$L(f_m) = 10 \log \left\{ \left[ 1 + \frac{f_0^2}{(2f_m Q_L)^2} \right] \frac{FkT}{2P_{sav}} \right\}$$

shown here without flicker and tuning component terms. The formula above gives the spectral density ratio to the carrier power at offset  $f_m$ .  $f_0$  stands for the carrier power,  $Q_L$  is the loaded Q of the resonator,  $F$  stands for a noise factor and  $T$  for the absolute temperature.  $P_{sav}$  represents the oscillator output power, and  $k$  is Boltzmann's constant.

The theory can be extended to more complicated circuits as the one shown below:

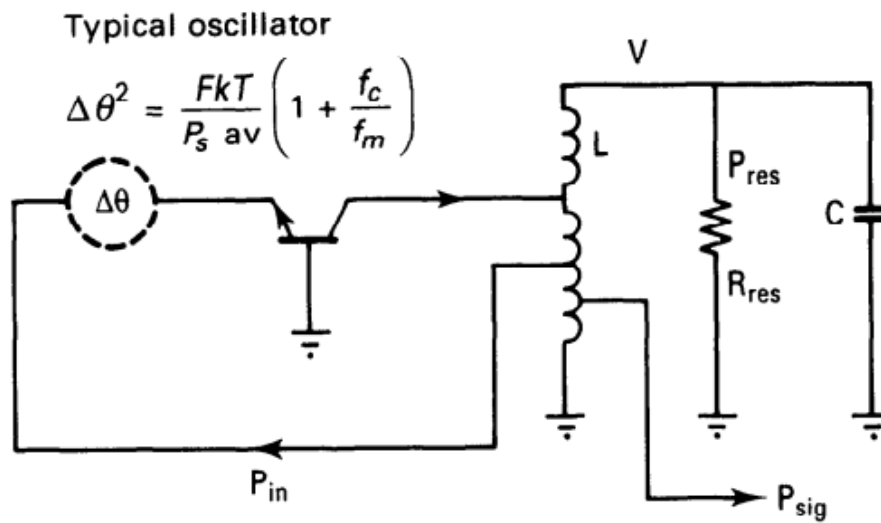


Figure 13 - Oscillator with Gain Stage and Feedback Network [2]  
Picture from [2]

By using individual noise contributions, a sum formula for all noise components can be given [2, p215]. The flicker term was added by Dieter Scherer [3] from Hewlett Packard.

The complete formula runs:

$$L_{\omega_m} = \frac{1}{8} \frac{FkT}{P_s \text{ av}} \frac{\omega_o^2}{\omega_m^2} \left( \frac{R_n}{\omega_o W_e} + \frac{1}{Q_{\text{unl}}} + \frac{P_{\text{sig}}}{\omega_o W_e} \right)^2 \left( 1 + \frac{\omega_c}{\omega_m} \right)$$

Phase  
Perturbation

Resonator Q

Flicker  
Effect

Input power  
over  
Reactive Power

Signal power  
over  
Reactive Power

Figure 14 - Phase Noise Formula Including All Relevant Noise Sources (Scherer)  
Picture from [2]

While a breakthrough for the time, the Leeson formula has its problems. First, there are amplifiers that work using a negative resistance, not using a feedback loop (e.g., a Clapp oscillator frequently used in USOs). Next,  $Q_L$  and  $F$  are not the well-defined stationary RF or DC values of the resonator and the amplifier transistor, but they are cyclostationary averages taken over a period of oscillation (and, in practice, no measurable quantities). In fact, they are fitting parameters to reconcile simulation to measurements, so the Leeson formula can hardly be used to design oscillators from scratch.

## References

- [1] D. B. Leeson, "Oscillator phase noise: A 50-year retrospective," in *2015 Joint Conference of the IEEE International Frequency Control Symposium & the European Frequency and Time Forum*, Denver, CO, USA, Apr. 2015, pp. 332–337, doi: [10.1109/FCS.2015.7138853](https://doi.org/10.1109/FCS.2015.7138853).
- [2] U. L. Rohde, *Microwave and wireless synthesizers: theory and design*. New York: Wiley, 1997.
- [3] Dieter Scherer, "Design Principles and Test Methods for Low Phase Noise RF and Microwave Sources," presented at the RF&Microwave Measurement Symposium and Exhibition, 1978, [Online]. Available: [http://hparchive.com/seminar\\_notes/Scherer\\_Low\\_noise\\_source\\_design\\_and\\_test.pdf](http://hparchive.com/seminar_notes/Scherer_Low_noise_source_design_and_test.pdf).

### 3.3 A Phasor Approach to Noise and Phase Noise

Phase noise is a random deviation of the frequency, not the amplitude of a signal source (see [1] for definitions and an introduction to terminology). To illustrate the principle using phasors, we draw a phasor diagram for a pure and a noisy signal.

When looking at the noiseless signal, the length of the phasor stays is constant, and the phase increases evenly by the product of the circular frequency and time.

In the noisy signal, the phasor end point moves around in a "cloud" of random values and has no constant amplitude nor a linearly increasing phase. Both amplitude and phase deviation are random quantities with a spectral distribution defined by the nature of the random process (white noise, flicker, spot, ...). The "gravity center" (i.e., a mean value) of the cloud, we may assume, still rotates with an average frequency. This assumption is valid for all random processes that have a defined mean value (true for all relevant physical noise processes).

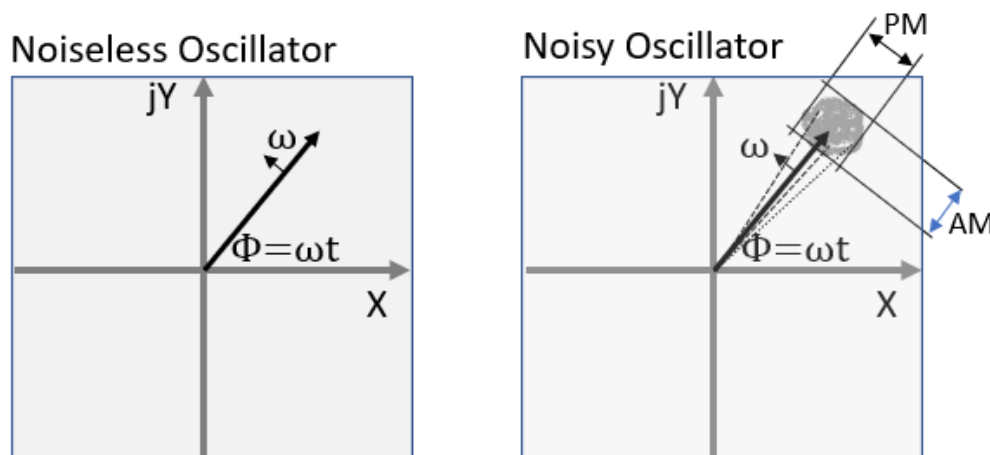


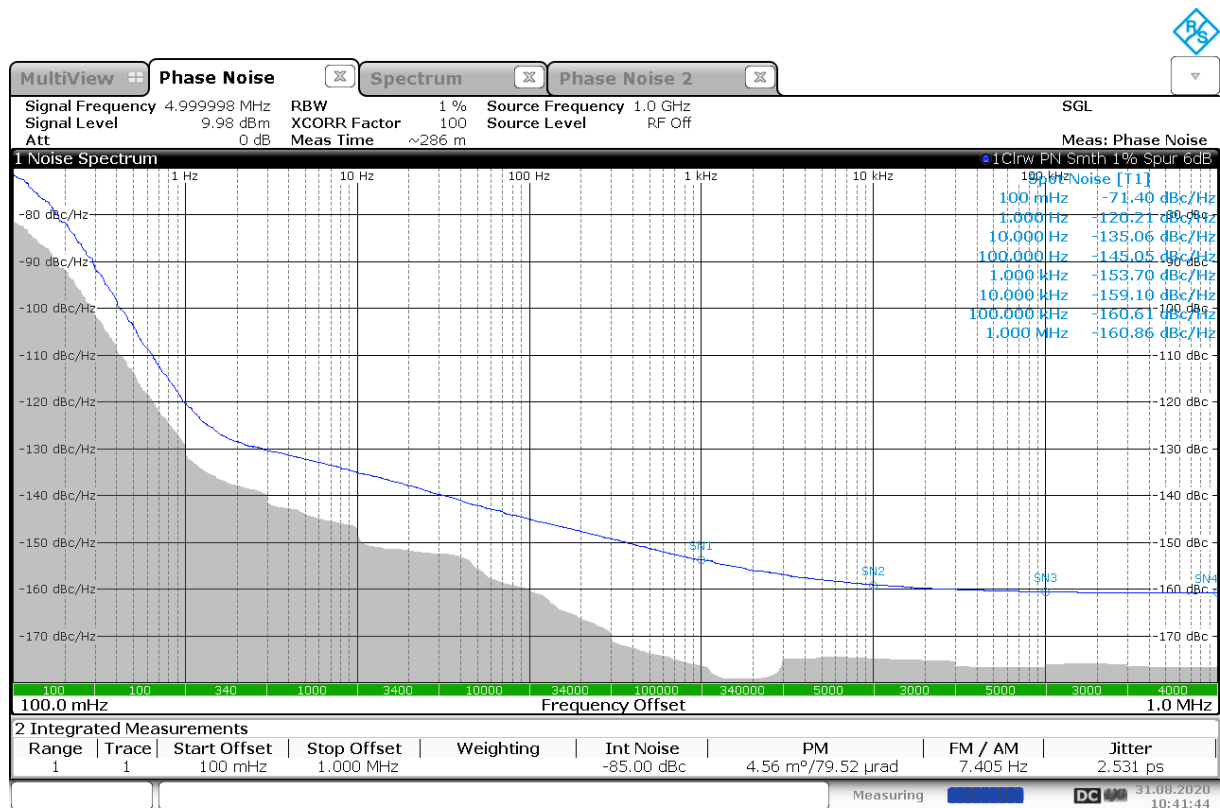
Figure 15 - Phase Plane Plots of a Noiseless and a Noisy Oscillator

The random deviations from the endpoint of the phasor vector have two observable effects; first, the amplitude of the signal (i.e., the length of the phasor) now varies over time in a random way. This is called AM noise because it looks like a noiseless carrier multiplied by a random variable with a mean value of 1. Second, the angle of the phasor now fluctuates around the value of  $\omega t$  defined by a random variable with mean zero. This is called FM or phase noise (PM).

If we ask for the resulting spectrum of a signal with AM and PM noise, unfortunately only white (frequency-independent) noise can be treated exactly by pencil and paper math. Flicker noise, e.g., with an  $1/f$  spectrum and other colored noise spectral densities must be handled using numerical methods ([1] has a derivation for spectra following negative and positive power laws). The bottom line

is still that all physically relevant processes create both AM and phase noise, only the proportions differ.

A realistic phase noise curve is shown below:



10:41:44 31.08.2020

Figure 16 - Example of the Measured Phase Noise of a 5MHz USO

### 3.3.1 Why is Phase Noise an Important Problem?

It is instructive to see what happens to the spectrum of a signal if phase noise is present in a signal. Depending on the amount of the random phase fluctuations, the single tone spectrum now flattens out into peak with sidelobes, where the slope and width of the decay happens according to the spectral density of the phase fluctuations. If we assume a white distribution, the decay is following an inverse square function of the frequency offset, as Leeson has shown.

Such a broadened curve has several negative effects on RF signal processing systems. We will discuss them one by one.

**Masking of weak signals.** A sidelobe in a strong transmitter with a lot of phase noise could cover up a small signal in close vicinity to the carrier, making the small signal impossible to receive. [2]

A graphical example for the masking effect is shown below:

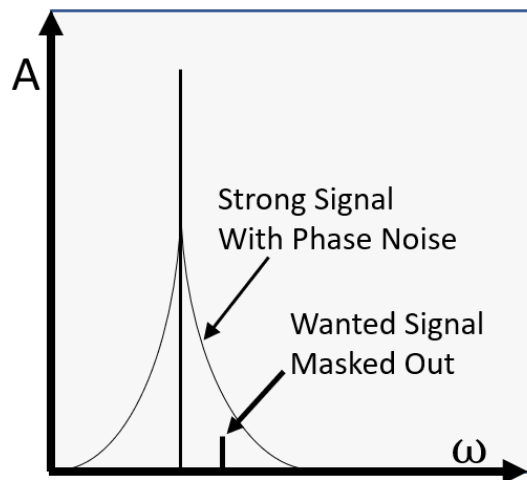


Figure 17 - A Strong Signal with Phase Noise Masks out a Wanted Signal

**Reciprocal Mixing.** If a noisy signal (e.g., from an LO or synthesizer), is used as an input source for a mixer with a given output IF frequency, not only LO plus IF signals will appear at the output of the mixer, but also signals in the neighborhood. This process (called reciprocal mixing) reduces receiver sensitivity and enables strong signals close to the desired signal to punch thru and reach the IF signal processing chain. [3, section 5.7 and 6.2.2] The reciprocal mixing effect is shown next:

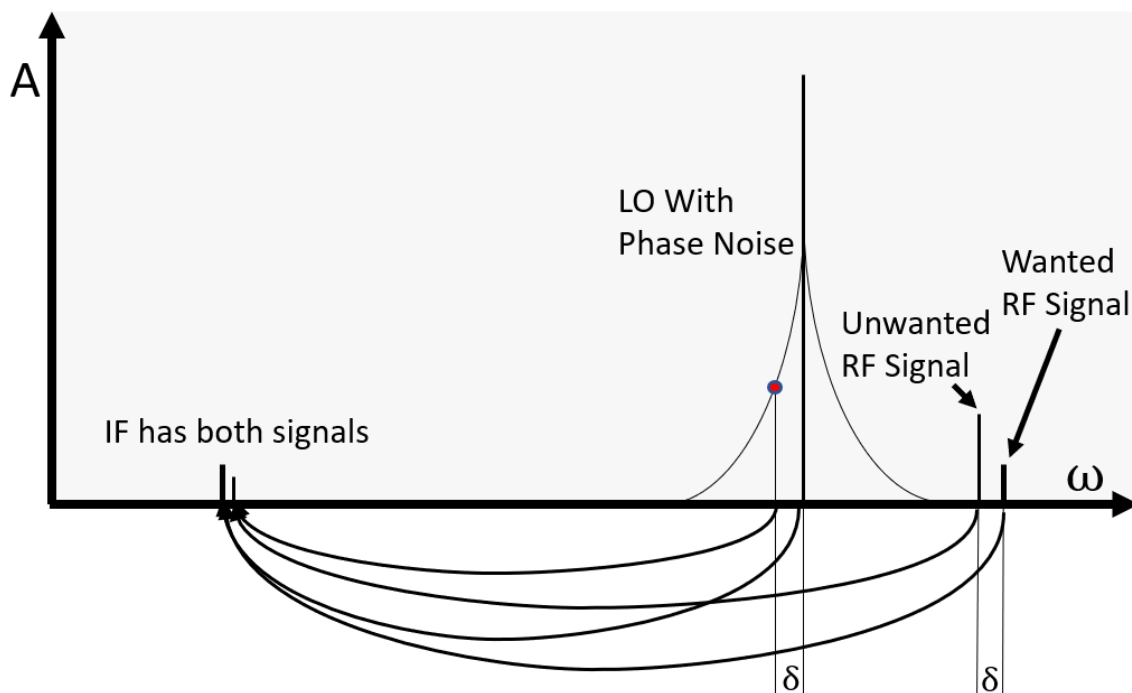


Figure 18 - Reciprocal Mixing Effect due to Local Oscillator with Phase Noise

**Jitter.** In telemetry where time is measured as the span between two zero transitions of a signal, phase noise leads to a random fluctuation of the measured timespan called jitter. Jitter, in space applications, sets a limit to how precise distances can be measured. The same effect applies to radar, where phase noise results in broadened target echoes and inaccurate distance results (this was the reason why Leeson started research on the mechanisms of phase noise in the first place).



**Adjacent Channel Congestion.** When thinking of crowded cellular networks with many digital channels, sidelobes into the neighboring channels rise the bit error rate there, calling for more elusive error corrections and/or reduced data throughput. This effect is specified in the ACPR (adjacent channel power ratio) figure of merit.[4]

**Frequency Multiplication.** If an USO is used as a master oscillator for all other systems, like on board of a satellite, the USO frequency at 5 or 10MHz is multiplied many times to reach, e.g., a VHF, UHF or microwave transmitter frequency. Every multiplication step adds 20dB phase noise per decade of the multiplication factor, so the starting point of a multiplier chain must have really low phase noise. It is worth mentioning that properly designed multiplier chains can have less phase noise than oscillators running natively at a higher frequency (see [5] for multiplying techniques).

### 3.3.2 Phase Noise in the Signal Processing Chain

The signal processing chain of RF systems (amplifiers, mixers, filters, detectors, ...) contains components that are (at least slightly) nonlinear, and none of them is completely noiseless. It is important how a noisy input signal is transformed by the building blocks inside an RF system.

Linear components like amplifiers, when reverting to the phasor model, just extend the length of the phasor. Phase is shifted by a constant amount defined by the group delay, but that would be it. A closer look needs to include amplifier noise, which is added to the input and then amplified along with the input signal. A chain of perfectly linear amplifiers with noise factors  $F_i$  and Gains  $G_i$  then behaves according to the Friis formula [9]:

$$F_{TOT} = 1 + (F_1 - 1) + \frac{F_2 - 1}{G_1} + \frac{F_3 - 1}{G_1 G_2} + \frac{F_4 - 1}{G_1 G_2 G_3} + \dots$$

If a linear system only adds phase noise (this is a theoretical case, i.e., by a lossless capacitance with a fluctuating value), it is intuitive that the phase fluctuations would add up more in a mean square way and not anymore by the Friis formula, as found by Rubiola [1, p49ff]. Addition now depends on the spectral power densities of the noise, and for flicker (1/f) noise the noise terms just add.

Now let us introduce some nonlinearity and see what happens. Under the assumption that the system output can be expressed as a polynomial function of the input (with complex coefficients), the output phasor now contains a piecewise vector sum with one vector at the base frequency, plus further vector components added, with their harmonically related angular frequencies.

Leaving noise out for a moment, the result in a spectrum view would be a carrier plus all the mixer products defined by the coefficients of the transfer polynomial function, as shown below:

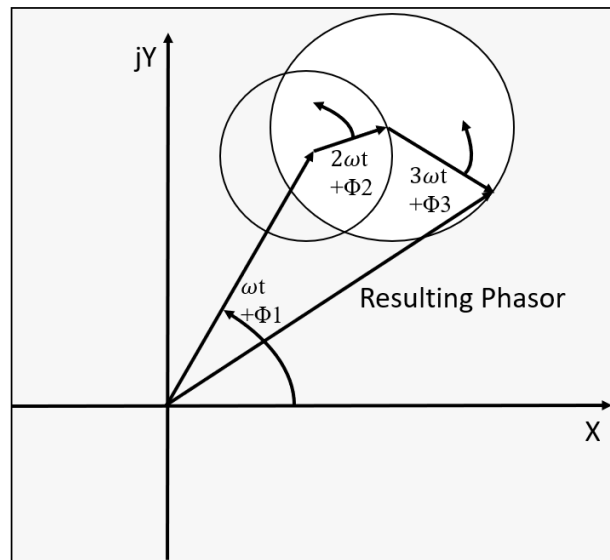


Figure 19 - Resulting Phasor After Nonlinear Amplification

To round things up, we now submit a general input signal containing AM and phase noise to a nonlinear system approximated by a polynomial. In principle, the same mixing occurs like in the noiseless case, but the output spectral lines will inherit the sidelobes of the input signal, only wider (multiplied by their harmonic number). Another effect is that even a theoretically pure AM noise signal will be converted in both AM and phase noise due to the nonlinear conversion process (remember that the higher order phasor components rotate several times faster than the fundamental phasor, covering a broader range of phase angles in the resulting vector sum).

The following plot shows this effect:

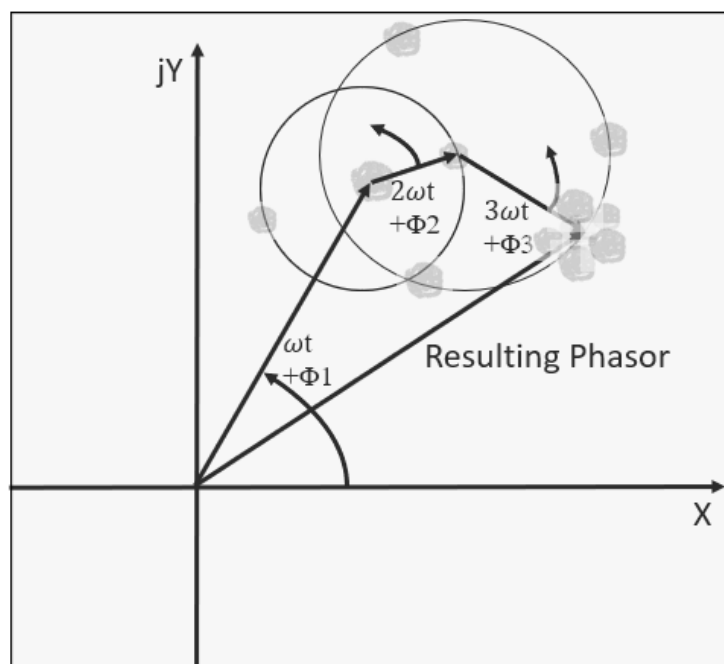


Figure 20 - Nonlinear Amplification Including Phase Noise

This process is called AM/PM conversion (for some mechanisms see [7]) and is the main reason why the oscillator *and* the amplifier chain of an USO should be designed as linear as possible.

## References

[1] E. Rubiola, *Phase noise and frequency stability in oscillators*. Cambridge, UK; New York: Cambridge University Press, 2009.

[2] J. Rutman and F. L. Walls, "Characterization of frequency stability in precision frequency sources," *Proc. IEEE*, vol. 79, no. 7, pp. 952–960, Jul. 1991, doi: [10.1109/5.84972](https://doi.org/10.1109/5.84972).

[3] T. J. Roupheal, *RF and digital signal processing for software-defined radio: a multi-standard multi-mode approach*. Amsterdam; Boston: Newnes, 2009.

[4] Signal Hound Corp, "What is Channel Power and Occupied Bandwidth", Website <https://signalhound.com/news/what-is-channel-power-and-occupied-bandwidth/> Snapshot Dec. 28<sup>th</sup>, 2020

[5] I. Rosu, "Frequency Multipliers," p. 24., Website Snapshot Jan. 10<sup>th</sup>, 2021. [https://www.qsl.net/va3iul/Frequency\\_Multipliers/Frequency\\_Multipliers.pdf](https://www.qsl.net/va3iul/Frequency_Multipliers/Frequency_Multipliers.pdf)

[6] H. T. Friis, "Noise Figures of Radio Receivers," in *Proceedings of the IRE*, vol. 32, no. 7, pp. 419-422, July 1944, doi: 10.1109/JRPROC.1944.232049.

[7] S. Golar, "Identifying Mechanisms of AM-PM Distortion in Large Signal Amplifiers," Master Thesis at UCLA, 2015.

### 3.4 Physical Effects in Oscillators

A major objective of this work is to understand and possibly improve USOs in the 5MHz range. The theoretical background regarding the principles of operation of these oscillators was found to be incomplete because the limiting mechanisms are only partly included in the formulas used so far. An experimental approach was used to identify the physical phenomena that really occurred in a running oscillator at different conditions, and based on this information, an understanding of the effects was sought. To get a complete picture we run the oscillator in a wide parameter range of bias conditions and record all relevant data, like bias voltages and currents, output amplitudes and spectra, voltages inside the oscillator as well as phase noise. The data obtained shows strong deviations from the signals predicted by simplified oscillator theory. For some phenomena, classic simulation software also delivers unrealistic results and necessitates model enhancements, like in the case of BE breakdown. We discuss the gain reduction by Bessel function bias shift, the Early effect, saturation as well as BE breakdown, their influence on oscillator performance as well as modeling approaches. A sample topology for the circuit analyzed is shown below. The transistor, the resonator, all capacitors and resistors are socketed can be easily exchanged (the circuit shows a 10MHz design):

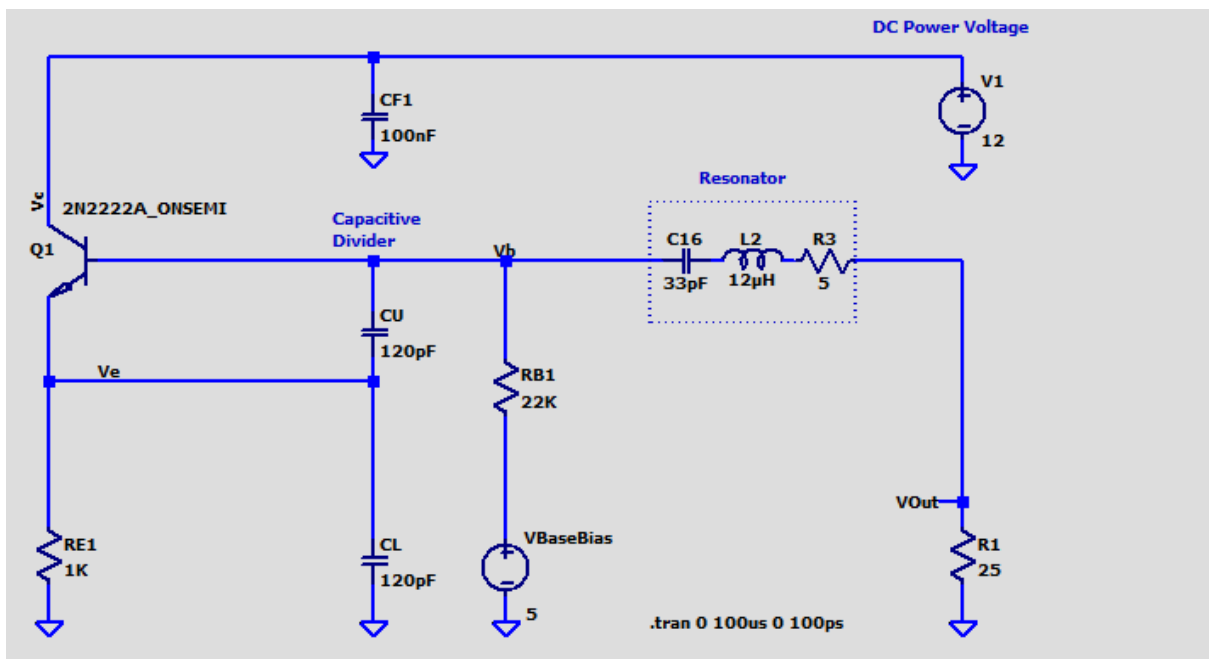


Figure 21 - Sample 10 MHz Oscillator Circuit for The Testing of Physical Effects

#### 3.4.1 Existing Approaches to Explain and Design USO Clapp Oscillators

All USOs made in recent times (at least no exceptions were found) use series-resonant crystals in a Clapp oscillator configuration. This applies to products made by HP (the famous 10811A, e.g.), Wenzel, Morion, Oscilloquartz and probably many others, and has been shown by several reverse-engineering projects and for some from schematic diagrams provided by the manufacturers (HP, Morion, ... see [1] for the HP10811A discussed in appendix A)

Another common denominator is the finding that the optimum way to extract oscillator power is not from a (transformer coupled) load at the collector, but directly via the resonator. This circuit was first proposed by Rohde [2] and provides significantly better phase noise than any other coupling method. The reason is obvious; the resonator of an USO has an extremely high Q, and by decoupling thru the resonator this high Q is used as an extra filter that extremely effectively dampens any off-carrier signals.

All known<sup>2</sup> modern oscillators work with this topology, most of them with a common base amplifier as the next buffer stage.

For the points we want to demonstrate in the following the exact parameters of the resonators are not important, because they play only a small role in the physics developing in nonlinear operation. It can be shown that all the effects to be discussed appear likewise in LC and crystal oscillators. LC oscillators, with their lower Q, are much easier to simulate using time domain and harmonic balance software (will be explained later). So, to illustrate the critical points, we use an LC oscillator as a first choice. The circuit is identical to the thru-resonator version used in the chapter about LC oscillators. Another aspect is that probing oscillator nodes at 5MHz can be done without loading and/or detuning (see chapter “Oscillator Measurement Techniques”).

### 3.4.2 Small Signal and Simple Nonlinear Approaches, Bessel Function Bias Shift

The first thorough theoretical attempt how the limiting processes in an oscillator work and how the shape of the transistor currents look like was undertaken by Rohde in his PhD thesis [3]. The thesis also derived predictions about the noise level generated by the different noise sources present inside the active device and the surrounding circuitry. Finally, Rohde proposed design procedures for practical oscillators based on his theoretical analysis, something left to pure heuristics before.

Even if this theory is incomplete, it does explain one limiting mechanism, which we nicknamed as “Bessel function bias shift”. The idea behind this (see [3], p70ff) works as follows:

If we assume<sup>3</sup> that the base emitter voltage is sinusoidal (around a mean bias voltage) with angular frequency  $\omega$ , we obtain a collector current of

$$I_C = I_S e^{\frac{V_{BE}}{V_T}} \text{ where } V_{BE} = V_{BE0} + V_{BE1} \cos(\omega t)$$

Where  $I_S$  stands for the saturation current,  $V_T$  is the temperature voltage  $kT/q$  and  $V_{BE0}$  and  $V_{BE1}$  are the bias and swing amplitude components of the base-emitter voltage. This formula has no closed form expression, but it can be expanded into a spectral sum using modified Bessel functions  $I_N$  by the identity

$$e^{x \cos(\omega t)} = I_0(x) + \sum_{n=1}^{\infty} I_n(x) \cos(n\omega t)$$

The use of the letter  $I_N$  for the modified Bessel functions is not to be confused with currents, but to make them discernible from the unmodified Bessel functions with the standard symbol  $J_N$ .

$x$  stands for  $V_{BE1}/V_T$ . So, for the collector current  $I_C$ , we get

$$I_C = I_S e^{\frac{V_{BE}}{V_T}} = I_S I_0(x) + I_S \sum_{n=1}^{\infty} I_n(x) \cos(n\omega t)$$

Not coming as a surprise, the exponential collector current formula converts a sinusoidal base drive into a periodic sequence of narrow collector pulses. The characteristic quantity is the ratio of the AC component of the base drive voltage to the temperature voltage,  $V_T$ . An increase or decrease of just

<sup>2</sup> Not all manufacturers publish their circuits.

<sup>3</sup> This assumption is fairly crude because a sinusoidal input voltage will be clipped by the onset of base current. Another limitation can be negative clipping in case the negative base-emitter breakdown voltage is exceeded (can happen in very modern transistors with a low breakdown voltage). The formula for the current further assumes the absence of high-current effects or spreading resistances which does not hold for small transistors and larger amplitudes. The peak currents must stay below the current ranges where beta begins to drop. Despite its limitations, the qualitative result that the oscillator current is pulse-shaped is still correct.

one  $V_T$  (ca. 25mV at room temperature), will double or half the collector current, so making a strong effect.

Apart from generating a pulse-like collector current, there is also a shift in DC base bias caused by the component  $I_s I_0$ . This current shift is negative and works along the base drive impedance, effectively reducing bias to smaller currents, and, consequently, reducing the transconductance of the transistor. This is clearly an amplitude-limiting mechanism.

In his paper Rohde shows how, starting from a given  $x$ , the other design values of the oscillator can be derived under plausible assumptions [3]. The bias conditions, the capacitive divider, the emitter resistor, the average currents can then be computed by a practical cookbook procedure based on the theory explained.

As we will show, several implicit assumptions we have taken as granted do not hold in practice at medium and higher power levels.

### 3.4.3 Sanity Checks by Observing Waveforms - Surprises

The strongest validity check of any form of theory is the direct comparison of predicted results with observed data. With oscillators, this is easier said than done. In the VHF region and above, it is simple not possible to probe waveforms or currents directly, because probe loading would destroy measurement integrity by parasitic capacitance and inductance effects.

In the HF region, we can successfully attack this problem by using ultra-low capacitance probes, without loading or detuning the oscillator. This is plausible; when we have  $C_1$  and  $C_2$  values in the range of hundred(s) of picofarads, a probe with 1-2pF will not cause an intolerable error. To judge the operating state of the transistor, we also need absolute voltages, i.e., DC modes with a sense resistance high enough not to influence the biasing. 1M $\Omega$  has been used here. Details of the probes can be found in the chapter "Oscillator measurement techniques".

The key statement is that for HF (up to 10-20MHz) we can *really measure an oscillator at work* at all circuit nodes if we want. Especially the base and emitter nodes are interesting; the collector is grounded regarding HF and at the supply voltage level regarding DC, so the transistor device voltages can be derived by subtraction.

An example set of waveforms observed for a Clapp oscillator at higher amplitudes is shown here:

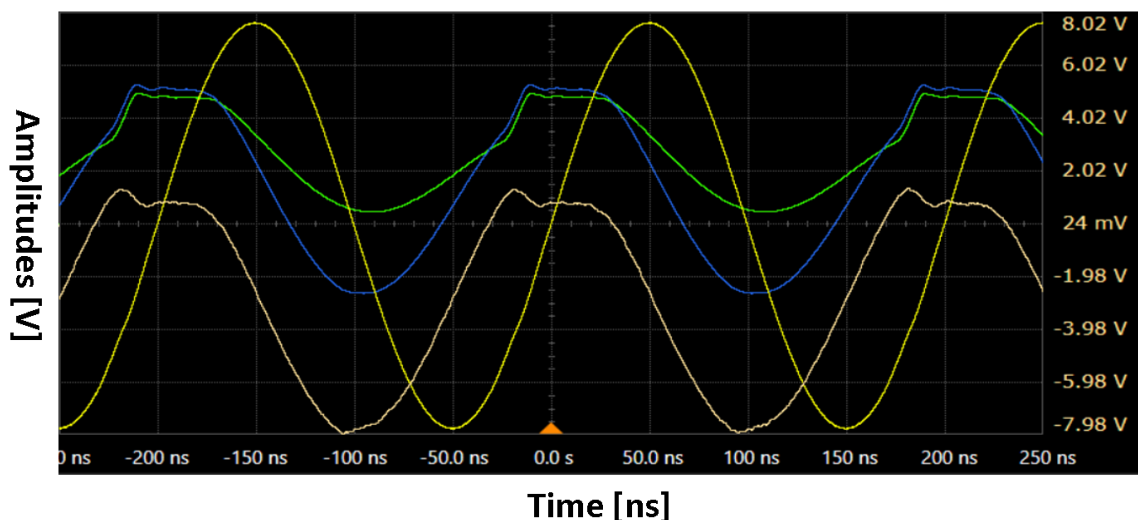


Figure 22 - Sample Voltages in a Running Clapp Oscillator at 5V Base bias and 20V Collector Voltage.

The waveforms of the base (blue), emitter (green) and BE difference (white) show a very nonlinear shape, pointing to several physical effects we have not included in the Bessel bias shift computation:

1. The assumption of a sinusoidal base emitter voltage is incorrect.
2. The transistor saturates. The collector/emitter voltage falls to extremely low values.
3. The base voltage turns negative, and the base-emitter differential voltage exceeds the datasheet breakdown limit. There is also a suspicious “dent” in the base voltage curve at the minimum.

The output voltage (yellow) still looks clean despite all nonlinear processes happening. This is a consequence of the filter effect of the resonator, which elegantly cleans up the output signal.

All above suggests that a much more complete understanding of the physics is necessary to explain what we see.

A video where the waveforms are plotted for a grid of operating points that are stepped through can be downloaded at [4]:

<https://electronicprojectsforfun.wordpress.com/crystal-papers/spice-simulation-techniques-for-difficult-circuits/colpitts-clapp-oscillator-waveform-videos/>

#### 3.4.4 Improvements to the Completeness of Transistor Models

We need to expand the transistor models into several directions:

1. **Early Effect**, i.e., the Influence of the Collector voltage on collector current [5]. While not directly visible from the screenshot above, this effect plays an important role with RF transistors and can even stop an oscillator from oscillating at all. This effect is included in SPICE transistor models (but sometimes with a considerable parameter variation even for the same part).
2. **Saturation**. When the base-collector voltage drops towards zero, the normally blocked BC diode opens and base current “runs out” to the collector, not playing part in the amplification process. This means that inside deep saturation there is no gain. The DC datasheets of transistors show this (example 2N2222A, see appendix L). There is also an effect caused by quasisaturation not discussed here. SPICE includes the saturation effect in its models.
3. **BE breakdown**. This is a complex effect involving either a tunnel effect (like low-voltage Zener diodes) or an avalanche breakdown (for higher voltages), with an overlapping range. The datasheet values are normally conservative; the real breakdown voltage of a transistor is 1-2V above what is guaranteed. In most SPICE models, the parameters for modeling this effect (VBBE) is missing, so it was necessary to model this by using behavioral sources. BE breakdown also introduces permanent damages to a device by ruining low-current beta. See appendix J for curves and explanations.

The list of effects above is far from complete. The more accuracy is asked for, the more fitting parameters and physical effects will need to be included (quasisaturation, CE breakdown, punch-thru, ...). We do not pursue this here, because:

1. The simulation models available from manufacturers cover only a set of basic parameters, so even if we have the formulas, the parameter values would be missing
2. The effort to extract complex model parameters from packaged devices is extremely large and difficult due to the thermal (time constants) and (parasitic) electrical properties of the package.
3. The parameter variation between individual transistors can be huge, so that standardized models are inaccurate. See SPICE models in appendix I where different models for the same transistor type show strong parameter variations.
4. In an USO, transistors are operated in regions where extremely exotic effects do simple not occur, so we could exclude them from modeling also.

After we have decided about the physics to be included in our models, the next logical step is to systematize experiments to verify our predictions, also in view to identify suitable transistors for an USO application and to find optimal operating conditions.

### 3.4.5 Systematic Measurements of Oscillator Conditions

To get a quantitative grip on the various physical effects involved in oscillations, an experiment was designed to collect as much data as possible for a broad range of bias points. One of the most common transistors was chosen (2N2222A [6], a space qualified part with good characteristics, as will be explained later). The experiment collects the following data:

1. The bias conditions (collector voltage, base bias voltage) are set for a matrix of  $V_C/V_{Bias}$  combinations.
2. Collector and base currents are measured by precise multimeters (Keysight 34461A [7])
3. The output waveform is measured on a scope (Keysight DSOS604A [8], Rigol DS1104Z [9])
4. The base voltage waveform is measured using a low-capacitance FET probe and a scope
5. The emitter voltage waveform is measured using a low-capacitance FET probe and a scope
6. The output frequency, carrier power and a phase noise curve are measured on a top-class phase noise analyzer (R&S FSWP [10])

All measurements do not require any user interaction and are computer controlled by a Python program. The results are then processed to create contour plots showing:

1. Collector and bias currents for all operating points (with a surprise, see later)
2. Output Amplitude for all operating points
3. Conduction angle, saturation angle and BE breakdown angle for all operating points
4. Max. BE voltages for all operating points
5. Output power and phase noise for all operating points



A contour plots of the base bias current is shown below:

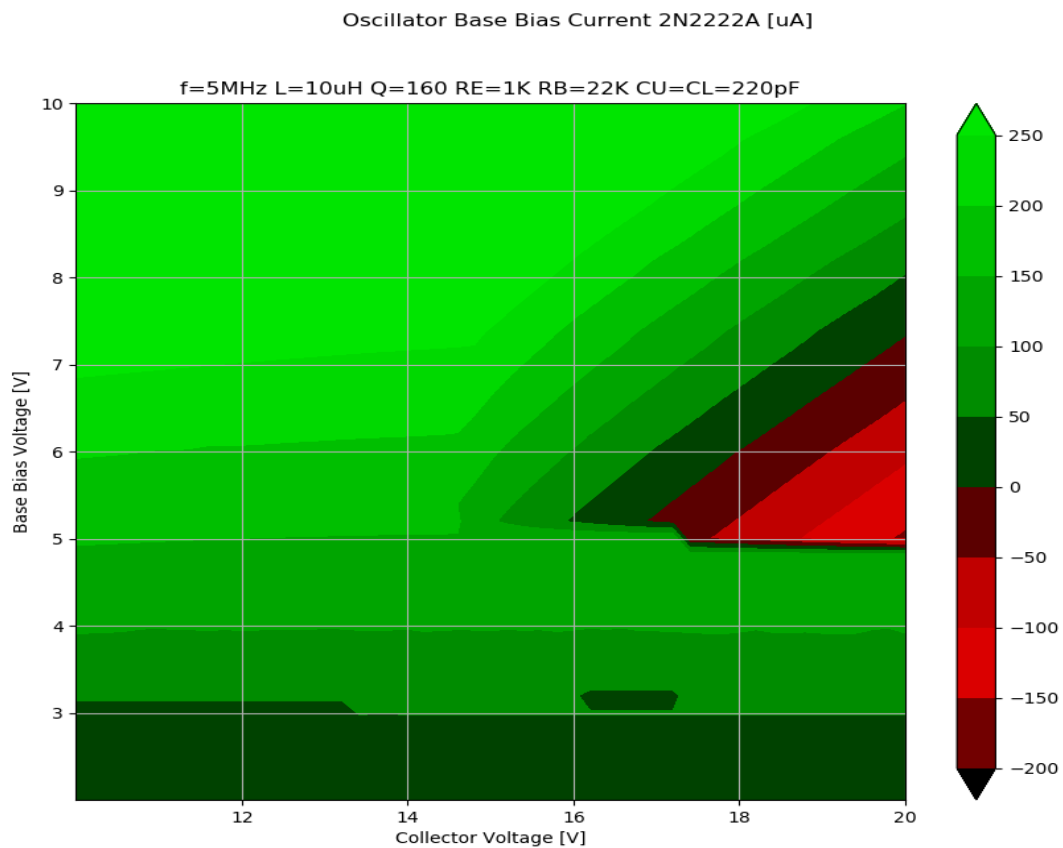


Figure 23- Base Bias Current Depending on Bias Conditions

As a surprise, we see a red region where the base bias current is *negative*. The resulting negative resistance at the base could, in practical oscillators, lead to instabilities of the bias network. A look at the waveforms in this region shows that the allowed BE breakdown voltage was exceeded in this part of the plot.

The collector current also shows a “split” behavior. At low base bias levels ( $<4\text{V}$ ), the collector current is almost independent of the collector voltage; at higher drive ( $\geq 6\text{V}$ ) the collector current only depends on collector voltage for  $V_C > 15\text{V}$  and is not controlled by base bias anymore, as shown here:

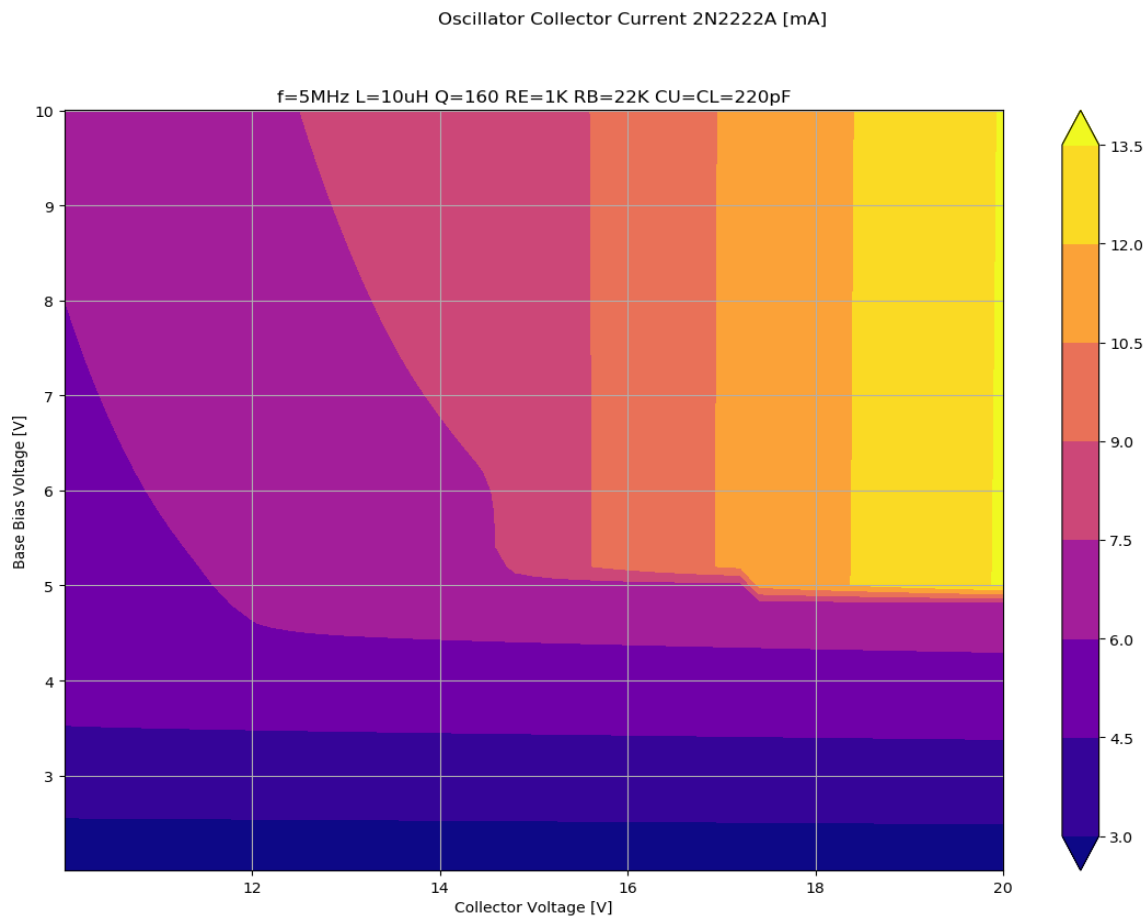


Figure 24 - Collector Current Depending on Bias Conditions

Further analysis will show that this is correlated to BE breakdown effects.

Next, we could see where the point with the maximum output power is found and what waveforms and phase noise is obtainable there for the 2N2222A (we also tried a 2N2857 [11]. No surprise, the output power of the 2N2222A was higher and the phase noise was lower, also due to the higher voltages allowed).

The power output is shown below:

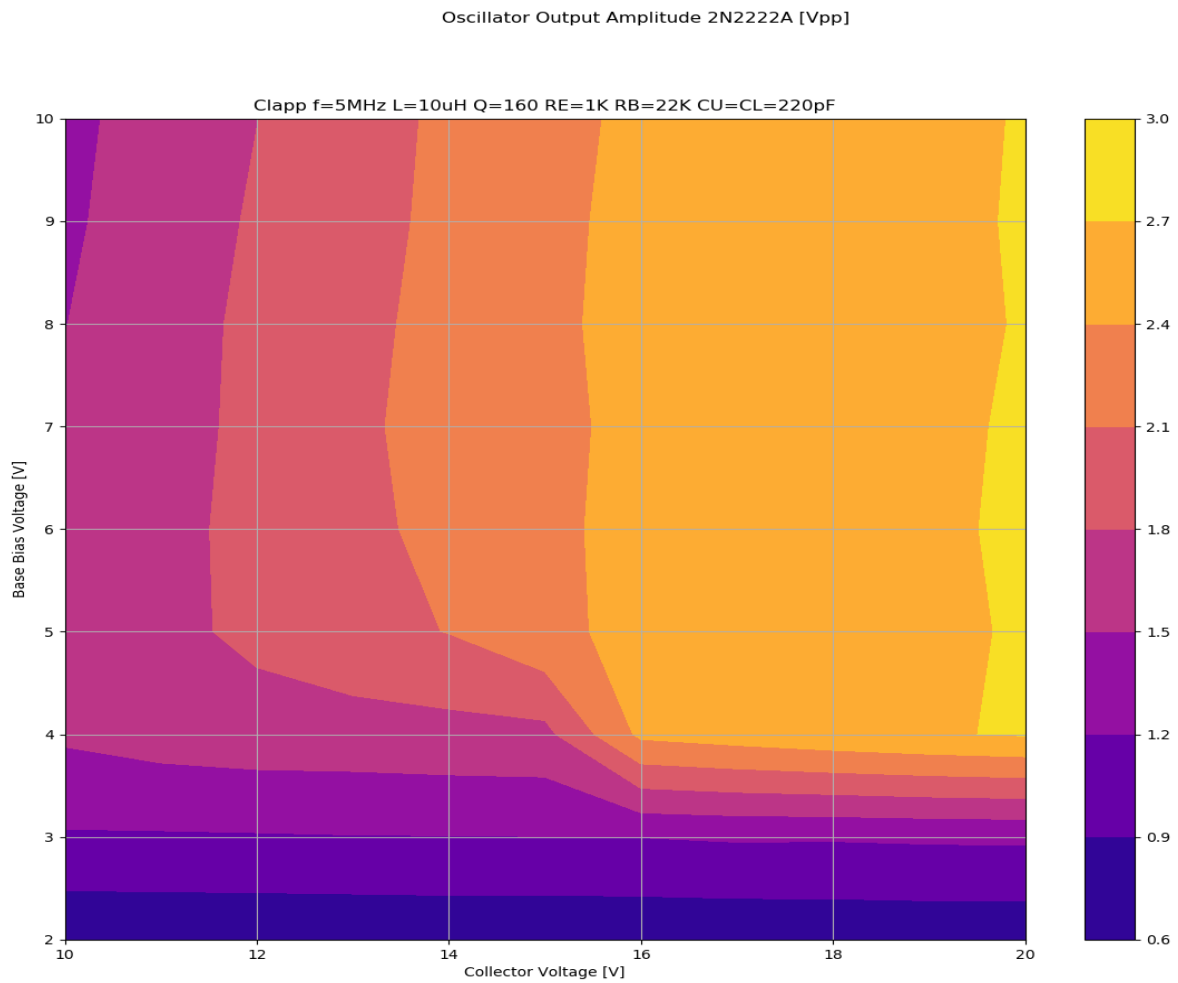


Figure 25 - Output Amplitude Depending on Bias Points

The shape of the contours of the output power resembles the collector current; what is surprising is that at high voltages an increase in base drive does not significantly increase output power anymore.

The minimum phase noise point is the next candidate. Best phase noise is obtained outside BE breakdown, but including (mild) saturation. This is a contradiction of recommendations in the literature that suggest avoiding saturation completely [12, p23.]. Classic theory also does not cover BE breakdown, so the theory would predict a phase noise minimum to the right of the dark blue zone, which is wrong.

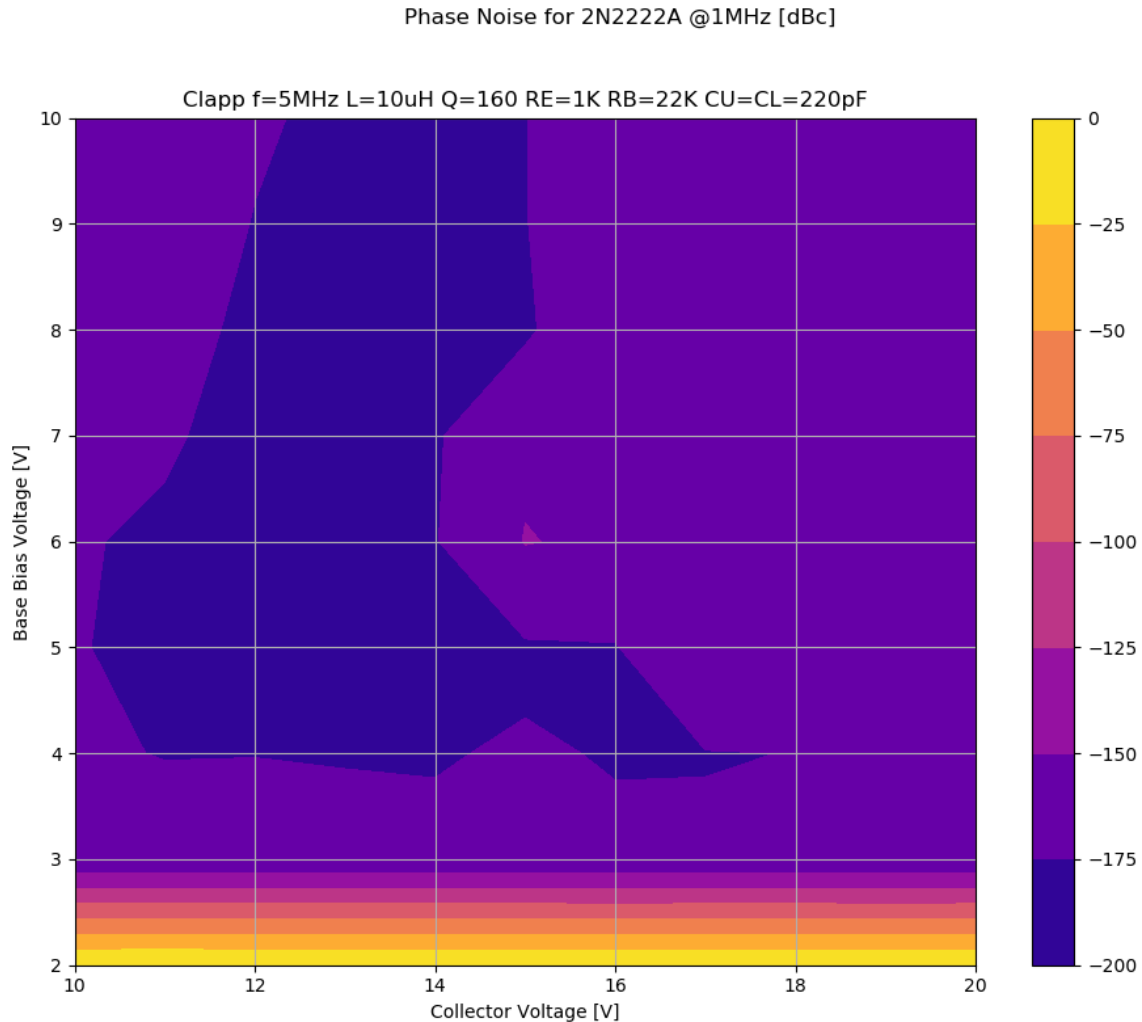


Figure 26 - Phase Noise Depending on Bias Conditions

What is worth mentioning is that minimum phase noise does *not* appear at the points of maximum output power, as the Leeson formula would suggest.

### 3.4.6 Simulations, Models, Parameters

There are two flavors of simulators we tried to reproduce my experimental results:

1. Time domain (LTSpice, ADS)
2. Harmonic Balance (Serenade, ADS)

To correctly interpret results, we need to understand which physical effects are modelled by the programs. For the effects we investigated we have:

1. The Early effect is modelled in both programs (VAF, VAR in SPICE, in Serenade probably the same, but models are not published)

2. Saturation is also modelled (BR, NR in SPICE, same with Serenade)
3. BE Breakdown is not modelled in neither SPICE nor Serenade. The predictions where this occurs are probably completely off, from DC to phase noise.

As a first approach, we will try what the unmodified simulation programs with existing manufacturers models will do. If needed, we will enhance existing device models to obtain realistic projections.

### 3.4.7 The Influence of Early Voltage on Oscillators

Every transistor output curve array shows a certain degree of “bending up” the collector current at higher voltages. This effect is called “Early Effect” [after James Early of Bell Labs] and is the result of a modulation of the length of the BC space charge zone at different collector voltages. A graph shows this (also see [5]):

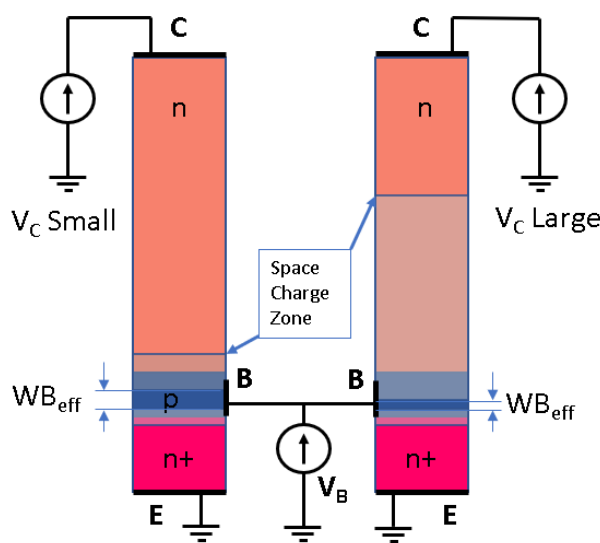


Figure 27 - The Early Effect

Note that the growth of the space-charge region at the base-collector boundary (grey shaded area) extends *mostly, but not completely* into the collector side. This is important because the base is much thinner than the collector (picture is not to scale) and when its thickness is all filled by the BC space charge zone, the transistor loses controllability by the base. This state is called punch-through. In punch-through the gain falls to zero.

The strength of the early effect and a potential punch-through depends on the transistor type; Again, LF types show (at moderate collector currents) little Early effects and are relatively immune to punch-through, while RF types are much more prone to these effects.

Very recent microwave SiGe, HBT or comparable transistors can show considerable Early effects.

The first-order oscillator theory approximations using pencil-and paper algorithms and the formula

$$I_C = I_S \exp\left(\frac{V_B - V_E}{V_T}\right)$$

as the core of their derivation of conductance [3] do not incorporate this effect. SPICE (and very probably HB, but models are mostly encrypted) does model this effect, even in reverse operation, but we do not need that here. The formula in forward mode now runs (see [14] for a good explanation of how SPICE models bipolar transistor physics):

$$I_C = I_S \exp\left(\frac{V_B - V_E}{V_T}\right) \left(1 + \frac{V_{CE}}{V_A}\right)$$

Where  $V_A$  is the Early voltage.

It is instructive to see some output curves with different extremes regarding Early effects (see the transistor measurement chapter for the hardware setup). First, a common LF transistor (2N2222A, 45V/800mA,  $f_T$  300MHz, space qualified) shown below:

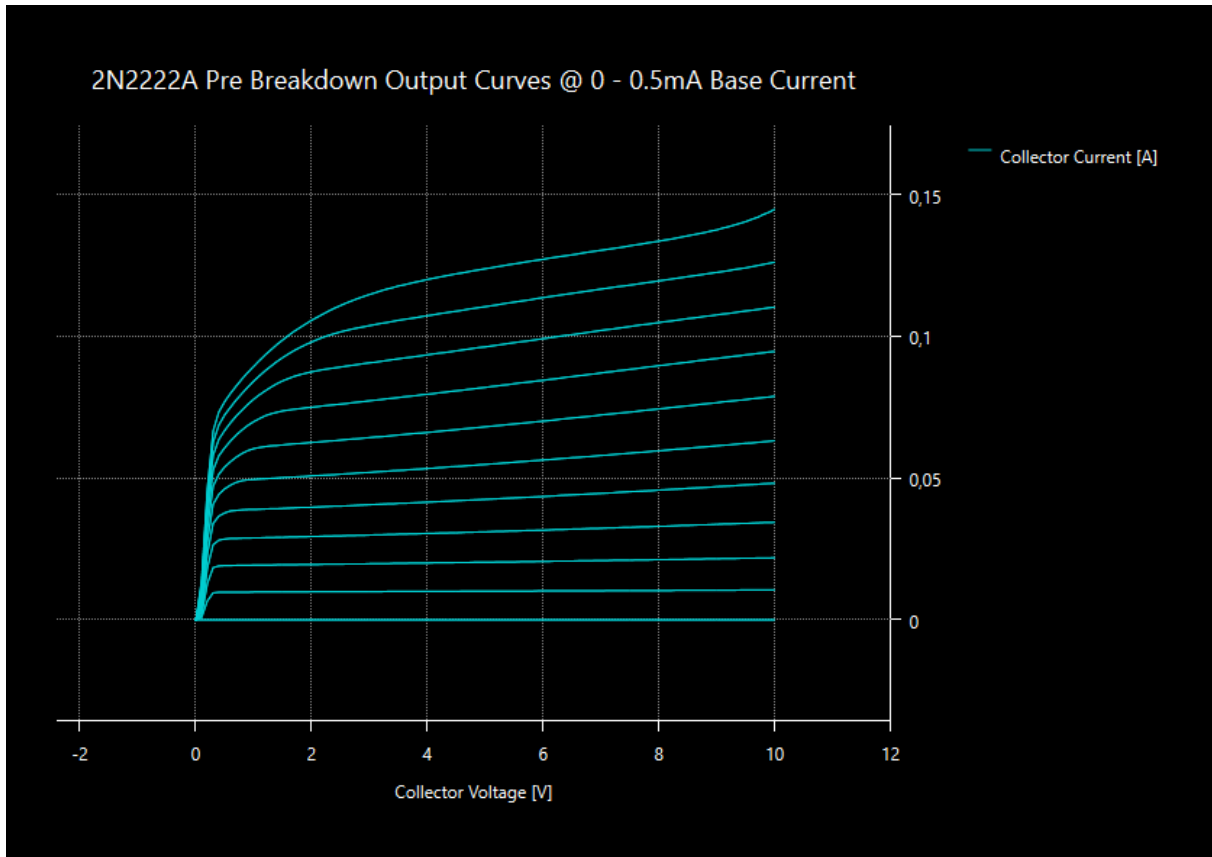


Figure 28 - 2N2222A Output Curves with Early Effect

Below 50mA of collector current the lines are very straight and (tangents extended to the left) meet at a point on the negative axis at around 60-100V. This is the Early voltage  $V_A$ , and SPICE parameters for this is ranges from 75 to 250, depending on manufacturer (see appendix I). There is another effect at higher collector currents where a second slope zone develops before the curves get straight (top curve, 0-2V). This is called quasisaturation, a high current effect. It is not always treated in SPICE (using the RCO parameter), but for the oscillators we are looking at, we normally should not operate in regions where that happens, so we will not consider this effect. If it happens, however, it is a linearity issue.

The output curves of an RF transistor (2N2857, 15V/40mA,  $F_T$  1.4GHz, space qualified) are shown here:

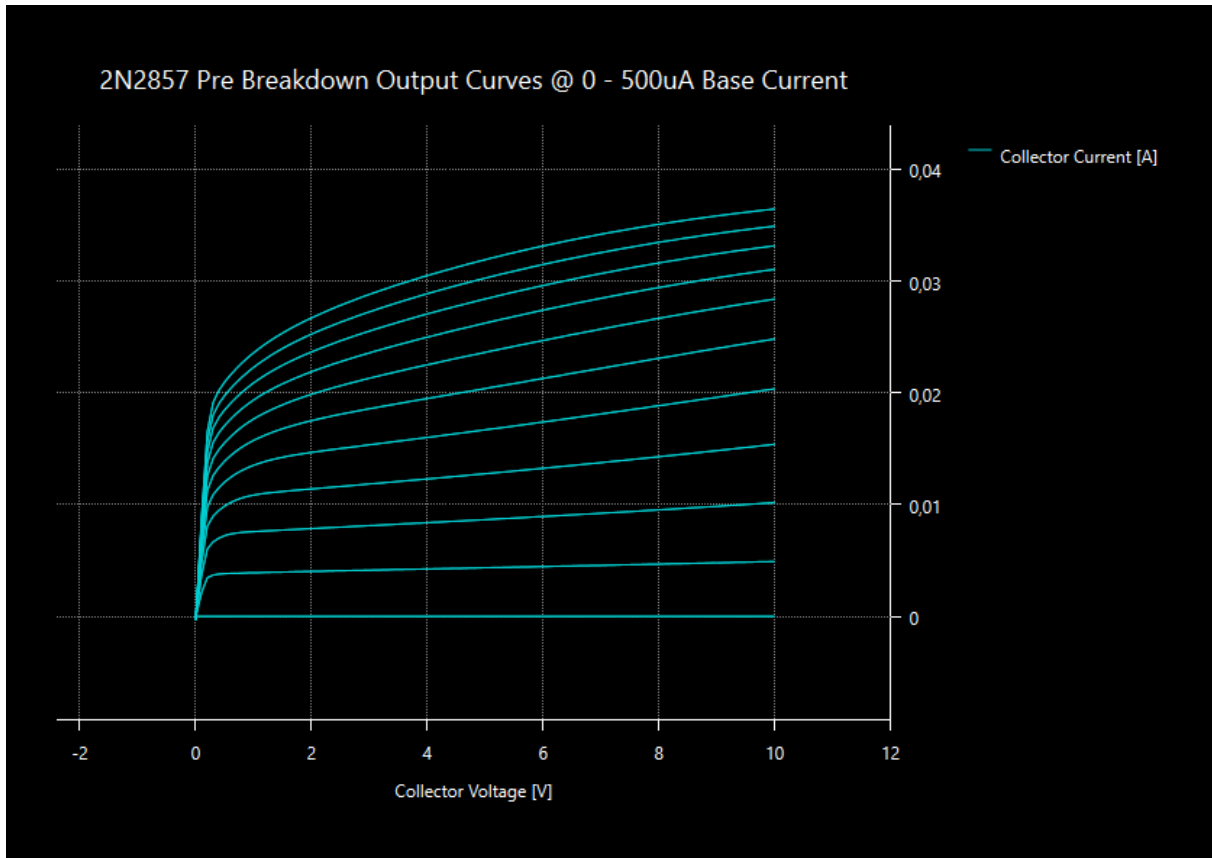


Figure 29 - 2N2857 Output Curves with Early Effect

Apart from much lower gain (watch the current axis), the Early voltage is much lower than with the 2N2222A, and if we assume that we use the part in an oscillator with  $60^\circ$  of conduction angle, pulses into the tens of mA are likely to occur. These pulses reach out into areas where the Early effect is non-negligible anymore. SPICE models have between 10V (MicroSemi) and 120V (IntuSoft, unrealistic) values for VAF (see SPICE model in appendix I). Depending on which base current you look at, about 10-30V is OK here. At the top curves, we see a variation of, e.g., 10mA over 9V of collect voltage span at the same base current, equivalent to a differential resistance of only  $900\Omega$ .

This differential resistance adds to the losses that need to be compensated by the transistor's negative impedance. We can compute that by assuming a cold-collector Clapp circuit with an emitter resistance  $R_E$ , a static collector voltage  $V_C$  and (imprinted over a large base resistance, neglecting base current) a collector current  $I_C$ . Where the Early effect is important, we stay clear of saturation and breakdown, so we can ignore these effects.

With  $V_{CE} = V_C - R_E I_C$  and  $V_{BE} = V_B - V_E$

We obtain for  $I_C$ :

$$I_C = \frac{I_S \exp\left(\frac{V_{BE}}{V_T}\right) \left(1 + \frac{V_C}{V_A}\right)}{1 + \frac{R_E}{V_A} I_S \exp\left(\frac{V_{BE}}{V_T}\right)}$$

If we introduce an idealistic collector current  $I_{C0}$  defined as

$$I_{C0} = I_S \exp\left(\frac{V_{BE}}{V_T}\right)$$

The formula simplifies to

$$I_C = \frac{I_{C0} \left(1 + \frac{V_C}{V_A}\right)}{1 + \frac{R_E}{V_A} I_{C0}}$$

The transistor input transconductance is defined by

$$g_M = \frac{dI_C}{dV_{BE}} \cdot \text{Using } \frac{dI_{C0}}{dV_{BE}} = \frac{I_{C0}}{V_T}$$

We get

$$g_M = \left(1 + \frac{V_C}{V_A}\right) \frac{\frac{I_{C0}}{V_T} \left(1 + \frac{R_E}{V_A} I_{C0}\right) - \frac{R_E}{V_T V_A} I_{C0}^2}{\left(1 + \frac{R_E}{V_A} I_{C0}\right)^2}$$

The nominator squares cancel, so we get

$$g_M = \frac{I_{C0}}{V_T} \frac{\left(1 + \frac{V_C}{V_A}\right)}{\left(1 + \frac{R_E}{V_A} I_{C0}\right)^2} = g_{M0} \frac{\left(1 + \frac{V_C}{V_A}\right)}{\left(1 + \frac{R_E}{V_A} I_{C0}\right)^2}$$

For an LF transistor (2N2222A), with a high Early voltage much larger than  $V_C$  (and  $V_E$ ), both terms are close to one ( $V_C \ll V_A$ ,  $V_E = R_E \cdot I_C \ll V_A$ ) and we get classic non-Early transconductance  $g_{M0}$  of  $I_{C0}/V_T$ .

If, on the contrary, we now have an RF transistor (2N2857) with  $V_A \sim V_C$  and  $V_E = 0.8V_C$ , say, we get only ca. 60% of the original transconductance, and that can be too small for safe oscillations.



### Experimental Verification

To make a sanity check on the calculations, the oscillator waveforms were extracted for both an LF and an RF transistor across a wide set of collector voltages and base bias points. The LF transistor always oscillated, even in the most exotic combinations of collector voltages and base bias. For the RF 2N2857, this was not the case, as the output amplitude contour plot shows:

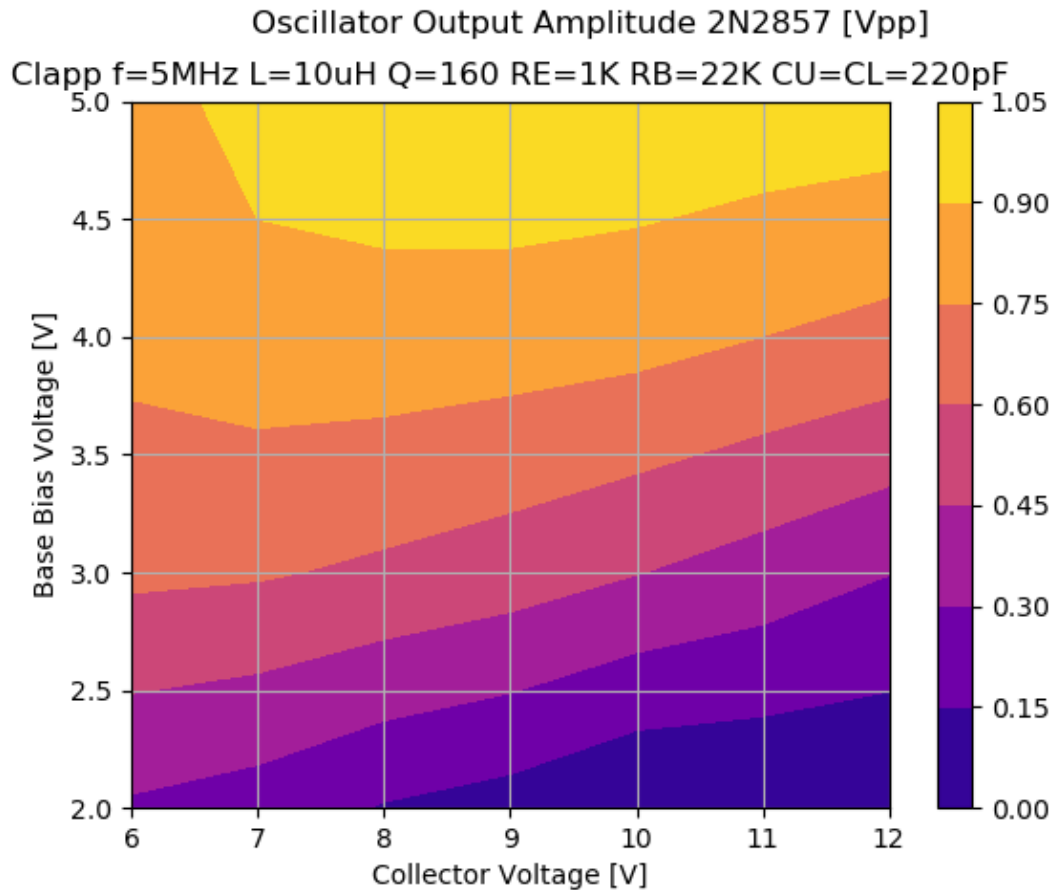


Figure 30 - Oscillator Amplitude with Early Effect Anomaly

At low bias points, but high voltages there is a dead zone (dark blue) where the circuit does not oscillate at all. This means, that if you start with a base bias of 2V and 6V collector voltage, the circuit oscillates. When base bias is left at 2V, but collector voltage is increased the amplitudes go down and for more than 8V oscillations subside completely, which is quite counterintuitive. This effect could be called “Early Quenching”.

### Conclusions for the Early Effect

The following derivations could be made from the points above:

1. Keep the transistor out of areas with strong Early effect by using an appropriate operating point where the output curves show no significant bending.
2. If frequency range permits, use a transistor with a small Early effect (as found in LF transistors with not too small maximum collector current (e.g., > 200mA).).

### Outlook for the Early Effect

What has not been investigated is base punch-thru, because this has no significance in USOs. Just for completeness it could be investigated if such effects are properly modelled in SPICE and HB programs.

### 3.5 Saturation and its Effect of Oscillator Performance

The literature discourages to let the oscillator transistor reach saturation [12, p23.]. While this is intuitively understandable (effects discussed below) measurements with different collector and base bias conditions where saturation did occur in some operating points did *not substantiate* that (moderate) saturation is resulting in worse performance.

The reasons given why saturation should be avoided are:

1. Transistor beta drops to extremely low values, effectively reducing  $g_m$ .
2. Transition frequency drops as well
3. It takes a while to clear the flooded space charge regions, so getting back out of saturation takes time
4. Conduction angle increases, suggesting worse phase noise [20]
5. Transistor capacitances soar when approaching saturation, potentially giving rise to varactor pumping and, in the worst case, parametric oscillations.

On the other hand, at only 5MHz, we could argue that

1. The capacitances are still small compared to the rest of the circuit ( $C_1, C_2, \dots$ )
2. Low frequency transistors have high beta values to start, so some degradation is acceptable
3. The varactor effect is not as disturbing, because the fixed capacitances are large enough ( $C_1, C_2$ ).
4. The fall time is still low enough to allow oscillations even when saturation occurred.

An interesting point is the noise issue. The transistor in saturation effectively floods the potential barriers that create Schottky noise at a normal active operating point. It could be (measurements follow) that this results in *less noise* than an active operating point outside of saturation.

If we look at the mechanism of saturation according to the Gummel-Poon model [14], we see that a saturated transistor consists of not just one, but two diodes that conduct simultaneously. The collector current is then expressed by (still without Early voltage terms):

$$I_C = I_S \left\{ \exp\left(\frac{V_B - V_E}{V_T}\right) - \left(1 + \frac{1}{B_I}\right) \exp\left(\frac{V_B - V_C}{V_T}\right) + \frac{1}{B_I} \right\}$$

And the base current now is

$$I_B = I_S \left\{ \frac{1}{B_N} \left( \exp\left(\frac{V_B - V_E}{V_T}\right) - 1 \right) + \frac{1}{B_I} \left( \exp\left(\frac{V_B - V_C}{V_T}\right) - 1 \right) \right\}$$

If we compare this with the simplified approach out of saturation where  $I_C$  is just

$$I_C = I_S \exp\left(\frac{V_B - V_E}{V_T}\right)$$

This can be off by orders of magnitude. A consequence is that the small-scale negative resistance of

$$Z_{IN} = -g_m X_{CU} X_{CL}$$

Is also off target.

To illustrate that, let us have a look at an operating point where no saturation, BE breakdown or other effects occur and see the waveforms there:

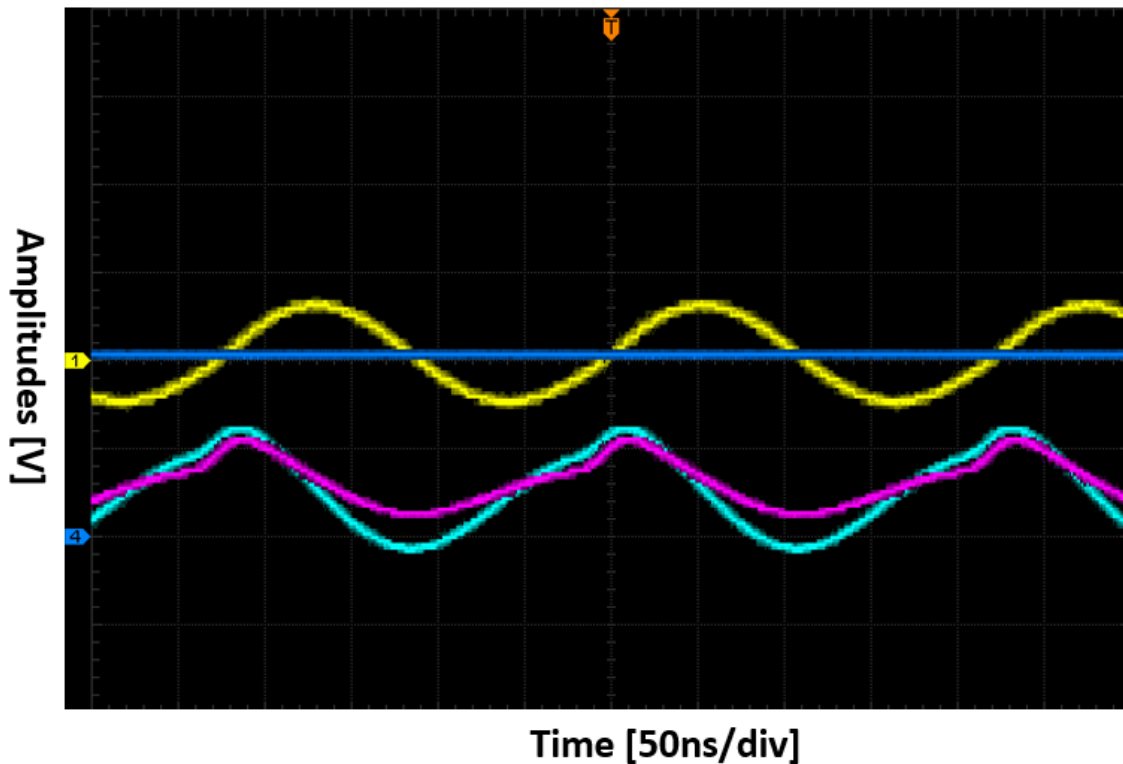


Figure 31 – Clapp Oscillator Waveforms without Saturation or BE Breakdown. The collector supply voltage is in blue, the output RF is in yellow, the cyan trace is the base voltage and pink is the emitter voltage.

Vertical scale is 5V/div for blue, 4V/div for pink ( $V_E$ ) and cyan ( $V_B$ ) and 500mV/div. for yellow (output signal) trace. Base and emitter are far enough away (more than 4V of headroom) from the collector so there is no saturation.  $V_C$  was 10V, bias was 2V,  $C_1=C_2=220\text{pF}$ .

The base voltage swings below the emitter voltage. As long the negative values stay below the specified datasheet maximum (2N2222A:6V), this is normal. Here we have ca. 2V, so OK.

Even at this small output level (500mVpp into 50Ohms, -2dBm) the base voltage is still not perfectly sinusoidal, but the base voltage distortion is small. Output looks like a perfect sinewave.

When we (this is arbitrary because the collector current never is really zero due to the exponential  $I_C/V_{BE}$  dependency) define the conduction angle as the ratio of the time where  $V_B > V_E$  over the total period length, we see an approximate  $180^\circ$  angle. This is not what is considered an optimal operating point regarding noise, and this is confirmed by a phase noise measurement below:

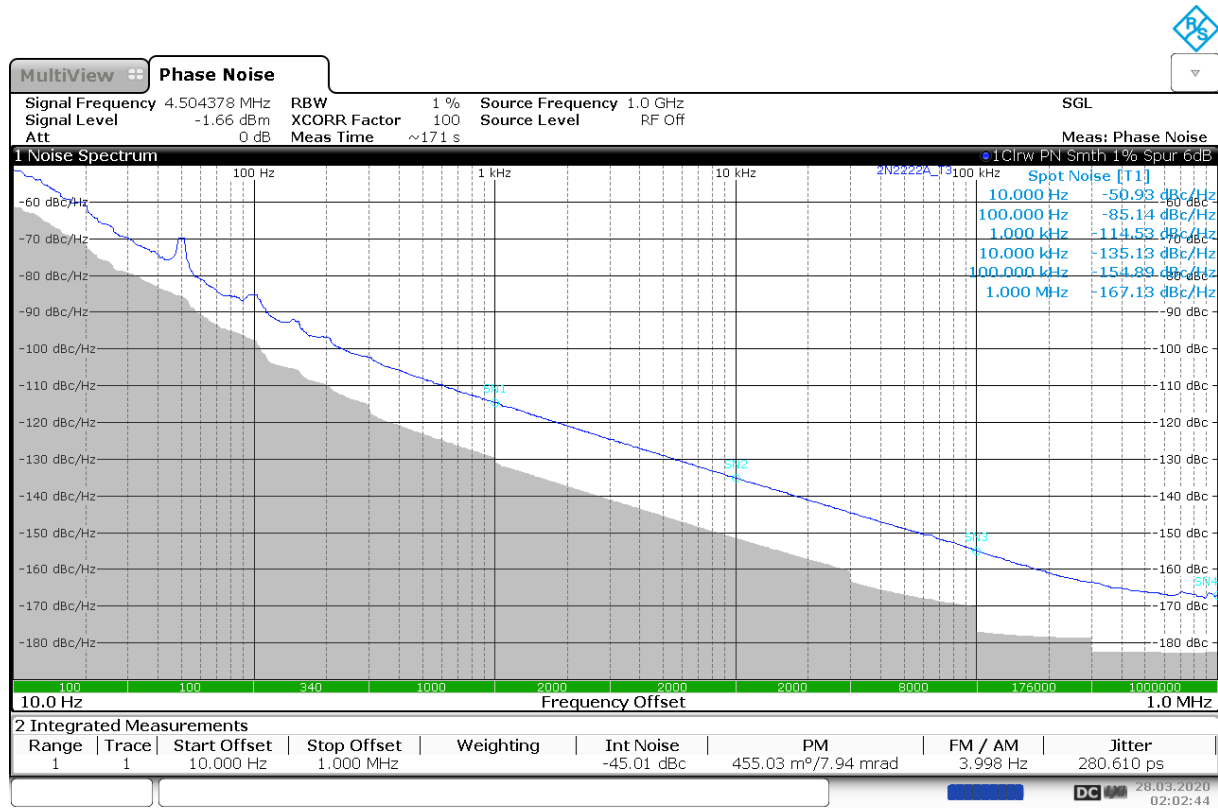


Figure 32 - Phase Noise for an Oscillator With no Saturation or BE Breakdown

Only  $-50\text{dBc}@10\text{Hz}$  is not a good result. The output power is too low, and the conduction angle is much higher than the  $30\text{-}60^\circ$  we need for a good phase noise oscillator.

Now we choose an operating point with an undisputable saturation (5V Base bias, 15V at the collector, other parameters unchanged). The waveforms change dramatically as shown:

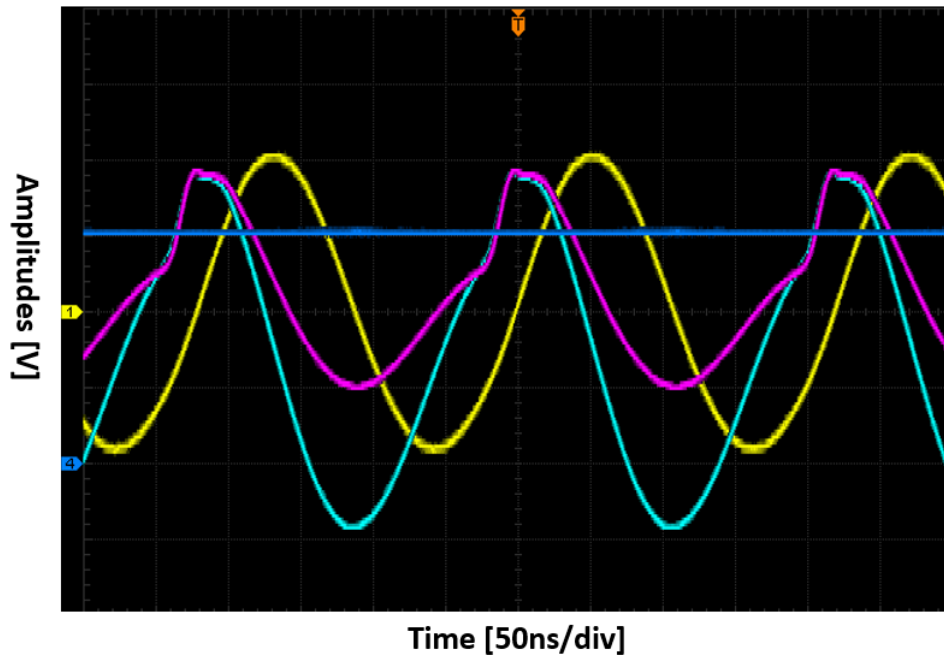


Figure 33 - Clapp Oscillator with Saturation without BE Breakdown. Collector voltage is in blue, RF output is in yellow, base voltage is in cyan and emitter voltage is in pink.

The base and emitter voltages now “collide” with the collector voltage (watch different scale factors for collector and base/emitter due to probing). All three voltages are within a few 100mVs around the collector voltage, clipping off the top of both emitter and base voltages.

Conduction angle is drastically reduced to some 10 degrees, not easy to see because of the overlapping curves (shown in contour plot later).

Negative BE voltage has increased as well, we see ca. -7V, which is above the datasheet value (6V), but probably inside the safety margin of our DUT transistor. This must be closely watched and will be discussed in the following.

The phase noise curve for the saturated oscillator is shown below:

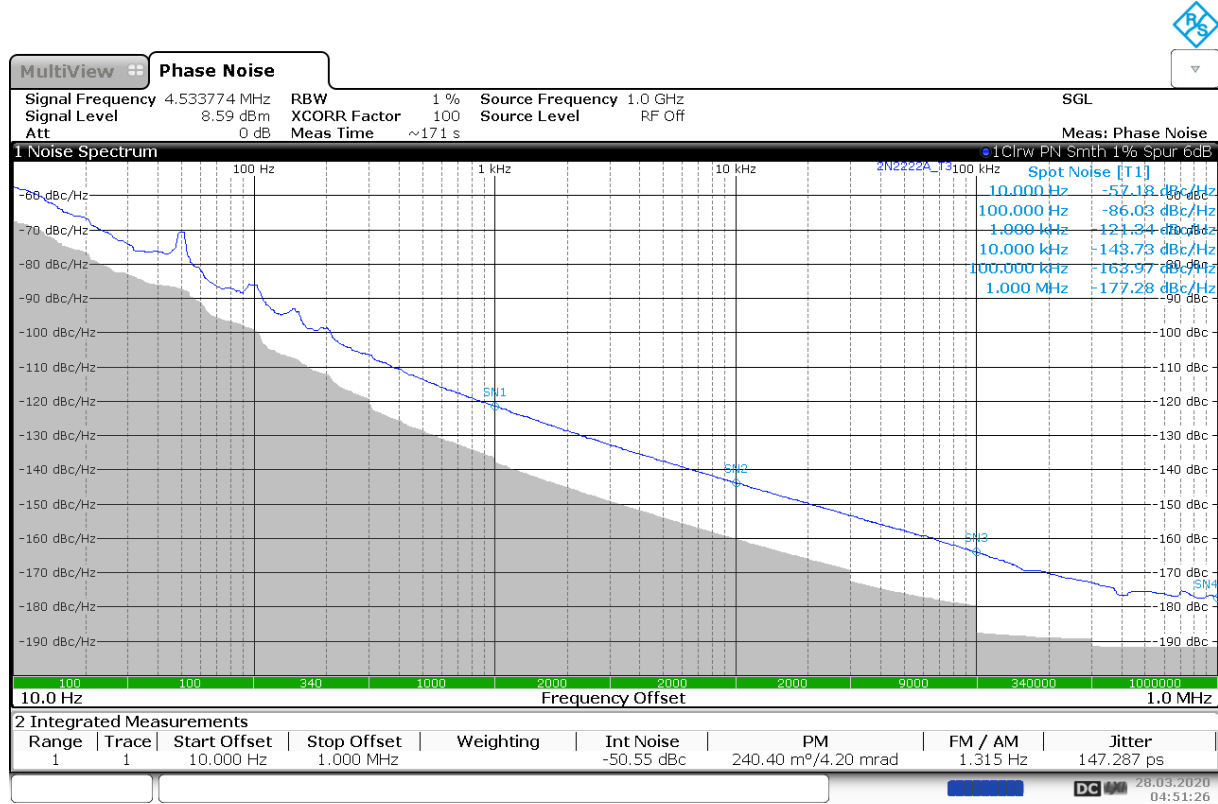


Figure 34 - Phase Noise of Oscillator with Saturation without BE Breakdown

We see a better output power at +9dBm, less phase noise, -59dBc@1Hz, -177dBc@1MHz even with saturation taking place. It seems that at least a modest amount of saturation is no reason why better phase noise is not reachable.

Conduction and saturation angles were measured for all bias points in our experiment and visualized in contour plots in the two plots below:

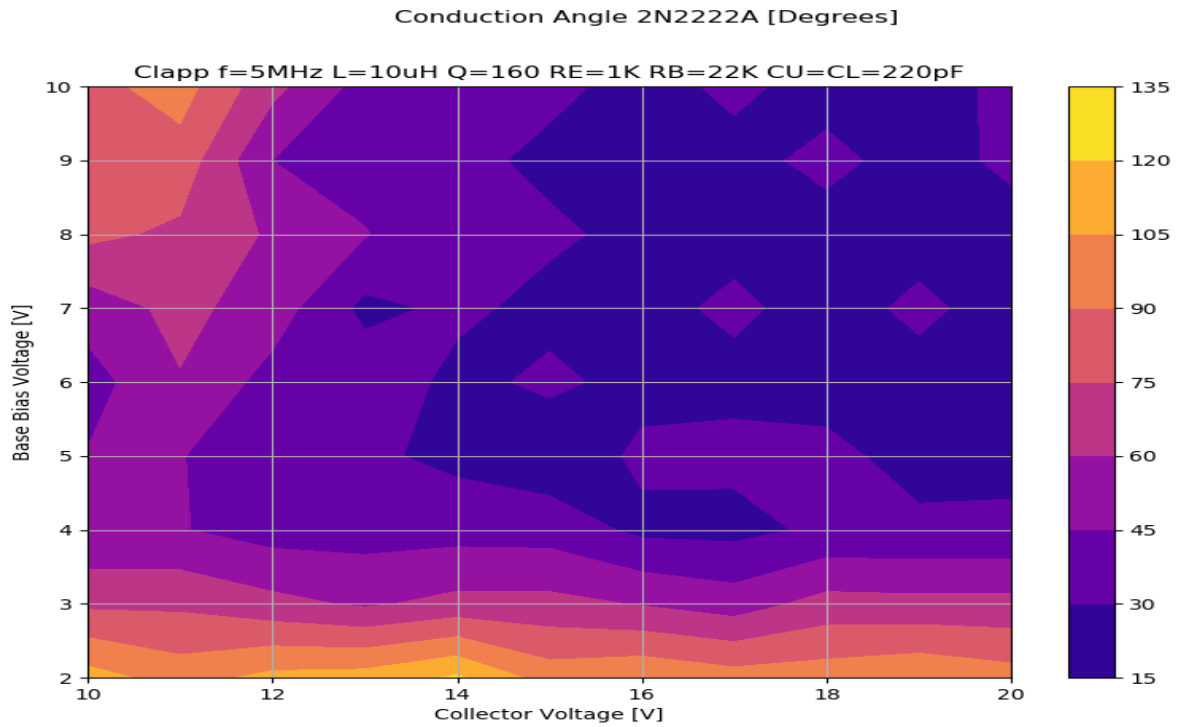


Figure 35 - Clapp Oscillator Conduction Angles

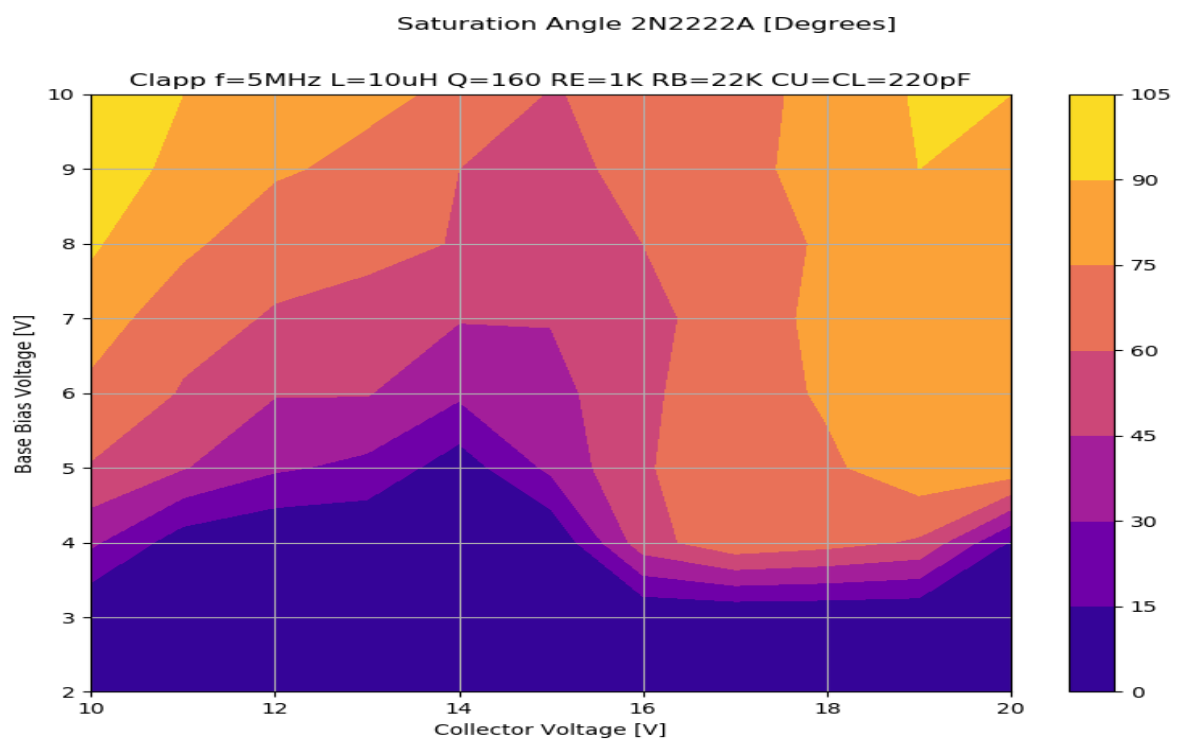


Figure 36 - Clapp Oscillator Saturation Angles

When we compare the operating points 2V/10V and 5V/15V we see a strong change in conduction angle and saturation. At 2/10 we see almost full conduction but no saturation at all. At 5/15, we see a small conduction angle and a not much smaller saturation angle, indicating that the transistor operates as a saturated switch most of the time.

If we try a (completely unpractical) operating point with a deep and long saturated period (8V/10V), we get:

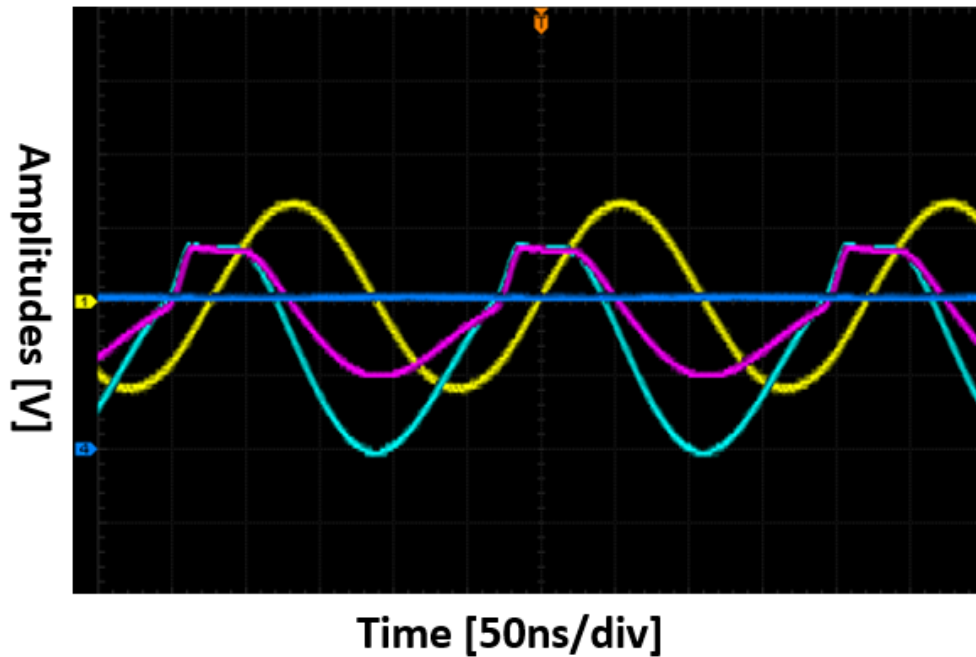


Figure 37 - Deeply Saturated Clapp Oscillator Waveforms without BE Breakdown. Collector voltage is in blue, RF output is in yellow, base voltage is in cyan and emitter voltage is in pink.

Conduction angle has now increased to ca. 3 times the last value, not what we want. Saturation and conduction almost coincide, indicating that the transistor is still acting as a saturated switch most of the time.

Negative base emitter voltage is less than before and below the datasheet limit, so OK.

The output power is a bit less than with the 5/15V case, but the waveform still looks sinusoidal.



Phase noise for the deeply saturated oscillator is shown below:

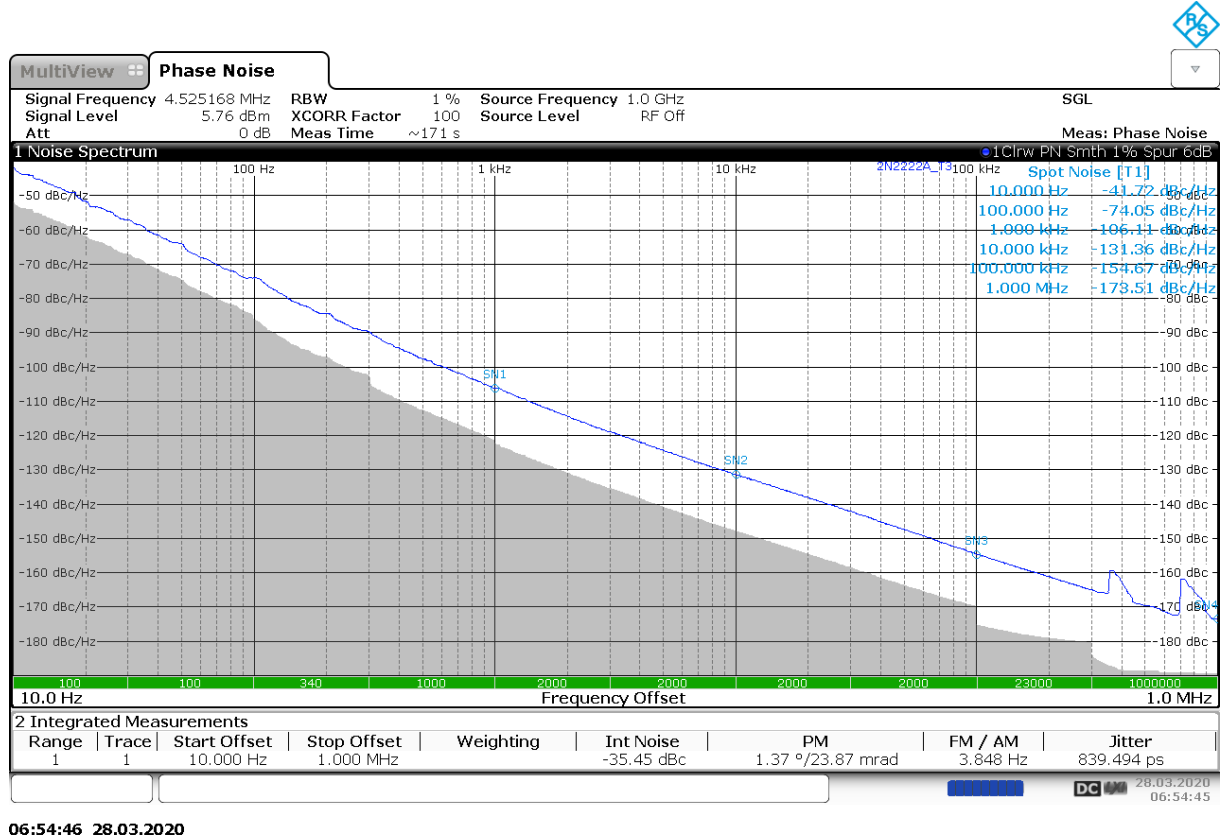


Figure 38 - Phase Noise of a Deeply Saturated Oscillator

This bias point, in contrast to the output amplitude, has an exceptionally bad close-to-carrier phase noise ( $-40\text{dBc}@10\text{Hz}$ ), even worse than the non-saturating oscillator we measured first.

The measurements suggest that saturation seems to be OK as long the conduction angle stays short.

### 3.5.1 Simulation Results for Saturation

SPICE time domain simulators incorporate saturation in their standard models. The most relevant parameters are [14]:

1. ISR reverse saturation current
2. BF and BR forward and reverse current amplification factor
3. VAF and VAR forward and reverse early voltage
4. IKF and IKR corner points for high-current beta roll off
5. NF and NR forward and reverse emission efficiency coefficients

To model the transistor including the saturation effect we could use a Gummel/Poon or transport model as employed by PSPICE. Ignoring resistances, the equations run (derived from the official PSPICE manual, using SPICE notation):

$$I_B = I_S \left\{ \frac{1}{BF} \left( \exp\left(\frac{V_B - V_E}{NF V_T}\right) - 1 \right) + \frac{1}{BR} \left( \exp\left(\frac{V_B - V_C}{NR V_T}\right) - 1 \right) \right\}$$

The NF and NR (“injection efficiency”) factors were assumed as 1 according to the 2N2222A spice model. The “non-ideal” base currents forward and reverse (ISE and ISR...) terms were set to zero for the same reason. For the collector we have:

$$I_C = I_S \left\{ \frac{1}{K_Q} \left( \exp\left(\frac{V_B - V_E}{V_T}\right) - 1 \right) - \frac{1}{K_Q} \left( \exp\left(\frac{V_B - V_C}{V_T}\right) - 1 \right) - \frac{1}{BR} \left( \exp\left(\frac{V_B - V_C}{V_T}\right) - 1 \right) \right\}$$

The term  $K_Q$  is the base charge factor,

$$K_Q = \frac{1 + \left[ 1 + 4 \left\{ \frac{I_S}{IKF} \left( \exp\left(\frac{V_B - V_E}{V_T}\right) - 1 \right) + \frac{I_S}{IKR} \left( \exp\left(\frac{V_B - V_C}{V_T}\right) - 1 \right) \right\} \right]^{NK}}{2(1 - (V_B - V_C)/VAF)}$$

For the 2N2222A model, there is no specific  $IKR$  and  $NK$  (default 0.5) available, so we can simplify to

$$K_Q = \frac{1 + \left[ 1 + 4 \left\{ \frac{I_S}{IKF} \left( \exp\left(\frac{V_B - V_E}{V_T}\right) - 1 \right) \right\} \right]^{NK}}{2(1 - (V_B - V_C)/VAF)}$$

If we want to express the base voltage as a function of base current and collector voltage (needed for comparative output plots) we get (derivation not shown):

$$V_B = V_T \ln \left\{ \frac{\frac{I_B}{I_S} + \frac{1}{BF} + \frac{1}{BR}}{\frac{1}{BF} + \frac{1}{BR \exp(V_C/V_T)}} \right\}$$

An example for the 5V/15V case is shown below:

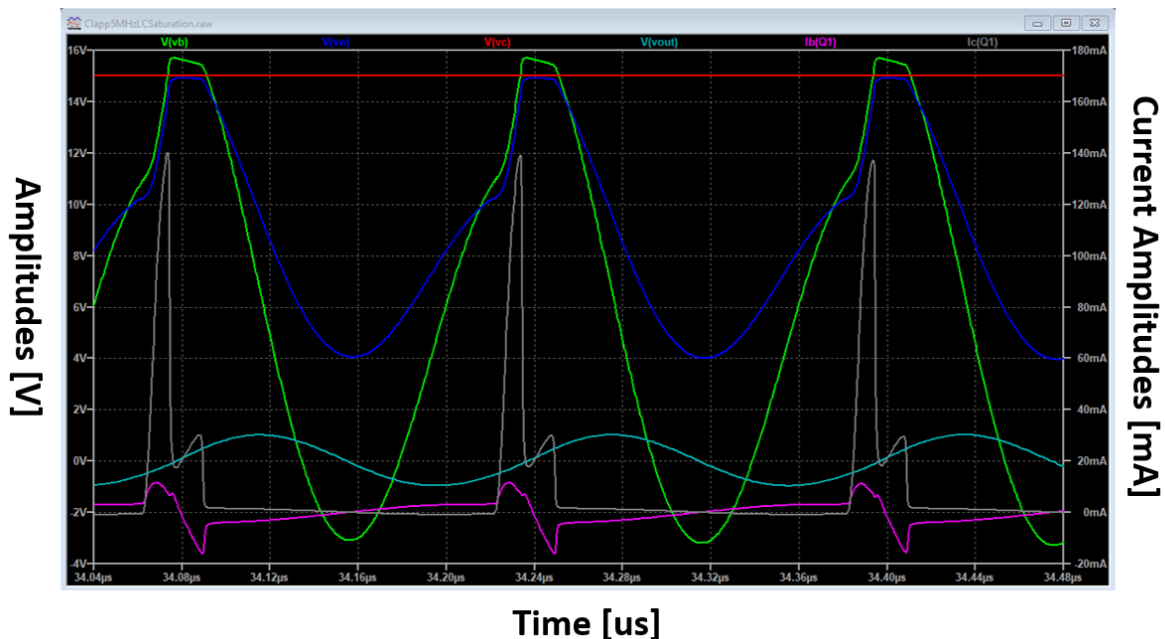


Figure 39 - Simulated Clapp Oscillator with Saturation and without BE Breakdown. Base voltage is green, emitter voltage is blue, collector voltage is red, collector current is grey and base current is pink.

A comparison with the measured waveforms (see above) shows a good agreement. The simulated oscillator shows squegging, so the screenshot is taken at the maximum of a squegging period. Squegging and oscillator operating point stability will be discussed as a separate topic.

The peak collector current is 140mA. It would be favorable if high current effects would not already set in at this current level, so this sets a limit for the transistors that are usable for this high-level oscillator. A collector current reserve of several times the peak current is a good idea to be on the safe side (2N2222A: 800mA maximum, so OK).

For the 2V/10V case (shown below) we get no saturation, confirming our measurement.

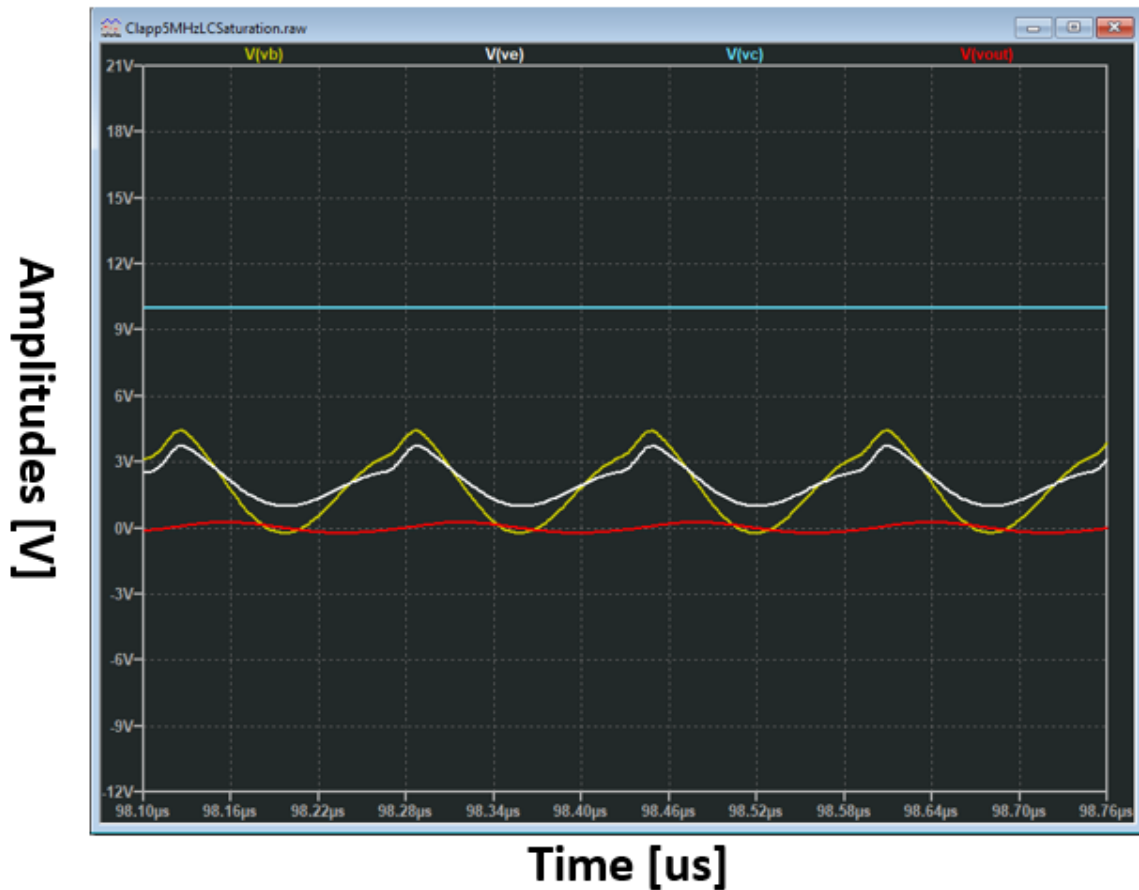


Figure 40 - Simulated Clapp Oscillator without Saturation and BE Breakdown. Collector voltage is in blue, RF output is in red, base voltage is in yellow and emitter voltage is in white.

Due to squegging in the simulator, the resistor RB1 was reduced to 10K for this simulation, the waveform is still very close to the measured ones.

Another interesting phenomenon is the shape of the base current, shown here in greater detail for the test case with saturation in the pink curve:

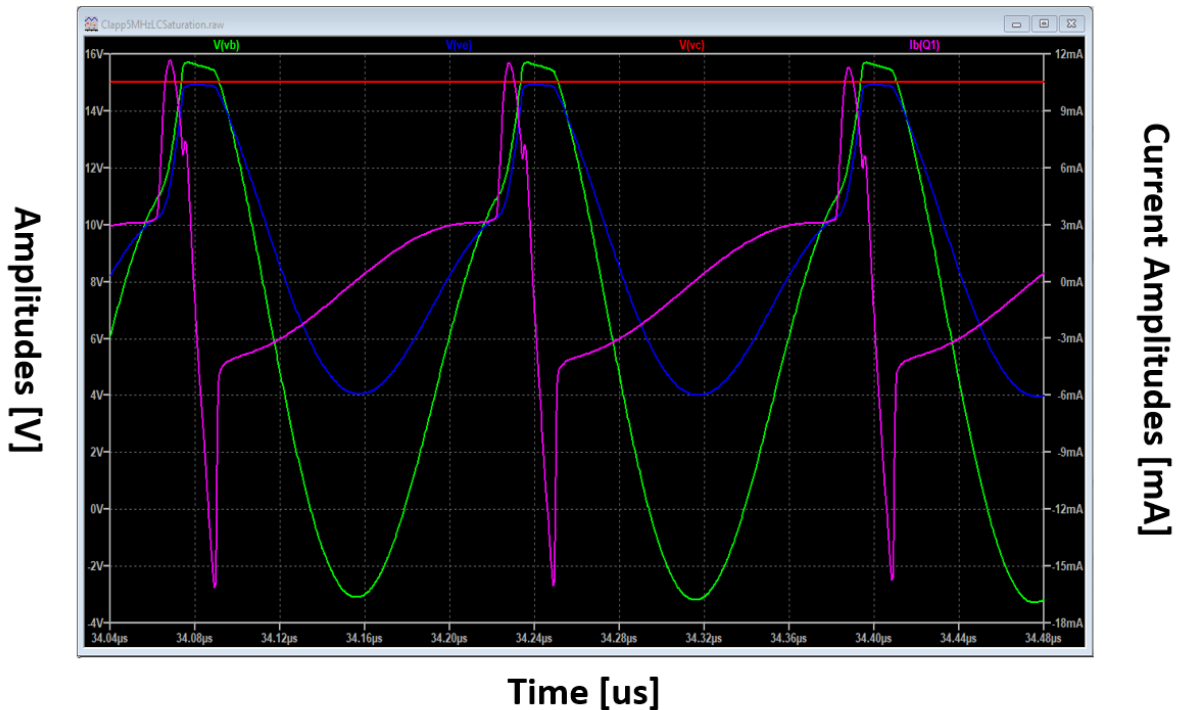


Figure 41 - Simulated Clapp Oscillator with Saturation Base Current without BE breakdown. Base voltage is in green, emitter voltage in blue, collector in red, and base current in pink.

During the upswing phase we see a sharp positive current spike, then a steep fall downwards, with a fall time of only ca. 18ns (minimum 7<sup>th</sup> harmonic). The back spikes at the bottom are even faster.

The location of the spike is naturally correlated to the point in time where the base-emitter voltage becomes positive and reaches a few 100mV. The physics of the smooth part of the curve looks like a constant value capacitor; the spike could be conduction (base) current as well as charging and discharging the diffusion capacitance as well as the nonlinear CB capacitor.

The peak value of the base current is +12/-18mA, ca. 1/10 of the collector current. The low-level DC gain of the 2N2222A is around 160, confirming that we operate in a saturated state.

A try to simulate the same circuit at 5V/15V with an HB simulator gave the following result for the base current (Serenade 8.7.1, 11 harmonics), the BE and CE voltages:

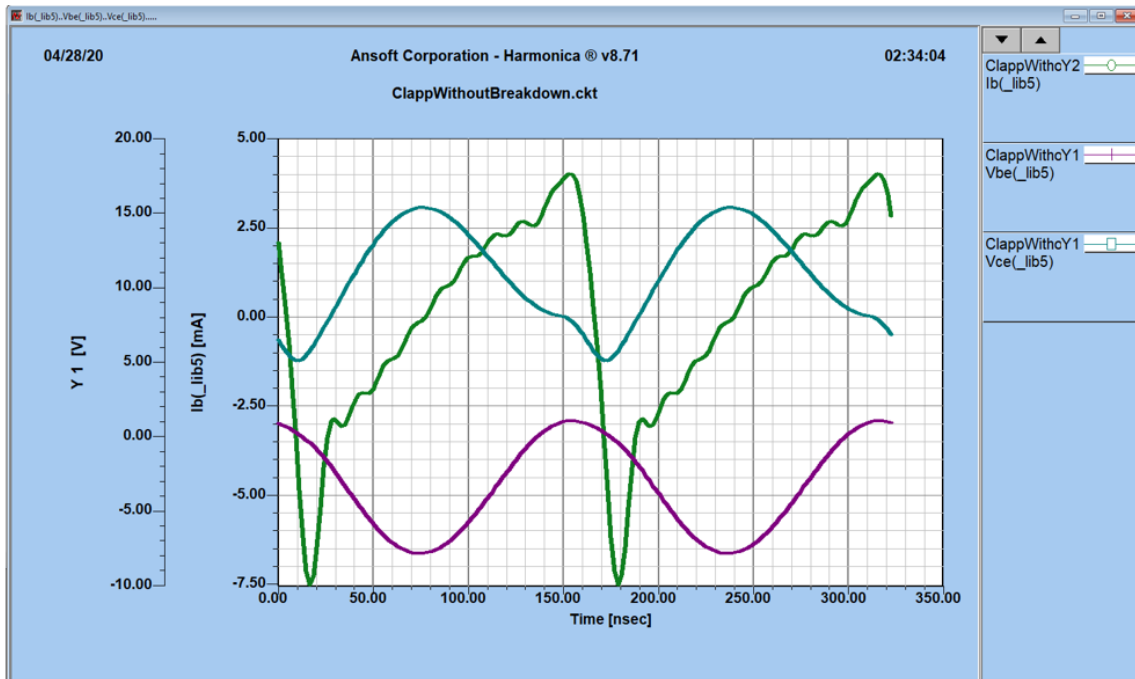


Figure 42 - HB Simulation of Clapp Oscillator Waveforms with Saturation and BE Breakdown

This is clearly not a good agreement with the measurements, not just for the base current. Reports (in the PhD thesis of A. Apte [15] that HB simulators can be off by up to 10dB regarding output power become credible because the waveforms are so unrealistic. The base emitter voltage is an almost perfect sinewave, which is certainly not true. The fact that the emitter/collector voltage never falls below 5V here is also completely wrong. The measured and SPICEd values are a few 100mV.

### 3.5.2 Saturation and Noise

DC tests are described in the transistor measurement chapter. The bottom line is that saturation reduces noise, by about 2dB from the unsaturated state.

This result could be a motivation to investigate switching transistors (e.g., 2N2369A, also a space qualified part) as oscillator cores.

## Conclusions Regarding Saturation Effects

Regarding the influence of saturation on oscillator performance, we could state that:

1. Moderate saturation does not seem to deteriorate oscillator performance
2. Saturation provides a hard-limiting mechanism, which is good [12]
3. Pencil-and-paper derivations without the additional currents occurring in saturation result in completely unrealistic predictions. This includes bias shift, waveforms, and amplitudes.
4. SPICE has a good coverage of saturation effects, and the curves predicted agree reasonably with the measurements.
5. Saturation seems OK if the conduction angle stays small. Deep saturation increases the conduction angle and phase noise, as measurements have shown.
6. The base current in a saturated oscillator has steep spikes from the loading and unloading of the BE and BC space charge zones including the charging and discharging capacitances. The

rise times involved are very short, suggesting that an accurate modeling in an HB simulator will be difficult. This was verified with an example where SPICE was OK, but HB was not.

7. Saturation has no negative effects on noise performance. On the contrary, at the same collector current the noise in saturation is ca. 2dB less than at an active operating point.

### 3.5.3 Outlook regarding Saturation Effects

Our present analysis did not take capacitive effects at very low voltages inside the transistor into account. With the large capacitances of the oscillator circuit at 5MHz, this is probably OK, but should be verified by extracting transistor models from real DUTs. Measurements have been made, but the incorporation into the simulations should be done. At higher frequencies, these effects are expected to become more influential.

## 3.6 Base Emitter Breakdown and its Effect of Oscillator Performance

When stepping thru a field of collector and base bias points and observing the output, there are several observations that suggest that there is a BE breakdown problem at higher amplitudes:

1. The difference between the probed base and emitter voltages measured exceeds the allowed negative base emitter voltages in the datasheets.
2. There is a “dent” in the negative swing of the base voltage, indicating a limiting mechanism.
3. Normally, far-off phase noise decreases with increased output power, but in the moment the VBE breakdown voltage is active this trend is reversed and there is a broadband increase in phase noise.

To illustrate this, a classic Clapp circuit in the MHz range was designed with probes attached and measured. The circuit looks like this:

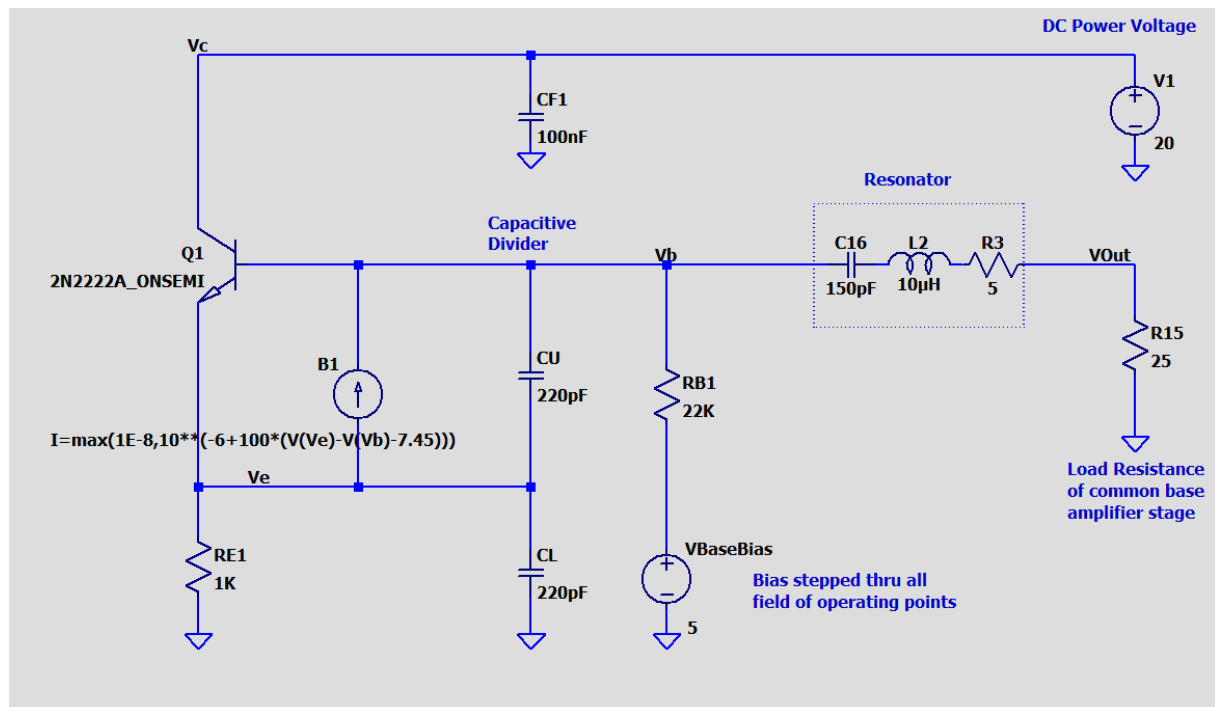


Figure 43 - Clapp Oscillator Simulation Schematics with BE Breakdown Effect Included

The details of this arrangement are discussed in the oscillator measurement chapter and in an IETE paper on the subject [17].

A contour plot of the measured 10Hz offset phase noise depending on the operating point is shown below:

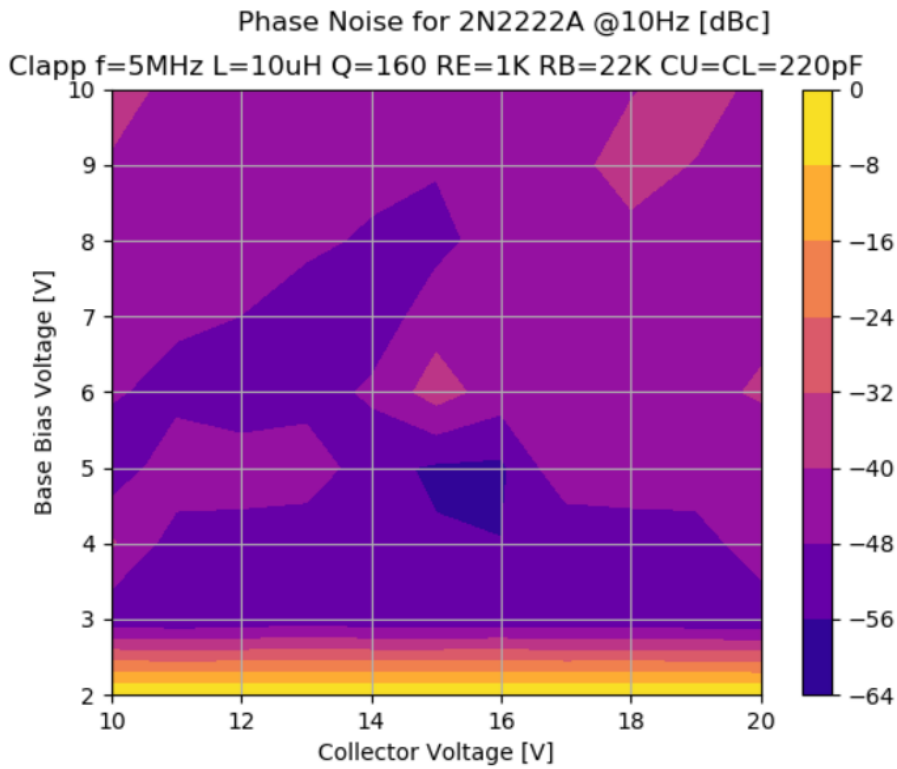


Figure 44 - Contour Plot of 10Hz Phase Noise Depending on Operating Point (2N2222A)

The 5/15 point is dark blue (-64 to -56), and the 5/18 point is in (-48 to -40). The same for 1MHz offset:

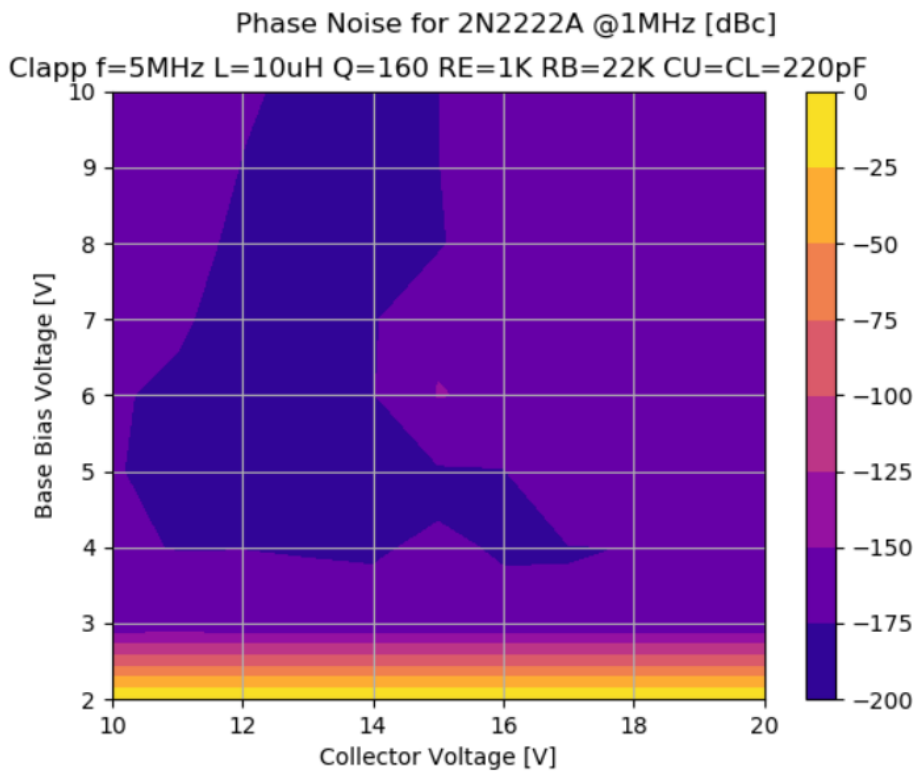


Figure 45 - Contour Plot of 1MHz Phase Noise Depending on Operating Point (2N2222A)

Same trend is visible; We have between -200 and -175 for 5/15, but ca. 20dB worse for 5/18, contradicting the Leeson formula.

Some points regarding the BE breakdown effect are worth mentioning:

1. The datasheets of the manufacturers are conservative about breakdown voltages. Measured voltages are 10% to 20% above the specifications
2. The measured BE breakdown voltages of LF transistors are significantly higher (up to 10V and more) than RF parts (a few volts). Modern high-ft RF parts (BFP Series, e.g.) can have BE breakdown voltages below 1V.
3. BE breakdown damages parts in the sense of a permanent reduction of beta at low collector current. The damage effect is much more pronounced at RF parts (see appendix E). The first mention found about this effect was published in 1969 (see [16]).
4. Only highly complex (and not generally available) simulation models (VBIC3, HICUM) contain parameters (VBBE) that include BE breakdown effects. Regular SPICE or HB models do not include this effect.
5. The BE breakdown consists of a tunnel mechanism (like low voltage Zener diodes) and an avalanche mechanism (for higher voltages). There is an overlapping range around 5-7V. The noise contribution of the tunnel and avalanche processes are different, and not documented in any known simulator device model.

### 3.6.1 Squegging Related to BE Breakdown, Semi-Isolated Topologies

As a sanity check, we could remove the breakdown (by removing the IB behavioral current source) from our simulation and see what the LTSpice simulation results would look like then:

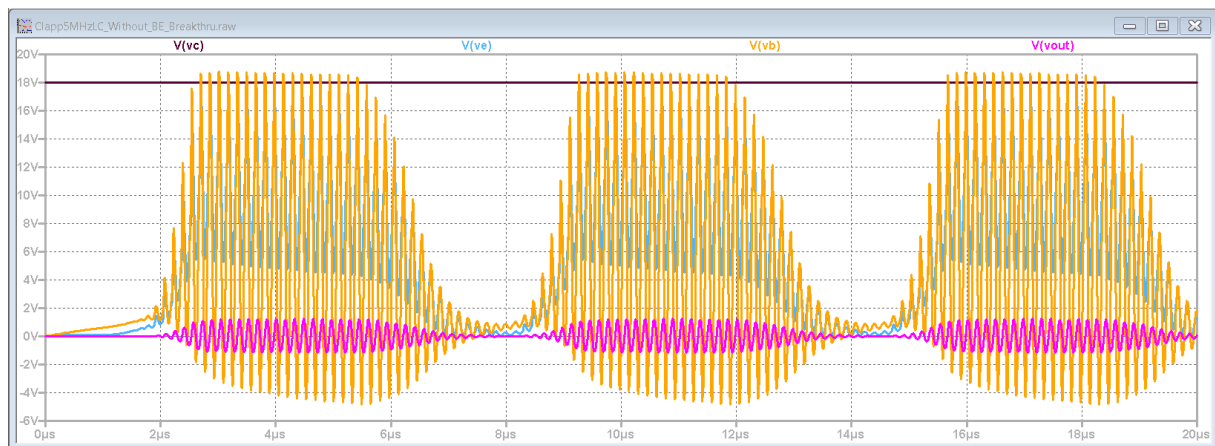


Figure 46 - Squegging Signal Example with Unstable Bias

In this case squegging occurs, and if we look in detail the VBE voltages reached are now at -9V, which is not possible for a real device. The occurrence of squegging is typical for a “one-sided” (saturation) limiting process with a lot of headroom on the other side (low voltages); According to Driscoll [12] any “soft-limiting” (and he considers one-sided limiting to automatically be soft limiting) is not as good regarding stability as “hard” limiting (with saturation and BE breakdown), but from a noise perspective this statement is incorrect.

Yet another sanity check is a slightly modified circuit where the coupling of the output is performed via a transformer coupled load at the collector side (semi-isolated type).



The schematics is show below:

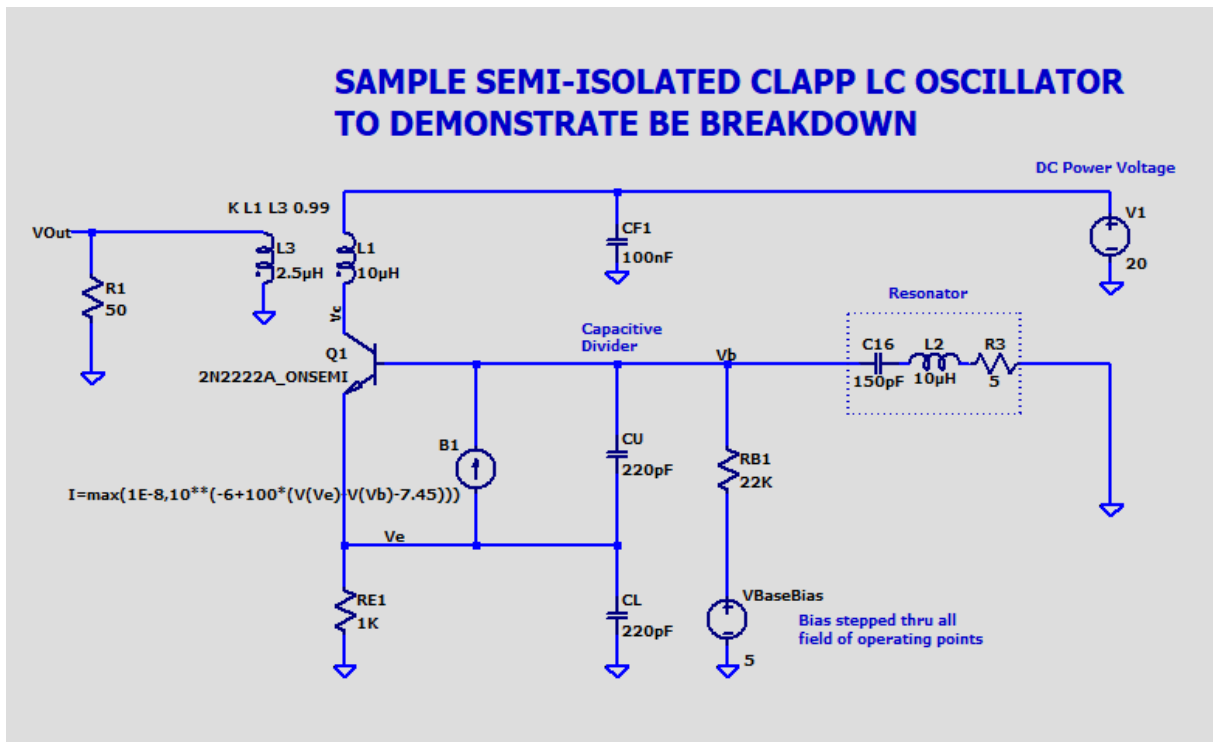


Figure 47 - Semi-Isolated Clapp Oscillator with BE Breakdown

And here are the waveforms:

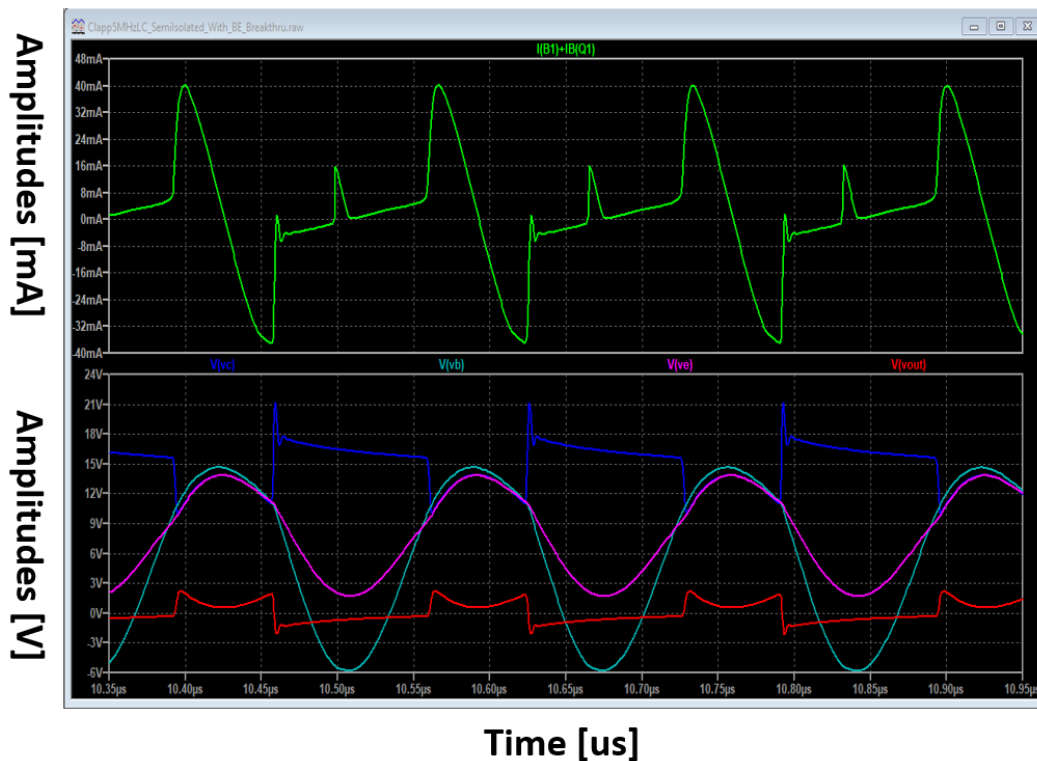


Figure 48 – Simulated Waveforms of a Semi-Isolated Clapp Oscillator with BE Breakdown. The upper plot shows base current in green. The lower plot shows base voltage (cyan), emitter voltage (pink), output voltage (red) and collector voltage (blue).

The BE breakdown effect can be clearly seen (the sharp spike in the IB(Q1) + IB1 curve). It should be noted that this circuit is not half as good as the decoupling through the resonator because the filtering

effect of the resonator has no “cleaning” effect on the output here. The output voltage (red) is extraordinarily rich in harmonics, a very unclean signal compared with decoupled Clapp we tried before.

In other words, the superior design of the decoupling thru the resonator is also capable of covering up internal oscillator problems, because the output is so clean and looks good even if the design is flawed and device limits are exceeded. Only the phase noise tells that something is fundamentally wrong. When the resonator Q is really high (e.g., 2.5 Million for a 5MHz SC part), the bandwidth is just a few Hz, and this will mask up almost all out-of-carrier signals.

### 3.6.2 Harmonic Balance Simulator Results

HB (Here Ansoft Serenade 8.71) has no BE breakdown implemented, so we should expect that the phase noise curve is drastically wrong. We tried this for the original circuit with the power picked off at the resonator, at 5V/18V, and the result is shown below:

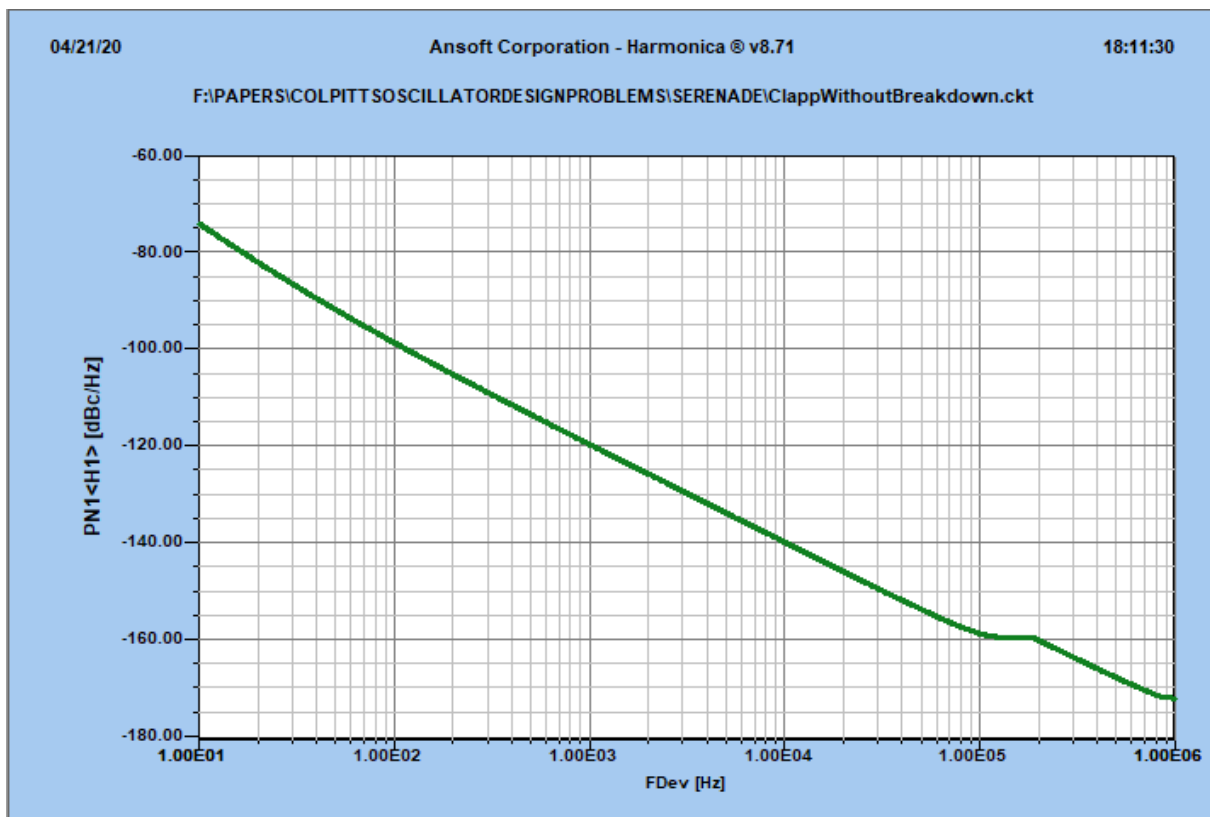


Figure 49 - Harmonic Balance Simulation of a Semi-Isolated Clapp with BE Breakdown

The *measurement* above at the same bias conditions was -40dBc@10Hz and -155dBc@1MHz. The output amplitude prognosed by Serenade was also off by 5dBm. In order to be fair, we tried to get a reasonable agreement without breakdown at 5/15V and got the fitting parameters  $AF=1.6$  and  $KF=5.E-11$ . These parameters were also used in the 5/18V simulation. Even at 15V, output power was off by ca. 3.6dB.

Some general words of warning regarding harmonic balance simulators; The precision is crucially dependent on the nature of the signal and the number of harmonics used in the simulation. When looking at the BE breakdown current spike (15ns/160ns), it is clear that a lot of harmonics would be needed to accurately model this waveform. People working at microwave frequencies where high harmonics are unlikely to occur to the limited bandwidths of the active components and circuit losses usually work with 5 or 7 harmonics; in this case here, that is by far not enough.

Bottom line for all simulation methods: missing physics in a model will create artefacts and grossly wrong data. On top of that, phase noise estimate formulas (Leeson) are completely off target if the BE breakdown mechanism is left out. This could be fixed by a “yet another Leeson extension” (YALE) term.

### 3.6.3 What about RF Transistors?

As discussed, “real” RF transistors provide worse performance in low frequency 5-10MHz USOs than classic low frequency types. The same measurements as above with the 2N2222A were carried out with a 1.4GHz  $f_T$  2N2857 transistor (at adapted voltage and currents) The outcome was that over all combinations of operating points the phase noise was 10 and sometimes more dB worse than the 2N2222A, especially at the low end where the higher  $1/f$  corner of RF parts hurts most. Regarding BE breakdown, we have to accept that we now are in the tunnel domain, with a much smoother breakdown curve; This means that the sharp “dent” as in the 2N2222A will be rounded off in the 2N2857 oscillator, and that the effect on phase noise will already occur at lower voltages and be less pronounced.

### Conclusions for BE Breakdown

BE breakdown can play an important role in the oscillation mechanism of Clapp oscillators at higher power levels. Until now, these effects have been left out from modeling, with the consequence of grossly false predictions about oscillator power, waveforms, and phase noise. The situation can be remedied by the inclusion of BE breakdown effects into simulation model, where the breakdown data was obtained by precision DC measurements. At 5-10MHz, it is possible to verify simulations by means of special low-capacitance active voltage and current probes. With the breakdown augmented transistor model, a good agreement between all waveforms and the output power was found.

### 3.6.4 Outlook for BE Breakdown

Even if the measurement techniques available at 5-10MHz are not directly applicable at VHF or even microwave frequencies, the underlying physical effects are still the same. Techniques like EBM could replace the physical probes and make the waveforms of microwave oscillators available for measurements. My expectation is that the principles above still hold, with the much lower VBE values of microwave transistors taken into account. What is needed is a method where reliable phase noise predictions are possible with BE breakdown present; The theory for this needs to be developed as well as measurement methods designed. Missing data about the nature of the breakdown process and the mechanisms involved present a major challenge for better simulation. On the software side, we need an incorporation of the BE breakdown effects into circuit simulators including not just the time domain, but also the noise generated. The next steps here would be measure breakdown noise for LF and RF transistors and to incorporate this into simulation models.

## 3.7 Phase Plots

A very intuitive and striking tool for understanding oscillator phenomena is to make phase plots of the variables involved in the oscillation process, like the transistor voltages and currents as well as the output. Emerging from small-bias starting points it is easy to see where classic oscillator theory still holds and where the underlying assumptions (like sinusoidal base emitter voltage for the Bessel function shift approach) are no longer valid.

To show the evolution from a small-signal case to a high-level oscillator incorporation all nonlinear limiting effects let's start with a low-power case. To run at a really low level, we set the base bias resistor to 1.8K $\Omega$ , the bias to 2V, and we increased the emitter resistor to 4.3K $\Omega$ . Supply voltage was set to 9V. All other parameters were left unchanged. The startup and the phase plot are shown below:

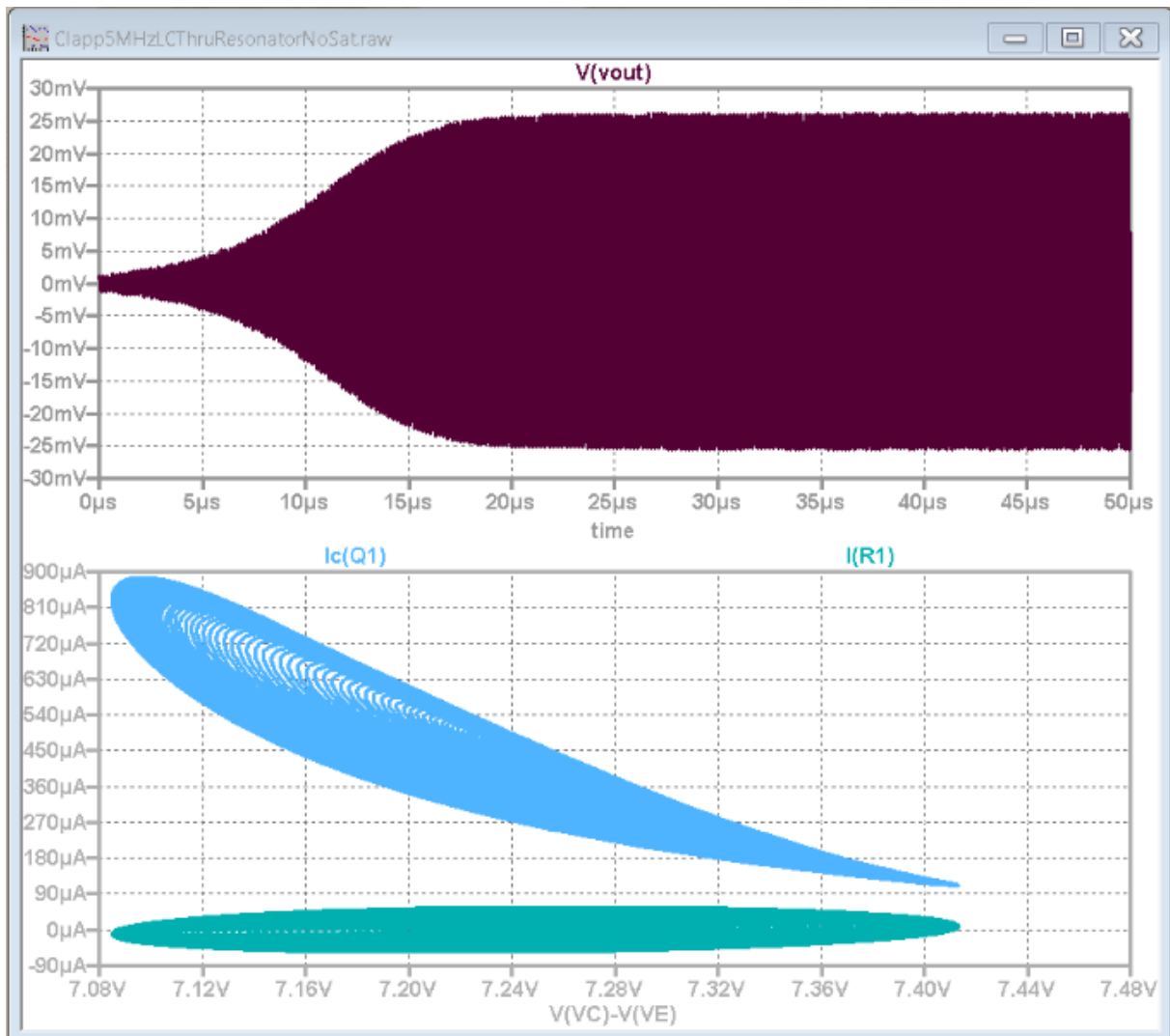


Figure 50 - Phase Plot of a very Low-Level Oscillator

The steady-state orbits are the outer contours, and we can see the startup from some center point. The curves show output voltage (brown) over time, and collector (blue) and base (green) current over emitter-collector voltage. The transistor never saturates, and the collector current never completely drops down to zero. If we would add the output curves of the transistor, everything happens around a small zone not even 500mV and 800uA wide.

Now let us use more power; the base resistor is set to 10K, the base voltage is 5V, the emitter resistor is now 1K. Supply voltage is 12V. The plot below shows a drastic change:

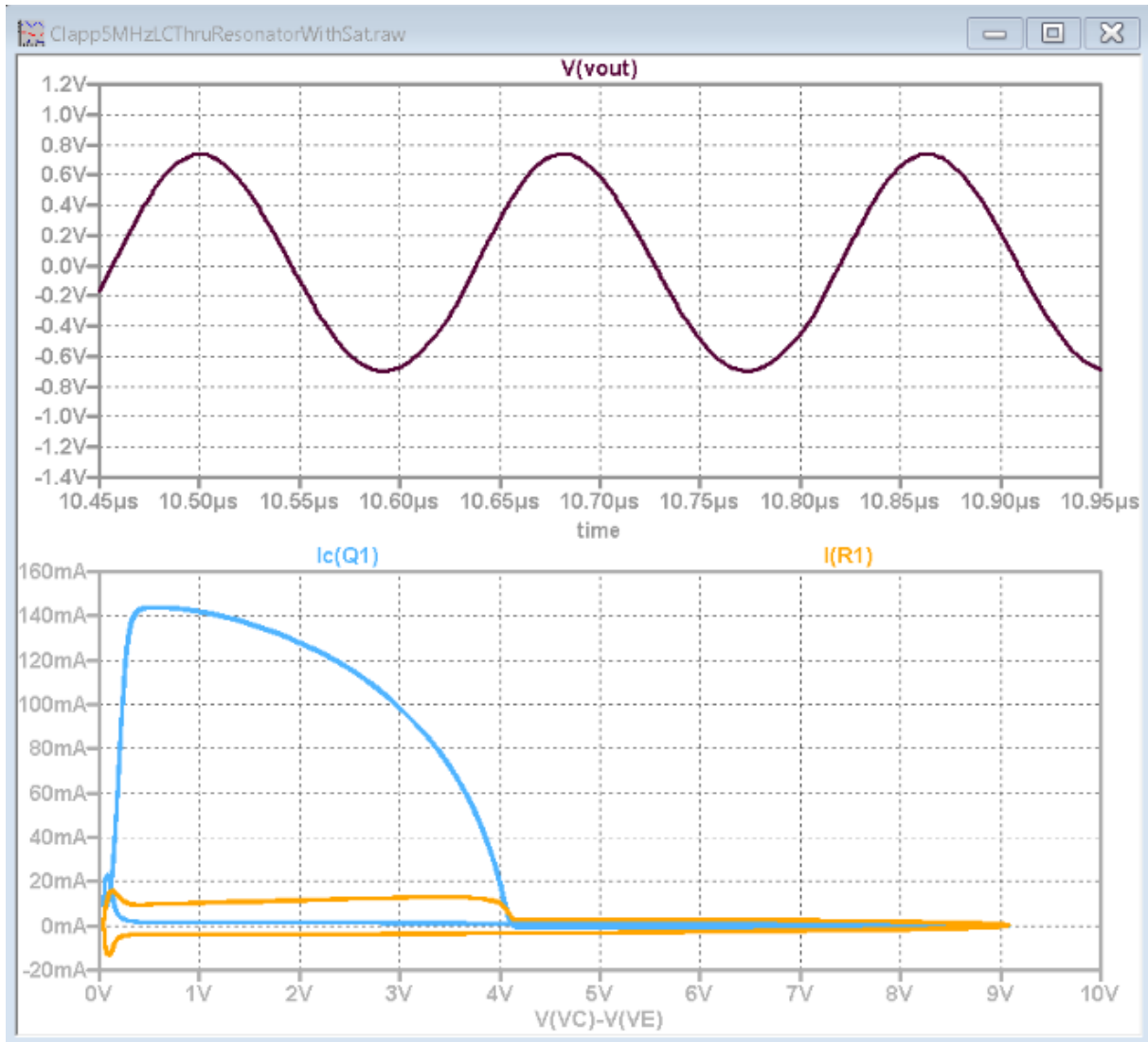


Figure 51 - Phase Plot of a Medium Power Oscillator. The upper plot shows the output voltage. The lower plot shows the collector current in light blue and the base current in yellow.

Only the steady state is shown here. The trace colors are the same as in the previous figure. We see that:

1. The collector current varies over a range of almost 0 to 140mA. This is (almost) in the high-current domain of the transistor.
2. Output voltage is much higher than in the low power case. We have ca. 1.4Vpp, or 7dBm.
3. The transistor goes into complete cutoff
4. There is a significant base current, especially when the transistor saturates.
5. Even with a “quasi-switching” behavior and a low-Q resonator, the output waveform contains only little harmonic content.

The Bessel function approach would not deal with base current at all, nor does it take the saturation phase into account. The onset of a massive base current when the transistor approaches saturation is, however, the reason for the clipped voltages in the oscilloscope screenshots shown.

We could now further increase bias, so we run into BE breakdown. The supply voltage is now 20V, the base resistor is 22K and the base voltage is 5V. The collector load line “blows up” even more:

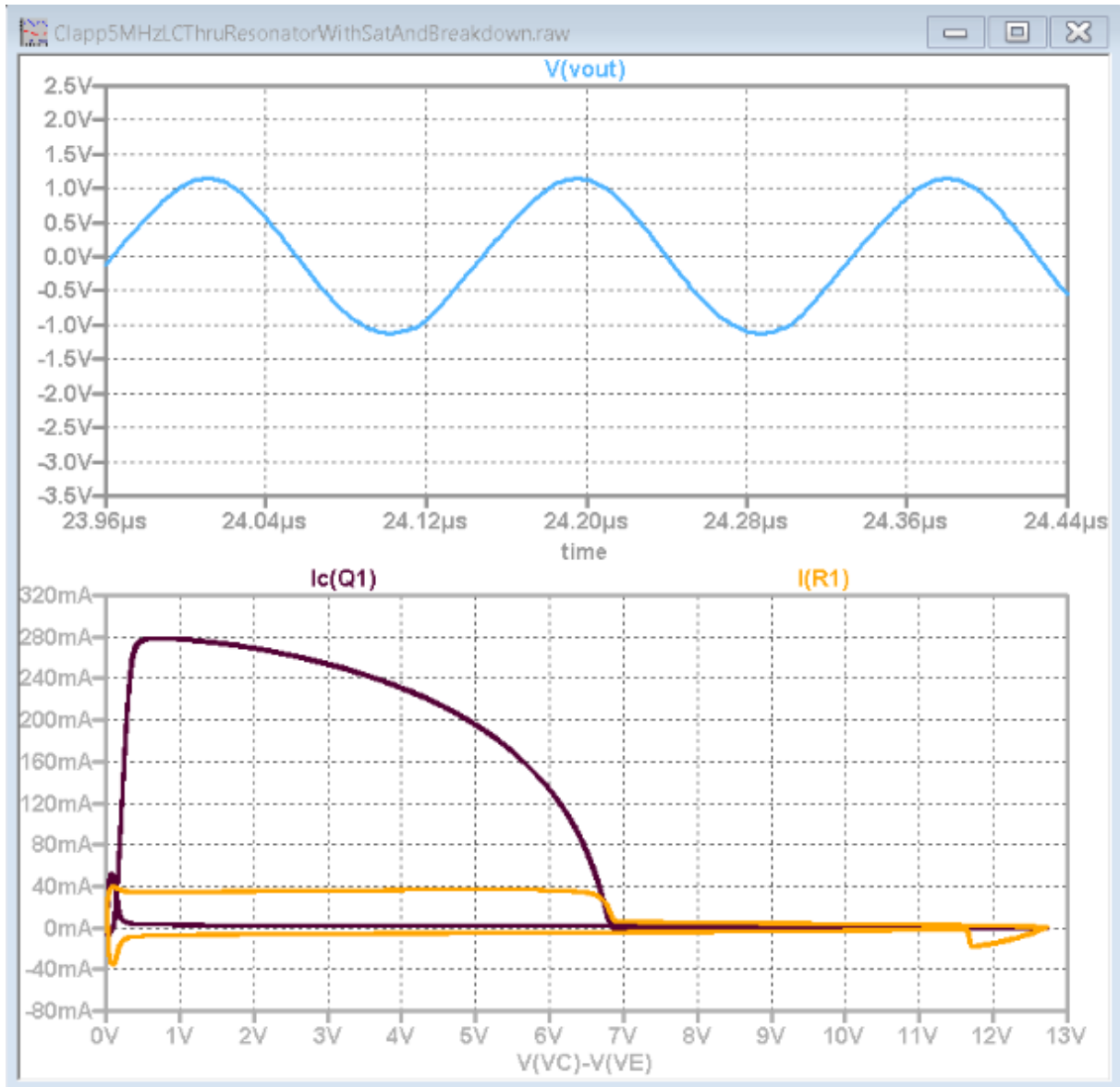


Figure 52 - Phase Plot of a Very High-Power Oscillator Showing Saturation and BE Breakdown. The curve types displayed are the same as in the preceding figures.

The curves are wider, the peak current is now 280mA, definitely a value where high-current effects become significant for the 2N2222A transistor used. Output voltage has climbed to 2.2Vpp, or 10.8dBm. Saturation and base current are massively increased, and, for the first time, we see a BE breakdown at the far right of the yellow base current line. The base breakdown current is -20mA, almost half of the positive maximum value. The transistor will suffer beta degradation caused by this, so this is not an acceptable oscillator design, leave alone the massively increase in phase noise caused by the breakdown.

### 3.8 Next Steps

The next chapter will cover LC oscillators, where the physical effects discussed can be practically examined and related to the theoretical models we discussed so far.

## References

- [1] Hewlett Packard Co., “10811A/B Quartz Crystal Oscillator Operating and Service Manual.” Aug. 1980, Accessed: Nov. 16, 2020. [Online]. Available: <http://literature.cdn.keysight.com/litweb/pdf/10811-90002.pdf>.
- [2] Ulrich L. Rohde, “Crystal Oscillator Provides Low Noise,” *Electronic Design*, vol. 21, Oct. 1975.
- [3] Ulrich L. Rohde, “A New and Efficient Method of Designing Low Noise Microwave Oscillators,” TU Berlin, Berlin, 2004.
- [4] “Colpitts/Clapp Oscillator Waveform Videos,” *Electronic Projects for Fun*, Mar. 17, 2020. <https://electronicprojectsforfun.wordpress.com/crystal-papers/spice-simulation-techniques-for-difficult-circuits/colpitts-clapp-oscillator-waveform-videos/> (accessed Nov. 17, 2020).
- [5] R. C. Jaeger and T. N. Blalock, *Microelectronic circuit design*, Fifth edition. New York, NY: McGraw-Hill, a business unit of The McGraw-Hill Companies, Inc, 2015., Early Effect on p5.8.6ff
- [6] Microsemi Corp., “2N2222A Technical Data Sheet.” Accessed: Nov. 17, 2020. [Online]. Available: [www.microsemi.com/index.php?option=com\\_docman&task=doc\\_download&gid=8898](http://www.microsemi.com/index.php?option=com_docman&task=doc_download&gid=8898).
- [7] Keysight, “Digital Multimeters 34460A, 34461A, 34465A (6½ digit), 34470A (7½ digit),” p. 28.
- [8] Keysight, “Infiniium S-Series Oscilloscope Datasheet.” Accessed: Nov. 17, 2020. [Online]. Available: <https://www.keysight.com/us/en/assets/7018-04261/data-sheets/5991-3904.pdf>.
- [9] Rigol, “Rigol DS1000Z Series Oscilloscope Datasheet.” Accessed: Nov. 17, 2020. [Online]. Available: <https://www.rigol-uk.co.uk/jg/wp-content/uploads/2020/09/Rigol-DS1000Z-Datasheet.pdf>.
- [10] R&S, “R&S FSWP Phase Noise Analyzer Specifications.” Accessed: Nov. 17, 2020. [Online]. Available: [https://scdn.rohde-schwarz.com/ur/pws/dl\\_downloads/dl\\_common\\_library/dl\\_brochures\\_and\\_datasheets/pdf\\_1/FSWP\\_d at-sw\\_en\\_3607-2090-22\\_v0900.pdf](https://scdn.rohde-schwarz.com/ur/pws/dl_downloads/dl_common_library/dl_brochures_and_datasheets/pdf_1/FSWP_d at-sw_en_3607-2090-22_v0900.pdf).
- [11] Pulse Microwave, “2N2857 Datasheet Pulse Microwave.” Accessed: Nov. 17, 2020. [Online]. Available: [http://www.mpulsemw.com/Pdf\\_files/2N2857.pdf](http://www.mpulsemw.com/Pdf_files/2N2857.pdf).
- [12] Michael M. Driscoll, “Low Noise Oscillator Design and Performance,” presented at the 2002 IEEE Frequency Control Symposium, New Orleans, LA, USA, Jun. 2002.
- [13] R. C. Jaeger and T. N. Blalock, *Microelectronic circuit design*, Fifth edition. New York, NY: McGraw-Hill, a business unit of The McGraw-Hill Companies, Inc, 2015., Early Effect on p5.8.6ff.
- [14] G. Massobrio and P. Antognetti, *Semiconductor device modeling with SPICE*. New York: McGraw-Hill, 2009.
- [15] Anisha Apte, “A New Analytical Design Method of Ultra-low-noise Voltage Controlled VHF Crystal Oscillators and it’s Validation,” TU Cottbus, Cottbus, 2020.
- [16] B. A. McDonald, “Three hFE Degradation Mechanisms and their Associated Characteristics,” in *8th Reliability Physics Symposium*, Apr. 1970, pp. 288–297, doi: [10.1109/IRPS.1970.362473](https://doi.org/10.1109/IRPS.1970.362473).
- [17] Wolfgang Griebel, Matthias Rudolph & Ulrich L. Rohde (2020) Added Noise in Oscillators Caused by the Transistor Base Emitter Breakdown Phenomenon, IETE Journal of Research, DOI: [10.1080/03772063.2020.1847702](https://doi.org/10.1080/03772063.2020.1847702)



### 3.9 LC Oscillators

The first oscillator (built with a vacuum tube triode as the active element) was invented by Meissner [1] in 1913. The schematics is shown below (from the original patent application):

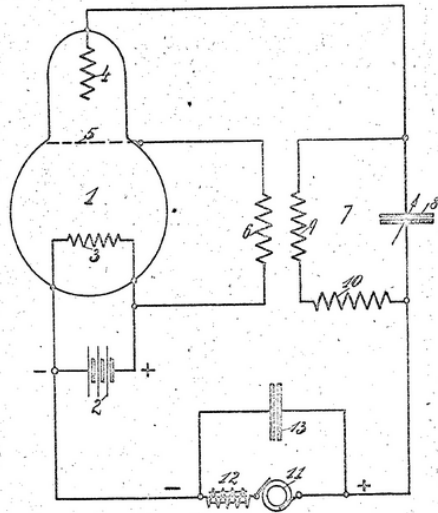


Figure 53 - Meissner Oscillator Patent  
Picture from Patent Application [1]

(initial) class A operation around this bias point.

The innovative idea at the time was to create a feedback path from an amplifier output (anode tank) to the input (the grid) so that a self-excitation of a small disturbance would be amplified until oscillations occurred and some sort of limiting mechanism set in. This principle is still at work in modern oscillators.

Meissner's (in the USA also called Armstrong's circuit because it was independently invented at the same time) feedback idea could be extended to all kinds of feedback mechanisms, not just transformers. As long as there is a frequency where the circuit had a positive loop gain and the phase was exactly right, oscillations would automatically start.

In 1913, standard symbols were not used yet, so what is looking as a resistor here are in fact inductors or transformers. The only resistor is #12.

The circuit consists of a vacuum tube triode at the left (#1), with a battery powered heater, a parallel tank at the anode (right side, #8, #10), and a feedback transformer (#6, #9). There is no extra grid bias, but at the time tubes that did not need a negative bias were common (like the 6B5, e.g., They still exist today in class A/AB power tubes, like the Eimac 3CX10000H7). The grid-cathode bias is even slightly positive, because the grid sits on the positive end of the heater supply and not in the middle, and the winding #6 probably has a small resistance only. Both these facts help to place the bias point of the tube into the active area, resulting in an



### 3.9.1 Oscillator Topologies

A vast variety of feedback networks that have been invented since Meissner's circuit. There are Hartley [4], Colpitts [5], Clapp [6], Vackar [7], Pierce [8], and many others (see below):

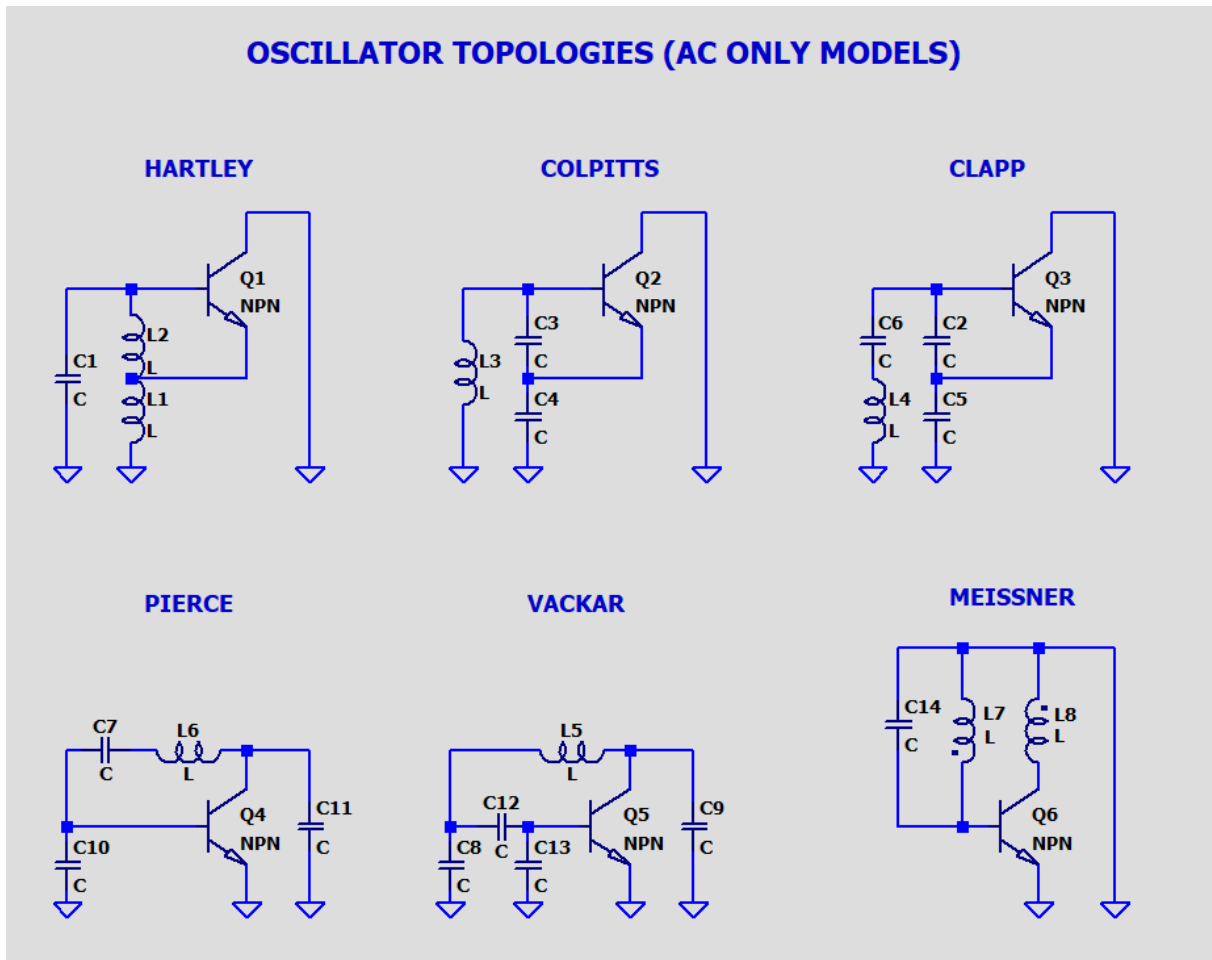


Figure 54- Oscillator Topologies

Picture was redrawn from the Circuits made by the respective Inventors named on top.

We need to concentrate on the most important and common types. For the purposes interesting here (space USOs), Colpitts or Clapp types almost have a complete monopoly<sup>4</sup>. A Colpitts or Clapp oscillator (invented 1918) uses a capacitive divider for feedback. Colpitts uses a parallel resonator, and Clapp uses a serial one, very suitable for ultra-high-Q crystals discussed later.

### 3.9.2 Colpitts/Clapp Varieties, Input Impedance

Within the Colpitts/Clapp topology, we still have several options to extract the output power from the oscillator:

1. On the collector side (probably with a matching transformer)
2. By a split lower capacitor in the divider
3. Through the resonator.

All three varieties will be discussed and simulated. Before we start with that, let us derive the input impedance of the oscillator as seen from the resonator side. The resonator is lossy and thus has an impedance with a *positive real part*. The active side of the oscillator must compensate for these losses,

<sup>4</sup> For pragmatic reasons: Only 1 coil, capacitors have a much higher Q than an inductive divider, are smaller, lighter, not sensitive to magnetic stray fields and vibrations, ...

so it must exhibit an impedance with a *negative real part* at the frequency of resonance that is larger than the losses by absolute value. To ensure a safe start of oscillations, we need some margin on the size of the negative part (usually chosen between 3 and 5)<sup>5</sup>.

As a basis for the analysis of the input impedance, we assume the following circuit:

A round a given operating point in the active domain with collector IC we get using KVL and KCL:

$$V_E = V_B - I_{in}(X_{C_U} || r_i)$$

$$V_E = (I_{in} + I_C)(X_{C_L} || R_E)$$

$$I_C = g_M(V_B - V_E)$$

$$r_i = \beta/g_M$$

Simplifying gives:

$$Z_{in} = (Z_B + Z_E)(1 + g_M Z_B || Z_E)$$

Where

$$Z_E = X_{C_L} || R_E \text{ and } Z_B = X_{C_U} || r_i$$

In the minimalist model applied here, there is no Early effect, no saturation, no breakdowns, so the output impedance of the current source is infinite, and the output loading  $R_C$  does not appear in the calculation. Nonideal effects will be discussed in detail later. In Rohde ([9], p380) there is a detailed derivation with parasitic elements included, but without the emitter resistor. At only a few MHz like in the USOs here, parasitics are much less of a problem than nonlinearities (discussed later).

A downside of Clapp oscillators is the dependency of output amplitude on the tuning capacitor. For USOs with an amplitude regulator this is not an issue, but LC VCOs are better off with a tapped parallel tank architecture like in the HP or Rohde circuit (See [10], p214).

### 3.9.3 Optimization

We have chosen some standard values for the components, a quite common transistor, an oscillation frequency of around 10MHz, and a common supply voltage and bias. No optimization or component selection whatsoever was made at this point; the aim is to see and understand what the theory predicts and what the simulation (and later actual measurements) show.

Optimization should take place *after* having a complete picture and not before, because otherwise prejudice could exclude effects from optimization that are in fact influential (e.g., BE breakdown). Optimization is always *subject to constraints* in the sense that the optimization target must be maximized in an area where certain conditions (e.g., maximum crystal current, supply voltage, power dissipation, BE breakdown voltage, ...) are not exceeded. This again puts more importance on having a simulation model including *all* these parameters and not just some.

A classic case for Clapp optimization is a derivation of how to set the best ratio of  $C_L$  over  $C_U$ . For a Bessel function approach (assuming a sinusoidal base emitter voltage) Rohde [11] has given a derivation explaining that a high  $C_L$  over  $C_U$  ratio has many positive effects, like less noise and less negative base swing leading to potential breakdown. Even if the assumption of a sinusoidal base

---

<sup>5</sup> This is needed, e.g., for crystals showing a DLD (drive level dependency) effect where the losses at small amplitudes are higher (up to several times) than normal. With not enough gain reserve, this could prevent a startup.

emitter voltage is (sometimes drastically) wrong, a tendency towards the effects predicted still exists, but the simplified formulas cannot really predict the best values accurately.

It is the job of a better and more complete theory to perform an optimization without unrealistic assumptions and without leaving out physics that may be hard to handle but is nevertheless important. We will try to follow this path in the next chapters, with the help of numeric math and simulations instead of pencil and paper algorithms limited in complexity.

Let us now analyze some Clapp LC oscillators with different pickoff methods and look at waveforms and spectra.

### 3.9.4 Semi-Isolated Colpitts/Clapp

First, we take the variant where we pick off the oscillator power at the collector, corresponding to an  $R_C$  in the calculation above, called a semi-isolated circuit Rohde ([10], p260), shown below:

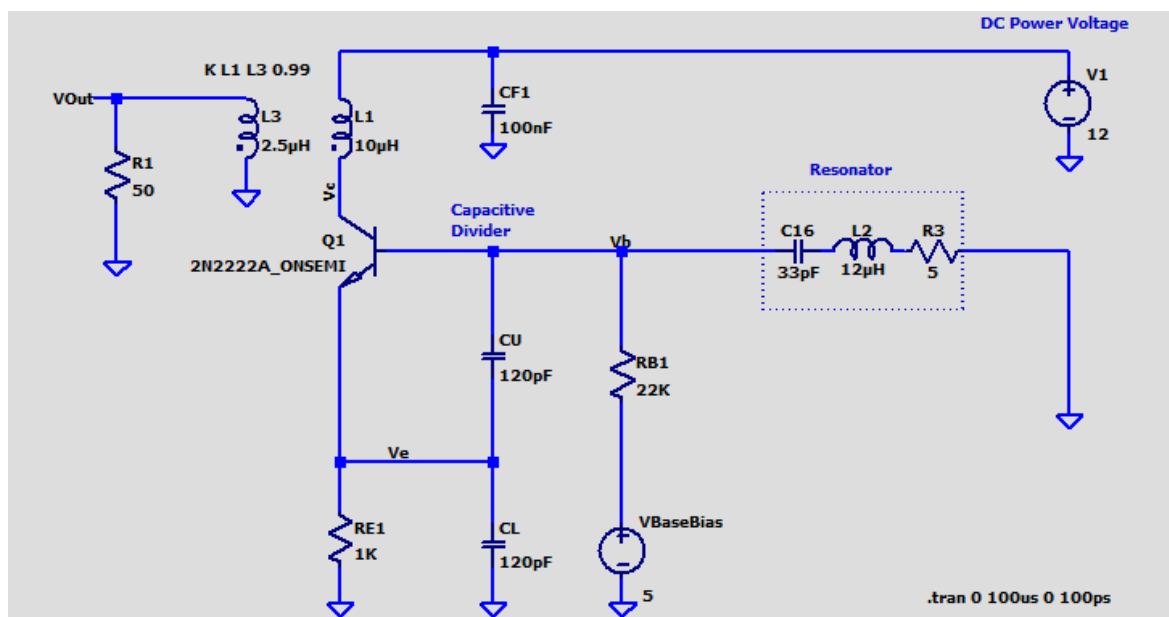


Figure 55 – 10 MHz Clapp Oscillator in Semi-Isolated Decoupling

This circuit was common when a frequency multiplication was intended at the collector side. A lot of crystal oscillators ran at, say, a 28.8MHz 3OT crystal frequency, and a tank tuned to 144MHz filtered the 5<sup>th</sup> harmonic out at the collector. For fundamental frequency output the circuit is less attractive because the Q of the output has only a small filter effect due to the 50Ohm secondary termination.

In case decoupling through the resonator is not possible, the emitter-tapped variety (see later) has a better signal quality because the decoupling point is inside the resonating loop, acting as a filter.

The waveforms of our sample oscillator look like this:

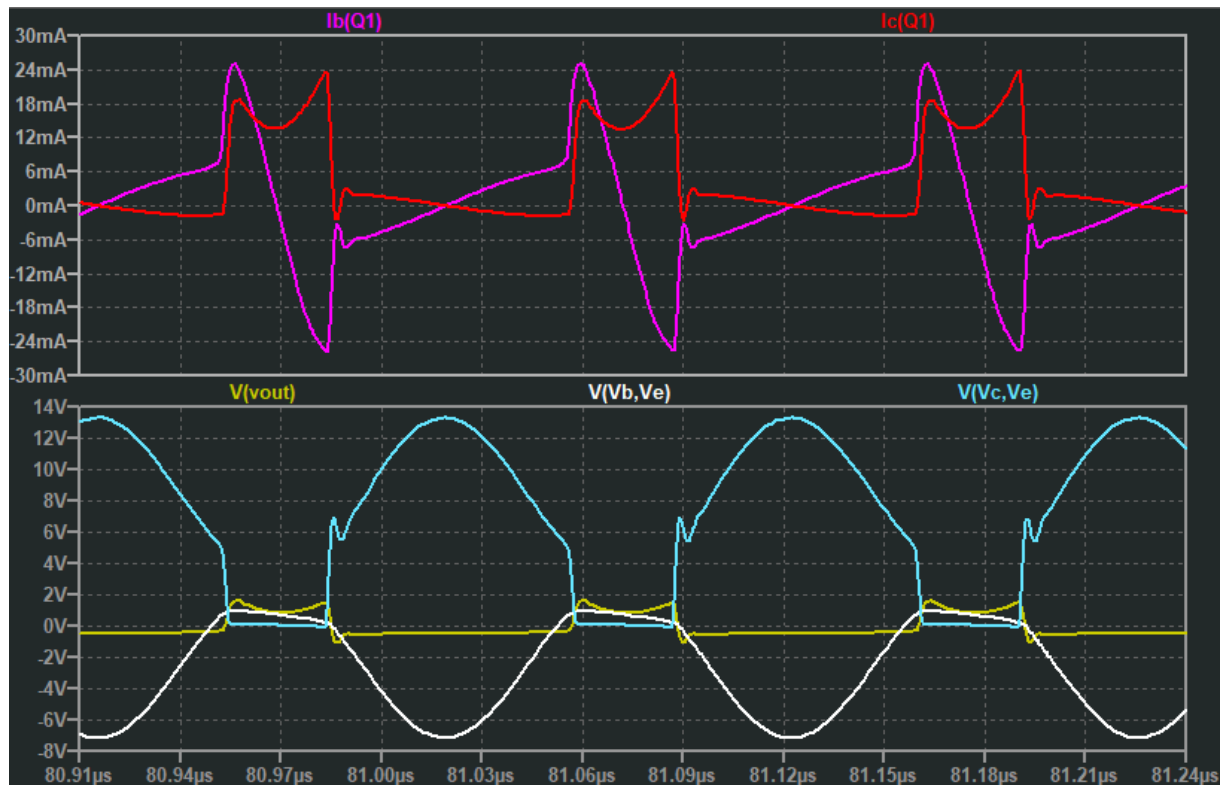


Figure 56 - Waveforms of the Semi-Isolated Clapp Oscillator. The upper plot shows base current (pink) and collector current (red). The lower plot shows the output voltage (yellow), the base-emitter voltage (white) and the emitter-collector voltage (cyan).

Even from this simple circuit, it is obvious that the small signal derivations made above won't hold. The transistor saturates (look at  $V_{CE}$ ), the base voltage is not really sinusoidal but capped, and the base emitter voltage exceeds the allowed voltage in the datasheet (see appendix D). The saturation voltage is only around 200mV, and the conduction angle is not much larger than the saturation angle. The output (yellow) looks not very pretty, with a lot of high harmonics, as the spectrum shows:

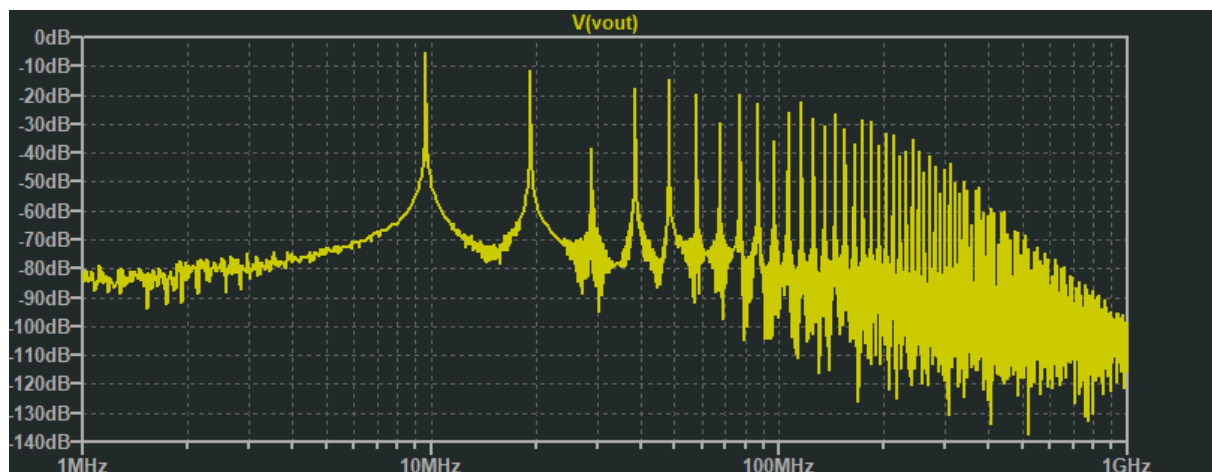


Figure 57 - Semi-Isolated Clapp Oscillator Output Spectrum

A possible BE breakdown effect was not included in the simulation (yet, see later). A lot of filtering will be necessary to convert this into a clean output spectrum, with the second harmonic only ca. 6dBc down. In case we want to extract higher harmonics, this circuit makes more sense.

### 3.9.5 Emitter-Tapped Colpitts/Clapp

The next variety is the decoupling of the output power via a split emitter capacitor, shown here:

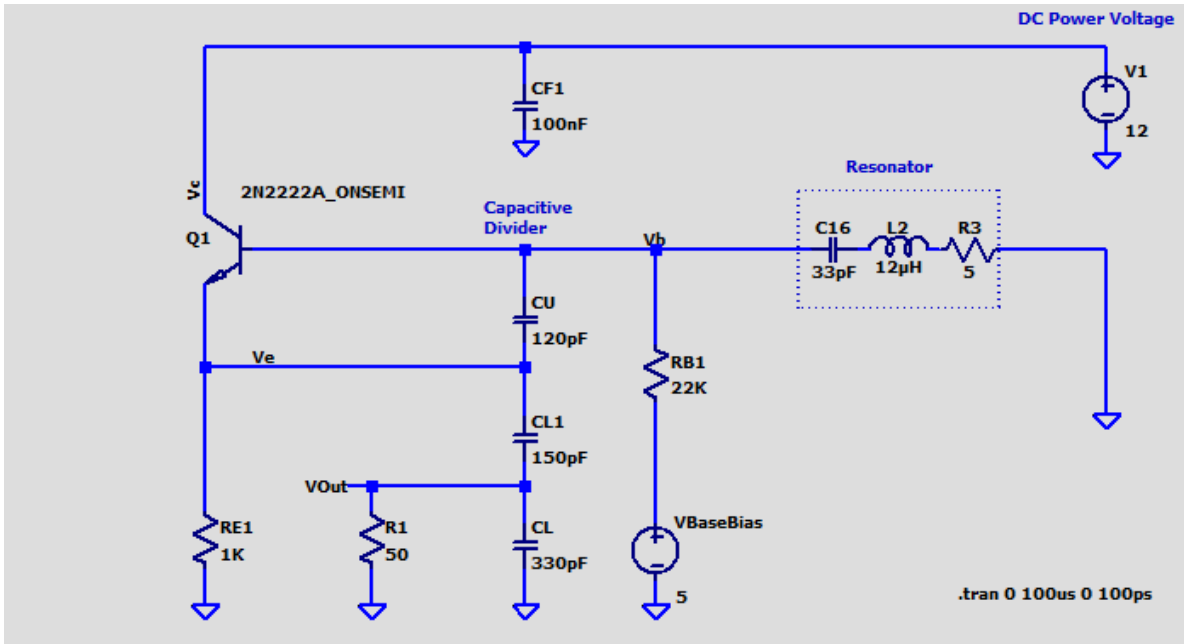


Figure 58- 10 MHz Emitter-Tapped Clapp Oscillator

This variety is common in the microwave range where the series tank is replaced by a quarter wave stripline or ceramic resonator and transformers are no viable choice due to parasitic inductances. A capacitive splitter can still be implemented with very small parts that have little parasitic effects. The output impedance at  $V_E$  is the load multiplied with the square of the  $C_L/C_{L1}$  ratio. This circuit is not very stable due to the dependency on reactive load impedance, but it is normally used in phase locked loops only.

The waveforms are shown here:

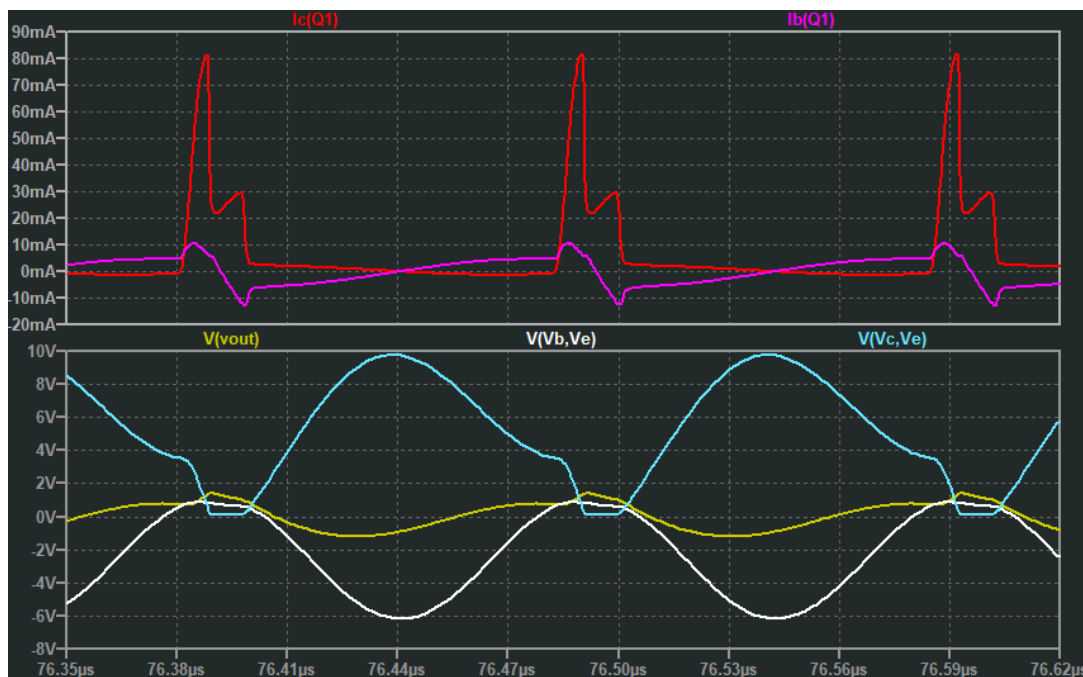


Figure 59- Emitter Tapped Clapp Oscillator Waveforms. The colors in this graph mean the same as in the previous one.

Again, the transistor saturates, but not as much as in the semi-isolated version. This is understandable because the collect voltage is not reduced the transformed load here. Negative  $V_{BE}$  is still ample, but not as close to the BE breakdown voltage as in the semi-isolated case.

And here is the output spectrum:

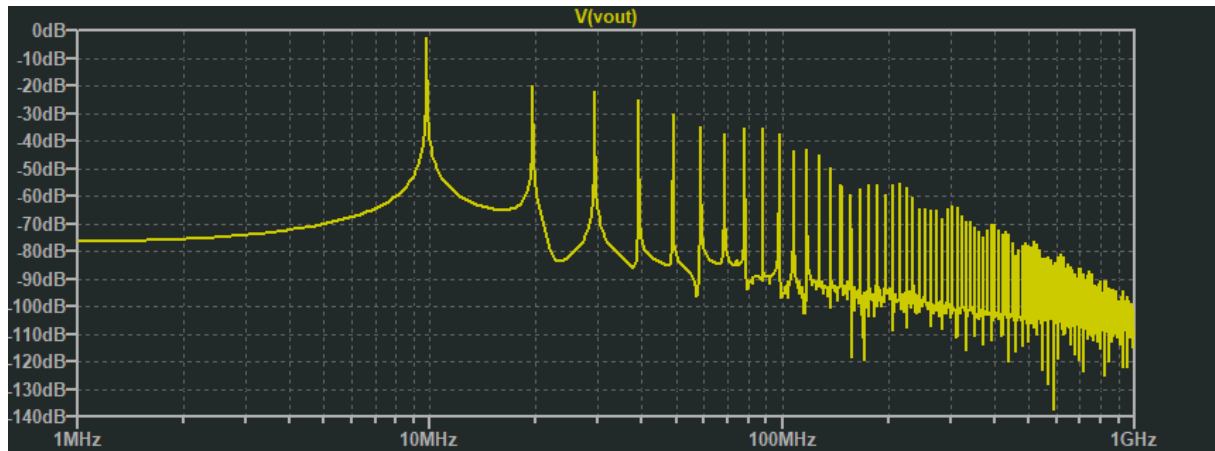


Figure 60 - Emitter Tapped Clapp Oscillator Output Spectrum

Better than before, but still not very pure. The spectrum looks a bit improved as well, the second is now down by ca. 17dBc, the 3<sup>rd</sup> by 20dBc.

### 3.9.6 Resonator-Decoupled Colpitts/Clapp

Now to the third variant, with the extraction of the output power via the resonator. This circuit was first published by Rohde [12] and has a lot of advantages over the other types. All modern USOs have this circuit topology (using a crystal instead of the series LC tank) as their oscillator core (HP, Keysight, Wenzel, Morion, ...). The schematics looks like this:

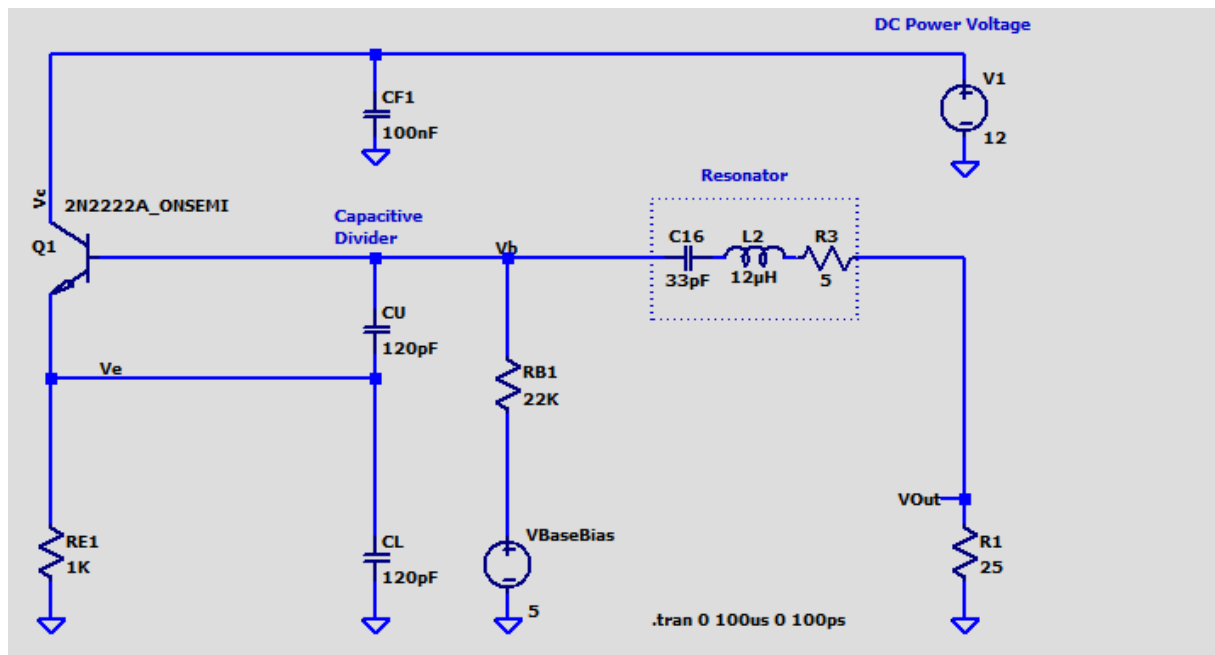


Figure 61 – 10 MHz Clapp Oscillator with Decoupling through the Resonator

The load R1 is either an output resistor (50Ohms for S22) in parallel with 50Ohms external load, or the input resistance of a following buffer stage (for an example see [13]). This stage is usually a common-base stage with a very low input impedance (in the range of a few to 10 Ohms).

This variety only works as a Clapp (series) configuration, and the resonator impedance and the load should be in the same order of magnitude.

The major benefit of this circuit is that the resonant element not only oscillates, but also filters the output before it goes to the next stage. Depending on  $Q$ , this filtering can be extremely effective (e.g., a  $Q$  2.5 Million 5MHz SC cut crystal has a bandwidth of only 2Hz!), completely masking out everything not very close to the carrier. As desirable this is, it has led to bad oscillator designs because people would only look at the output (in time domain and HB simulators not having the complete physics included), but not at the waveforms inside the core. If, e.g., unwanted limiting by BE breakdown occurs, this is barely recognizable as a uniform increase of phase noise. Even on a good scope, no changes in waveforms can be observed. Nonlinear mixing, however, spoils top performance close to carrier as it is required for premium space USOs, so clean waveforms are a must even if the output seemingly looks alright.

The waveforms of the oscillator with through-resonator decoupling are shown below:

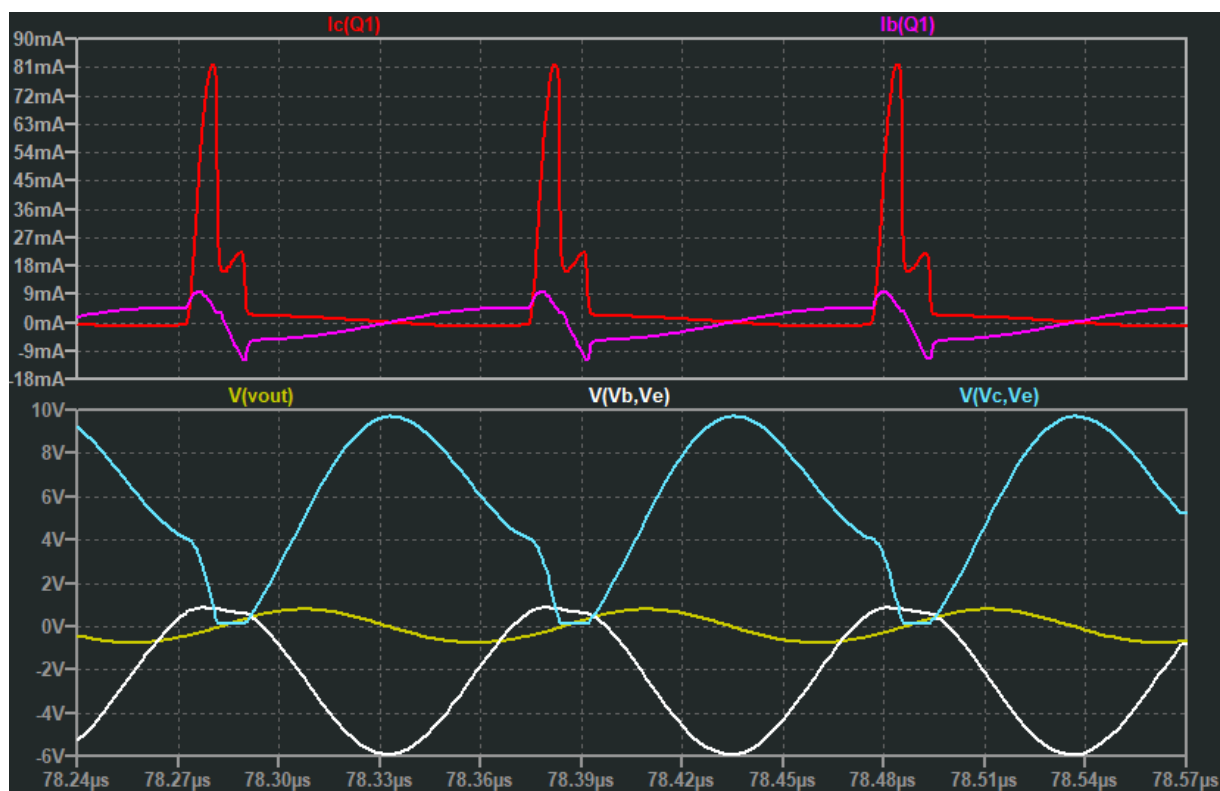


Figure 62 - Clapp Oscillator with Decoupling through Resonator Waveforms. The trace colors used are the same as in the previous waveform plots.

Negative VBE is lower and definitively out of the datasheet danger zone, there is still some saturation, otherwise nothing special occurs.

What does change much is the output voltage, as the spectrum confirms:

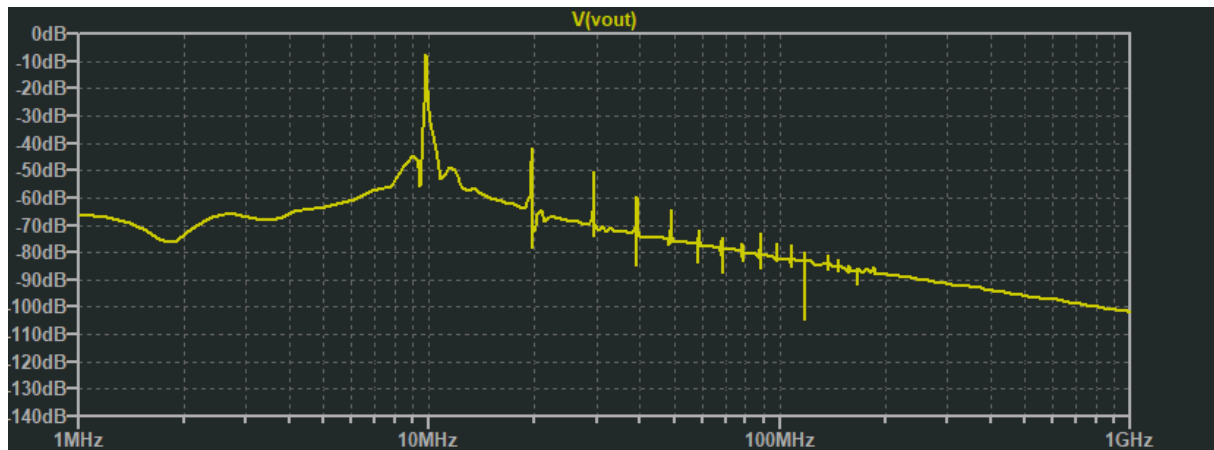


Figure 63 - Clapp Oscillator with Decoupling through Resonator Spectrum

This is, compared to the other variants, a pure sinusoid.

The next harmonic is 30dB down from the carrier, not too bad for the rather low  $Q_L$  of the resonator, in this case only ca. 25. As will be shown phase noise also profits a lot from the extra filtering effect.

### 3.9.7 Phase Noise

An important parameter of an oscillator is the phase noise characteristic. The Single Sideband Phase noise (a dimensionless quantity) specified at a given carrier offset, is the ratio of the power density measured at this offset expressed in a one Hz bandwidth divided by the transistor oscillator carrier power. The principal concept formulas for phase noise were derived in 1966 by Leeson, a radar engineer trying to explain where the noise sidelobes of his radar signals came from.

It uses feedback system with an active device, a mixer, a resonator and various noise sources. The principal formula was derived by D. Leeson [14], D. Scherer [15] added the flicker noise term, J. Everard [16] introduced the loaded  $Q$  and U.L. Rohde extended the formula with a voltage-controlled oscillator (VCO) component [11]:

$$L(f_m) = 10 \log \left\{ \left[ 1 + \frac{f_0^2}{(2f_m Q_L)^2} \right] \left( 1 + \frac{f_c}{f_m} \right) \frac{FkT}{2P_{sav}} + \frac{2kTRK_0^2}{f_m^2} \right\}$$

Where

$L(f_m)$  = ratio of sideband power in a 1 Hz bandwidth at  $f_m$  to total power in dB

$f_m$  = frequency offset

$f_0$  = center frequency

$f_c$  = flicker corner frequency

$Q_L$  = loaded  $Q$  of the tuned circuit

$F$  = noise factor

$kT$  =  $4.1 \times 10^{-21}$  at 300 K<sub>0</sub> (room temperature)

$P_{sav}$  = average power oscillator output (W)

$R$  = equivalent noise resistance of tuning diode (typically 50 Ω - 10 kΩ)

$K_0$  = oscillator voltage gain, MHz/V



The formula is a *fitting* formula, because some parameters like  $Q_L$ ,  $f_C$  and  $F$  are *not readily available* but chosen to fit the experiment. They are “cyclostationary” quantities, meaning averages over an oscillation period and *not* the static datasheet values for a single operating point. Another source is Lee and Hajimiri [17] who have shown that the creation of phase noise is the result of a nonlinear mixing process, where (white or other) noise somewhere in the spectrum is mixed up to the oscillator carrier by a multiplication process. A more heuristic derivation of phase noise for a practical oscillator can be found at Rohde [11].

In our case we did not use a tuning diode, so the VCO term can be omitted. Space USOs never use tuning elements. All “tuning” is done by selecting fixed value components before launch. The reason is better stability, immunity to vibrations, size, and aging.

The formula above indicates that phase noise power should be inversely proportional to output power squared. For oscillators with *small* RF amplitudes, this is a widely used approximation and corresponds well with the measured values and their trend, also confirmed by the measurements in this paper at low to medium bias conditions.

For the general, high amplitude case, we must question the meaning and significance of the fitting parameters:

First, what is the definition of a quality factor  $Q$  in a cyclostationary (nonlinear but periodic with a *single* period) circuit where the resonator is undamped by a strongly time varying negative resistance, working like a flywheel with short pulses? Not easy to answer, leave alone to measure. See “Oscillation Measurement Techniques” chapter, section “What is loaded  $Q$ ?”.

Next, the use of a noise factor  $F$  and a flicker corner frequency  $f_C$  is, strictly speaking, a misnomer. These values are *not* the same as the parameters extracted from a transistor device measurement even if they carry the same name. What they mean here are cyclostationary mean values of a noise factor and a flicker frequency corner of one period of oscillation. When we look at the waveforms encountered in the pages above the operating cycle of an oscillator covers a rather large part of its transistors complete output curve field, from saturation to several volts of collector and base voltages, from cutoff to current spikes in the tens of mA, it becomes clear that the variations of these parameters are greater than their mean value. The types of noise generated (thermal noise, Schottky noise, flicker noise, ...) effect that noise sources are effective only in (small, see conduction angle) parts of a period. To make a long story short,  $F$  and  $f_C$  are fitting parameters where a credible connection to physics is missing in high amplitude oscillators.

The VCO term is more plausible, but as space USOs have no tuning elements (who should fly up there and tune it), it is left out of discussion.

On the other hand, BE breakdown adds a strong noise source missing in the current formula. Formally, this could be fixed by a new extension term. This will be discussed later (and in a forthcoming paper).

For LC oscillators with not too high Q ( $< 1000$ ) and a practical transistor, a typical phase noise curve has the following shape:

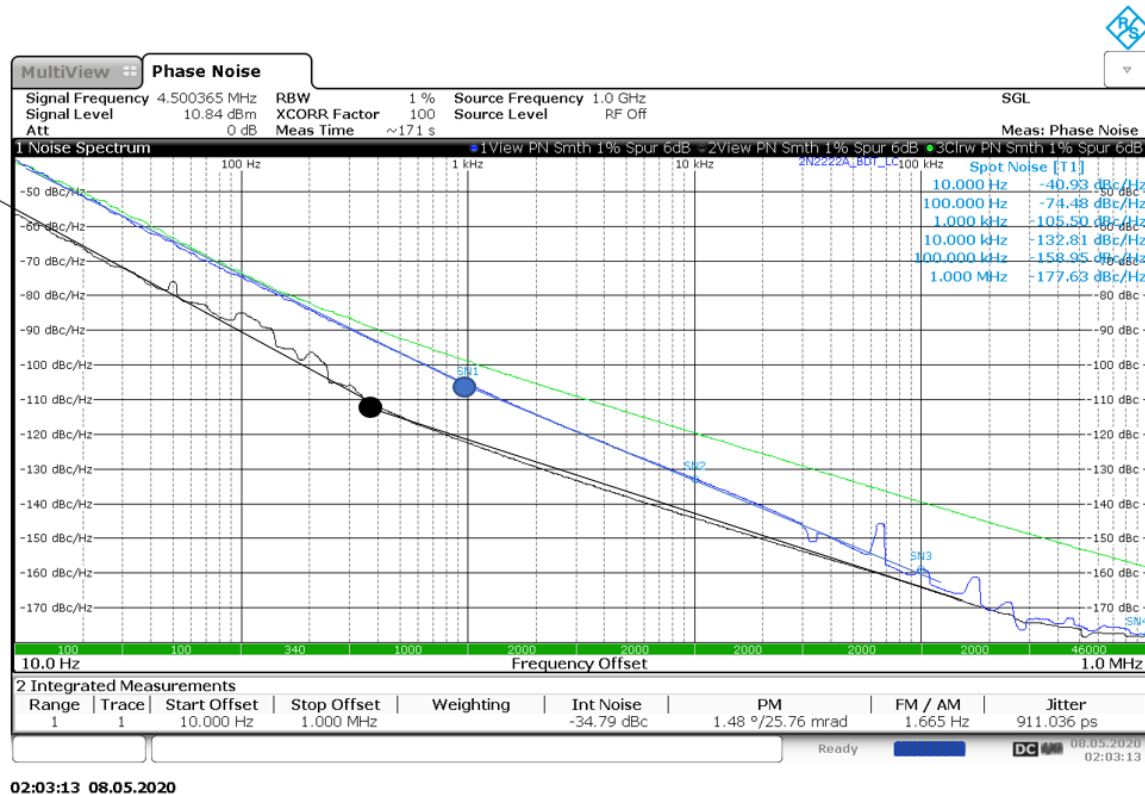


Figure 64 - Phase Noise Plot of a Clapp Oscillator without BE Breakdown (black curve):  $C_L=C_U=220\text{pF}$ ,  $R_E=1\text{K}$ ,  $R_B=22\text{K}$ ,  $V_{Bias}=5\text{V}$ ,  $V_{Collector}=15\text{V}$

By applying tangents, a soft  $1/f$  corner is visible at around 1kHz, the curve dips into the thermal floor at around 1MHz, the far offset value is about thermal floor ( $-177\text{dBm SSB}$ ) minus oscillator power in dBm.

For higher Q resonators, the  $1/f$  corner gets masked out by the bandwidth of the resonator.

From a mathematical point of view, the Leeson formula offers a “fit-friendly” structure where tuning  $Q_L$ ,  $f_C$  and  $F$  provide enough parameters to fit measured phase noise curves to a measurement. An agreement of below a dB between fit and measurement is no exception, what is much harder to achieve is a good prediction of the resulting oscillator power. 10dBs (!) off are considered acceptable.<sup>6</sup>

The unsatisfying accuracy of Leeson formula and simulator power predictions come from both incomplete physics in the models as well as the numerics of simulation programs. This will be demonstrated in the following chapters, where actual measurements of waveforms and output are related to the theoretical and simulator predictions.

<sup>6</sup> It should be noted that even a premium signal analyzer (Rohde&Schwarz FSWP) specifies a 3dB uncertainty on phase noise measurements.

Anticipating results of the chapters to follow, the following example plot shows an oscillator phase contour plot where both saturation and BE breakdown occur. The transistor with its exponential dependencies exhibits a much more complex behavior than the simple cubic nonlinearity in the Van der Pol equation:

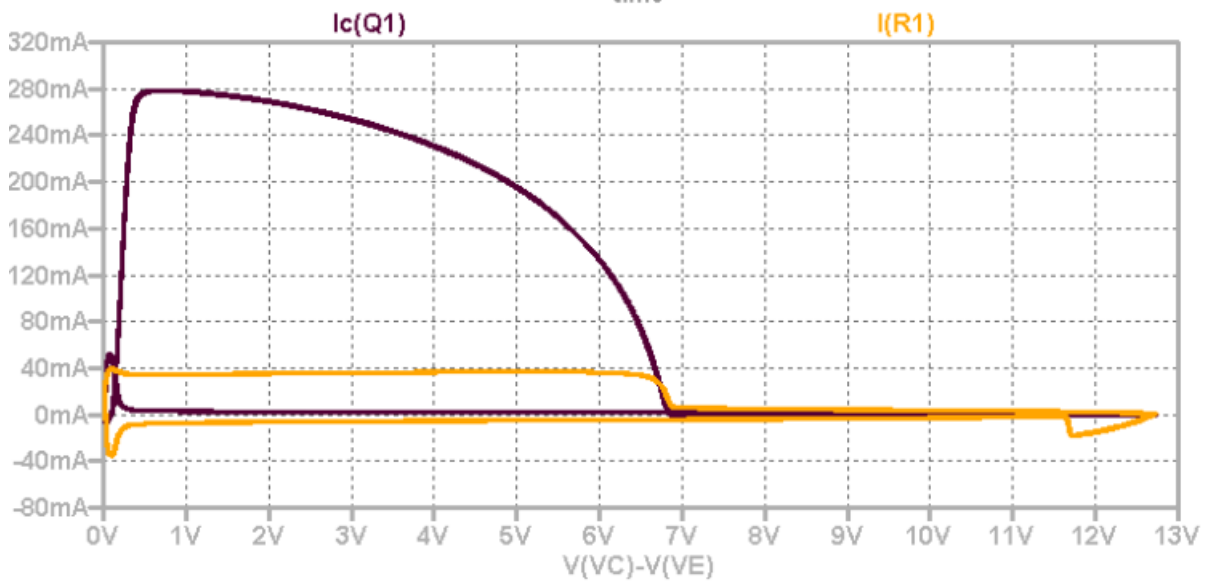


Figure 65- Collector and Base Voltage/Current Load Line Phase Plots

The saturation part occurs far left, with collector voltages of only a few 100mV at peak currents of 280mA. On the right part ( $V_{CE} > 7V$ ) of the plot the transistor is operating in cutoff with collector current dropping to almost zero. At the far right we see a negative BE breakdown with a breakdown current of ca. 20mA. The extreme deviations of voltages and currents suggest that this problem is no good candidate for a small signal approach centered around a well-defined operating point.

### Conclusions for LC Oscillators

The classic theory of oscillator operation is not very well suited for accurately predicting the performance of practical circuits.

Nonlinear general dynamic approaches are much better, but they are numerics-only approaches. If all physics is properly included in the simulation formulas, predictions are fairly accurate for LC oscillators. SPICE time domain simulations are a good starting point.

All relevant, not just some physical effects observable in oscillators must be included in simulations. What is relevant or not should be substantiated by measurements, not by assumptions.

The most important quality measure of a simulator is the agreement of *all* waveforms in the time domain, not just a match of a phase noise curve. With the large number of fitting parameters, the reverse conclusion that the physics is understood if the phase noise is fittable (not the same as correct) is wrong.

Screening tests are needed to identify problems with model accuracy and to find optimum operating points under constraints. Pencil-and-paper predictions are unreliable.

### 3.9.8 LC Oscillators, A Pragmatic Design Method

When we need to design an HF LC oscillator with minimum phase noise, the approach would be to simulate and measure different configurations for a grid of bias points,  $C_1$  and  $C_2$ , extract their waveforms and phase noise, and to go for a “legal” phase noise point where all datasheet limits of the transistor are duly respected.

This approach is safe but time-consuming because of the large number of parameter grid points, so a rule of thumb / pragmatic cookbook approach would be helpful as well. Here we go:

If our main objective is minimum phase noise, the Leeson formula suggests that the output power should be as high as possible. We are, of course, limited by power dissipation, the deterioration of beta at higher currents, the possibility of a BE breakdown and current limits.

As shown previously, classic NPN LF transistors provide better noise than modern RF types. From what we learned from the simulations and measurements we could state that an output power of 7-15dBm is OK for a 2N2222A transistor. The maximum collector current is 800mA, which provides ample reserves for the around 100mA of peak collector currents that are likely to occur. Maximum collector voltage is above 40V, which has found to be always on the safe side, even in BE breakdown conditions.

When we think of the limiting mechanisms that occur at the different operating points, the measurements show that the optimum phase noise points occurred at moderate levels of saturation. Bessel function shift and the Early effect were not visible, nor did a BE breakdown occur.

The next question is the  $C_1$  (upper) to  $C_2$  (lower) ratio.  $C_1$  and  $C_2$  act as a capacitive divider, so the remaining swing amplitude at the BE junction is approximately the base swing amplitude multiplied by  $ZC_1/(ZC_1+ZC_2)$ . The top will always be capped by the onset of base current, but a large  $C_1/C_2$  ratio will reduce the chance of a BE breakdown. A ratio of 1-6 is possible, with a design center ratio of about 3 to start.

The supply voltage should be not too small to allow for a reasonably strong DC stabilization resistor in the emitter. A good starting point is the DC base voltage a little less than half of the supply voltage, so we could use a bias of 5V, and 1K of emitter resistance, giving ca. 4mA of DC bias current, with a total supply voltage of 12V. Temperature stability is important because dissipation is substantial, in our case we have DC-wise around  $4\text{mA} \cdot (12\text{V} - 4.3\text{V}) = 30\text{mW}$ , which leads to a temperature increase of ca.  $10^\circ\text{C}$  and a corresponding bias shift of ca. 25mV, less than a percent of the static emitter bias and therefore OK.

Base DC bias current is in the range of 25uA (beta of 2N2222A is around 160), which should cause no large drop across the base bias resistor. On the other hand, the base bias resistor lies in parallel to the resonator, reducing Q. If we ask for a drop which is smaller than half the  $V_{BE}$  voltage, we get  $R_B < \text{ca. } 10\text{K}$ . Too small  $R_{BS}$  reduce Q, too large values can cause squegging and instabilities.

The output amplitude is very sensitive to the Q of the series tank. A Q of around 160 resulted in an output amplitude of 8dBm. When looking at the contour plot of phase noise, we find an optimal zone around 11-15V of collector voltage, not very much dependent on base voltage (i.e., resulting bias current). Power in this collector voltage range has an approximately quadratic dependency on base bias, and collector current increases about linearly with base voltage.

Conduction angles and saturation angles were around 60 and 30 degrees, respectively. This is in line with the fact that low conduction angles produce less noise.

The final recipe for a low noise HF LC oscillator would run like this:

1. Use an LF transistor (e.g., 2N2222A)
2. Around 9-15V of supply voltage
3.  $C_1/C_2$  around 3-4 (tests were done with 1:1, but this does not change amplitude much)

4. Base voltage 40-50% of collector voltage for stability
5. Base resistor around 10K
6. Q around 150
7. Emitter resistor around 1K, i.e., around  $V_{\text{SUPPLY}}/(2*1\text{K})$  of DC supply current

Then we may expect an output power that follows the supply voltage in a square fashion, so

$$P_{\text{OUT}}[\text{dBm}] \cong K_p + 10 \log(V_{\text{SUPPLY}}^2 * 2.5)$$

With  $K_p$  needs a fit from the contour plots.  $K_p$  depends on the transistor type,  $C_1/C_2$ , the emitter resistor and resonator Q. For the circuit investigated, we have

$$K_p \cong -15 \text{dBm}$$

As a caveat, the formula above is a starting point only, but not a precise design rule.

### Next Steps

The next steps will be to analyze crystal oscillators.

### References

- [1] Alexander Meissner, "EINRICHTUNG ZUR ERZEUGUNG ELEKTRISCHER SCHWINGUNGEN." Accessed: Nov. 26, 2020. [Online]. Available: <https://worldwide.espacenet.com/patent/search/family/000546471/publication/DE291604C?q=pn%3DDE291604>.
- [2] H. Barkhausen, *Elektronen-Röhren, 3. Band Rückkopplung*, 4. Leipzig: S.Hirzel, 1931.
- [3] H. Nyquist, "Regeneration theory," *The Bell System Technical Journal*, vol. 11, no. 1, pp. 126–147, Jan. 1932, doi: [10.1002/j.1538-7305.1932.tb02344.x](https://doi.org/10.1002/j.1538-7305.1932.tb02344.x).
- [4] E. Rubiola, *Phase noise and frequency stability in oscillators*. Cambridge, UK; New York: Cambridge University Press, 2009.
- [5] R.V.L. Hartley, "Oscillation Generator." [Online]. Available: <https://docs.google.com/viewer?url=patentimages.storage.googleapis.com/pdfs/US1356763.pdf>.
- [6] E.H. Colpitts, "Oscillation Generator." Accessed: Nov. 26, 2020. [Online]. Available: <https://patentimages.storage.googleapis.com/5a/95/f0/832baa7af5edf1/US1624537.pdf>.
- [7] J.K. Clapp, "Frequency Stable LC Oscillators." Accessed: Nov. 26, 2020. [Online]. Available: [https://ietlabs.com/pdf/GR\\_Appnote/A65%20Clapp.%20Freq.%20Stable%20LC%20Oscillators.pdf](https://ietlabs.com/pdf/GR_Appnote/A65%20Clapp.%20Freq.%20Stable%20LC%20Oscillators.pdf).
- [8] Jiri Vackar, "LC Oscillators and their Frequency Stability." Accessed: Nov. 26, 2020. [Online]. Available: [http://www.f6evt.fr/f6evt\\_fr/vackar\\_wholepaper.pdf](http://www.f6evt.fr/f6evt_fr/vackar_wholepaper.pdf).
- [9] George W. Pierce, "Piezoelectric Crystal Resonators and Crystal Oscillators Applied to the Precision Calibration of Wavemeters." Proceedings of the American Academy of Arts and Sciences, Oct. 1923, Accessed: Nov. 26, 2020. [Online]. Available: <https://www.jstor.org/stable/pdf/20026061.pdf?refreqid=excelsior%3Afa0351f79a0a9ec1e7ad973eb7e163e0>.
- [10] U. Rohde, J. Whitaker, and H. Zahnd, *Communications Receivers: Principles and Design, Fourth Edition*, 4. Edition. New York, NY: McGraw-Hill Education, 2017.
- [11] U. L. Rohde, *Microwave and wireless synthesizers: theory and design*. New York: Wiley, 1997.

- [12] Ulrich L. Rohde, “A New and Efficient Method of Designing Low Noise Microwave Oscillators,” TU Berlin, Berlin, 2004.
- [13] Ulrich L. Rohde, “Crystal Oscillator Provides Low Noise,” *Electronic Design*, vol. 21, Oct. 1975.
- [14] Hewlett Packard Co., “10811A/B Quartz Crystal Oscillator Operating and Service Manual.” Aug. 1980, Accessed: Nov. 16, 2020. [Online]. Available: <http://literature.cdn.keysight.com/litweb/pdf/10811-90002.pdf>.
- [15] D. B. Leeson, “Oscillator phase noise: A 50-year retrospective,” in *2015 Joint Conference of the IEEE International Frequency Control Symposium & the European Frequency and Time Forum*, Denver, CO, USA, Apr. 2015, pp. 332–337, doi: [10.1109/FCS.2015.7138853](https://doi.org/10.1109/FCS.2015.7138853).
- [16] Dieter Scherer, “Design Principles and Test Methods for Low Phase Noise RF and Microwave Sources,” presented at the RF&Microwave Measurement Symposium and Exhibition, 1978, [Online]. Available: [http://hparchive.com/seminar\\_notes/Scherer\\_Low\\_noise\\_source\\_design\\_and\\_test.pdf](http://hparchive.com/seminar_notes/Scherer_Low_noise_source_design_and_test.pdf).
- [17] “Ultralow Phase Noise 10-MHz Crystal Oscillators - IEEE Journals & Magazine.” <https://ieeexplore.ieee.org/document/8540461> (accessed Nov. 27, 2020).
- [18] Thomas H. Lee, Member, IEEE, and Ali Hajimiri, Member, IEEE, “Oscillator Phase Noise: A Tutorial.” *IEEE JOURNAL OF SOLID-STATE CIRCUITS*, VOL. 35, NO. 3, Mar. 2000, Accessed: Nov. 26, 2020. [Online]. Available: [https://web.ece.ucsb.edu/~long/ece145b/HajimiriLee\\_JSSCtutorial00.pdf](https://web.ece.ucsb.edu/~long/ece145b/HajimiriLee_JSSCtutorial00.pdf).

### 3.10 Crystal Oscillators

In the last chapter we analyzed classic LC oscillators and showed that several physical effects play an important role in its function, especially in the amplitude limiting process. We were able to show that simple analytical models are inaccurate but satisfying results can be obtained by time domain simulation including all relevant physical effects like saturation, the Early effect or even BE breakdown.

Just like with LC oscillators, many ways to obtain a crystal oscillator are possible by varying the feedback path. We will not fully discuss all of them because just one type is really used in USOs, and that is the Clapp type. This type has several advantages that made it so popular:

1. Use of ultra-stable series resonant SC cut crystals including filter effect, but now with an extremely efficient filter with a Q in the range of millions at 5MHz.
2. Good independence of the frequency from the properties of the surrounding circuit, but using a high-values capacitive divider, also reducing noise
3. Few, reliable and well-proven components

We will go into detail about these benefits in this chapter. The underlying physics of crystals and their measurements are explained in a separate chapter.

#### 3.10.1 The Behavior of Precision Crystal Oscillators

If we stick to the Clapp type, the only thing to do to convert a series LC oscillator to a crystal oscillator, so it seems, is to remove the L and the C and replace it by a crystal. For low-precision (AT mode) crystals in fundamental mode this statement is correct. For precision crystals (SC cut), this can result in a series of surprising effects, like the generation of chaos, the simultaneous generation of two frequencies, squegging and so on.

The obvious reason for the added complexity in behavior is the much more complex impedance a precision crystal has over frequency. Instead of just one L and one C as in the LC oscillator, we now have an equivalent circuit with (see Rohde [1], p247):

1. A series RLC with high Q at the crystal fundamental mode frequency. The fundamental frequency is never used in USOs, however, because its Q is less than the 3<sup>rd</sup> overtone and because mechanic stability and ruggedness of a 3<sup>rd</sup> OT thicker slab is better.
2. A series RLC with an extremely high Q at the nominal frequency of interest (3<sup>rd</sup>, rarely 5<sup>th</sup>).
3. Another series RLC at ca. 8% above the overtones of interest, with a Q that is often larger than all other resonances, and with a strong DLD effect. This frequency is called "B Mode".
4. A parallel capacitance originating from packaging and the crystal disk itself.

An equivalent circuit of an SC cut crystal including fundamental mode, nominal frequency ( $3^{\text{rd}}$  OT), b Mode and the parallel capacitance is shown below:

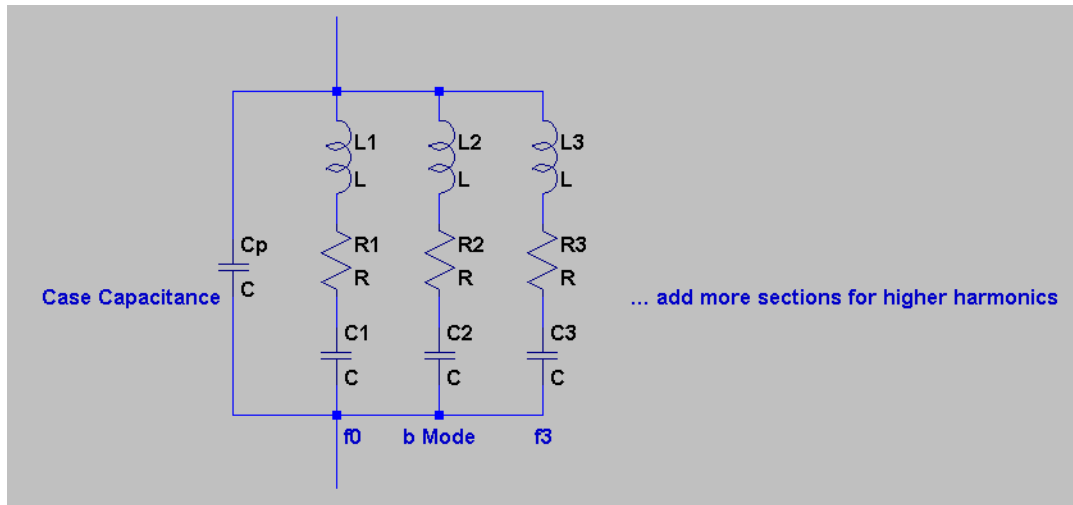


Figure 66 - Equivalent Circuit of an SC Cut Precision Crystal

A look at the network suggests that every series branch has an impedance minimum where  $X_L$  and  $X_C$  cancel (series resonance), plus an impedance maximum (“parallel” resonance) with the parallel capacitance  $C_p$ . The impedance of the total circuit starts capacitive with low frequencies, turns inductive at the series resonance frequency of the lowest frequency branch (here: the fundamental frequency), becomes capacitive again beyond the “parallel” fundamental resonance frequency until the next higher series resonance frequency is reached, and so on.

The  $Q$  of the branches differs for practical crystals; The  $Q$  of the fundamental was found in the range of several 100K, the nominal frequency reaches about the maximum possible for good crystals according to the Vig curve [2], which is about 2.2 Million for 5MHz SC, and the B Mode can go even higher to ca. 8 Mio., but shows a strong DLD effect and must be measured with extremely low power. Measurement techniques and actual crystal measurements are discussed in the crystal chapter.



If we measure transmission in series connection on a VNA (no impedance analyzer was available when the measurement was needed, see section about crystal measurements), we see several deep dips in uncomfortably close vicinity of our 5MHz nominal frequency (Croven 5MHz SC HC-40, [3]), as shown here:

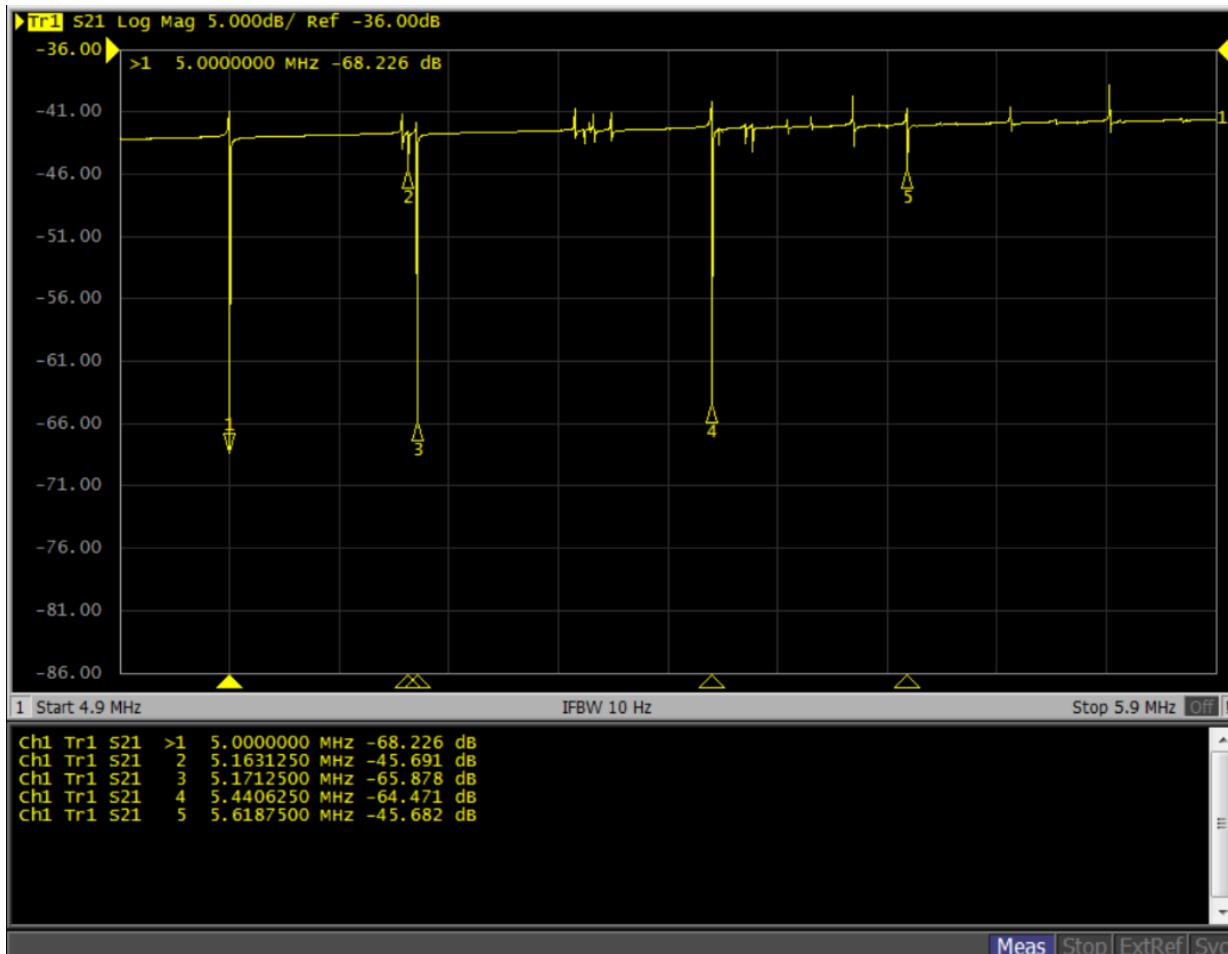


Figure 67 - Resonances of a 5MHz Precision SC Cut Crystal

Due to the log scale the impedance minima (= S21 maxima) are a bit hard to see, but it shows that the nominal frequency minimum is less than the B Mode at 5.44MHz. Another observation is that numerous spurious resonances and dips occur as well.

Even if we ignore the side resonances and dips the number of circuit elements has now gone up from 3 (AT crystal, or RLC resonator) to at least 10 (SC precision crystal). Adding the rest of the Clapp oscillator plus a realistic transistor model including at least Early effect and saturation results in a large, strongly nonlinear system of differential equations that cannot be solved by pencil and paper algorithms, leaving computer simulations as the only viable alternative.

### 3.10.2 What Kind of Solutions to Expect from a Complex Oscillator Circuit?

Even if an elegant (or even inelegant) closed form solution of our SC crystal Clapp oscillator's equations is impossible, we could still employ concepts of general dynamics theory to classify *types* of possible solutions:

1. Asymptotic approach to a steady state. – oscillator does not “start”. Unusable, probably caused by insufficient gain. No (repetitive) Poincaré map intersections exist.
2. Approach to a periodic attractor of order 1 (limit cycle, as in the Van der Pol equation). This is what we want. The steady-state Poincaré map has two single points (one in, one out), a phase plot would show a closed curve with no inner loops.
3. Approach to a periodic attractor of higher order (limit cycle, subharmonics, ...). The Poincaré map shows several single points, and the phase plot shows a curve that takes more than one period to reach its starting point again. Such a curve is typical for a squegging oscillator, where a subharmonic waveform modulates the oscillator output, but the subharmonic frequency has an integer (or at least rational) relation to the nominal frequency of oscillation.
4. Chaos. The Poincaré map shows an infinite set of points, and a phase plot looks like a “knurl” of intertwined lines. The “butterfly principle” applies here; two extremely close starting points take curves that diverge more and more from each other as time proceeds, just like physical particles in a turbulent flow (also called independence of initial conditions). The rate of separation of neighboring initial conditions can be derived from the Eigenvalues of the systems Jacobian matrix for a given phase space point (called Lyapunov exponents [3], but due to mathematical complexity no closed form expression is available for a realistic case). The existence of a limited phase space volume (guaranteed by a finite amount of energy available in the system) plus the existence of positive Lyapunov exponents are a practically sufficient proof that chaotic solutions exist. If we leave out the active element (the transistor), the rest of the circuit is dissipative, and its total energy (stored in capacitors and inductors) decreases over time until all voltages and currents become zero, i.e., the phase volume contracts. The total of all losses is dependent on the squares of current and voltage amplitudes in the network; if this loss is replenished *on average* by an active element like a transistor the system reaches a state where the time average of the total energy becomes a constant as observation time increases, i.e., the assumption of a bound phase space volume is plausible.

The Colpitts (or Clapp) oscillator topology is well known in the literature for chaotic behavior. [4]. Many papers derive stability criteria, output waveforms and Lyapunov exponents from an oversimplified transistor model having no other dependency except an exponential collector current over base emitter voltage. Such models are unrealistic, but a high accuracy cannot be expected from a chaotic system in general. The existence of chaos nevertheless is a reality.

All the above effects discussed above are actually observable in practical oscillator circuits. An example circuit (modelled after the industry standard HP10811A adapted for 5MHz, from my website, [5]) is shown below:

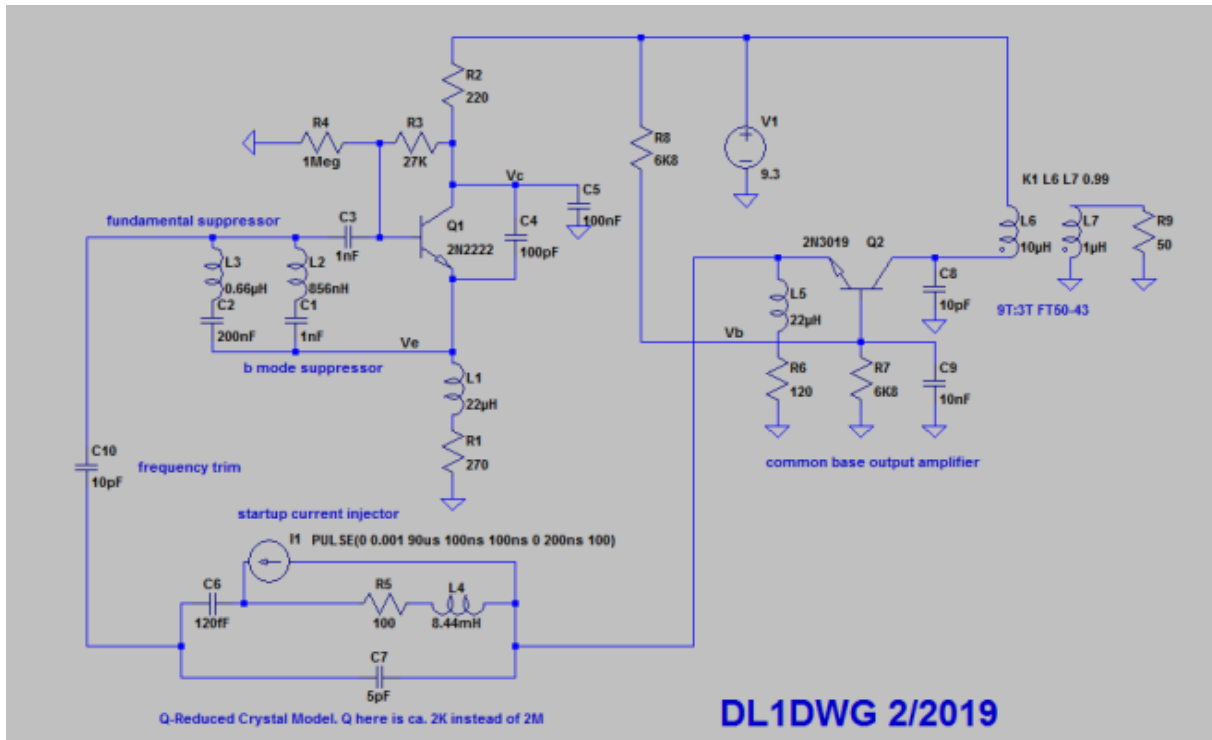


Figure 68- Crystal Oscillator HP10811A adapted for 5MHz Original Circuit from HP Journal, [5]

The video at the link below shows a chaotic oscillation in phase space:

[https://videos.files.wordpress.com/kRVWQEVO/modifiedhp10811aoscillator5mhzwithtrimmermultiplefrequencieschangingscope\\_dvd.mp4](https://videos.files.wordpress.com/kRVWQEVO/modifiedhp10811aoscillator5mhzwithtrimmermultiplefrequencieschangingscope_dvd.mp4)

The video was created on a scope with the base and emitter tapped with low capacitance probes.

A snapshot of the waveforms and a phase plot in white is shown below:

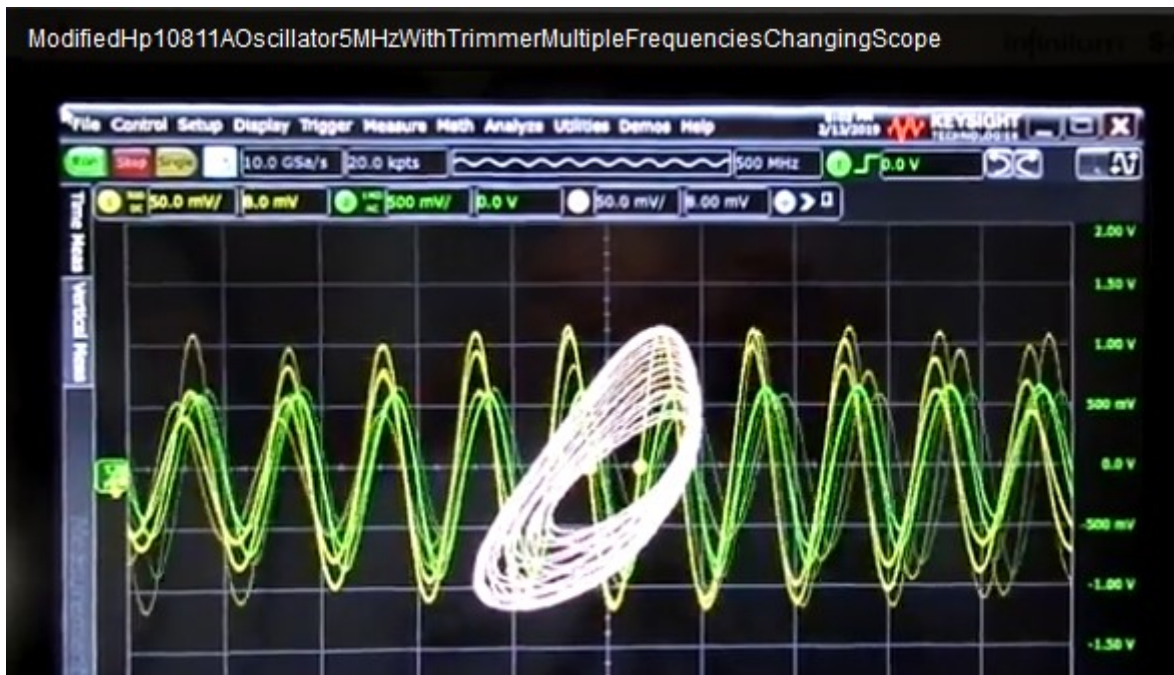


Figure 69 - Chaotic Clapp Oscillator Waveforms and Phase Plot

The “knurl” is the base and emitter signal displayed in XY mode.

As a conclusion, we need to be very aware of the temperamental and complex behavior of simple-looking SC crystal Clapp oscillator circuits, and we need to make sure that our USO designs do not exhibit any of the unwanted effects.

Results from simplified oscillator design rules are to be taken with great caution, as always with potentially chaotic systems. As we will see, the design process of an USO involves many methods and solutions that are not standard tools, because the predictions of the standard tools like SPICE or Harmonic Balance simply do not work.

### 3.10.3 An Example Clapp Oscillator with a Multiresonator Model

Being warned by the large and diverse solution space the theory of general dynamics predicts, as well as by experimental results that the predicted phenomena are real and can be observed in practical circuits, it makes sense to create an exemplary circuit to study and simulate all signals in the time and frequency domains. Such a circuit is shown below:

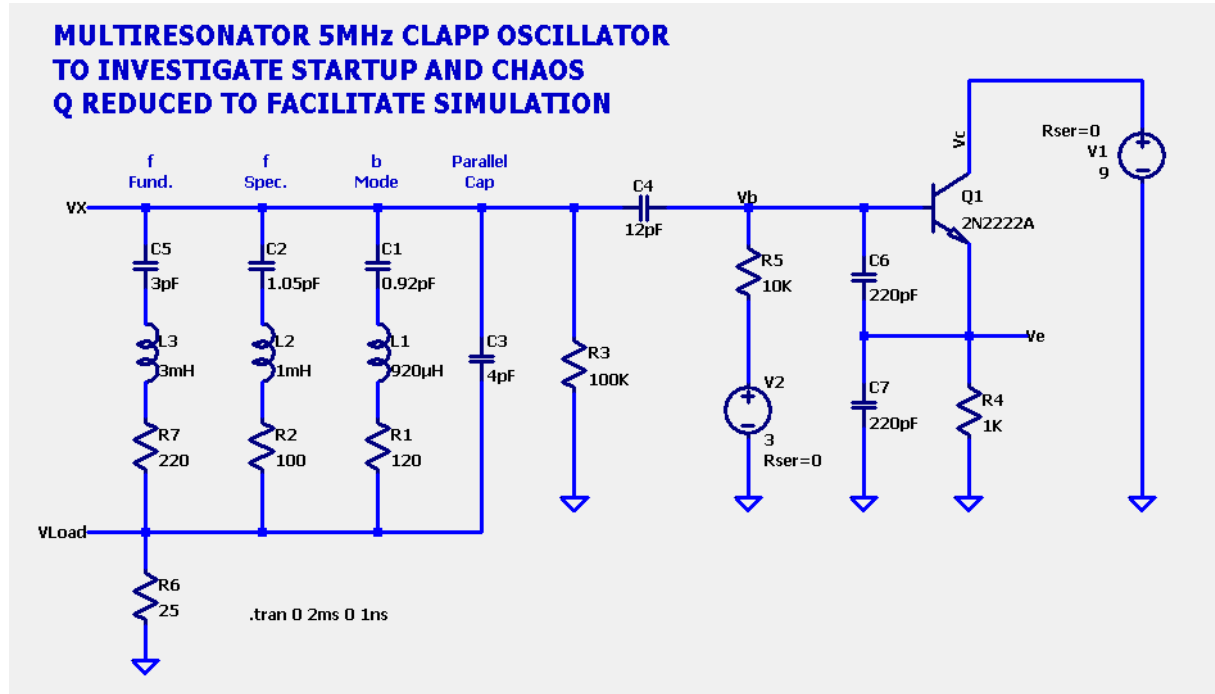


Figure 70- Multiresonator Clapp Oscillator

To the left we see a multiresonator crystal model to a hypothetical 5MHz SC crystal. The  $Q$  of all branches has been reduced to make simulation times acceptable<sup>7</sup>. Resistor  $R_3$  keeps SPICE happy because it avoids a floating node  $VX$ , plus it would also be needed in a practical circuit because SC crystals do not tolerate a DC voltage across them [2]. The output signal is extracted through the resonator (the 25Ohms resistor stands for a 50Ohm output resistor in parallel with a 25Ohm load). The capacitor  $C_4$  is the crystals series tuning resistor. The right-hand side of the circuit is a classic Clapp oscillator with ca. 2mA steady state current and 9V operating voltage. The transistor chosen is the trusty 2N2222A, identified as a well-suited part to low HF frequency oscillators, and with a proven space mission history [6].

<sup>7</sup> The simulation problems associated with extremely high  $Q$  oscillators will be cover later.

The first thing to simulate is the crystal/output circuit impedance as seen from the oscillator side at the right of C4. The SPICE plan has no surprises, as shown here:

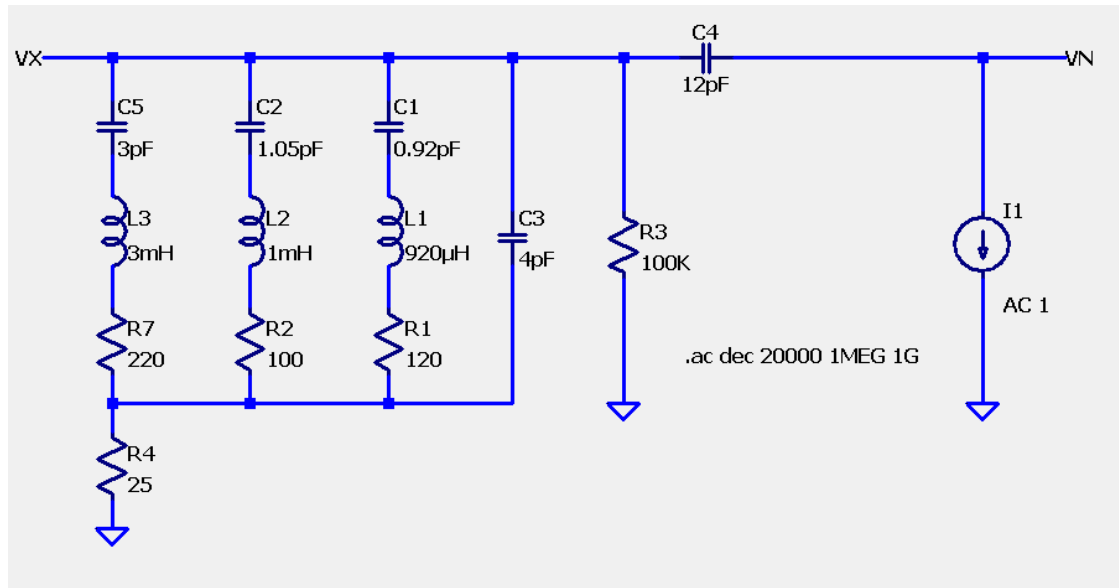


Figure 71 – 5MHz Multiresonator Network Input Impedance Simulation Circuit

The impedance looks similar to (except for the lower Q we used in the simulation and the spurs) the measured plot on the VNA above.

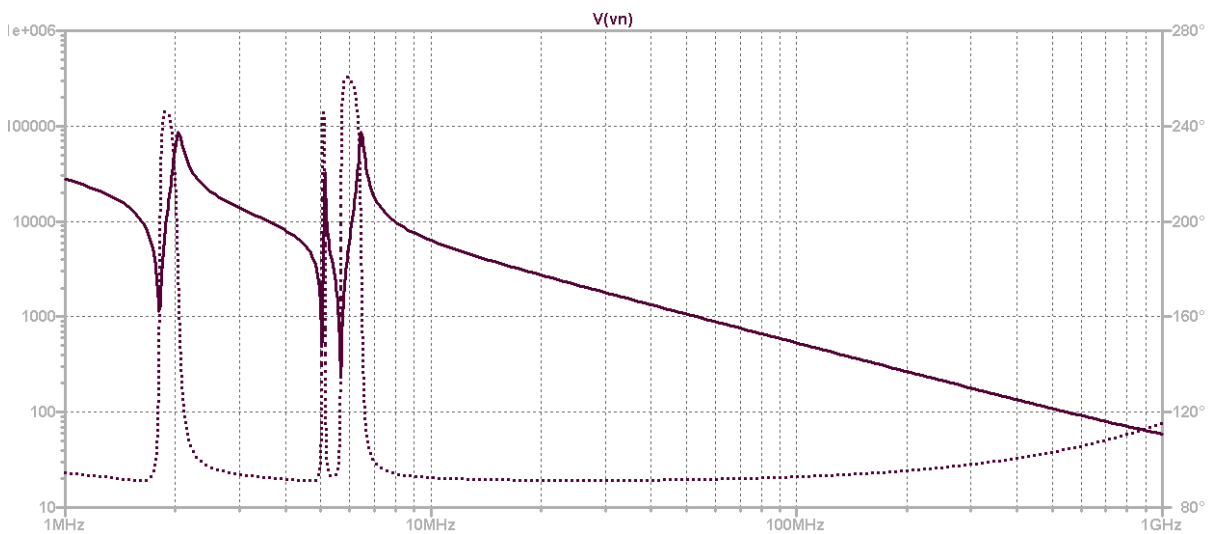


Figure 72- 5MHz Multiresonator Impedance Results. The left axis shows the impedance in a log scale, the right axis shows the phase, and the horizontal axis shows the frequency. The full line is the impedance, the dots are the phase.

As any normal crystal, we start off as a capacitor at low frequencies, at the series resonance frequency the impedance has a minimum and we are now inductive until the “parallel” resonance frequency, and then capacitive again. With three sections for our SC crystal, this repeats three times, with different Q values. The input impedance of the transistor circuit is capacitive; we therefore can expect low-level startups only at frequencies where the crystal is inductive. Unfortunately, the oscillator now has three inductive ranges to choose from.

The next step is to start our oscillator in the time domain simulator and see what happens. With enough negative resistance available, there is no startup problem, but, opposed to single resonator oscillators, there is no simple asymptotic approach to a steady state frequency:

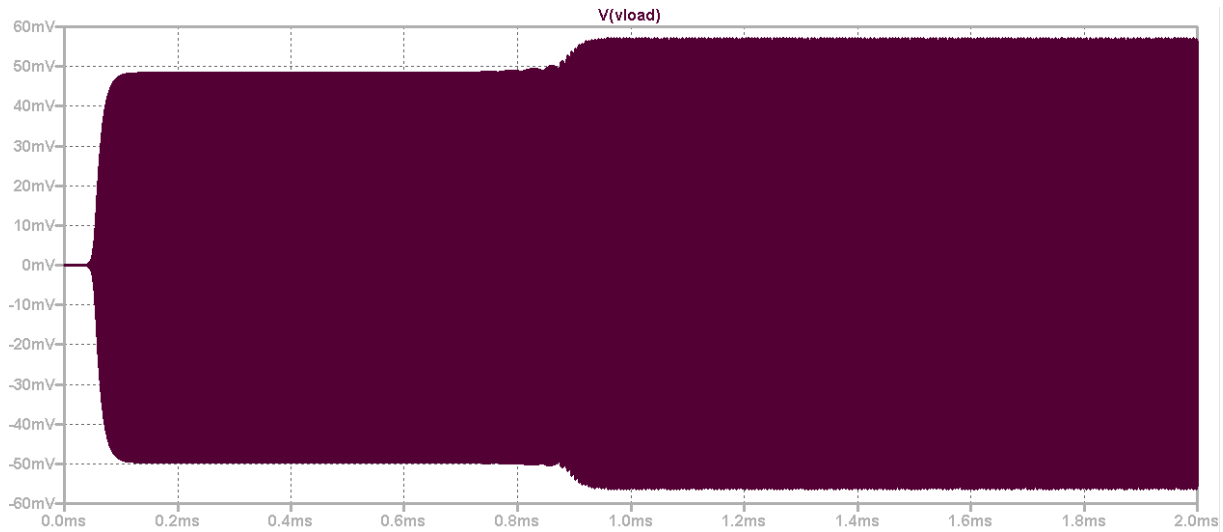


Figure 73 - Multiresonator Clapp Oscillator Startup

The simple rule of thumb that the startup time constant is about  $Q/2f_0$  seconds (see derivation from the Van der Pol equation in the previous chapter) seems to be not valid in this case, because startup occurs in two steps. The first step occurs in ca. 30us, which is compatible with a Q of ca.  $300@f_0$ , but there is second step occurring at 900us (4500 periods) later. A closer look at an FFT shows that between ca. 100us and ca. 800us the spectrum looks like the oscillator has started in B Mode:

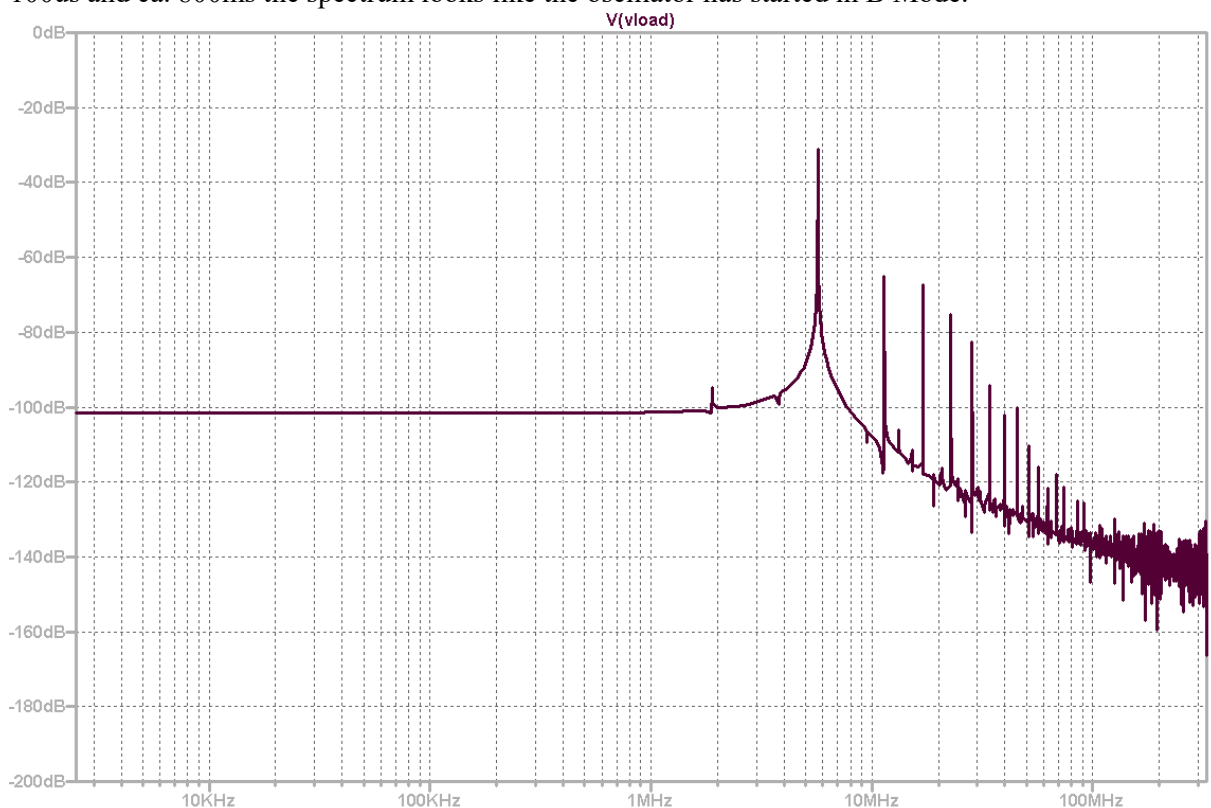


Figure 74 - Multiresonator Clapp Oscillator First Startup Phase between 0.3 and 0.6ms

This is confirmed by a look at a phase plot showing multiresonator (C4) current over resonator voltage:

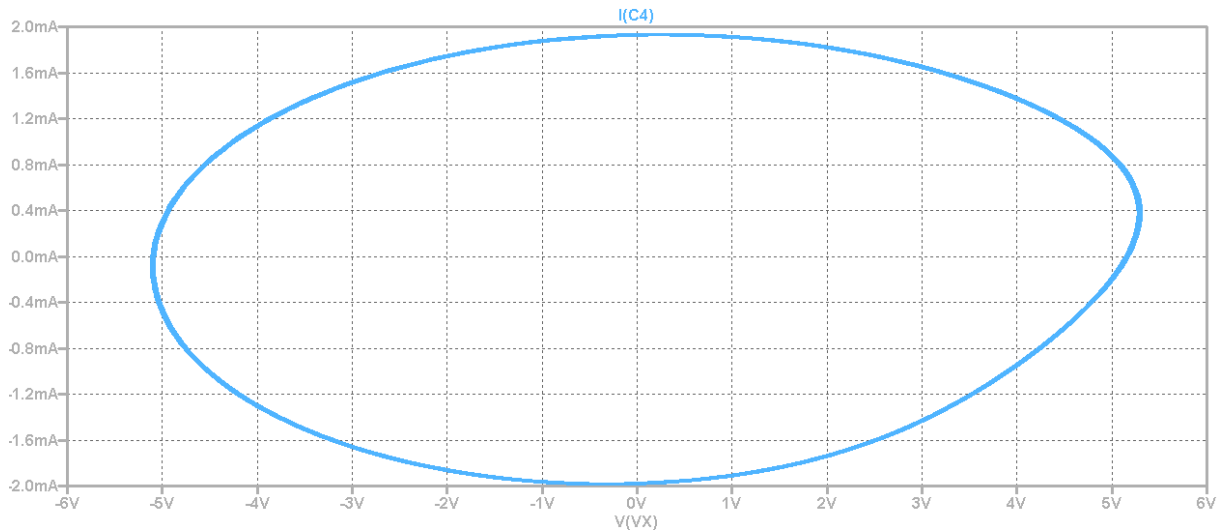


Figure 75 - Multiresonator Clapp Oscillator First Startup Phase between 0.3 and 0.6ms Phase Plot

That looks like a standard oscillator, not at the frequency we would like it to be, but otherwise very normal, with a close to harmonic oscillator curve.

Now let us see what happened to the output after the second startup phase:

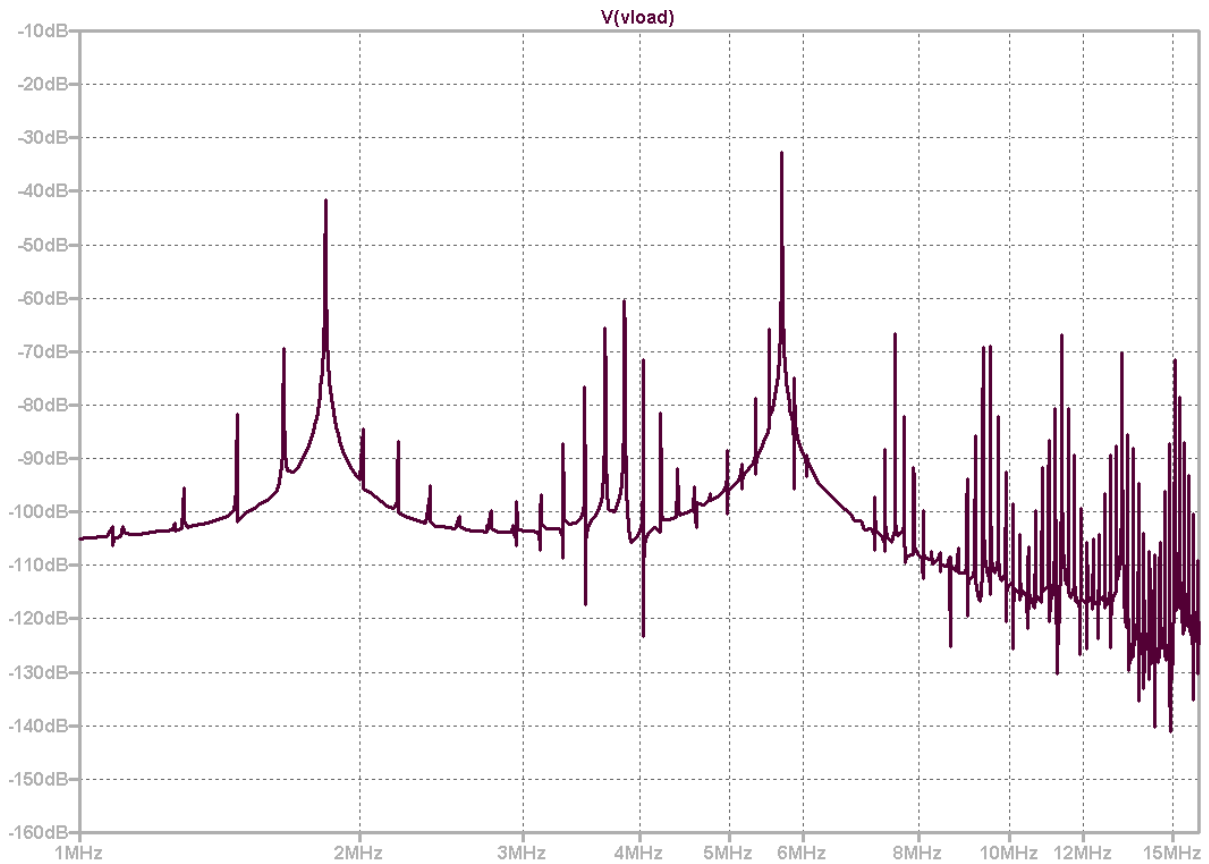


Figure 76- Multiresonator Clapp Oscillator Second Startup Phase between 1.3 and 2ms Spectrum

Instead of one dominant output signal there is now a fundamental signal visible, plus the B Mode plus some mixer products.



This looks like an interesting output signal:

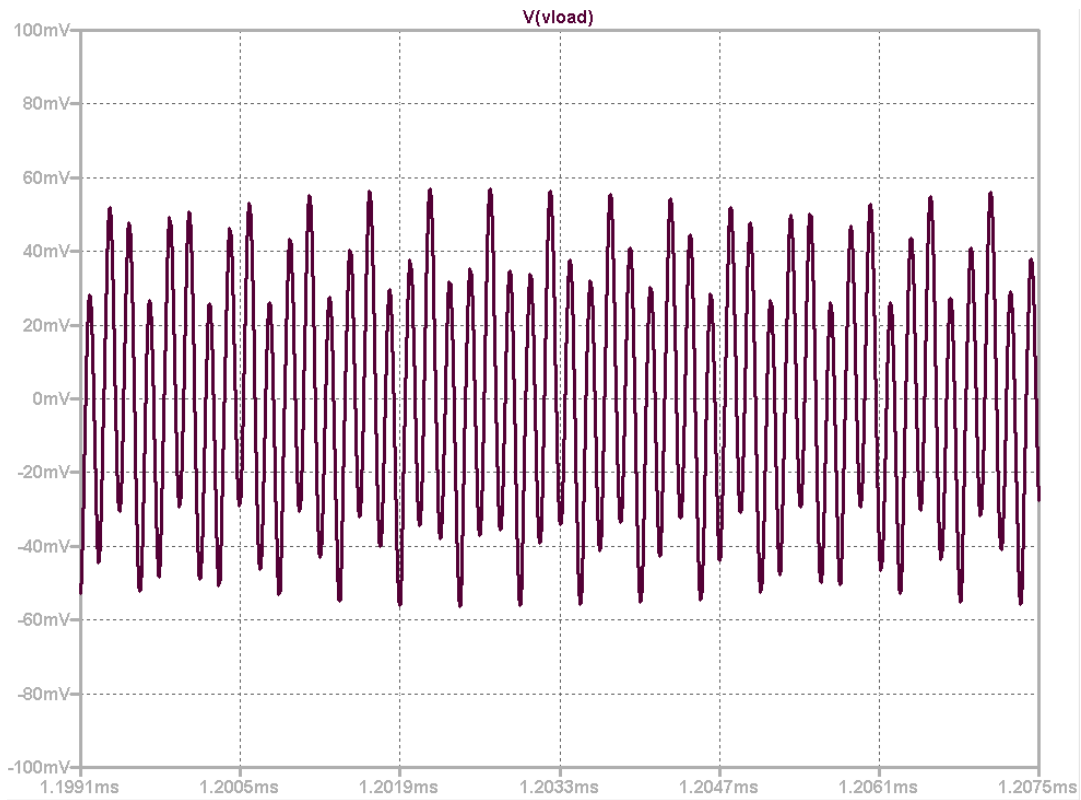


Figure 77- Multiresonator Clapp Oscillator Second Startup Phase Output Signal in the Time Domain

There are some dominant frequencies visible, but the signal is definitely not periodic. This is chaos. A phase plot confirms this (between 1.3 and 2ms):

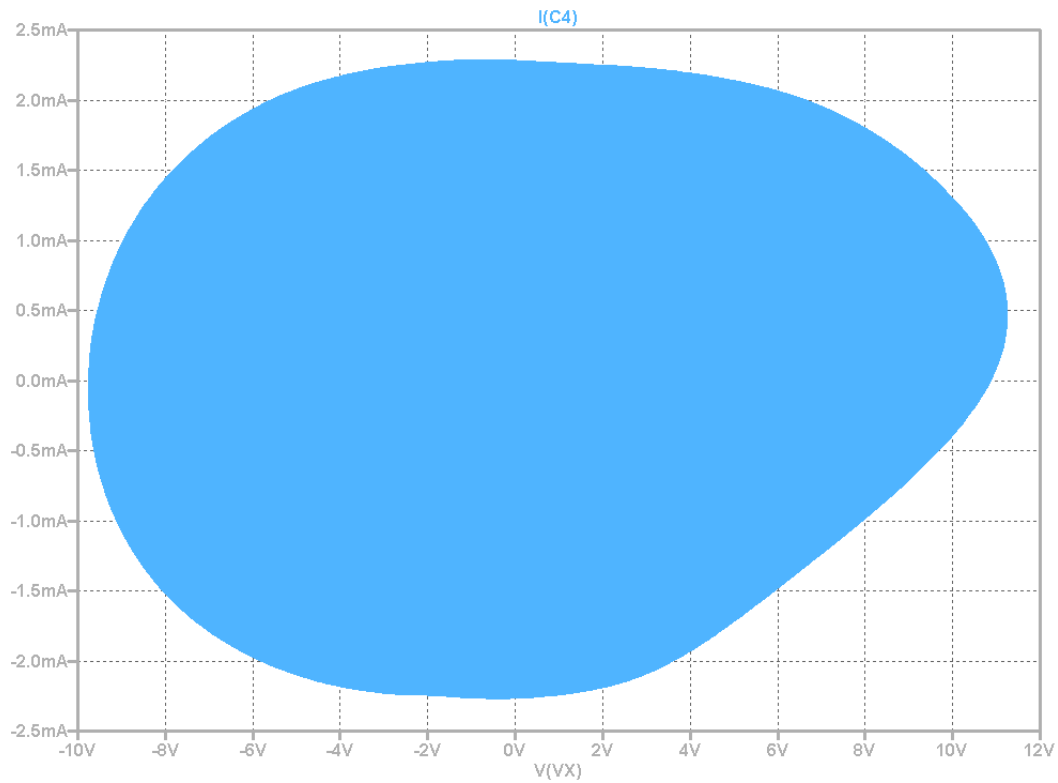


Figure 78 - Multiresonator Clapp Oscillator Second Startup Phase Output Signal Phase Plot

The phase space volume does not contain a clear single trajectory, but is completely filled, confirming that the solution is bound but not periodic, so it must be chaos.

### 3.10.4 Other Possible Multiresonator Clapp Oscillator Solutions

The repertoire of output waveforms of the multiresonator oscillator is considerable. The following other phenomena have been observed by varying circuit component values, especially  $C_4$  and the bias resistor  $R_5$ :

1. Squegging. The output comes in packets of oscillations with no signal in between. Especially prone if  $R_5$  has a high (very soft bias) value above 10K.
2. No output. That happens if  $C_4$  is made too small ( $< 4\text{pF}$ , depending on other component values).
3. Fundamental Output only. Depends on the Q values for the multiresonator branch inductors.
4. Meandering between B Mode and the specified frequency. Happens depending on the resistor values of the pertaining multiresonator branches ( $Q_s$ ), and  $C_4$ .
5. Stationary, simultaneous generation of B Mode and specified frequency. Looks like chaos but has two discrete line spectra.

The measurement video above also shows some of the effects discussed.

### 3.10.5 Limitations

For completeness it should be noted that we left out some (possibly important) physical effects in our simulation:

1. The B Mode of the crystal shows a strong DLD effect we have not modelled. This nonlinearity could give rise to new, amplitude dependent effects or frequency shifts.
2. The transistor model is a standard SPICE model using default parameters including Early effect and saturation, but no BE breakdown.
3. Generally, the crystal mode was assumed to be linear. Pulling and other Duffing-like DLD nonlinearities were not modelled.

### 3.10.6 Mathematic Approaches to the Problem of Multiresonator Oscillators

In principle, we could follow the same path as we did in the derivation of the solutions of the Van der Pol equation, but we will need to deal with a massively increased complexity.

The procedure would run as follows:

1. Establish a set of nonlinear differential equations for all nodes and loops of the oscillator circuit, similar to what SPICE would do. The nonlinearity is confined to the transistor model, everything else is linear.
2. Reformulate the equation system to take the form  $S' = F(S)$  using auxiliary variables, in the same way as in the van der Pol case.
3. For a stability analysis, we need fixed points. These need to be found numerically because no closed form solutions will be available. Unlike basic Van der Pol, we must expect more than one of these points, and the Poincaré-Bendixson theorem does not apply.
4. At the fixed points, we need to compute the Jacobian matrix (large, but could be done by symbolic math) and its Eigenvalues (no algebraic solution available because the rank of the Jacobian is larger than 4 [7]). Anyway, we now know the stability of the fixed points. The multiresonator structure suggests that there could be several fixed points, with imaginary Eigenvalues defined by the branch resonant frequencies).

5. To determine whether chaos is possible or not, we need to compute Lyapunov exponents at the fixed points. This again has no close form solution but needs numerical techniques.
6. Based on all steps above, we could determine parameter spaces (i.e., component values) where our circuit behaves steady-state, periodic, multiperiodic or chaotic. We could use this information to find operating points and component values that result in clean signals and a safe non-chaotic operation.

The effort for the steps above is considerable and provides no general solution for an oscillator with arbitrary component values. Another problem not yet discussed is the successful simulation of extremely high Q resonators with industry standard simulation software (they notoriously fail with Qs above several 100K). Therefore, the pure mathematical approach was not pursued further. Instead, some more practical, and heuristic approaches were sought to suggest and improve oscillators. Experimental verification and proper measurement techniques play a critical role in this process, along with problem-specific simulations where possible.

### 3.10.7 Design Steps for a High Stability / Low Power Oscillator

The following is a suggestion how to create a first design for a space USO that can be optimized and improved later. Based on the chaotic nature of the oscillator we refrain from computations based on linearized or simplified physical models and make pragmatic suggestions instead.

#### *USO Power*

The major design criterion of a crystal for a space mission is mission lifetime and allowed frequency deviation, i.e., the crystal aging rate. This rate is dependent on the power level used; for deep space USOs we need to get along with 10, maximum 30uW of power to obtain the aging rates guaranteed by the manufacturers [3]. Aging of SC crystals always lets the frequency go up (due to the vibrating crystal “shrugging of “surface particles damping oscillations and the release of crystal stress over time). To reach the nominal frequency, the crystal is made for a frequency slightly *lower* than the nominal frequency, and a series capacitor rises the frequency up to the nominal frequency. If the crystal ages too fast, it will overrun the nominal frequency requiring a zero series cap (or inductor) to compensate, so this is the end of useful lifetime. 10uW with a crystal series resistance of ca. 100Ohms (Croven SC 5MHz HC-40, e.g.) is a crystal current of

$$I_{XT} = \sqrt{\frac{P}{R}} = \sqrt{\frac{10^{-5}}{100}} = 316\mu A_{RMS}$$

The crystal voltage then is

$$V_{XT} = R I_{XT} = 31.6mV_{RMS}$$

If we add the voltage across the load of 25 Ohms, we have

$$V_{XTL} = (R + R_{LOAD}) I_{XT} = 39.5mV_{RMS}$$

The whole assembly of crystal, load and series resistor in total is still inductive at the series mode resonance frequency. When looking inside the transistor, we see a capacitive divider and an approximate negative impedance of

$$Z_{IN} = -g_M X_{CU} X_{CL} \text{ with } g_M = \frac{I_C}{V_T}$$

The base emitter voltage is the  $V_{XTL}$  split by the ratio of the divider capacitors  $C_1$  and  $(C_1+C_2)$ , so it is even smaller than the crystal voltage (estimated between 0.5 and 0.2). The consequence is that the resulting variation in BE voltage is not a lot more than the thermal voltage

$$V_T = \frac{kT}{q} = 25mV \text{ at room temperature}$$

A further consequence is that the collector current variation will also be small, and the conduction angle will be  $180^\circ$ , i.e., we operate in class A and there is no cutoff period. Provided the collector voltage is not too low for saturation to occur Bessel bias shift (see previous chapters) is the only (and weak) significant limiting mechanism.

Summing up, the small power level has created us a list of problems:

1. The voltage variation at the base is so small that the transistor operates in class A, which is bad for a low phase noise level. The collector current cannot be made too small, otherwise transconductance will be insufficient to start oscillations.
2. We cannot dimension the capacitive voltage divider with large capacitors, otherwise the resulting negative resistance cannot overcome the crystal losses
3. A large top divider capacitor would be beneficial for low phase noise and a small conduction angle, but it would further decrease AC base drive.
4. With no hard-limiting effect we need to care about bias shift and stabilization. For startup, we need to have enough gain (a margin of  $Z_{IN}$  of 3...4 is often used), but then we need a quenching mechanism that is driven from a post-buffer amplified signal. The power level coming out of this oscillator is too small to be rectified in a diode rectifier with acceptable accuracy.
5. The power coupled into the next stage is very small (5uW at best). If we choose a common-base stage at the next amplifier stage, we can enjoy a very selective output filter, but due to the mismatch of the very low input impedance (a few ohms) to the crystal impedance (100Ohms), we lose even more available power. This, again, worsens phase noise.

A sample oscillator design for a low power / high stability variant is shown here:

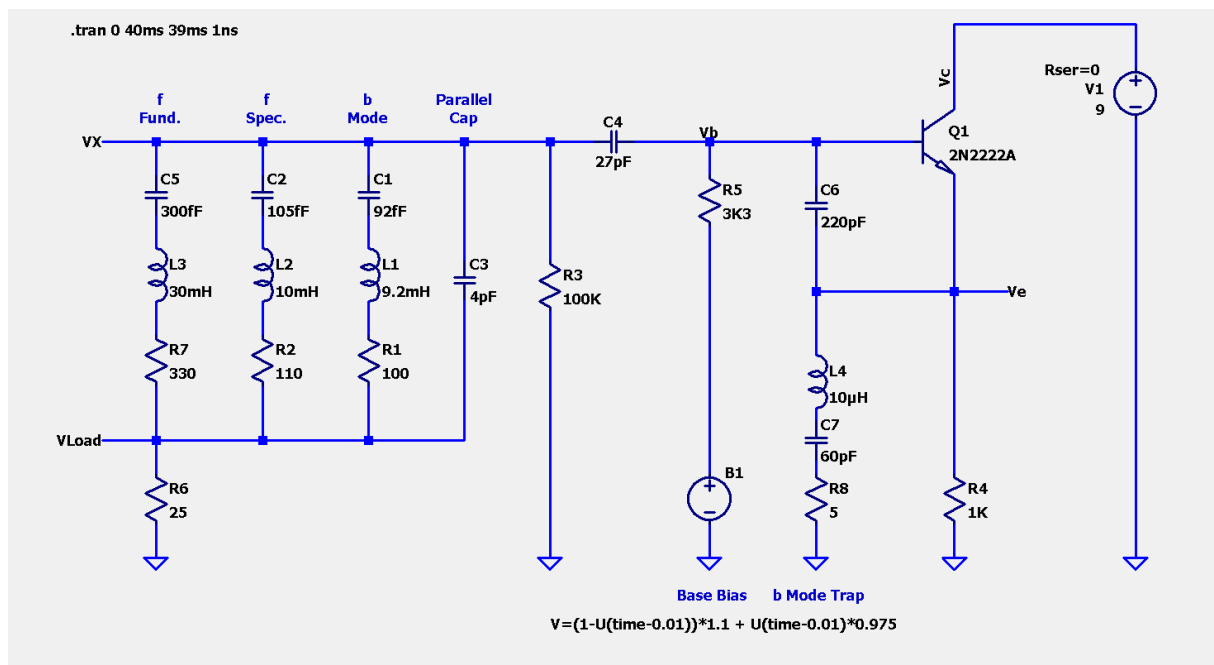


Figure 79 - Low Power Clapp Oscillator Schematics

To reduce simulation times, the circuit was “kick-started” by a larger base bias value (here: 1.1V) that was replaced by the final bias voltage value. Below 0.975V, no sustainable oscillations were found within 40ms of simulation time; at 0.975V we obtained a crystal power level of 25uW, and at 0.977V

the crystal power went up to 50uW. Phase plots at 25uW and 50uW are shown in the following figures:

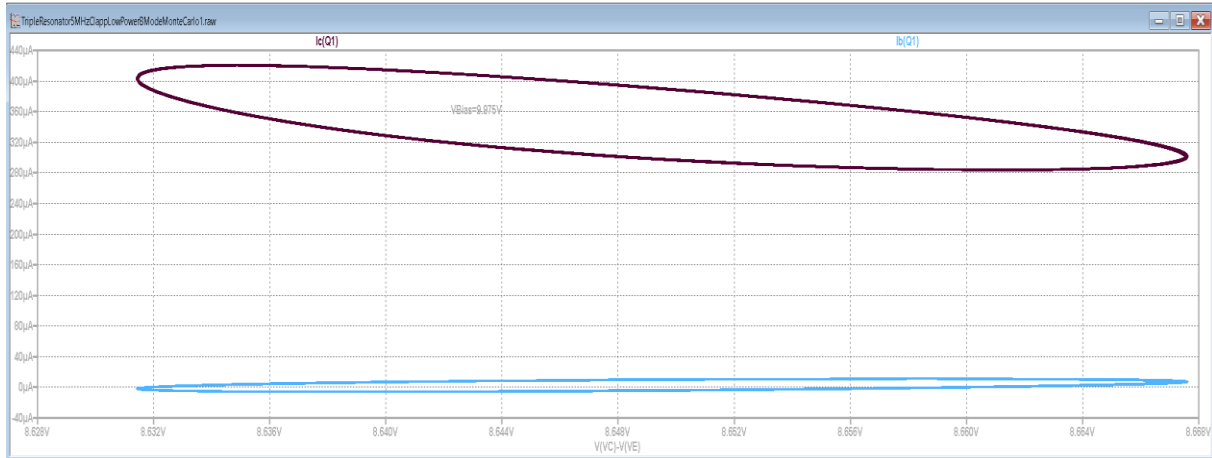


Figure 80 - Phase Plot ( $I_C$  brown /  $I_B$  blue over  $V_{CE}$ ) at 25uW Crystal Power

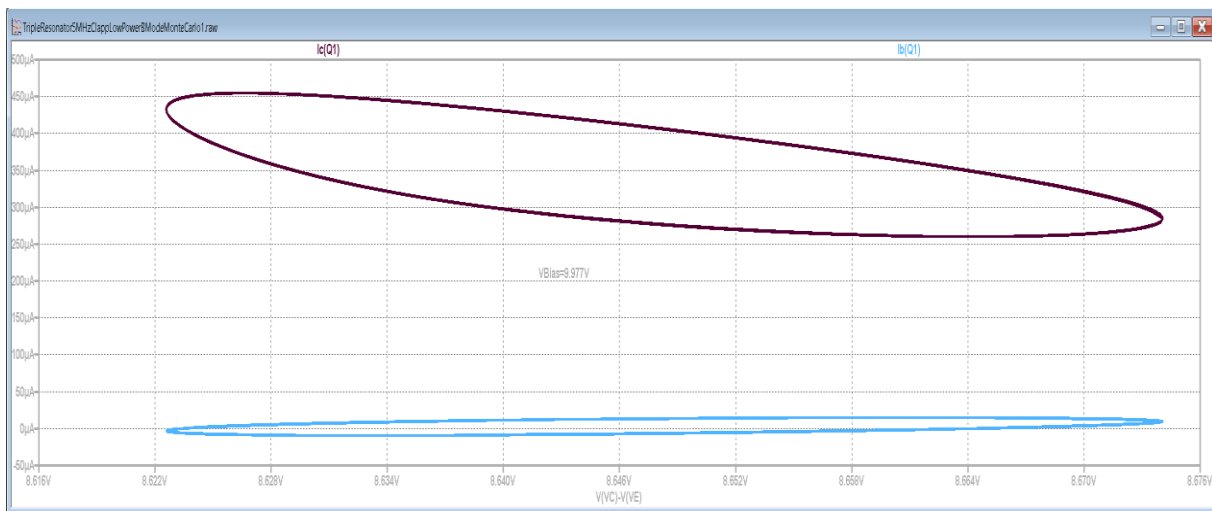


Figure 81 - Phase Plot ( $I_C$  brown /  $I_B$  blue over  $V_{CE}$ ) at 50uW Crystal Power

The plots show that:

1. No hard-limiting mechanism is present. There is no saturation, no cutoff, and no BE breakdown. There is also no visible Early quenching. Bessel bias shift is the only remaining amplitude limiting mechanism here, and the limiting caused is extremely gradual.
2. Collector current variation over an oscillation cycle is 250uA over an average value of 350uA at 50uW, at 25uW we only have 100uA swing.
3. The conduction angle is 180° in both cases, with the negative consequences discussed previously.

### 3.10.8 Consequences

The circuit is extremely sensitive to changes in base bias. A voltage variation of just +2mV doubles the output power, and -2mV will prevent the oscillator from starting up. 2mV is *less* than the decrease of the base-emitter diode voltage drop for 1°C. With a thermal resistance of ca. 300K/W the static bias currents will also cause a temperature increase of around 1K changing output power. If we need a safe startup and a very low but constant crystal power, we cannot work without an amplitude stabilizer circuit.

With very low crystal powers around 20uW or less, we have no chance to run a Clapp oscillator in an operating point where the conduction angle is small. For the sake of stability, we must accept a higher phase noise level.

### 3.10.9 Design Ideas

When looking at commercial OCXOs a common solution to stabilize the oscillator core amplitude is to pick off the signal after it has passed some amplifier stages, rectify it and use the rectified DC to reduce oscillator core base bias [8]. The lower the crystal power gets the more gain stages (often with a not very well-defined gain) are needed to obtain a minimum voltage for rectification.

A better idea is to use an accurate log amp to monitor output (and consequentially) crystal power. These amps (AD8307, e.g.) are accurate to ca. 1dBm in a range from at least -65dBm to +5dBm and a useful frequency range up to 100MHz. The output of a log amp is a DC voltage proportional to the log of the input power. This voltage can then be compared to a reference (setting the oscillator power wanted), and the difference can drive the base bias. A compensation network is required to avoid loop oscillations. Such a solution was built and is discussed in the USO prototype chapter.

### 3.10.10 B Mode Trapping

As discussed in the crystal properties chapter low-frequency USO crystals with an SC cut have a strong side resonance called B Mode, at just ca. 8% above the nominal frequency. This mode must be reliably suppressed. The circuit responsible for this purpose is called a B Mode trap.

There are several places where a B Mode trap can be implemented. The trick is always the same, as the HP paper from [9] explains: Make sure that the loop condition (Gain=1, Phase=Zero) is met at the nominal frequency, but not at the frequency at the B Mode, or, if we think of a Clapp oscillator type, the whole transistor circuit at the nominal frequency must be capacitive, and at the B Mode frequency it must appear inductive, because the crystal is inductive at the nominal frequency (just between its series and parallel resonances there, apart by just 100Hz or so).

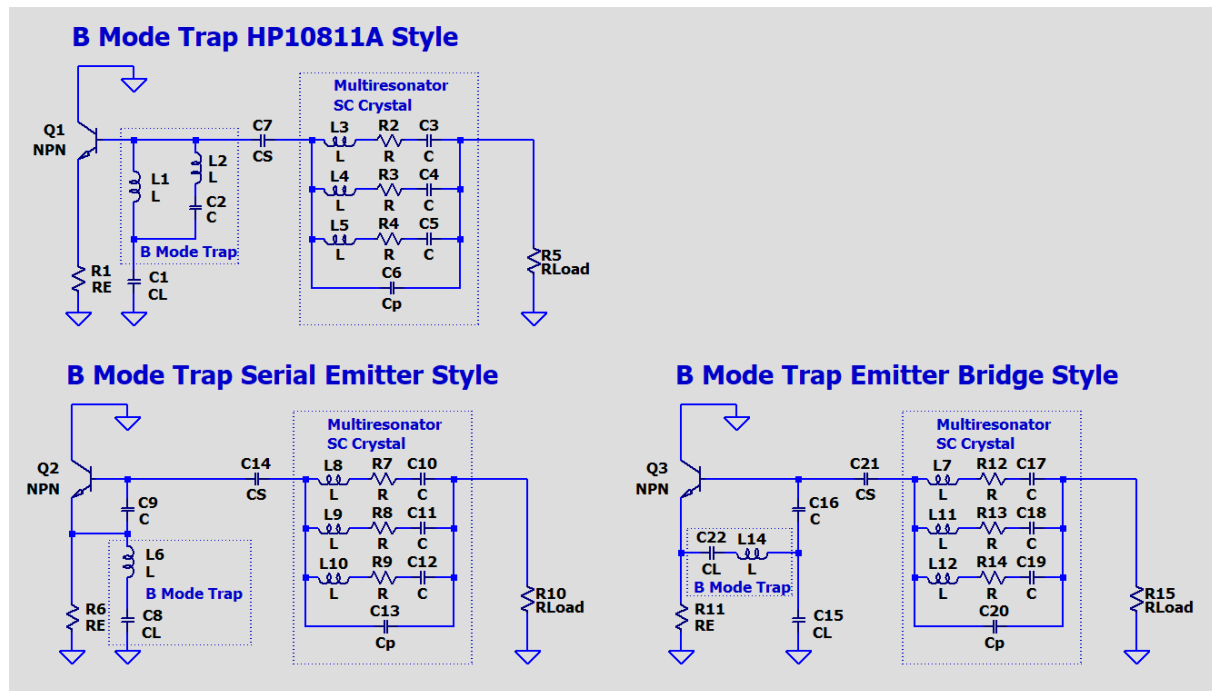


Figure 82 - B Mode Trap Locations

Some facts about these traps are important:

1. The inductors in the trap are molded types with a Q between 30 and 100 (rare case on toroids). Better Q inductors are either too bulky or simply not obtainable.
2. The loss resistors are not shown in the schematics.
3. B Mode trapping was argued coming from a linear domain theory, i.e., it does *not reliably exclude* chaos or frequency hopping for large-amplitude oscillators.

Another issue of B Mode is that the traps cost phase noise performance and output amplitude. To prove this, a simulation was performed using a crystal equivalent where a B Mode trap would not even be needed because the Q of the B Mode is slightly smaller than the Q of the nominal frequency.

Ansoft Serenade was used for the simulation, with the schematics shown below:

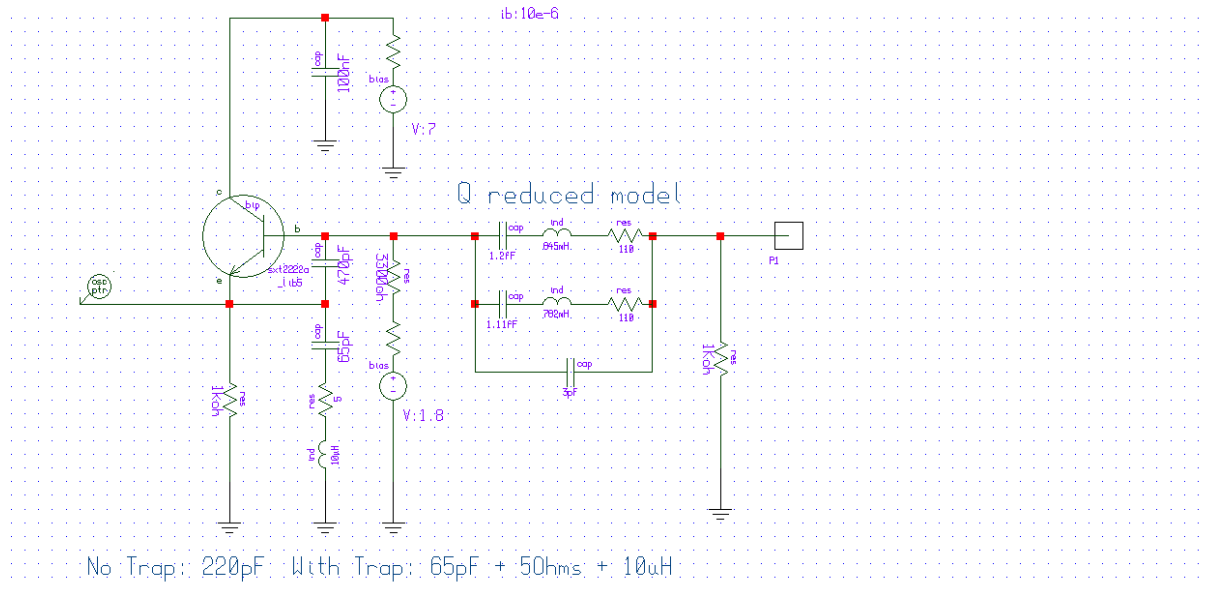


Figure 83 - Phase Noise Effect of B Mode Traps

The circuit is a classic Clapp using a 5MHz SC crystal with an 8% above B Mode. The serial trap variety (65pF + 50uH + 10uH) was simulated and compared to a simple capacitor (220pF).

The simulated phase noise plot is shown below:

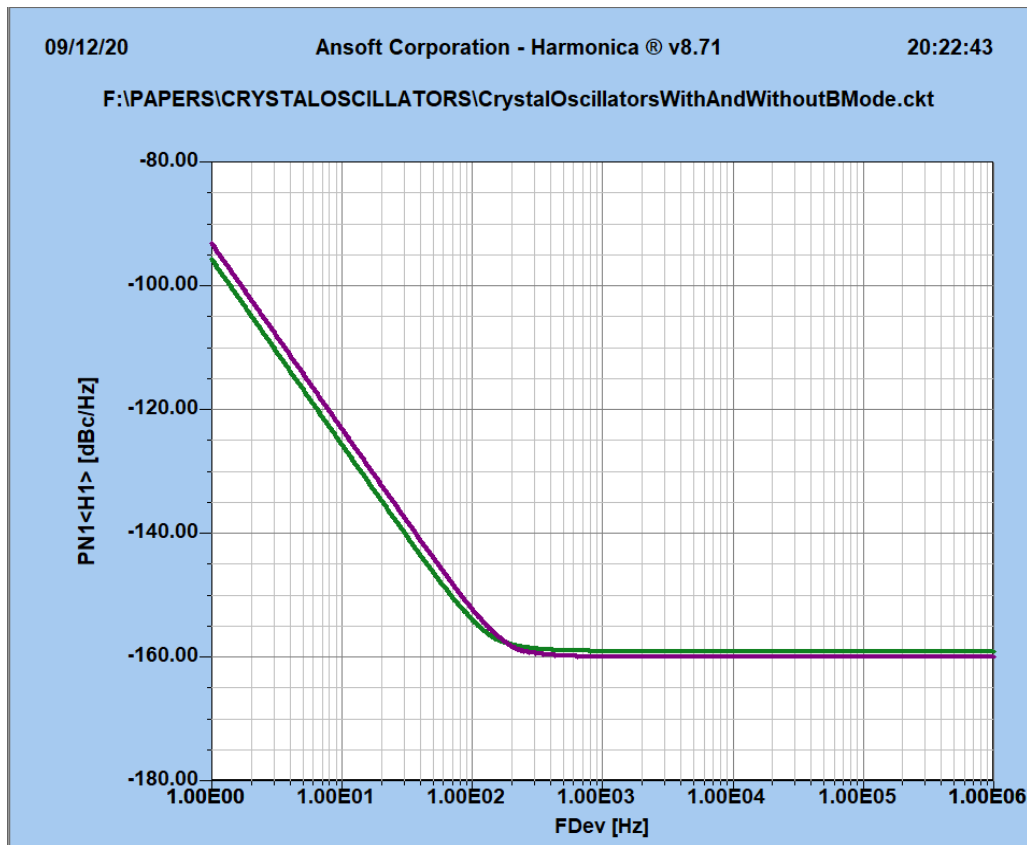


Figure 84 - Phase Noise with and Without B Mode Trap

The red curve is with the trap in place, the green curve is without the trap. As expected, the losses in the emitter branch cause a ca. 3dB rise in close to carrier phase noise. The difference at large offsets is not even 1dB.

Similar tests were made with other topologies of B Mode traps, and the results were always the same, i.e., the trap deteriorates phase noise and should be used only where a strong B Mode dictates it.

As a concluding remark, the B Mode is going out of fashion anyway due to the appearance of new premium quality crystals with better cuts where the B Mode has a low enough Q not to interfere with the nominal frequency or is not present at all.

The statement (often heard from crystal makers) that suboptimal oscillator performance is due to bad trap design is unsubstantiated. Its inherent, because the losses in the trap will be noticeable, and the equivalent loss resistance are in a similar range of magnitude as the crystal serial resistance (Trap coil: 5-10Ohms, crystal 100Ohms).

## References

- [1] U. L. Rohde, *Microwave and wireless synthesizers: theory and design*. New York: Wiley, 1997.
- [2] John Vig, "Quartz Crystal Resonators and Oscillators." Accessed: Nov. 19, 2020. [Online]. Available: <http://www.resonal.com/Downloads/John%20R.%20Vig%20-%20tutorial%20on%20Quartz%20Crystals%20and%20Oscillators.pdf>.
- [3] Croven Crystals Inc., "Croven HC-40 Crystals Datasheet." Accessed: Nov. 19, 2020. [Online]. Available: [https://crovencrystals.com/wp-content/uploads/HC-40\\_Crystal\\_Holder\\_Rev\\_00.pdf](https://crovencrystals.com/wp-content/uploads/HC-40_Crystal_Holder_Rev_00.pdf).



- [4] Fadhil Rahma Tahir, “Chaotic Colpitts Oscillator.” ResearchGate, Accessed: Nov. 25, 2020. [Online]. Available: [https://www.researchgate.net/publication/319912711\\_Chaotic\\_Colpitts\\_Oscillator/link/59c14dd9a6fdc69b92bbee2/download](https://www.researchgate.net/publication/319912711_Chaotic_Colpitts_Oscillator/link/59c14dd9a6fdc69b92bbee2/download).
- [5] W. Griebel, “Chaotic Colpitts/Clapp Oscillator.” Accessed: Nov. 26, 2020. [Online]. Available: [https://videos.files.wordpress.com/kRVWQEVO/modifiedhp10811aoscillator5mhzwithtrimmermultiplefrequencieschangingscope\\_dvd.mp4](https://videos.files.wordpress.com/kRVWQEVO/modifiedhp10811aoscillator5mhzwithtrimmermultiplefrequencieschangingscope_dvd.mp4).
- [6] Microsemi Corp., “2N2222A Technical Data Sheet.” Accessed: Dec. 27, 2020. [Online]. Available: <http://math.uchicago.edu/~may/REU2019/REUPapers/Mrinal.pdf>
- [7] Mishan Mrinal, “Galois Theory and the Abel–Ruffini Theorem.” Accessed: Nov. 26, 2020. [Online]. Available: <http://math.uchicago.edu/~may/REU2019/REUPapers/Mrinal.pdf>
- [8] Hewlett Packard Co., “10811A/B Quartz Crystal Oscillator Operating and Service Manual.” Aug. 1980, Accessed: Nov. 16, 2020. [Online]. Available: <http://literature.cdn.keysight.com/litweb/pdf/10811-90002.pdf>.
- [9] Robert Burgoon et a., “SC-Cut Oscillator Offers Improved Performance,” *HEWLETT-PACKARD JOURNAL*, vol. 32, no. March 1981, p. 20ff.

## 4 Oscillator Components

This chapter deals with the most important components of an oscillator, i.e., crystals and transistors. The other parts (resistors, inductors, and capacitors) do by far not have a comparable influence on oscillator performance as the former two (provided quality parts are used). Crystal and transistor properties are discussed, and several appendices contain information about the historic background, manufacturing techniques, and measurements.

### 4.1 Quartz Properties

This chapter covers the physics and the resulting device properties of Quartz crystals in detail, covering the resonances that can be obtained, cutting techniques, equivalent circuits, temperature dependence, vibration sensitivity and other aspects. We concentrate here on crystal properties that are relevant for our purpose (i.e., the electrical parameters relevant to build USOs), because we have to work with standard parts without access to manufacturing details. The following appendices provide additional information:

Appendix B, **Quartz Crystal Physics** covers the theory of piezoelectricity, modes of resonance, cuts, temperature curves, geometries, defects and aging processes in more detail.

Appendix C, **Crystal Measurements** covers the measurement of crystal parameters, like the motional constants, spurs, B Mode, DLD and noise.

### 4.2 Transistor Properties

The field of transistor technology is even larger than that the crystals, because so many effects influence oscillator behavior. This starts from the amplification process, limiting mechanisms, and, most important for USOs, the creation of white and flicker noise. The transistors used in this thesis were standard industry types, so we had to live with the (somewhat sparse) information available from device manufacturers, or we had to extract the parameters needed by dedicated measurements. The following appendices deal with transistor properties:

Appendix E, **Measurement of Transistor DC Parameters** explains how important characteristics are obtained for a specific part. Datasheet information is not always usable because it is mostly incomplete (e.g., for noise data) and pessimistic (showing worst-case limits and not the values for a specific parts), so device extract techniques must be developed to obtain realistic parameters.

Appendix F, **Measurement of Transistor AC Parameters** explains the extraction of transistor AC parameters works. For packaged devices like the ones used here, this is much more complicated and less rewarding than the usual VNA wafer-based measurements the industry performs as a standard.

Appendix G, **Transistor Noise Measurements** explains the measurement of white and flicker transistor noise under different bias conditions. A direct method and an indirect method using an LC oscillator are presented and results are compared.

### 4.3 Crystal Properties

This chapter deals with crystals used in precision oscillators. Their material properties, manufacturing, and application aspects are investigated. Equivalent circuits are explained, and practical crystal measurements are performed.

For the purposes of oscillator building, we need to treat crystals as prefabricated parts with properties that we need to understand but we cannot change.

The most relevant electrical characteristics of crystals are their (complex) equivalent circuit covering several resonances, their power handling capabilities, temperature behavior and aging.

For the physics of the relevant effects that take place in a crystal please refer to appendix B, **Quartz Crystal Physics**. This section covers piezoelectricity, modes of resonance, cuts, temperature curves, geometries, defects and aging processes in more detail.

We measured several crystals. Measurement data and methods are covered in appendix C, **Crystal Measurements**.

#### 4.3.1 Electric Properties of Packaged Crystals, Equivalent Circuits

Generally speaking, a packaged crystal looks like a collection of very high-Q series tank circuits in parallel with a holder capacitance. An equivalent circuit would look like this:

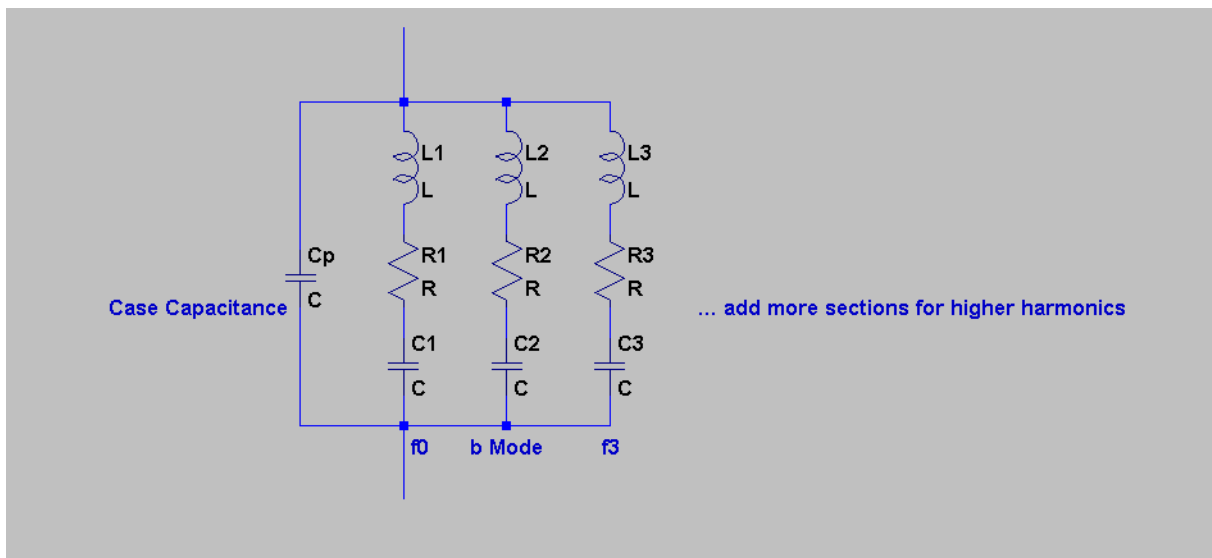


Figure 85 - Crystal Equivalent Circuit

The resonant sections correspond to the most important resonant modes the crystal disk can have.

This can be a lot more than the ones generally to be expected (fundamental and overtones), but there are (depending on the type of cut) all kinds of side resonances without an integer multiplier relation to the fundamental frequency.

To make things manageable for a simulator (and even more for pencil and paper math) only the strongest resonances are usually modelled.

An example of the S21 of such crystal in a series connection (SC cut precision crystal 5MHz, 3<sup>rd</sup> overtone, cold-weld, Croven HC-40) is shown below:

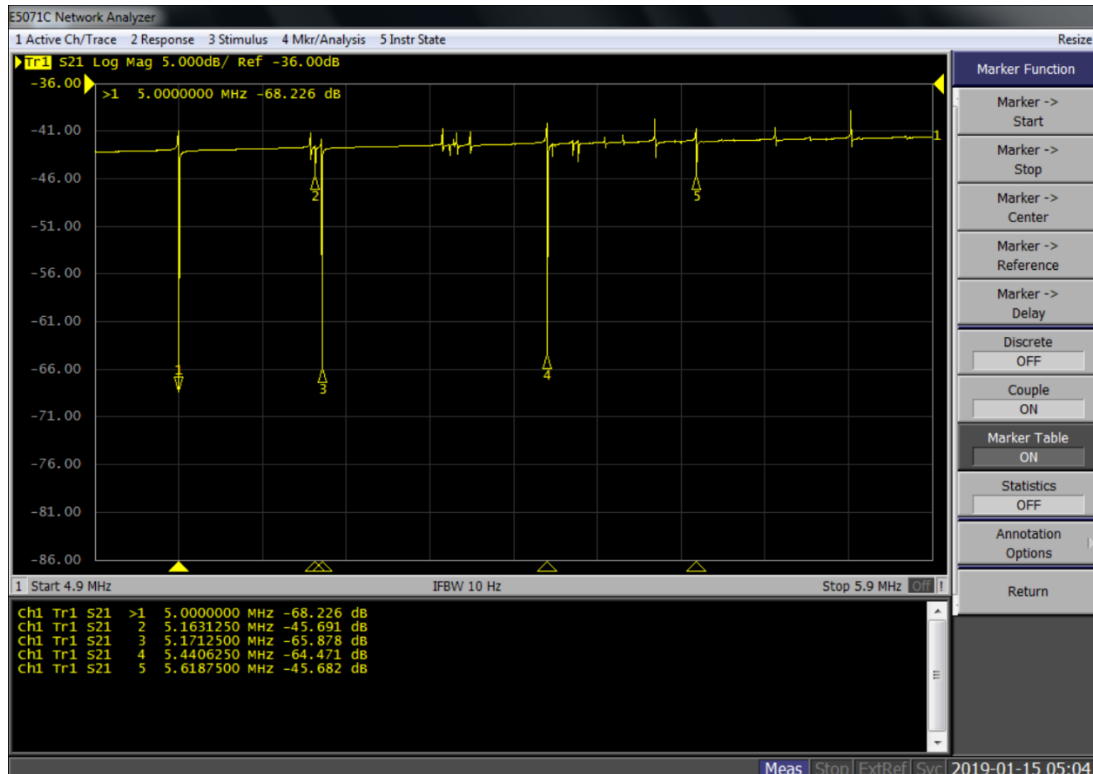


Figure 86 - SC Cut Crystal Resonances Measured on a VNA

The crystal is measured in series mode using an adapter (IEC444). The dips are the “parallel” resonances. Series resonances are the peaks, not very well visible due to the log scale). What is visible is that for this crystal the peak is somewhat larger than the peak at the nominal frequency.

The measurement above was performed on a standard, general purpose VNA (Keysight E5071C 8.5GHz, [1]). For crystals with Q values in the millions the resolution and accuracy of such an instrument is not sufficient for reliable measurements. We would need frequency resolutions in small fractions of an Hz and the possibility to work with extremely low power levels to avoid (or detect) DLD effects in a crystal.

Professional crystal measurements are done using a dedicated impedance analyzer working with a so-called auto-balancing bridge (e.g., Keysight E4990A [2]). Such an instrument can measure extremely wide impedance spans in mHz frequency ranges with extremely small power levels.

Measurements in detail are covered in the appendix C, **Crystal Measurements**.

For comparison, an ordinary performance AT cut crystal has a lot less resonances and look like this:

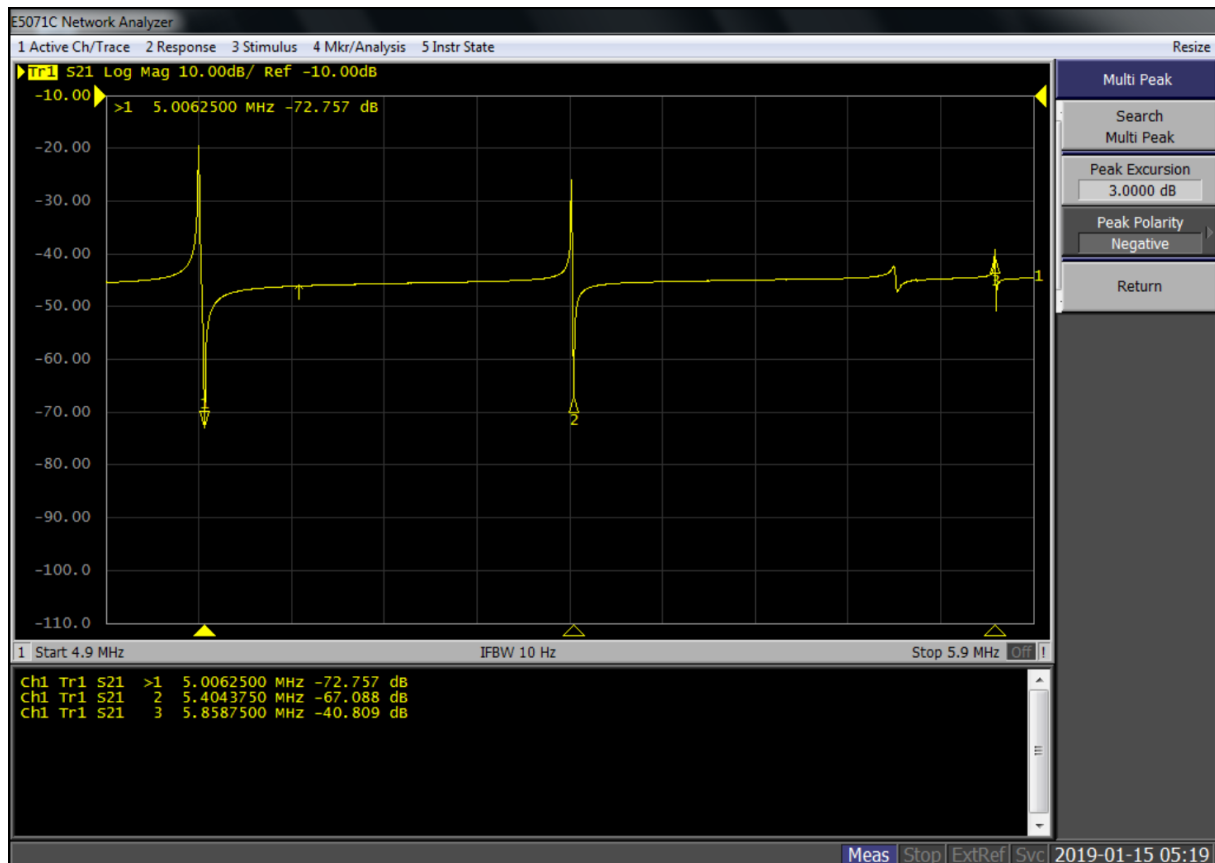


Figure 87 - Resonances in an AT Cut Crystal

The simulation models including *all modes* and spurs would come out prohibitively complex, and determination of all model parameters would be a difficult task. Most simulation models encountered so far only incorporate the intended main frequency of resonance. For SC cut crystals, these models are certainly not enough to predict oscillator behavior. B mode, the fundamental and (if used) the 3<sup>rd</sup> overtone should be included in realistic SC cut models, otherwise startup problems, chaos or subharmonics cannot be found in a simulation output, but much more so in implemented circuits. This will be demonstrated later in this paper.

A word of warning: due to the extreme Q measuring the resonances is tricky; bandwidth, number of points, sweep time, ... must be carefully chosen in order not to skip a resonance or to measure an incorrect amplitude. This will be discussed later when crystal measurements are covered.

### 4.3.2 Nonlinear Effects

Crystals are normally considered linear devices; this not exactly true, neither at the very low and the very high end of the power range applied.

### 4.3.3 Drive Level Dependency (DLD)

At the low end, an effect called DLD (drive level dependency) makes the internal equivalent series resistance for a given resonance frequency dependent on applied AC voltage. At extremely low AC voltages, this resistance increases, sometimes to several times its value at medium power levels. This effect could cause a failed start for an oscillator circuit because the overall gain is too low. Premium crystals have these values specified in their datasheets, as in the BQOTY HC30 glass crystals from

Bliley which states a maximum of 1ppm for a power range from 50nW to 100uW (REF Bliley BQOTY Datasheet, [3])

The physical reason for the DLD behavior is not completely understood but has something to do with impurities deposited on the surface. When vibration amplitude is low, they are not “shrugged off”, but keep attached to the surface and perform a “dangling” movement, resulting in a damping effect (see [4] for a more formal investigation).

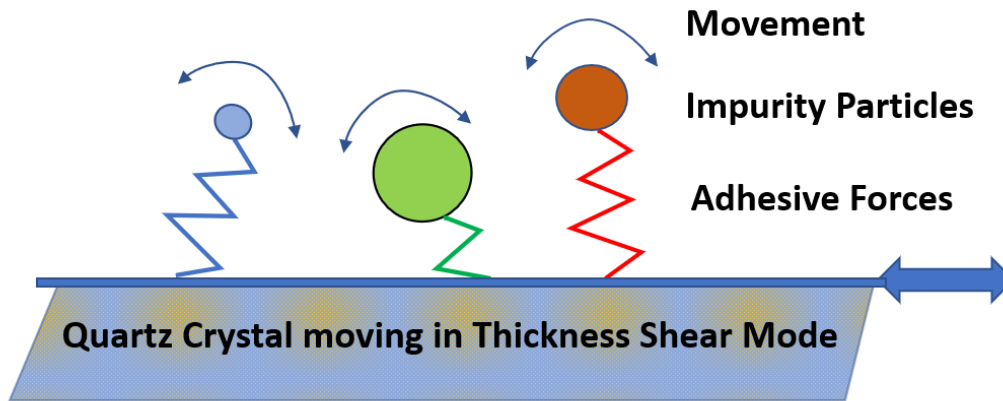


Figure 88 - DLD Effect Caused by Surface Impurities  
Picture redrawn from Rubiola [4]

With increasing amplitude, the impurities on the surface fall off, and Q and frequency increase. At very high amplitudes, the Quartz medium is driven into the nonlinear domain and additional amplitude limiting effects set in (analogous to the nonlinear spring example). This can go as far as exceeding the mechanical stress limits of Quartz, and then the disk gets cracks, or the contacts peel off. A hint that mechanical stress might be a problem comes from the observation that premium crystals can have Q values in the millions. Q is the ratio of the stored energy inside the crystal over the dissipated Energy in 1 cycle. If we assume that we run a crystal at 1mW at 1MHz with a Q of 1 Million (this is an example with very high power), we have

$$W_{stored} = \frac{QP}{f} = \frac{10^6 10^{-1}}{10^6} = 10^{-1} J$$

This energy is confined in the active area between the electrodes, which is only a few ten mm<sup>2</sup> in size. The thickness of this crystal would be less than a mm depending on cut. If we assume a volume of 50mm<sup>3</sup> (ca. 8mm electrode diameter), the energy density is

$$DE_{stored} = \frac{W_{stored}}{V} = \frac{10^{-1}}{50 * 10^{-9}} = 20kJ/m^3 = 20mJ/cm^3$$

If we assume that, for a given moment in the oscillation period, all energy is stored in an electrical field instead of mechanical stress, and if we apply the dielectric constant of Quartz, we have (for the same geometry, 50mm<sup>2</sup> and 1mm of thickness) a static capacitance of

$$C_{Active} = \frac{A * \epsilon_0 * \epsilon_r}{d} = \frac{50 * 10^{-6} * 8.85 * 10^{-12} * 3.8}{10^{-3}} = 1.681pF$$

Where

$C_{Active}$  is the static capacitance,

$A$  is the active area size,

$\epsilon_0$  is the permittivity of the vacuum,

$\epsilon_r$  is the relative permittivity of Quartz and

$d$  is the distance between the electrodes.

When computing the voltage from the energy stored and the capacitance, we get

$$U_{Active} = \sqrt{\frac{2W_{stored}}{C_{Active}}} = \sqrt{\frac{2 * 10^{-1}}{1.681 * 10^{-12}}} = 34kV$$

which is not a lot below the punch-thru voltage of Quartz (ca. 40kV/mm)<sup>8</sup>, this is the DC value, however).

The calculations above show why large crystal power levels will result in massive nonlinearities, fast aging, and other undesirable effects, even if they might be advantageous for minimum phase noise oscillators from a theoretical point of view.

A sample graph containing extreme DLD curves can be seen here (j. Vig [5], p4-58):

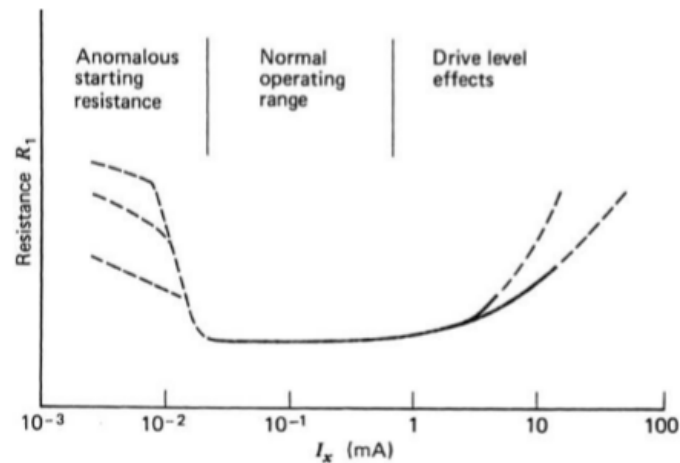


Figure 89 - DLD Effect for a Sample Crystal  
Picture from John Vig [5]

Several sample crystals and their DLD were measured (described later). In the range of interest for low power long-term stable space oscillators (ca. 20 $\mu$ W max, this translates to RMS currents of 0.3 $\mu$ A assuming a resistance of 1000 $\Omega$ ) the DLD effect of the crystals measured is manageable and can be easily compensated by amplitude levelling. Bliley, e.g., guarantees a DLD effect of less than a percent down to 50nW (see datasheet above).

<sup>8</sup> This is a DC value. RF punch-thru in thin layers has a higher voltage because charged particle acceleration is not as efficient in a field that rapidly changes polarity, make the avalanche effect occur at a higher voltage.

#### 4.3.4 Frequency Pulling

Another nonlinear effect is frequency pulling with increasing signal amplitudes. The effect observed in crystals look like this:

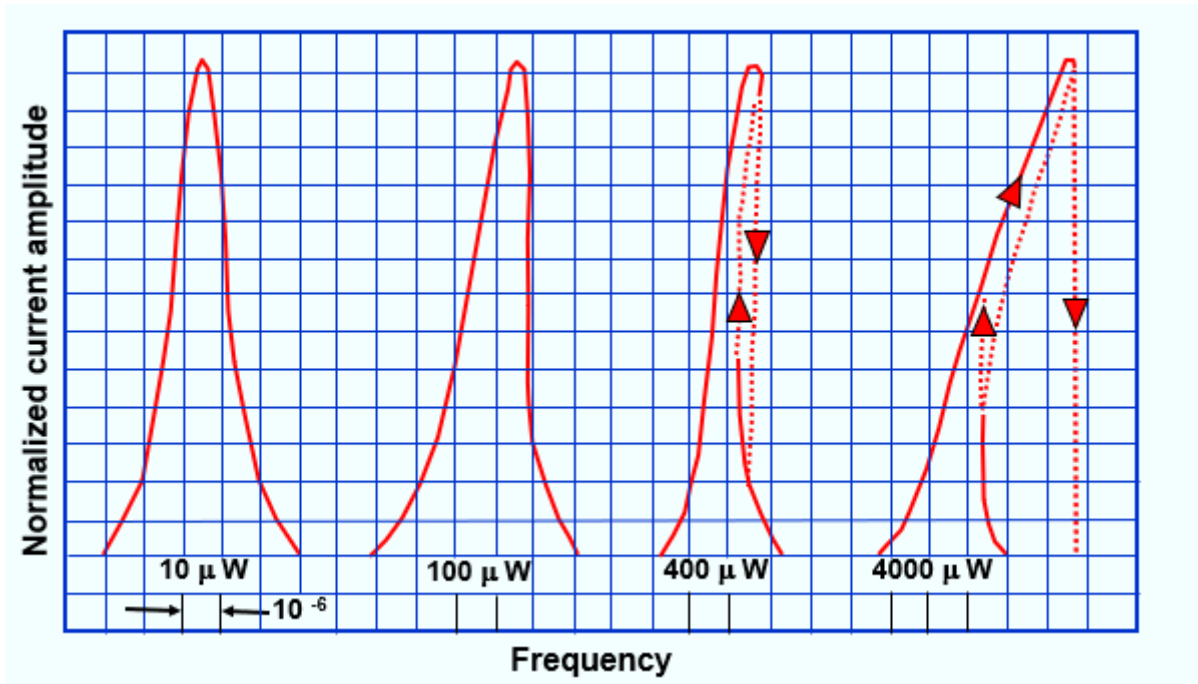


Figure 90 - Nonlinear Frequency Pulling Effect (Picture by John Vig, [5])

This very much corresponds to the resonance curves of a nonlinear spring oscillator, as shown here:

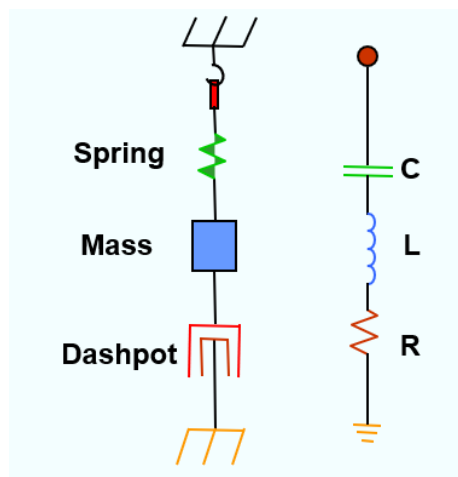


Figure 91 - A Mechanical Equivalent for a Crystal Oscillators

where  $C$  is amplitude dependent in the nonlinear case. The mechanic equivalent is a nonlinear (not obeying Hooke's law) driven spring oscillator. Systems like this can be described using the *Duffing equation* (using a third-power nonlinear term) [6]:

$$x'' + \delta x' + \alpha x + \beta x^3 = \gamma \cos(\omega t)$$

where

$x''$  stands for the acceleration,

$x'$  for the velocity,



$x$  for the position  
 $\gamma$  is the externally applied signal amplitude,  
 $\omega$  is the circular frequency and  
 $t$  is the time.

In mechanical terms,  $\alpha$  and  $\beta$  are the linear and nonlinear stiffness, and  $\delta$  is the damping factor. Despite its simplicity, this equation exhibits all nonlinear effects also observable in crystals:

1. Pulling
2. Frequency jumps, hysteresis
3. Creation of subharmonics, period doubling, bifurcation
4. Chaos

For the non-driven case (autonomous oscillator, *not* a practical crystal oscillator) we would have

$$\alpha < 0 \text{ (undamping) and } \gamma = 0.$$

Some possible waveform outputs and phase space attractors of a Duffing oscillator can be seen here [13]:

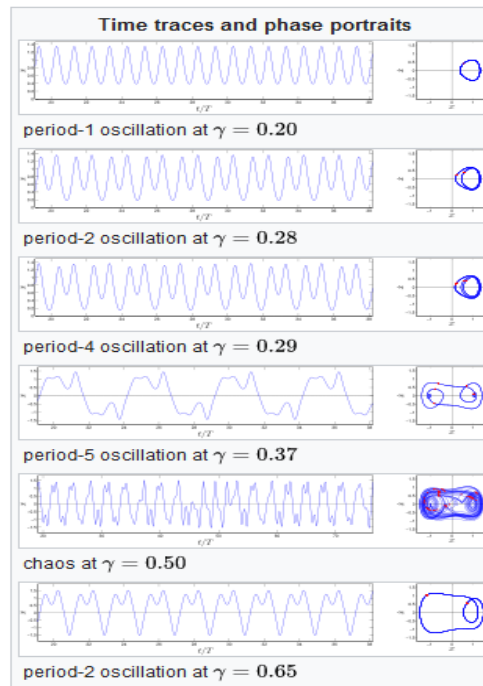


Figure 92 - Chaotic Solutions for a Duffing Oscillator (Calculated from [13], Picture from Wikipedia, [14])

Only the first type is what we need in a precision oscillator.

Under the assumption of a *bound periodic solution* an analytic equation for the possible frequencies and steady-state amplitudes depending on the equation parameters can be derived. The solutions of this equation can be single (no pulling), or double (hysteresis). The equation runs [6]:

$$\left[ \left( \omega^2 - \alpha - \frac{3}{4} \beta z^2 \right)^2 + (\delta \omega)^2 \right] z^2 = \gamma^2.$$

where  $z$  is the steady-state amplitude. This explains pulling (1 solution), and hysteresis (2 solutions), but no chaotic phenomena. This changes when the system is excited by an external signal; then chaotic solutions can occur.

Measurements on 5MHz SC crystal samples have shown that the nonlinear effects above can occur in practice, especially at high amplitudes in the mW range for the nominal frequency. For the B Mode, the nonlinear effects can start at very low amplitudes in the microwatt ranges (See appendix C, **Crystal Measurements**). For oscillators, the power levels in USOs are too small to enable pulling; for filter crystals in the oscillator output circuitry this is another story and hysteresis has been observed.

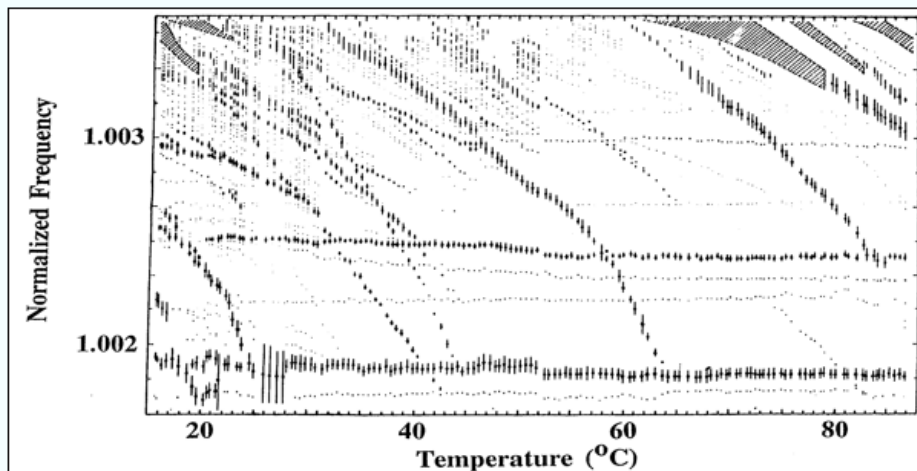
#### 4.3.5 Dips, Mode Coupling

Crystals are normally considered free of mode coupling; this seems to be not realistic (at least for SC cut crystals having a “B Mode” resonance) when looking at an oscillator startup process that will be explained later.

Dips manifest themselves as *abrupt* changes in amplitude and frequency when operating parameters (power, temperature) are *continuously* changed at a slow rate. The reason for dips is that there is some (very weak) coupling from thickness shear mode to other modes.

These couplings have small bandwidth and a small coupling constant, but when the conditions are exactly met energy is transferred from the main mode to some parasitic other mode, lowering Q and slightly pulling the frequency. A plot of a sample AT cut crystal is shown below:

(3 MHz rectangular AT-cut resonator, 22 X 27 X 0.552 mm)



Activity dips occur where the  $f$  vs.  $T$  curves of unwanted modes intersect the  $f$  vs.  $T$  curve of the wanted mode. Such activity dips are highly sensitive to drive level and load reactance.

Figure 93 - Activity Dips in a Crystal (Picture by John Vig) [5]

The value of resistance change caused by dips is specified in the crystal datasheet value RLD, either in Ohms or in percent of the resonance resistance. 10-15% of the static resistance maximum is normal.

### 4.3.6 Memory Effects

#### Retrace

Crystals also “memorize” their oscillation amplitude and temperature in the past and will change frequency slightly if the amplitude is changed, recovering them after a while. This applies to cycling in temperature *and/or* power level. Example curves are shown below:

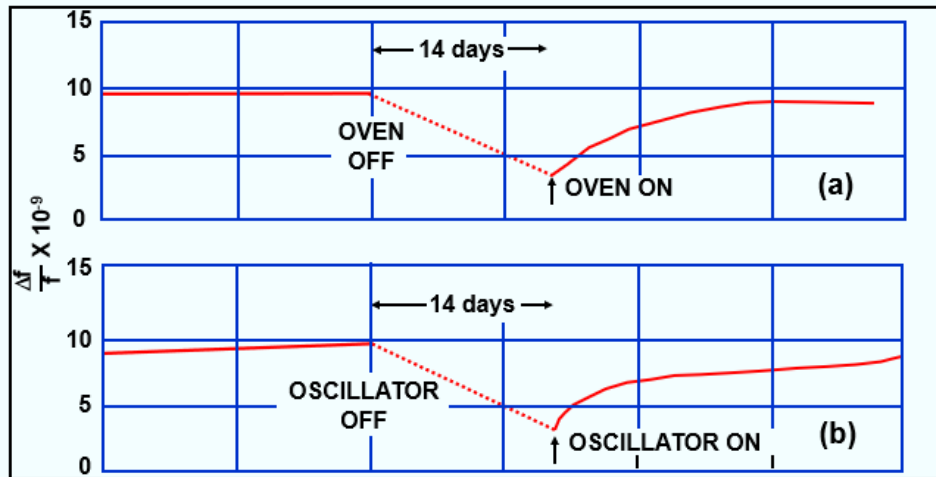


Figure 94 - Memory Effects in a Crystal (Picture by John Vig) [5]

The top curve shows the behavior when just the oven was switched off, but the oscillator was kept running. In the lower curve the oscillator was switched off as well.

If a crystal is subjected to temperature cycling, the frequency changes on the heating branch will be slightly different than the cooling branch (according to Neubig, [7]), like here:

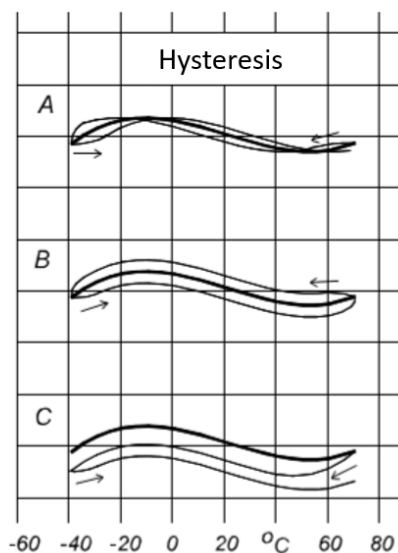


Figure 95 - Temperature Hysteresis (Frequency over Temperature, from Neubig Quarzkochbuch [7])

Hysteresis is much less pronounced in SC cut parts.

In space applications the master clocks are (almost) never shut down or their heaters turned off, so this effect is not very disturbing.

### 4.3.7 Crystal Ageing

Another important effect observed in crystals is ageing, i.e., the shift of the resonant frequency over time. Aging depends a lot on temperature and power applied, to some extent also on radiation and mechanical influences. There are many effects that influence aging, the most prominent ones being:

1. By constant movement mechanical stressed left over from manufacturing (polishing, clamping, electrode applications, ...) levels off and becomes less. This increases the frequency. Natural grown crystal does not suffer from this effect but is never used for space crystals for other reasons.
2. Deposited atoms (metal from the case or welding, ...) sitting on the crystal disk get “shrugged off” due to vibrations. This can take a while, and crystal manufacturers of precision crystals asks for a 30-day run-in period before guaranteeing specs. This effect also increases frequency, but all space applications have so long burn-in periods that this effect is almost nonexistent.
3. There are also frequency-decreasing effects which are normally associated with contamination (e.g., in a high vacuumed crystal) from outgassing components like glass seals or even metals.

Aging can be accelerated by high temperature and temperature cycling. Cycling also shows a hysteretic effect on frequency. A typical ageing curve (*after* burn-in is over) is shown below:

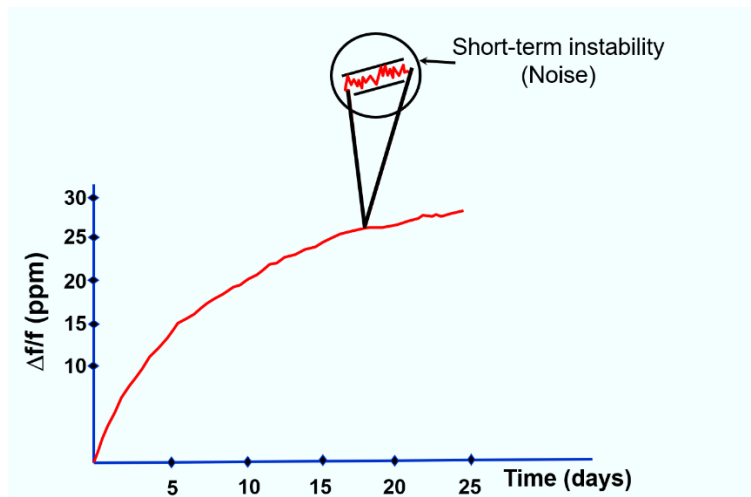


Figure 96 - Crystal Aging over Time (Picture by J. Vig [5])

Aging strongly depends on oscillator power level. For minimum aging, the power level should be in the range of 10uW to 50uW maximum. The lower practical limit of the crystal power level is given by the DLD effects, safe startup as well as allowable phase noise according to the Leeson formula, where phase noise is inversely proportional to power level.

In an oscillator circuit the desired frequency can be fine-tuned by a series capacitor (e.g., Clapp type) or by a parallel pulling capacitor (e.g., Colpitts, never used for precision oscillators). In the Clapp case there is a minimum value of the series capacitor, limiting the down tuning range and the amount of aging deviation that can be compensated. In space oscillators, there are no trimmable components (who should come by and tune them?), and a (selected) fixed series capacitor must be chosen that guarantees specs with aging effects included over the intended lifetime of the spacecraft.

Simulation of the aging process *after the burn-in period* can be described by a logarithmic law of the form (Arrhenius approach [8] using an “activation energy”)

$$\Delta f/f = K_0 e^{-E/RT} \ln(t)$$

where

$\Delta f/f$  stands for the relative frequency change,

$E$  is the activation energy, to be determined for the type of crystal *and power level*

$R$  is the universal gas constant (8.314J/ (mol K)),

$T$  is the absolute temperature and

$t$  is the time.

Aging rates are valid for stable conditions, and in case of changes (switching on/off, change in power level and/or temperature, shock, ...) they show *retrace effects*.

With the parallel capacitance remaining constant, what changes is the series capacitance of the mode of interest. A simulation of this effect can be done using a time-elapsd dependent series capacitor, with a change rate equal to the root of the frequency change rate.

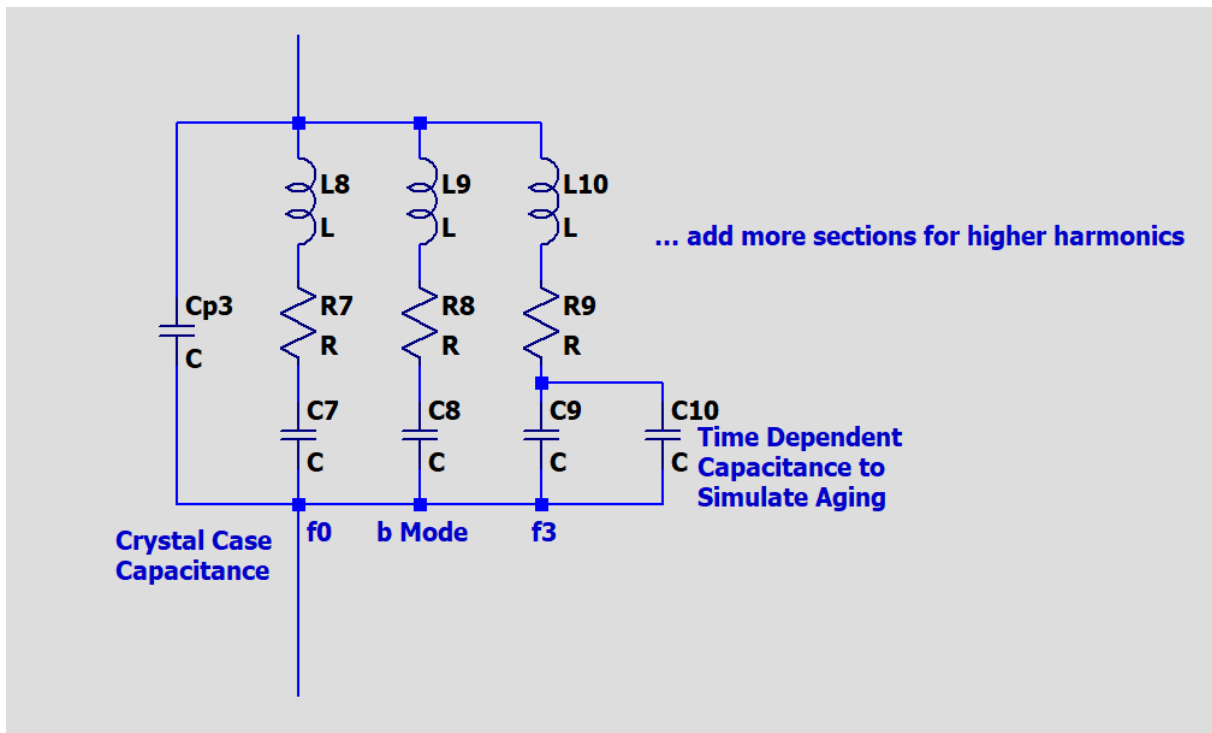


Figure 97 - Simulation of Aging Using a Time Dependent Capacitance

#### 4.3.8 Crystal Noise

Crystals also exhibit noise, not just caused by the equivalent series resistance(s) of the modes, but also by other effects (e.g., flicker).

The resistive noise has a “white” Spectrum (originating from thermal and Schottky components) and a  $1/f$  (flicker) component as well. The amount of crystal noise is hard to predict because the mechanisms of its creation are not very well understood. Manufacturing aspects (cleanliness of the base material, surface quality, impurities, the modes, ...) play a role, but to my knowledge a profound theory allowing quantitative predictions about the noise spectrum of a crystal has not been developed yet.

Measuring crystal noise *outside* of an oscillator is tricky (see crystal measurements), but reverse-fitting methods use a “noisy capacitor” (i.e., a varactor with a noisy bias voltage) to simulate the effect. [9] This is a behavioral model, of course, having no physical background. The static capacitance of D1 must be deducted from Cp1 to keep the resonance frequency as before. The circuit looks like this:

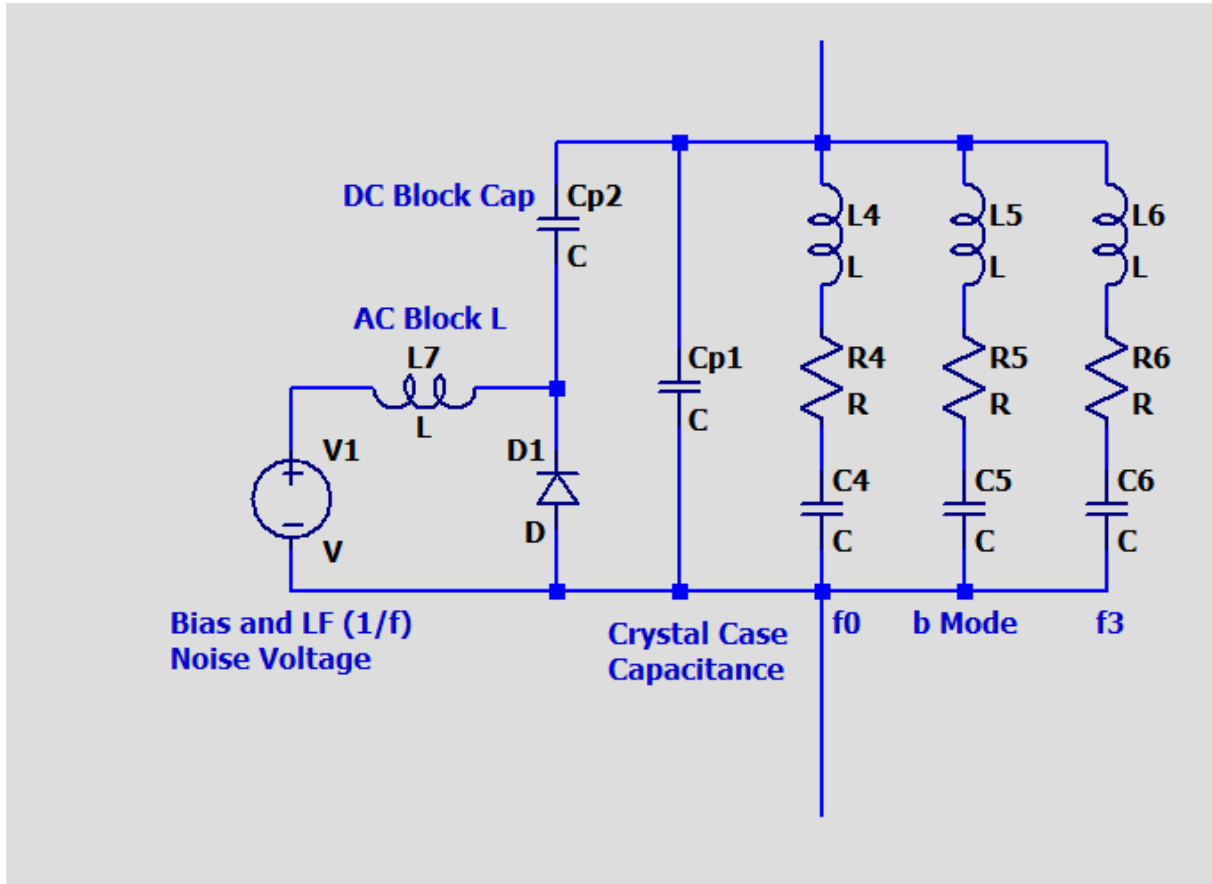


Figure 98 - Modeling Crystal Phase Noise Using a Varactor Biased from a Noise Voltage

Another idea is to use crystals as filters and to check if a white noise input signal appears at the filter output with a noise level larger than the crystals equivalent series resistance would explain (discussed later).

### 4.3.9 Environmental Effects

#### *Acceleration and Vibrations*

Crystals due to their piezoelectric properties are obviously sensitive to acceleration. For space crystals, acceleration is not just the strong (several g), linear acceleration during the launch phase of a spacecraft, but also all kinds of small, low-to medium frequency mechanical noise with a probable power spectrum up to a few kHz. Motors, actuators, pumps, valves, thruster rockets and other parts of a spacecraft create a considerable sound level. Vibrations of the crystal body create FM and sidebands in the output spectrum, and they alter the phase noise behavior. This effect can be seen in the following graph:

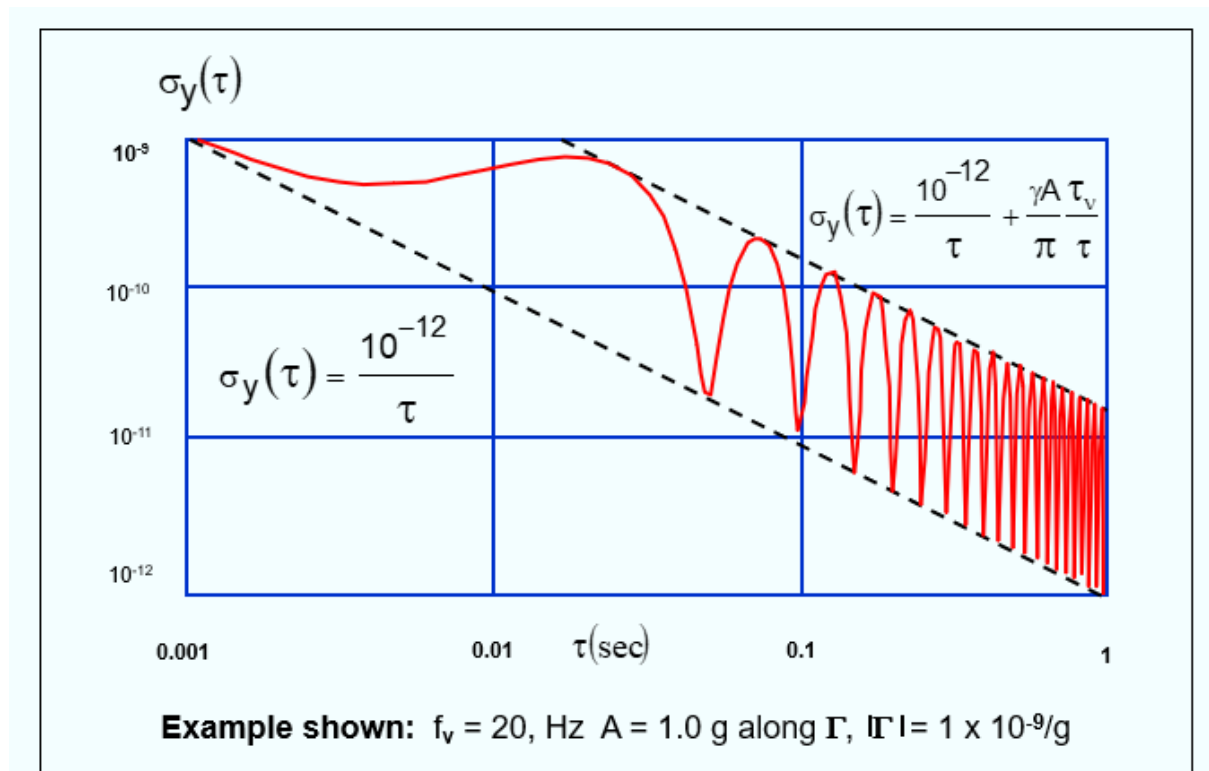


Figure 99 - Deterioration of Allan Variance due to Vibrations (Picture from John Vig) [5]

Details depend on the size and mass of the crystal disk, the method of clamping, and the mechanical frequency of self-resonance of the disk within its holder (usually between several 10Hz and ca. 1kHz).

Damping materials could be used, but they are ineffective at low frequencies, adding weight and size to oscillator units. By using more than one crystal vibrations can be compensated by cancellation (invented by Driscoll, 10).

Another technique is to compensate vibrations electronically by using a motion sensor and actively regulating out the vibration influence on the Quartz.

Space crystals are tested for vibration sensitivity according to a military test norm, MIL-PRF-55310 [11].

### *Mechanical Shock*

Shock events are a special, nonrepetitive, short form of strong acceleration. Depending on amplitude, permanent deformation can result, but even if this is not the case a frequency “jump” will occur, plus a recovery phase where it takes a while for the crystal to return to frequency before the shock event, sometimes the change may be even permanent:

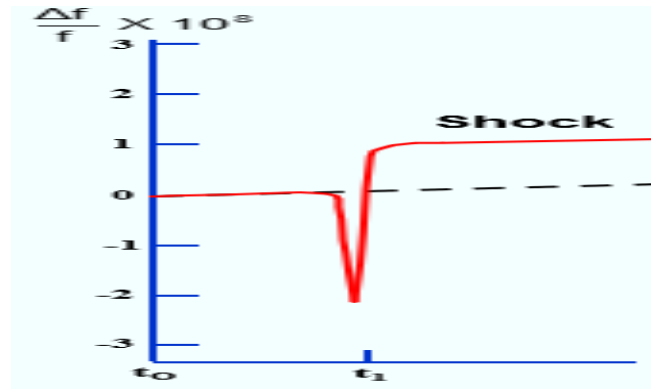


Figure 100 - Crystal Frequency Change after Mechanical Shock (Picture from John Vig [5])

To my knowledge, there are no massive mechanical shocks on board of a spacecraft after the launch phase. Nevertheless, shock testing is part of the space qualification program for crystals, according to MIL-PRF-55310.

A series of experiments with commercial and self-made SC and AT cut crystal oscillators, measuring their reactions to gravity, swept vibration, random vibration, and shock were carried out. The measurements are described in the crystal measurements chapter.

### *Radiation*

Outside the protective atmosphere of the earth and its Van Allen belt the level of ionizing radiation can be several times higher than on earth. The radiation sensitivity depends on the type of radiation involved (alpha, beta, neutrons, gamma, ...), intensity, but also on the type (natural, synthetic) and manufacturing process (e.g., sweeping) of the crystal in question. The cut is also important; SC cut is much less sensitive to radiation than AT, another good reason why it is now used exclusively.

The physical effects of radiation on the crystal structure are

1. Dislocation of atoms, creating vacancies, interstitials, and other crystal defects (this is caused by neutrons colliding with grid atoms, e.g.)
2. Trapping charges when a particle creates electron-hole pairs, and the holes find an impurity atom to stick to
3. Lowering Q

A crystal grid can be reconstructed (“annealed”) by using an elevated temperature (240 °C), but this temperature is far beyond the operating temperature of SC cut crystals in space OCXOs. Therefore, radiation effects on space OCXOs must be considered cumulative.

Space crystals can be pre-radiated before use. Radiation hardening is a part of the MIL-norm testing procedures.



### *Temperature Shock*

A sudden change in temperature will lead to an inhomogeneous distribution of crystal temperature over the disk, building up mechanical stress, and therefore resulting in frequency and amplitude changes in an oscillator. With space crystals normally running in ovens with long thermal time constants (minutes), this is not a prominent concern.

Still, the space MIL norms require testing this, probably to make sure that no fatigue or cracking occurs and puts a mission at risk.

#### 4.3.10 Crystal in Oscillator Circuits

This will be treated with a lot more detail later, but there are two fundamentally different modes of application of a crystal:

1. Low-impedance mode, also called series resonance
2. High-Impedance mode, often called “parallel resonance”

In series mode, the frequency is determined by the very high Q of the RLC part and only to a small amount by the parallel capacitance. The tuning range (and therefore, the dependency on external and maybe not so stable circuit elements) is very small, most welcome for precision oscillators. This is especially true for overtone oscillators.

In parallel mode, a tunable “burden” capacitance forms a shunt for the impedance of the RLC part, and as long as this RLC impedance is inductive an impedance maximum can be built, but with a much lower Q and at a higher frequency than in series mode. The electromechanical resonance frequency of the crystal disk does not change by this trick, obviously, so the term “parallel resonance” is in a way a misnomer but is nevertheless used frequently in the industry.

All known precision oscillators use *series* resonance, and most of them run in 3<sup>rd</sup> or 5<sup>th</sup> overtone mode. Parallel resonance is something for applications where a wide tuning range is needed, and stability and signal purity is unimportant.

### 4.3.11 Crystal Q Limitations

There is a curve originating from John Vig [5] showing that the product of achievable Q and oscillating frequency is a constant.

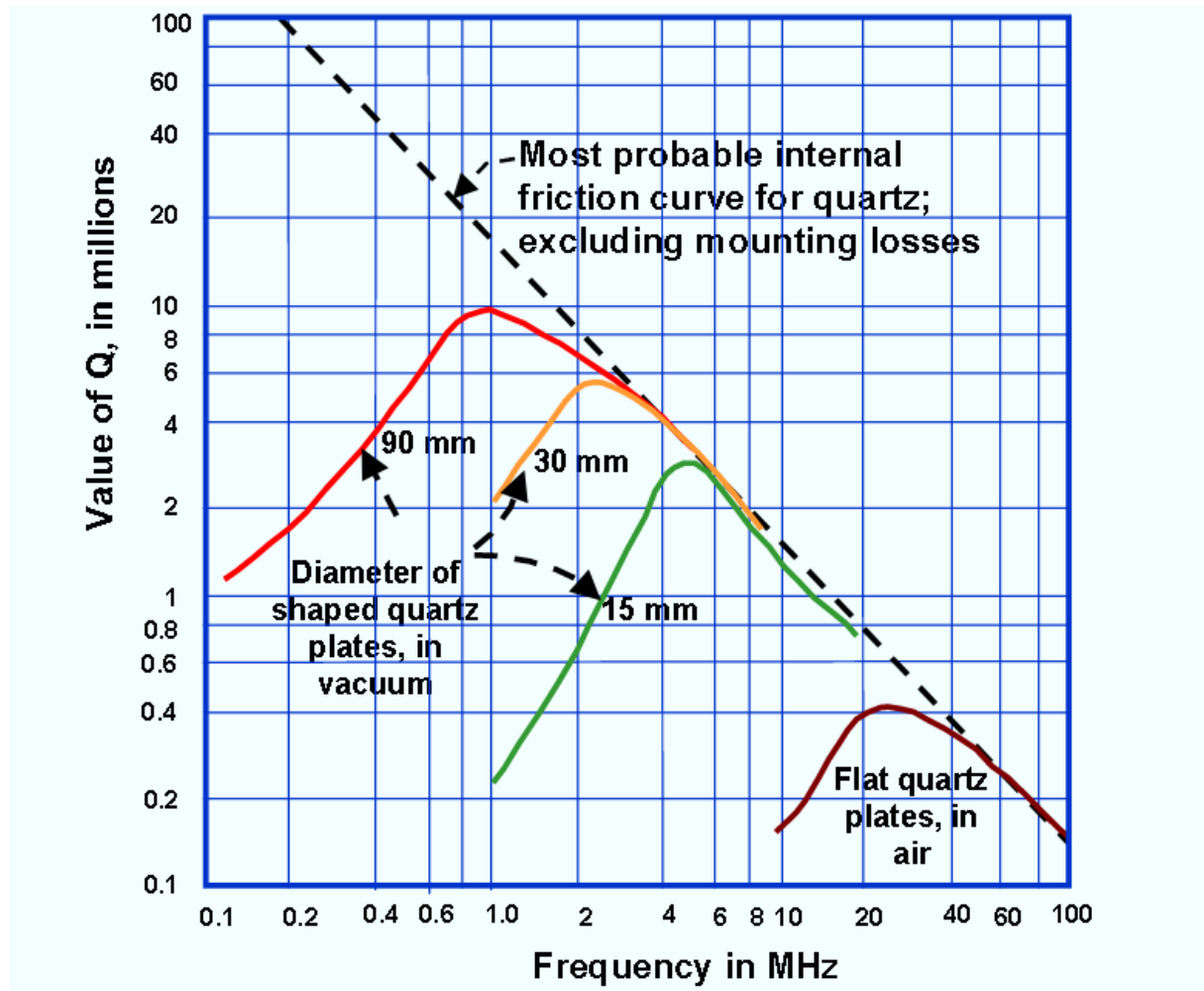


Figure 101 - Frequency/Q Curve (Picture from John Vig [5])

According to Bernd Neubig [12] these limits have a theoretic background and are not purely empirical, resulting from losses by Phonon scattering ( $\sim$  “viscosity”) in a crystal disk of a given thickness, size, and temperature. The Vig curve assumes a given crystal disk diameter and a planar shape. BVA crystals which are pill-shaped can have a higher Q. Current production crystal are close to the dashed line, provided their datasheet values are correct.

Several precision crystals were measured (see crystal measurements chapter) and all of them observed the  $Q \cdot f$  maximum relation proposed. A BVA crystal was unfortunately not available for measurements. Rumors that the crystals of the industry standard 10MHz HP10811A OCXO oscillator violate these rules seem to be wrong.

## References

- [1] Keysight Inc., “E5071C ENA Vector Network Analyzer Datasheet.” Accessed: Nov. 24, 2020. [Online]. Available: <https://www.keysight.com/us/en/assets/7018-01424/data-sheets/5989-5479.pdf>.
- [2] Keysight Inc., “E4990A Impedance Analyzer Datasheet.” Accessed: Nov. 26, 2020. [Online]. Available: <https://www.keysight.com/us/en/assets/7018-04256/data-sheets/5991-3890.pdf>.
- [3] Bliley Corp., “BQOTY-XXMXX-XXXB–HC-30/U Crystals Datasheet.” Accessed: Nov. 26, 2020. [Online]. Available: [https://cdn2.hubspot.net/hubfs/2222150/Assets/Datasheets/01\\_Crystals/BQOTY-XXMXX-XXXB\\_v2.0.pdf](https://cdn2.hubspot.net/hubfs/2222150/Assets/Datasheets/01_Crystals/BQOTY-XXMXX-XXXB_v2.0.pdf).
- [4] M. Addouche et al., “Low drive level sensitivity (DLS) of quartz crystal resonators.” Accessed: Nov. 27, 2020. [Online]. Available: <http://rubiola.org/>.
- [5] John Vig, “Quartz Crystal Resonators and Oscillators.” Accessed: Nov. 19, 2020. [Online]. Available: <http://www.resonal.com/Downloads/John%20R.%20Vig%20-%20tutorial%20on%20Quartz%20Crystals%20and%20Oscillators.pdf>.
- [6] I. Kovacic and M. J. Brennan, Eds., “The Duffing equation: nonlinear oscillators and their phenomena”. Chichester, West Sussex, U.K.; Hoboken, N.J: Wiley, 2011.
- [7] B. Neubig et al., “DAS GROSSE QUARZKOCHBUCH.” Accessed: Nov. 26, 2020. [Online]. Available: <https://www.axtal.com/Deutsch/TechnInfo/Quarzkochbuch/>.
- [8] S. Arrhenius, “Über die Dissociationswärme und den Einfluss der Temperatur auf den Dissociationsgrad der Elektrolyte,” *Zeitschrift für Physikalische Chemie*, vol. 4U, no. 1, Jan. 1889, doi: [10.1515/zpch-1889-0408](https://doi.org/10.1515/zpch-1889-0408).
- [9] U.L. Rohde, “Rohde Idea how to Model Crystal Phase Noise by a Varactor Diode.” Private communication.
- [10] Michael M. Driscoll, “LOW VIBRATION SENSITIVITY CRYSTAL RESONATOR ARRANGEMENT.” Accessed: Nov. 27, 2020. [Online]. Available: <https://patentimages.storage.googleapis.com/f3/6e/76/07117512fd12f6/US5250871.pdf>.
- [11] NASA, “MIL-PRF-55310 PERFORMANCE SPECIFICATION FOR OSCILLATOR, CRYSTAL CONTROLLED.” 1998, Accessed: Nov. 27, 2020. [Online]. Available: <https://nepp.nasa.gov/DocUploads/1F3275A6-9140-4C0C-864542DBF16EB1CC/MIL-PRF-55310.pdf>.
- [12] B. Neubig, “Phonon Scattering is the Reason that there is a Maximum Q for Quartz Crystals.” Private communication.
- [13] D. W. Jordan and P. Smith, *Nonlinear ordinary differential equations: an introduction for scientists and engineers*, 4th ed. Oxford [England]: New York: Oxford University Press, 2007.
- [14] Wikipedia, “Duffing Equation”, Snapshot on Dec. 28<sup>th</sup>, 2020, [https://en.wikipedia.org/wiki/Duffing\\_equation](https://en.wikipedia.org/wiki/Duffing_equation)

## 5 Oscillator Measurement Techniques

The following chapters deal with the difficulties and remedies encountered when trying to measure voltages and currents in a running oscillator, at low and high signal levels and bias conditions.

### 5.1 How to Probe an Oscillator Without Unacceptable Loading or Detuning

This chapter deals with methods that allow to measure even “hot” points in an oscillator without (capacitive and/or resistive) loading. Most commercial probes are unsuitable due to either excessive capacitance or too low resistance, due to insufficient voltage range (we need DC measurements plus HF), missing robustness and high cost. Self-made FET probes were able to solve all aspects for a 5MHz oscillator.

If we need to analyze waveforms inside a running oscillator, we would like to use probes to tap the interesting circuit nodes. Unfortunately, some nodes are extremely sensitive against capacitive (and partly also resistive) loading. This effect can be immediately verified by watching the output change as a classic oscilloscope probe (like 10M || some pF) probe is attached.

What is needed is a probe, that is small and has an exceptionally low capacitance. Such active FET probes are commercially available (from Keysight, Rohde&Schwarz, Tektronix, Rigol and many others), but their common drawbacks are

1. Low voltage range (+/-8V, e.g.), sometimes too small for oscillators at high power levels
2. Not forgiving. Overvoltage can instantly destroy the probe.
3. Sometimes only AC or with low input resistance (especially in the GHz range).
4. Higher frequency parts often have a small DC input resistance, like 100KOhms or less. This would shift the bias point if applied to the base.
5. Expensive (>1K€ for 1GHz, prices increase rapidly with frequency).

After an idea by Bob Pease (see [1], p159ff) a homebrew FET probe was developed and used for all voltage probing in oscillators. The characteristics are:

1. -40V to +20V input voltage range with a division factor around 20 into 50 Ohms.
2. Ca. 2pF of capacitive loading including stray capacitances
3. 1MOhm input resistance
4. 100MHz bandwidth (-3dB), good enough for 5-10MHz oscillators)
5. Total parts value is a few €.

The schematics of this probe is shown here:

### HOW GOOD ARE OUR PROBES – THE SCHEMATICS

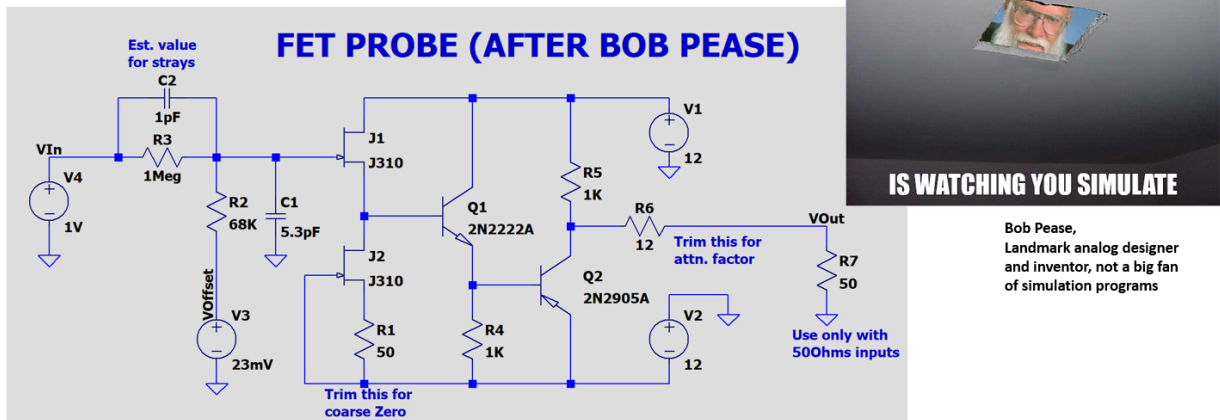


Figure 102 - FET Probe Schematics. Picture Redrawn from Bob Pease [1]

The input consists of a compensated divider with rise time and offset trimming, just as a normal scope probe. The lower J310 JFET ([2] selected as pairs for equal  $I_{DSS}$  and cutoff voltage) acts as a current source, the upper one as a source follower. The two emitter follower stages with a 2N2222A and the 2N2905A [3] serve as impedance buffers and a driver to a 50 $\Omega$  coaxial output.

A sample of such a probe is shown below:



Figure 103 - Photo of a FET Probe in a Test Oscillator

The probe tip is shown in red. The probes were calibrated using a Keysight B2902A SMU [4], a scope (Keysight DSOS604A, [5]) and a VNA (Keysight E5071C [6]).

The DC transfer curves are shown below:

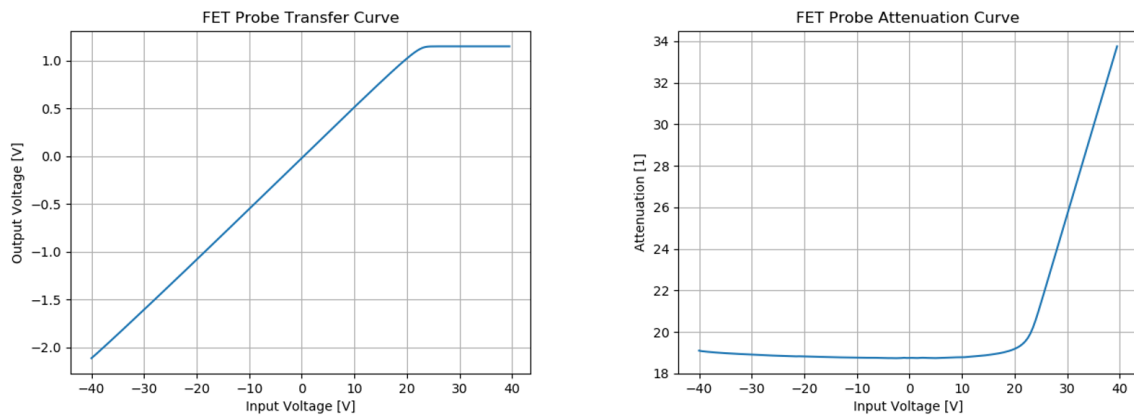


Figure 104 - Probe DC Transfer Curves Measurement

The linear range stretches from -40V to over +20V and the attenuation within this range is 19dB. This is enough for the voltages found in any oscillator we have been testing. The asymmetric clipping is a result of the work resistor  $R_5$ , which we set at 1K. When  $Q_2$  does not conduct at all,  $R_5$  sets the maximum current that can flow into the output load, and consequentially the maximum attainable output voltage. The positive range could be increased by either a larger supply voltage and/or a smaller resistance  $R_5$ , with an added penalty that the current consumption (and self-heating) of the probe would increase.

Resistor  $R_6$  is there to fine-tune the amplification factor. When we look at the cascade  $J_1$ ,  $Q_1$  and  $Q_2$  we see that the voltage gain of all stages is less than one, because all stages are just voltage followers. The cumulated loss is partly compensated by the ratio of the input divider (1M/68K instead of 900K/100K), and then  $R_6$ .

Pulse rise and fall times were also measured using a fast rise time generator (Tektronix AFG3252 [7] with 1-2ns) and a 6GHz scope, as shown here:

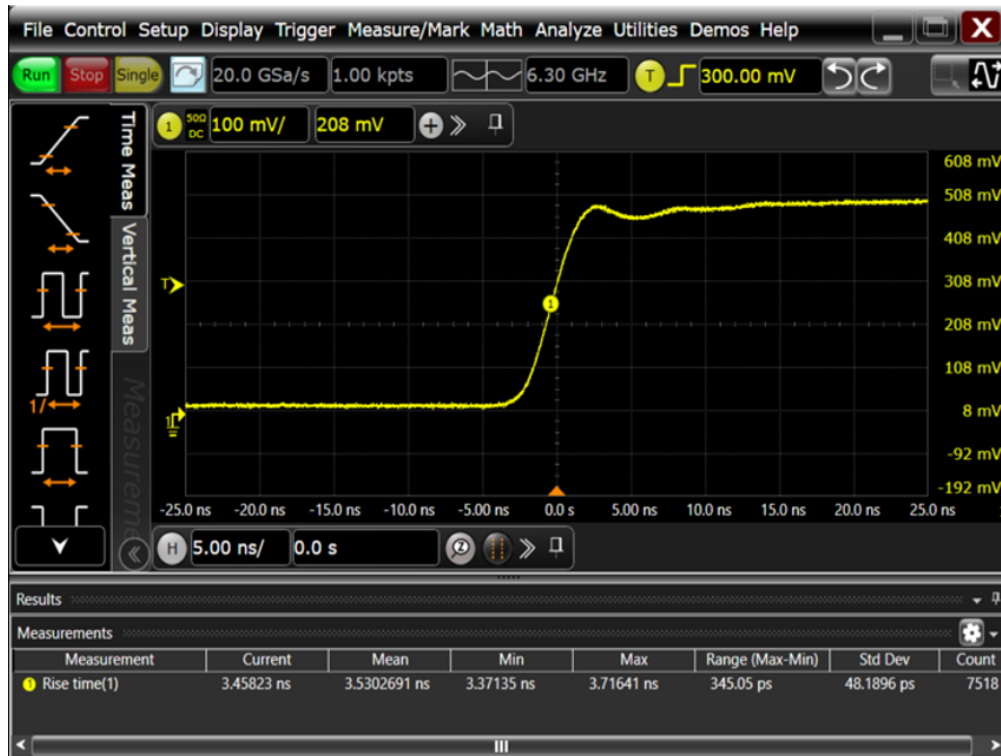


Figure 105 - Rise Time of the FET Probes

The probe was directly connected to the pulse generator output. Rise time is 3.5ns, an expected value for a 100MHz bandwidth. Ringing is moderate, and the settling time is less than 10ns within 5%.

Via the capacitor C2 the probe can be aligned just like a normal passive scope probe for a good compromise between rise time and flatness.

The falling edge looks comparable:



Figure 106 - Fall Time of the FET Probes

The fall time is about 3.5ns, with a little bit more pronounced ringing.

As a last sanity check, we could measure the probe using the VNA and map the input impedance as well as the transfer function.



The rise time and the bandwidth are consistent with the bandwidth, as a VNA plot shows:

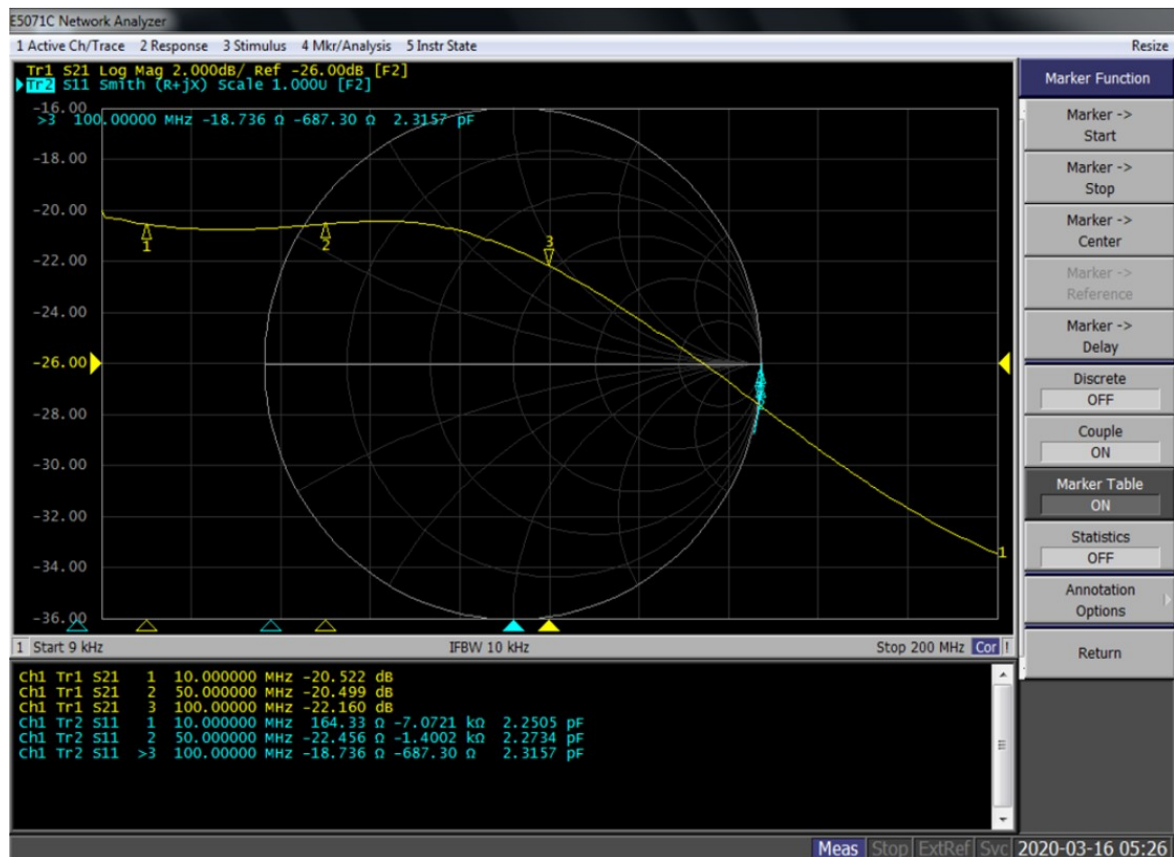


Figure 107 - FET Probe Input Impedance and Transmission on a VNA

The capacitance including all strays is 2.3pF (blue spots in the Smith chart), and we see a transmission down -2dB at 100MHz. This concludes the FET probe measurements.

A picture of the FET probe calibration fixture is shown below:

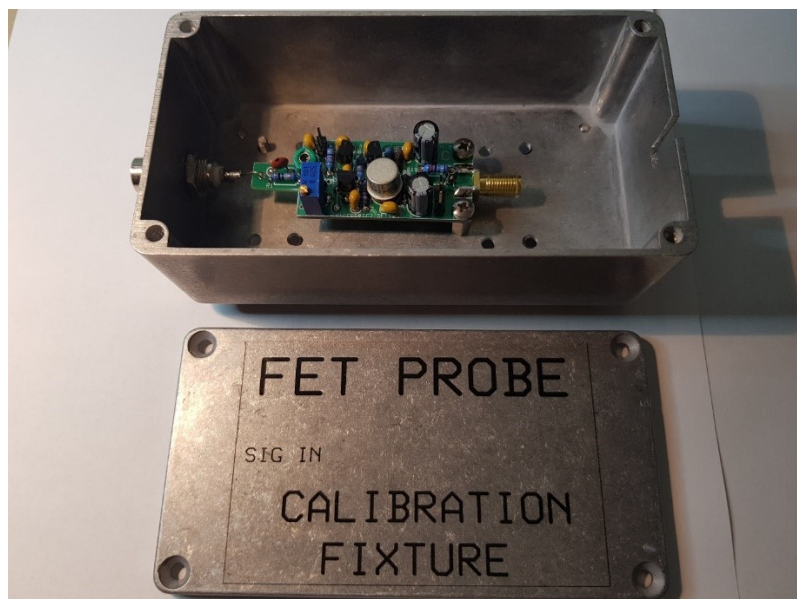


Figure 108 - The FET Probe Calibration Fixture

A mounted DUT probe PCB is shown inside, the enclosure with the output, power and offset adjustment cabling removed for better visibility. The signal enters from the left thru a BNC socket,

and the buffered signal exits thru the SMA connector at the right side. The probe hovers ca. 1cm above ground to keep capacitances low, and the total measured capacitance of 2.3pF includes the ca. 1-1.5pF capacitance of the BNC connector, leaving a net probe capacitance of around 1pF.

## Conclusions

The probes worked quite well and reliable. Some usability aspects must be observed, however:

1. In the interest of a fast rise time and sufficient bandwidth, the probes run at considerable collector currents, causing a warmup temperature drift. The probes should be powered up 30 minutes before measurements to stabilize.
2. Offset nulling should be performed prior to use. After warmup and nulling, residual drift stays within a range of a few mV.
3. The scale factor is fine-tuned by the output resistor and should be accurately measured before use. As the charts show it is almost constant across the input voltage range.

## References

- [1] Bob Pease, "Troubleshooting Analog Circuits," *EDN Magazine, Jan1989*, Jan. 1989.
- [2] On Semiconductor, "J310 N-Channel JFET Transistor Datasheet." Accessed: Nov. 25, 2020. [Online]. Available: <https://www.onsemi.com/products/discretes-drivers/jfets/j310>.
- [3] On Semiconductor, "2N2905 Datasheet." Accessed: Nov. 25, 2020. [Online]. Available: <https://www.onsemi.com/pub/Collateral/2N2905A-D.PDF>.
- [4] Keysight Inc., "B2900A Series Precision Source/Measure Unit Datasheet." Accessed: Nov. 29, 2020. [Online]. Available: <https://www.keysight.com/us/en/assets/7018-02794/data-sheets/5990-7009.pdf>.
- [5] Keysight, "Infiniium S-Series Oscilloscope Datasheet." Accessed: Nov. 17, 2020. [Online]. Available: <https://www.keysight.com/us/en/assets/7018-04261/data-sheets/5991-3904.pdf>.
- [6] Keysight Inc., "E5071C ENA Vector Network Analyzer Datasheet." Accessed: Nov. 24, 2020. [Online]. Available: <https://www.keysight.com/us/en/assets/7018-01424/data-sheets/5989-5479.pdf>.
- [7] Tektronix, Inc., "AF 3252 Arbitrary Function Generator Datasheet." Accessed: Nov. 25, 2020. [Online]. Available: <http://www.testequipmenthq.com/datasheets/TEKTRONIX-AFG3252-Datasheet.pdf>.

## 5.2 Measuring Base Current

This chapter Current discusses a technique to measure the base current of an oscillator transistor and to correlate these measurements with the probed voltage measurements above and the measurement of generated phase noise, depending on bias conditions. It could be demonstrated that the BE breakdown phenomenon creates massive base current spikes, and that a very good agreement between scope measurements and SPICE simulations is reachable by augmenting the simulations with the math for the breakdown process.

The probing of oscillator *voltages* is covered by low-capacitance FET probes, but the probing of *currents* is also needed in some cases, e.g., for BE breakdown measurements.

There are some candidate current probe solutions from Keysight and others that can provide sufficient bandwidth (e.g., DC to 150MHz, [1]), but the problem is that commercial probes are so large that they cannot physically attach to a circuit that is made with RF design rules in mind.

Especially the transistor base is a sensible point where long wire lengths can lead to parasitic oscillations in the VHF or higher range, so a multi-cm wire extension is no valid option.

What we need is:

1. A small probe preferably introducing not more than 5mm in additional wire length at the base lead of the transistor.
2. Probe bandwidth from ca. 1MHz to > 100MHz.
3. Coax 50Ohm output
4. Low stray capacitances.

A possible choice for this requirement is an RF current transformer on a tiny ferrite core. We chose a FT23-43 Amidon toroid core [2] with 10 secondary windings and a 50Ohms resistor termination immediately at the secondary. A 50Ohms coax line was used to attach the probe to the VNA, spectrum analyzer or scope, where a 50Ohm termination was used as well.

The current probe transmission (S21, yellow) and reflection (S11, blue) were then measured on a Keysight E5071C [3] VNA from 9kHz to 200MHz, as shown:

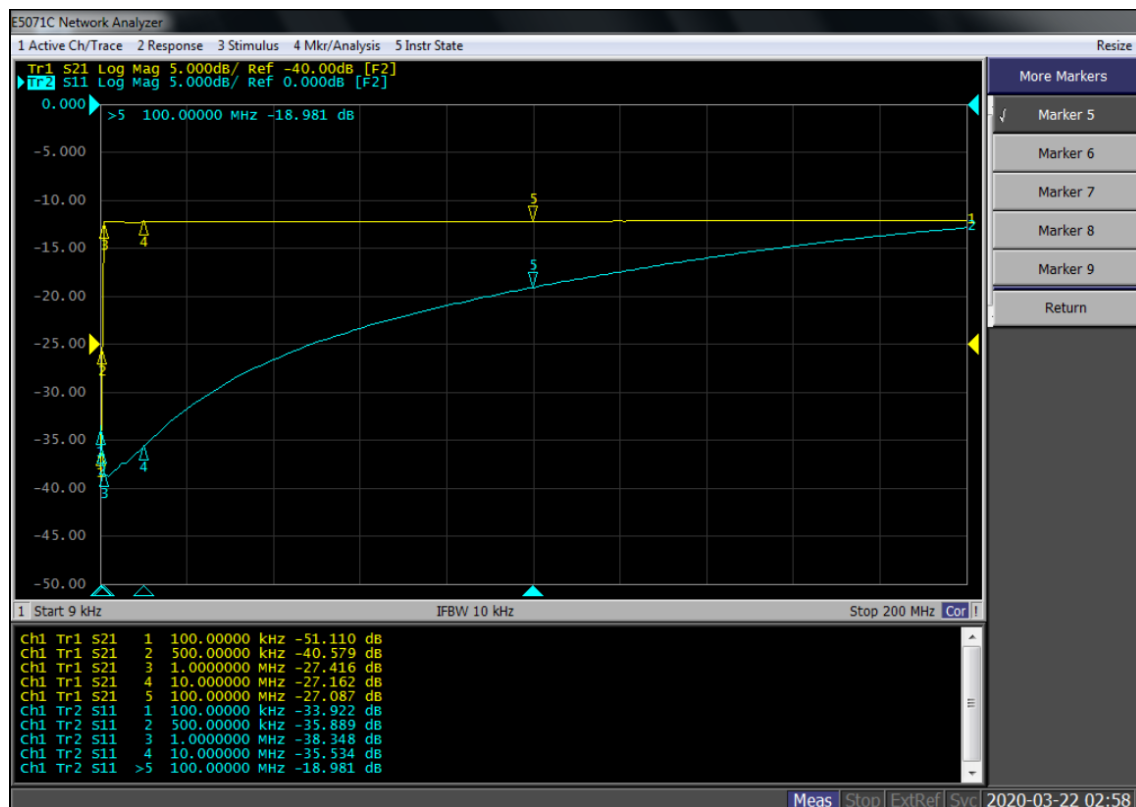


Figure 109 - VNA Measurement of Base Current Probe Transmission with Terminated Outputs

From 1MHz to 100MHz the transmission to the probe port is -27dB with variations of less than 0.4dB. Matching is 19dB or better in the same range. This is sufficient to make reasonably quality measurements in the 5MHz oscillators we are working on, even if higher harmonics (up to the 20<sup>th</sup>) should occur.

For 10MHz, the performance is also acceptable.

The next interesting quantity is to see how the transmission between input and output port looks like when the probe port is terminated with 50 Ohms. This is shown here:

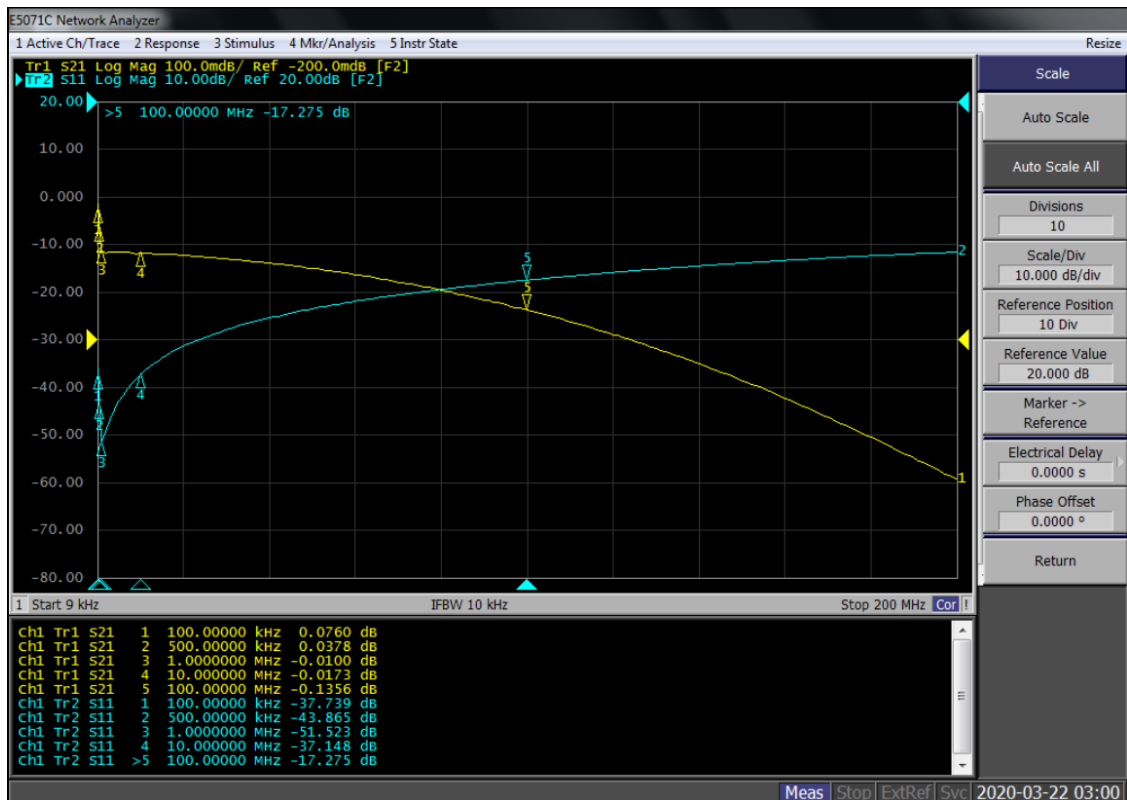


Figure 110 - VNA Measurement of Base Current Probe Thru Characteristics

No significant loss is caused by the probe (only  $-0.13\text{dB}@100\text{MHz}$ ).

As a conclusion, we could assume that the proposed current probe will provide usable measurements in the range of 1MHz to at least 100MHz with no prohibitive inaccuracies.

The stray capacitances and inductances are dependent on how the probe is located in the oscillator; when a compact layout is implemented, we could estimate an extra base lead length of ca. 5mm (a few nH) and a coupling capacitance in the range of few pF.

A frequency domain simulation was performed to cross-check the measurements, as shown:

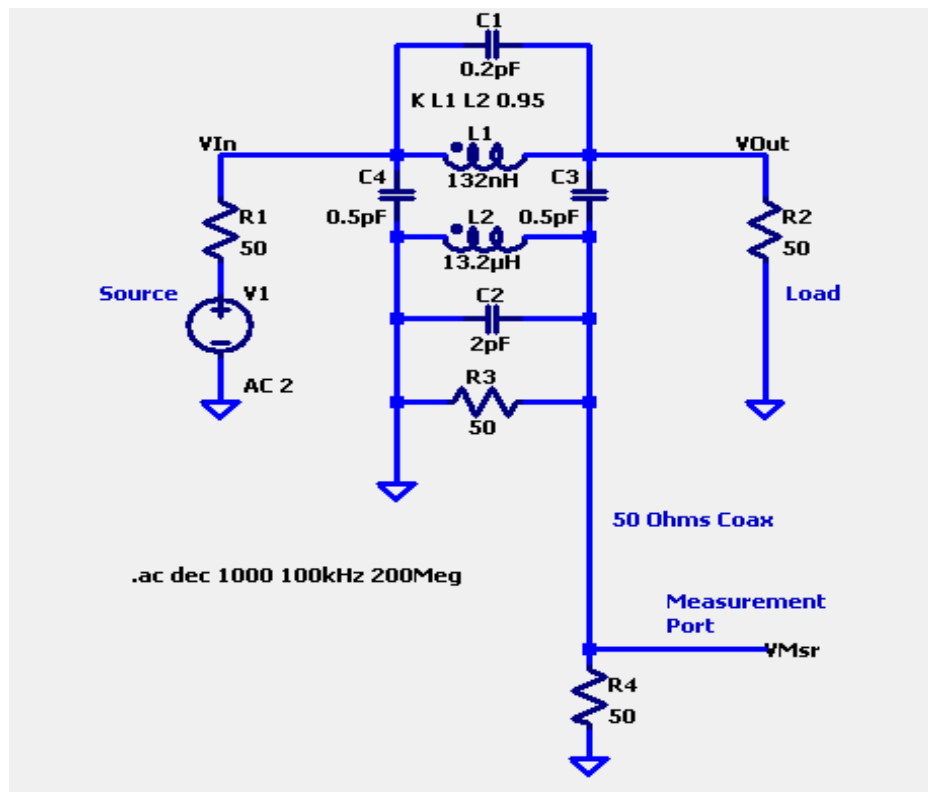


Figure 111 - Simulation Model of the Base Current Probe

The circuit includes some values for stray capacitances (C1, C2) and the stray inductances are modelled by less-than-one coil coupling factor. The factor of 0.95 is a common guess for a toroid. The output transmission line needs no modeling because perfect terminations were assumed (plausible for industry grade VNA input ports, a Keysight E5071C used here).

The transformer has a winding ratio of 1 (primary, just the base lead) to 10 (windings). The total secondary impedance including probe termination, coax cable to the VNA and its input impedance is 25 Ohms, which will be transformed into a 0.25 Ohm series impedance loading on the through line. This impedance is so much smaller than all other resistances in the base circuit branch that a damping influence at 5 MHz is highly unlikely.

The secondary inductance for 10 turns on an FT37-43 is 42  $\mu$ H.

The simulated results show a very good agreement with the measured values:

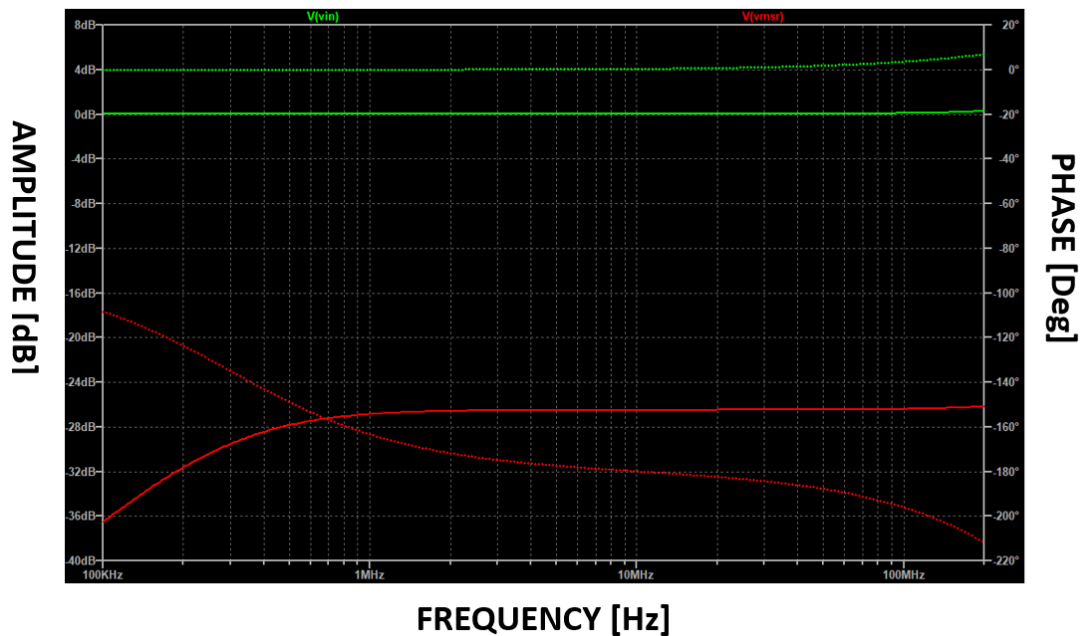


Figure 112 - Simulated Probe and Thru Frequency Response

The coil coupling factor and the stray capacitances were educated guesses from the geometry. From 1MHz to 200MHz the -27dB measured is with ca. 0.5dB of the simulation result (red curve).

## Conclusions

The miniature current probe presented here is a usable instrument to measure currents inside a working oscillator from 1 to 100MHz. The frequency range must cover not just the nominal frequency of the oscillator, but also all harmonics with a significant amplitude. This, in case of very non-sinusoidal current waveforms, limits the oscillation frequency that can be accurately measured to 5-10MHz.

## References

- [1] Keysight Inc., “N7026A AC/DC high sensitivity clamp-on current probe, 150MHz.” Accessed: Nov. 25, 2020. [Online]. Available: <https://www.keysight.com/en/pd-2877490-pn-N7026A/ac-dc-high-sensitivity-clamp-on-current-probe-150mhz?nid=-32553.1229527&cc=US&lc=eng>.
- [2] Amidon Corp., “Amidon 43 Material Specifications.” Accessed: Nov. 25, 2020. [Online]. Available: [http://www.amidoncorp.com/product\\_images/specifications/43\\_Material.pdf](http://www.amidoncorp.com/product_images/specifications/43_Material.pdf).
- [3] Keysight Inc., “E5071C ENA Vector Network Analyzer Datasheet.” Accessed: Nov. 24, 2020. [Online]. Available: <https://www.keysight.com/us/en/assets/7018-01424/data-sheets/5989-5479.pdf>.

## 5.3 Noise Caused by Base Emitter Breakdown

Noise Caused by Base Emitter Breakdown discusses an effect not predicted by classic oscillator theory (Leeson formula). Normally, noise should decrease as a square function of oscillator output power. With no breakdown present, this is approximately correct and in a good agreement with measurements. With BE breakdown present, the noise level drastically increases. The reason is the emergence of new and strong noise sources based on the tunnel and/or avalanche effect.



Please refer to the paper “Noise Caused by the Base Emitter Breakdown Phenomenon” now published on IETE:

Wolfgang Griebel, Matthias Rudolph & Ulrich L. Rohde (2020) Added Noise in Oscillators Caused by the Transistor Base Emitter Breakdown Phenomenon, IETE Journal of Research, DOI: [10.1080/03772063.2020.1847702](https://doi.org/10.1080/03772063.2020.1847702)

#### 5.4 What Does “loaded Q” Mean?

This chapter investigates the term “loaded Q” from a theoretical and measurement point of view. The loaded Q term appears in many derivations involving phase noise, but its definition is questionable, as has been found. A pragmatic, but methodically robust method to define and measure loaded Q also for extremely high-Q, nonlinear oscillators with a low conduction angle is presented.

In RF circuitry, the term Q denotes a quality measure of a resonator. It is defined as ratio of resonance frequency  $f_0$  and bandwidth B, or to the ratio between the energy (W) stored in a resonator and the energy dissipated in one oscillation cycle (V), like

$$Q = 2\pi \frac{W}{V} \text{ or } Q = \frac{f_0}{B} \text{ or (LC tank) } Q = \frac{\omega L}{R}$$

There is no dependency of Q on the amplitude the oscillations actually have. Now let us consider a very primitive nonlinear circuit like the simple series LCR van der Pol type oscillator [1] governed by the equation

$$RI + L \frac{dI}{dt} + \frac{1}{C} \int_0^t I dt = -\alpha I + \gamma I^3$$

From the structure of the “undamping” term  $\alpha$  consisting of a linear negative resistance and a positive cubic damping  $\gamma$  it intuitively follows that the negative resistance will supply net energy to the resonator as long amplitudes are small, effectively compensating all losses in the resonator and creating, by classic measures, an indefinite high Q, because the total R will be zero or even negative.

As the amplitude rises, some energy will be now dissipated as described by the cubic damping term, limiting the amplitude growth until the losses over time compensate the gain provided by the negative resistance term. Thinking in small signal, Q will vary widely over an oscillation cycle, from infinity to some finite value, not a particularly useful idea. If we would like to think of an “effective” negative resistance it would be exactly as large as the loss resistance of the resonator, creating a stable oscillation amplitude and a total effective resistance of zero. The total Q of such an arrangement according to the classic definitions like  $\omega L/R$  would be infinite, which is again useless.

When thinking of a Clapp oscillator instead of the van der Pol circuit and its pulse-shaped transistor current (see Rohde [2]), the energy lost in the resonator is replenished by short pulses, more like a switch than a smooth nonlinearity like in the van der Pol case. A good comparison to mechanics is a flywheel, where a short periodic “kick” keeps the wheel spinning. A classic Q like in the linear or at least almost linear case makes no sense here.

A suggestion that can also be used in the case of nonlinearities is the idea of Wang and Roychowdhury [3] to define a meaningful Q by the following process:

1. Let a nonlinear system start up and reach an equilibrium, strictly periodic state (no chaos allowed, this is essential. The phase plane contour must be a single closed line of thickness zero and no intersections).
2. Apply a small amount of extra energy to the circuit (method is unimportant as long periodicity is maintained, you could use more bias, more collector voltage, whatsoever). The amplitude of

the oscillations should increase. This is more subtle than it sounds, because in a resonator system with hysteresis (nonlinear crystals with DLD, e.g., this is not guaranteed).

3. After removal of the extra stimulus, the amplitudes should fall back to the original oscillation waveshape and amplitude. The time constant of this decay (assumed exponential but this does not have to be the case) can be used to define an “operating point Q” (hence called  $Q_{OP}$ ) as

$$Q_{OP} = \frac{\text{Extra Energy Applied}}{\text{Extra Energy Dissipated in 1 Cycle}}$$

The following properties of this  $Q_{OP}$  definition are noteworthy:

1.  $Q_0$  is dependent just on the resonator,  $Q_{OP}$  depends on the complete circuit
2.  $Q_{OP}$  is operating point and amplitude dependent,  $Q_0$  is not
3.  $Q_{OP}$  assumes that the oscillator output is strictly periodic with a single characteristic frequency. Any deviation from this requirement (subharmonics, sragging, b-Mode, chaos, hysteresis, ...) make a definition of  $Q_{OP}$  meaningless.  $Q_0$  is always well defined.
4. There are no combination rules like  $Q_{eff} = Q_1 Q_2 / (Q_1 + Q_2)$  for combined nonlinear resonators. Such rules *only work for the linear case*.

When thinking of the Leeson formula,  $Q_{OP}$  is the term that should be used instead of the term loaded  $Q_L$ , because it does have a measurable and well-defined derivation from physics, which the classic  $Q_L$  term does not have. Derivations relating  $Q_0$  and  $Q_L$  by the idea of a power match are heuristic and have no derivation traceable to physics for larger amplitudes.

A key advantage of  $Q_{OP}$  is the fact that it can be exactly measured, which ends the fitting/guessing game necessary to obtain plausible phase noise curves with an educated guess on  $Q_L$ .

Sample measurements were done running an LC and a crystal sample oscillator and by measuring the decay time constant.

A sample result of a measurement of an AT crystal is shown below:

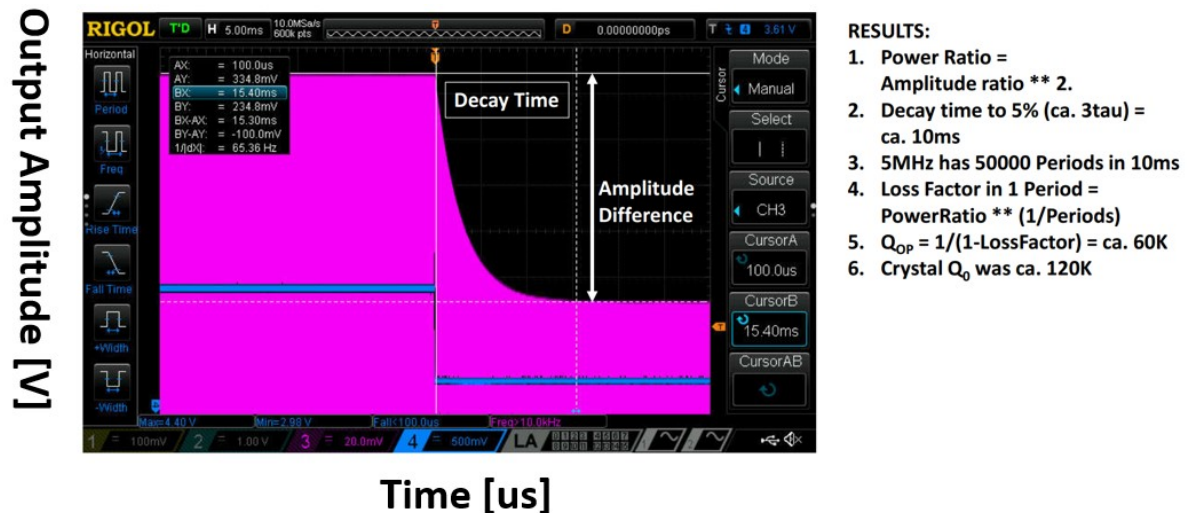


Figure 113 - Measuring QOP from the Delay Time Constant of an Oscillator

Measuring low-Q resonators is not possible when the decay times approach the rise and fall times of the bias applied (here: 5us). This unfortunately excludes LC oscillators where Q is just a few hundred.

Bias rise and fall times cannot be reduced beyond limits because RF blocking capacitors must stay in place to ensure that the collector, e.g., is grounded regarding RF signals.



A Caveat: Normal power supplies have rise and fall times that are much longer than 5 $\mu$ s. This is a consequence of output filter capacitors that are built-in into lab power supplies to reduce ripple and to guarantee a low output impedance at frequencies where the regulating loop inside has no or little gain anymore.

The solution is to use a standard low frequency waveform generator, and to amplify the output voltage with a precision power amplifier having a bandwidth of at least 300kHz. This method was chosen here. A Rigol DG1022Z LF generator [4] created the square wave signals with a few seconds repetition rate and rise times of 10ns, and a discrete booster amp amplified the output up to +30V/150mA, enough for the oscillators we tested. The base voltages were low enough so that they could be used directly from the LF generator, or another precision power amp could be used.

The schematics of the power amp is shown below:

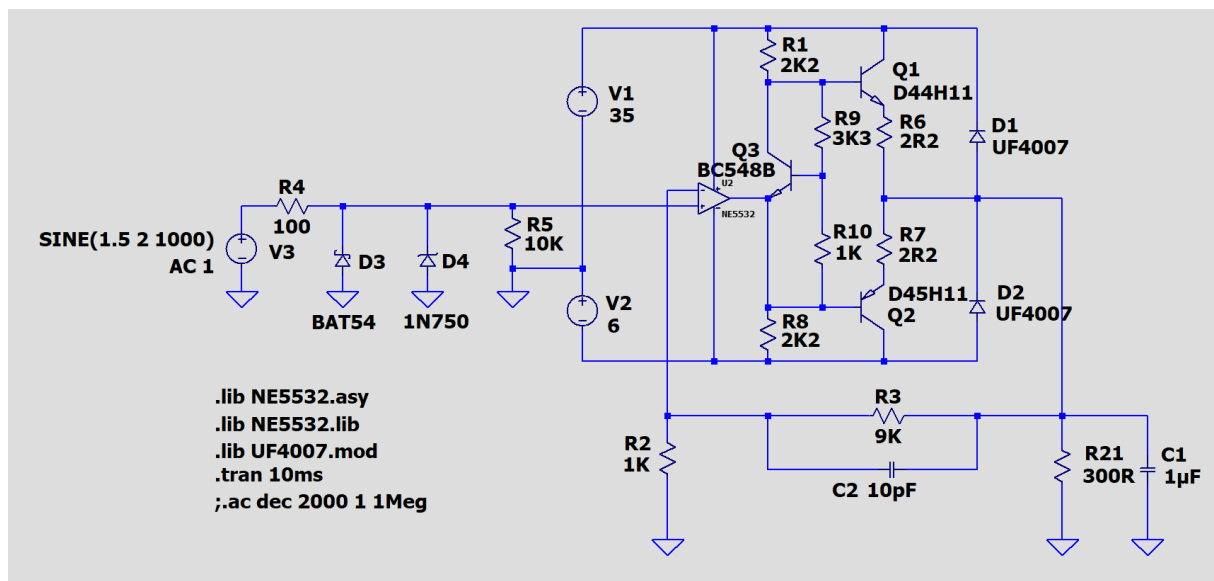


Figure 114 - DC Power Amp to Drive Oscillator Voltages

The circuit is a straightforward compensated op amp stage driving a complementary output buffer made from Q<sub>1</sub> and Q<sub>2</sub>. Q<sub>3</sub> sets the bias so the final stage operates with low crossover distortion. The voltage gain is set by R<sub>2</sub> and R<sub>3</sub> and is set to 10. C<sub>2</sub> is used for frequency response tuning.

The NE5532 op amp is a classic high voltage type commonly used in audio amplifiers [5]. It features low noise, low distortion, a gain bandwidth product of 10MHz and is a low-cost part.

The transistors in the final stage (D44H11, D45H11) are fast power types with maximum currents of 10A and transition frequencies 50MHz [6]. Note the asymmetric power supplies so an output voltage range of 0 to 30V can be accommodated without clipping (all oscillators and buffers are normally operated with positive supplies only). Input resistance is 10kOhms, and input is protected by D<sub>3</sub> and D<sub>4</sub>. R<sub>6</sub> and R<sub>7</sub>, along with Q<sub>3</sub> work as an output current limiter as well. Further limiting is provided by an LM723-based power supply regulator with current limiting (not shown).

To avoid oscillations, it can be necessary to insert a small damping resistor before the load. This resistor was not included as a fixed component to allow fastest rise times with ohmic or low-capacitance loads. It can be added externally.

A simulation shows that 0 to 30V are produced into 300Ohms without clipping:

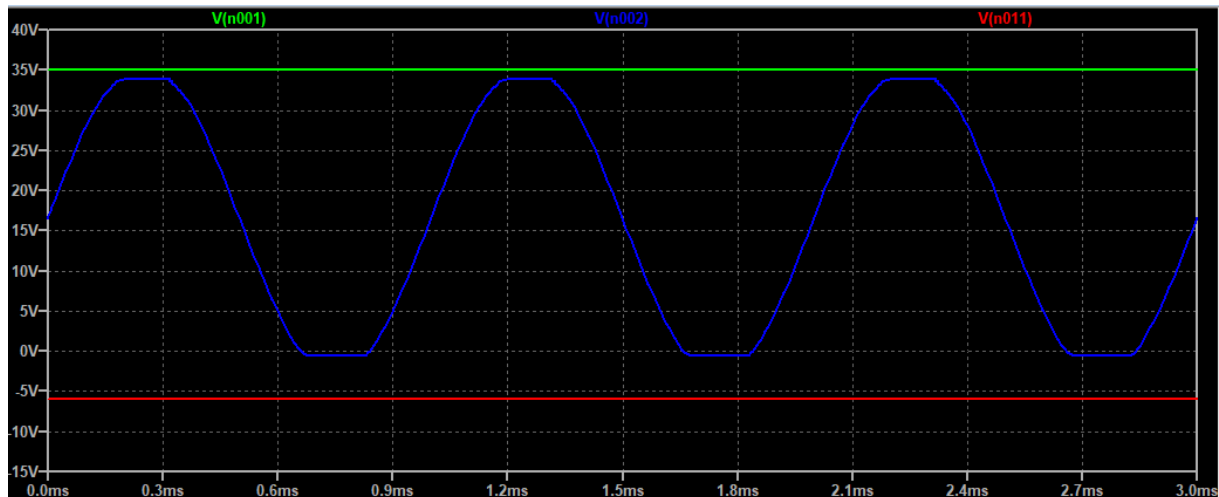


Figure 115 - DC Power Amp Overdriven Waveforms – Simulation. The blue curve shows the output waveform. Supply limits are in red (lower) and green (upper).

Clipping occurs below 0V (by the input diode  $D_3$ ) and at 33V (by saturation of  $Q_1$ ), so we have enough safety margin here.

Dynamic behavior is also important because we plan to drive oscillator circuits that contain RF blocking capacitors, e.g., so we have capacitive loads ( $C_1$  above). If we have 100nF, the rise and fall times are shown below:

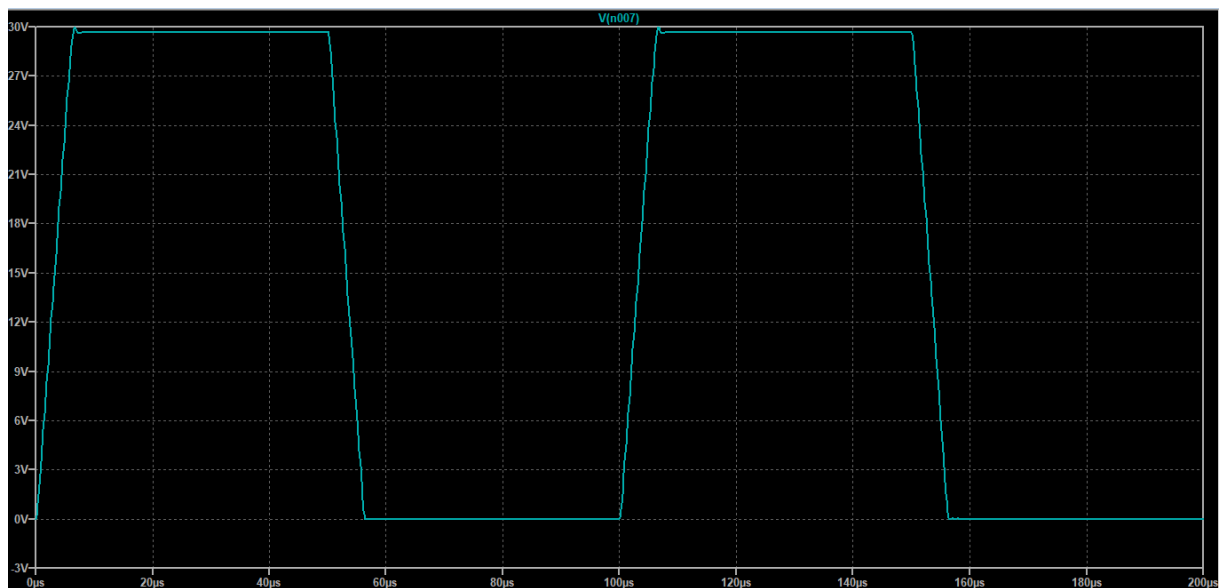


Figure 116 - Rise and Fall Times with Capacitive Load - Simulation

It is 6.5µs from 0 to 30V and 6µs from 30V back to zero. At 100nF, overshoot is minimal. The rise time is small enough to test the Q time constant for all crystal oscillators measured.

To verify the rise times, a square wave was injected into 300Ohms with no capacitance. The result is shown below:

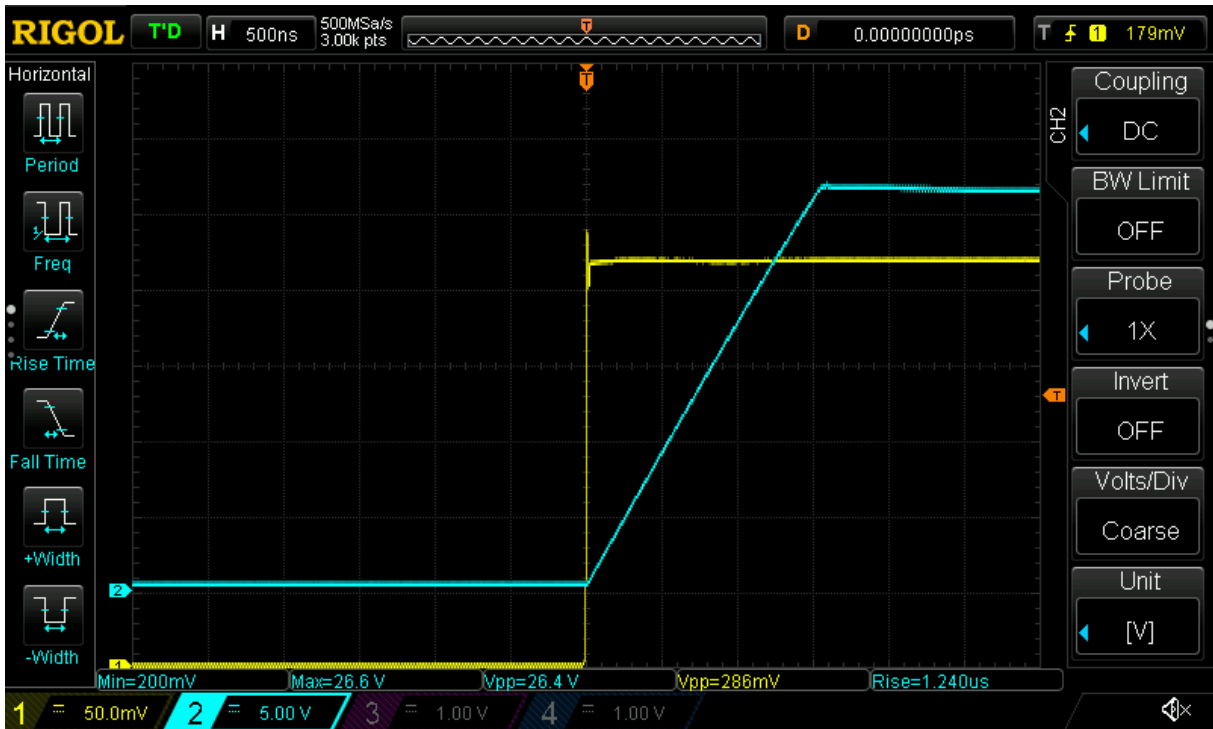


Figure 117 – Rise time with 300Ohms Ohmic Load - Measurement

Without the capacitor, we have 1.24us here. The difference is explained by the current absorbed by the capacitive load (100nF at 30V in 6us draw 500mA). With 100nF in parallel with 300Ohms (100mA range) plus a series resistor of 100Ohms shows this:

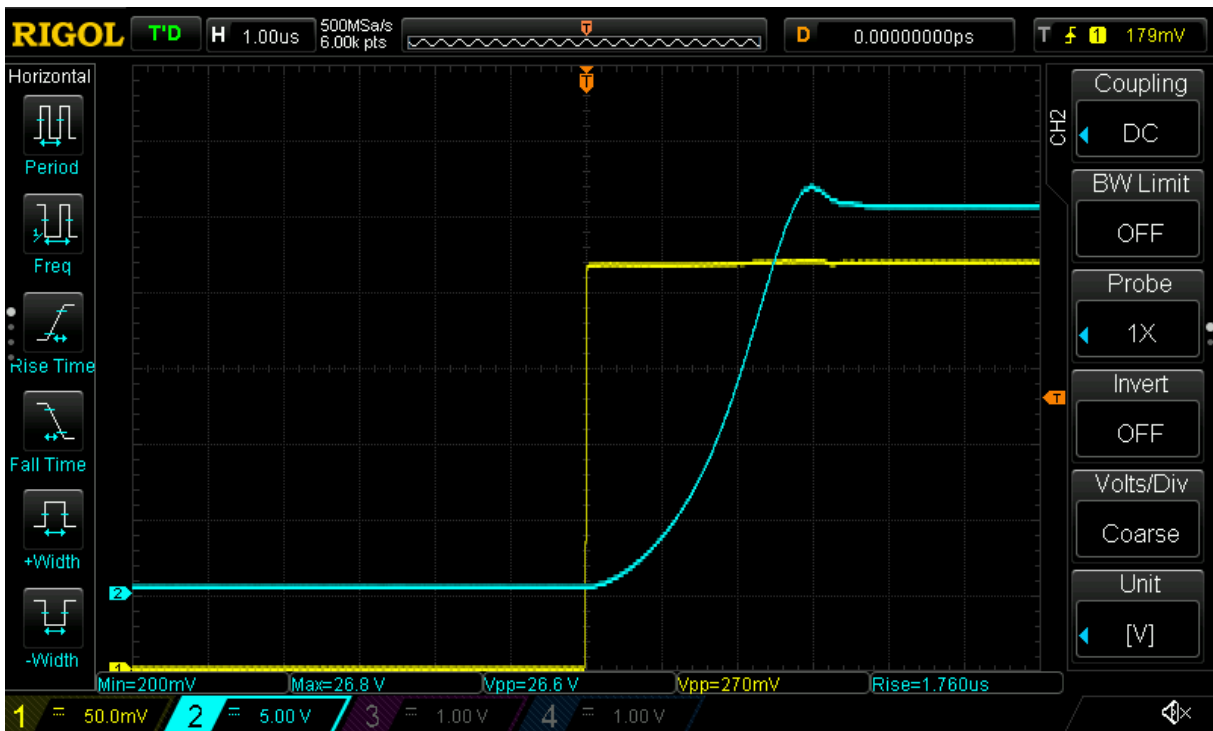


Figure 118 – Rise time with Ohmic and Capacitive Load – Measurement

Rise time has increased to 1.76us. There is a moderate overshoot for one microsecond. The observed voltages on the scope screenshots above confirm that we are fast enough for the measurements we need to do.

## References

- [1] B. van der Pol, "On oscillation hysteresis in a triode generator with two degrees of freedom," *Philos. Mag.*, vol. 6, no. 1922.
- [2] Ulrich L. Rohde, "A New and Efficient Method of Designing Low Noise Microwave Oscillators," TU Berlin, Berlin, 2004.
- [3] Tianshi Wang and Jaijeet Roychowdhury, "Rigorous Q Factor Formulation and Characterization for Nonlinear Oscillators." Cornell University, Oct. 04, 2017, Accessed: Nov. 25, 2020. [Online]. Available: <https://arxiv.org/pdf/1710.02015.pdf>.
- [4] Rigol, "Rigol DS1000Z Series Oscilloscope Datasheet." Accessed: Nov. 17, 2020. [Online]. Available: <https://www.rigol-uk.co.uk/jg/wp-content/uploads/2020/09/Rigol-DS1000Z-Datasheet.pdf>.
- [5] Texas Instrument, "NE5532 Dual Low-Noise High-Speed Audio Operational Amplifier Datasheet." Accessed: Nov. 25, 2020. [Online]. Available: <https://www.ti.com/product/NE5532>.
- [6] On Semiconductor, "D44H11 D45H11 Power Bipolar Transistors Datasheet." Accessed: Nov. 25, 2020. [Online]. Available: <https://www.onsemi.com/products/discretes-drivers/general-purpose-and-low-vcesat-transistors/d44h11>.

## 5.5 Phase Noise Measurement Techniques at 5MHz

Phase Noise Measurement Techniques discusses the methods available to measure phase noise and their implementations in practical instruments. Sensitivity and precision of the available instruments has increased drastically over the recent years; for ultra-performance oscillators the frontier lies at  $10^{-14}$  (tau for 1s) and uses cryogenic references, hardware mixers and correlators.

Accurate phase noise measurements are difficult due to the fact that large (carrier) and very small signals (phase noise) need to be measured in close spectral vicinity. For a top performance USO like the RAKON 5MHz HSO14 with a 1Hz offset phase noise of -130dBc the measurement precision should be better than 140dBc, or less than  $10^{-14}$  Allen deviation for 1s (see [1] for a datasheet). This chapter discusses the evolution of phase noise measurement techniques and test equipment over time and the performance levels achieved, plus the effects that impose limits on the accuracy that can be guaranteed. Techniques and equipment that are restricted to frequencies outside of 5MHz are not discussed.

### 5.5.1 The Discovery of Phase Noise

One of the first encounters with the disturbing effect of phase noise was the observation that reflected radar signals showed an inexplicable jitter, making the distance measurement to the targeted object inaccurate. Leeson [2] derived a mathematical explanation of what happened, resulting in the famous Leeson formula relating the phase noise to physical quantities like a resonator Q, oscillator power, noise figures, and so on. In a few words, inevitable nonlinearities in the operation of an oscillator mix noise components anywhere in the spectrum into the carrier frequency (see Rubiola, [3]).

### 5.5.2 Measuring Phase Noise – Spectrum Analysis

An obvious approach to measure the phase noise would be to use a classic spectrum analyzer, tune it to the oscillator center frequency and setting it to the smallest IF bandwidth available (1Hz in most cases). What you then get is a carrier signal at the center, plus some sidelobes left and right containing the phase noise components. This approach is possible, but only usable for rather low-performance oscillators. Here is why:

The noise at the end of the spectrum analyzers IF strip contains phase noise from your DUT, but also phase noise from the local oscillator(s) inside the spectrum analyzer. While standard units (e.g., Keysight N9000A CXA, [4]) have noise floors of only -110dBc at 10kHz, premium analyzers go below -135dBc at 10kHz (Keysight UXA, R&S FSW, [5]). Close to carrier phase noise is a lot worse than that and often not even specified. These values are orders of magnitude worse than even mediocre crystal oscillators. The local oscillator in a spectrum analyzer is based on VCO, PLL, DDS, and/or YIG, technology, so it does not have the spectral purity and low phase noise of a high-class crystal USO signal.

1. The spur free dynamic range (SFDR) of classic spectrum analyzers ranges from around 70dBc (standard units) to up to 85dBc (top instruments, R&S FSW/FSWP [5], Keysight UXA [6]). This range is not sufficient to measure signal to noise ratios that can easily exceed 100dB. Anything below the SFDR could be an artefact.
2. Frequency resolution of most spectrum analyzers is limited to 1Hz. ADEV measurements to 10s are therefore not feasible with such a spectrum analyzer.
3. Some commercial spectrum analyzers (e.g., Keysight X-Series) provide licensed software to make automatic phase noise plots within the instrument, but as shown these tools are strictly for low-quality oscillators.
4. Noise bandwidth and flat or gaussian filter bandwidth are not the same and this introduces some systematic measurement error (which some analyzers can correct automatically).

### 5.5.3 Measuring Phase Noise – The Phase Shifter Method

An idea that works without the use of a local or other external oscillator is the phase shift method. The input signal is split in two by a power splitter, one branch is sent to a delay line and the other to an adjustable phase shifter (compensating the delay line and creating a 90° phase angle). Then, both branches are mixed, and the baseband signal is filtered and analyzed by an FFT signal analyzer.

The block diagram is shown in below, from [8], p38.

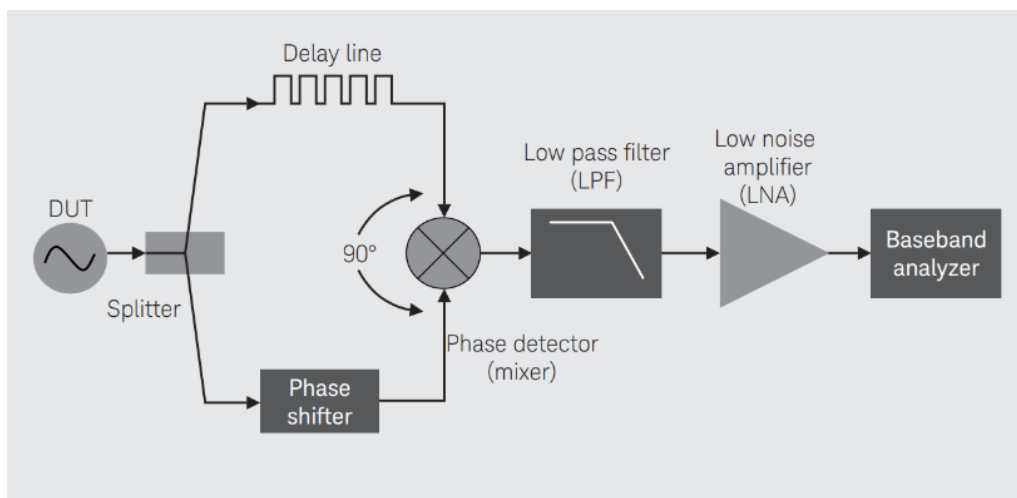


Figure 119- Measurement Setup for a Phase Shifter Phase Noise Measurement. Photo from [8].

The disadvantage of the method is that the length of the delay line limits the offset frequency range that can be measured. Another negative point is the minimum oscillator power needed to run the mixer in its usable power range (ca. 7dBm for standard parts, up to 27dBm for extremely high-performance mixers). The delay line and the phase shifter are lossy, and those losses must be balanced and create noise. To my knowledge, no commercial system that still uses this method today for HF frequencies.

#### 5.5.4 Measuring Phase Noise – The Mixer Method

This method is still in used today. You need an exceptionally good LO to get acceptable results, however. The input signal is mixed with an LO signal at the same frequency with the input signal. The down converted signal is filtered and used to tune the LO frequency and phase to the input signal. The remaining mixer output signal must be noise, but from both the DUT and the LO. This noise is FFTed and displayed.

The block diagram is shown below, from Rohde ([7], p2):

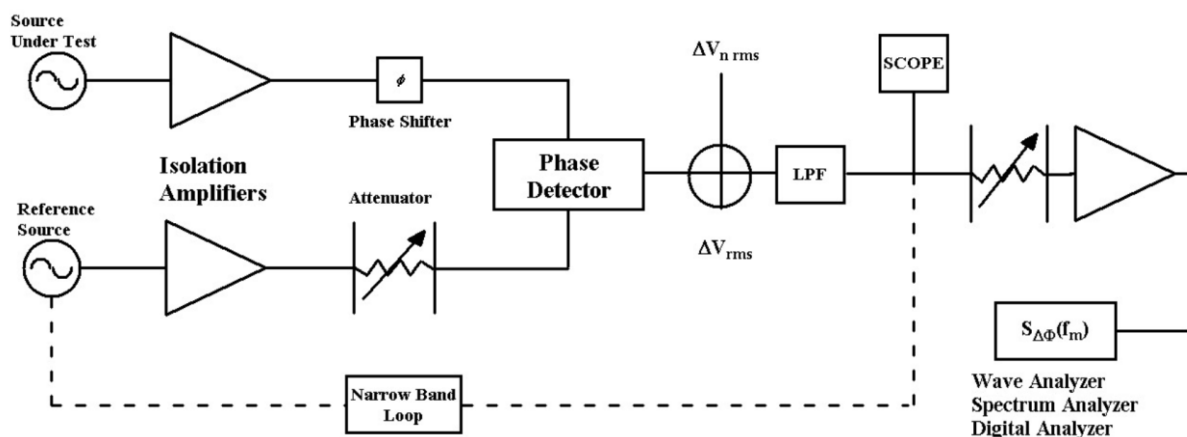


Figure 120- Phase Noise Measurement Using an LO Reference and a Mixer  
Photo from Rohde, [7]

The disadvantage of the method is the dependence on a premium LO, preferable a lot better than the DUT oscillator. For very long ADEV times the filter loop bandwidth becomes a limit to the retuning the LO.

#### 5.5.5 Measuring Phase Noise – Modern Correlator Analyzers

With oscillators getting better and better the measurement instruments had to stay ahead of the phase noise of the test objects. A widespread approach is to employ two independent high-quality local oscillators and mixers and to filter the DUT noise out of the baseband result using correlation techniques. The noise from the two independent LOs will cancel out if integration time is increased, and only the DUT noise will remain. This concept is employed by the leading phase noise test instruments like the R&S FSWP, or the older FSUP. Keysight E5052B series would be usable as well in principle but needs a minimum of 10MHz carrier frequency. With a 0dBm source, measurements very close to the thermal noise floor of -177dBc (L(f) single sideband) become possible. Close to carrier noise levels can be measured down to approximately -125dBc at 1Hz offset at 5MHz under normal lab conditions.

A block diagram is shown below from [8]:

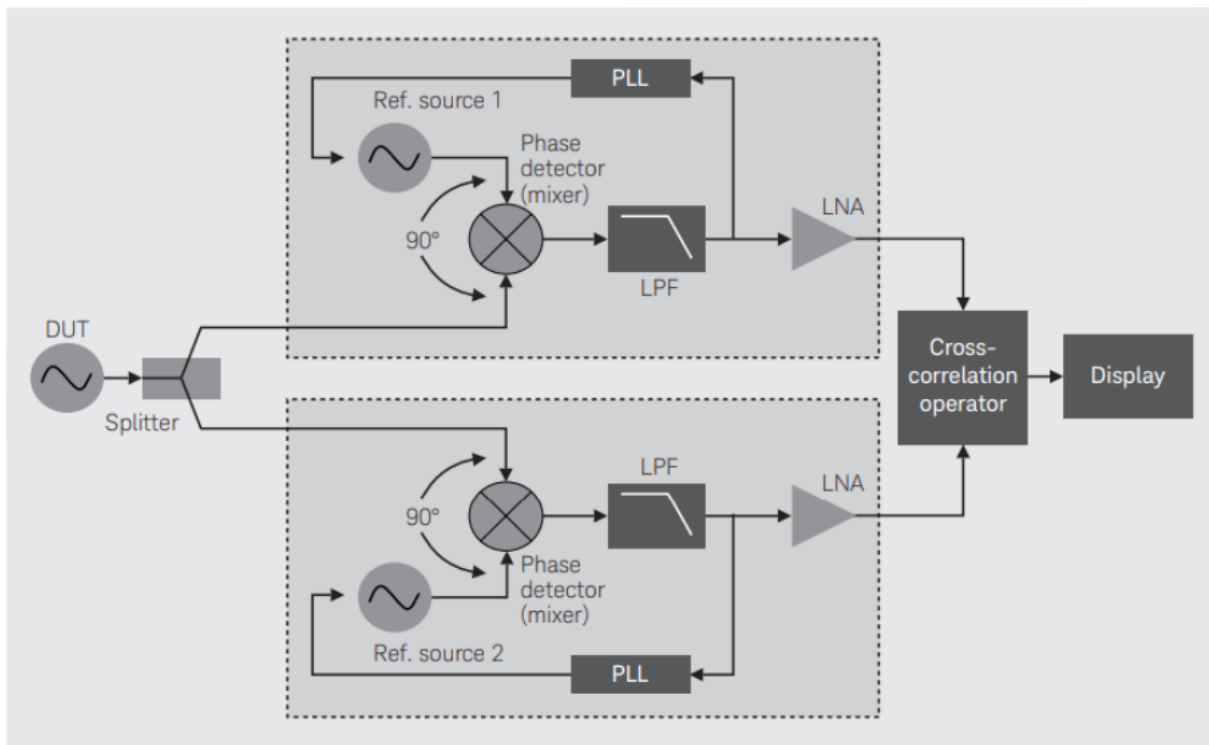


Figure 121- The Operation of Modern Correlating Phase Noise Analyzers  
Picture from [8] p39

It should be noted that the phase noise of the two internal sources does cancel out on average, but that would need many correlations if the LO noise is significantly larger than the DUT noise.

The total noise  $N_{MEAS}$  can be expressed by the formula:

$$N_{meas} = N_{DUT} + \frac{N_1 + N_2}{\sqrt{M}}$$

Where  $N_{DUT}$  is the noise factor of the DUT,  $N_1$  and  $N_2$  are the noise contributions of the internal reference sources and  $M$  is the number of correlations.

For extremely low noise DUTs, this is not a practicable option. The number of correlations cannot be indefinitely increased because the assumption that the two LOs are absolutely independent holds only up to a correlation factor of ca. 100 for the FSWP [9].

### 5.5.6 Measuring Phase Noise – Measuring Extreme Performance USOs

Extreme performance parts need specialized hardware to lower the measurement instrument phase noise figure low enough so that the DUT phase noise can be identified with confidence. The system that was employed to measure the HSO14 and other extreme performance USOs employed the following components:

1. A cryogenic sapphire whisper-gallery reference oscillator source (CSO) with (divided) 5MHz and an Allen deviation of  $1E-14$  for 1 and 10 seconds. Phase noise at 1Hz was below -140dBc. For the technology, see Giordano [10].
2. A mixer/digitizer hardware [11] with no built-in sources. This hardware can accommodate not just one reference source, but also several USOs. It is possible, e.g., to use 3 or 4 HSO14s as reference sources for a new DUT USO. The frequency of the references can be different from each other and from the DUT frequency, which is a big advantage.



3. A PC to do the correlations. The workload for a HSO14 measurement using a CSO is 8 hours according to the paper of the design team [12].
4. Last, but absolutely not least an absolutely perfectly shielded environment is mandatory. This applies to electric, magnetic, mechanic and temperature conditions as well as lab equipment like cables, connectors, power supplies, ...

A test setup using three BVA USOs is shown below (From a Microsemi Application Note AN3526, see [12]):



*Figure 122 - Test Setup for a 3-Oscillator Correlation Phase Noise Measurement  
Picture from [12]*

On top we see the DUT, and the two reference oscillators, all BVA USOs. The silver box is the mixer/ADC hardware, and the PC at the right does the correlation and the graphics.

The downside of the architecture is a limited frequency range from 1 to only 200MHz, the need for top performance and very expensive external references as well as a powerful external computer to keep correlation times acceptable.

### 5.5.7 Measuring Phase Noise – The Direct Method using a Precision Counter

A completely different approach from the spectrum-based measurement methods discussed so far are direct timing measurements. Provided we have a counter with an extremely high resolution at hand, we could directly measure the time of two consecutive zero transitions of our test signal and its variance, which leads directly to an estimate of the Allen deviation.



A counter product from Keysight, the 53230A [13], has a 20ps resolution that can be used to measure the Allen deviation of oscillators. A photo of the instrument is shown here:



Figure 123 - Keysight 53230A Counter with 20ps Resolution. Picture from Keysight Website [13]

The instrument also comes with a MATLAB PC application to present the measured values in an Allen deviation diagram. As the 20ps resolution suggests, the end of the measurable range is in the ballpark of  $10^{-11}$ , so it is not suited for real USOs. A possibility (hopefully not needed) is to measure higher order deviation measures like the 3-point Hadamard deviation.

What it is good for, however, are long-term stability measurements. The counter uses a sliding window technique to increase measurement rate and accuracy, so measurements down to a mHz are possible at frequencies of 5 or 10MHz. Despite the internal OCXO, a GPS input source is needed to achieve a mHz accuracy. This instrument was also used to determine the sensitivity of the output frequency of commercial USOs on XYZ orientation, and that worked well.

## Conclusions

The development of phase noise measurement techniques has made huge progress over the past few decades. The technological limits of today's (national standards grade labs) test equipment allow even the best oscillators to be measured reliably, but with considerable cost and effort.

Unfortunately, we have no access to the extreme performance equipment described. With the very good, but not cutting-edge crystals we have to work on the limits of the R&S FSWP instrument are absolutely acceptable.

## References

- [1] RAKON Corp., “Ultra Stable Oscillators HSO14 and HSO13 for Ground Based Applications.” Accessed: Nov. 19, 2020. [Online]. Available: <http://www.rakon.com/corporate/about/news/43-rak-news-product/432-rakon-introduces-ground-station-uso>.
- [2] D. B. Leeson, “Oscillator phase noise: A 50-year retrospective,” in *2015 Joint Conference of the IEEE International Frequency Control Symposium & the European Frequency and Time Forum*, Denver, CO, USA, Apr. 2015, pp. 332–337, doi: [10.1109/FCS.2015.7138853](https://doi.org/10.1109/FCS.2015.7138853).
- [3] E. Rubiola, *Phase noise and frequency stability in oscillators*. Cambridge, UK ; New York: Cambridge University Press, 2009.
- [4] Keysight Inc., “CXA X-Series Signal Analyzer N9000A Datasheet.” Accessed: Nov. 26, 2020. [Online]. Available: <https://www.keysight.com/us/en/assets/7018-02222/data-sheets/5990-4327.pdf>.
- [5] R&S, “R&S FSWP Phase Noise Analyzer Specifications.” Accessed: Nov. 17, 2020. [Online]. Available: [https://scdn.rohde-schwarz.com/ur/pws/dl\\_downloads/dl\\_common\\_library/dl\\_brochures\\_and\\_datasheets/pdf\\_1/FSWP\\_d\\_at-sw\\_en\\_3607-2090-22\\_v0900.pdf](https://scdn.rohde-schwarz.com/ur/pws/dl_downloads/dl_common_library/dl_brochures_and_datasheets/pdf_1/FSWP_d_at-sw_en_3607-2090-22_v0900.pdf).
- [6] Keysight Inc., “N9040B UXA X-Series Signal Analyzer, Multi-touch Datasheet.” Accessed: Nov. 26, 2020. [Online]. Available: <https://www.keysight.com/us/en/assets/7018-04541/data-sheets/5992-0090.pdf>.
- [7] Ulrich L. Rohde et al., “Phase Noise Measurements and its Limitations.” Accessed: Nov. 26, 2020. [Online]. Available: [https://www.synergymwave.com/articles/2013/04/full\\_article.pdf](https://www.synergymwave.com/articles/2013/04/full_article.pdf).
- [8] Keysight Inc., “Phase Noise 101: Basics, Applications and Measurements.” Accessed: Nov. 26, 2020. [Online]. Available: [https://www.keysight.com/upload/cmc\\_upload/All/20180720\\_KEE7\\_PhaseNoise.pdf](https://www.keysight.com/upload/cmc_upload/All/20180720_KEE7_PhaseNoise.pdf).
- [9] A. Roth (R&S), “FSWP Internal Oscillator Independence.” Private communication, Nov. 26, 2020.
- [10] V. Giordano et al., “The Autonomous Cryocooled Sapphire Oscillator: A Reference for Frequency Stability and Phase Noise Measurements,” *Journal of Physics: Conference Series*, 723, 2006
- [11] Microsemi Inc., “53100A Next Generation Phase Noise Analyzer.” Accessed: Nov. 26, 2020. [Online]. Available: <https://www.microsemi.com/product-directory/phase-noise-and-allan-deviation-testers/5565-53100a>.
- [12] Microsemi Inc., “Dual Reference Noise and Stability Measurements with the 53100A Phase Noise Analyzer Application Note AN3526.” Accessed: Nov. 26, 2020. [Online]. Available: <https://www.microsemi.com/product-directory/phase-noise-and-allan-deviation-testers/5565-53100a#resources>.
- [13] Keysight, “Keysight 53220A/53230A 350 MHz Universal Frequency Counter/Timer.” Accessed: Nov. 19, 2020. [Online]. Available: <https://literature.cdn.keysight.com/litweb/pdf/53220-90001.pdf>

## 6 Simulation Problems and Strategies

When working on space-grade USO oscillator design topics (using extremely high-Q crystals) a very common problem is that the circuits fail to be simulated either completely or the simulations take prohibitively long. The predictions of simulators regarding waveforms, output amplitudes and even noise (where not fitted a posteriori) are notoriously off the results obtained by measurements. An explanation why these rather simple circuits are so hard to simulate and what can be done to improve the situation is badly needed. The problems encountered apply to both time domain and frequency domain simulators.

### 6.1 A stripped-down Circuit to test Simulators

Practical circuits contain quite some components that are needed (ALC, mode suppression, ...) but are not the root cause why simulations fail (just try this). To explain what is going wrong, a very basic circuit has been used in order to characterize simulation results.

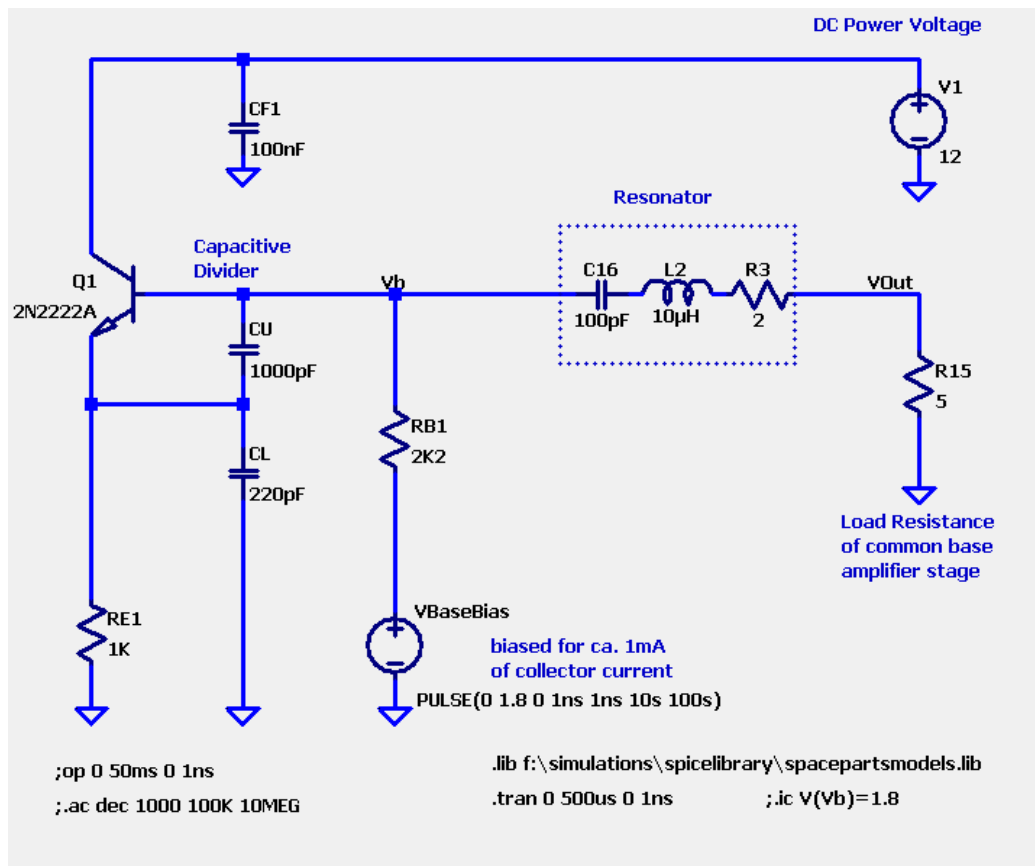


Figure 124 - Simple Clapp Oscillator to Test Simulators

The resonator in this schematic can be anything from an SC cut space-grade crystal (5MHz,  $L=8.44\text{H}$ ,  $C=0.12\text{fF}$ ,  $R=80\text{Ohms}$ ,  $Q$  ca. 2.5Millions) to a cheap AT-cut part ( $L=\text{ca. } 80\text{mH}$ ,  $C=12\text{fF}$ ,  $R=50\text{Ohms}$ ,  $Q$  some 10K) or an LC tank as shown above. Following a Rohde design [1], the crystal is used as a resonator and a filter at the same time; the output goes directly into a low-impedance input of the next stage, a common base amplifier. This trick results in an exceptionally clean signal with low close-to-carrier noise, caused by the very small resonator bandwidth.

### 6.1.1 Simulators and Q Values

Simulator (LTSpice handbook see [2], but online information is more current) parameters were left at their defaults (discussed later), and the maximum timestep was set to 1ns, which is 1/200 of a full oscillation period. When starting with a low-Q LC circuit and increasing the resonator Q step by step, without changing other parameters, the following effects can be observed:

1. The higher Q is, the longer the oscillator takes to start up. This is in line with the (linearly) derived rule-of-thumb that the startup time constant is approximately  $Q/(2*\omega)$ .
2. At some Q (ca. 1000), the startup time in the simulator takes a lot longer than expected
3. The simulation times become prohibitive above Q of ca. 25.000 (tens of minutes on a modern PC workstation (8-Core i7,4GHz) using LTSpice.
4. At some Q values above ca. 100K there is no startup at all.
5. Startup depends on the values of the capacitive divider. While all combinations (even silly ones) seem to work in practice, they fail in the simulators.
6. Predicted waveforms were completely off from measured results, surprising for such a primitive schematic.
7. Tuning simulation parameters (RELTOL, ABSTOL, GMIN...), minimum timestep or integration method (TRAP, Mod TRAP, GEAR) does not change much.
8. Changing transistor models also does not make qualitative changes.
9. Frequency-Domain (Harmonic Balance) Simulators (like Ansoft Serenade) cannot model startup. They also fail to simulate some capacitor combinations, and their predictions of power and waveforms are equally inaccurate. This problem is also Q dependent and manifests itself by the program being unable to find a starting point with negative impedance and a zero-phase crossing.

Valuing the facts above the idea is the principal difficulty must be some immanent mathematical property of the equation systems we want to solve, and not something we need to look for in special component values or SPICE models. A look at a few design aspects will make this plausible.

## 6.2 Oscillator Abstractions

When we look at the resonator and the load (input impedance of the following stage) we see a pure passive circuit made from an inductor, a capacitor and a (internal and load) resistor. If we ask for oscillations, the base point must present a negative resistance of at least the same value as the internal resonator resistance and the load. Using a classic transistor h model, this (small signal) negative resistance has the value of

$$Z_{IN} = -g_M X_{CU} X_{CL} \text{ with } g_M = \frac{I_C}{V_T}$$

$I_C$  is the collector current and  $V_T$  is the temperature voltage  $kT/q$ . For larger amplitudes, the negative input resistance will become smaller until at a certain amplitude it will become the same as the positive resistances, stopping the growth of the oscillation amplitudes. In a real-life transistor, we have many amplitude-limiting effects, like

1. The onset of base current clipping amplitudes (normal)
2. Transistor saturation (no more  $I_C$  because  $V_{CE}$  drops to zero, unwanted when too deep)
3. Negative breakdown of  $V_{BE}$  junction (should never happen, destructive)
4. Reduction of  $g_m$  due to high current effects (not ideal for phase noise, to be avoided)

Some of these effects are extremely hard to handle accurately in a simulator; For our simulation startup problems it is clear, however, that the exact form of limiting is unimportant for the simulation troubles, simply from the fact that at startup the amplitudes are almost zero so that no limiting level is ever reached. Note that the following derivations have been discussed in the “oscillator principles”

chapter, but now we work towards realistic resonator values. We could therefore use a simple (cubic, starts late enough) nonlinear term to incorporate nonlinear damping into our model. From an AC perspective, the circuit now looks like this (a type of a van der Pol equation [3]):

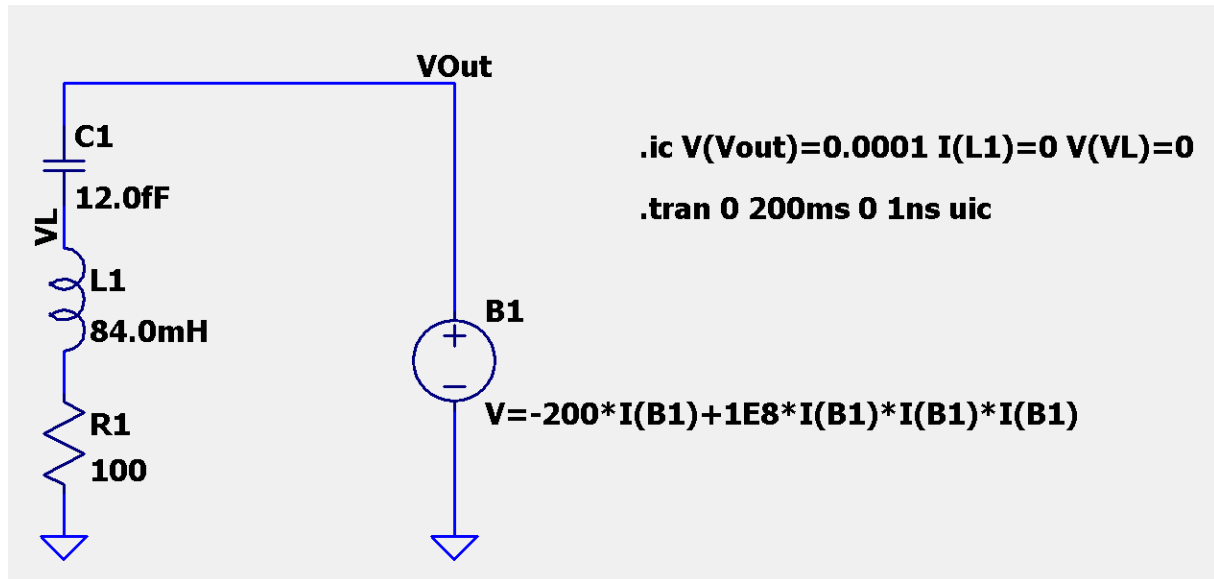


Figure 125 - Nonlinear Van der Pol Oscillator for Simulation

The “behavioral” voltage source incorporates the negative resistance and the cubic damping factor, the rest is a resonator with a Q of about 25.000. When we treat this analytically using the KVL, we get an equation like

$$RI + LI' + \frac{1}{C} \int_0^t Idt + \alpha I + \gamma I^3 = 0$$

where R, L and C are the resonator parameters and  $\alpha$  and  $\gamma$  are the parameters of the nonlinear resistance. Differentiating over time, normalizing, and reordering gives a van der Pol type equation:

$$I'' + I'(a + bI^2) + \omega_0^2 I = 0$$

where

$$a = (R + \alpha)/L, b = 3\gamma/L \text{ and } \omega_0^2 = 1/(LC).$$

As all sufficiently interesting nonlinear circuits, the van der Pol equations have no closed form solution.

Any useful *oscillator* design must be *unstable* and capable to start itself from a powerless, steady state (e.g.,  $I=0$ , and  $I'=0$ ). Heuristically, we can assume that I is so small at startup so that the square I term can be neglected. The equation then becomes a linear harmonic oscillator:

$$I'' + aI' + \omega_0^2 I = 0$$

and the conditions for an increasing amplitude over time is that the total damping is negative, meaning that a is smaller than 0 and subsequently

$$\alpha < -R$$

must be fulfilled. Then we get a solution over time of the form:

$$I(t) = e^{-\delta t} \{ I_{t=0} \cos(\omega_d t) + (I_{t=0} \delta + I'_{t=0} \sin(\omega_d t) / \omega_d) \}$$

Where

$$\delta = a/2 \text{ and } \omega_d^2 = \omega_0^2 - \delta^2$$

If we assume that

$$I_{t=0} = 0 \text{ and } I'_{t=0} = 0$$

the consequence is that the current  $I$  will always be zero, too, not what we like. We seem to need an external stimulus, even if the damping is negative. For a more profound analysis we can use the theory of dynamic systems to assess the fixed point (there is only one) of the van der Pol equation and its stability. To do this, we convert the second order differential equation into a set of two differential equations by substituting a variable  $X = I'$ . We then get (by substituting into the original equation and solving for  $X'$ ):

$$\begin{pmatrix} I' \\ X' \end{pmatrix} = F(I, X) = \begin{pmatrix} f_i(I, X) \\ f_x(I, X) \end{pmatrix} = \begin{pmatrix} X \\ -X(a + bI^2) - \omega_0^2 I \end{pmatrix}$$

which is a just a reformulation as a system of two first-order differential equations where we can compute the derivatives  $I'$  and  $X'$  at a given point from the coordinates  $I$  and  $X$ , using the vector function  $F$ . If we ask for local properties, we need to take the total derivative (the Jacobian matrix) of our equation system, by  $I$  and  $X$ , like

$$J = \begin{pmatrix} \frac{df_i(I, X)}{dI} & \frac{df_i(I, X)}{dX} \\ \frac{df_x(I, X)}{dI} & \frac{df_x(I, X)}{dX} \end{pmatrix} = \begin{pmatrix} 0 & 1 \\ -2XbI - \omega_0^2 & -(a + bI^2) \end{pmatrix}$$

The Jacobian acts as a “tangent” to our matrix function at a given point [4] and can be used to approximate the vector function in the vicinity of the point we have computed the Jacobian for.

The Eigenvalues of this matrix determine the local behavior around a given point (see [5] for a practical introduction about this). Several possibilities exist:

5. All Eigenvalues have a real part smaller than 0. This corresponds to a stable point where a neighboring point to our given starting point move closer to the given point over time (a “sink”).
6. If one Eigenvalue is 0, we have a “saddle point” some points around move in, and some out. The other Eigenvalue determines the direction.
7. If both Eigenvalues have a real part  $> 0$ , we have a “source” where points would move away from the starting point.
8. Imaginary Eigenvalue components indicate a rotation of a neighboring point around the point  $(I, X)$ . Together with the sign of their real parts we get inbound or outbound spirals.

If we compute the equation for the Eigenvalues of  $J$  we obtain

$$\text{Det}(J - \lambda E) = \begin{vmatrix} -\lambda & 1 \\ -2XbI - \omega_0^2 & -(a + bI^2) - \lambda \end{vmatrix} = 0$$

Solving this for  $\lambda$  results in

$$\lambda = -\frac{(a + bI^2)}{2} \pm \sqrt{\frac{(a + bI^2)^2}{4} - 2XbI - \omega_0^2}$$

For the starting fixed point with  $X = 0$  and  $I = 0$  we have:

$$\lambda = -\frac{a}{2} \pm \sqrt{\frac{a^2}{4} - \omega_0^2}$$

If we go back to the definition for our SC cut model crystal with 5MHz from the circuit diagram above, we obtain a  $\lambda$  that has a small positive real part (remember  $a$  is negative, and  $O(1)$ ) but the expression under the root is a huge negative number, giving a result which is almost completely imaginary. So, the point  $(0,0)$  is an unstable fixed point, yes, but the movement of neighboring points is a spiral with an extremely small slope, again explaining the long startup times. The derivation above confirms the common rule of thumb formula for an oscillator startup which is

$$\tau = \frac{Q}{2\omega_0} \text{ with } Q = \omega_0 L / (R + \alpha)$$

Another result (not derived here) is that the oscillations have a stable limit cycle as an attractor, plus that the simple case here has no chaotic attractors.

For a further mathematical treatment and simulation effort, it makes sense to transform the equation into a form with less parameters. If we start from

$$I'' + I'(R + \alpha + 3\gamma I^2)/L + I/LC = 0$$

The first step is to introduce a normalized time

$$T = \frac{t}{\sqrt{LC}} \text{ so we have } \frac{dI}{dt} = \frac{dI}{dT} \frac{1}{\sqrt{LC}} \text{ and } \frac{d^2I}{dt^2} = \frac{d^2I}{dT^2} \frac{1}{LC}$$

And our equation now reads:

$$\frac{d^2I}{dT^2} \frac{1}{LC} + \frac{\frac{dI}{dT} \frac{1}{\sqrt{LC}} (R + \alpha + 3\gamma I^2)}{L} + \frac{I}{LC} = 0$$

Cleaning up gives:

$$\frac{d^2I}{dT^2} + \frac{dI}{dT} \sqrt{\frac{C}{L}} (R + \alpha + 3\gamma I^2) + I = 0$$

We could get rid of some more parameters by setting

$$x = I \sqrt{\frac{-3\gamma}{R + \alpha}} \text{ remembering } \alpha \text{ is negative and larger than } R$$

Rewriting results in where the

$$\frac{d^2x}{dT^2} \sqrt{\frac{R + \alpha}{-3\gamma}} + \frac{dx}{dT} \sqrt{\frac{C}{L}} \sqrt{\frac{R + \alpha}{-3\gamma}} \left( R + \alpha + 3\gamma \frac{R + \alpha}{-3\gamma} x^2 \right) + x \sqrt{\frac{R + \alpha}{-3\gamma}} = 0$$

And finally

$$\frac{d^2x}{dT^2} + \frac{dx}{dT} \sqrt{\frac{C}{L}} (R + \alpha)(1 - x^2) + x = 0$$

If we now set

$$\varepsilon = -(R + \alpha) \sqrt{\frac{C}{L}} = \frac{-(R + \alpha)}{\omega_0 L} = \frac{1}{Q_U} \text{ where } Q_U \text{ stands for undamped } Q$$

and revert to the prime notation, now for T, we get:

$$x'' - \varepsilon(1 - x^2)x' + x = 0$$

which is the van der Pol differential equation in classic notation known for over a century and extensively treated in the literature. In fact, this is bad news because, depending on  $\varepsilon$ , this differential equation is notorious for bringing simulators to their limit.

The range of  $\varepsilon$  for the oscillator types we are trying out therefore is in the order of  $10^{-1}$  (LC tank) to  $10^{-6}$  (SC cut crystal).

So, as a conclusion for now, we have derived that the Colpitts/Clapp circuit used in USOs can be modelled by a van der Pol type nonlinear oscillator, at least when looking at the startup process.



### 6.2.1 Stiffness and Startup Values

A good reason while a differential equation is hard to solve is when it describes physical phenomena at a large range of timescales (the smallest one limits the size of the maximum timestep a simulation can use without introducing unacceptable errors). For large values of  $\epsilon$ , this can be immediately seen from the shape of the limit cycle and the corresponding waveforms<sup>9</sup> (shown here for an  $\epsilon$  of 5, an  $x$  startup value of  $10^{-6}$ ) with normalized coordinates):

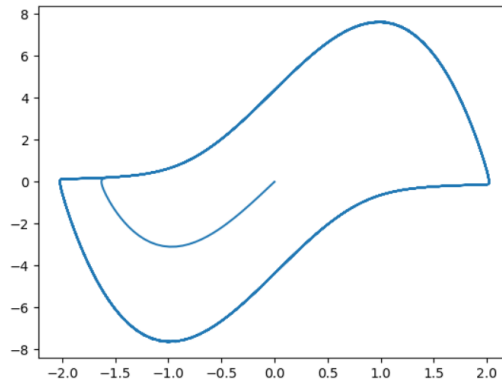


Figure 126 - Limit Cycle of a Van der Pol Oscillator with a large epsilon

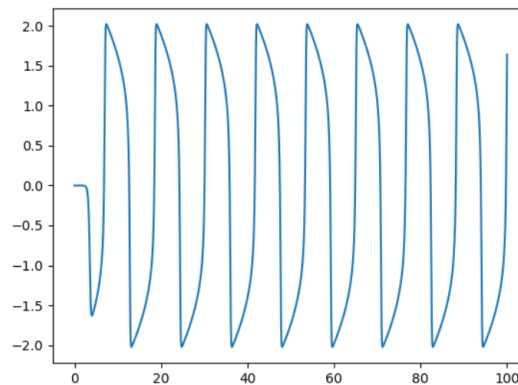


Figure 127 - Waveform of a Van der Pol Oscillator with a large epsilon

The phase plot shows that startup and joining the limit cycle seems to happen within less than one period of oscillation, and the waveform is relaxation oscillations with very sharp edges and some smoother phases between. To reasonably resolve the steep edges, the maximum timestep there is only a very small fraction of the period. For a harmonic balance approach, this translates to the requirement that a lot of harmonics need to be included into the simulation.

For our case of high-Q oscillators, stiffness as such can hardly be the problem. The  $\epsilon$  values there are extremely small, the limit cycle resembles a perfect ellipsis (i.e., the waveform is almost a perfect sinusoid), and the startup process is a spiral taking many rounds until it approaches the limit cycle.

<sup>9</sup> All the examples were programmed in Python using the NumPy and SciPy packages and the ODEINT solver method. This works by a factor of 100 faster than circuit simulators and can handle a larger range of circuit Q.

The picture below shows the startup close to the origin ( $Q=25K$ ,  $X_0=10^{-6}$ , normalized coordinates):

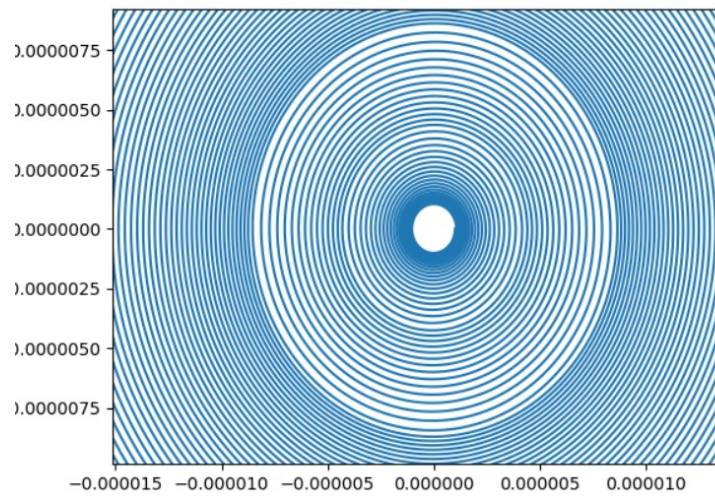


Figure 128 - Startup of a Van der Pol Oscillator with small epsilon

And the log plot of X looks like this:

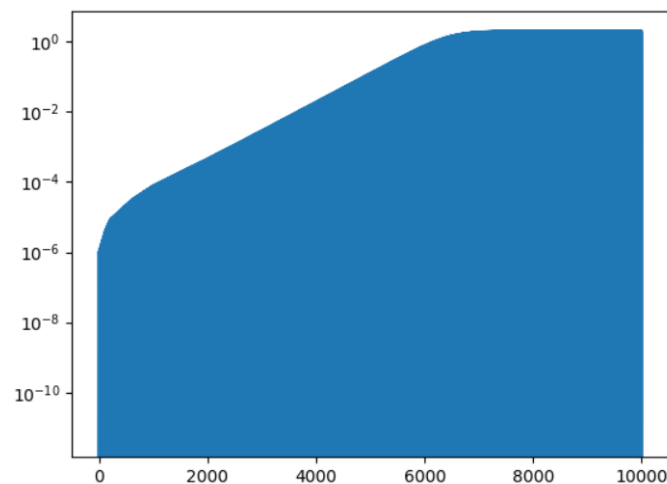


Figure 129 - Amplitude over Time for a Van der Pol Oscillator with small epsilon

Some interesting phenomena can be observed:

1. There seems to be more than one time constant at small amplitudes (spiral growth rates). This must be caused by numerics (i.e., a change in integration methods), not by physics.
2. The “large amplitude” time scale is fairly consistent.
3. A start value of  $x(0) = 0$  and  $x'(0) = 0$  never starts off (no surprise).

So, the conclusion is that van der Pol equations for high  $Q$  oscillators are not difficult because they are *stiff*, they are problematic because they are *lazy* (in terms of amplitude growth at very small amplitudes). In order to substantiate that, we could try to have an even closer look at the startup process at a very small number of periods and even smaller starting points.

For the choice of  $X_0=10^{-8}$  we get the following picture:

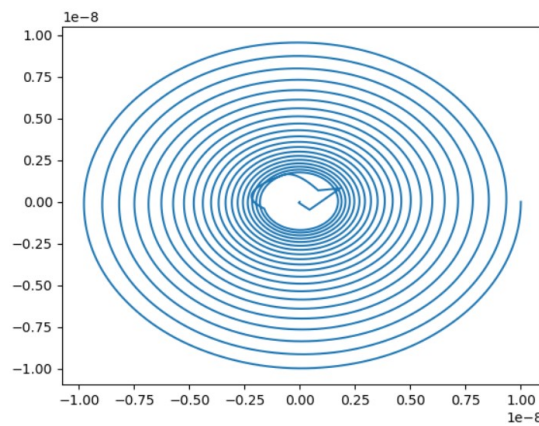


Figure 130 - Start Failure for a Van Der Pol Oscillator with small epsilon

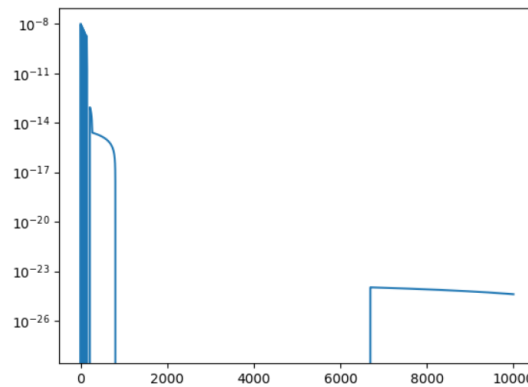


Figure 131 - Start Failure for a Van der Pol Oscillator with small epsilon - Amplitudes

Everything in the phase plot looks familiar except for the fact that the spiral is now going *inwards* instead of outwards, i.e., the oscillations die out instead of grow as it should be. At very low amplitudes, some awkward numeric effects are visible as well. The output amplitude plot confirms this. If we choose a start value of  $10^{-7}$  is still the same, it only dies out at a slower pace. It's also no successful idea to use an  $x'$  offset instead of  $x$  (or even both) as a start value.

The key question now is how we can explain if a simulation with a start value of  $(x(0)|x'(0))$  with a given  $\varepsilon$  will work or not and why, preferably independent of the details of specific integration methods used.

### 6.3 Integration Methods, Precision

All ODE solvers rely on numerical integration methods, the approaches varying by software and type of problem. The common denominator is that the function to be approximated is replaced by lower-order (linear, polynomial, ...) curve defined over a timestep interval. The coefficients of the lower order curve are computed, and an error estimate is made. The timestep is adjusted until a limit for the permitted error is fulfilled. This adjusted timestep is used to compute the next point of the integrated curve, and so on. Especially for stiff problems higher order methods were developed that can better express fast-changing function behavior without making the timestep too small (e.g., GEAR [6]). For our high-Q van der Pol startup problem higher order methods are of no big help, because the start

values are so small that all higher powers quickly fall into irrelevance<sup>10</sup>. If we remember that due to the high Q the waveform is very much similar to a sinusoid, we could use the simplified equation around a very small x, making  $x^2$  even smaller than 1 and can be ignored.

$$x'' - \varepsilon(1 - x^2)x' + x = 0 \text{ becomes } x'' - \varepsilon x' + x = 0$$

This is a harmonic oscillator equation, with a transient solution of

$$x(T) = e^{\left(\frac{\varepsilon T}{2}\right)} \left\{ x_0' \sin \left( T \sqrt{1 - \frac{\varepsilon^2}{4}} \right) + x_0 \cos \left( T \sqrt{1 - \frac{\varepsilon^2}{4}} \right) \right\}$$

Where the values of  $x_0$  and  $x_0'$  are the start values and T stands for the normalized time. We are only interested about very small values of  $x$ ,  $x_0$ , T and  $x_0'$ , so we can replace all functions by expansions, ignoring all terms with powers larger than 1. We get

$$e^{\frac{\varepsilon T}{2}} \sim 1 + \frac{\varepsilon T}{2}, \quad \sin \left( T \sqrt{1 - \frac{\varepsilon^2}{4}} \right) \sim \left( T \sqrt{1 - \frac{\varepsilon^2}{4}} \right), \quad \cos \left( T \sqrt{1 - \frac{\varepsilon^2}{4}} \right) \sim 1$$

When Q is very high, the root term approaches 1.

$$x(T) \sim \left( 1 + \frac{\varepsilon T}{2} \right) \{ x_0' T + x_0 \}$$

Now we look at a (very small) increment in time after T, called  $T + \Delta T$ .

$$x(T + \Delta T) \sim \left( 1 + \frac{\varepsilon(T + \Delta T)}{2} \right) \{ x_0'(T + \Delta T) + x_0 \}$$

Subtracting the two gives

$$x(T + \Delta T) - x(T) \sim \left( 1 + \frac{\varepsilon(T + \Delta T)}{2} \right) \{ x_0'(T + \Delta T) + x_0 \} - \left( 1 + \frac{\varepsilon T}{2} \right) \{ x_0' T + x_0 \}$$

Which can be simplified to (ignoring a square of  $\Delta T$ ):

$$x(T + \Delta T) - x(T) = \Delta T (x_0'(1 + \varepsilon T) + x_0 \varepsilon / 2)$$

So, the estimate for the derivative becomes for small  $x_0$ ,  $x_0'$ , T and  $\Delta T$  becomes:

$$\frac{x(T + \Delta T) - x(T)}{\Delta T} = x_0'(1 + \varepsilon T) + x_0 \varepsilon / 2$$

This result explains the following phenomena:

1. If  $T=0$ , either  $x_0$  or  $x_0'$  must be different from zero so that oscillations can start, so no surprise
2. The change is proportional to time, as expected for an exponential system.
3. In order to be accurate as a growth factor, the term  $\varepsilon T$  must be **considerably** larger than  $10^{-p}$  where p is the precision of the computer arithmetic available, otherwise no correct amplitude growth will result.
4. This also explains that the numeric computations of startup times result in values longer than the math predicts. The factor  $1 + \varepsilon T$  is always *underestimated* from its real value by rounding down errors.

<sup>10</sup> This is substantiated by the fact that the maximum order of polynomial approximation in the ODE solver has to *reduced* when Q increases to enable convergence. In the same vein, supplying the Jacobian does not help much either (if you don't, the software uses a linear approximation).

For an SC crystal at 5MHz and 15 digits we have  $\varepsilon$  ca.  $10^{-5}$ , which means that the normalized T must be larger than about  $10^{-5}$  if we want to keep 5 valid digits for the time dependent growth factor. This calculation is probably still optimistic because error propagation issues were not covered, but this would ask for detailed analysis of the integration methods used.

A remedy for this problem could be using a higher precision math or simulator package.

## Conclusions

It has been shown that the classics Colpitts/Clapp circuit is extremely hard to simulate with classic simulation programs when the resonator has a high Q. Starting from a simple equivalent circuit it could be shown that the Clapp circuit is (in the startup phase) structurally equivalent to a van der Pol nonlinear oscillator. The properties of this equivalent oscillator are investigated, and an explanation of the numerical problems encountered is found. It is not the stiffness of the equation in this particular case, but a matter of insufficient numeric precision that makes classical simulators fail to start an USO circuit.

To summarize, benefits of time domain simulator are

1. Can simulate the startup process
2. Can reveal chaos and squegging
3. Shows realistic waveforms
4. If models are complete, results are reliable and close to measurements.
5. BE breakdown can be added to the model and delivers realistic results close to measurements.

the main difficulties for time domain simulators are:

1. Startup problems due to insufficient numeric precision
2. Failure of the timestep determination algorithm (minimum time step error) related to the above
3. Nonlinear noise cannot be (realistically) computed at all.
4. Unacceptably long simulation times due to long simulation times dictated by the large Q, in conjunction with extremely small timesteps because of the precision required.

For frequency domain (HB) simulators, the strengths are:

1. The method can accommodate nonlinear noise.
2. Simulation times are much shorter than for time domain simulators

And the downsides are:

1. Only the steady state can be simulated. Startup cannot be treated at all.
2. Chaos and squegging cannot be detected by the simulator.
3. Fast processes (saturation, ...) require a lot of harmonics and waveforms are still not as accurate as the time domain simulators
4. The Gibbs phenomenon creates artefacts on steep transitions.
5. For some software products, the models are undisclosed and cannot be examined and augmented. Some demo results gave rise to the concern that high-current effects are not realistically modelled.
6. BE breakdown cannot be modelled at all (at least not in Serenade HB, maybe possible with handwritten C expansion modules, this has not been checked).

There is no unproblematic simulator for extreme Q oscillators. Much more progress was possible using time domain methods than with harmonic balance, because of their openness and expandability and the chance to immediately match results with waveform measurements.

## 6.4 Further Research

The efforts here could be continued in the following directions:

1. Experiments with higher precision math software (MATLAB, MPMATH, ...)
2. More complex models of the nonlinear component (square term in VdP, ...)
3. Gummel-Poon transistor model instead of the nonlinear resistance model used
4. Investigations regarding the different integration schemes available and their effects on the solvability of our problem (TRAP, GEAR, BDF, ...)
5. Better resonator model involving side resonances and fundamental mode. (B-Mode for SC cuts). This will probably show a lot more interesting phenomena like mode coupling, chaos or the simulation excitation of two frequencies, as can be observed in experiments.

## 6.5 The Simulation Program

The Python simulation program is shown below. It was run on a Windows10 PC with 12GB memory in 64Bit mode (32Bit Python runs out of memory). The Python version used was 3.8.2. Different ODE solver parameters can be activated by uncommenting the relevant program lines.

```
import numpy as np
import matplotlib.pyplot as plt
from scipy.integrate import odeint

L          = 0.0844
R          = 100
alpha     = -200
gamma     = 1E8
omega0    = 2*np.pi*5E6
omega0Sq  = omega0**2
Q         = omega0*L/R
epsilon   = -(R+alpha)/Q

print ('Q=',Q,'epsilon=',epsilon)

def vdP(x, t):
    res = np.zeros(2)
    res[0] = x[1]
    res[1] = epsilon*(1-x[0]*x[0])*x[1] - x[0]
    return res

def vdpJac(x, t):
    res = np.zeros((2,2))
    res[0,0] = 0
    res[0,1] = 1
    res[1,0] = -2*x[0]*x[1]*epsilon - 1
    res[1,1] = epsilon*(1-x[0]*x[0])
    return res

ts = np.linspace(0.0, 10000, 5000000)
# xs = odeint(vdP, [1E-9, 0], ts,Dfun=vdpJac)
# xs = odeint(vdP, [1E-7, 0], ts,mxordn=10,mxords=4)
# Works xs = odeint(vdP, [1E-6, 0], ts,Dfun=vdpJac,mxordn=10,mxords=4)
xs = odeint(vdP, [1E-6, 0], ts, Dfun=vdpJac,mxordn=10,mxords=4)
plt.plot(xs[:,0], xs[:,1])
plt.show()
plt.plot(ts, xs[:,0])
plt.yscale('log')
plt.show()
```

## References

- [1] Ulrich L. Rohde, "Crystal Oscillator Provides Low Noise," *Electronic Design*, vol. 21, Oct. 1975.
- [2] Analog Devices, "LTSpice User Manual." Accessed: Nov. 23, 2020. [Online]. Available: <https://ltspice.linear.com/software/scad3.pdf>.
- [3] B. van der Pol: "A theory of the amplitude of free and forced triode vibrations", *Radio Review* (later *Wireless World*) 1 701–710 (1920)
- [4] [Weisstein, Eric W.](https://mathworld.wolfram.com/Jacobian.html) "Jacobian." From *MathWorld*--A Wolfram Web Resource. <https://mathworld.wolfram.com/Jacobian.html>
- [5] Engineering Libre Texts, "Using eigenvalues and eigenvectors to find stability and solve ODEs." Accessed: Nov. 23, 2020. [Online]. Available: [https://eng.libretexts.org/Bookshelves/Industrial\\_and\\_Systems\\_Engineering/Book%3A\\_Chemical\\_Process\\_Dynamics\\_and\\_Controls\\_\(Woolf\)/10%3A\\_Dynamical\\_Systems\\_Analysis/10.04%3A\\_Using\\_eigenvalues\\_and\\_eigenvectors\\_to\\_find\\_stability\\_and\\_solve\\_ODEs](https://eng.libretexts.org/Bookshelves/Industrial_and_Systems_Engineering/Book%3A_Chemical_Process_Dynamics_and_Controls_(Woolf)/10%3A_Dynamical_Systems_Analysis/10.04%3A_Using_eigenvalues_and_eigenvectors_to_find_stability_and_solve_ODEs).
- [6] Y X Wang and J M Wen, "Gear Method for Solving Differential Equations of Gear Systems." IOP Publishing (Open Access), Accessed: Nov. 23, 2020. [Online]. Available: <https://iopscience.iop.org/article/10.1088/1742-6596/48/1/026/pdf>.

## 6.6 A Simulated High Q Clapp Oscillator

After unsuccessful attempts to simulate a Colpitts/Clapp USO with a space-grad crystal using standard simulation tools, an attempt was made to understand the nature of the difficulties encountered (see separate paper). With several failed attempts using standard software for Q values larger than ca. 250K, it was decided to attack the problem by formulating all nonlinear differential circuit equations in the time domain and to create a dedicated solver for the problem. That worked for Q values of 2.5 Million.

### 6.6.1 A stripped-down Circuit to test Simulators

Practical circuits contain quite some components that are needed (ALC, mode suppression, ...) but are not the root cause why simulations fail (just try this). To explain what is going wrong, a very basic circuit can be used with the same results, like this one:

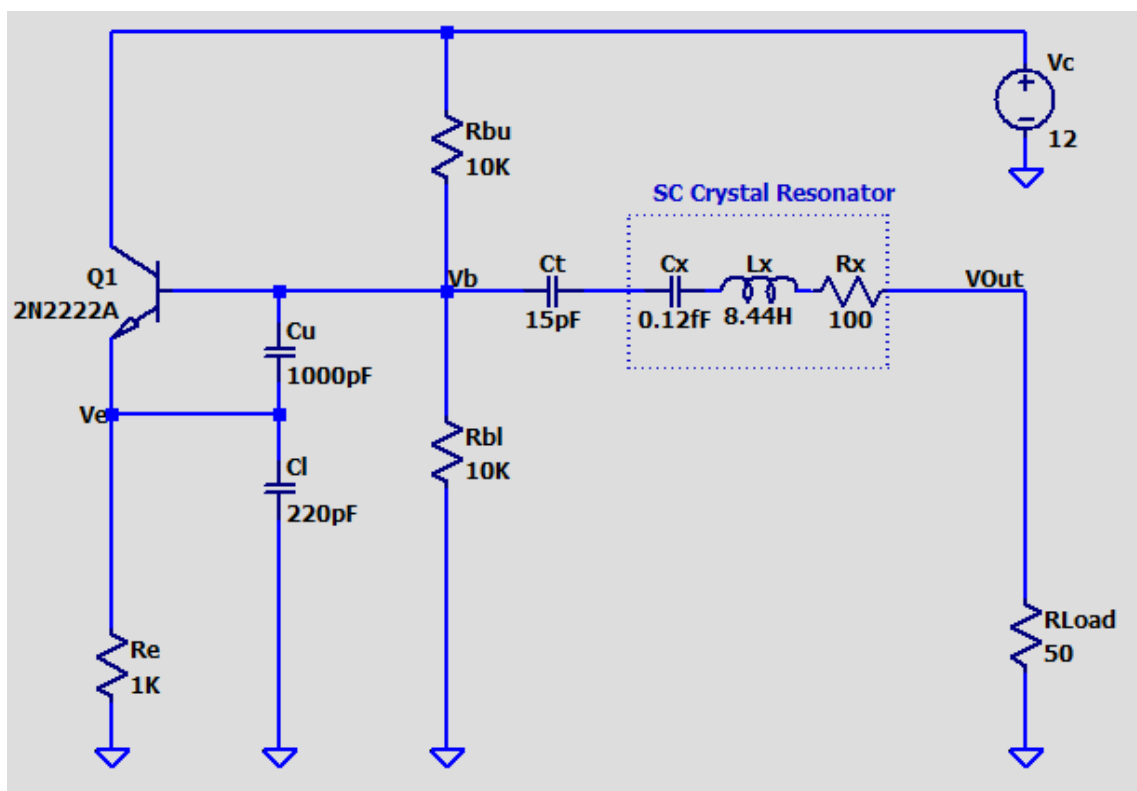


Figure 132 - A Sample Clapp Oscillator with a High Q Resonator

The resonator in this schematic represents a simplified (b mode and fundamental not modelled) SC cut space-grade crystal (5MHz,  $L=8.44\text{H}$ ,  $C=0.12\text{fF}$ ,  $R=80\text{Ohms}$ ,  $Q$  ca. 2.5Million). Following a Rohde design [1], the crystal is used as a resonator and a filter at the same time; the output goes directly into a low-impedance input of the next stage, a common base amplifier. This trick results in a very clean signal with low close-to-carrier noise, caused by the very small resonator bandwidth.

This circuit has failed to simulate in LTSpice and Serenade, so an attempt was made to use specialized simulation programs. These (Python) programs work differently from standard simulators by deliberately not using higher-order ODE solvers that run out of significant digits. Details why extremely high Q circuits fail in standard simulators are explained in another paper.



### 6.6.2 A Simplified Model for Simulation

Some simplifications were performed to make simulation easier. These have no impact on functionality but reduce the number of components.

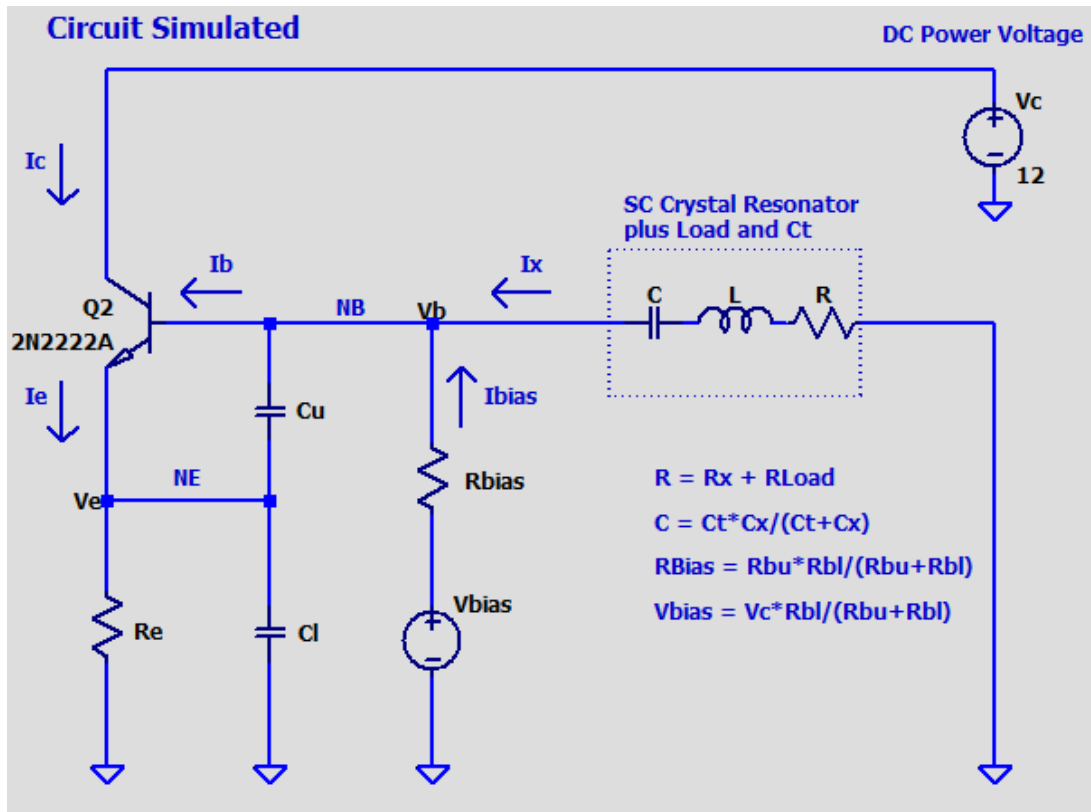


Figure 133 - A Simplified Clapp Oscillator for Simulation

The simplifications were:

1. The tuning cap was integrated in the series cap of the resonator  
 $C = C_x * C_T / (C_x + C_T)$ .
2. The base bias resistors were put into a single resistor and a voltage bias source  
 $V_{BIAS} = V_c * R_{BL} / (R_{BU} + R_{BL})$ ,  $R_{BIAS} = R_{BU} * R_{BL} / (R_{BU} + R_{BL})$ .
3. The load resistor was integrated in the crystal series resistance. The crystal equivalent circuit elements are named R, L and C without suffixes (C see above).

So, if we collect equations with KVL and KCL, we end up with (using KVL, with  $I_X$  as crystal current):

$$V_B = RI_X + L \frac{dI_X}{dt} + \frac{1}{C} \int_0^t I_X dt$$

Next, we use KCL for the base node NB. We get:

$$I_X + \frac{V_{BIAS} - V_B}{R_{BIAS}} = I_B + C_U \frac{d(V_B - V_E)}{dt}$$

For the emitter node NE the KCL gives:

$$C_L \frac{dV_E}{dt} + \frac{V_E}{R_E} = I_E + C_U \frac{d(V_B - V_E)}{dt}$$

Now we need to decide on a transistor model. For a start, we choose a simplified Gummel-Poon model with

$$I_C = I_S * \exp\left(\frac{V_B - V_E}{V_T}\right) + \frac{V_C - V_E}{r_a}$$

Where  $V_T$  is the temperature voltage,  $I_S$  is the saturation current and  $r_a$  is the output resistor. Furthermore, we assume a constant current amplification factor  $B$ , so

$$I_B = I_C/B \quad \text{and} \quad I_E = I_C (1 + 1/B)$$

It should be noted that this simple model has no provisions for high current effects, saturation, BE breakdown, internal capacitances and so on. For the intended purpose (to successfully simulate the *startup* of extremely high Q oscillators) these effects are insignificant. *After* the startup phase, however, it must be checked if the waveforms obtained are still OK regarding the assumptions made.

The KVL equation for IX is an integro-differential equation. We differentiate again to get a second-order differential equation:

$$\frac{dV_B}{Ldt} = \frac{RdI_X}{Ldt} + \frac{d^2I_X}{dt^2} + \frac{1}{LC}I_X$$

What we would like to see is a first order, vector equation system of the form

$$\frac{dX}{dt} = F(X)$$

with all derivatives on the left and all other terms on the right. To obtain this, we define

$$\frac{dI_X}{dt} = Y$$

Our equation then reads:

$$\frac{dY}{dt} = \frac{1}{L} \frac{dV_B}{dt} - \frac{R}{L}Y - \frac{1}{LC}I_X$$

We now need to get rid of the derivative of  $V_B$  on the righthand side. Subtracting the KCL equations for NB and NE we get

$$\frac{dV_E}{dt} = \frac{1}{C_L} \left( I_C + I_X + \frac{V_{BIAS} - V_B}{R_{BIAS}} - \frac{V_E}{R_E} \right)$$

And

$$\frac{dV_B}{dt} = \frac{1}{C_L} \left( I_C + I_X + \frac{V_{BIAS} - V_B}{R_{BIAS}} - \frac{V_E}{R_E} \right) + \frac{1}{C_U} \left( I_X + \frac{V_{BIAS} - V_B}{R_{BIAS}} - \frac{I_C}{B} \right)$$

The bold printed terms can be inserted in the equation of the derivative of  $Y$ .  $I_C$  can be expressed from the transistor model above, only depending on  $V_C$  (a constant),  $V_B$  and  $V_E$ . We ended up with a system of 4 nonlinear differential equations with state variables  $I_X$ ,  $Y$ ,  $V_B$  and  $V_E$ , put into a state vector called  $X$ . This can now be used for numeric computation. What we want to do is to compute the evolution of our state variables over time. We can approximate the value of the state vector at a time  $t + \Delta t$  by

$$X(t + \Delta t) = X(t) + \Delta t \frac{dF}{dt}$$

where the term  $dF/dt$  is the vector of derivatives we just computed, evaluated at time  $t$ . There will be an error term in the order of magnitude of  $\Delta t^2$ . We know from physical arguments that the components

of  $F$  are well-behaved (i.e., have no extremely steep gradients) so a  $\Delta t$  that is a reasonably small fraction of an oscillation cycle should ensure that the square and following terms can be safely ignored.

This should do what we need. What is still missing are initial conditions for our variables. We could choose those according to physics; a “cold” start would mean that all  $X$  currents and voltages are zero (only the bias and supply voltages would be present). If everything works well (not as in standard simulators) the circuit should startup to its operating point and commence oscillations. This is also a test for the realism of the assumptions made.

### 6.6.3 Results

A first run was made, using the values in the diagrams. The results in a few words:

1. The circuit starts up from DC and establishes a reasonable operating point
2. Oscillations set in and grow exponentially, as it should be in the startup phase.
3. The waveforms of the collector current show spikes, as predicted and desired for low phase noise.
4. The simulation was stopped after startup was demonstrated, because we have not implemented any limiting mechanisms. This must be done by improved transistor modeling.

A collection of screenshots follows:

The operating point is established:

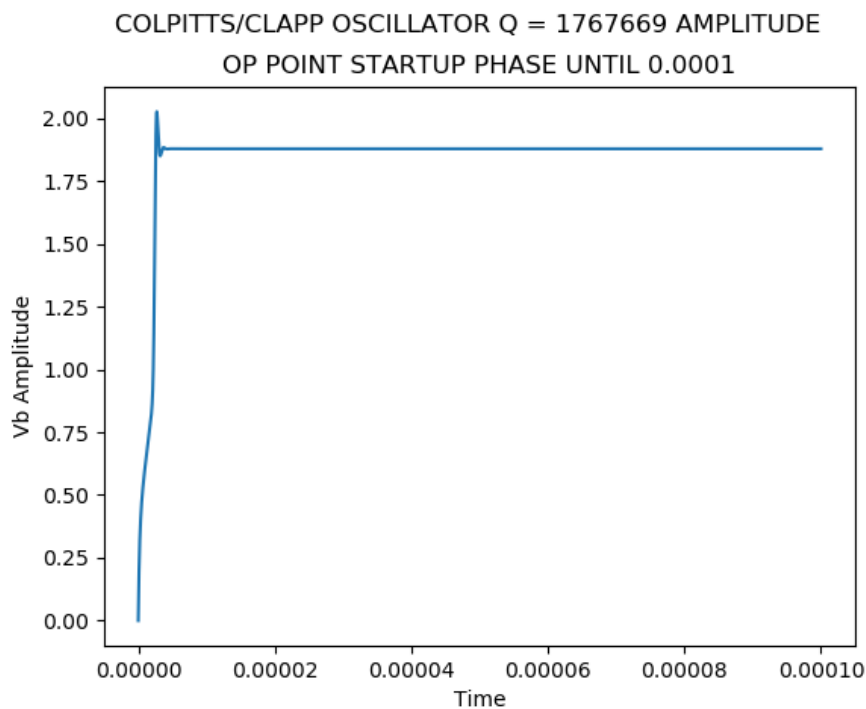


Figure 134 - Simulated Establishment of the Operating Point

The oscillations start off:

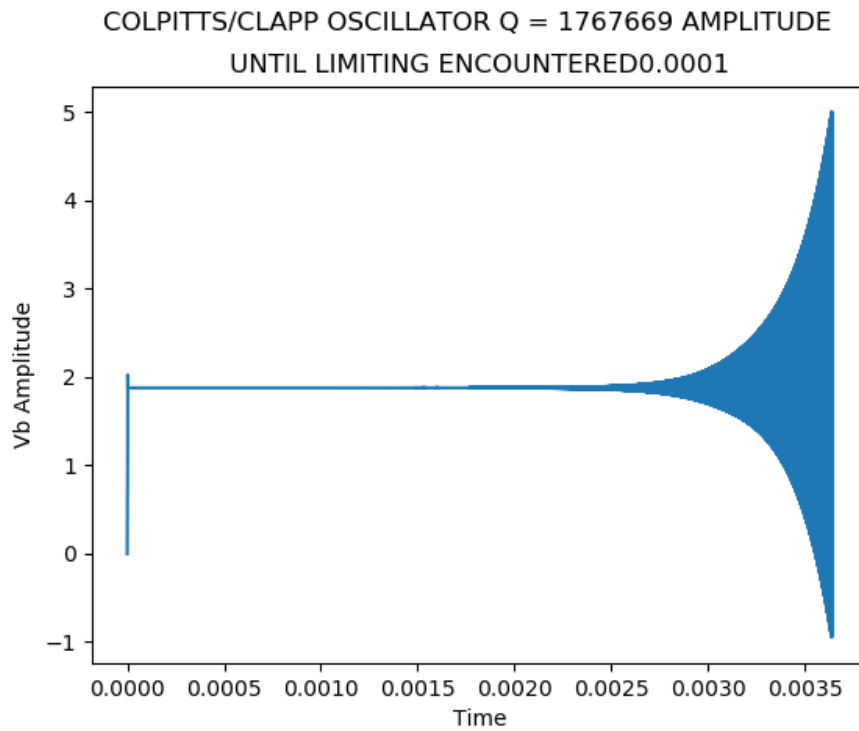


Figure 135 - The Startup of a High Oscillator

Note that lack of limiting makes the curve unrealistic at high amplitudes. Successful startup is demonstrated, however. Now the collector current:

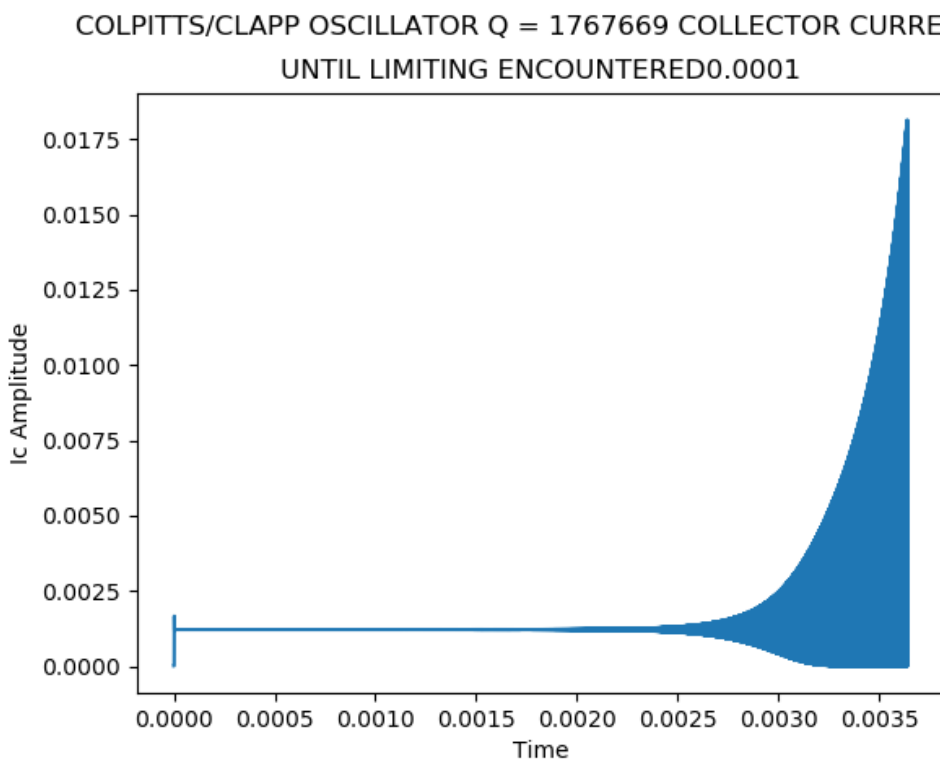


Figure 136 - Collector Current During Startup

For amplitudes see comment above.

The collector waveform in detail is next:

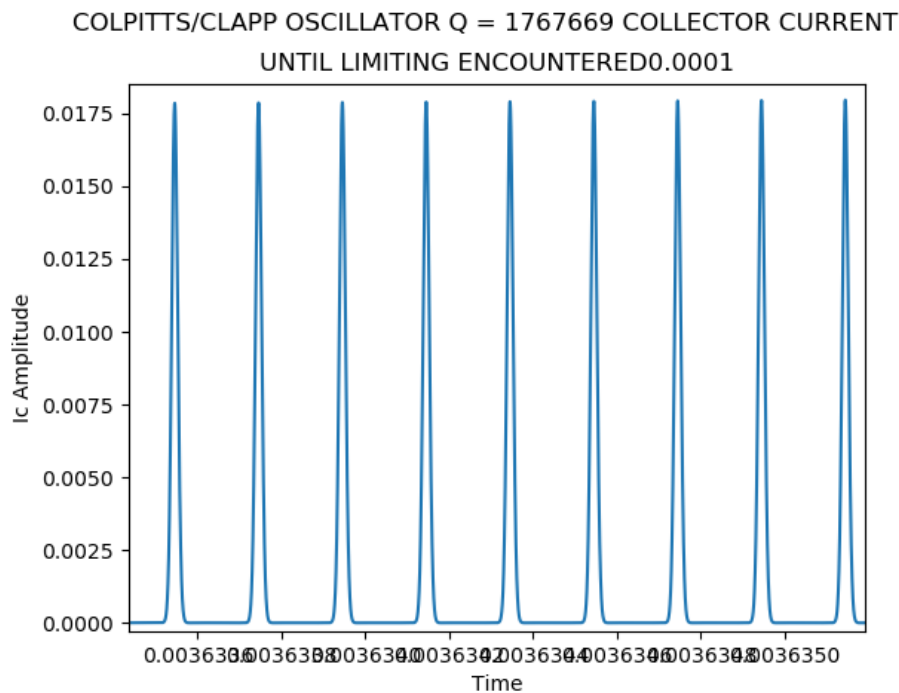


Figure 137 - Collector Current Waveforms

As it should be.

## Conclusions

It could be demonstrated that the simulation of Colpitts/Clapp oscillators with extremely high Q (2.5 Million) is indeed possible. What is needed, however, is a tailored solution instead of standard circuit simulator software. When everything is written from scratch, full control over timesteps and the interpolations methods is possible. The disadvantages of refined higher-order interpolation methods (no output due to precision loss problems) are avoided by using a single-step approach with suitable step sizes. The next steps would be to include realistic amplitude limiting mechanisms into the simulation (saturation, VB breakdown, ...) so that, ideally, a complete simulation of oscillator behavior including the steady state will become possible.

The unrealistic amplitudes are a clear indication that the limiting effect of Bessel bias shift is not able to stabilize an oscillator amplitude in a general case. Other limiting effects must be included in the model to reproduce experimental results.

### 6.6.4 The Next Step - Limiting Mechanisms

As discussed, the following amplitude limiting effects can play a role:

1. Shift of bias towards smaller transconductance (“Bessel function shift”)
2. Saturation
3. High current effects (beta degradation)
4. Negative VBE breakdown

If we want to make our simulation more realistic, these effects need to be included in the simulation. For the bias shift no further action is necessary; this effect is automatically modelled by defining an exponential collector current formula.

### Saturation

Saturation, however, is not included so far. To incorporate this effect, we need to implement a model for the base current running into the collector instead of the emitter in case the collector voltage becomes close to or even lower to the base voltage. The classic Ebers-Moll [2] or the Gummel-Poon [2] transistor transport model (also used in SPICE) solves this issue by computing both the diode currents from base to emitter and from base to collector. The equations for the terminal currents are:

$$I_B = I_S \left\{ \frac{1}{B_N} \left( \exp\left(\frac{V_B - V_E}{V_T}\right) - 1 \right) + \frac{1}{B_I} \left( \exp\left(\frac{V_B - V_C}{V_T}\right) - 1 \right) \right\}$$

$$I_C = I_S \left\{ \exp\left(\frac{V_B - V_E}{V_T}\right) - \left(1 + \frac{1}{B_I}\right) \exp\left(\frac{V_B - V_C}{V_T}\right) + \frac{1}{B_I} \right\}$$

$$I_E = I_S \left\{ \exp\left(\frac{V_B - V_C}{V_T}\right) - \left(1 + \frac{1}{B_N}\right) \exp\left(\frac{V_B - V_E}{V_T}\right) + \frac{1}{B_N} \right\}$$

Where  $B_N$  and  $B_I$  are the normal and inverse current amplification factors (called BF and BR in SPICE for forward and reverse). The forward factor is ca. 160 for the transistor used, and the reverse factor is close to 1.

### High Current Effects

High-current effects are, in the case of the transistor used, extremely unlikely. The maximum collector current is 800mA, and the spikes have an amplitude of a few ten mA at the top. The current for maximum beta is ca. 80mA, as can be seen from a gain over collector current plot:

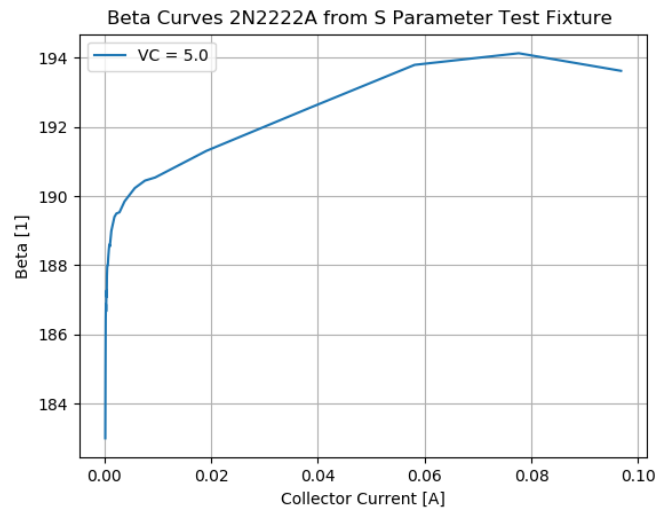


Figure 138 - Beta Curve over Collector Current

Furthermore, the curve is very flat when looking at the left axis scale, i.e., there is almost *no* dependency of current gain on collector current. We therefore will not model this effect for the 2N2222A transistor. For other parts, this can be very different.

*Base Emitter Breakdown*

The base emitter breakdown at negative base voltages can be modelled by a Zener diode in series with a normal diode that prevents current to flow under normal bias conditions. So, the simplified transistor model including saturation and BE breakthrough looks like this:

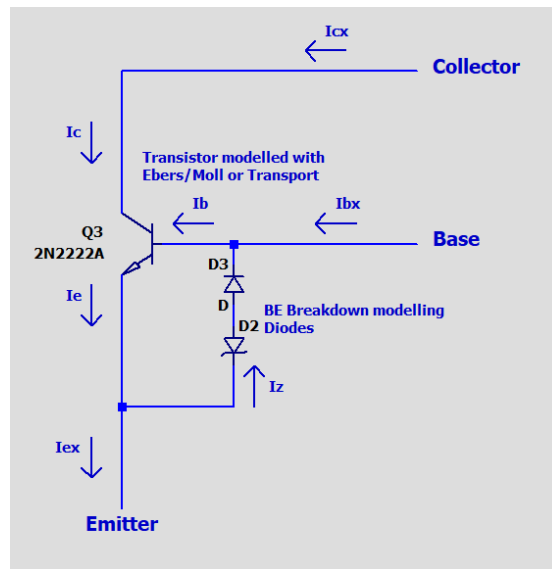


Figure 139 - Base Emitter Breakdown Effect Simulation

$I_C$ ,  $I_B$  and  $I_E$  now come from the Gummel/Poon model, and the new terminal currents are now  $I_{CX}$ ,  $I_{BX}$  and  $I_{EX}$ .

The formula for the Zener current is not straightforward because the nature of the breakdown depends on voltage; below a few Volts we see a tunnel breakthrough with a gentle slope and a negative temperature coefficient, above ca. 6-7V the avalanche effect dominated with a much steeper breakthrough and a positive temperature coefficient. An example of measured Zener currents is shown below:

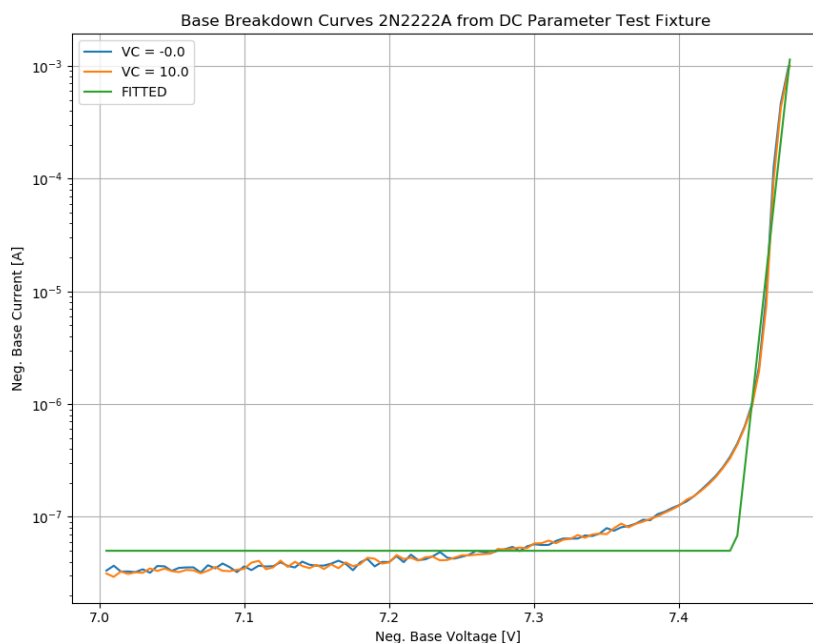


Figure 140 - Breakdown Current over Negative BE Voltage

The interesting part of the curve is where significant currents occur (i.e., the branch from 1uA upwards); for the part in question (will be different for other types) the fitting formula would run

$$I_Z = 10^{(-6. + 116 \cdot (V - 7.45))}$$

Experiments with different transistors have resulted in an empirical Zener current formula for the 2N2222A used (will be different for other types):

$$I_{CX} = I_C$$

And for the base we have

$$I_{BX} = I_B - I_Z$$

The emitter current is just the sum of the two, so

$$I_{EX} = I_{CX} + I_{BX} = I_C + I_B - I_Z$$

This can now be used in the software model.

It should be mentioned that VBE breakdown causes a permanent degradation of transistor beta. This is caused by hot carrier being injected into the oxide layer of a planar transistor and is more prominent with RF parts. The degradation there can go up to almost 50%, as measurements have shown. The BE breakdown is treated in detail in a separate chapter.

### 6.6.5 Modeling of the Transistor including Saturation

To model the transistor including the saturation effect we could use a Gummel/Poon or transport model as employed by PSPICE. Ignoring resistances, the equations run (derived from the official PSPICE manual, using SPICE notation):

$$I_B = I_S \left\{ \frac{1}{BF} \left( \exp\left(\frac{V_B - V_E}{NF V_T}\right) - 1 \right) + \frac{1}{BR} \left( \exp\left(\frac{V_B - V_C}{NR V_T}\right) - 1 \right) \right\}$$

The NF and NR (“injection efficiency”) factors were assumed as 1 according to the 2N2222A spice model. The “non-ideal” base currents forward and reverse (ISE and ISR...) terms were set to zero for the same reason. For the collector we have:

$$I_C = I_S \left\{ \frac{1}{K_Q} \left( \exp\left(\frac{V_B - V_E}{V_T}\right) - 1 \right) - \frac{1}{K_Q} \left( \exp\left(\frac{V_B - V_C}{V_T}\right) - 1 \right) - \frac{1}{BR} \left( \exp\left(\frac{V_B - V_C}{V_T}\right) - 1 \right) \right\}$$

The term  $K_Q$  is the base charge factor,

$$K_Q = \frac{1 + \left[ 1 + 4 \left\{ \frac{I_S}{IKF} \left( \exp\left(\frac{V_B - V_E}{V_T}\right) - 1 \right) + \frac{I_S}{IKR} \left( \exp\left(\frac{V_B - V_C}{V_T}\right) - 1 \right) \right\} \right]^{NK}}{2(1 - (V_B - V_C)/VAF)}$$

For the 2N2222A model, there is no specific IKR and NK (default 0.5) available, so we can simplify to

$$K_Q = \frac{1 + \left[ 1 + 4 \left\{ \frac{I_S}{IKF} \left( \exp\left(\frac{V_B - V_E}{V_T}\right) - 1 \right) \right\} \right]^{NK}}{2(1 - (V_B - V_C)/VAF)}$$



If we want to express the base voltage as a function of base current and collector voltage (needed for comparative output plots) we get (derivation not shown):

$$V_B = V_T \ln \left\{ \frac{\frac{I_B}{I_S} + \frac{1}{BF} + \frac{1}{BR}}{\frac{1}{BF} + \frac{1}{BR \exp(V_C/V_T)}} \right\}$$

As a sanity check we can make a Gummel plot and some output curves:

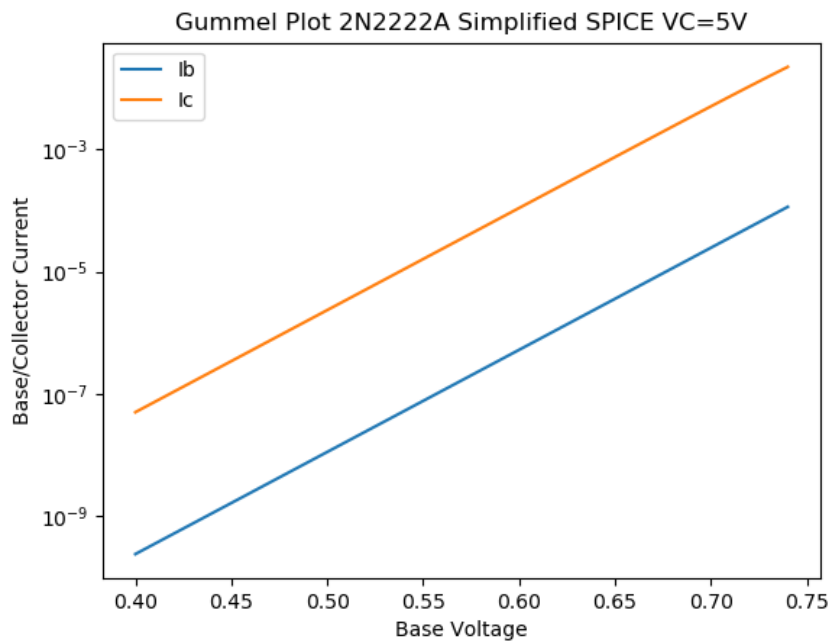


Figure 141 - Gummel Plot of the Simulated 2N2222A Transistor

Not including high current and recombination effects this looks as expected.

Now the output curves:

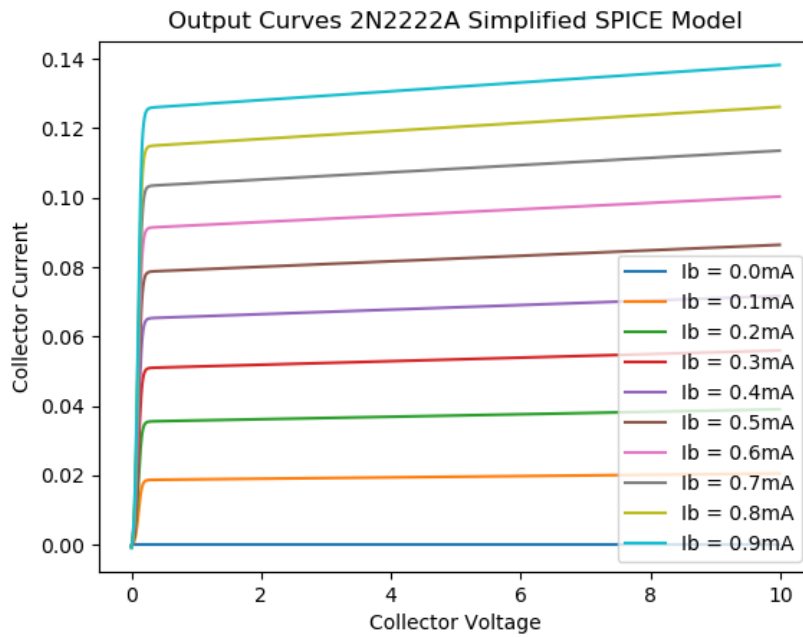


Figure 142 - Output Curves of the Simulated 2N2222A Transistor

Saturation looks plausible as well. This means the model can be used as a candidate in a time domain simulator. The inaccuracies are mostly in the quasisaturation domain, as shown previously.

## References

- [1] Ulrich L. Rohde, "Crystal Oscillator Provides Low Noise," *Electronic Design*, vol. 21, Oct. 1975.
- [2] G. Massobrio and P. Antognetti, *Semiconductor device modeling with SPICE*. New York: McGraw-Hill, 2009.

## 7 Thermal and Environmental Aspects

This chapter deals with temperature management and stabilization, the properties of space qualified electronic components, the effects of shock and vibration as some practical recommendations for successful measurements and operation.

### 7.1 Temperature Regulator

Space oscillators run inside a double or at least a single thermostat, so temperature effects are regulated out to a large degree ( $0.01^{\circ}\text{C}$  or even less); Outside temperature differences can be huge, however (e.g.,  $-150^{\circ}\text{C}$  in the shade of a moon or planet,  $+150^{\circ}\text{C}$  in direct exposure to the sun). The core part does not see much of this inside a Dewar flask, but the buffers and regulators around must perform well under much less regulated conditions. Frequency pulling due to changed properties of buffer amps (input impedance, ...) is a threat to premium stability.

Thermal Design covers the construction and operation of temperature stabilized single and double ovens. The underlying math is discussed, and the implications on regulator designs are explained and simulated. A practical case is discussed in the “A Prototype USO Design” chapter.

The crystal temperature and its fluctuations have a direct influence on frequency stability and close to carrier phase noise. The temperature regulator must therefore be

1. Extremely stable with minimal long-term drift and aging.
2. Low noise, at least what arrives as temperature fluctuations at the crystal after being low pass filtered by the huge thermal mass.

Several reference designs have been published; all newer ones use a PI (proportional-integral) regulator design with long time constants. Attempts to speed up response by a D (differential) regulator component were found to be unsatisfactory (by creating a lot of extra noise, see [6]).

The control variables of the regulator have very small active ranges; if we assume an  $80^{\circ}\text{C}$  SC cut crystal controlled by a Platinum type temperature sensor with  $1\text{K}\Omega$ , the resistance value changes are in the range of  $3\ \Omega$  per  $0.1^{\circ}\text{K}$ . For premium frequency stability, the temperature should be kept constant better than  $1\text{mK}$ , however, making the resistance range of a few ten milliohms.

Premium voltage references, low-tolerance metal film or foil resistors, metrology-grade operational amplifiers and a careful low noise design are critical success factors. Extended burn-in and pre-aging is necessary to ensure reliable performance.

A modest example of a regulator design for an USO prototype is shown below:

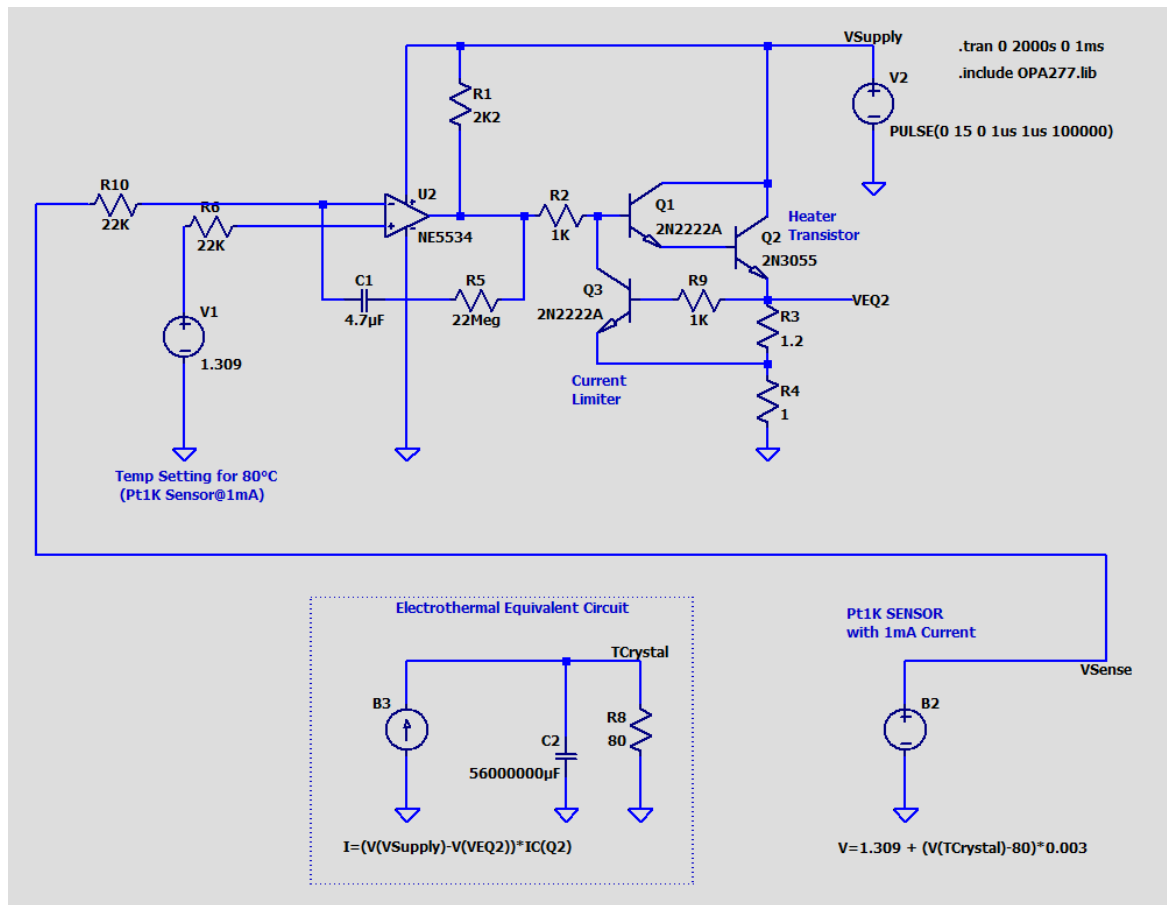


Figure 143 - A Simulated USO Heater with an Electrothermal Equivalent Circuit

The precision temperature setting voltage reference sources (V1) are not shown (REF02 from Analog Devices was used [7]). The Op amp drives a Darlington transistor configuration where Q2 acts as the heater transistor. The two emitter resistors serve as current measurement shunt (R4) and as a maximum current limiter (R3). As long as the desired temperature is not yet reached, the circuit runs with the maximum current set by R3/Q3 and provides several Watts of heater power with no further regulation. If the preset temperature (defined by the voltage across a Pt1K sensor driven with 1mA) is reached, the op amp starts to reduce transistor bias and keeps the temperature constant. The large RC circuit (C1/R5) ensures stability (time constant is 103 seconds).

The behavior of the thermal mass is modelled by an electrothermal equivalent circuit at the bottom. The heater power is modelled by a behavioral current source, the thermal resistance is modelled by an electrical resistance and the capacitor is used to model the thermal time constant. The voltage value across the thermal resistance is the temperature above 0°C.

The sensor circuit is modelled by another behavioral voltage source converting the temperature to a Pt1K sensor voltage.

The startup of the circuit is shown here:



Figure 144 - Heater Current and Crystal Sense Voltage over Time. The red curve is the collector current of the heater transistor, the green curve is the crystal temperature, and the blue curve is the op amp output voltage.

Some percent of overshoot are visible. For more details see appendix K, “Thermal Design”.

Further zoom-in measurements can be seen in the “USO Prototype” chapter.

## 7.2 Influence of Mechanical Vibrations

Vibrations can be a real threat to oscillator phase noise, and spacecraft are not as quiet places as one could assume. Even after the launch phase, thrusters, actuators for solar cells or antennas, pumps, ... can create a vibration level that can disturb the spectral purity of oscillator signals. Crystals are an obvious target of mechanically induced dirt effects due to their piezoelectricity, but also other parts are susceptible (inductors, air capacitors, ...). A very solid, well damped mechanical construction is a must, and the mechanical arrangement should not have sharp resonances anywhere.

Crystals and crystal oscillators react to mechanical vibrations and shock. A measurement apparatus that allows to correlate phase noise with acceleration is discussed. The apparatus is able to create single-tone, shock and random acceleration pulses and is described in detail, along with measurements that clearly show why acceleration is a strong limiting factor to USO performance.

It is in the very nature of piezoelectric materials that there is a coupling between electrical and mechanical quantities. What has very desirable properties when we try to make extremely high Q resonators has a downside as well: our resonators (Quartz disks) are sensitive to acceleration and shock. As it turns out, this property is a serious limiting factor of oscillator phase noise performance [1]. Details are discussed in the crystal properties chapter.

An environment for testing vibration sensitivity was constructed, with an overview in the following picture:

**FSWP MEASURING MICROPHONIC OSCILLATORS**

**A MICROPHONICITY MEASUREMENT SETUP NEEDS ...**

1. A VIBRATION GENERATING DEVICE
2. A TEST TABLE
3. A DRIVER AMPLIFIER
4. A SIGNAL GENERATOR
5. AN ACCELERATION SENSOR
6. A SCOPE

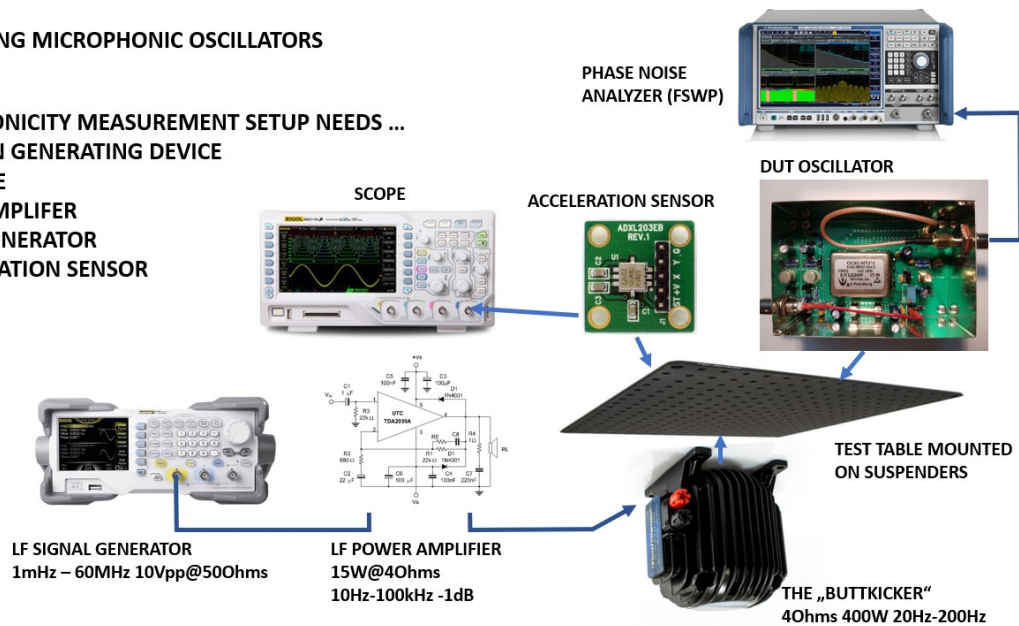


Figure 145 - The Key Components of the Vibration Test Environment

For more details see appendix K, **Thermal Design**.

Several commercial OCXOs were measured, and a frequent phenomenon was increased phase noise in the range below ca. 1kHz from the carrier.

A HP10811A example is shown below:

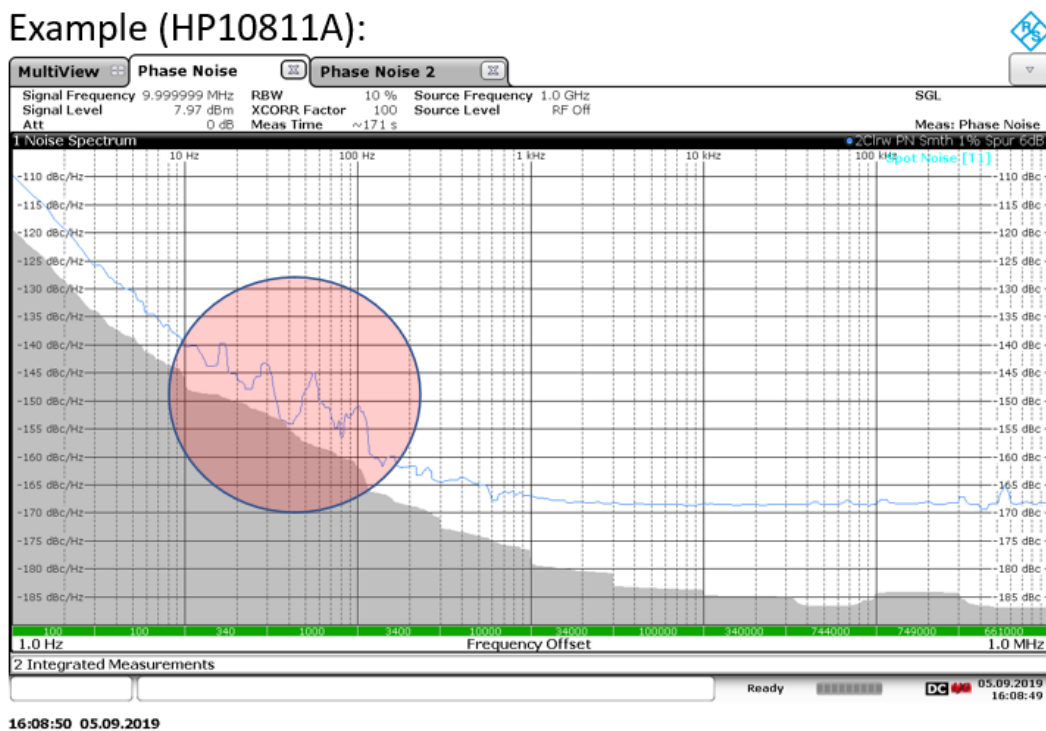


Figure 146 - HP10811A Phase Noise with Suspected Vibration Peaks

The red zone shows the suspect area. Electrical causes (interferences) were ruled out as complete as possible by using an all-shielded environment (the HP10811A was encapsulated in a further shielded tinfoil box with coaxial connectors only) and low-noise power supplies. Only high shield factor cables were used to make the connections (Sucoflex or EnviroFlex 400). The spurs remained, however. Other OCXOs were tried, with similar, but not sufficiently clear results. What was clearly missing was an environment that allowed vibrations to be accurately controlled and measured.

### 7.3 Black Magic

Black magic normally means something that cannot be rationally explained. Oscillator design is a well investigated area, but the selection of components is not always obvious and well understood. Several critical parts do not have specifications detailed enough to simulate the final design with sufficient accuracy. The mission critical parts are discussed here, along with some heuristic practical recommendations. The same goes for measurements. The more precise we need to be, the more uncontrollable effects come into play and influence our results.

#### 7.3.1 Crystals

Premium crystals (all SC cut running in overtone modes) do come with a datasheet, including values measured for each individual part, like saddle point temperature, series inductance, capacitance and resistance, parallel capacitance and Q factor for the main resonance. Even good crystals exhibit noise not only caused by their series resistance, but also a flicker component (normally modelled by a varactor driven by a noise voltage in parallel [1]). Unfortunately, this value is missing in the datasheets in most cases. A selection of crystals is the only countermeasure left (and this method, on a large scale) was used to select space qualified crystals for a lot of space programs.

Parts selected by the JPL, e.g., come in handwritten boxes with some remarks on it. To my knowledge there is no method available today that allows to *make* these parts instead of hand-picking the best of a large lot.

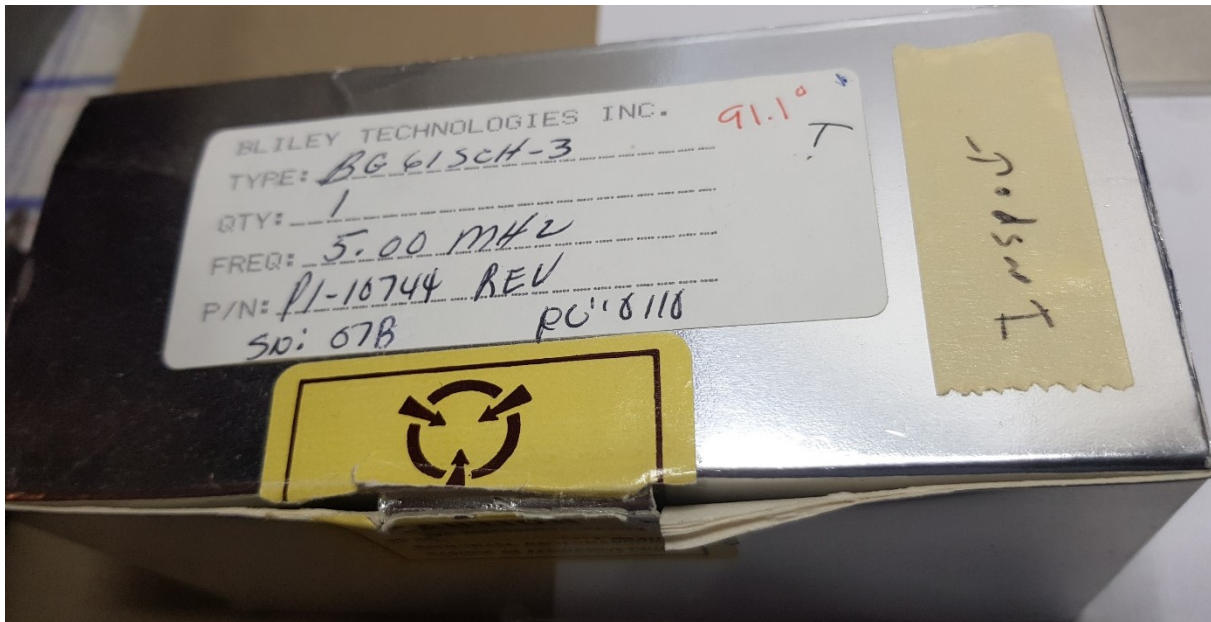


Figure 147 - A JPL Space Tested Bliley BG61SCH-3 Crystal



### 7.3.2 Transistors

Space Qualified Transistors are available for space USO designs. Apart from the default radiation and environmental specs enforced by the space/MIL procurement and test procedures an overview of available types and their properties is given in appendix L, **Space Qualified Transistors**.

The transistor properties we need for a 5MHz oscillator core are

1. Low flicker noise corner
2. Low noise figure at the operating point (a few V, a few mA)
3. Linearity, constant gain over a broad current range
4. High gain at medium collector currents (1-20mA).
5. Sufficient, but not too high  $f_T$  (20x the oscillation frequency minimum).

We run into several difficulties here:

1. Often noise figure values are only specified for a single operating point, if at all
2. Flicker noise specifications are missing completely for most parts. If they exist, they are given for a single bias point only.
3. Datasheet values are normally pessimistic and contain a (sometimes huge) safety margin.
4. Noise values are given for a room temperature environment, not for 80-90°C inside a thermostat.
5. Space transistors need to be radiation hardened. For those, post-radiation noise figures are not specified (exceptions welcome).
6. For most transistors, the manufacturing process is not published, and (except for JANS parts) can be changed anytime at the discretion of the manufacturer. While datasheet values are still valid after a process change, unspecified characteristics like noise and flicker can change to the better or worse. This has happened multiple times due to “improved” processes with less chip area and faster processing times, but worse low-end noise figures. [2]

The only remedy here is to boil down the transistor selection to some promising parts and then to test every single part individually.

From my personal experience, the rules of thumb (Parts of this is guesswork, but exact information is unavailable) for a promising part are (with a heuristic reason where available):

1. For 5MHz, old parts perform better than new parts.  
Why: most modern transistors have very smaller chips, and those seem to have higher 1/f noise due to higher dopant levels and a more disturbed lattice.
2. Low frequency parts are a lot better than RF transistors.  
Why: Maybe also larger chips, lighter base doping resulting in lower flicker noise exponent (AF 1.4 instead of 2)
3. Medium current parts ( $I_c \text{ max} > 100\text{mA}$ ) perform better than low current parts  
Why: If the gain curve over collector current is very nonlinear, this is an extra nonlinearity causing increasing mixing of 1/f noise up to the carrier. This happens for most small-signal parts close to their current limit (see beta curves).
4. Higher voltage parts are better than low voltage parts  
Why: BE breakdown will probably not occur in an oscillator with a transistor with several volts of VBE breakdown. Microwave transistors have breakdown voltages in the range of 1-2V, the general use ones in the range of 5-7V. BE breakdown causes extra noise. [3]

The bottom line is that for best results quite a lot of experimental work is required, and a good explanation why a transistor is a lot better than others is normally unavailable.



### 7.3.3 Passive Components

#### *Resistors*

Not a lot of black magic is required here; good quality, precision metal film resistors create (almost) no noise apart from the inevitable Johnson noise and Schottky noise. There are no trimmer resistors in space projects; all value fitting must be done by selection. Resistors other than precision metal film are to be treated with caution; especially carbon composite or film types are noisy.<sup>11</sup> A paper discussing resistor noise can be found in [4].

#### *Capacitors*

There are ceramic capacitors that are prone to create noise. The ones affected are the types with high-epsilon dielectrics, like X7R and Z5U (noise comes from leakage and tunneling, see [5]). Furthermore, these parts are nonlinear with applied voltage, age over time, have huge tolerances, and they are microphonic (see [6] for a discussion of high-capacitance ceramic materials). Ceramic caps should be avoided completely where possible or only implemented as NP0 types (Exception: allowed as blocking caps or in parallel with a large non-ceramic type cap).

Noise data from datasheets regarding noise is very sparse if present at all. Again, only experiments can ensure that a part is safe to use.

Non-inductive foil capacitors are much better regarding noise than the ceramic ones. There is no significant voltage coefficient, noise is negligible, they are not microphonic and aging over time is low. There is no capacitor that is absolutely noise free (see [7]).

Electrolytic capacitor noise is normally very low (for measurements see [8]). They show a flicker noise component, however.

Variable capacitors are not used in space missions due to transport problems with the service personnel. Critical caps must be chosen by selection and/or paralleling.

#### *Inductors*

Are normally noise free, leave alone their core and resistive losses. They can be microphonic. Fixing windings is critical. Only fixed valued inductors and transformers are used in space projects.

### 7.3.4 Radiation

Apart from long time exposures to low-level radioactivity that degrades components properties gradually (e.g., the gain and leakage currents for transistors), there are rare but high-energetic events caused, e.g., by solar flares that can cause instantaneous circuit malfunction like glitches or runt pulses in digital logic. Apart from screening the only remedy against these events is a robust circuit design that does not work with very low-level currents that could be significantly overridden by an ionizing event. This precludes an ultra-low energy consumption oscillator design. Useful predictions of circuit behavior under high-energy particle bombardment depend on the type of mission and are, to some degree, guesswork. Crystal based USO failures were not frequent, but did occur in the Voyager (1 USO out of two died after 40 years) and Cassini missions (see [9]).

## 7.4 Measurement Problems Without a Clear Cause

Extremely low-level measurements as close to carrier phase noise are prone to dirt effects of all kinds, among those:

**Vibrations.** A gentle tap on the lid of an FSWP can immediately ruin a measurement (1Hz-1kHz offset range is most sensitive). The same goes for the DUT USO. Anti-vibration rubber mats

---

<sup>11</sup> Using ultra low noise Op Amps like the LT1028 with around  $1\text{nV}/\sqrt{\text{Hz}}$  it is possible to analyze the Johnson and flicker noise of DUT resistors by using an amplifier with the input shorted to ground with the resistor. The DUT resistor should be soldered into the circuit to avoid contact noise.

(originally designed for washing machines) plus thick foam packaging were able to provide some soundproofing. The important point is high absorption plus a strong acoustic mismatch between the layers of the damping material. For extremely low levels, even busy roads in front of your house can ruin your day.

**Loud talking.** Same as above, with a bit broader frequency range affected up to 10kHz.

**RFI.** There should be no neon lights, cheap LED lighting with insufficient RFI suppression, heavy pulsed loads like compressor refrigerators (sic!), mobile phones, remote controls or any other similar RF source closer than a few meters from the instruments and the DUT. Line filters have proven beneficial but will never remove all the interference.

**Cabling.** This is an often neglected, but especially important issue. The screening factor of lab coaxial cables can vary widely, depending on how the outer shield is made. Simple, cheap RG58 with a sparse outer braid is sure way to have spurs in your measurements. ENVIROFLEX400 from Huber and Suhner is recommended, a double shielded cable with a foil and braid outer shield [10]. The French group working on the HSO14 types of oscillators explicitly recommend SucoFlex, a metrology grade cable with extremely good shielding [11].

**Connectors.** The best cabling cannot prevent RFI from outside if the connectors are shaky. For threaded connectors like SMA using a torque wrench this is hardly a problem, but budget BNC sockets sometimes have large gaps between socket and shell, plus weak springs for the inner conductor. This can cause interference and, even worse, contact noise.

**Thermal oscillations.** On a hot summer day inexplicable periodic aberration were found in a long-term stability measurement. After some hours of research, the culprit was found in an oscillating room fan in the other corner of the lab. With USOs, thermal shielding must be close to perfect, also for the non-Dewar parts, if possible.

**Power Supply Problems.** With USOs, it is always a risk to use switching power supplies because of their broadband noise output. Only classic linear regulated types with ca. 350uVRMS of PARD voltage (e.g., Rigol DP832A, [12]) should be used. When you need to not only supply power, but also to make accurate measurements (6 ½ digit precision for all set and measured voltages and currents, e.g., for the base bias), a source measure unit (SMU) is a must. These expensive instruments can be used for device characterization (transistor curves, BE breakdown, Gummel plots, gain over current, ...) and for USO collector and base bias supply. Additional filters can further lower SMU noise levels to values below any linear lab power supply [13]. You cannot send SMUs into space; but what is needed is a power supply chain filter that ends up with similar noise levels, in the 10uV range in a bandwidth of ca. 100kHz. When building sensitive equipment, “board power” is always regulated by an on-board regulator, even if the input comes from a stabilized power supply. Another issue is ground loops; if possible, all instruments should be powered from a single line power phase, and from a common outlet.

**Shielding.** All sensitive electronics must be shielded. “Schubert” tinfoil metal boxes were used for all my prototypes [14], and Hammond Aluminum boxes [15] for larger test setups and homebrew instruments. Both provide excellent shielding. All RFI sensitive connections are coaxial, and this includes power.

## References

[1] U.L. Rohde, “Modeling of Varactor Noise by adding a white noise voltage drive.” Private communication, Nov. 21, 2020.

[2] I. Eisele, “Causes of the increase of noise in semiconductor devices due to rapid thermal processing (RTP).” Private communication, Nov. 20, 2020.

- [3] Wolfgang Griebel, Matthias Rudolph & Ulrich L. Rohde (2020) Added Noise in Oscillators Caused by the Transistor Base Emitter Breakdown Phenomenon, IETE Journal of Research, DOI: [10.1080/03772063.2020.1847702](https://doi.org/10.1080/03772063.2020.1847702)
- [4] Yuval Hernik, "Strategies for minimizing resistor-generated noise." EETimes, Jan. 31, 2006, Accessed: Nov. 20, 2020. [Online]. Available: <https://www.eetimes.com/strategies-for-minimizing-resistor-generated-noise/>.
- [5] M. Tacano et al., "Poole Frenkel Currents and 1/f noise Characteristics of High Voltage MLCCs," presented at the 21st International Conference on Noise and Fluctuations, 2011.
- [6] T.L. Jordan, "Piezoelectric Ceramics Characterization." Langley Research Center, Accessed: Nov. 21, 2020. [Online]. Available: <https://apps.dtic.mil/dtic/tr/fulltext/u2/a395517.pdf>.
- [7] H. Nyquist, "Thermal Agitation of Electric Charge in Conductors," *Phys. Rev.*, vol. 32, no. 1, pp. 110–113, Jul. 1928, doi: [10.1103/PhysRev.32.110](https://doi.org/10.1103/PhysRev.32.110).
- [8] J. SIKULA et al., "LOW FREQUENCY NOISE OF TANTALUM CAPACITORS," *Active and Passive Elec. Comp.*, vol. Vol. 25, no. 2002, p. pp 161-167, 2002.
- [9] P. J. Schinder, "A numerical technique for two-way radio occultations by oblate axisymmetric atmospheres with zonal winds." AGU Publications, Jul. 28, 2015, Accessed: Nov. 21, 2020. [Online]. Available: <https://agupubs.onlinelibrary.wiley.com/doi/epdf/10.1002/2015RS005690>.
- [10] Huber und Suhner, "ENVIROFLEX 400 Datasheet." Accessed: Nov. 20, 2020. [Online]. Available: [https://www.koax24.de/storage/datasheet/de/050118\\_Datenblatt\\_Enviroflex\\_400\\_Enviroflex\\_400.pdf](https://www.koax24.de/storage/datasheet/de/050118_Datenblatt_Enviroflex_400_Enviroflex_400.pdf).
- [11] Huber + Suhner, "Sucoflex 102 Cable Datasheet." Accessed: Nov. 21, 2020. [Online]. Available: [https://ecatalog.hubersuhner.com/?fcode=m\\_cs\\_catitmg&m\\_cs\\_gv\\_itmguid=051MWOIs7kgQsJ4EjPxO5G&m\\_cs\\_gv\\_with\\_navi=X](https://ecatalog.hubersuhner.com/?fcode=m_cs_catitmg&m_cs_gv_itmguid=051MWOIs7kgQsJ4EjPxO5G&m_cs_gv_with_navi=X).
- [12] Rigol Inc., "DP800 Series High Performance Linear DC Power Supplies." Accessed: Nov. 20, 2020. [Online]. Available: <https://www.rigolna.com/products/dc-power-loads/dp800/>.
- [13] Keysight Inc., "B2962A 6.5 Digit Low Noise Power Source." Accessed: Nov. 20, 2020. [Online]. Available: <https://www.keysight.com/en/pd-2149912-pn-B2962A/65-digit-low-noise-power-source?cc=DE&lc=ger>.
- [14] Otto Schubert GmbH, "Weißblechgehäuse." Access: Nov. 21, 2020. [Online]. Available: <http://www.schubert-gehaeuse.de/weissblechgehaeuse.html>.
- [15] Hammond Manufacturing, "Diecast Aluminum Enclosures (1590 Series)." Accessed: Nov. 21, 2020. [Online]. Available: <https://www.hammpg.com/electronics/small-case/diecast/1590.pdf>.

## 8 A Prototype USO Design

In this chapter we present a design for a USO prototype consisting of an oscillator and a postprocessing filter to improve noise floor. The purpose of this prototype is to sanity check the conclusions of the theoretical derivations, to gain experiences with the operating parameters and, if possible, to optimize the design for maximum stability in the range of 1 to 10s and lowest possible phase noise. This chapter refers to the chapter “Crystal Oscillators” and “LC Oscillators” for the theoretical foundations.

The goals to be achieved with the prototype were:

1. Build a working low-noise oscillator with all peripheral systems like power supplies, temperature regulator, buffer amplifiers, amplitude control and output filtering.
2. Facilitate experimentation by a “service friendly”, modular design with the possibility to make changes easily and by providing a large number of test access points to monitor circuit and environmental parameters.
3. Measure Allen deviation and phase noise for some design parameters like crystal dissipation, linearity resistances, supply voltages and temperatures.
4. Find solutions to some design problems of the past like power level stability and safe oscillator startup.
5. Compare what we found to the performance of commercial/military/space oscillators.
6. Discuss results in relation with theoretical predictions.

The Not-Goals of the prototype were:

1. Deliver a space-ready product. The prototype is made with quality, but not space qualified parts (“engineering model” approach). The reason is that space parts take a long time to procure, cost orders of magnitude more money than industrial parts, and, in some cases, cannot be bought from outside of space program organizations.
2. Use “unobtainium” components to reach top performance. We must do with parts that are available on the market for all researchers. This excludes, e.g., special crystal cuts made in single-number quantities or precision capacitors with customer-specified values sealed in glass, ...
3. Fine-tune the output frequency to an exact 5MHz value. The reason is that this would require multi-week burn-in periods which would block other experiments. Furthermore, phase noise does not change by adjustment, and the premier goal is stability, not accuracy in the first place.
4. Use of metrology-grade lab equipment. For accurately measuring lowest phase noise levels close to the carrier, even top-notch general-purpose instruments like the FSWP come to its limits. No CSOs (cryogenic sapphire oscillators), ultra-precise reference sources (like selected RAKON HSO-14 oscillators with  $6 \cdot 10^{-14}$  Allen Deviation at 1s) or dedicated ultra-low noise multi-source mixer/digitizer hardware (Microsemi 53100A, e.g.) was available. No perfectly climatized, vibration shielded EMI proof lab room was available either.
5. Make environmental measurements like vibration, radiation, or ambient temperature cycling. The reason is that the available crystals did not have their vibration specifications published, and the available vibrator was not large enough to accommodate the USO prototype. A lab-grade climatized environment that would allow temperature cycling also was not available.





The DC voltages of the core circuit are RF blocked by ceramic capacitors, but not by electrolytics. This is a concession to longevity because the heater temperature can be quite high, up to 95°C, leading to short electrolytic capacitor lifetimes. Space circuits avoid electrolytics whenever they can. In our prototype electrolytics can be used for blocking DC, but they are 105°C types and enabled by a jumper only (to enable stand-alone tests outside the USO environment here).

All connections from the core PCB are coaxial using SMA connectors. The crystal is mounted in an Aluminum heater block with pluggable contacts to the core PCB, so it can be easily exchanged without soldering. On top of the heater block there is a heater transistor and a precision Platinum temperature sensor with 1kOhms of nominal resistance. A photo of the core PCB with a heater block is shown below:

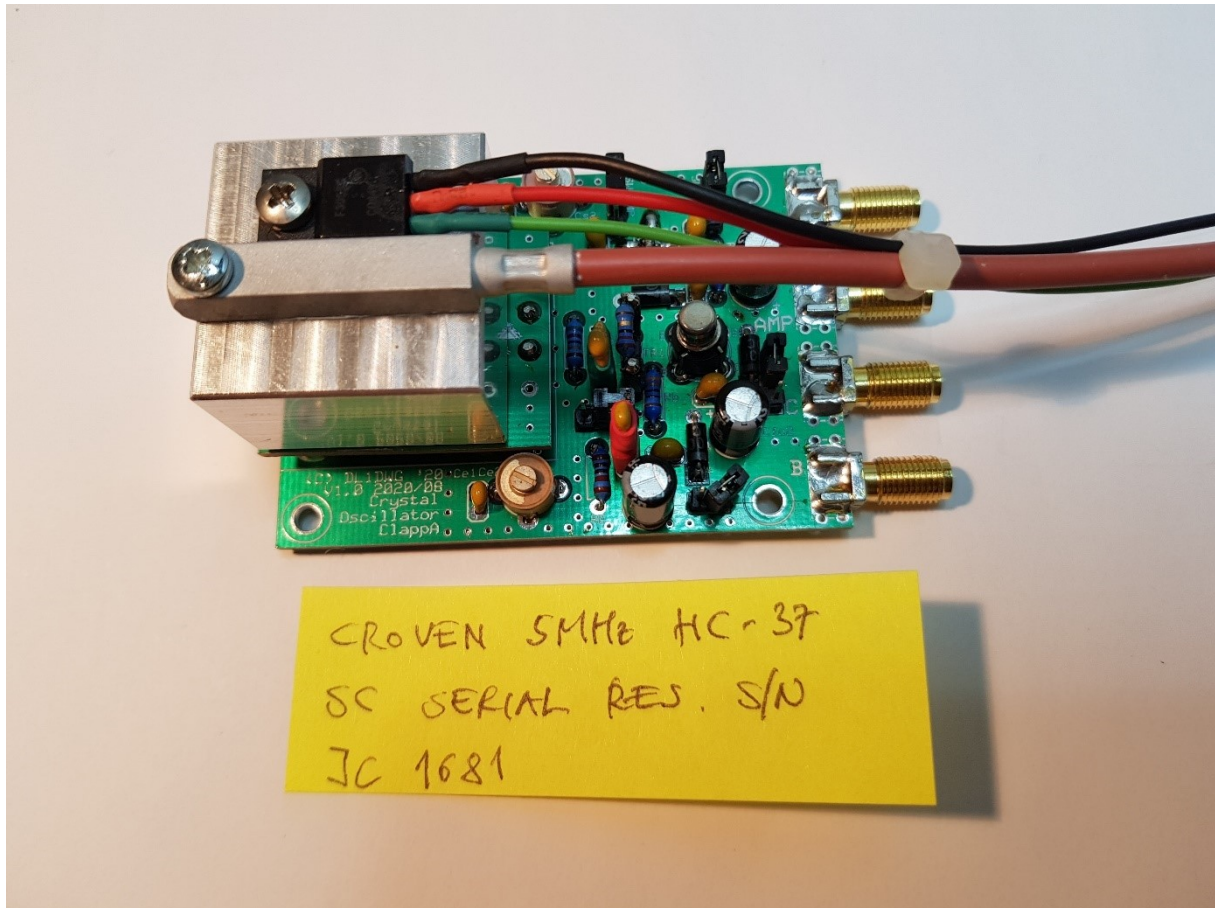


Figure 149- A Sample Oscillator Core PCB with Heater Block

Heater blocks are available for HC-30 (Bliley glass), HC-40, HC37 and HC49/U crystal cases.

### 8.1.1 Amplitude Regulation

A major issue of the design of an USO is the definition of the starting point. For the present problem, the starting point is not voltage, bias, or some other quantity, but the maximum acceptable crystal power, which sets the aging rate (datasheet example in [3]). Setting a limit to the aging rate consequentially limits the allowed crystal dissipation, and, in the topology above, this automatically determines the AC amplitudes at the base of the oscillator circuit. There is no reliable pencil-and-paper algorithm that would compute a proper operating point that will result in the AC amplitude we need. The circuit could be simulated using a time domain or harmonic balance simulator (Which does normally not work without applying some tricks), but even this will not solve the problem in a satisfying way, because it can be shown that the solution is extremely sensitive to circuit parameter tolerances, like resistor values, transistor parameters and temperature (see the phase plots in the crystal

oscillator chapter). In other words, even if an operating point could be found it would be extremely *unstable* and of no practical use, or – in other words, a regulator circuit instead of a statically fixed operating point approach is needed.

The novel regulator presented here uses the *real* output power picked off after the first amplifier stage. A dedicated log amplifier IC converts the level into a DC voltage that is then compared to a target value. An op amp drives the base bias voltage of the oscillator core which closes the regulating loop. Loop compensation is critical in two ways:

1. Any instabilities in the loop cause AM that would be converted to PM due to the AM/PM conversion mechanism (caused by nonlinearities).
2. The loop must be slow enough so no noise from the op amp reaches the base bias.

The plant transfer function has a delay of a few milliseconds due to bias deblocking capacitors and the log amp with rectified output. The op amp gain is very high ( $O(10^6)$ ) so we need to make sure that gain drops off fast enough to keep the loop stable. The regulator operates almost as a pure PI regulator in this mode. Several tests were performed; 1 $\mu$ F of integration capacitance worked well for the loop but created a 20dB phase noise “bump” in the range between 10Hz and 1kHz. Increasing the capacitors to 10-20 $\mu$ F made the loop very slow, but the phase noise returned to a clean curve.

A long time constant is not a practical USO problem, because all power sources are extremely well filtered, and temperature is kept constant. Apart from slow warm-up drift there are no disturbances that need to be ironed out by a fast loop. Low noise has priority.

The loop was found to be extremely effective, however. In a test where the oscillator was cold started and then kept on for two about two hours the deviations from the set power level were less than 0.05dBm, displayed here:

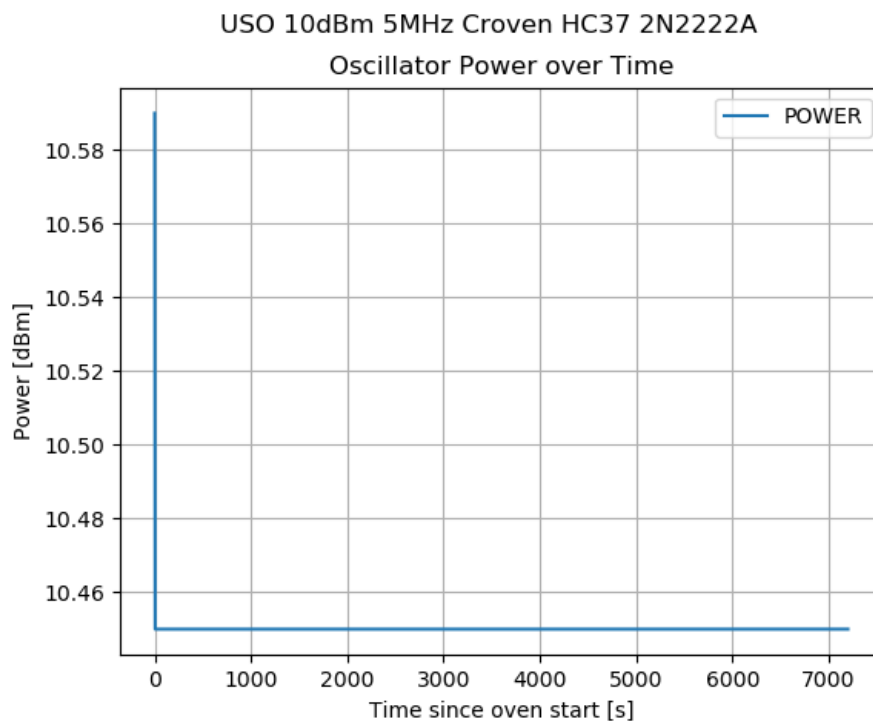


Figure 150- USO Oscillator Output Power over Time

A small overshoot occurs at startup (less than 0.2dB), but within the resolution of the power meter ( $\pm 0.05$ dBm) there were no fluctuations. The method employed could be used to further reduce crystal power (here: around 10 $\mu$ W) so that aging is kept to a minimum. Output power levels of 0dBm have

been tried (see graphs later), giving a 1Hz phase noise of -120dBc/Hz, but the noise floor gets worse with less power.

The amplitude was measured with an AD8307 based power meter (and, for validation, a Keysight U2004A RF power sensor specified from 9kHz to 6GHz). The advantage of using a log-detector based meter is the possibility to calibrate it against signal sources that are significantly more accurate than classic RF generators (e.g., Keysight N5171B has +/- 0.6dB uncertainty, and the U2004A has 4% tolerance of the power). Such a signal source could be a low frequency arbitrary function generator, which have uncertainties of about 1% (Rigol DG1062Z [4], Keysight 33622A [5], e.g.). The U2004A would be suitable but suffers from unforeseeable self-calibration activities that last 20 seconds and would confuse the timescale of our measurements. A further advantage of log-detector based meters is the strong independence from temperature changes.

As we need only 5MHz, we could calibrate just a curve for this frequency to obtain the best accuracy.

The simplified (!) circuit diagram of the amplitude regulator is shown here:

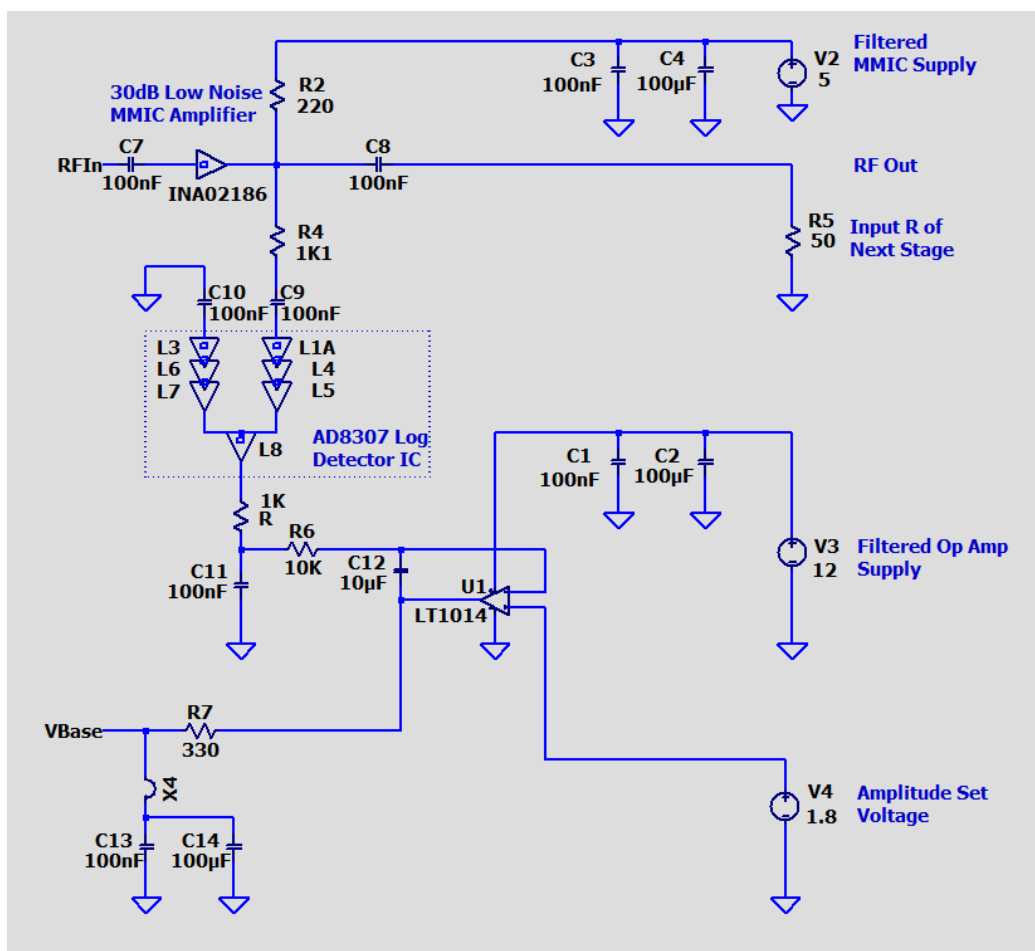


Figure 151- Simplified Schematics of the Amplitude Regulator

The incoming RF is amplified by 30dB using a INA02186 Silicon MMIC amplifier [7] that does not show strong flicker noise as modern parts using HBT or PHEMT technology (for an example of an otherwise very low noise amplifier MMIC see [6]. The catch is that the device does not even specify data below 50MHz where flicker noise sets in).



Unfortunately, no SPICE model of the INA02186 was available. By analogy, the IC highly likely looks internally like a lot of other MMICs shown below:

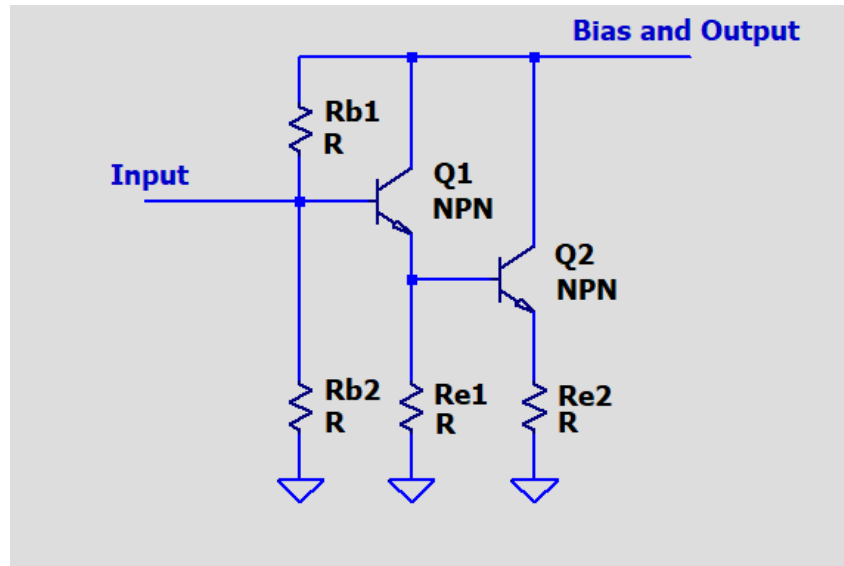


Figure 152- MMIC internal Structure

The INA02186 datasheet claims the use of a 10GHz  $f_T$  Silicon process, so we could assume that the transistors are approximate equivalents of 8-10GHz discrete devices like the BFR series. The key point is the flat noise figure curve with no visible flicker noise increase at low frequencies, as found in the INA02186 data sheet [7]:

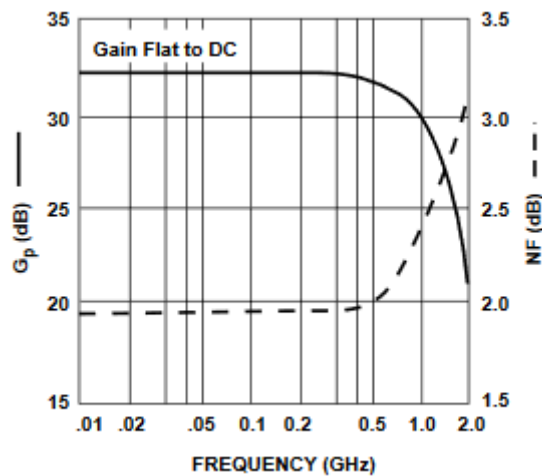


Figure 153 - INA02186 Gain and Noise Figure Over Frequency  
Picture from the INA02186 Datasheet [7]

The use of a MMIC was the result of trying several buffer amplifier topologies like common base, Norton, shunt-series pair, emitter degenerate stages and some others. The combination of high linearity and the low noise including flicker of the MMIC was hard to beat, however. A problem might be to include the MMIC inside the thermostat because of operating temperature limitations (+85°C max), but this is not a must.

A photo of the amplitude regulator inside its shielded box is shown below:

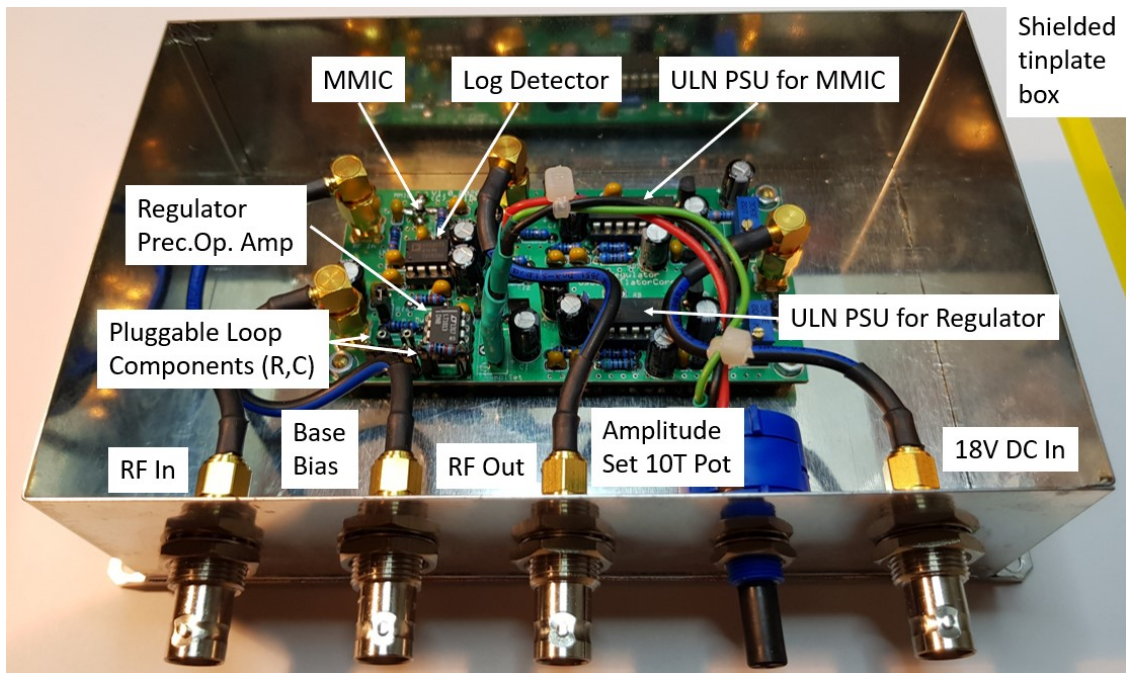


Figure 154 - Photo of the Boxed Amplitude Regulator

After amplification, the output signal is sampled via the  $R_4$  resistor (see the schematics above) and fed into a log amp level detector IC, the AD8307 [8]. This IC has differential inputs with an input impedance of around 1.1K, matched with  $R_4$ . The output of the AD8307 is a rectified DC voltage which is proportional to the logarithm of the input power. The slope is 25mV/dBm, and the smallest detectable signal is as low as -80dBm. Dynamic range is supply voltage dependent but is more than we will ever need here, as the plot from the AD8307 datasheet shows:

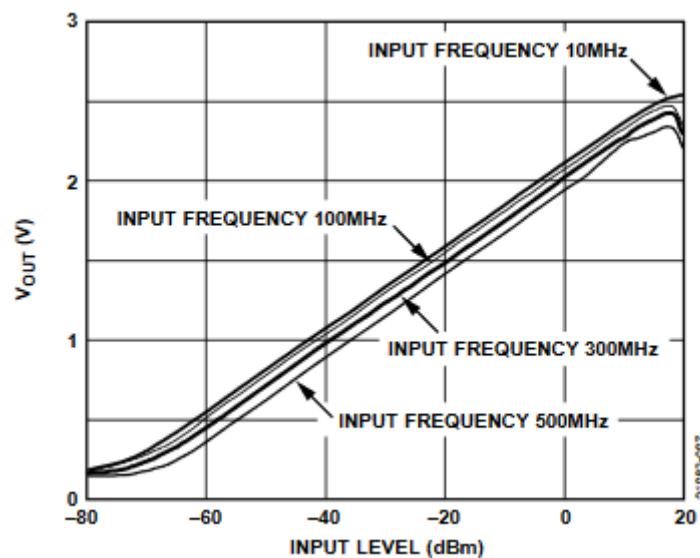


Figure 155 - AD8307 Output Voltage over Input Power  
Picture from the AD8307 Datasheet [8]

The curves show a drop in sensitivity at higher frequencies; for the 5MHz used here we found no difference to the topmost 10MHz curve in the diagram. The maximum linear power at the IC is around 15dBm, but we have a resistive divider at the input that attenuates by another 6dB, so 10dBm of oscillator power are definitely inside the linear range.

The output of the log amp is further smoothed by an RC filter. The regulation itself is done in an LT1013 precision, low noise op-amp with a reference voltage at the positive input and the log output at the negative. The circuit acts as a PI regulator with a large integration time defined by  $C_{12}$  and  $R_6$  (pluggable, set for e.g., 100ms). The regulator output is used to drive the base of the oscillator transistor, with optional RC filtering with  $C_{13}$  and  $C_{14}$ . The  $R_s$  and  $C_s$  of the regulator are pluggable so an optimal value can be found experimentally. If the time constant is too short, oscillator phase noise will increase within the regulator bandwidth (happens at  $C < 1\mu\text{F}$ ).

The usual linear approach for designing control loops cannot be used because the plant is inherently nonlinear due to the log detector. A consoling thought, however, is the fact that the dependency of oscillator power on base bias voltage (at a given collector voltage) is also nonlinear, but with a strong positive coefficient on the square (and probably also on higher) terms. This partly compensates the log behavior around the operating point and makes the loop manageable. A full simulation can be found later in this chapter.

What is missing in the schematics is the power conditioning part of the circuit. All “Filtered Supplies” in the schematics above are using an LM723J regulator with a PNP pass transistor, a filtered reference, an RC output filter, and, in case of the oscillator collector supply, additional noise cancelling circuits like a capacitance multiplier [9] and a Wenzel clean-up shunt [10]. The first regulator state with the LM723J (low-drift military version, [11]) is shown here:

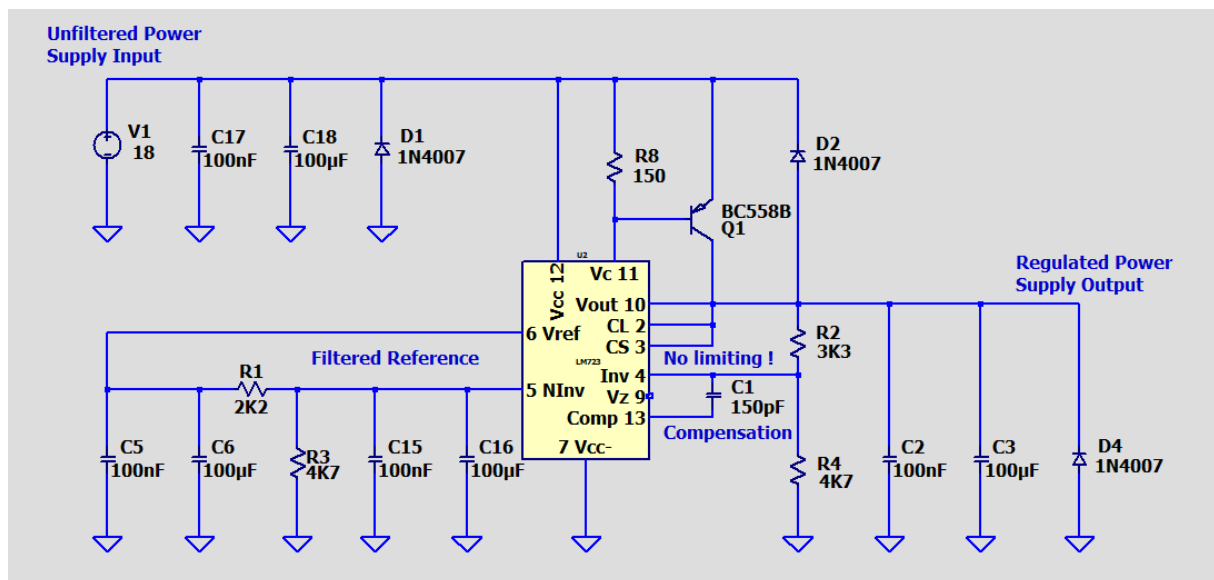


Figure 156 - Low Noise Regulated Power Supply for MMIC, Collector and Regulator

According to tests by other researchers [12] this vintage circuit performed best in comparison with several other voltage regulators (probably due to the possibility to filter the reference). A PNP pass transistor keeps the dissipation (not much anyway) away from the LM723s internal reference. The PNP solution adds less noise than an emitter follower NPN transistor normally employed. No current limiting was implemented, also because we found that it would add noise to the output. Limiting must be done at the input side, if needed.

The post-supply filters are shown below:

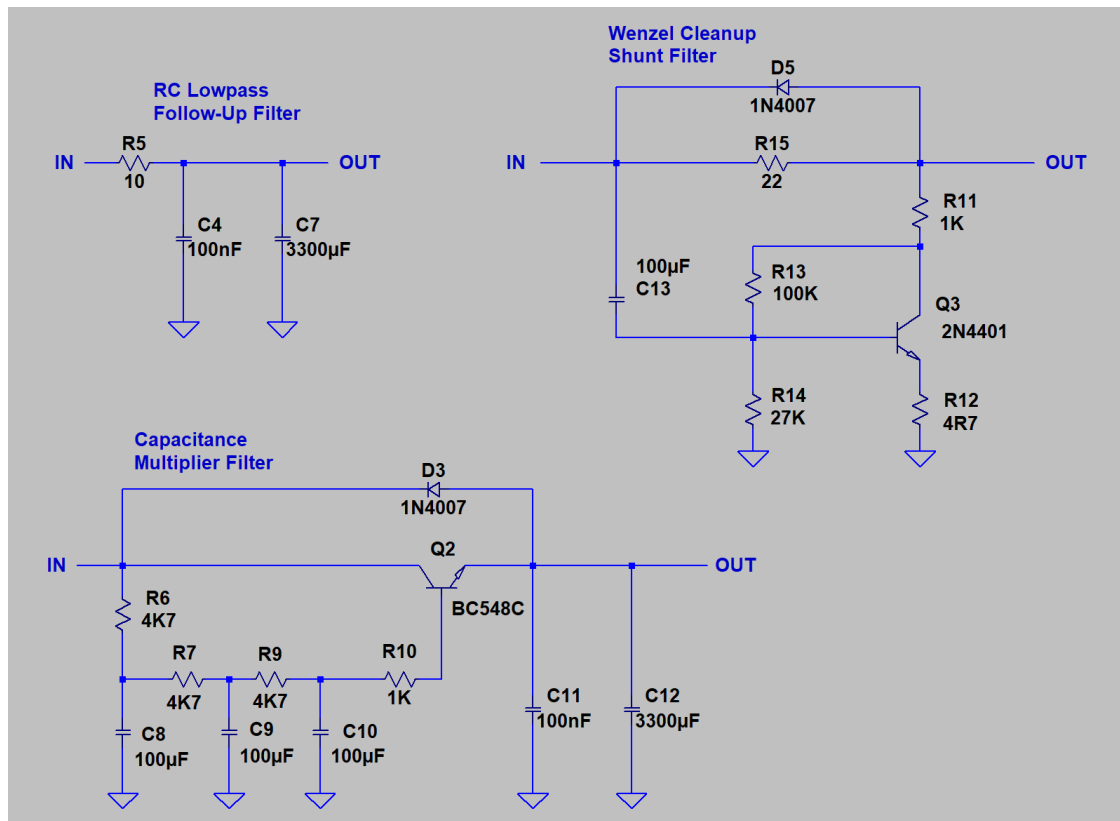
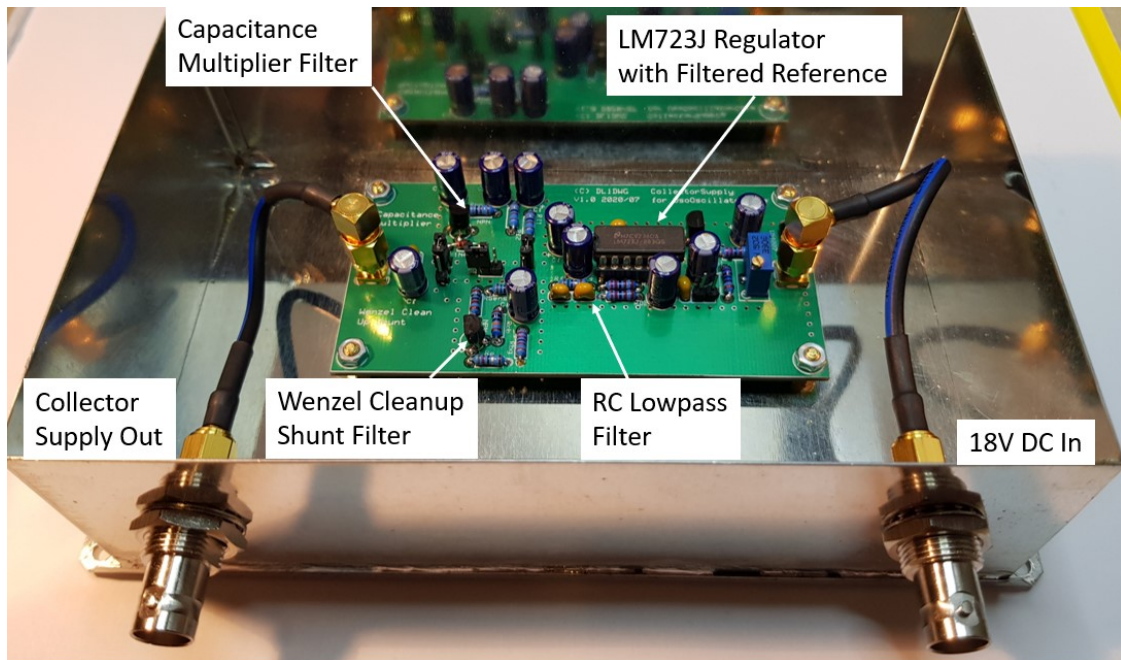


Figure 157 - Post-filter Schematics  
Redrawn from [9].

The RC lowpass needs no further comment, but the Wenzel shunt filter is not as trivial. Let us assume a steady state with a DC current flowing thru  $R_{15}$ , causing a (small) voltage drop. If a positive spike or noise appears at the input, the output would also rise, but the transistor inverts the spike and pulls more current thru  $R_{11}$ , (partially) eliminating the spike at the output. Component values must be determined depending on average current. In the case of the USO collector supply we may assume an almost constant current drain, so this circuit makes sense. The last possibility is a well-known circuit called a capacitance multiplier [9]. It works fine for not too high interference frequencies and output currents, so in case of the collector supply it is suitable.

The filtering and shielding techniques employed made it possible to run the complete USO assembly from a standard lab power supply (Rigol DP832A, [13]) instead of a high-precision SMU with special output filters (Keysight B2962A with LNF, [14]). Without extra filtering, spurs would prevent achieving low phase noise at small offsets (<100Hz).

A picture of the completed and boxed collector supply regulator unit can be seen here:



*Figure 158 - The Collector Supply Regulator with RC Lowpass, Capacitance Multiplier and Wenzel Cleanup Shunt*

As discussed, all connections are coaxial. The use of high-shield factor cables (ENVIROFLEX 400 from Huber&Suhner [15]) and quality connectors is extremely important. A good sanity check is to take a mobile phone with an active call and put it into the vicinity of the cabling. If nothing or very little can be seen on the phase noise curves, cabling and shielding is OK. A range of 10Hz to 1MHz is enough to see the effects, so measurement times can be kept short.

### 8.1.2 The Heater Regulator

The heater regulator is another important part to USO performance. Again, a slow PI loop is used, along with a large thermal mass acting as a low pass to suppress fluctuations in heater current before they can penetrate to the crystal disc. The heater regulator circuit is shown below:

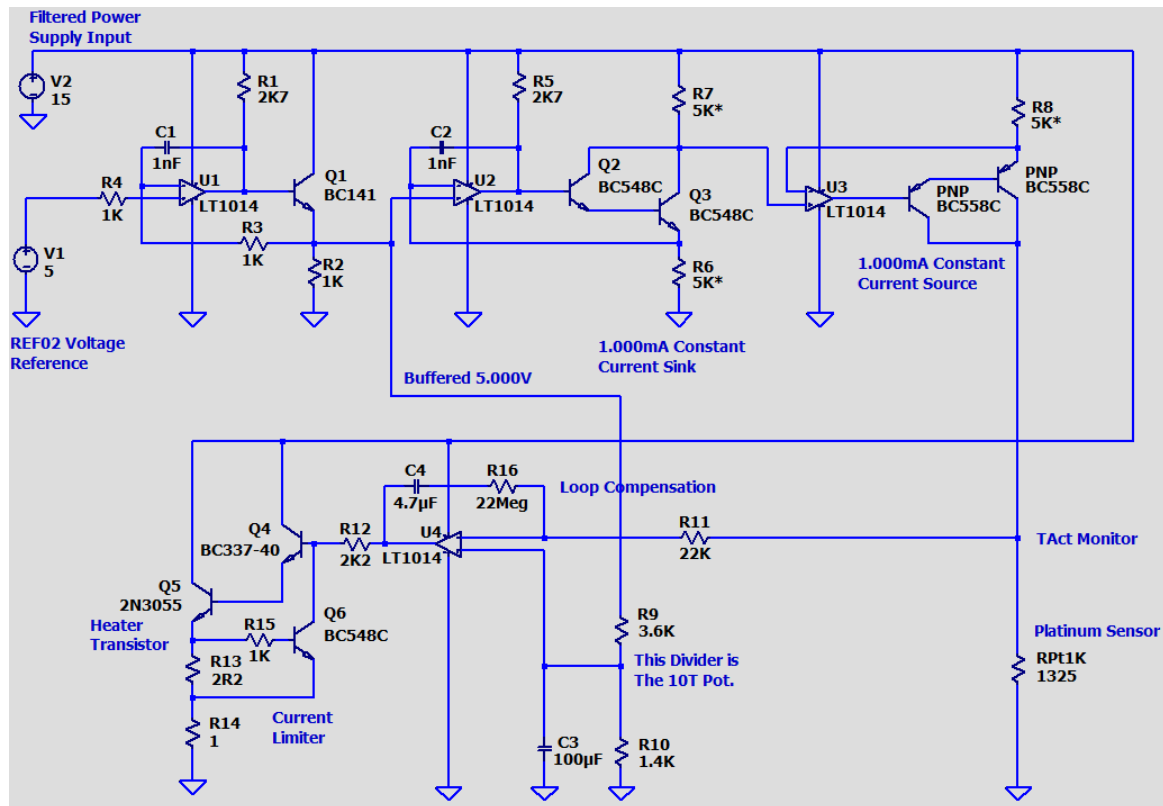


Figure 159 - Heater Regulator Schematics (Simplified)

The regulation process is partly nonlinear for the sake of a reasonably (but not too short to avoid thermal stress in the crystal) startup time. Below the set temperature, the heater works in a current limited mode that has a few Watts of heat created (i.e., the limited current times the collector/emitter voltage). The startup current is set by R<sub>13</sub>. The loop is not active during this period due to error amplifier saturation.

When the desired temperature is reached, the current drops below the limited amount and, after a small overshoot, the linear loop takes over and stabilizes the temperature, as shown here:

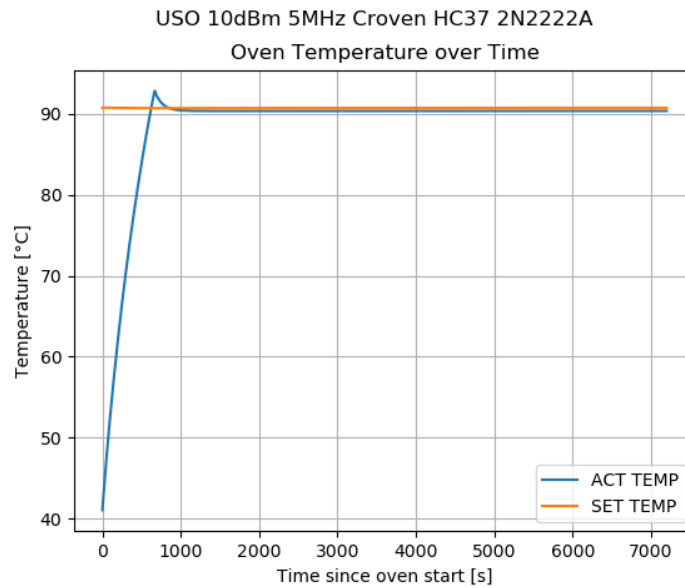


Figure 160 - Oven Temperature over Time

The climb rate of the temperature during the constant current phase is approximately  $52^{\circ}\text{C}/700\text{s}$ , which is about  $4.5^{\circ}\text{C}/\text{minute}$ . We found no data about the permissible rate of crystal temperature changes, but a warm-up time of a bit more than 10 minutes is not uncommon for other commercial oscillators, even shorter times are quite common.

After a short overshoot, the big picture suggests that equilibrium is reached after 1000s.

The set and actual temperatures differ by a very small offset. This offset is a static error caused by the tolerances of the Platinum sensor (here:  $1^{\circ}\text{C}$ ) and could be reduced by using sensors with a smaller tolerance ( $0.1^{\circ}\text{C}$  or less, expensive).

The overshoot is magnified in the picture below:

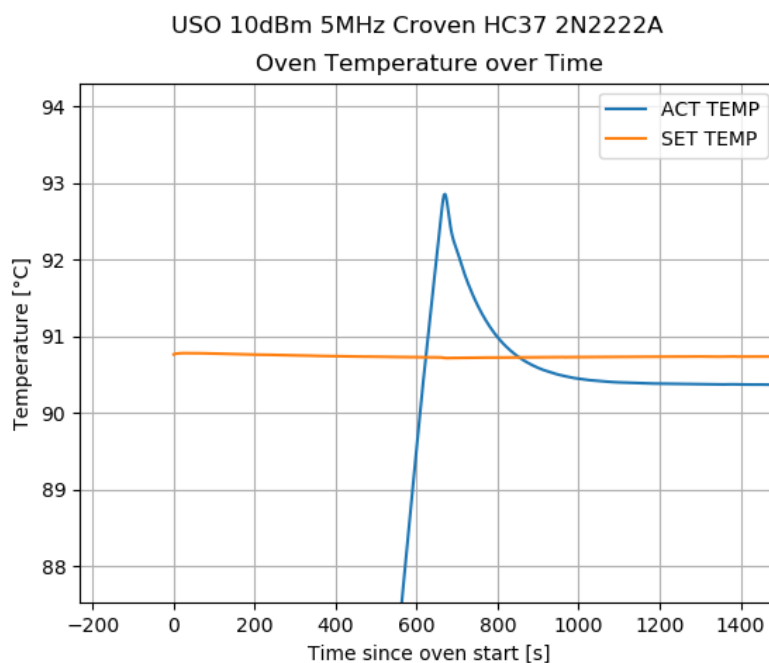


Figure 161 - Oven Temperature over Time - Overshoot



The overshoot magnitude is about 2.5 °C.

The zoom also shows the static offset in more detail, we have ca. 0.4°C between set and actual measured value. With the sensor (1°C) and the measurement current ( $10^{-3}$ ) tolerance this is absolutely within limits.

The settled temperature is shown below:

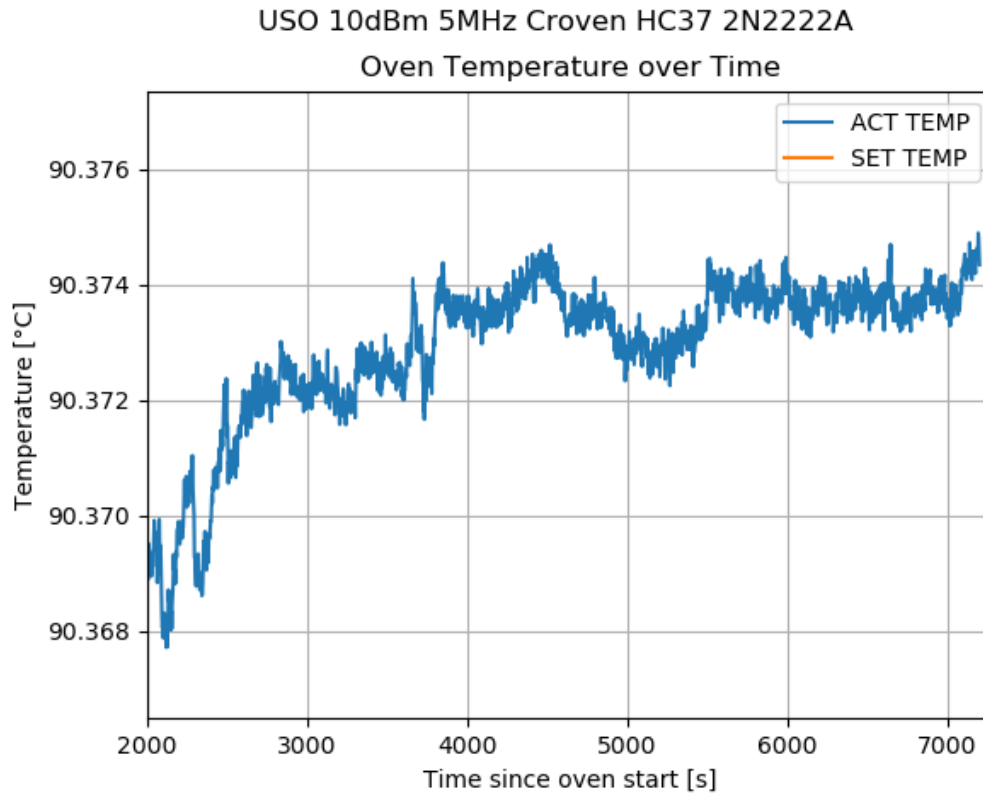


Figure 162 - Oven Temperature over Time - Steady State & Noise

After around an hour the temperature stays within 2mK. This value is pessimistic, because it is measured by a digital multimeter at its resolution and noise limit, despite the 7 ½ digit resolution (Keysight 34470A [16]). What is measured is the voltage drop across a 1kOhm Platinum temperature sensor with exactly 1.000mA driven into it. The temperature fluctuations shown above are in the range of the instruments accuracy (16ppm) and noise floor.

For more exact temperature measurements a standard lab grade multimeter and sensors would be necessary (e.g., a Keysight 3458A 8 ½ digit 4ppm multimeter, Class A (0.1°K) or even better sensors). Special cables with low thermal EMF would also be needed, and the influence of the cable resistances would then need compensation.

As long as the circuit is operated at or around the crystals lower turning point the performance gain is probably not worth the extra effort.



Using an SC crystal means that the frequency first rises when temperature increases, until the lower turning point is reached. The frequency over time can be seen in the following picture:

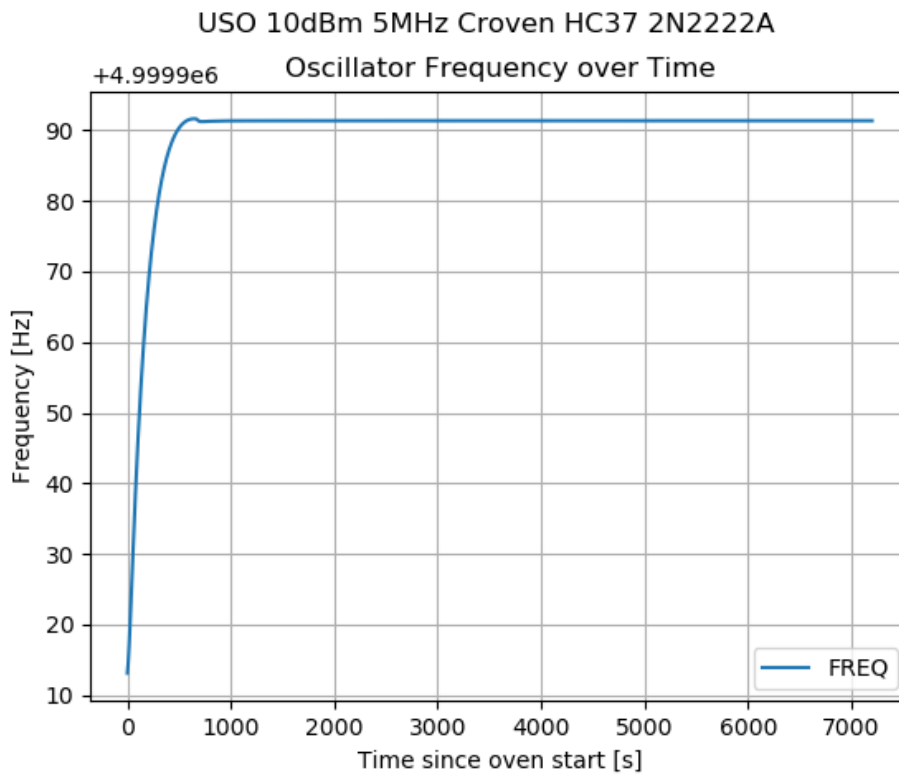


Figure 163 - Oscillator Frequency over Time

A small overshoot occurs, indicating that the LTP temperature was maybe set a very small bit too low.

The long-term value is very stable, as the detailed view shows:

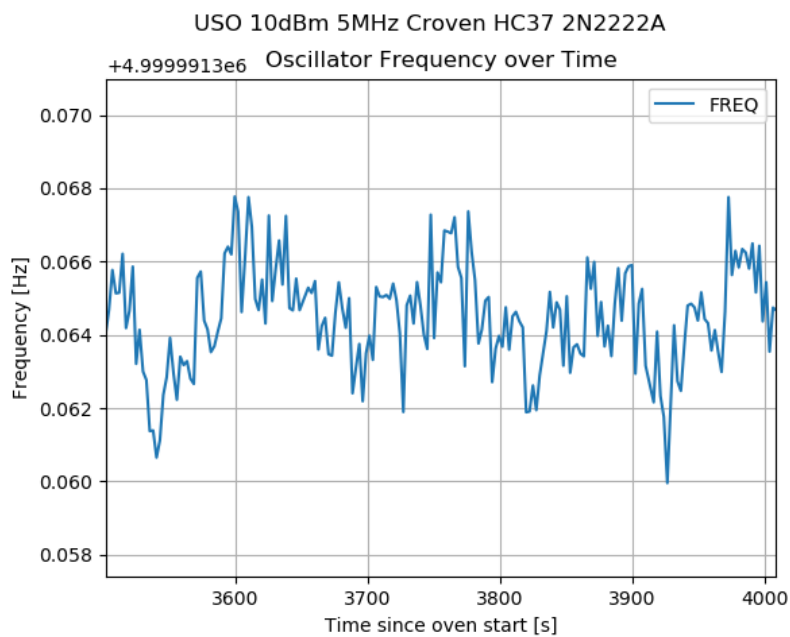


Figure 164 - Oscillator Frequency over Time - Steady State & Noise

The total deviations stay within a range of 8mHz peak-peak, on average less than 4mHz. The frequencies were measured using a Keysight 53230A 6GHz counter with a resolution of 20ps. The counter was additionally stabilized by a GPS receiver.

For a sanity check, the counter was fed with the same GPS signal at the input and at the reference. The measured frequency deviation was below  $10^{-11}$ Hz for a 10s gate time, confirming the specifications.

The dependency of the crystal frequency on temperature is shown in the next graph:

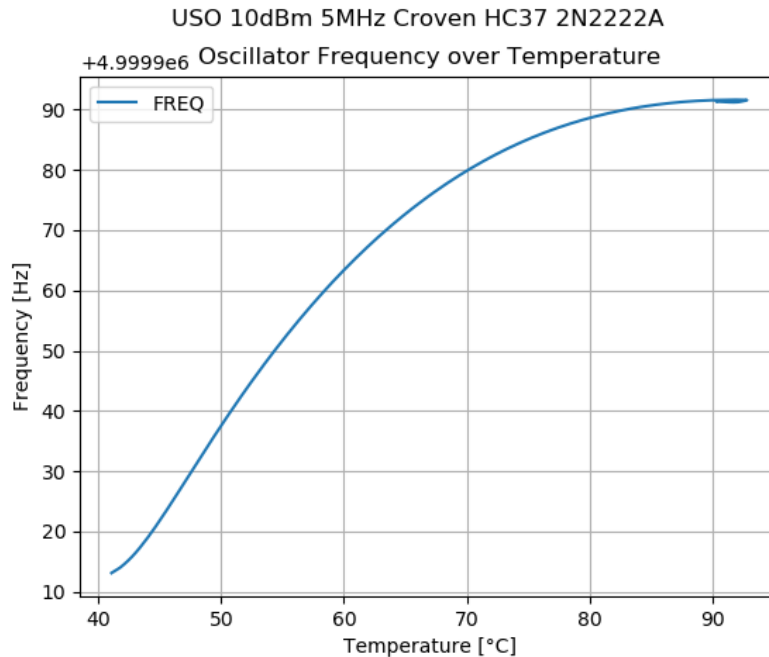


Figure 165 - Frequency over Temperature

This curve is typical for an SC cut crystal. The almost flat top indicates that the temperature is almost exactly at the lower turning point (LTP), as it should be for maximum temperature stability.

The little loop at the upper end comes from the temperature overshoot and shows some minimal retrace effect:

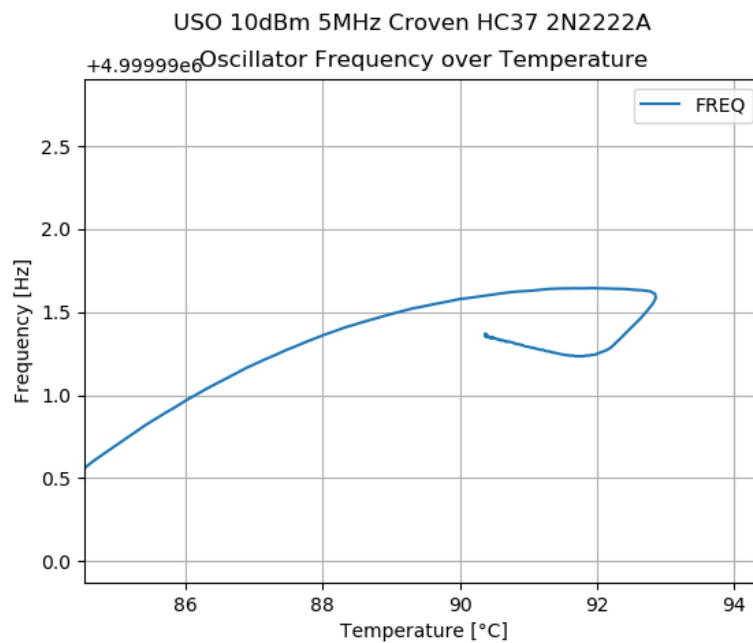
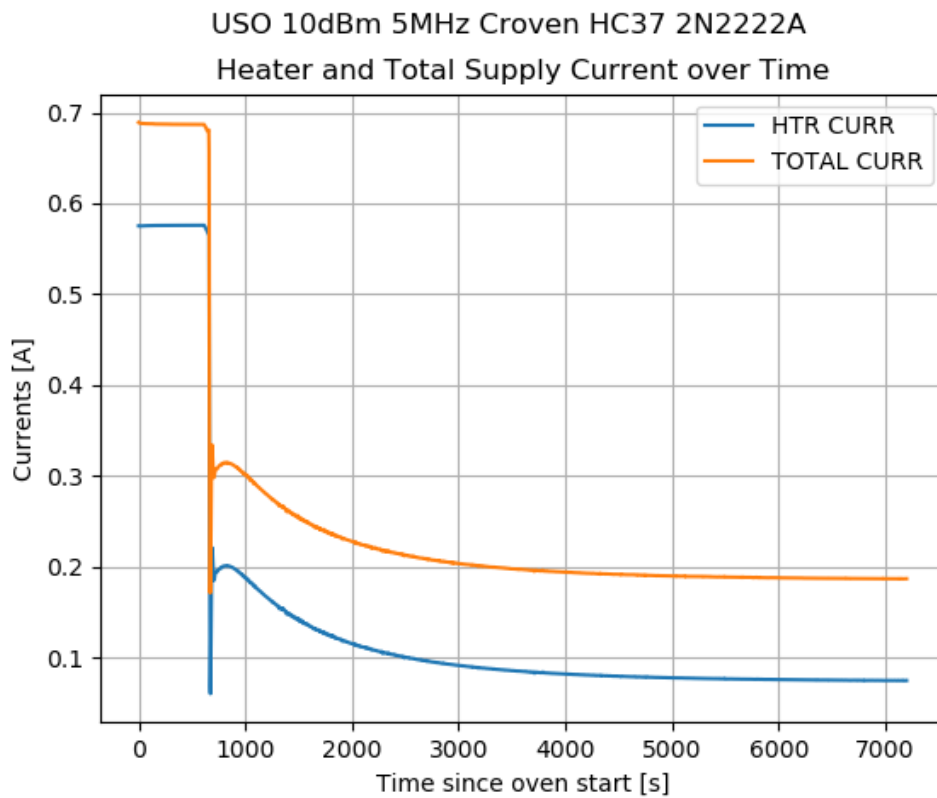


Figure 166 - Frequency over Temperature - Details

This is not real “retrace” (SC crystals almost do not show this effect, unlike AT parts), but the little delay in sensing heater block temperature and the temperature inside the crystal metal can and the crystal disk inside itself.

The heating process also reveals some properties of the thermal environment. Consistent with the partly nonlinear heater regulator, the heater current looks like this:



*Figure 167 - Heater and Total Supply Current over Time*

After the linear loop takes over, there is another 2000s until the current approaches a stable value. This is not the slow reaction time of the regulator, but due to the fact that the rest of the oscillator PCB, the innards of the Dewar flask, and also the heat-conductive cabling still warm up after the crystal has already reached its nominal temperature.

The statement above can be substantiated by showing the takeover process in detail:

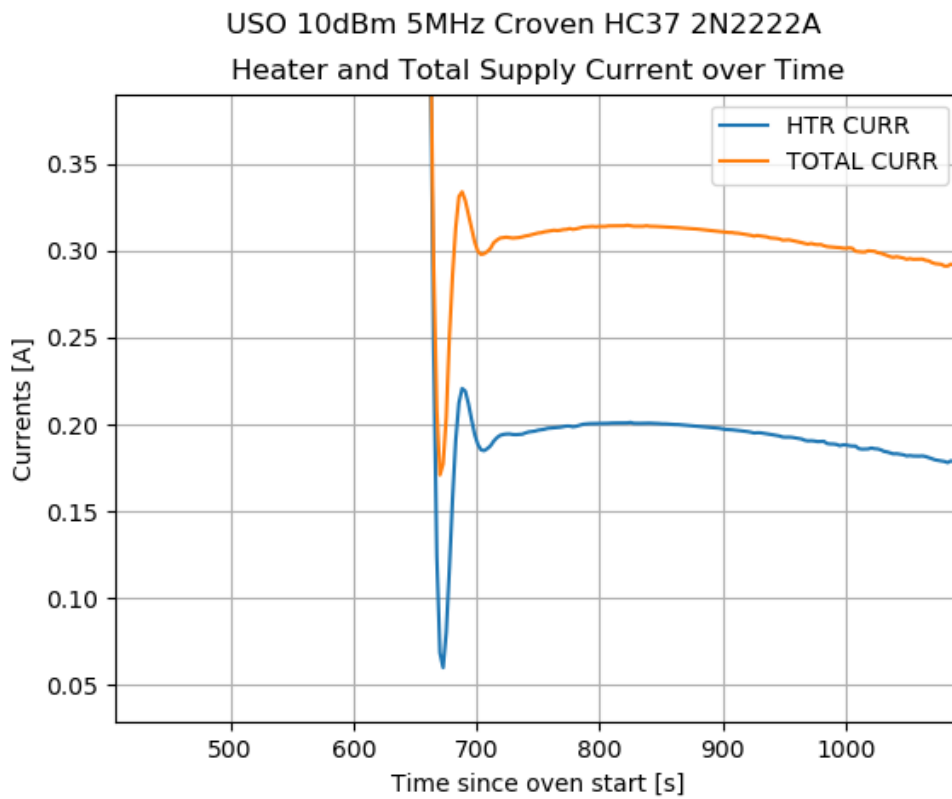


Figure 168 - Heater and Total Supply Current over Time - Regulator Settling Time

The overshoot is small and over in a few ten seconds (this is the regulator PI integration time), but the plant still needs power until everything within the Dewar is finally hot enough.

The heater current has some noise on it, but the large thermal mass flattens that out:

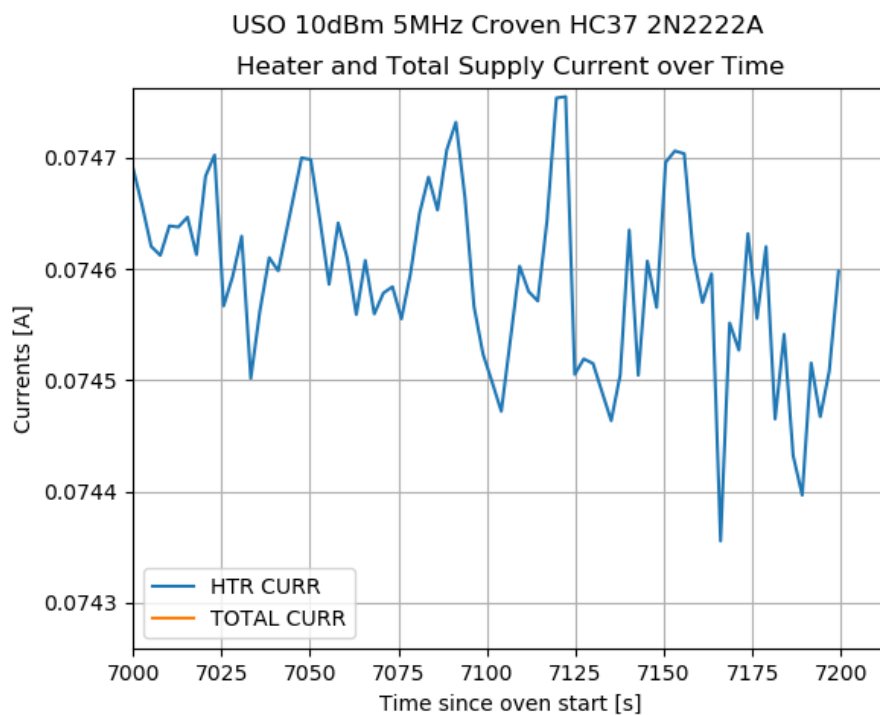


Figure 169 - Heater and Total Supply Current over Time - Steady State and Noise

This about 200uApp at a current at the end of the experiment of 74.5mA, so a noise level of less than 0.3%pp. Even after two hours the current still drops gently.

The complete heater controller unit is shown in the picture below:

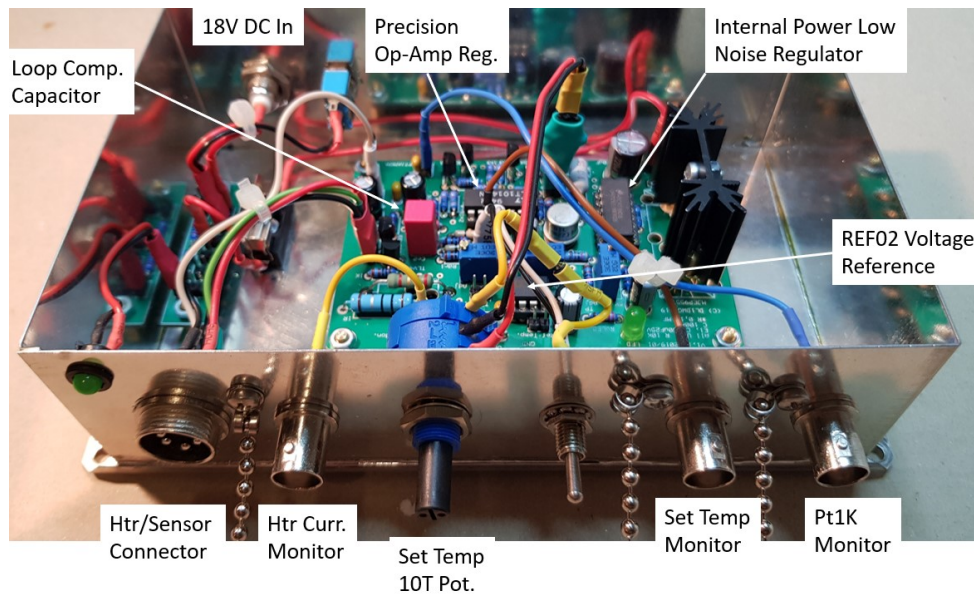


Figure 170 - Picture of the Boxer Heater Regulator

The heatsink at the right of the PCB belongs to the PNP pass transistor of the LM723J regulator. With total currents of more than 0.5A and a voltage drop from external 18V to internal 15V a larger transistor (MJE2955) is needed, and must it dissipate 1.5W safely, therefore it is heatsinked.

All external connections go through shielded coaxial (all signals) or shielded multiwire (heater and sensor) cables.

A last interesting point is the initial and permanent power consumption of the whole USO including heating, oscillator power supply, amplitude regulation and buffering:

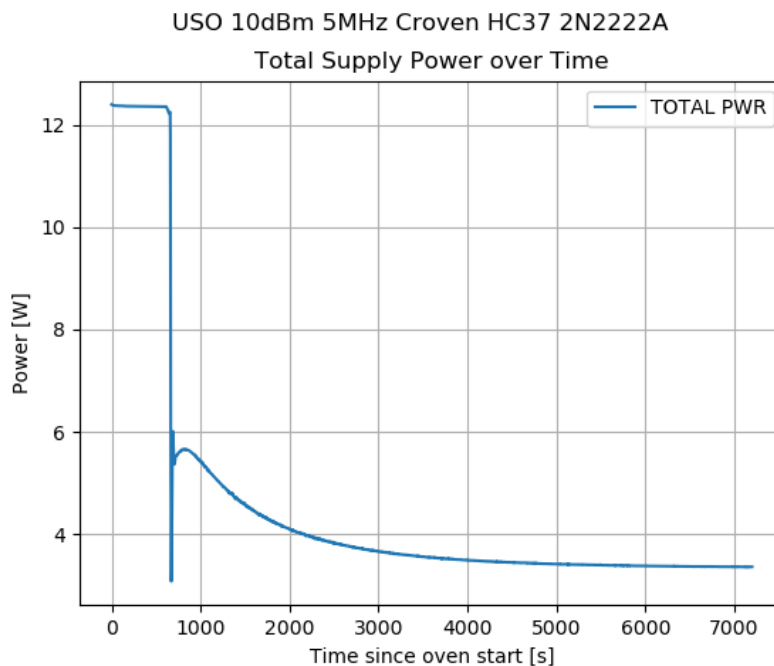


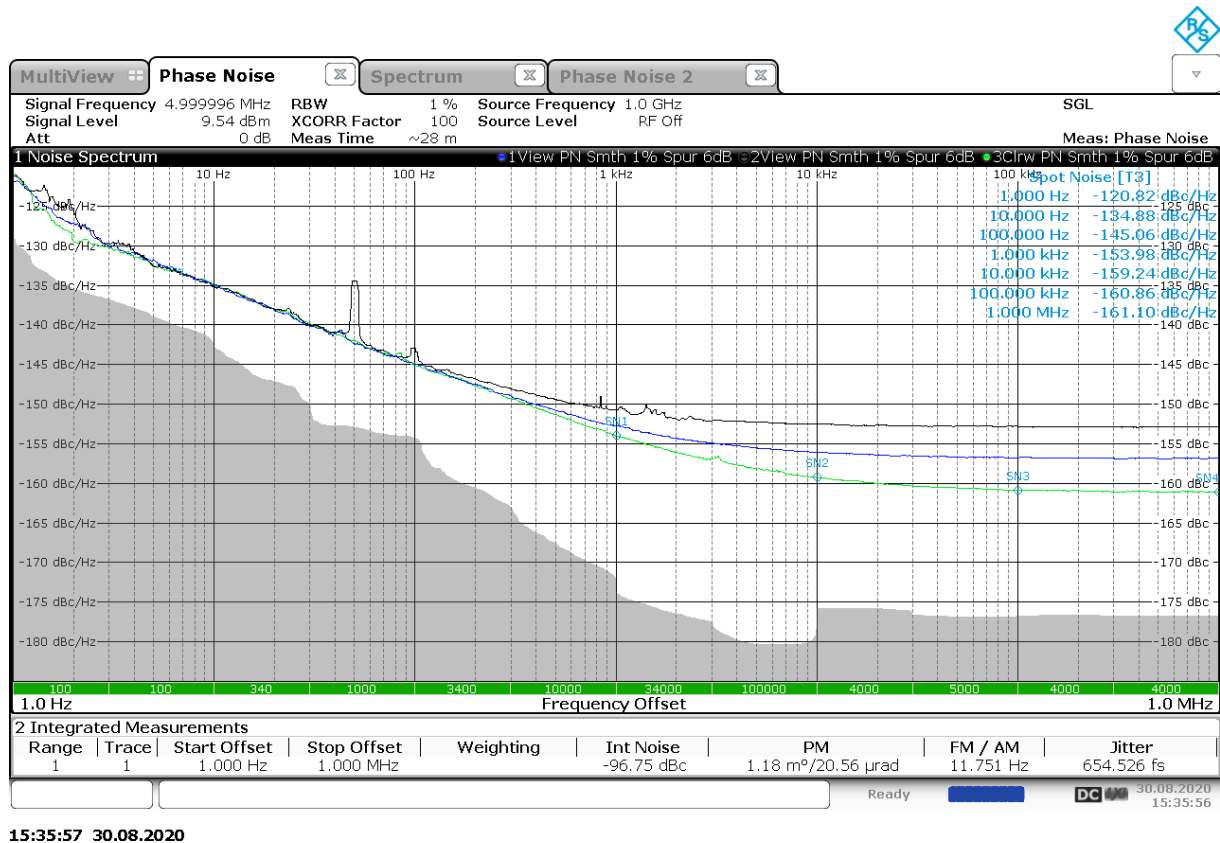
Figure 171 - Total Supply Power over Time

At startup power consumption is a little bit more than 12W, and the final value with at 23°C room temperature is around 3.5W. These values are in the range what other commercial products have (e.g., Wenzel HF Citrine: Start uses 8W, permanent power is 5W).

The top value can be easily reduced by setting a smaller startup heater current (here: 0.6A) if needed. This would increase warmup time, however.

### 8.1.3 Phase Noise and Allen Deviation

Now to a very important result, phase noise and Allen deviation in the range from 100mHz to 1MHz:



15:35:57 30.08.2020

Figure 172 - Phase Noise at 2,5, and 10mW Output Power

This plot shows phase noise for 2mW (black), 5mW (blue) and 10mW (green) of oscillator output power. The crystal used was a Croven HC-37 5MHz SC cut part, with the standard circuit. The table at the top right belongs to the 10mW version. What can be noted is:

1. There is only a small difference in 1Hz phase noise levels. At all power levels, it stays below 120dBc/Hz, not a bad value for a commercially available crystal
2. The floor at high offsets follows the predictions of the Leeson formula and drops with increasing power. 10dBm is just below the compression limit of the post-oscillator amplifier, so no further attempts for more power were carried. We are interested in extremely low aging, so the crystal power level of between 10uW and 20uW associated with a 10mW output power is still low (datasheet has 50uW as default power), but about the limit for high-stability operation.
3. The grey zone (marking a confidence limit) is just 7dB below the measured values at low frequencies, so these values should be taken with a grain of salt (the FSWP has a datasheet tolerance of 3dB on phase noise values). A longer measurement (4.8h) confirmed the values, however.

The classic space oscillators like the ones of the Apollo and following missions have no crystal power specified (only output power). All known circuits (e.g., see Greg Weaver, HP10811A, Morion MV89, ...) use a simplistic amplitude stabilization scheme rectifying AC after a buffer stage and diverting base drive of the oscillator transistor if the amplitude becomes too high. This mechanism is not very precise, explaining the large tolerances of datasheet output levels.

Linearity resistors do make a difference. As experiments have shown (tried all E12 values from zero to 470 Ohms), a value of 220 Ohms gave the best results for the 2N2222A transistor used.

The same test as above was repeated with Bliley BG61SCH-3 crystals, with about identical results. These glass case (HC-30) parts are much larger than the modern HC-37 types, and some need a B Mode trap circuit. The thermal time constants are longer than the cold-weld parts, partly due to the better insulating glass case and the larger heater block. Bliley did not respond to a request for sample parts, so we did not pursue this approach.

HC40-type Croven SC crystals were tried as well but resulted in a worse phase noise level at 1 Hz and below. No further experiments were done with those.

The next test (HC37 again) used just 10mW but was conducted down to 100mHz:

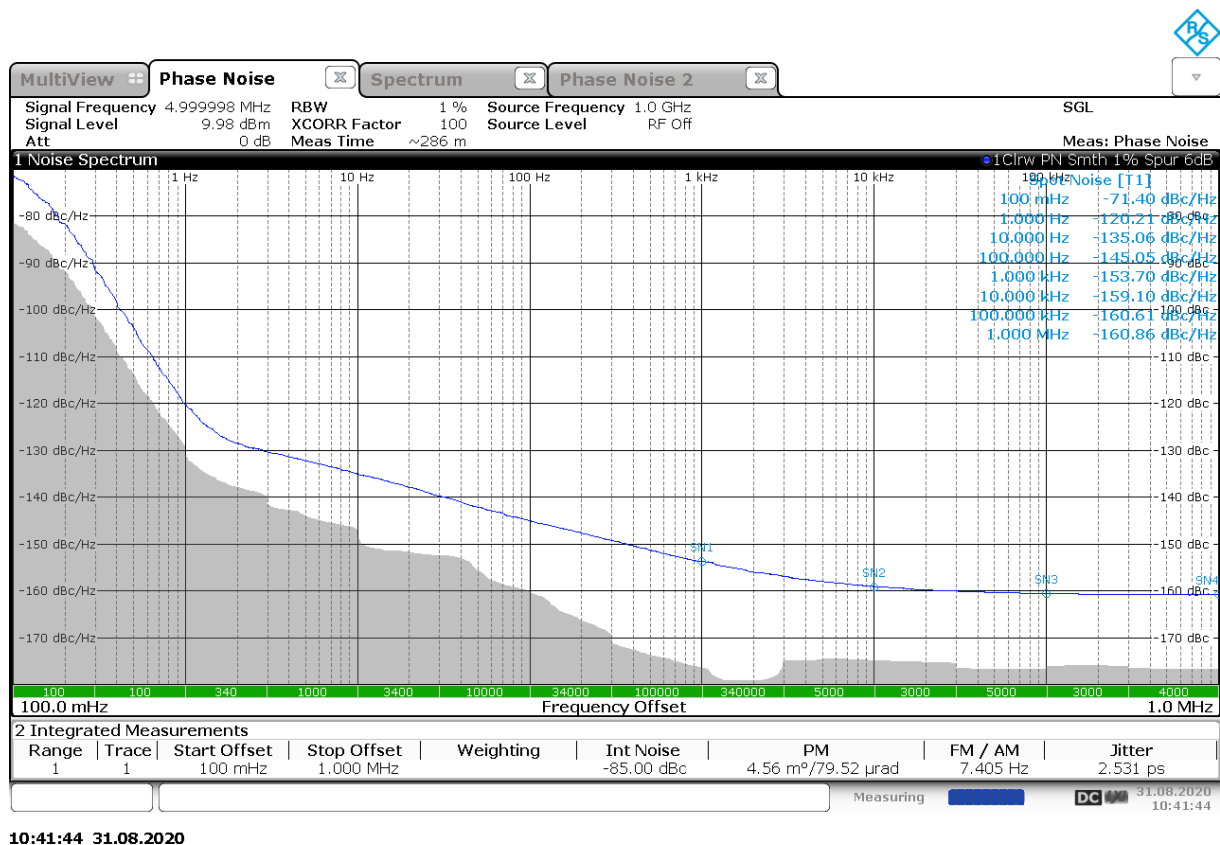


Figure 173 - Phase Noise from 100mHz to 1MHz (Oscillator Power 10mW)

The previous down to 1 Hz results were confirmed, and the 100mHz phase noise level was -71.4dBc. At 100mHz a slight flattening of the curve occurs; This could be the influence of the amplitude regulator time constant. Due to the extremely long measurement times of 4.8h this was not further investigated.

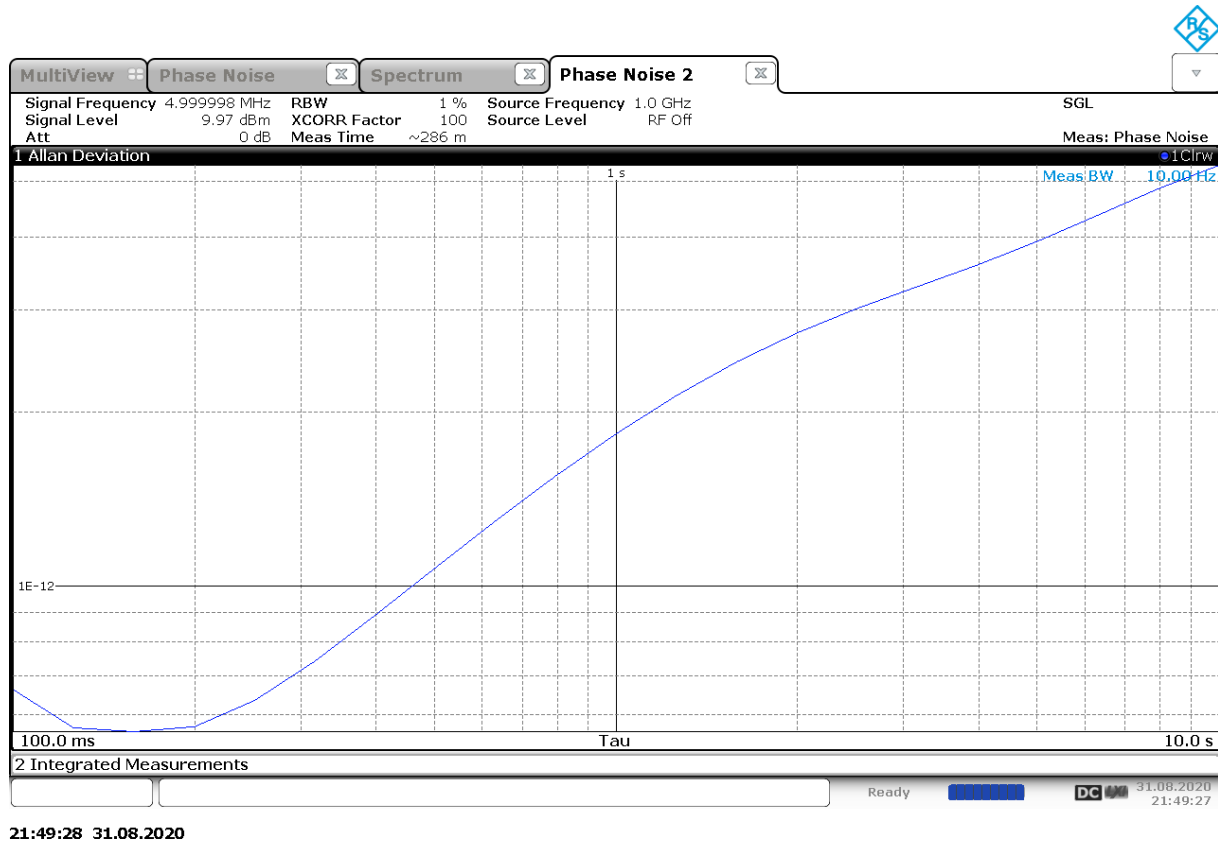
Measurements like this do not always work out so smooth as shown above. All kinds of vibrations, like closing doors, handling equipment on the same table as the experiment, loud talking and probably all kinds of other interference like mobile phones in the vicinity can litter the curves with numerous



spurs and invalidate the measurement. In order to avoid these effects, the experiments were started remotely and after midnight were nobody was working in the lab.

For a continued research into ultra-low close to carrier phase noise a shielded and vibration-proof room is a must.

In Allen deviation terms we see a minimum between 100ms and 1s:



21:49:28 31.08.2020

Figure 174 - Allen Deviation from 100ms to 10s at 10mW Oscillator Power

The Allen deviation minimum occurs at ca. 150ms and reaches down to  $5.5 \cdot 10^{-13}$ . In the complete range we stay below  $2 \cdot 10^{-12}$  until 1s and below  $5 \cdot 10^{-12}$  until 10s.

The phase noise and Allen deviation results compare well with commercial parts, as can be seen from the following table:

Specification	PN@1Hz spec.	PN@1Hz typ.	PN@10kHz spec.	PN@10Khz typ.
RAKON RK410	-110	-120	-145	-146
USO Prototype	-120.21	-122 (best)	-160	-162 (best).

To be fair, the prototype only shows what is possible with the new crystal generation, but it is not space qualified. On the other hand, the RAKONs have been measured with specialized correlators that have a lower internal noise limit, so the prototype values on the FSWP are probably pessimistic.

### 8.1.4 The Complete Setup

A block diagram of the USO Prototype, plus all test equipment used in the experiment is shown here:

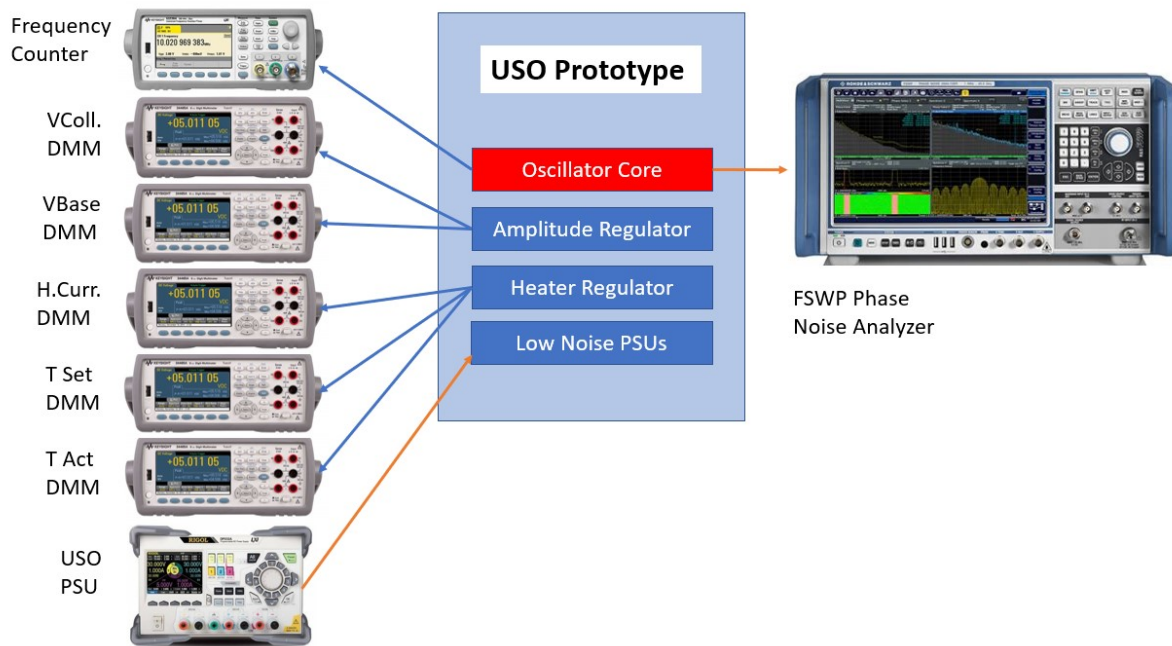


Figure 175 - The Complete USO Prototype Measurement Setup  
Pictures of Instruments from respective Manufacturers (see text)

The counter at the top of the left tower is fed from a 30dB tap (not shown). This tap has a through attenuation of only 0.3dB and is usable up to 100MHz, so by far good enough for the 5MHz we have here.

Below the counter are the DMMs used in the USO experiment. The multimeters are all from Keysight (a 34470A 7 ½ digits for T Act, 3x 34465A 6 ½ digit for T Set, H. Curr. and VBase, and a 34461A 6 ½ digit for the collector voltage).

The PSU at the bottom of the left tower is a Rigol DP832A (2\*30V/3A, 1x5V/5A). Due to the internal filtering efforts an SMU (Keysight B2962A) is no longer needed.

On the right side the FSWP signal analyzer measures phase noise. It is placed on a dual layer of vibration damping material (rubber, Styrofoam). The USO prototype is located on top of the FSWP, with another foam package between the FSWP and the prototype.

What is not included in the picture is the PC that controls all instruments remotely. First, the PSU is switched on and stabilized for 10 seconds. Then, a timed loop reads all data from the power supply, all multimeters and the counter and collects it in a database.

After a successful run (7200 seconds were chosen for a start, 2hours) a postprocessing program reads the database and creates all graphs needed (as shown in this chapter).

For phase noise measurements, the process is a bit different, because the startup phase is unimportant and even annoying for a phase noise measurement due to frequency drift. A stabilized state (at least a few hours) is needed to make meaningful phase noise plots, especially for measurements very close to the carrier like 100mHz. The PSU is powered up manually, so are the DMMs, and after a few hours a FSWP scan is triggered and the screenshot is taken after the run is completed (up to 4.8hours).

### 8.1.5 A Full Simulation of the Amplitude Regulator

This section discusses the oscillator/amplitude regulator circuitry in more detail. As discussed, there are no manufacturers models for the MMIC and the AD8307 logarithmic detector circuit. What can be done is to create behavioral models, gauge them on calibration models (standard power levels, same output as the datasheets suggest), and model a regulating loop with the newly created models.

The modeling circuit looks like this (enlarged for clarity):

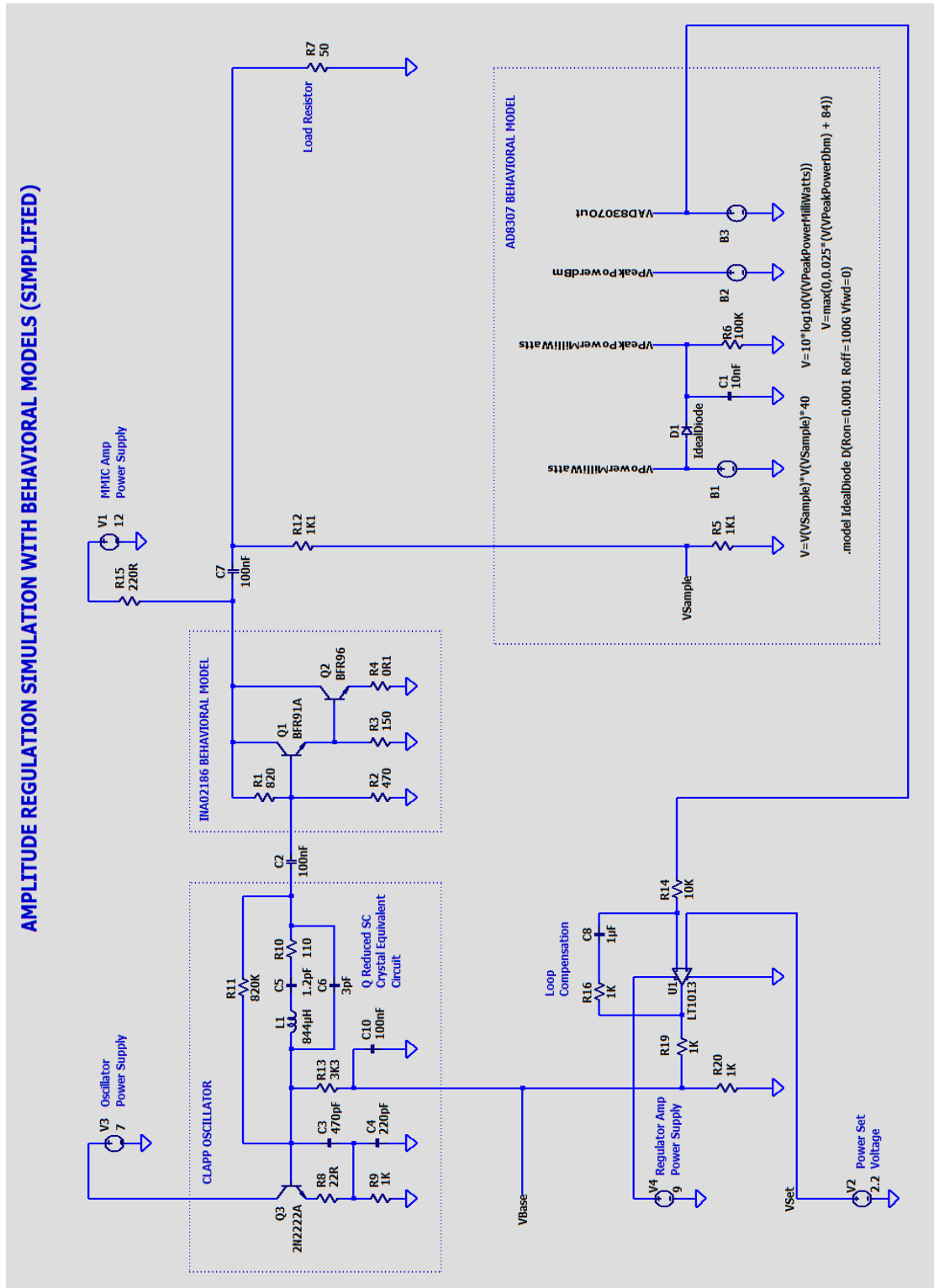


Figure 176- USO Amplitude Regulation Simulation with Behavioral Models

The Clapp oscillator is found on the upper left corner, then comes the MMIC to the right, the detector part is on the lower right and the amplitude regulating loop is below the Clapp oscillator.

To make this circuit work in the time domain simulator, several parameters had to be changed:

1. The crystal Q had to be reduced drastically to reduce startup times (and to enable startup at all). This effect is discussed in detail in the simulation/numeric chapters included in this thesis.
2. The MMIC was emulated using discrete transistors of the same  $f_T$  range as have been used in the original part. The resistors were chosen to provide the expected gain at 5MHz and a reasonable input match to 50Ohms.
3. The work resistor of the MMIC and the headroom were increased to provide less distortion.
4. The AD8307 was emulated in a cascade of behavioral sources with their formulas attached. In the end a good match for the log curve of the AD8307 was obtained, with a slope of 25mV/dB and a -85dBm intercept point.
5. The PI regulator loop time constant worked for the simulation, but it will need to be reality checked against the startup times of a real SC cut crystal oscillator.
6. Minimum timestep was 10ns, which would be by far too long for a high Q resonator.

The simulation worked, as the curves below show:

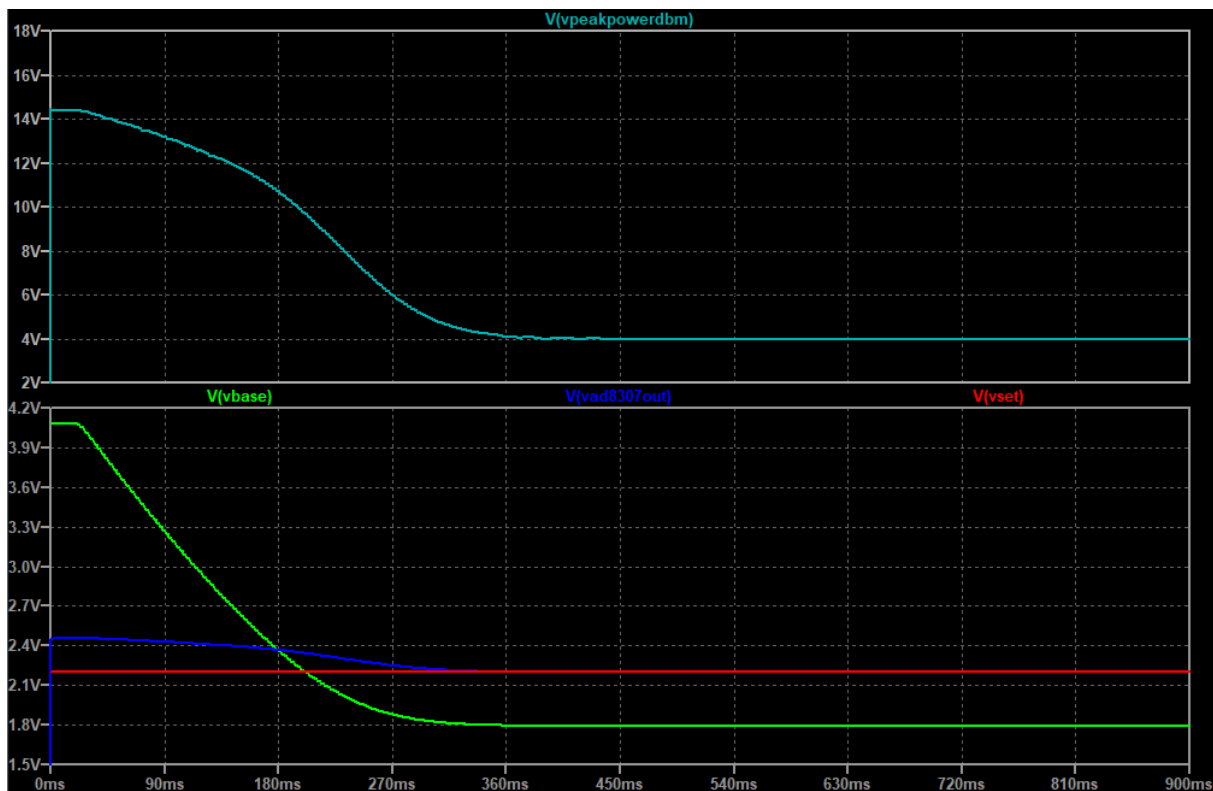


Figure 177 - Waveforms for the USO Amplitude Regulator - Base, Set Power, Detected Power. The top plot shows the output power in dBm (1V corresponds to 1dBm). The bottom plot shows the base drive voltage (green), the set log voltage (red) and the measured log voltage (blue).

As seen, the loop stabilizes after ca. 300ms.

If we look directly at the oscillator output before the DC blocking cap, the settling of the power level can be seen as well:

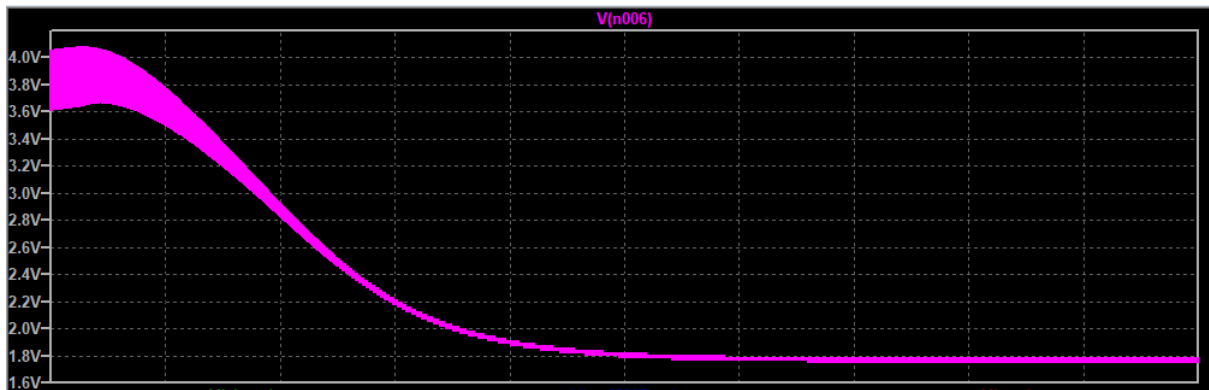


Figure 178- Regulated USO Base AC and DC Voltage during Startup

The unregulated level is about 400mVpp (about -4dbm, 400uW). The stabilized level is shown next:

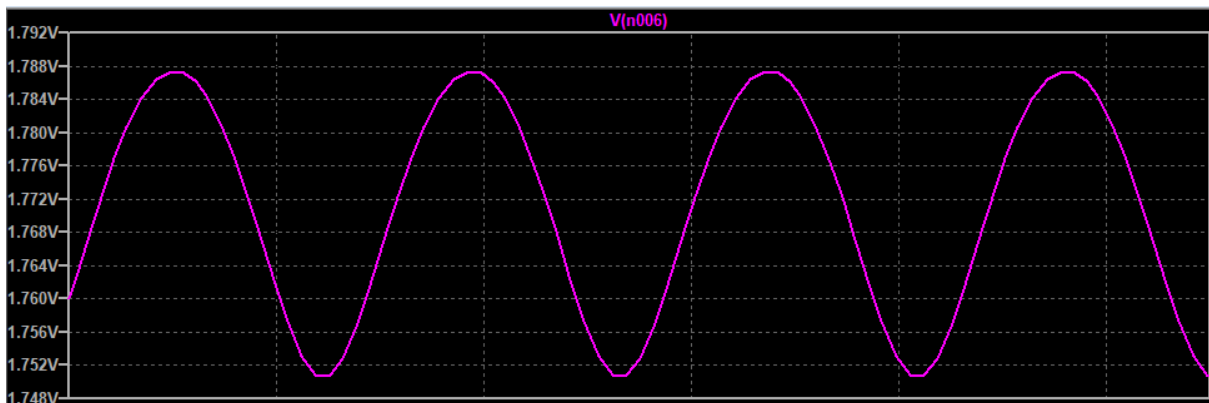


Figure 179 - Regulated USO Base AC Voltage Stabilized - Detail.

This is 38mVpp, or -24dBm or 3,61uW.

This proves that even small amplitudes can be very well regulated by a log-detector based loop. The startup with 400uW is no problem at all, and (in case of crystals that have been sitting unpowered for a long time and have a large DLD effect) it will safely start the oscillator with a large gain reserve.

## Conclusions

It is possible to build a high performance ultra-stable oscillator at 5MHz from commercially obtainable, but high-quality parts.

Success was reached by paying attention to critical components (crystals, transistors), ultra-low noise power supplies (with special noise reduction techniques), well-controlled thermal management (a Dewar flask, high thermal inertia heater blocks, and a precision temperature regulator), plus an amplitude stabilization scheme with a precise power regulator. Premium performance does not tolerate a single error, as was found out the hard way.

Environmental and peripheral influences (vibration proofing, cables, connectors, power supply filtering, ...) are key factors to success.

The prototype has a better performance than several commercial USO products (under the restrictions described under “Not-goals”).

There are ideas for further improvements regarding components (even better SL2 or IT crystals), mechanical design (milled isolator components in the Dewar flask, more precise temperature measurements, milled Aluminum housing for all circuits), power handling (lab-grade power supplies with extremely low drift and noise), magnetic shielding, vibration proofing and many others, but this would exceed the lab capabilities presently available. Some of the suggestions are described in the chapter “Suggestions for Further Research”.

## References

- [1] Ulrich L. Rohde, “Crystal Oscillator Provides Low Noise,” *Electronic Design*, vol. 21, Oct. 1975.
- [2] U. L. Rohde, *Microwave and wireless synthesizers: theory and design*. New York: Wiley, 1997.
- [3] “Bliley BG-61 Glass Unit Crystals.” Accessed: Nov. 20, 2020. [Online]. Available: <http://www.quartz1.com/price/techdata/HC30U.pdf>.
- [4] Rigol, Inc, “DG1000Z Series Rigol Waveform Generators.” Accessed: Nov. 20, 2020. [Online]. Available: <https://www.rigolna.com/products/waveform-generators/dg1000z/>.
- [5] Keysight Inc., “33500B and 33600A Series Trueform Waveform Generators.” Accessed: Nov. 20, 2020. [Online]. Available: <https://www.keysight.com/de/de/assets/7018-05928/data-sheets/5992-2572.pdf>.
- [6] Hewlett Packard Co., “INA02186 Low Noise, Cascadable Silicon Bipolar MMIC Amplifier.” Accessed: Nov. 19, 2020. [Online]. Available: <https://www.qsl.net/n9zia/metricom/ina02184.pdf>.
- [7] Mini Circuits, “PGA-103+ Monolithic Amplifier.” Accessed: Nov. 20, 2020. [Online]. Available: <https://www.minicircuits.com/pdfs/PGA-103+.pdf>.
- [8] Analog Devices, “AD8307 Datasheet.” Accessed: Nov. 20, 2020. [Online]. Available: <https://www.analog.com/en/products/ad8307.html>.
- [9] Cadence Corp., “Designing a Capacitance Multiplier as a Power Supply Filter.” Accessed: Nov. 20, 2020. [Online]. Available: <https://resources.pcb.cadence.com/blog/2019-designing-a-capacitance-multiplier-as-a-power-supply-filter>.
- [10] Steve Hageman, “Simple circuits reduce regulator noise floor,” *EDN*, Oct. 15, 2013.
- [11] Texas Instrument, “LM723QML Voltage Regulator.” Accessed: Nov. 20, 2020. [Online]. Available: <https://www.ti.com/lit/ds/symlink/lm723qml.pdf>.
- [12] Jörn Bartels DK7JB, “Rauschen von Spannungsreglern.” Accessed: Nov. 20, 2020. [Online]. Available: <https://www.bartelsos.de/dk7jb.php/rauschen-von-spannungsreglern>.
- [13] Rigol Inc., “DP800 Series High Performance Linear DC Power Supplies.” Accessed: Nov. 20, 2020. [Online]. Available: <https://www.rigolna.com/products/dc-power-loads/dp800/>.
- [14] Keysight Inc., “B2962A 6.5 Digit Low Noise Power Source.” Accessed: Nov. 20, 2020. [Online]. Available: <https://www.keysight.com/en/pd-2149912-pn-B2962A/65-digit-low-noise-power-source?cc=DE&lc=ger>.
- [15] Huber und Suhner, “ENVIROFLEX 400 Datasheet.” Accessed: Nov. 20, 2020. [Online]. Available: [https://www.koax24.de/storage/datasheet/de/050118\\_Datenblatt\\_Enviroflex\\_400\\_Enviroflex\\_400.pdf](https://www.koax24.de/storage/datasheet/de/050118_Datenblatt_Enviroflex_400_Enviroflex_400.pdf).
- [16] Keysight, “Digital Multimeters 34460A, 34461A, 34465A (6½ digit), 34470A (7½ digit).” Accessed: Nov. 20, 2020. [Online]. Available: <https://www.keysight.com/de/pdx-2891643-pn-34470A/digital-multimeter-7-digit-truevolt-dmm?pm=rsc&nid=-32051.1242961&cc=DE&lc=ger>.



## 8.2 A Tracking Crystal Filter

When making premium crystal oscillators, there is a tradeoff between minimum aging and lowest phase noise. Minimum aging asks for the minimum possible crystal dissipation, and lowest phase noise asks for the maximum permissible output power, as expressed by the Leeson formula where the phase noise level decreases with the square of the oscillator output.

When maximum stability is prime, as in deep space USOs, the oscillator design has to live with less-than-optimal phase noise. Massive amplification is necessary to provide a standard output level of around 10dBm.

The idea implemented here was to insert a premium filter crystal into the amplifier chain where it can purify the spectrum from relatively close to the carrier up to the thermal floor. This crystal now runs at a high dissipation and must be stabilized against the effects of accelerated aging. This was done by controlling the crystal temperature instead of the series capacitance.

In the following the relevant properties of the crystal, the filter circuit, and the tracking regulator are described. Effectively, the circuit forms a “temperature locked loop (TLL)”. Measured performance improvements are presented as well.

### 8.2.1 Overall Architecture

The oscillator core is an amplitude-controlled Clapp oscillator housed in a thermostabilized Dewar flask. Its output amplitude was set to about -30dBm. This signal is amplified by a linear, low-noise amplifier stage with a gain of around 30dB, so we arrive at a power level of around 0dBm, a good compromise between allowed crystal power, aging rate, and insensitivity to processing stage noise. A photo of the setup is shown below:

### The Tracking Crystal Filter Test Environment

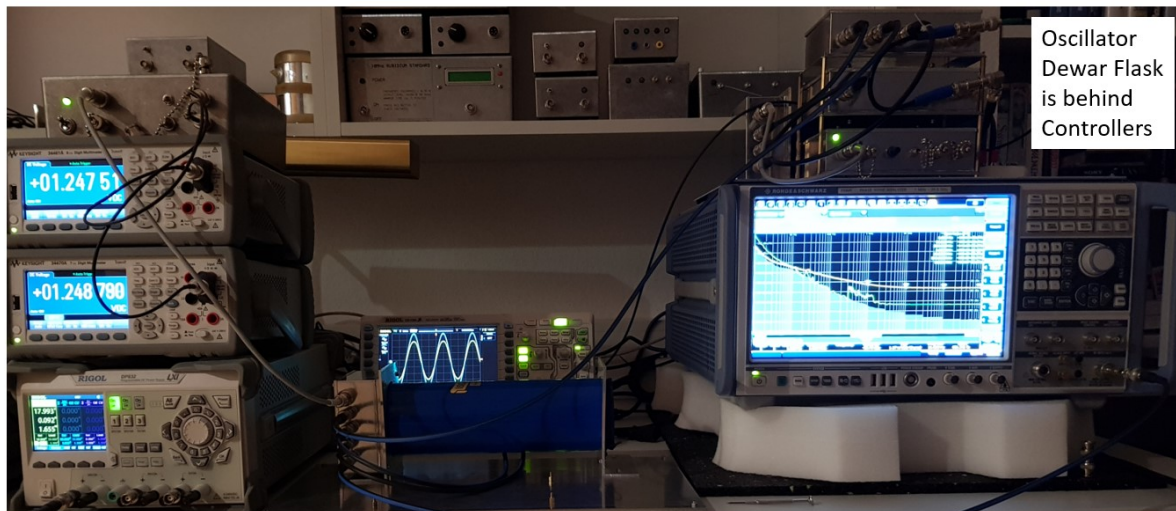


Figure 180 - The Tracking Crystal Filter Environment

Starting with the left stack, we have the filter temperature regulator on the top left (using the same circuit as the temperature regulator for the oscillator), below we have precision multimeters showing the set and measured Dewar temperatures inside via the voltage over a Platinum 1K sensor driven with exactly 1mA. The temperature can then be computed from the standard published Pt1K curves.

An 18V power supply for the heater regulator can be seen at the bottom.

In the middle we have the Dewar arrangement for the filter. The scope behind the Dewar flask was used to control the phase difference, here the tuned-in state with zero degrees is shown.

The USO arrangement discussed previously and the FSWP phase noise analyzer can be seen on the right. The signal is routed through the filter and is then analyzed for phase noise.

A photo of the filter PCB that sits inside the Dewar flask is shown here:

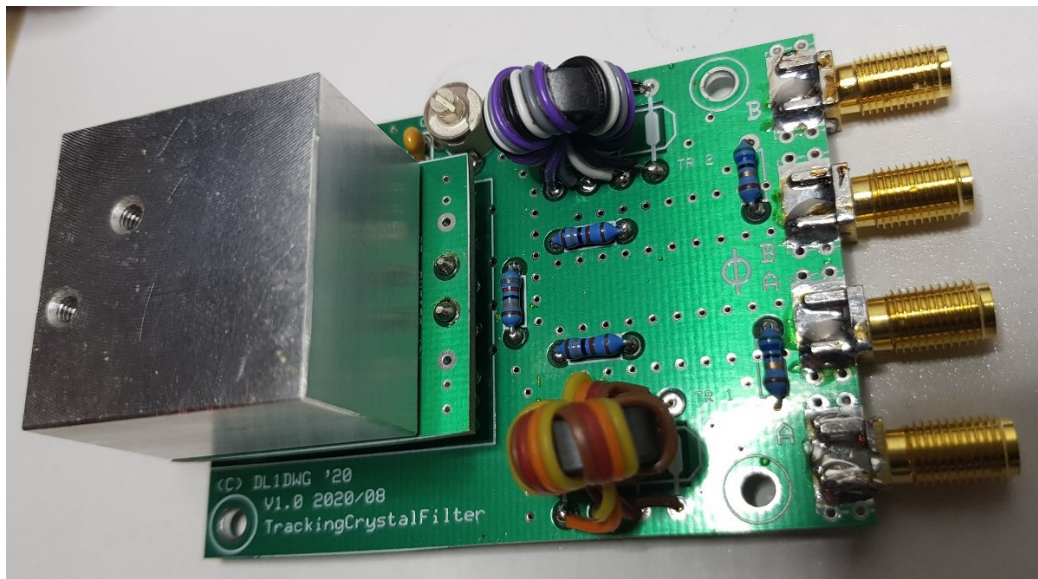


Figure 181 - Filter PCB with Mounted Crystal Inside the Heater Block

The heater block has the same design as the ones used in the USO prototype. Versions for HC-30, HC-37, HC-40, and HC-49 are available. The heater transistor and the Platinum temperature sensor are removed from the heater block for better visibility.

### 8.2.2 Designing the Filter Stage

For the filter stage, we can define the following requirements:

1. Bandwidth as small as possible.
2. Allowable input power level up to 1-2dBm minimum.
3. Minimum loss possible (less than 6dB at the center frequency)
4. VSWR needs not to be perfect but should stay below 10 to avoid stability problems with the feeding and following amplifiers (safety measure).
5. Automatic adjustment of the filter center frequency to follow the input signal in a range of 5ppm.

At the nominal frequency of 5MHz premium SC cut crystals (Crown used here, [1]) have a Q of about 2-2.5Million, a series resistance in the range of ca. 100Ohms (3. OT), and an inductance of several Henrys, with a motional capacitance of ca. 1/10 of a fF. At series resonance, the crystal circuit can be replaced by the series resistance, which is larger than the 50Ohms we normally use (dependent on part. Range is between 80 and 120 Ohms).

Therefore, it makes sense to use impedance matching networks that create a higher impedance level. In this case a 1:9 impedance transformer was used, which creates a 450Ohm environment. The simulated (and measured) minimum attenuation was around 4-4.5dB, which is acceptable.



The schematics of the filter is shown here:

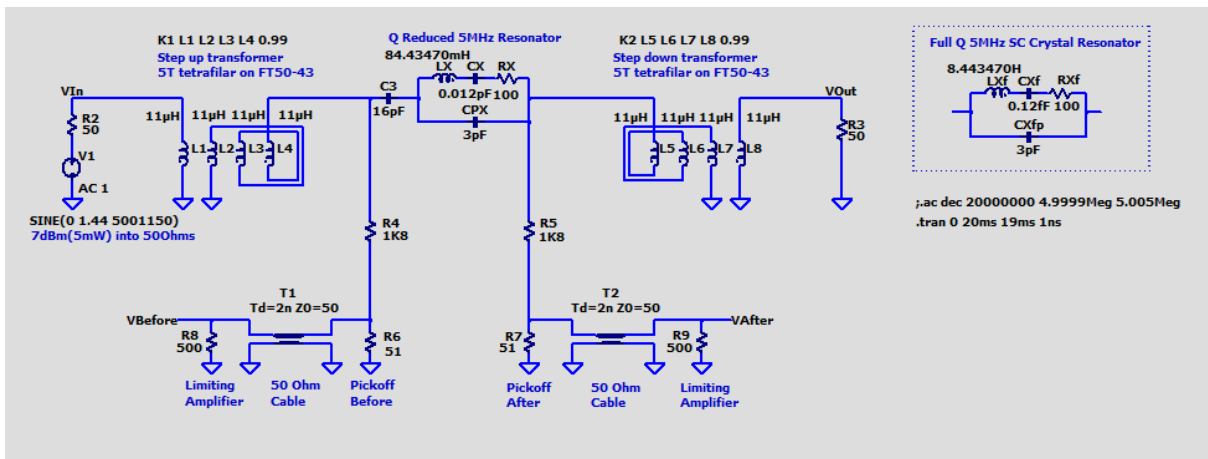


Figure 182 - Tracking Crystal Filter Schematics

The  $R_4$  and  $R_5$  resistors are a compromise between acceptable losses and sufficient isolation of the “hot” parts of the series circuit from the phase detection circuitry.

A simple crystal equivalent circuit could be used here because the signal arrives as a very pure 5MHz sine tone. B Mode or other resonances play no role here.

$V_{Before}$  and  $V_{After}$  are measured by a scope with 50Ohm input terminations to avoid reflections. No extreme performance scope is needed, it should be only sensitive enough to determine the phase of two signals in the mV range accurately. The 1mV/div sensitivity of the Rigol DS1054Z was sufficient.

### 8.2.3 Crystal Properties

The SC cut provides on the best temperature stabilities available after it has been set to the appropriate operating temperature, which is a square maximum so (locally) the temperature dependency vanishes completely.

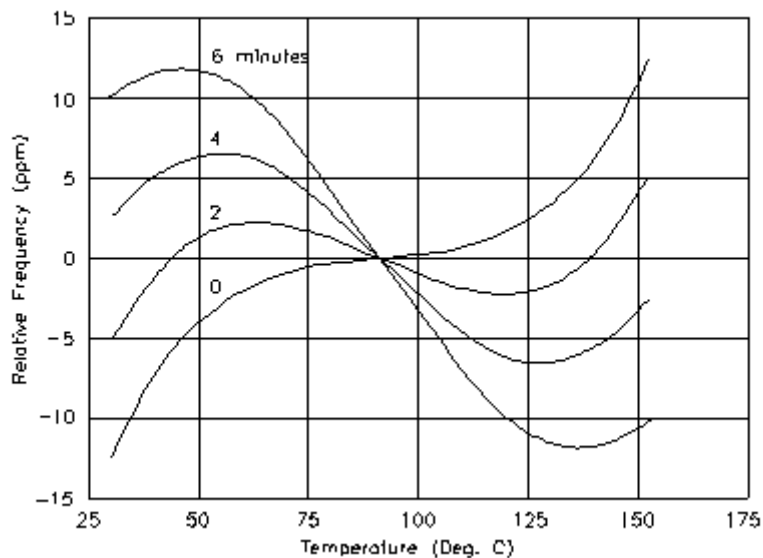


Figure 183 - SC Cut Crystal Frequency over Temperature depending on Cutting Angle  
Picture from Neubig Quarzkochbuch

Electronic tuning is done with a series capacitance (value is supplied on the crystal datasheet). The smaller the external series cap, the higher the frequency will be.

When heating up an SC crystal from room temperature, the frequency increases until the nominal frequency is reached. The frequency difference between cold (20°C) and hot (around 80°C) is around 100-150Hz, which is more than 10 times the bandwidth and about 30ppm of the nominal frequency. One of the sweet spots of the SC cut is a very low thermal hysteresis and retrace effects (compared to AT and other cuts), so when heating up the frequency will not show an overshoot (says nothing about the thermal regulator, however).

Power level dependent aging at low power levels (max. 50-100uW) is about 0.1-0.2ppm/year. Datasheets give no information what happens at high powers. If we assume that at 1mW we have 10 times the aging of 100uW we must cope with 1-2 ppm per year. As long this can be compensated by changing the crystal temperature, we are fine. All SC cut crystals age by *increasing frequency* (this is valid after the burn-in period is over. Before that, frequency decrease effects are possible). This also implies that the circuit cannot be used with AT crystals (would not make sense anyway due to the lower Q).

What is needed is an operation inside the *left falling range* of the curve above, where the temperature coefficient of the resonant frequency is positive. In other words, we need to stay below the lower turning point (called LTP in the datasheets). If we overrun this point, we would lose regulation.

#### 8.2.4 Regulation

The best filter effect occurs if the signal coming from the oscillator and the series resonance frequency of our filter are exactly the same. The Q involved is the loaded Q of the crystal plus the attenuation of the impedance matching networks and the driving and input impedances. A Q of about half the unloaded Q can be assumed (and measured), so for an SC cut 5MHz crystal at 5MHz we have something around 1-1.2 Million and a 3dB bandwidth in the range of 10Hz.

At the nominal frequency, the output amplitude reaches its maximum (hard to regulate because it can go down both sides), but we have a much better quantity to observe: The phase of the signals before and after the crystal. Phase crosses zero from capacitive to inductive at the series resonance frequency, stays inductive until the parallel resonance frequency, and becomes capacitive again above.

What is needed is an accurate phase detector that is reasonably insensitive to amplitude variations. After detecting the phase, a control loop compares the phase to its set value (0°) and adjusts heater power accordingly.

Some characteristics of the control loop make an implementation difficult:

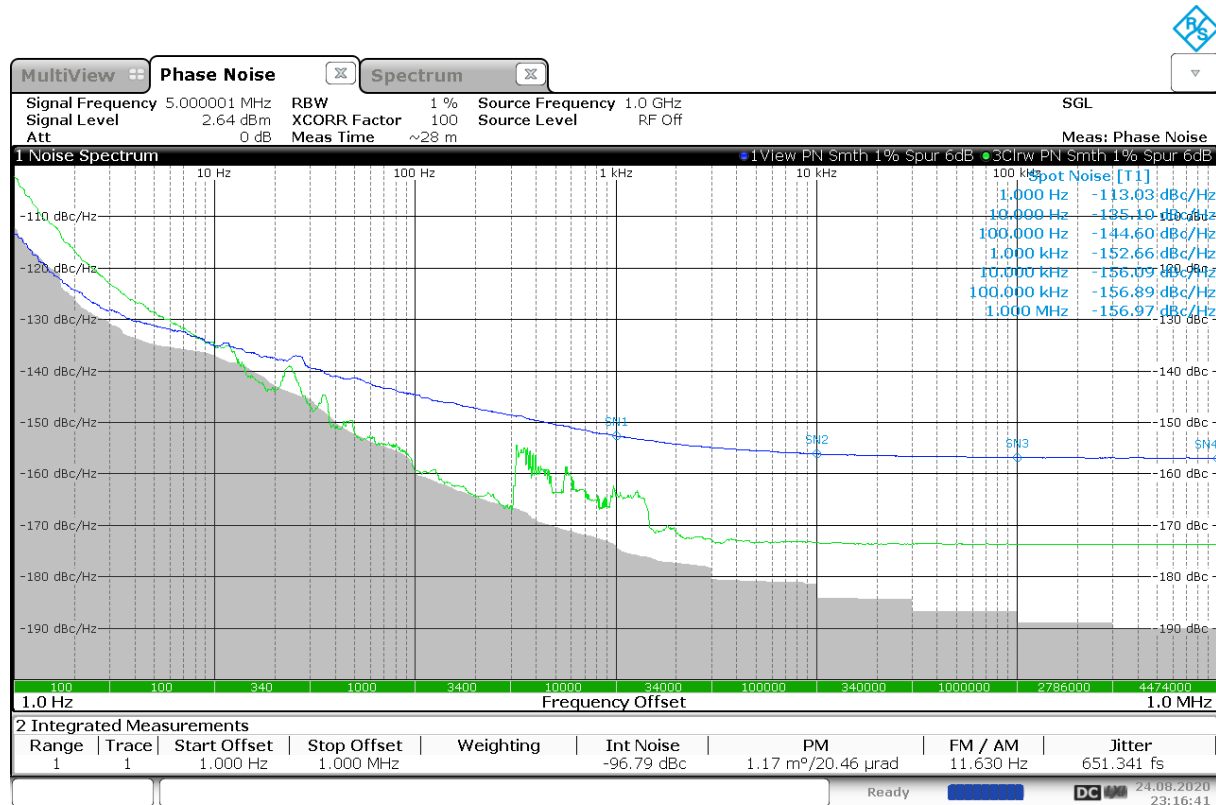
- The thermal time constant of the crystal and the surrounding thermal block is very long (>> 100s).
- We need an accelerated heat-up procedure that with a lower time constant (a few minutes). After reaching equilibrium, heater power must be reduced fast enough so no, or just a small temperature overshoot occurs.
- There must be a limiter to the maximum heater power, so no thermal gradient stress is induced on the crystal
- If the thermal loop overshoots, the phase beyond parallel resonance will be capacitive, but the output amplitude will be very low. In this case, a cooling down must be performed.

An analog approach was tried first, involving limiting amplifiers, a phase detector that could measure positive and negative phase values with a midpoint at zero degrees, and a regulator. With the exceptionally long thermal time constants involved, but with the high gain provided by the phase detector finding a proper compensation design proved to be difficult.

A software-based regulator provided better results and was then used for the measurements of filter performance. The trick was here to “measure” the rate of phase change and to drive back heater power even before the zero-phase point was reached.

## 8.2.5 Results

The following curves from the FSWP signal analyzer show the performance improvement achieved:



23:16:41 24.08.2020

Figure 184 - Unfiltered and Filtered Phase Noise Curves

The blue curve is the unfiltered signal, achieving a noise floor of ca. -157dBc/Hz. With the filter (green curve), a considerably better noise floor is achieved, at -173dBc. The spurs around a kHz are artefacts (vibration?). At 10Hz, a crossover point can be seen where below the unfiltered signal has better phase noise, plausibly explained by the filter losses.

We have been conservative here with the allowable power dissipation inside the filter crystal. Luke Mueller of Croven Crystals stated that his new HC37 crystals could cope with 5mW without causing reliability problems. If the crystal losses are calculated back to the allowable filter input power, a 10dBm input would be easily permissible, giving a boost in close to carrier phase noise performance.

A further welcome effect of the filter is that it effectively suppresses harmonics that might have been generated in the preceding amplifier. On the other hand, it could be argued that the crystal itself could become nonlinear and generate harmonics on its own, but this effect was not (yet) observed at the (conservative) power levels measured so far.

## References

[1] Croven Crystals Inc., “Croven HC-40 Crystals Datasheet.” Accessed: Nov. 19, 2020. [Online]. Available: [https://crovencrystals.com/wp-content/uploads/HC-40\\_Crystal\\_Holder\\_Rev\\_00.pdf](https://crovencrystals.com/wp-content/uploads/HC-40_Crystal_Holder_Rev_00.pdf).

## 9 Suggestions for Further Research

This chapter contains suggestions about further research, mostly in areas that were not central to this PhD thesis and/or where no required resources were available, like extremely accurate measurement equipment or supercomputer resources. During the research several challenges that might be interesting problems were found, so each of them is described in a short exposé.

### 9.1 Refine and Improve the In-Oscillator Measurement Capabilities to Higher Frequencies.

The techniques developed in this thesis that made the waveforms inside a running oscillator accessible to direct measurements were extremely valuable to clarify the real-world behavior of oscillator circuits as opposed to simulations including only incomplete physics. Many discrepancies were found, and for some effects like the BE breakdown and deep saturation it could be demonstrated that only an extension to existing simulation models would produce accurate results.

The techniques usable at 5MHz become more and more problematic as frequency increases; A plausible estimate is that the frequency limit even for improved probes is about 30MHz. The physical phenomena, however, are highly likely to occur at frequencies up to the microwave range. In other words, what is needed is a technique which allows to measure all voltages, preferably also currents, inside a running VHF, UHF or microwave oscillator *without detuning or loading the circuit*.

Due to parasitics the probing of microwave circuits with commercial probes (that are available to 30GHz) are no option because they are usable for low impedance, digital circuits only. Their input capacitance is down to fractions of a pF, but the voltage range is limited, and they often have a small DC impedance that would change bias conditions.

A viable way would be to adopt the technology of on-chip probing by electron microscopy. This technique is used today in the development process of fast integrated circuits where test pads are not available and the potential on some chip area needs to be measured. Sampling techniques can be used to obtain waveforms at a frequency that can be handled by available lab equipment. By using this technique, the range of waveform-measurable oscillators could be extended to the 10-20GHz range.

There are some technical difficulties to surmount before electron microscopy-based measurements can be made:

1. The circuits must be made from vacuum-enabled parts and components
2. This excludes some part types like normal electrolytic capacitors and other components that can ooze gases or liquids into vacuum, such as some plastic packaged parts
3. The same goes for PCB materials, solder flux, ...
4. Beam focusing on a sculptured surface like a PCB with components needs to be solved

Lab equipment like electron beam microscopes is normally restricted to universities or large companies, so the research needs to be done at such a location.

### 9.2 Extend the Usability of Simulation Programs to Circuits with Extremely High Q Components

During the simulation runs for realistic Q USOs in this thesis, it was a normal case that the crystal Q had to be reduced for simulations that failed for the measured extreme Q values. It has been shown why this happens; the culprit is the way the numerical algorithms within commercial simulation software (LtSpice, Serenade) handles the discretized differential equations. Higher-Order ODE solvers normally do a good job for standard problems where higher-order polynomials do not need extremely

small timesteps; for ultra- high Q resonators they are responsible for the effect that not even the oscillator startup can be properly simulated, due to precision loss in the coefficient evaluation formulas of the polynomials.

The difficulties in commercial simulators when working on extreme-Q oscillators were overcome by writing specialized ODE solvers with two approaches:

1. Use a single-step approximation only, no higher polynomials
2. Increase precision beyond the 64bits normally available on IEEE-math CPUs.

These specialized computer programs written in Python or C worked and could explain the startup process, but they are limited to a predefined oscillator topology.

What would be needed is a “Extreme Q Oscillator Simulation Kit”, including

1. a collection of mathematical methods suitable for “stiff” differential equations,
2. a front-end where the equations are automatically extracted from a circuit,
3. a variable precision environment with a “quality control” mechanism for rounding and timestep errors
4. an efficient implementation on a multiprocessor computer architecture.

Even with a lot of optimization potential over general simulator it has to be expected that the needed computer power is considerable, maybe a candidate for GPU computing.

### 9.3 Take the Performance of USOs to New Frontiers

In this thesis the parts used were parts of high quality, but not what will be used for a real space mission. The reason clearly is availability, delivery time and cost for actual space parts. The most critical part obviously is the crystal itself; The best obtainable parts that could be used were Croyen HC37 SC/S2 5MHz.

Top performance products described today do not have the restrictions of standard parts. The crystal used is a swept QAS type, and made-to-order components were employed to squeeze out the last few dB in phase noise performance. Mechanical and thermal design is extremely elaborate and involves special manufacturing.

If one would like to close the gap to the absolute top class of today’s USOs and beyond, several preconditions apply:

1. A lab environment that is perfectly shielded, perfectly climatized and perfectly vibration-proof
2. Reference oscillators with -145dBc/1Hz or less phase noise (cryogenic sapphire oscillators, CSO), or the top line of the RAKON HSO-14 with 6.E-14 Allen deviation for 1s.
3. Techniques and equipment to control and measure temperature to fractions of a mK.
4. Extremely accurate and noise free power supplies, including 8 ½ digit precision DMMs and power sources with negligible noise (probably those must be built instead of bought).
5. Special phase noise measurement hardware (Microsemi 53100A or better) using several extreme-quality reference oscillators to determine DUT phase noise
6. Ample computer power to do the correlations in a reasonable time.
7. A supplied of made-to-order components like QAS crystal, passive and active precision resistors, inductors, and capacitors as well as ultra-low flicker noise linear transistors.

### 9.4 Develop a Time Domain Simulator that Incorporates Realistic Noise

In both harmonic balance and time domain simulators noise is treated by an approximation approach. There is white noise in resistors, there is current (Schottky) noise, and (only some) models use a heuristic flicker term with a coefficient and an exponent, but that is it.

Attempts have been made to start from a network consisting of L, Cs and Rs as well as a (SGP) transistor model including noise, like the paper from Kärntner [1]. The approach is an improvement over the classic linear noise models, because it starts from a set of stochastic nonlinear equations and derives noise performance from (in principle) measurable quantities, very much unlike the Leeson approach where a lot of parameters are fitted from measurements but have no connections to physics. Unfortunately, the Kärntner paper assumes an infinite Q resonator and it ignores flicker noise. Kärntner's approach, unfortunately, did not become very popular and is, as far as we know, not used in any commercial simulation program today.

The challenge would be to revert to the starting point of the problem, to make it complete regarding physics and to employ a solver of stochastic ODEs to determine the expected noise performance.

There are some foreseeable difficulties for such an endeavor, such as:

1. The intensities of noise voltages and currents depends nonlinearly on the operating point in which the transistor actually operates; This must be measured before the results can be used in a simulation. There are no datasheet or simulation models available where these values can be found.
2. The High-Q problem encountered with USOs still applies. Timesteps need to be extremely small, and the minimum timestep is not only determined by the steepest transitions / highest harmonics to be expected, but also by the bandwidth of the noise components to be incorporated. On the other hand, oscillator startup for an USO can be in the range of 1s and beyond, depending on Q.
3. In a time-domain approach, noise sources must be able to generate output with a given, non-white distribution, e.g., for flicker components.
4. What can be measured after solving the stochastic ODEs by simulation are all voltages and currents over time, including their fluctuations due to all kinds of (also nonlinear) noise. To take averages, many parallel simulations are needed.

## 9.5 Create a Theoretical Foundation to Determine the Character of the Solutions of the Equations Governing Ultra Stable Oscillators.

Colpitts/Clapp oscillators are very well known for their possibly chaotic waveforms. The chaos comes either from the bias network, from the multiresonator crystal (SC cut with B Mode), or both. The creation of chaos is no surprise; it is the default when combining high-Q components with strong linearities, the same as for other natural phenomenon like turbulence and parametric oscillations.

The exclusion of strong nonlinearities is a design option, but as Lee and Hajimiri have shown, a design with a low conduction angle will produce significantly less phase noise, so "quasilinear" oscillators are not what is needed.

For an USO, it is extremely important that no chaotic solutions occur at any time, so a safe method to provide the following information would be extremely valuable:

1. For a given topology and component values, is there a chaotic solution possible for any operating condition (startup, change in loading or supply voltages, temperature, or aging)?
2. If we find that we identified a "stable" solution without chaos, how far (in terms of component or operating parameter tolerances) are we away from the closest chaotic solution?

It is probably illusionary to expect a closed-form solution to this problem; what would be helpful is an algorithm that is able to identify problematic domains in the phase space depending on component values and their variability.

A starting point for research could be the van der Pol oscillator with a multiresonator crystal model (fundamental, nominal frequency and B Mode).

Monte Carlo techniques could be an approach to determine the effects of component parameter spreads in the vicinity of identified critical points.

## References

[1] FRANZ X. KAERTNER, "Determination of the Correlation Spectrum of Oscillators with Low Noise," *IEEE TRANSACTIONS ON MICROWAVE THEORY AND TECHNIQUES*, vol. VOL. 37, no. NO. 1, Jan. 1989.



## 10 Appendix A: An In-Depth Analysis of the HP10811OCXO

The HP10811 oscillator is a classic that no thesis on USOs even today should ignore. It was used to power generations of professional HP RF equipment like spectrum analyzers, VNAs, counters, for almost two decades. It was also sold as an OEM part to customers outside HP. It looks like this:



*Figure 185 - The Packaged HP10811A Crystal Oscillator  
Picture from HP Journal [1]*

It was first marketed around 1980 according to the manual but this model and successors (10811D and E) were still marketed under Agilent branding, so that must have been after 1999 but before 2005 where Agilent sold its precision oscillator division to Symmetricom.

HP devoted an article about this oscillator and the advantages of the new SC cut crystal technology in their HP journal [1].

The performance of these units (they came in a lot of variants) was outstanding for the time, and it was a really successful product. The HP10811A type, e.g., had the following specs (from a HP manual):

1. Output power ca. 8dBm into 50 $\Omega$
2. 10MHz with a drift spec of  $10^{-7}$  per year
3. Phase noise 90dBc down at 1Hz, improving to 160dBc down at 10kHz
4. Best Allen deviation  $5 \cdot 10^{-12}$  from 100mHz to 10Hz.

Another aspect very welcome for analysis is that the HP10811A is fully documented. There is a complete parts list, full schematics, a service manual, and an article in HP's journal highlighting the design principles applied and the performance achieved (see [3]). As will be shown later, not all information is consistent, however. The practice of documenting products to this level of detail has, unfortunately, long been given up, so today almost no design information is available for current commercial units, leave alone parts lists or schematics. From the information currently available the design principles of this part still apply today.



## 10.1 HP10811 Oscillator Building Blocks

The unit consists of the following building blocks:

1. The oscillator core
2. An output buffer amplifier
3. An amplitude regulation circuit
4. A thermostat circuit with a heater.
5. A voltage regulator for the tuning diode bias and the oscillator core

All these units are assembled on a series of flexible interconnected PCBs, shown here:

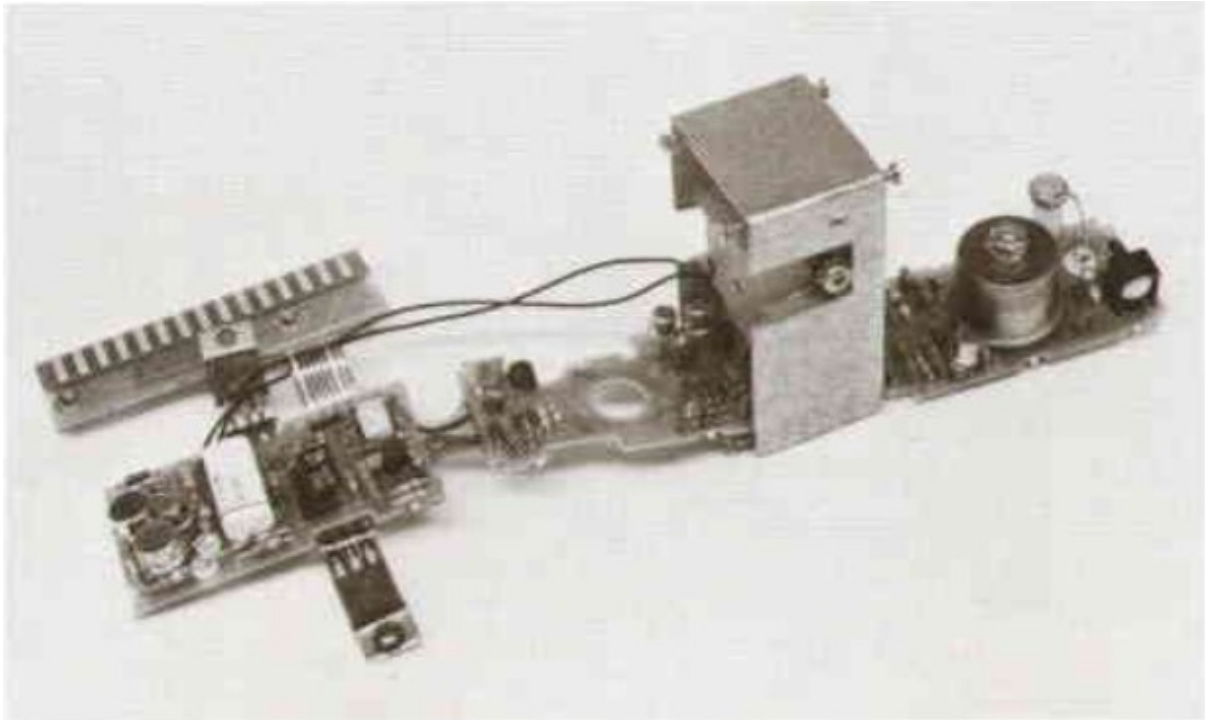


*Figure 186 - The Disassembled HP10811A Crystal Oscillator on Flexible PCBs  
(Photo HP Journal [1])*

Conventional, thru-hole components are used throughout, facilitating debugging and test. HP was very proud of the flexible PCBs and used some routing tricks to avoid and create track capacitances. All the PCBs are double sided with no shielding or ground plane. When you look at modern USO designs like the 8600 series there are flexible interconnects, but all PCBs are rigid FR4 (see [2] for a teardown). There is no compelling advantage of the flexible PCB design.

The heater block consists of cast, not milled Aluminum, and houses the crystal (on rightmost PCB) plus two heater transistors (on leftmost PCB). The thermal mass and weight of the heater block is surprisingly small, only ca. 25grams. The wall thickness is just a mm, no comparison to ultra-high performance USOs today with milled copper blocks weighing 300grams for the crystal alone (see [4] for a drawing).

The crystal is packaged in a (cold-weld?) copper case and mounted into the heater block with a central mounting screw. No thermal compound was used. The crystal leads were rather long (2-3cm) and were directly soldered into the PCB.

### 10.2 The Oscillator Part

The enlarged schematics can be seen below:

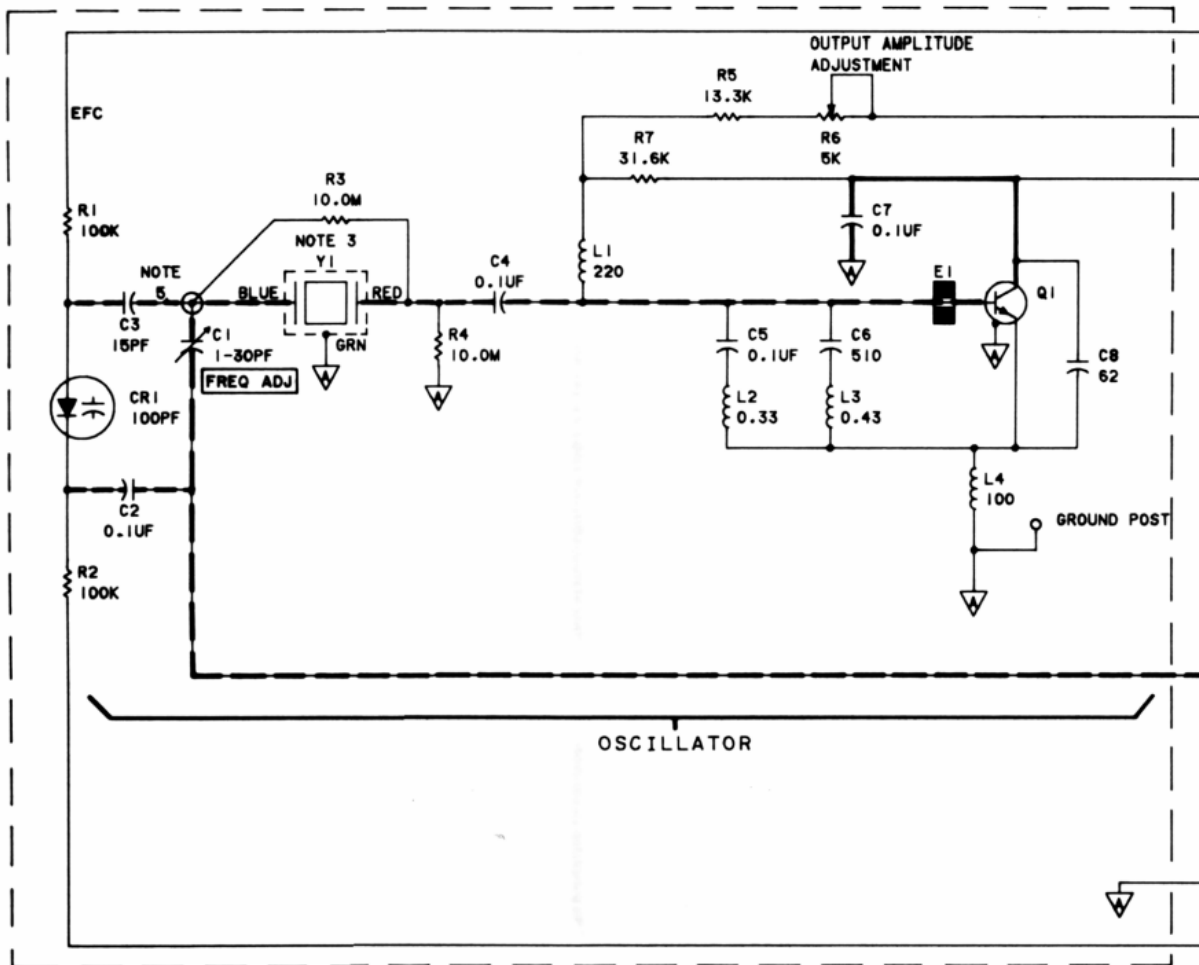


Figure 187 - The Oscillator Core of the HP10811A  
 Photo from HP10811A Service Manual

Maybe looking a bit in disguise, but it is a Clapp oscillator. The C8 cap goes to RF ground (via C7, the Q1 collector has a zero cap with 100nF), and the combined L2/C5 and L3/C6 tank impedances are capacitive at the operating frequency of 10MHz (see the HP article mentioned above). Their purpose is to prevent oscillations at the fundamental crystal frequency (10MHz is the 3rd OT) and the B Mode resonance ca. 8-10% up from 10MHz.

At 10MHz we have an impedance of

$$Z_{C5L2} = j\omega L_2 + \frac{1}{j\omega C_5} = j20.7\Omega$$

in parallel with

$$Z_{C6L3} = j\omega L_3 + \frac{1}{j\omega C_6} = -j4.22\Omega$$

Giving

$$Z_{TOT} = \frac{Z_{C5L2}Z_{C6L3}}{Z_{C5L2} + Z_{C6L3}} = -j5.3\Omega$$

$Z_{TOT}$  corresponds to a capacitor of about  $3nF@10MHz$ .

The resonance frequencies are 875kHz at the low end and 10.75MHz at the high end, which is close to the B Mode frequency of 10.9MHz. The HP paper mentions that the intention was to make sure that only desirable frequencies will find a capacitive impedance in the filtered range, enabling oscillation. They also mention other crystal resonant frequencies like the fundamental or 7MHz, both also falling in this range so they would not be filtered. It is not clear why this was done; a higher low- end tank frequency could have cured this problem. It could be a typo, because the HP service manual mentions ([3], paragraph 8.15) a lower frequency limit of 9MHz, which would be a 1nF capacitor instead of the 100nF in the schematics and parts list. Reverse engineering showed that the parts list values were correct, but the 7MHz were not.

So, at 10MHz the two tanks behave like a base-emitter capacitor and the C8 capacitor also can be drawn so ground, completing the classic Clapp circuit.

The inductors used for filtering, as well as the  $L_1$  and  $L_4$  inductors are standard molded chokes ( $L_2$  and  $L_3$  with 1% tolerance) and they are not trimmable. The Q values are not documented. It makes sense to assume that  $L_4$  and  $L_1$  are ferrite chokes with a SRF of roundabout the oscillator frequency and a peak impedance of several  $k\Omega$  (compared with the RM10 THT inductors from, e.g., FASTRON, [5]). The DC series resistances of the 100uH and 220uH inductors today are in the range of a few Ohms, and their maximum currents are some ten mA, so no issue here.

The crystal is an SC type, mounted in a thermal heater socket. At the end near to the base there is a  $10M\Omega$  resistor to ground, plus there is another  $10M\Omega$  resistor across the crystal itself. These resistors are not discussed in the paper and not in the service manual either. Their obvious purpose is to keep the crystal disk itself free from DC voltages. This is necessary because for SC cut crystals randomly accumulated charge can change crystal resonance frequency and can also add low-frequency noise (see Vig, [6], p36ff). No specific crystal data is given; Q can be assumed to be in the range of 100000 to million by comparison to similar 10MHz SC crystals today. Crystal current in the HP paper is cited as 1mA, with 30uW of dissipation.

The tuning part consists of a mechanic capacitance trimmer plus varactor tuning. The diode used has a large capacitance (max. 100pF) that is reduced by a small series capacitor ( $C_3$ ). Ignoring the  $C_2$  DC block capacitor the usable tuning range is  $C_1$  (30pF max., the mechanic trimmer) plus a capacitor with a maximum value of ca. 12pF (100pF diode in series to 15pF), so we have some picofarads up to 42pF maximum.

Tuning DC is brought to the diode by  $100k\Omega$  resistors, the positive end sitting at the oscillator's internal stabilizer, and the negative end leading to the EFC (electronic frequency control) terminal. The diode type is a HP internal designation. Only 100pF maximum capacitance is known.

According to the service manual the transistor  $Q_1$  is a 2N5179 [7], a common RF transistor at the time, with an  $f_T$  of ca. 1.4GHz and a noise figure of 3dB at 200MHz, probably a lot better at 10MHz. The transistor is run off a 5.7V collector supply voltage, with base bias coming over an RFC ( $L_1$ ) and a bias network consisting of  $R_5$ ,  $R_6$  and  $R_7$ . There is no DC bias stabilization network; negative feedback is derived from buffered and rectified RF, lowering the base bias voltage by draining current via  $R_5$  and  $R_6$ .

When switching on, there is no RF, so we can expect a base current of

$$I_{Base} = \frac{V_C - V_{BE}}{R_7} = \frac{5.7 - 0.7}{31.3K} = 160\mu A$$

creating a collector current anywhere between 4 and 48mA (beta spread according to the 2N5179 datasheet is 25 to 300). The HP parts lists contains a hint ("SPL" for special) that this transistor is preselected (for gain and maybe noise, probably). A certain "kick" at startup is a good idea when

starting high-Q oscillators because crystal losses at very small amplitudes can exceed the normal series resistances when running due to the DLD effect. Despite these resistances, the oscillator must start safely, so some extra gain at startup is needed (no useful data available for very good crystals with negligible DLD, for a rough guess see Rohde [8]). We found by reverse engineering that the crystal used had no prominent DLD effect at the nominal frequency, so a large gain margin was maybe a safety design.

The crystal used in the HP10811A has triggered statements about having an inexplicable high Q or other properties that could not be replicated today (see Apte [9], section 5-25). The parts obtained from a reverse engineered unit with a broken heater were measured at AXTAL (Thanks to B. Neubig) using a precision impedance analyzer and it was found that it was *not unusual* at all regarding its motional parameters (see the crystal measurements section later). Parts like this (and better) can easily be made today.

### 10.3 The Buffer/AGC/Stabilizer Part

Is shown in detail here:

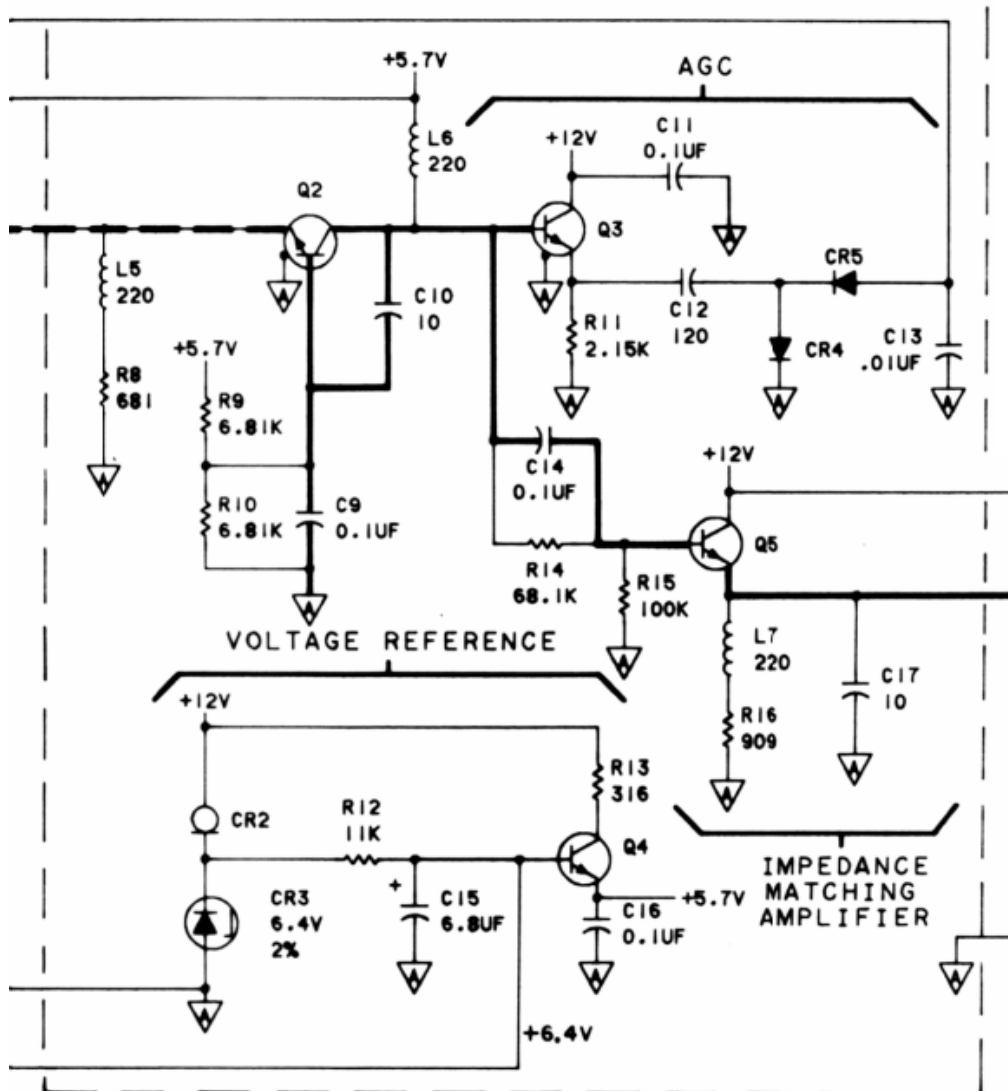


Figure 188 - HP10811A Buffer Amplifier and AGC Section  
 Photo from HP10811A Service Manual

The RF enters from the fat dashed line from the left. Q<sub>2</sub> is also a 2N5179 according to the parts list. Bias is established from the stabilized 5.7V line, just like the oscillator supply. The transistor is operating as a common base amplifier. Base is RF grounded by C<sub>9</sub>, the emitter is RF-isolated by L<sub>5</sub> and the collector by L<sub>6</sub>. The input impedance of Q<sub>2</sub> can be estimated (no detailed computation done here) as

$$Z_{IN} = \frac{V_T}{I_E} = \frac{kT}{qI_E}$$

with k as Boltzmann's constant and T standing for the absolute temperature and q for the electron charge. V<sub>T</sub> at 300K is about 25mV. If we compute I<sub>E</sub> (neglecting base current), we get

$$I_E = \left( \frac{V_S R_{10}}{R_9 + R_{10}} - V_{BE} \right) / R_8 = 3mA \text{ and } Z_{IN} = 8\Omega$$

This, compared to the crystal impedance in the range of 100 to 200Ohms, represents almost a short circuit and enforces a sinusoidal current into the emitter of Q<sub>2</sub>. This "filtering" approach was invented by Ulrich L. Rohde and is widely used in a lot of oscillators [10].

Q<sub>3</sub>, also a 2N5179 model, is configured as an emitter follower. Its collector now runs off the 12V supply rail, and the emitter current is approximately

$$I_E = \frac{V_C - V_{BE}}{R_{11}} = 2.3mA$$

The output impedance would be quite low, and it drives the voltage doubler rectifier made from the Schottky diodes CR<sub>1</sub> and CR<sub>2</sub> plus the C<sub>12</sub> and C<sub>13</sub> capacitors. The output voltage of the doubler is negative regarding to ground and drains current away from the oscillator transistor Q<sub>1</sub>'s base. Regulator time constants are best simulated.

Parallel to Q<sub>3</sub> we have Q<sub>5</sub>, another emitter follower/buffer stage. The collector runs from 12V, with an emitter current of (base currents neglected)

$$I_E = \left( \frac{V_S R_{15}}{R_{14} + R_{15}} - V_{BE} \right) / R_{16} = ca. 3mA$$

Q<sub>5</sub> is a 2N6429A [11], a common low noise audio transistor, like a BC549C. The f<sub>T</sub> of these transistors is in the range of ca. 200MHz, roughly, but gain is 300 or more. The emitter is RF decoupled by L<sub>7</sub>, and the 10pF cap (C<sub>17</sub>) is probably used for damping unwanted VHF oscillations.

At the bottom we have a voltage stabilizer circuit, also using a 2N6429A (Q<sub>4</sub>), a 1mA current regulator diode 1N5297 [12], and a precision Zener diode with no industry type specified. Zener voltage is low passed by R<sub>12</sub> and C<sub>15</sub> (cutoff frequency is ca. 13Hz). The collector resistor R<sub>13</sub> of Q<sub>4</sub> limits the output current to the 5.7V rail to less than ca. 16mA. This circuit is definitively not very precise, but probably has low noise. PSRR and noise will need to be simulated.

## 10.4 The Output Buffer

The last part of the circuit is shown here:

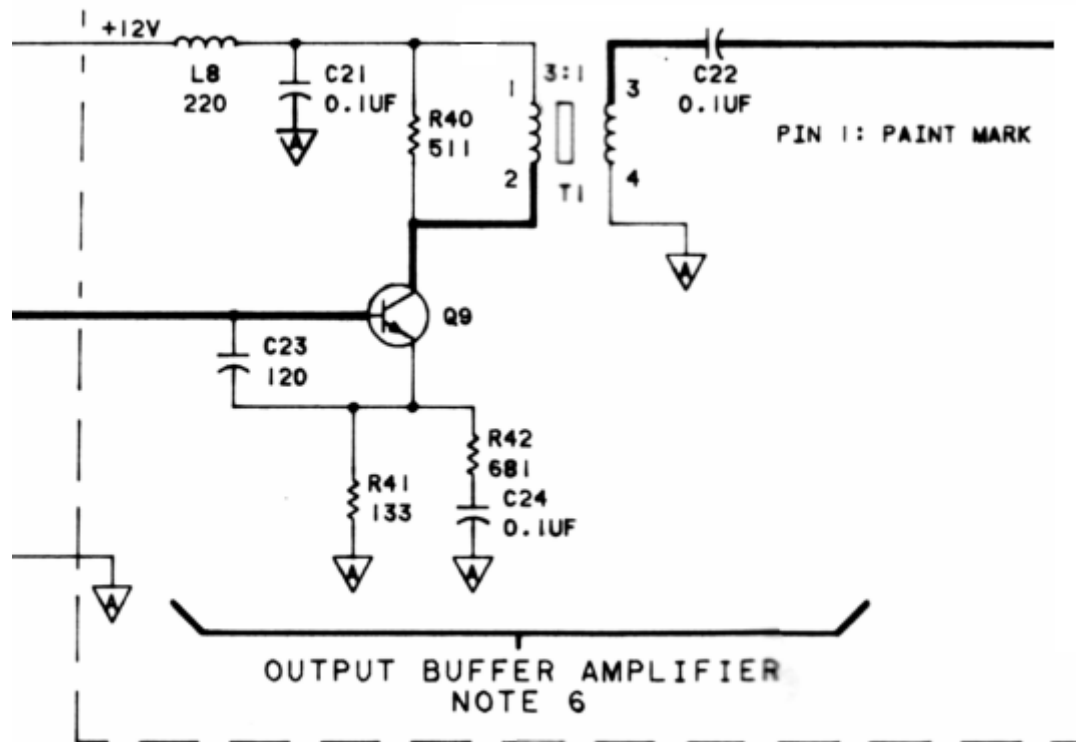


Figure 189 - The HP10811A Output Buffer Circuit  
Photo from HP10811A Service Manual

The fat line at the left comes directly from  $Q_5$ , so it sits at  $Q_5$ 's emitter voltage, DC-wise. The emitter current of  $Q_9$  is therefore

$$I_E = \frac{V_C - V_{BE}}{R_{41}} = 15mA$$

AC-wise the emitter resistor is smaller, and we must take  $C_{23}$  into account. The  $Q_9$  model is no industry type, but just defined as "600MHz 600mW". On the collector side we have a 3:1 transformer (described as "RF", no type, with 9T:3T), giving a 9:1 impedance transformation ratio. Using  $R_{40}$  and assuming a high output impedance of  $Q_9$  at a low frequency much lower than its  $f_T$ , we can assume an output impedance in the range of 50 Ohms. Gain is defined by the ratio of the collector impedance divided by the emitter impedance. Without  $C_{23}$ , we may assume a gain of around 2. At the collector we have:

$$Z_C = R_{41} \parallel (Z_0 * 9) = ca. 250\Omega$$

and at the emitter we have

$$Z_E = R_{41} \parallel R_{42} = ca. 113\Omega$$

so, including some transistor losses, we have a gain of about 2. The impedance of  $C_{23}$  at 10MHz is roughly  $130\Omega$ , adding to  $Q_{9S}$  unknown input capacitance. The reason to have a  $C_{23}$  is not documented, but it probably serves as a parasitic stopper cap.

$Q_{9S}$  power rail is filtered by  $L_8$  and  $C_{21}$ . The cutoff frequency of this lowpass is ca. 1MHz.

### 10.5 Heater Architecture

The heater circuit (not shown) consists of an op-amp based regulator sensing temperature via a thermistor and driving two TO-220 cased heater transistors. This design is unusual but is motivated by the need to avoid thermal asymmetry, as the HP article explains. The heater block is so light and thin that it would not be isothermal with just one transistor. It has been found that a large thermal mass design is less complicated and provides better results, an idea substantiated by the fact that nobody copied the HP design.

### 10.6 Phase Noise Performance

As a quick lookahead a measurement of a working 10811A oscillator on an FSUP phase noise analyzer is shown:

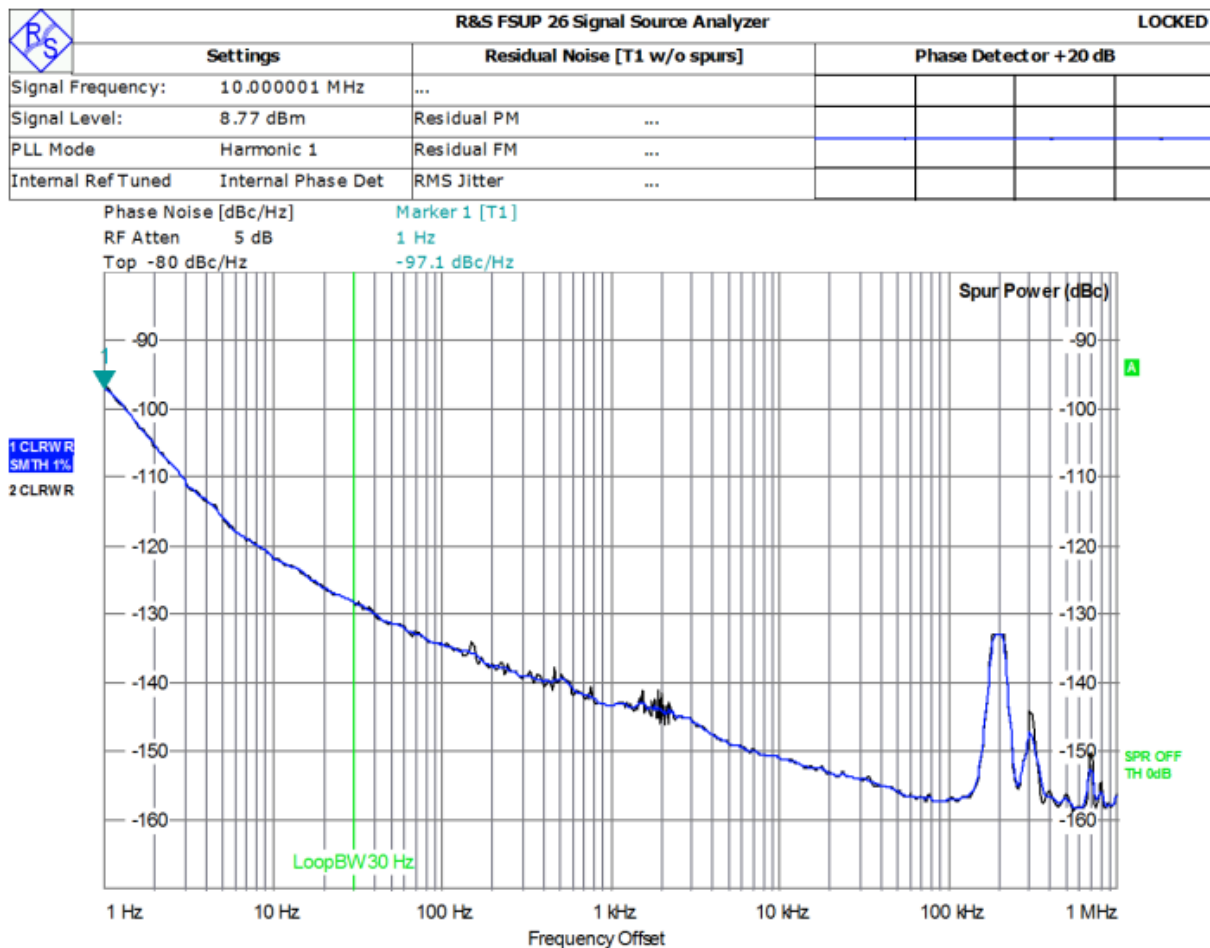


Figure 190 - HP10811A Phase Noise Performance

The curve is OK according to the specifications of the HP10811A, but it shows no exceptional performance by 2020 standards.

As a conclusion, the HP10811A was a landmark oscillator at the time it was introduced, but nowadays USO designs provide much better performance. The principal architecture, however (core, buffer, amplitude regulator, temp controller, output amplifier) is still quite common.

## References

- [1] Robert Burgoon et al., "SC-Cut Oscillator Offers Improved Performance," *HEWLETT-PACKARD JOURNAL*, vol. 32, no. March 1981, p. 20ff.
- [2] Ed Palmer, "Oscilloquartz 8601 BVA Oscillator Teardown." Accessed: Nov. 23, 2020. [Online]. Available: <http://www.leapsecond.com/museum/osa8601/view.htm>.
- [3] Hewlett Packard Co., "10811A/B Quartz Crystal Oscillator Operating and Service Manual." Aug. 1980, Accessed: Nov. 16, 2020. [Online]. Available: <http://literature.cdn.keysight.com/litweb/pdf/10811-90002.pdf>.
- [4] Vincent CANDELIER et al., "SPACE QUALIFIED 5MHz ULTRA STABLE OSCILLATORS," in *Proceedings of the 2003 IEEE International Frequency Control Symposium and PDA Exhibition Jointly with the 17th European Frequency and Time Forum*, 2003, p. 575ff.
- [5] FASTRON Group, "MICCS, MICCS/N Inductors Datasheet." Accessed: Nov. 24, 2020. [Online]. Available: <http://fastrongroup.com/uploads/datasheets/Series/Complete-DataSheet/MICCS.pdf>.
- [6] John R. Vig, "Introduction to Quartz Frequency Standards." U. S. ARMY LABORATORY COMMAND, Mar. 1992, Accessed: Nov. 24, 2020. [Online]. Available: <https://apps.dtic.mil/dtic/tr/fulltext/u2/a248503.pdf>.
- [7] SGS Thomson, "2N5179 VHF/UHF Transistor Datasheet." Accessed: Nov. 24, 2020. [Online]. Available: <https://pdf1.alldatasheet.com/datasheet-pdf/view/21690/STMICROELECTRONICS/2N5179.html>.
- [8] Ulrich L. Rohde, "A New and Efficient Method of Designing Low Noise Microwave Oscillators," TU Berlin, Berlin, 2004.
- [9] Anisha Apte, "A New Analytical Design Method of Ultra-low-noise Voltage Controlled VHF Crystal Oscillators and it's Validation," TU Cottbus, Cottbus, 2020.
- [10] Ulrich L. Rohde, "Crystal Oscillator Provides Low Noise," *Electronic Design*, vol. 21, Oct. 1975.
- [11] Central Semiconductor, "2N6429 Datasheet." Accessed: Nov. 24, 2020. [Online]. Available: <https://www.datasheets360.com/pdf/-3919446309018920913>.
- [12] Motorola Semiconductor, "Current Regulator Diodes 1N5283 to 1N5314." Accessed: Nov. 24, 2020. [Online]. Available: <https://pdf1.alldatasheet.com/datasheet-pdf/view/2827/MOTOROLA/1N5297.html>.



## 11 Appendix B: Quartz Crystal Physics

### 11.1 The Piezoelectric Effect

The basic effect of piezoelectricity originates from a breach of symmetry of the charge distribution inside the crystal caused by displacement of the atoms in the crystal induced by a mechanical force.

If, for instance, we take a crystal made from  $\text{SiO}_2$  (i.e., Quartz) we have Silicon (positive) and Oxygen (negative) atoms arranged in a hexagonal lattice (viewed from Z direction), and everything is symmetrical if no external force is present. If we pull or squeeze normal to the Z axis, symmetry breaks and there is a separation of charges to the top and bottom, proportional (within limits) to the pressure applied. This is shown below:

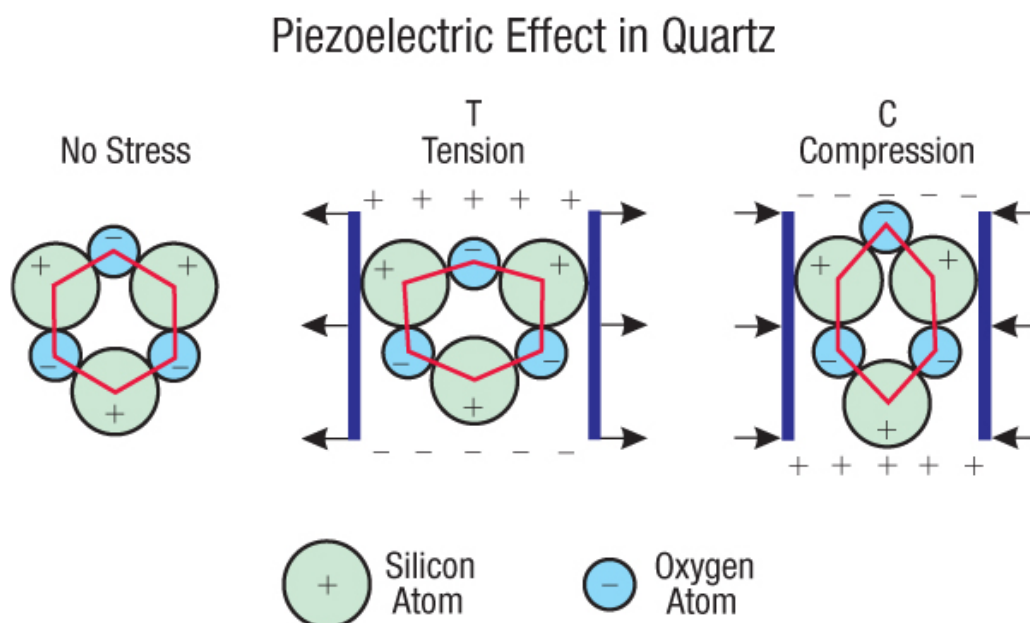


Figure 191 - The Effect of Stress on the Charge Distribution in Quartz  
Picture from [11]

[11] The Z axis is normal to the paper.

The proportionality factors of how much voltage is generated by a given force per square meter are dependent on the direction of the pressure vector in relation to the symmetry axes of the crystal.

In an isotropic material *unlike* Quartz, we would have Hooke's law in the simplest form (linear force, no shear)

$$S = sT$$

Where

$S$  is the strain (deformation, a vector),

$s$  is the compliance (a scalar quantity, or a diagonal matrix with identical elements) and

$T$  is the stress (a vector).

In case there is shear stress,  $\mathbf{T}$  becomes a symmetric 3x3 matrix, and the same goes for  $\mathbf{S}$ . The elements of  $\mathbf{S}$  can be computed from the basic mechanical properties of a material (young modulus, shear modulus, ...).

For the electric part in the isotropic case, we have

$$\mathbf{D} = \epsilon \mathbf{E}$$

Where

$\mathbf{D}$  is the electric displacement (a vector),  
 $\epsilon$  is the permittivity (a scalar quantity) and  
 $\mathbf{E}$  is the electric field strength (a vector).

As seen, there is no coupling between the electrical and mechanical parts here.

For an *anisotropic, piezoelectric* material like Quartz, things change in almost every aspect [12]:

1. The compliance  $\mathbf{S}$  is now a symmetric matrix with nonzero off-diagonal elements
2. The stress  $\mathbf{T}$  is now a matrix, containing mixed coordinate entries (shear)
3. The deformation  $\mathbf{S}$  is also a matrix, with its Eigenvectors *not* looking in the same directions as  $\mathbf{T}$
4. The same as above holds for  $\mathbf{D}$ ,  $\epsilon$  and  $\mathbf{E}$
5. There are coupling terms between electrical and mechanical quantities

We now have

$$\mathbf{S} = \mathbf{s}^E \mathbf{T} + \mathbf{d}^t \mathbf{E}$$

and

$$\mathbf{D} = \mathbf{d} \mathbf{T} + \epsilon^T \mathbf{E}$$

Where

$\mathbf{s}^E$  is the compliance tensor at no electric field,  
 $\mathbf{d}^t$  is a matrix for the converse (strain from electrical field) piezoelectric effect,  
 $\mathbf{d}$  is the matrix for the direct (displacement from stress) piezoelectric effect and  
 $\epsilon^T$  is the permittivity tensor at no external stress.

All coefficients above depend on the material, environmental conditions, and the crystallographic symmetry group. The formulas above assume linearity, which is not true outside of the elastic domain (not at extremely high field strengths either). All coefficients above are temperature dependent, in general with positive and negative coefficients depending on direction.

The fact that  $\mathbf{T}$  is symmetric ( $t_{12}=t_{21}$ ,  $t_{13}=t_{31}$ ,  $t_{23}=t_{32}$ ) and therefore has only 6 *different* elements can be used to combine  $\mathbf{S}$  and  $\mathbf{D}$  into one vector have a 9x9 matrix called  $\mathbf{C}$  compute this from  $\mathbf{T}$  and  $\mathbf{E}$ . The elements of  $\mathbf{C}$  come from  $\mathbf{s}^E$ ,  $\mathbf{d}$ ,  $\mathbf{d}^t$  and  $\epsilon^T$ . This is called Voigt notation after its inventor. [13]

$$\begin{Bmatrix} T_{11} \\ T_{22} \\ T_{33} \\ T_{12} \\ T_{23} \\ T_{31} \\ D_1 \\ D_2 \\ D_3 \end{Bmatrix} = \begin{bmatrix} c_{11}^E & c_{12}^E & c_{13}^E & 0 & 0 & 0 & 0 & 0 & -e_{13} \\ c_{12}^E & c_{11}^E & c_{13}^E & 0 & 0 & 0 & 0 & 0 & -e_{13} \\ c_{13}^E & c_{13}^E & c_{33}^E & 0 & 0 & 0 & 0 & 0 & -e_{33} \\ 0 & 0 & 0 & c_{66}^E & 0 & 0 & 0 & 0 & 0 \\ 0 & 0 & 0 & 0 & c_{44}^E & 0 & 0 & -e_{15} & 0 \\ 0 & 0 & 0 & 0 & 0 & c_{44}^E & -e_{15} & 0 & 0 \\ 0 & 0 & 0 & 0 & 0 & e_{15} & \epsilon_{11}^S & 0 & 0 \\ 0 & 0 & 0 & 0 & e_{15} & 0 & 0 & \epsilon_{11}^S & 0 \\ e_{13} & e_{13} & e_{33} & 0 & 0 & 0 & 0 & 0 & \epsilon_{33}^S \end{bmatrix} \begin{Bmatrix} S_{11} \\ S_{22} \\ S_{33} \\ S_{12} \\ S_{23} \\ S_{31} \\ E_1 \\ E_2 \\ E_3 \end{Bmatrix}.$$

[I think that in R5C5 it should read  $C_{55}$ .]

Which elements are nonzero is determined by the symmetry group of the crystal material [14].

## 11.2 Equations for a Piezoelectric Resonating Body

The next step would be to derive a set of equations describing the *motion* and the *electric field* of a working crystal resonator. This involves

1. Newton's law of inertia  $F = m \cdot a$ .
2. Maxwell's equations (magnetics can be left out)
3. The coupling relation between strain, stress, electric displacement, and field strength above
4. Electric and mechanic boundary conditions (thickness, size, electrodes, zero amplitude (attachment) points, ...)

According to John Vig these equations together were never able to be formulated in close-form mathematics (he called them *messy* [15]).

Furthermore, all interesting effects (temperature dependency, sensitivity on acceleration, DLD, RLD, pulling, ...) involve higher order "constants" (up to order 3 according to Vig, [15]) that make the equation systems extremely complicated. Only special cases (infinite disk of a given thickness, linear case, no electrode loading, no fixtures, ...) have approximate solutions.

Instead of diving into this extremely complicated matter we will use approximate results successfully applied in the industry, and give heuristic explanations were exact solutions are not available.

## 11.3 Modes

Even if we think of an infinite disk without boundaries a plethora of operating "modes" are possible, no wonder because of the complicated structure of the electric and mechanic material constants. An incomplete collection of actually *used* "modes" is shown below [16]:

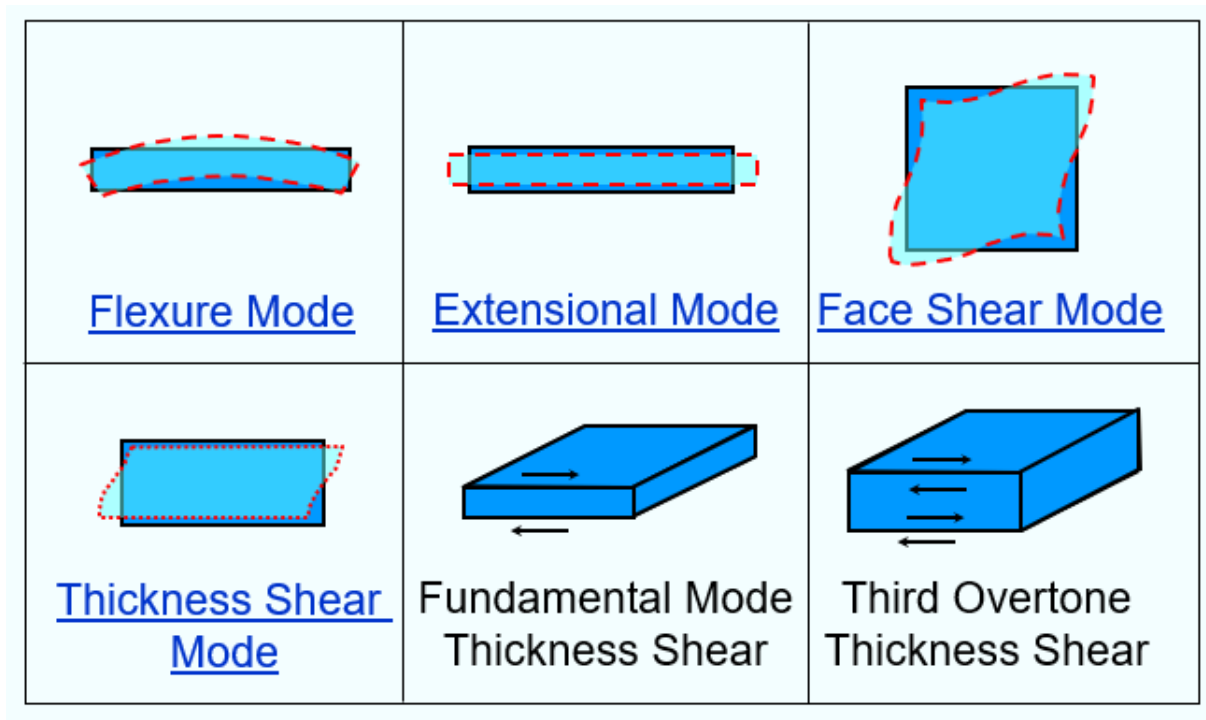


Figure 192 - Crystal Vibration Modes  
Picture by John Vig [16]

Unfortunately, there are other modes too, but they are normally not used in practical design or they are parasitic (e.g., twist mode, B Mode, ...). These modes do in general *not* have an integer frequency relation to the fundamental frequency (e.g., the very strong B Mode in SC cut crystals is a few percent above the intended frequency). For a volume with the dimensions  $d$ ,  $l_x$  and  $l_y$  the mode frequencies are given by [17]

$$f_{nmp} = \frac{1}{2\sqrt{\rho}} \sqrt{\frac{c_{66}n^2}{d^2} + \frac{c_{11}m^2}{l_x^2} + \frac{c_{55}p^2}{l_y^2}}$$

Where

$\rho$  is the density of Quartz

$c_{ij}$  are material constants of Quartz and

$n$ ,  $m$ ,  $p$  are integers, with  $n > 0$  and  $m, p \geq 0$ .

From this point on, we will focus on Quartz only as a base material, on disk-shaped precision crystals (no wristwatch tuning-fork, sheet, or other types). Furthermore, we will restrict ourselves to AT and SC cut crystals running in thickness shear mode(s), explained next.

## 11.4 Quartz Cuts

When we look at a Quartz crystal and its axes, we have z-Axis and a hexagon structure normal to it, as shown here [18]:

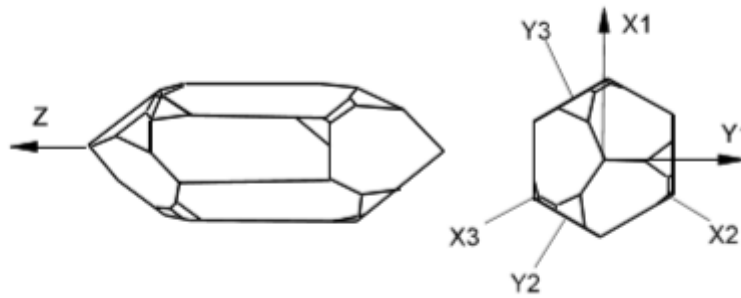


Figure 193 - Crystal Axis in Quartz

The X and Y axes can assume one of three identical positions, 120° apart. When planning to make a precision crystal we need to make the dependency of all the material constant matrices on temperature as small as possible. Fortunately, the temperature coefficients along the axes do have opposing signs, so a linear combination of angles could do the trick of cancelling temperature coefficients around a specified target operating temperature. Two temperature compensated “cuts” are widely used: AT cut and SC cut. Their positions regarding the axes are shown below (from John Vig [15]):

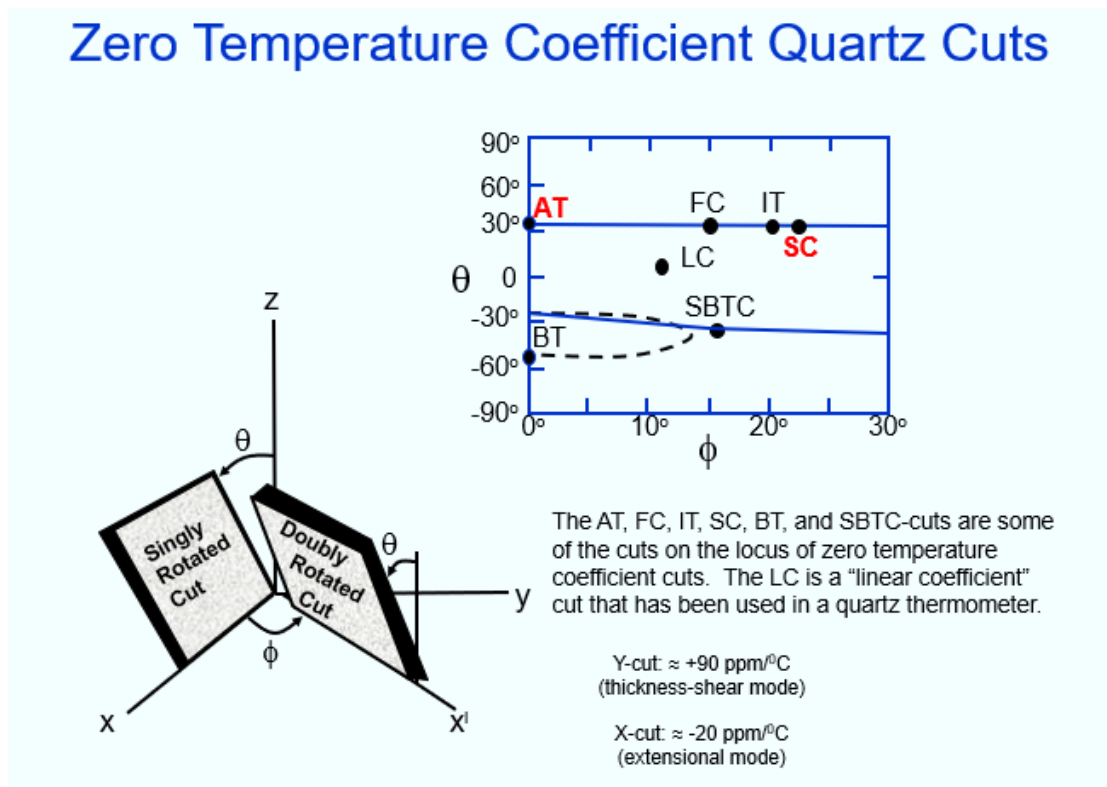


Figure 194 - Zero Temperature Coefficient Cuts in Quartz  
Picture by John Vig [15]

Combining directions can also be used to *maximize or linearize* temperature dependence, e.g., for use as temperature sensors).

The AT cut was invented first (in 1934) and is still in use today (It is safe to say that much of the 2019 crystal production is AT and tuning fork). Its comparatively easy to make, is tolerant of (slight) maladjustments of the cutting angles and delivers acceptable performance for most routine applications.

When it comes to premium oscillators with exceptional stability, the SC (stress compensated, since 1976) cut has distinct advantages [15]:

1. Compensation for planar stress and thermal transients
2. Lower temperature coefficient, less retrace, better repeatability
3. Low DLD effect
4. Very few dips
5. Low vulnerability to radiation
6. Higher Q

The downsides are

1. Much higher cost
2. Very small tolerances in manufacturing
3. Sensitive to static voltages (can be used for tuning) and, most important
4. B Mode. This is a spur (ca. 8-10% above the main frequency) that can have a *higher Q* than the specified frequency and that needs to be actively suppressed (or electronically separated from the oscillator output). See VNA screenshots in this chapter.

All up-to-date precision oscillators today run SC cut crystals. This includes BVAs (explained later).

## 11.5 Thickness Shear Mode

The thickness shear modes have some unique advantages over other modes:

1. There is no mechanical tension *within* the top and bottom surfaces of the disk (i.e., no stress on electrodes that may lead to cracks or open circuits)
2. Close control of the temperature dependencies is possible
3. Active zone and crystal holder structures can be separated (explained below).
4. Overtone modes can be used to obtain smaller bandwidths

In thickness shear mode (To my knowledge the only one used in precision oscillator crystals today) the movement of the crystal is *normal* to the electric field vector between the electrodes. This means that the attachment of the crystal to a support structure (holder pins plus contacts for the electrodes) at the disk boundaries is *not* located at a position where the mechanical displacement is zero, making it clear that the acoustic and electric short circuit by a clamp would distort the waveform, and therefore also have an effect on frequency. This needs to be avoided, see below.

## 11.6 Active Regions

When looking at a crystal from the side, we see a blank with electrodes attached above and below (exception BVA, will be treated later), like this:

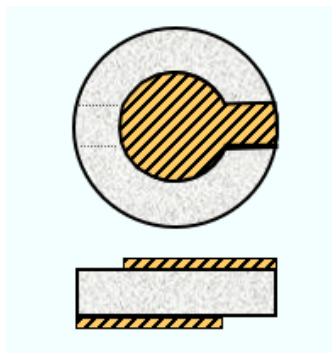


Figure 195 - Crystal Electrodes  
Picture from John Vig [15]

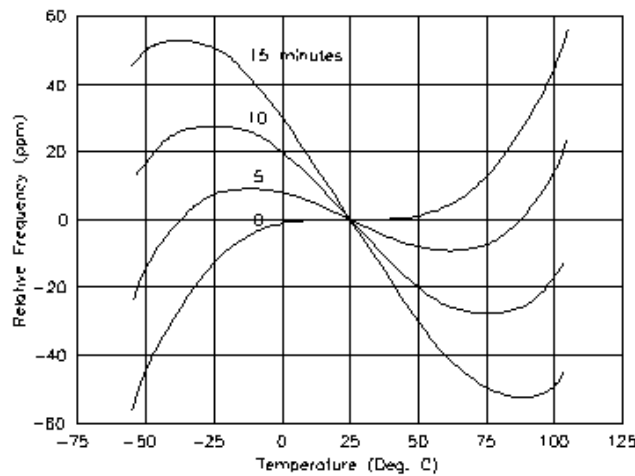
The active region is strongly confined to the volume located between the electrodes, with an exponential decay of activity beyond. The confinement can be improved even more by giving the Quartz disk a lens-like shape. Keeping the electrodes away from the disk boundary by a few mm minimizes this effect of the holder clamps on the waveform. This technique is used by all disk-shaped crystals used today. Neubig [10] recommends that the electrodes cover less than 70% of the area, and that the diameter of the disk is more than 60 times the thickness.

### 11.6.1 Fundamental Frequency, Overtones, Spurs

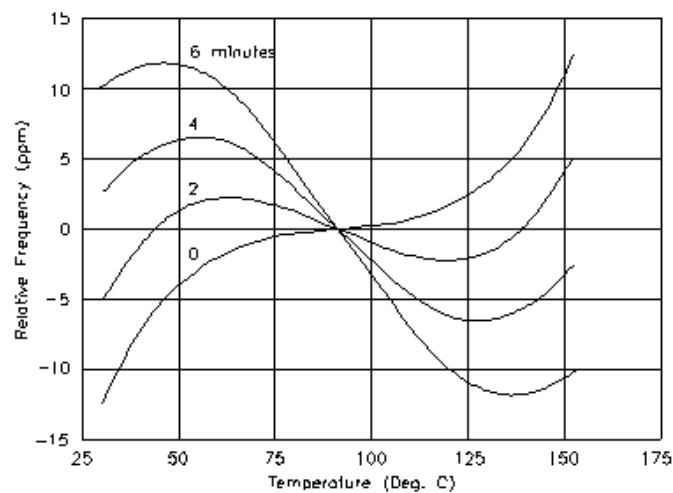
An infinite disk can resonate in a fundamental mode frequency, but also in (inexact) odd multiples of it. All *even* harmonic modes do not propagate because they would have no voltage across their end points. Unfortunately, there are a lot more non-thickness shear modes (spurs) with no integer frequency relation to the fundamental frequency that can resonate as well (e.g., the B Mode for SC cut crystals). See formulas on previous pages for possible frequencies.

### 11.6.2 Temperature Dependency, Compensation

By using the proper cut (AT, SC) it is possible to create a parabolic or third-order inflection point in the frequency over temperature curve. Sample curves for AT cut and SC cut temperature dependency curves are shown below [20]:



AT-cut Frequency vs. Temperature Curves



SC-cut Frequency vs. Temperature Curves

Figure 196 - Frequency over Temperature Curves for AT and SC Crystals  
Photo from <https://www.4timing.com/techcrystal.htm>

The parameter called “minutes” is the cutting angle. As seen, the “zero” point for AT cut is at about room temperature, while SC is between 75°C and 100°C. In case of an OCXO, the crystal temperature must always be safely *higher* than ambient temperature, because all temperature controllers can heat, but not cool. The SC lower turning point is also ideal because it is low enough to not cause problems for semiconductors running at the same temperature inside an ovenized oscillator. When we assume that we have 85°C inside, 20mW of transistor dissipation, and an  $R_{TH}$  of, say, 200K/W (small signal transistor), the Silicon runs at 89°C, which is absolutely no reliability problem. Running OCXOs at the upper turning point is normally not done due to stress on semiconductors and other parts.



### 11.6.3 Crystal Defects

Crystals made nowadays are exceptionally clean in terms of impurities and other chemical or physical defects; still, some of them do play a role in the resonant properties:

1. Aluminum ions in the grid (“clouds”, they lower Q but can be “swept out”, see later)
2. Grid defects (Interstitials, Offset lines or planes, corkscrew defects ...). This can be reduced by growing at a slow rate, and by using very pure seed crystals. Thermal annealing also helps.
3. Mechanical tension coming from the cooling phase of the manufacturing phase (not found so much in natural crystals because they had millions of years to anneal)
4. Impurities attached to the surfaces (from grinding, lapping, etching, polishing, handling, ...)

All these have a damping effect on oscillations, and therefore lower the Q factor and increase phase noise in oscillators. The effect on resonant frequency can be both ways, as will be discussed later.

## 12 Appendix C: Crystal Measurements

The measurement of high-Q precision crystal properties is tricky and needs some extra caution. If we start with impedance measurements, the extreme impedance range (series resonance has around 50-200 Ohms, “parallel resonance”<sup>12</sup> can have  $10^6$  Ohms or more) ask for appropriate tools. Standard VNAs could be used in principle, but they are not the best choice, because:

1. Resolution bandwidth must be very small so no peak or dip with an extremely low bandwidth is missed out (e.g., the BW of a 5MHz 3<sup>rd</sup> OT SC crystal is ca. 2Hz).
2. Frequency stepping must be fine enough (1/10 of bandwidth)
3. Sweep speed must be slow enough so that that a resonant frequency is excited long enough to stabilize the output level (so the effect on amplitude is not “swept out”).
4. Especially for the “parallel resonance” a test fixture with precisely defined capacitances is needed. Crystal series resonance can be measured in shunt-thru or series mode.
5. Most VNAs have no precision output amplitude. This can be a problem for amplitude dependent effects like DLD.

### 12.1 Measurement Set-up

See [1] for a discussion of a LF VNA based impedance measurements.

The two measurement possibilities with a VNA are shown below:



*Figure 197 - Crystal Parameter Measurements Using a VNA  
Photos of Instruments from Keysight Website*

Shunt is good for low impedances, series for high impedances. Around the system impedance (50 Ohms) both methods perform equally well. The impedance range of an SC crystal (a few 10 Ohms at series resonance up to several million Ohms) suggests that series mode is the method of choice.

As said, these techniques on a standard VNA are a compromise for high-Q crystal measurements.

---

<sup>12</sup> Physically speaking there is no parallel crystal resonance. It is just an impedance maximum, but not a maximum in the mechanic movement of the crystal. I will use the term here because of its widespread use in the literature.

A precision LF impedance analyzer is the best measurement tool for high quality crystals, much better than a 50Ohm VNA. The crystals are attached to IEC standardized test fixtures [2], and the impedance analyzers have a wider amplitude setting range so DLD and other nonlinear effects can be accurately measured. The measurement conditions are standardized in norm IEC444. A suitable measurement setup is shown below:

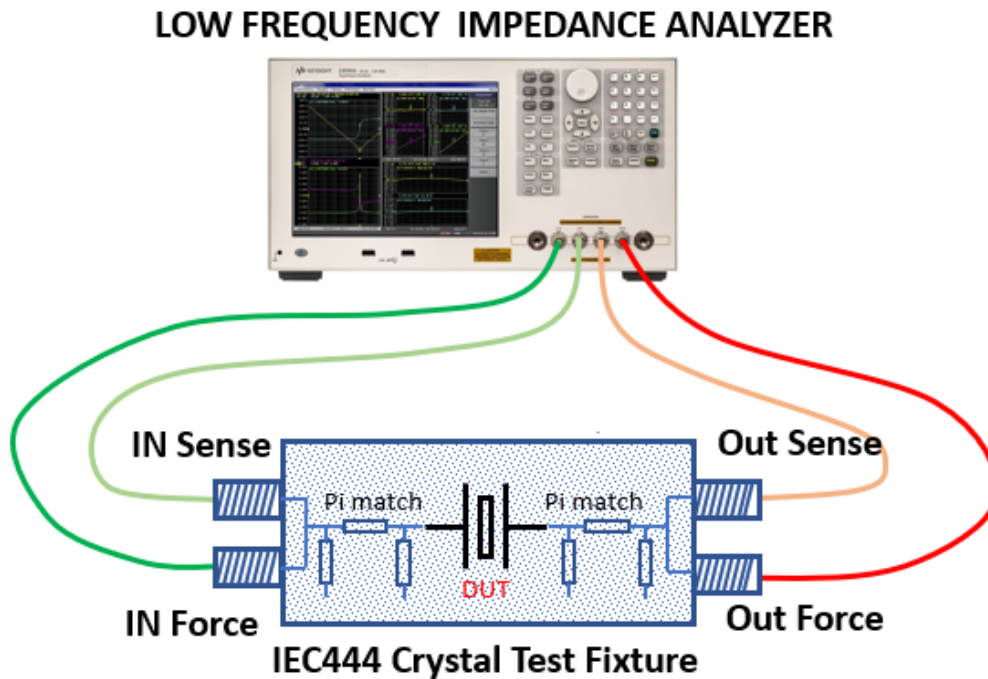


*Figure 198 - Standard Crystal Measurements Using an Impedance Analyzer  
Photos of Instrument from Keysight Website*

The essential difference between a VNA and an impedance analyzer is that the impedance analyzer measures using either a balanced bridge technique (best, [3]) or a *4-wire technique* instead of single 50Ohm cabling (classic). This drastically increases dynamic range, 25mOhms to 2MOhm (at 5MHz with 10% error) as compared to ca. 20kOhms for the VNA. More details about the measurement are described later in this chapter.

## 12.2 Results

At AXTAL (the company owned by B. Neubig, [4]) a set of different 5MHz and 10MHz crystal was measured on an autobalancing bridge impedance analyzer (HP E5100B), and the measured data was compared to the datasheet values from the manufacturers where available. DLD Measurements were also tried on a Kolinker KH1120 crystal test set [5].

The 5MHz types were HC-40 types from Croven Crystals [6], Inc., and two Bliley space qualified crystals provided by the Jet Propulsion Laboratory in USA (obtained via Prof. U. L. Rohde). These space qualified parts are also Bliley glass types (label says BG61SCH-3 [7]) but have undergone testing in a space parts lab using MIL testing procedures.

The crystal extracted from a 10MHz HP10811A OCXO and a consumer grade AT cut crystal were tested for comparison. All crystals were heated to the temperatures specified by the manufacturers. The heating was done using specialized milled Aluminum heater blocks (the same as used in my prototype USOs) and a precision temperature regulator (see chapter on thermal regulation).

The following crystals were measured:

1. Bliley glass from JPL 5MHz (BG61SCH-3) [7]
2. Croven HC-40 Cold-weld 5MHz [6]
3. HP10811A SC-Cut 10MHz

The following results were obtained:

Series resonant frequency, resistance, capacitance, and inductance were remarkably close to the datasheet values, for all parts.

1. Glass parts are slightly better than cold-weld parts (5-10% in Q). According to Luke Mueller from Croven this is plausible because Bliley used swept Quartz for their space products which the normal Croven line did not [6]. Newer Croven parts also made of swept material have the same datasheet Q as the Bliley parts, but could not be measured due to the lack of a premium impedance analyzer.
2. The DLD effect at 5MHz (10MHz for HP) is low ( $<10^{-3}$ ), even when measured starting in the nW range. This applies to the Bliley glass and the Croven cold-weld-types. This confirms datasheet information and makes extra caution about the lazy crystal effect unimportant.
3. The Kolinker equipment was not able to measure DLD at 5MHz and  $Q > 2 \cdot 10^6$ , only at 10MHz and up.
4. The B Mode of the glass crystals and the Croven parts is extremely power sensitive (more than 10uW creates jumps) and had a Q above  $5 \cdot 10^6$ , double the operating Q.
5. The HP10811A crystal has a Q around  $10^6$  and stays below John Vig's Q over f curve. No magic involved.
6. The HP10811A crystal has an untypical low series resistance, and a smaller capacitance and higher L than modern crystals. The undesirable effect is (even with the same Q) larger sensitivity on changes in external capacitances than obtainable with modern designs.

A screenshot (manually, hardcopy function did not work) from the impedance analyzer containing a nonlinear B-Mode DLD effect (Croven HC-40, 100uW, B-Mode) can be seen here:

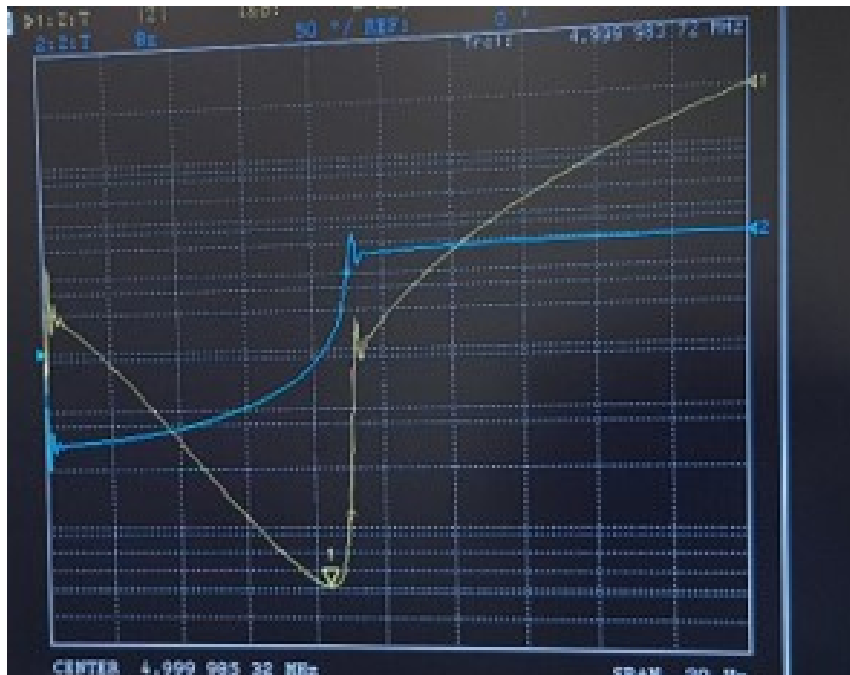


Figure 199 - B Mode Resonance Showing Strong DLD Effect

After reducing power, the curves smoothed out.

The HP10811A 10MHz crystal screenshot is shown here:

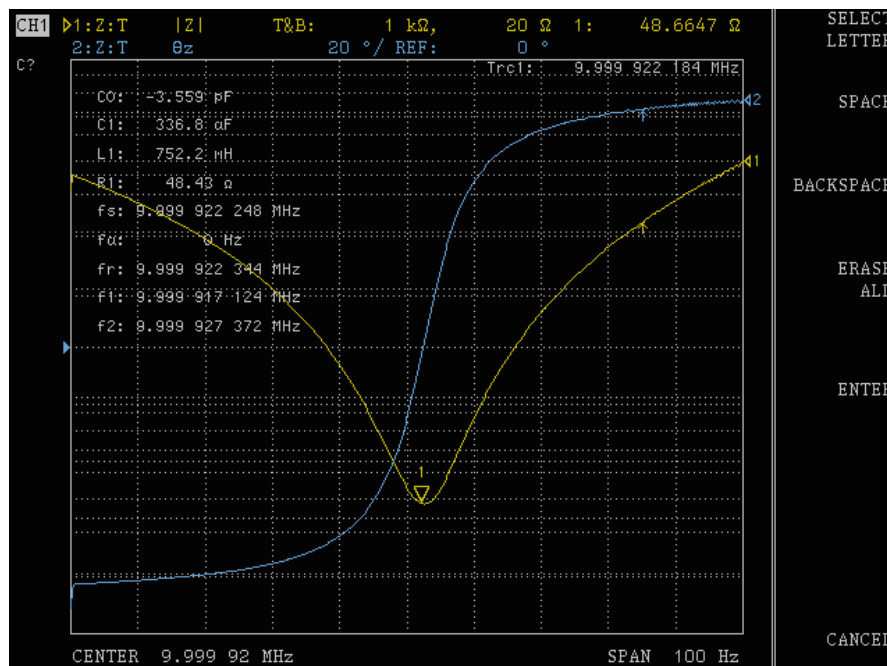


Figure 200 - The Resonance Curve of the HP10811A 10MHz Crystal

Measured Q was 975000. This is in line with the predictions of the Vig Q over curve.

## References

- [1] Keysight Inc., "Performing Impedance Analysis with the E5061B ENA Vector Network Analyzer." Accessed: Nov. 26, 2020. [Online]. Available: <https://www.keysight.com/us/en/assets/7018-03423/application-notes/5991-0213.pdf?success=true>.
- [2] Cathodeon Inc., "Cathodeon PI Network Mark II Quartz Test Fixture." Accessed: Nov. 26, 2020. [Online]. Available: <https://isolalab.com/pinetwork.html>.
- [3] Agilent Technologies, "New Technologies for Accurate Impedance Measurement (40Hz to 110MHz) Product Note." Accessed: Nov. 26, 2020. [Online]. Available: <https://literature.cdn.keysight.com/litweb/pdf/5968-4506E.pdf>.
- [4] AXTAL / B. Neubig, "AXTAL Corp.- Website." Accessed: Nov. 26, 2020. [Online]. Available: <https://www.axtal.com/>.
- [5] Kolinker Inc., "KH1800/ KH1820 PI-Network Crystal Measurement System." Accessed: Nov. 26, 2020. [Online]. Available: <https://www.kolinker.com/wp-content/uploads/images/cataloguePDF/KH1800.pdf>.
- [6] Croven Crystals Inc., "Croven HC-40 Crystals Datasheet." Accessed: Nov. 19, 2020. [Online]. Available: [https://crovencrystals.com/wp-content/uploads/HC-40\\_Crystal\\_Holder\\_Rev\\_00.pdf](https://crovencrystals.com/wp-content/uploads/HC-40_Crystal_Holder_Rev_00.pdf).
- [7] Bliley Corp., "Bliley Quartz Crystals." Accessed: Nov. 19, 2020. [Online]. Available: <https://de.slideshare.net/BlileyTech/bliley-takes-you-further>.

## 13 Appendix D: Measuring Crystal Properties

Top quality crystals are a challenge even to premium test equipment. The reason for this is the extreme Q factor, the associated very small bandwidth and extremely large and small values of the motional inductance and capacitance parameters. Another complication is that extreme impedance values must be measured at extremely small power levels to avoid nonlinear effects. This section covers measurement problems and techniques in more detail.

### 13.1 Instruments for Measuring Premium Crystals

The best choice for crystal parameter measurements is a dedicated impedance analyzer, like the Keysight E4990A. This instrument does not work like a classic VNA, but as a so-called auto balancing bridge, where a controllable feedback impedance in a sensitive difference amplifier is adjusted until a match is reached [1]. This instrument can measure impedance ranges from  $m\Omega$  to  $M\Omega$  with a maximum precision of below 0.1% at 5MHz [1]. The power level can be lowered to 500nW, so DLD effects can also be measured, and frequency resolution goes down to 1mHz. A further advantage of dedicated impedance analyzers is that the coefficients of Maximum frequency range is 120MHz, at a cost of ca. 60K€. The instrument is shown here:

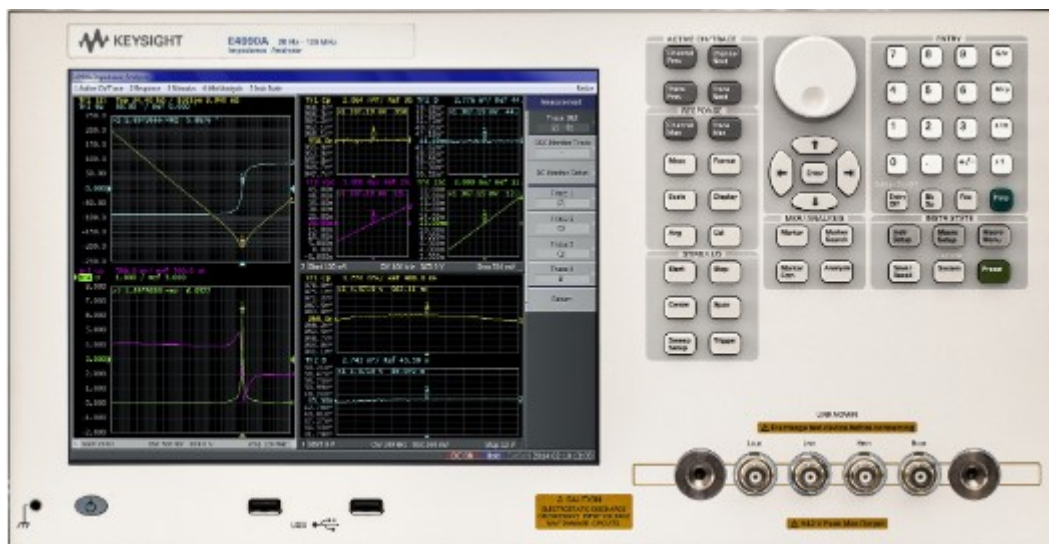


Figure 201 - Keysight E4990A Autobalancing Bridge Impedance Analyzer  
Photo from Keysight Website

If an auto balancing bridge analyzer is not available, a classic VNA can be used with less precision, range of power level and a smaller range of impedances that can be measured. For our application, it is important that the VNA also has good properties at low frequencies ruling out most microwave VNAs that start at 10MHz. A Keysight E5071C (9kHz to 8.5GHz) [2] was used here.

Gain/Phase analyzers can also be used, with further restrictions.

### 13.2 Standardized Measurement Procedures for Crystals

There is a new IEC standard for measuring crystals (IEC60444). This standard defines the measurement environment, the test fixtures, the error correcting methodology, calibration, and many more aspects). Unfortunately, these documents are only available for a license fee and must not be disclosed. Some important aspects, however, are discussed by B. Neubig in his “Crystal Cookbook” [3].

For precise crystal measurements, we need a reproducible test environment. For leaded crystals, this consists of two PI-type attenuators around a clamp with defined geometry, shown here:

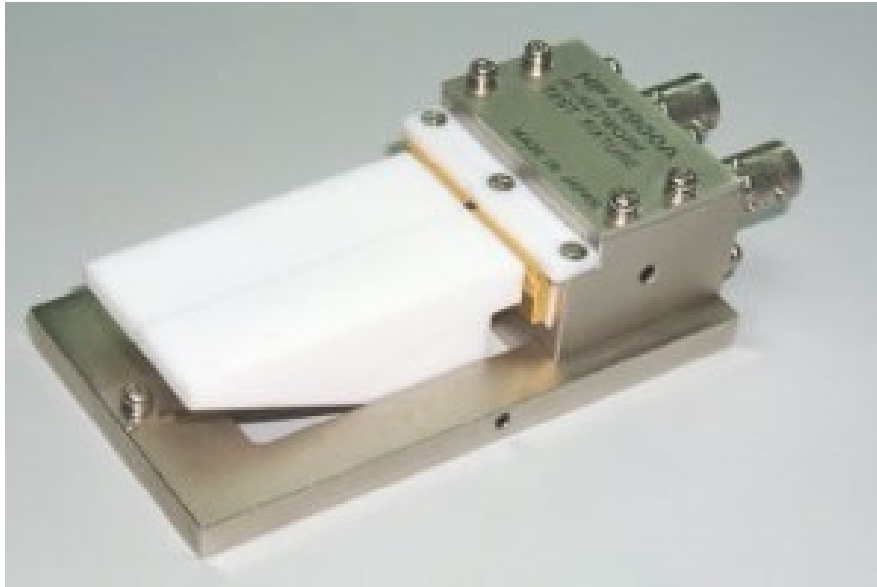


Figure 202- HP Leaded Crystal Test Fixture  
Photo from HP Website, also see [2]

The two big white PTFE levers clamp the wires of the crystal to large gold-plated contact areas. The resistor networks lead to the BNC sockets at the back. This adapter works well for the usual HC49/U and similar types with a small can and two leads. The white PTFE bar on top simulates the PCB with a thickness of ca. 1.5mm so the crystal measured will have a realistic nonzero lead length.

Unfortunately, there is no IEC standard fixture for the precision crystal cases HC-35/U and HC-40. Such an adapter needs to be built from scratch.

These adapters have become rare and expensive. New ones can be ordered from Cathodeon [7] for ca. 1200€.

The role of the PI attenuators is to create a low reflection low impedance environment so crystals with a low resistance can be measured accurately. The IEC defined the output impedance of the attenuators to be 12.5Ohms, resulting in the resistance values shown next:

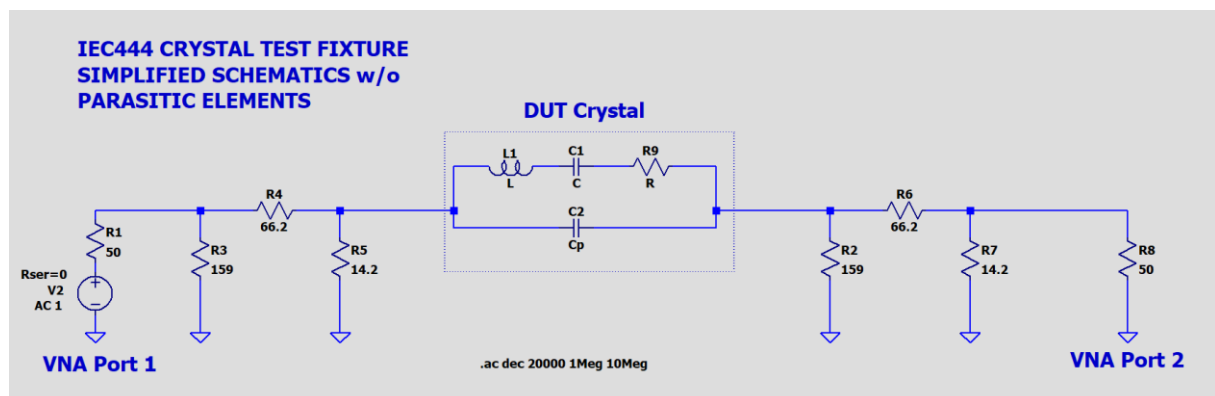


Figure 203 - IEC444 Crystal Test Fixture Schematics

The measurement is then done in the so-called Series-Thru mode where S21 is recorded over frequency. Assuming a VNA measurement, the following parameters are extracted:

1. Attenuation at the series resonance (gives R)
2. Q factor of the series resonance (gives L)



3. Series resonance frequency (gives C)
4. Parallel resonance frequency (gives  $C_p$ )

A modest self-made test fixture for the low HF range with a test crystal inside is shown here:



Figure 204 – Self-made Low HF IEC444 Crystal Test Fixture

An example of a 5MHz consumer grade HC-49 AT crystal is shown below (Max and Min, and Q factor). The VNA used was a Keysight E5071C (good, but not premium lab VNA) [2]

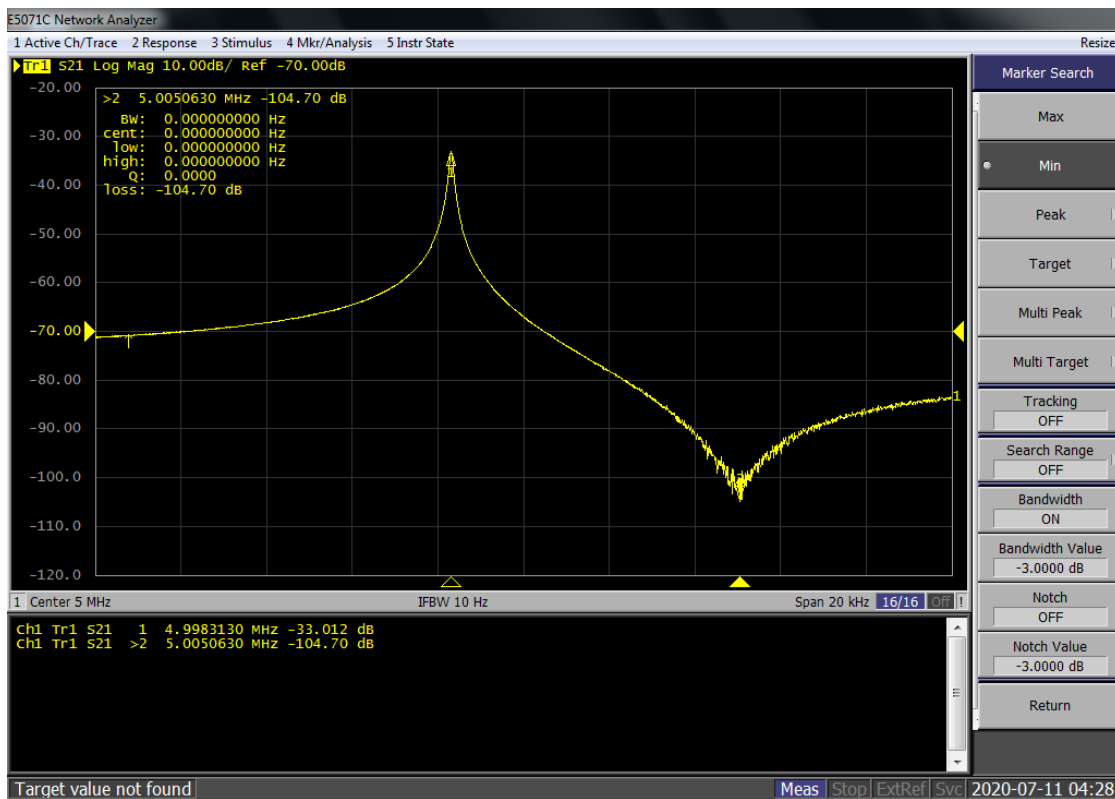


Figure 205- Impedance Minimum and Maximum of a 5MHz AT Crystal measured on a VNA



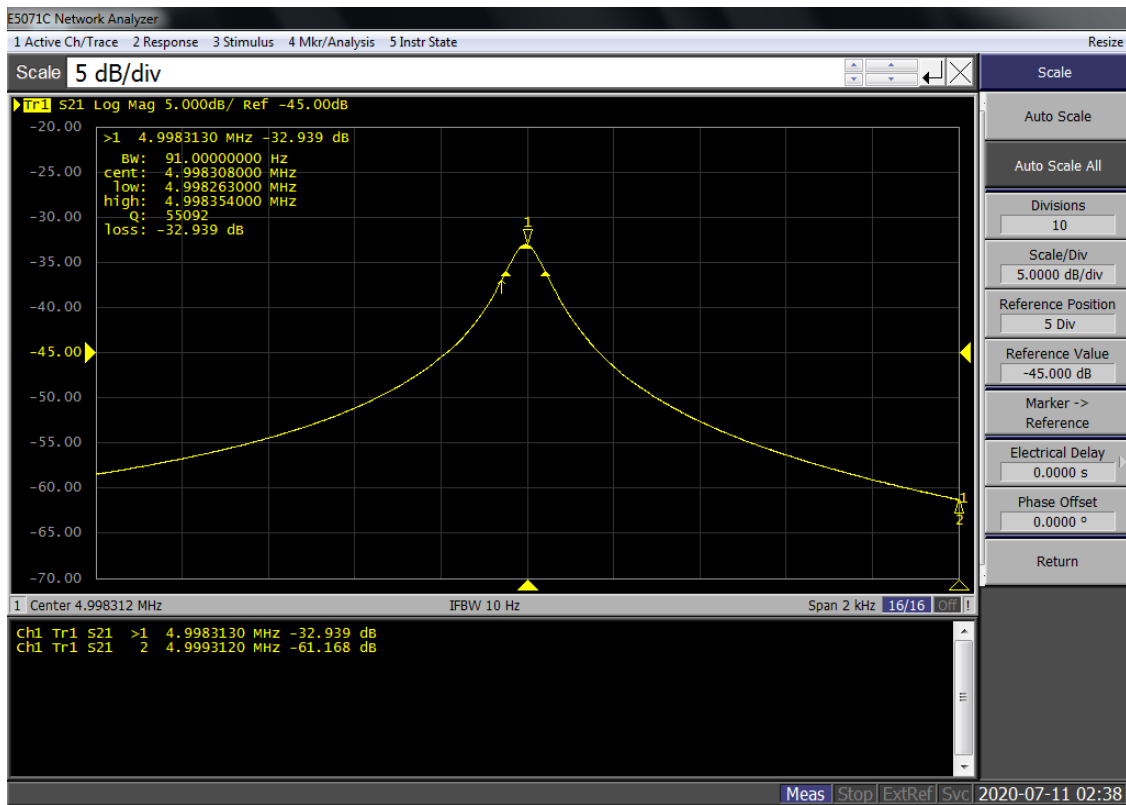


Figure 206- Series Resonance Measurement of  $Q$  Factor of a 5MHz AT Crystal Measured on a VNA

We can (leaving out stray capacitances and other parasitics that are handled in IEC40666) derive the motional parameters for this resonance.

For the measured  $Q$  we get

$$Q_M = \frac{2\pi f_S L}{R}$$

For  $f_S$  we have

$$f_S = \frac{1}{2\pi\sqrt{LC}}$$

And for  $f_P$  we have

$$f_P = \frac{1}{2\pi\sqrt{L(C||C_p)}}$$

$R$  needs to be derived from the maximum value of  $S_{21}$ .

For that, we compute two-port network matrices for the two PI attenuators and the DUT crystal. We start from  $Y$  matrices, convert them to  $ABCD$  matrices to concatenate, and then convert back to  $S$  matrices to measure. The  $Y$  matrix of the left attenuator is (resistors called  $R_I$  for input,  $R_S$  for series and  $R_O$  for output, corresponding admittances are called  $Y_I$ ,  $Y_S$  and  $Y_O$ ) is

$$Y_{\pi 1} = \begin{pmatrix} Y_I + Y_S & -Y_S \\ -Y_S & Y_O + Y_S \end{pmatrix}$$

Resulting in an  $ABCD$  matrix of

$$A_{\pi 1} = R_S \begin{pmatrix} Y_O + Y_S & 1 \\ (Y_O + Y_S)(Y_I + Y_S) - Y_S^2 & Y_I + Y_S \end{pmatrix}$$

The ABCD matrix of the right attenuator then reads (just applying symmetry):

$$A_{\pi 2} = R_S \begin{pmatrix} Y_I + Y_S & 1 \\ (Y_O + Y_S)(Y_I + Y_S) - Y_S^2 & Y_O + Y_S \end{pmatrix}$$

The ABCD matrix of a pure series element like our DUT crystal with Impedance  $Z_X$  is

$$A_{XT} = \begin{pmatrix} 1 & Z_X \\ 0 & 1 \end{pmatrix}$$

If we make a shorthand for the elements of  $A_{\pi 1}$  and  $A_{\pi 2}$  using

$$\alpha = \frac{Y_I + Y_S}{Y_S} \quad \beta = \frac{1}{Y_S} \quad \gamma = \frac{1}{Y_S} ((Y_O + Y_S)(Y_I + Y_S) - Y_S^2) \quad \delta = \frac{Y_O + Y_S}{Y_S}$$

Then we have

$$A_{\pi 1} = \begin{pmatrix} \alpha & \beta \\ \gamma & \delta \end{pmatrix} \quad \text{and} \quad A_{\pi 2} = \begin{pmatrix} \delta & \beta \\ \gamma & \alpha \end{pmatrix}$$

The total ABCD matrix for the whole circuit including the two PI attenuators plus the crystal is

$$A_{TOT} = A_{\pi 1} A_{XT} A_{\pi 2}$$

Which now reads after multiplying everything out

$$A_{TOT} = \begin{pmatrix} \alpha\delta + \beta\gamma + \alpha\gamma Z_X & 2\alpha\beta + \alpha^2 Z_X \\ 2\gamma\delta + \gamma^2 Z_X & \alpha\delta + \beta\gamma + \alpha\gamma Z_X \end{pmatrix}$$

We can now separate  $A_{TOT}$  into a constant and a variable part so that

$$A_{TOT} = U + Z_X V$$

With

$$U = \begin{pmatrix} \alpha\delta + \beta\gamma & 2\alpha\beta \\ 2\gamma\delta & \alpha\delta + \beta\gamma \end{pmatrix} \quad \text{and} \quad V = \begin{pmatrix} \alpha\gamma & \alpha^2 \\ \gamma^2 & \alpha\gamma \end{pmatrix}$$

and from this matrix we need the expression for  $S_{21}$ , which is done by using the standard conversion formula to convert an ABCD matrix to an S Matrix ( $Z_0$  is the system impedance,  $S_{21}$  as a factor and not in dB):

$$S_{21} = \frac{2}{A + B/Z_0 + CZ_0 + D}$$

Now using our separated U and V we get

$$\begin{aligned} S_{21} &= \frac{2}{u_{11} + u_{12}/Z_0 + u_{21}Z_0 + u_{22} + Z_X(v_{11} + v_{12}/Z_0 + v_{21}Z_0 + v_{22})} \end{aligned}$$

Using

$$\begin{aligned} S_U &= u_{11} + u_{12}/Z_0 + u_{21}Z_0 + u_{22} \quad \text{and} \quad S_V \\ &= v_{11} + v_{12}/Z_0 + v_{21}Z_0 + v_{22} \end{aligned}$$

Both  $S_U$  and  $S_V$  are real numbers derived from the values of the PI networks and the system impedance. The numeric values are 60.088 and -2.404, respectively for the standard IEC444 networks.

We can resolve for  $Z_X$  as

$$Z_X = \frac{2/S_{21} - S_U}{S_V}$$

and we are done with the measurement of the series resistance.

When looking at the formula for Q, the resistance/inductance ratio includes not just the resistance of  $Z_X$  but also the two output impedances of the PI networks. For the IEC444 network, the crystal side output impedance is

$$Z_\pi = R_O \parallel (R_S + R_I \parallel Z_O) \text{ giving } 12.5 \text{ Ohms}$$

We have two of those, so we measure  $Q_M$  with a resistance that is 25Ohms above the crystal resistance  $Z_X$  we have just derived from S21 above. The formula for the Q we measured is therefore:

$$Q_M = \frac{2\pi f_S L}{Z_X + 2Z_\pi}$$

Solving for L gives:

$$L = \frac{Q_M(Z_X + 2Z_\pi)}{2\pi f_S}$$

The  $Q_X$  of the crystal alone is then:

$$Q_X = \frac{2\pi f_S L}{Z_X}$$

which can be a lot more than what the value for  $Q_M$  indicates, especially for low-ohmic crystals. With L now determined we can compute the crystal motional capacitance by

$$C = \frac{1}{(2\pi f_S)^2 L}$$

And for the parallel capacitance we get

$$C_P = \frac{C}{\left(\frac{f_P}{f_S}\right)^2 - 1}$$

This completes the math behind the crystal measurement using a VNA.

### 13.2.1 Crystal Noise Measurements

Unfortunately, no crystal datasheet containing information about crystal noise was found. Noise is always measured in the context of a running oscillator, which, of course, adds its own noise sources like the transistor with its flicker component, and the resistors inside the transistor and in the rest of the circuit.

Rubiola [4] uses a technique with two identical (however that can be guaranteed) crystals and measures their noise by correlation, all other authors use an oscillator to measure crystal noise.

When plotting phase noise of an oscillator, we usually see the influence of classic white transistor noise (from the base spreading resistance  $R_{BB}$ , e.g.), transistor flicker noise (see transistor noise measurement chapter) plus, potentially, additional flicker noise from the crystal. Due to the extremely small bandwidth of premium SC cut crystals in the range of just 2Hz this effect becomes detectable only very close to the carrier.

Most USOs use the “resonator as filter” architecture from Rohde, having the pleasant side effect that the transistor flicker noise (with corner frequencies in the some 100Hz ranges for low noise low frequency transistors) is also ironed out by the extremely low filter bandwidth of the crystal, making it hard to determine where the noise around a few Hz from the carrier really comes from (as it is also very tricky to measure low-level transistor noise at a few Hz).

A dedicated experiment was designed to circumvent these difficulties and to measure crystal noise outside an oscillator. The key ideas of the experiment work like this:

1. We start from a calibrated, flat, broadband tube noise source [5]. The ENR of this noise source is 7dB and can be assumed exact because it is pure Schottky noise generated by a saturated tube diode. The amplitude flatness can be checked on a quality spectrum analyzer. The bandwidth of the noise is 200MHz.
2. The noise is amplified by ca. 58dB, using two battery powered INA02186 low noise amplifiers. These amplifiers have noise figures in the 1-2dB range and a good match at input and output. The level is now at  $-174 + 7 + 58 = -109\text{dBm/Hz}$ , so for 200MHz the power is -26dBm over the whole bandwidth. If needed the bandwidth can be further reduced by filtering. It is important that the amplifiers are not overdriven because this would ruin the flatness of the output spectrum.
3. The next step is to create a test fixture with 3 channels. Channel one is a through, channel two is a (pluggable) metal film resistor and channel 3 is the crystal. We can now calibrate the setup. For channel one, our spectrum analyzer (FSWP used here for its supreme dynamic range) shows a (hopefully) flat line. A zoom in at the series resonance frequency of the crystal shows a (more noisy) flat line at a level of -109dBm multiplied by the resolution bandwidth.
4. Having measured the crystal, its equivalent series resistance at the frequency of resonance is known. Using a quality metal film resistor (assumed flicker noise free) as a series element another noisy flat line as before is obtained but lowered by the added losses caused by the series resistance.
5. Finally, a channel 3 measurement uses the crystal in series instead of its resistor. If the crystal has no (added) noise, the top of its selection curve must exactly touch the line measured with its equivalent series resistance and the 3dB bandwidth must correspond to its loaded Q in the arrangement. If it creates amplitude noise, the curve must reach over the line with the equivalent series resistance, and if there is phase noise, the bandwidth should grow beyond the value the  $Q_L$  value would suggest.

To give an impression of the setup, the picture below shows the whole setup:

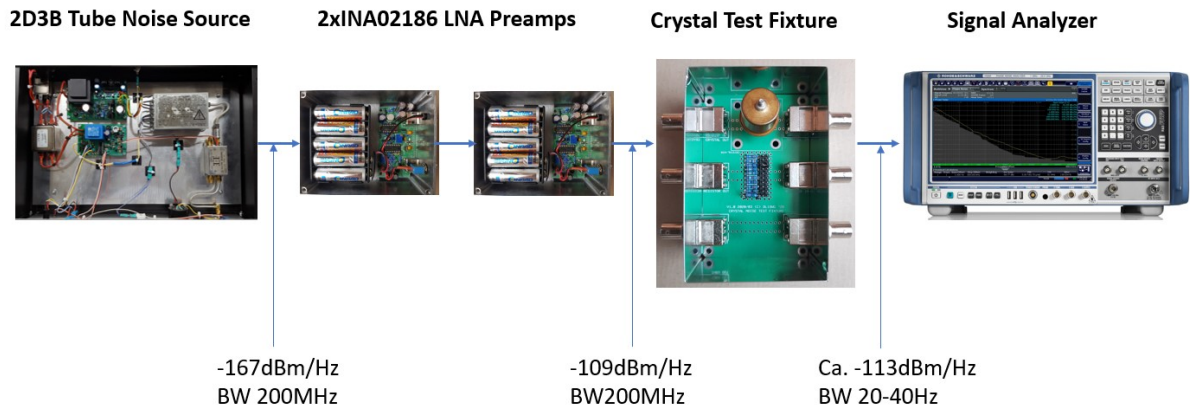
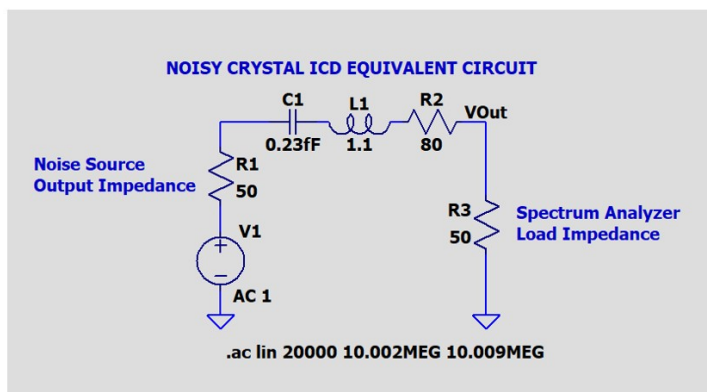


Figure 207 - The Crystal Noise Measurement Setup

The test adapter with an HP10811A crystal (copper cylinder on top) inserted is shown in detail:

**THE MEASUREMENT ENVIRONMENT SCHEMATICS, TEST ADAPTER**



**USING A MEASUREMENT ADAPTER**

**3 MODES:**

- THRU 1:1 FOR CALIBRATION
- TEST RESISTOR IN SERIES
- CRYSTAL IN SERIES

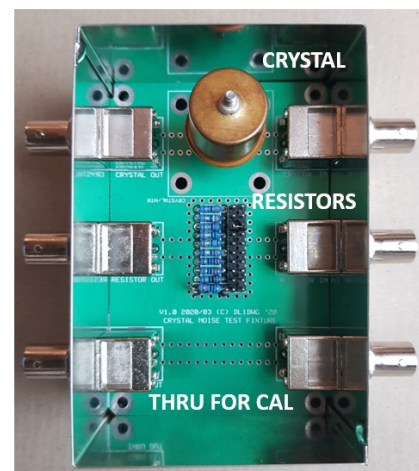
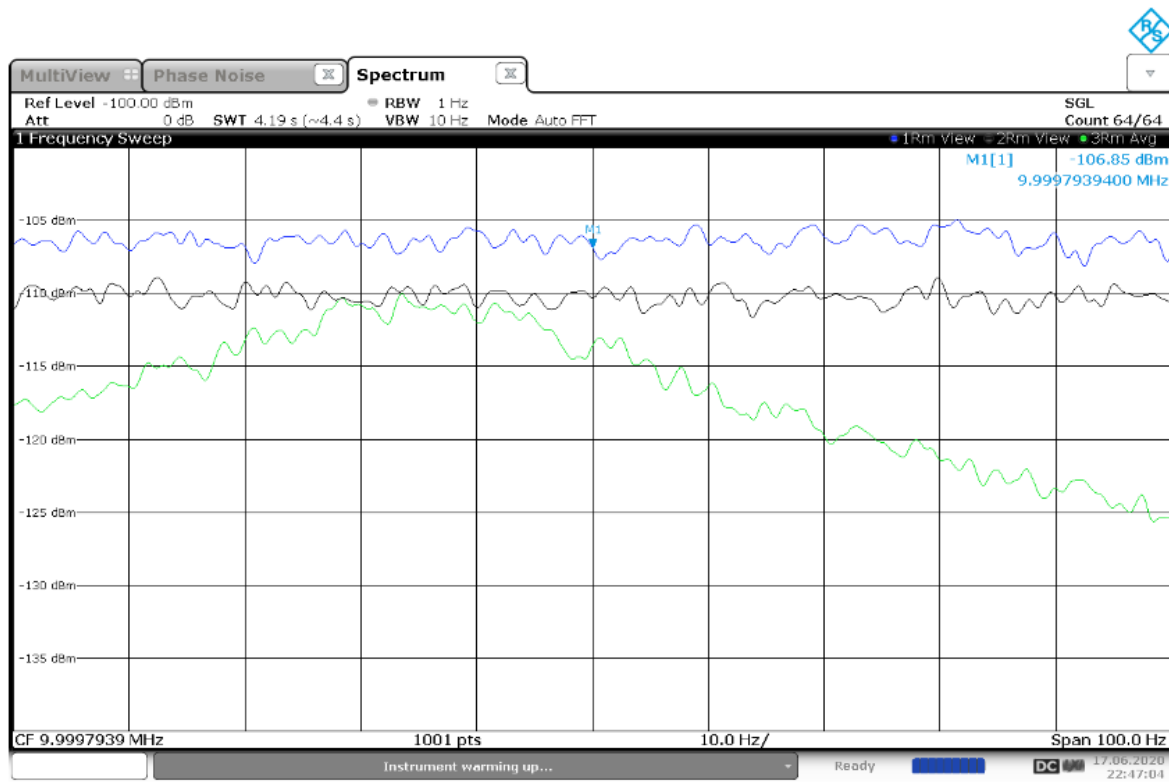


Figure 208 - Crystal Noise Test Adapter

The curves for the HP10811A crystal showed no excessive noise:



22:47:05 17.06.2020

Figure 209 - The HP10811A Crystal Noise Measurement Results

The through calibration is blue, the 470 Ohms resistance is black and the crystal curve is green. As seen, no excess noise is present.

The bandwidth (unloaded Q) of the HP10811A crystal was measured to be about 1 Million, translating to 10 Hz of bandwidth at 10 MHz. We must use a loaded Q here, with another total 100 Ohms from the source and spectrum analyzer input resistance, reducing Q to less than half (crystal resistance was 47 Ohms) and tripling the bandwidth to ca. 30 Hz, a plausible value looking at the picture above.

To make a long story short, *all SC premium crystals* measured showed no extra noise.

The only part with a slightly increased noise was a consumer grade 10MHz AT-cut part, shown here:

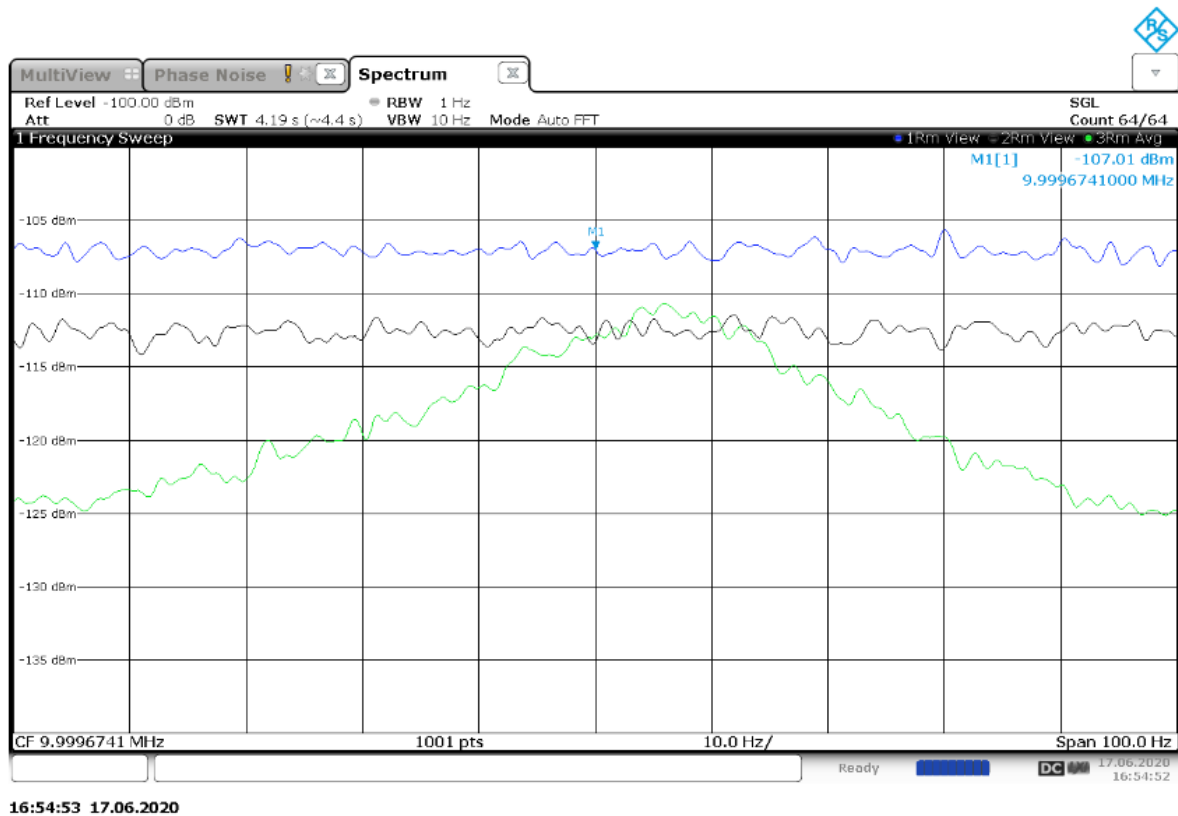


Figure 210 - Residual, Resistor and Crystal Noise

This is 1-2dB above its series resistance, so a solitary proof that noisy crystals do exist.

The next try was to ask manufacturers for crystals with known noise problems. B. Neubig of AXTAL was so kind to provide me with 100MHz samples that have proven noisy in oscillators, but for those no convincing evidence of added noise was found either.

Summing up the results, the conclusions are:

1. Noisy (1-2dB ENR) crystals exist, but seemingly not within premium SC parts used for OCXOs. This could simply be the result of better manufacturing and/or quality control.
2. The measurement technique works, but as any extremely low-level setup it is very tricky. Source flatness, excellent shielding, battery powered LNAs, and a premium spectrum analyzer with extremely high SFDR is required to avoid artefacts.
3. The measurements show either that 1) crystals are not noisy or 2) the 1/f noise only occurs in addition to a significant signal power.

### 13.2.2 General Caveats when Measuring Premium Crystals

While the procedure for a VNA is adequate for low to medium Q crystals, extremely high Q crystals (< 1 Million, e.g.) present additional challenges, among those:

**DLD and power sensitivity.** The power level of the VNA must be reduced so that the specified maximum power is not exceeded, otherwise nonlinear effects can occur (visible by asymmetric curve shapes at resonance, and/or ragged slopes). The input PI attenuator has an attenuation of ca. 15dB, which might not be sufficient. Overtone crystals can have power limits of just 10uW (50T SC 5MHz, e.g., [6]).

**Dynamic range.** The measurement of the series resonance frequency is normally not a challenge for the dynamic range of a VNA, but this is sometimes not true for the parallel resonance. If the crystal almost completely blocks the signal, a high noise level makes the measurement of the parallel resonance frequency difficult. Averaging might provide a solution. The idea to use the phase instead of the amplitude of  $S_{21}$  is no remedy because it will oscillate randomly when the level is too low.

**IF bandwidth, sweep speed.** With crystals passbands in the range of just around 1 to 5Hz, the IF bandwidth and sweep speed must be set to the smallest available value to avoid artefacts (e.g., BW 1Hz, sweep time several 10 seconds for a span of ca. 100Hz). The time constant of energy absorption by a crystal is in the range  $Q/2fs$ , that could be *seconds*. The E5071C does not go below 10Hz.

**Frequency accuracy.** The VNA should be driven by a GPS level precise frequency reference to avoid drift effects by the instruments internal clock.

**Measurement Temperature.** If possible, precision crystals should be heated to their specified operating temperature and stabilized for 30 minutes before measurement.

**Calibration.** An open and thru calibration around the series and parallel resonance frequencies is necessary, especially if the series resistance of the crystal is extremely small. One calibration is good enough for both because the frequency variation is low enough. Calibration can be verified using precise metal film resistors (e.g., Short, 20, 50, 100, 200Ohms) and checking the resulting attenuation and compute back R. Differences should be below 1%. At 5MHz we use here, parasitic inductances and capacitances are not yet a big problem.

## References

- [1] Keysight Inc., “E4990A Impedance Analyzer Datasheet.” Accessed: Nov. 26, 2020. [Online]. Available: <https://www.keysight.com/us/en/assets/7018-04256/data-sheets/5991-3890.pdf>.
- [2] Keysight Inc., “E5071C ENA Vector Network Analyzer Datasheet.” Accessed: Nov. 24, 2020. [Online]. Available: <https://www.keysight.com/us/en/assets/7018-01424/data-sheets/5989-5479.pdf>.
- [3] B. Neubig et al., “DAS GROSSE QUARZKOCHBUCH.” Accessed: Nov. 26, 2020. [Online]. Available: <https://www.axtal.com/Deutsch/TechnInfo/Quarzkochbuch/>.
- [4] F. Sthal et al., “About Quartz Crystal Resonator Noise: Recent Study.” Accessed: Nov. 26, 2020. [Online]. Available: [https://www.researchgate.net/publication/24168373\\_About\\_Quartz\\_Crystal\\_Resonator\\_Noise\\_Recent\\_Study/link/0deec526f669e75784000000/download](https://www.researchgate.net/publication/24168373_About_Quartz_Crystal_Resonator_Noise_Recent_Study/link/0deec526f669e75784000000/download).
- [5] W. Griebel, “A Tube Noise Source using the 2D3B Tube.” Accessed: Nov. 26, 2020. [Online]. Available: <https://electronicprojectsforfun.wordpress.com/making-noise/noise-sources-i-have-built/a-tube-noise-source-using-the-2d3b-tube/>.
- [6] Bliley Corp., “BQOTY-XXMXX-XXXB-HC-30/U Crystals Datasheet.” Accessed: Nov. 26, 2020. [Online]. Available: [https://cdn2.hubspot.net/hubfs/2222150/Assets/Datasheets/01\\_Crystals/BQOTY-XXMXX-XXXB\\_v2.0.pdf](https://cdn2.hubspot.net/hubfs/2222150/Assets/Datasheets/01_Crystals/BQOTY-XXMXX-XXXB_v2.0.pdf).
- [7] Cathodeon Inc., “Cathodeon PI Network Mark II Quartz Test Fixture.” Accessed: Nov. 26, 2020. [Online]. Available: <https://isolalab.com/pinetwork.html>.



## 14 Appendix E: The Measurement of Transistor DC Parameters

### 14.1 The Measurement Setup

When looking at the DC parameters of a transistor for application in an oscillator, we need the following information:

1. Output curves (i.e., collector current over collector voltage, stepped by base current)
2. Gummel plot (Collector and base current over base-emitter voltage)
3. Gain curve (DC current gain over collector current, at a fixed collector voltage)
4. Base-emitter breakdown voltage

Oscillator transistors are operated at low power levels, so the collector breakdown limits or the properties as extremely high currents are of no interest.

The currents vary over several orders of magnitude, from some pA to several 10mA. The exponential dependency of the collector currents on base voltage asks for a very high accuracy of the base voltage. In other words, we cannot use a standard power supply, we need an SMU with a sufficiently fine output resolution and a 6 ½ digit auto scale readback function for currents. The setup used is shown here:

#### TRANSISTOR BE BREAKDOWN MEASUREMENTS – MEASUREMENT ENVIRONMENT

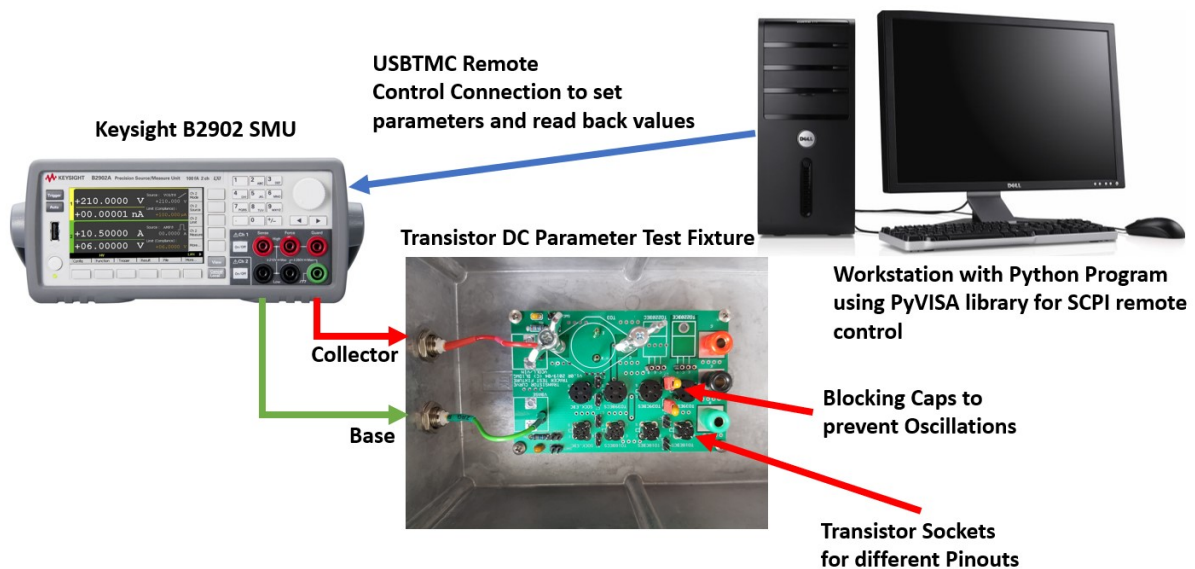


Figure 211 – Transistor DC Parameter Measurement Environment

The PC automates pulsed measurements to keep the thermal drift minimal (1ms pulses, 1%DC). The SMU used was a Keysight B2902A, which has a current resolution of 100fA [1]. The test fixture is fully shielded, and the connections to the SMU use coaxial cabling (otherwise the very small currents will have all kinds of RFI on them, spoiling the measurements). The test fixture has transistor sockets for TO-18, TO-39, TO-3, TO-220, TO-5, TO-92 in various pin configurations, plus an extender socket for SMD or other packages. Pluggable blocking caps (100nF) stop parasitic oscillations, important for high- $f_T$  parts.

## 14.2 USO Transistor Candidates

The datasheets of the transistors measured are shown below:

**2N2222A : 75V/800mA  $V_{BE}=6V, \beta=300, f_t=300\text{MHz}$**

**2N2857 : 15V/50mA  $V_{BE}=3V^*, \beta=30, f_t=1.4\text{GHz}$**   
 \* as low as 1.5V for some manufacturers

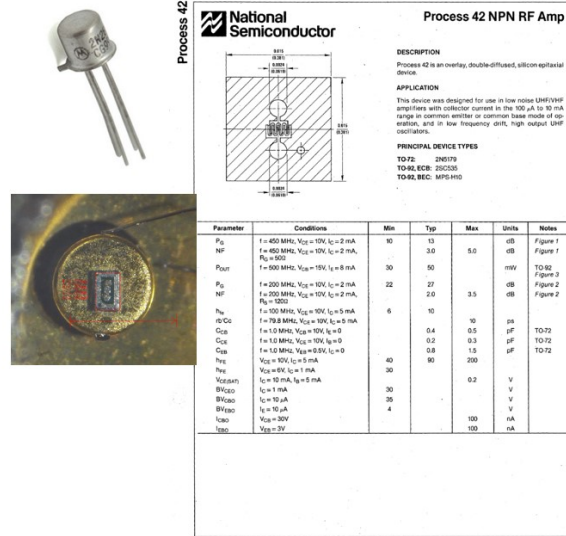
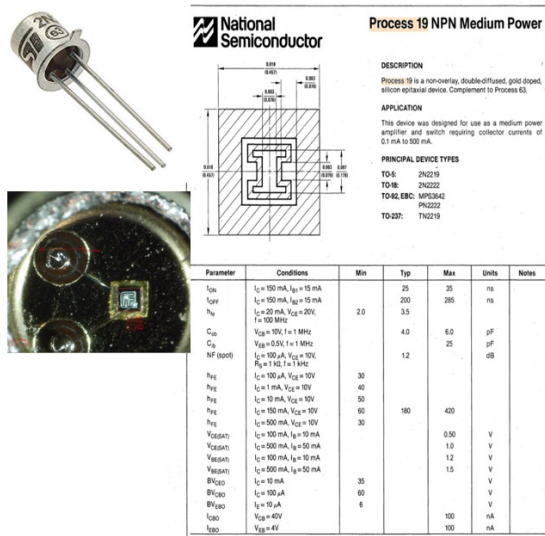


Figure 212 - Test Transistor Datasheets  
 Photo from Fairchild Data Book [3]

The datasheet extracts are from an old Fairchild transistor data book [3]. These old data books even specified chip layouts and the process technology used, something that was soon abandoned. Today's datasheets are often extremely rudimentary and therefore useless for a serious analysis.

The two transistors analyzed here are very different types made for very different application areas. Both are space qualified, however, and were used on numerous space missions (the earliest references are from 1966, see [2]).

The 2N2222A [3] is a general purpose, medium current (800mA), medium voltage (75V), medium gain (300) part with a rather low transit frequency of ca. 300MHz. It is made in planar technology and has a very simple chip layout (this is true also for later versions and versions from other manufacturers) [3]. Base emitter voltage is limited to 6V in the datasheet. The rather high maximum collector voltages mean that the base cannot be very thin, suggesting a light doping profile.

The 2N2857 [4] is a low-current (50mA), low voltage (15V), low gain (30), high frequency (1.4GHz) part intended for RF amplification and oscillators. The chip layout is much more complex; This part has an overlay emitter to keep inductances low and to increase  $f_T$ . Base emitter voltage is limited to 3V in the datasheet. To keep the base thin, doping profiles must be much steeper than for the 2N2222A. This definitely has an effect on the BE breakdown behavior.

### 14.3 2N2222A Measurement Results

The following picture shows output curves for the 2N2222A (before a base emitter breakdown occurred):

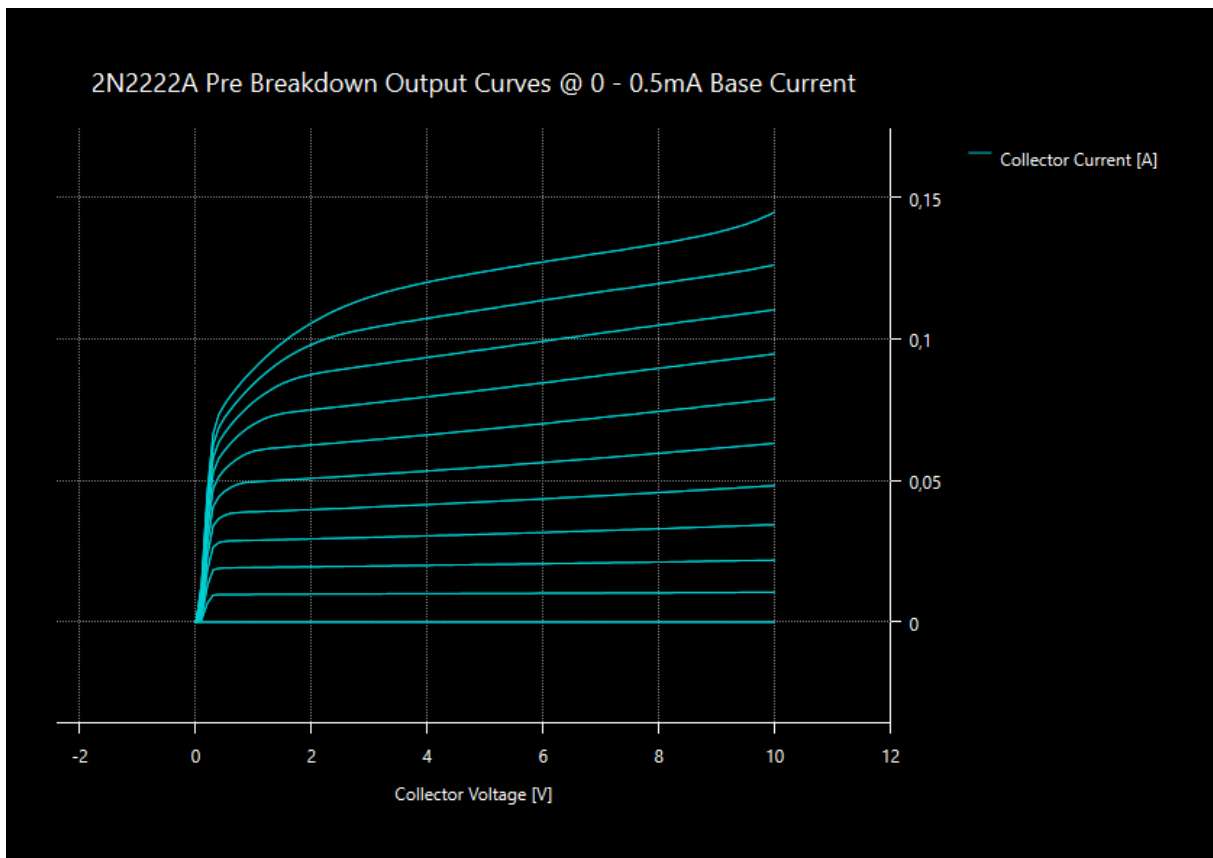


Figure 213 - 2N2222A Output Curves (0-500uA Base Current)

What can be said that the Early effect (discussed later) is very small below 30mA (lines are almost horizontal). Saturation looks standard below ca. 50mA, but shows a quasisaturation domain at 1V/100mA. We don't need to be concerned about this, because in an USO core we will never use currents this high.

A word of warning: Measuring at the high current / high voltage corner creates dissipation levels that will induce sufficient self-heating and bias shift to distort the curves. Pulse measurements are mandatory.

Next, we have a look at the Gummel plot at 5V of collector voltage:

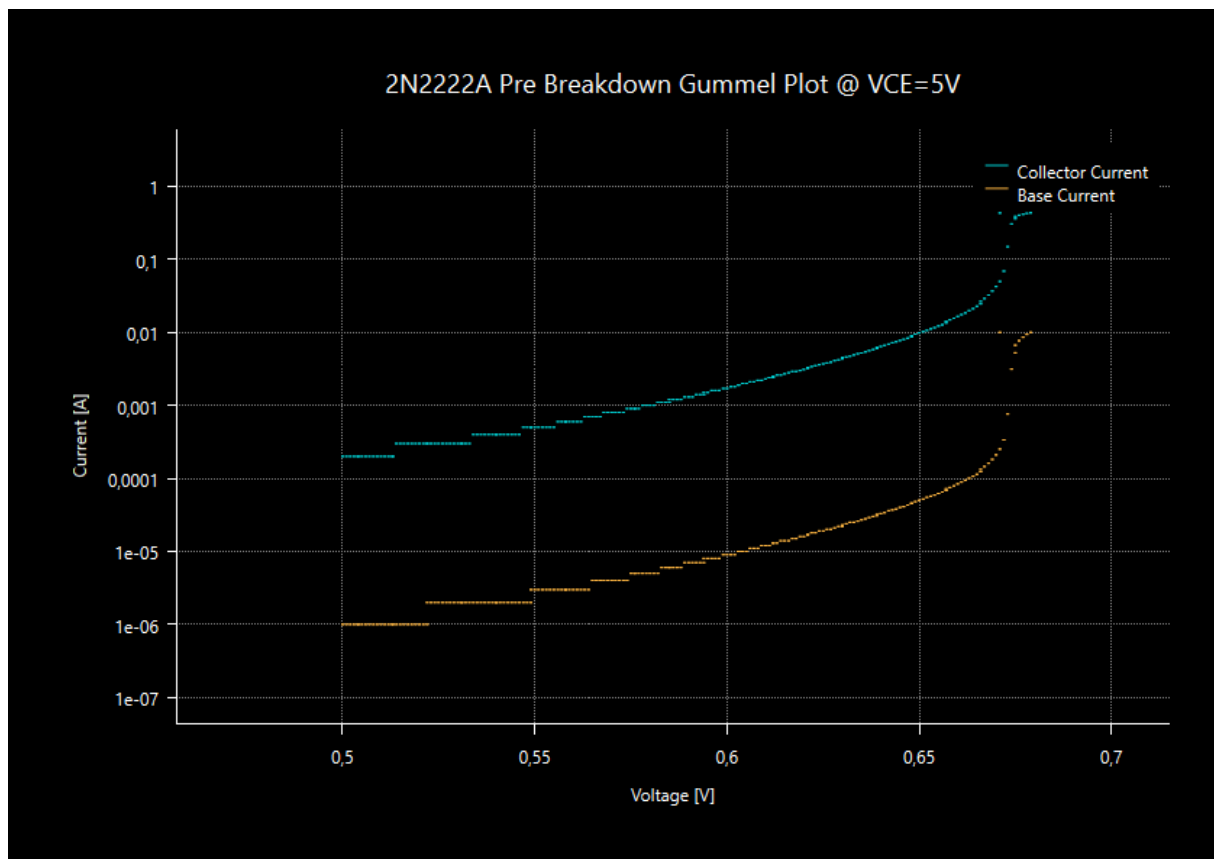


Figure 214 - 2N2222A Gummel Plot

Note the log scale on the left. The current gain is very linear from 0.5 to 0.66V, spanning 2 decades of collector current. The linear domain ends at ca. 20mA, OK for what we need for an USO core part.

The beta curve is last, taken at 5V:

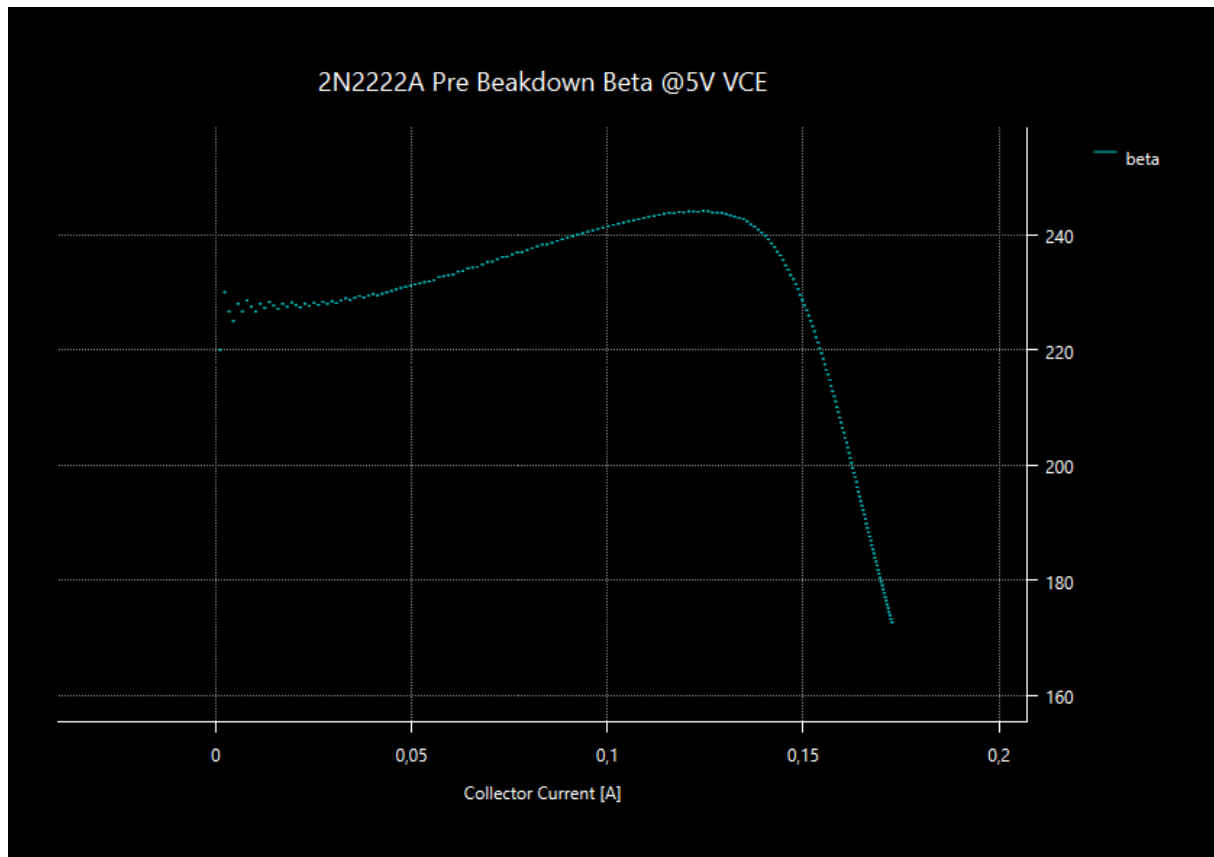


Figure 215 - 2N2222A Beta Curve

Looks very linear. Between 0 and 50mA gain variation is only a few percent.

As a conclusion, the 2N2222A transistor shows a very constant behavior around the usual bias points of USOs (a few volts, some mA). Gain is almost constant over current; the Early effect is negligible and there is no problem with gain at the low end.

## 14.4 2N2857 Measurement Results

The following picture shows output curves for the 2N2857A (before a base emitter breakdown occurred):

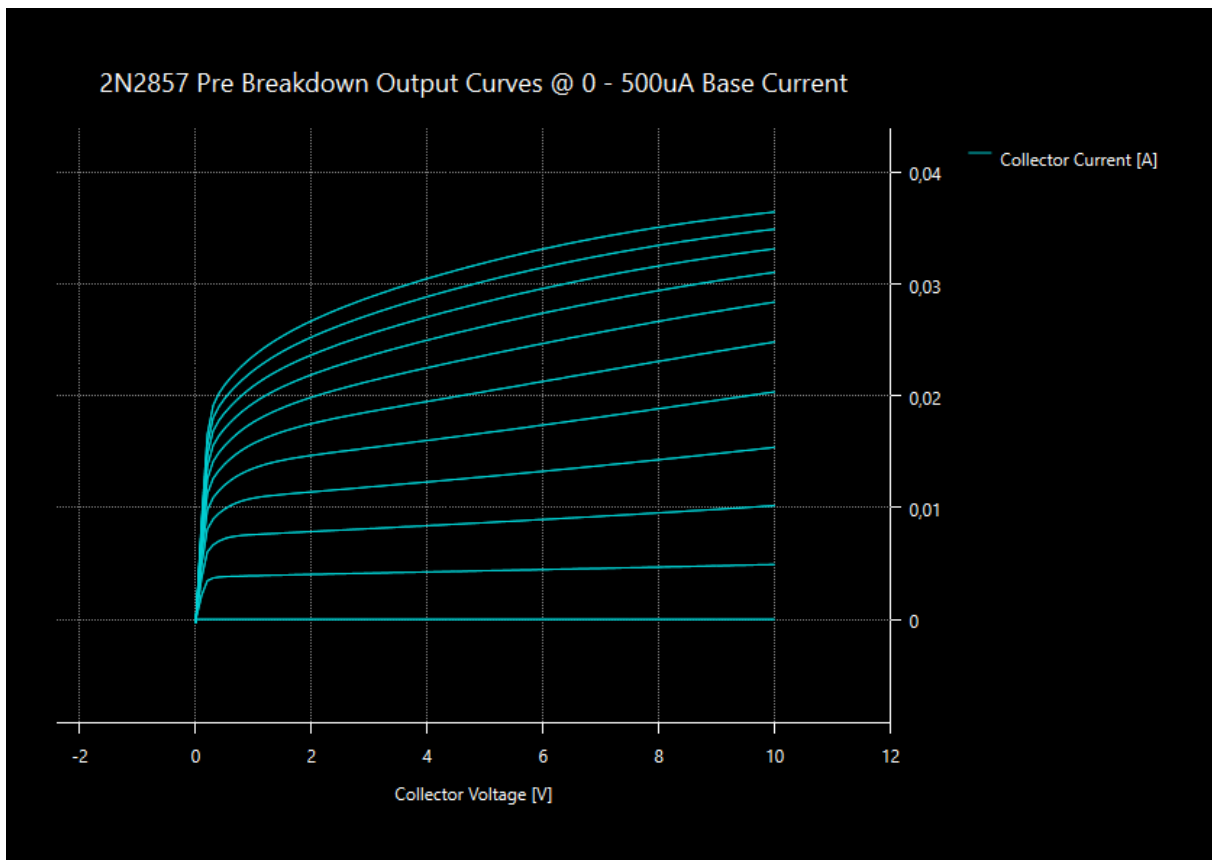


Figure 216 - 2N2857 Output Curves at 0-500uA Base Current

What can be said is that the Early effect is much stronger than for the 2N2222A (watch the current scale!). There is no visible quasisaturation effect, at least not to the maximum datasheet current of 40mA.

Next, we have a look at the Gummel plot at 5V of collector voltage:

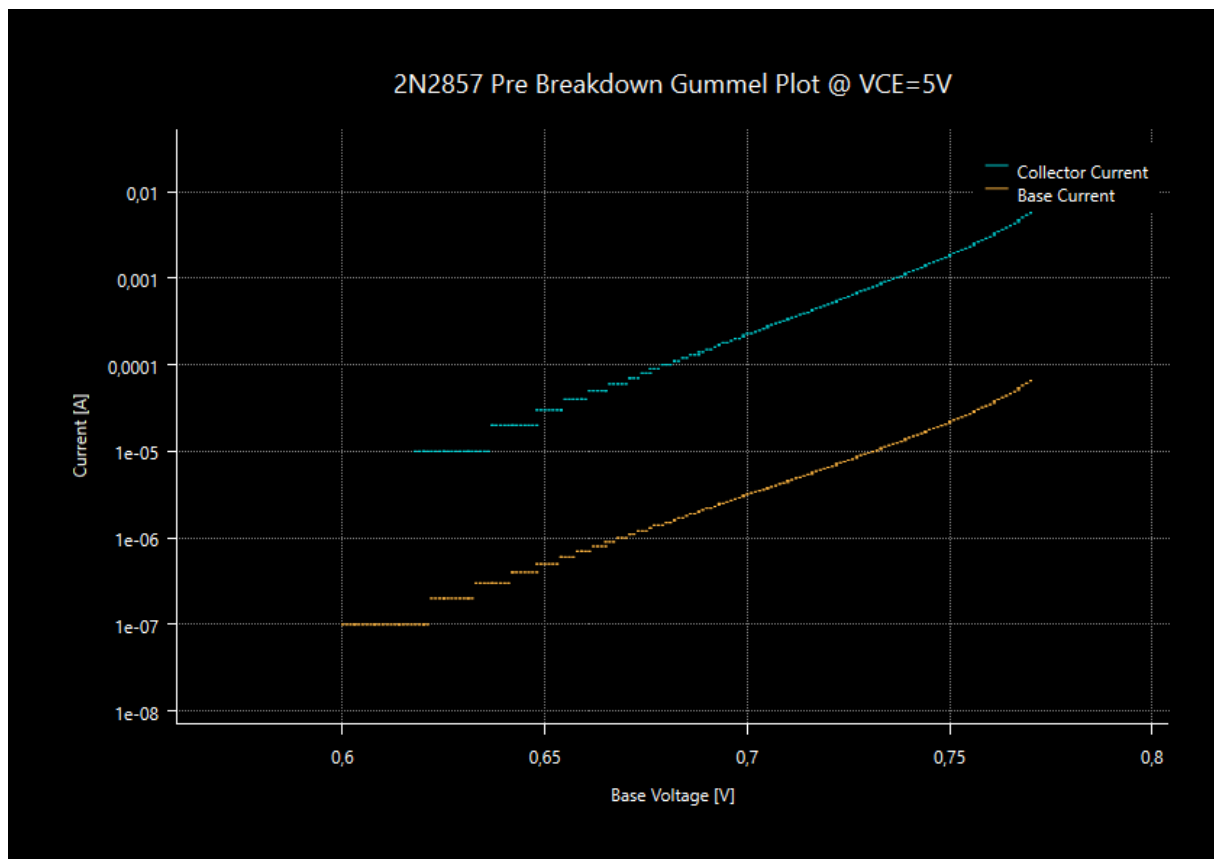


Figure 217 - 2N2857 Gummel Plot

There seems to be a problem at extremely small base currents (loss of low-end gain due to recombination, a consequence of gold doping), the rest of the plot looks normal.

The beta curve is last, taken at 5V:

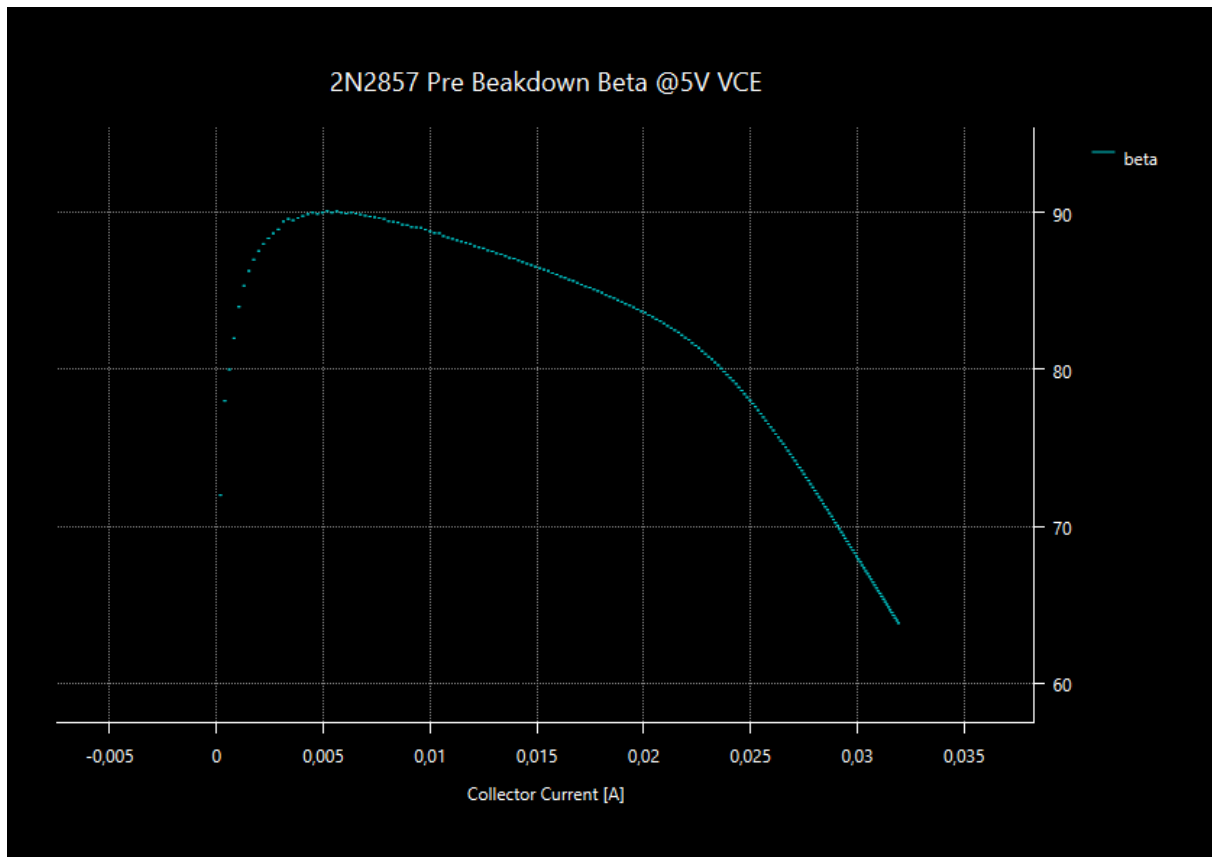


Figure 218 - 2N2857 Beta Curve

The beta curve shows much more nonlinearity than the 2N2222A. We have a maximum at 5mA, but a steep falloff to low and high currents. The gain is also only less than half of the 2N2222A value.



## 14.5 Base Emitter Breakdown

This effect occurs when the base is driven negative enough respect to the emitter. Since the BE junction is highly doped, it only has a small breakdown voltage which can be underrun in high amplitude oscillators. The effect on oscillator performance will be discussed in a separate chapter, but there is a destructive DC effect that makes it important to unconditionally avoid a BE breakdown condition. This effect [5] is the degradation of current gain even after very short exposure to breakdown. The breakdown curves of the 2N2222A are shown below:

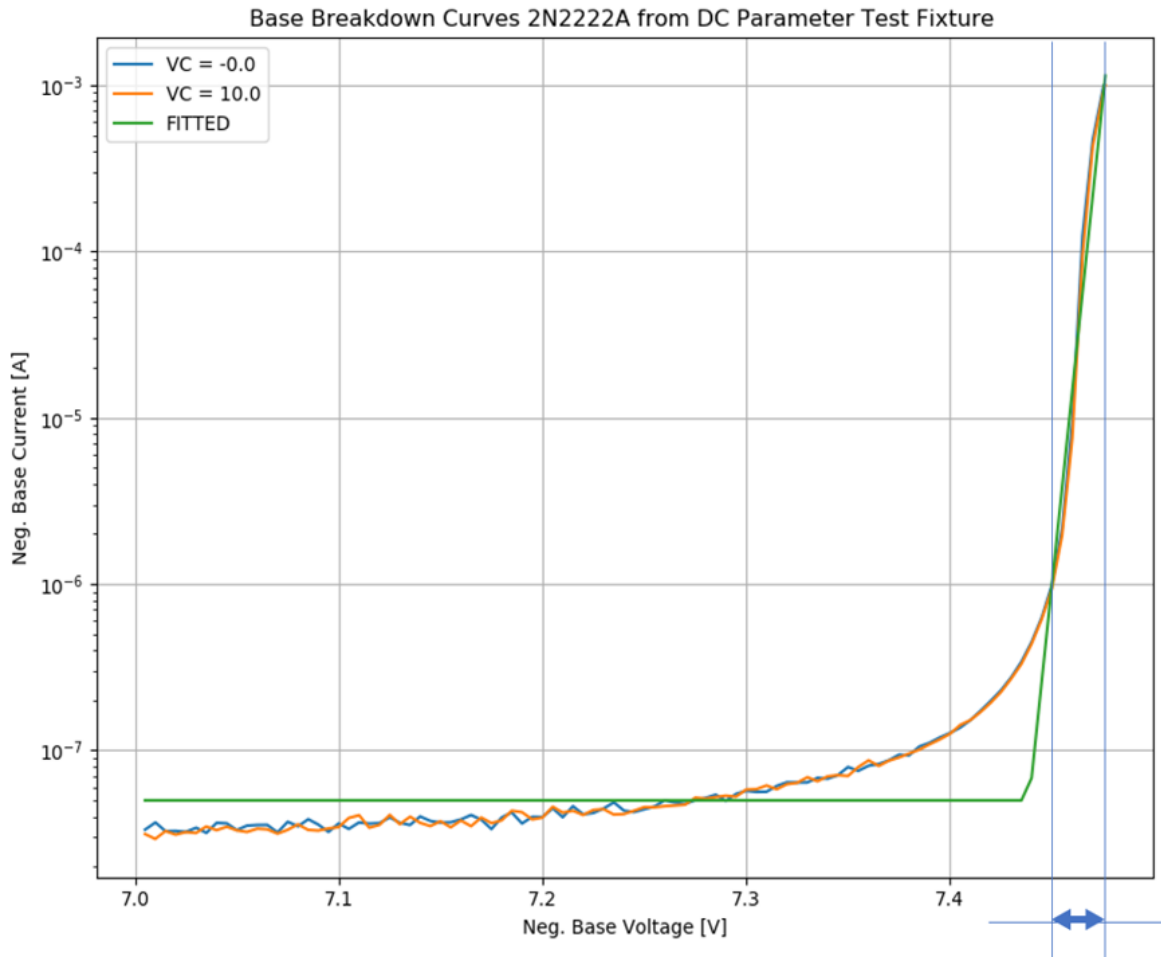


Figure 219- 2N2222A BE Breakdown Current over Voltage

That is a classic avalanche breakdown, very steep and with very little leakage current below the breakdown voltage. Three orders of base current magnitude are crossed in a span of just 30mV of base emitter voltage.

The 2N2857 breakdown is shown here:

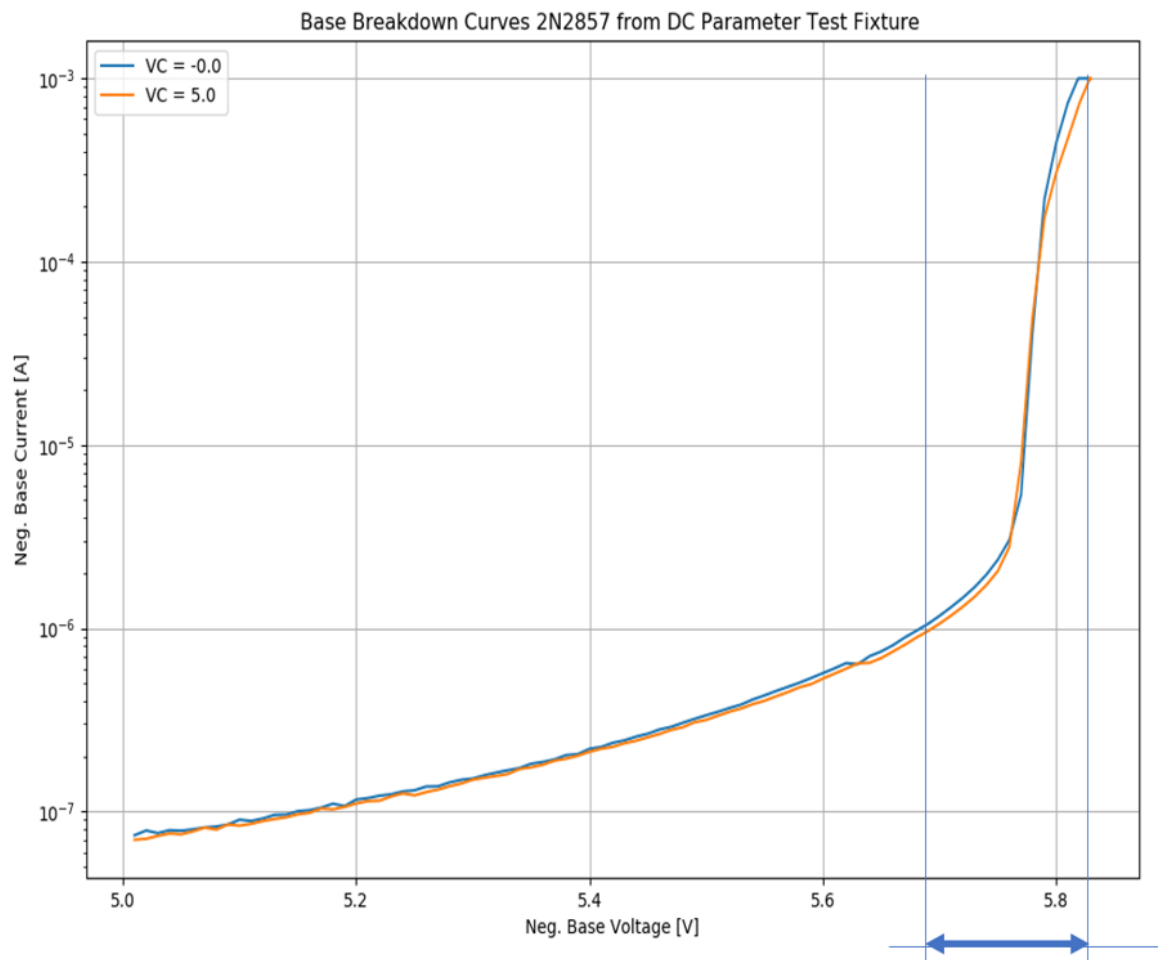


Figure 220 - 2N2857 BE Breakdown Current over Voltage

... a much smoother transition than the 2N2222A, at a lower voltage, not purely exponential. The voltage span for 3 orders of magnitude is now 130mV instead of 30mV, and there is a substantial leakage current even before breakdown occurs. This is, at least partly, a tunnel breakdown.

The permanent damage effect is shown first for the 2N2222A:

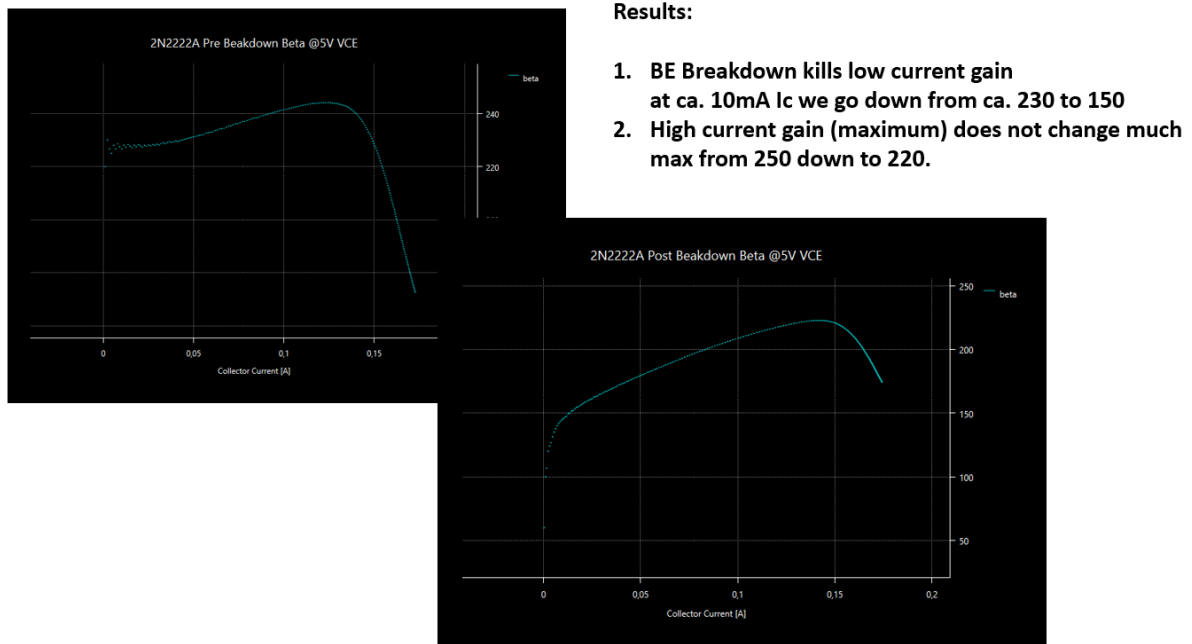


Figure 221- 2N2222A Permanent Gain Degradation After BE Breakdown

The effect on the 2N2222A is clearly visible, but not dramatic. Now the 2N2857:

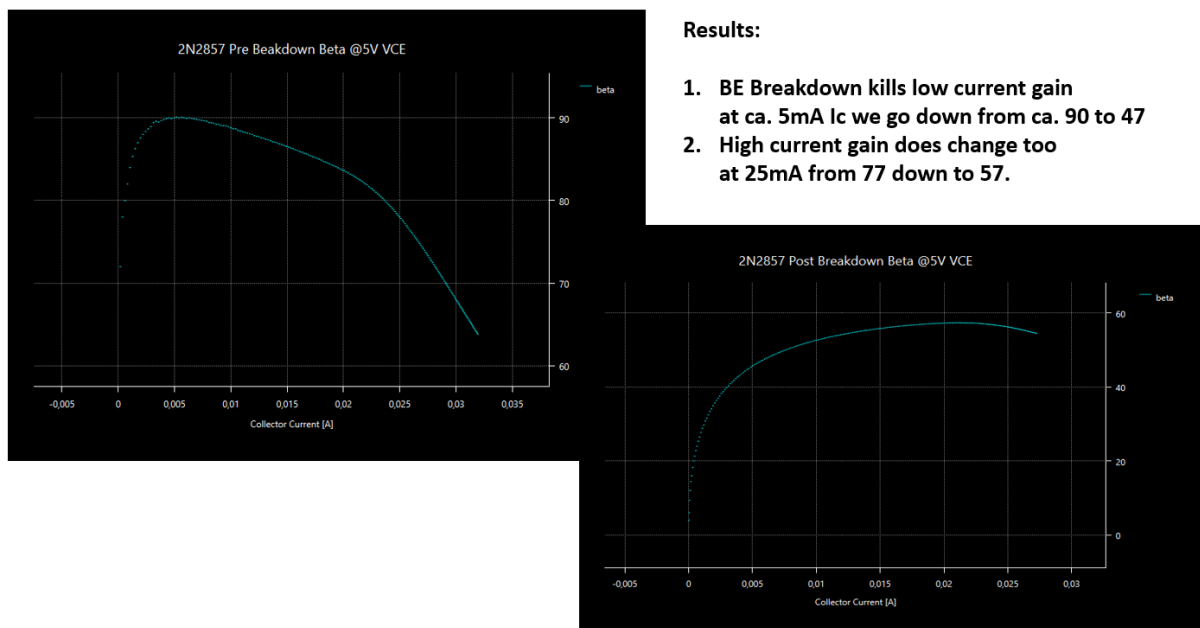


Figure 222 - 2N2857 Permanent Gain Degradation After BE Breakdown

A much higher drop occurs here. Low current gain is almost halved, with a significant loss at higher currents.

An interesting effect is that the junctions of both transistors emit visible light when sent into breakdown (Pictures from R. Kaußler, see acknowledgements [6]). The glowing 2N2222A is shown here:

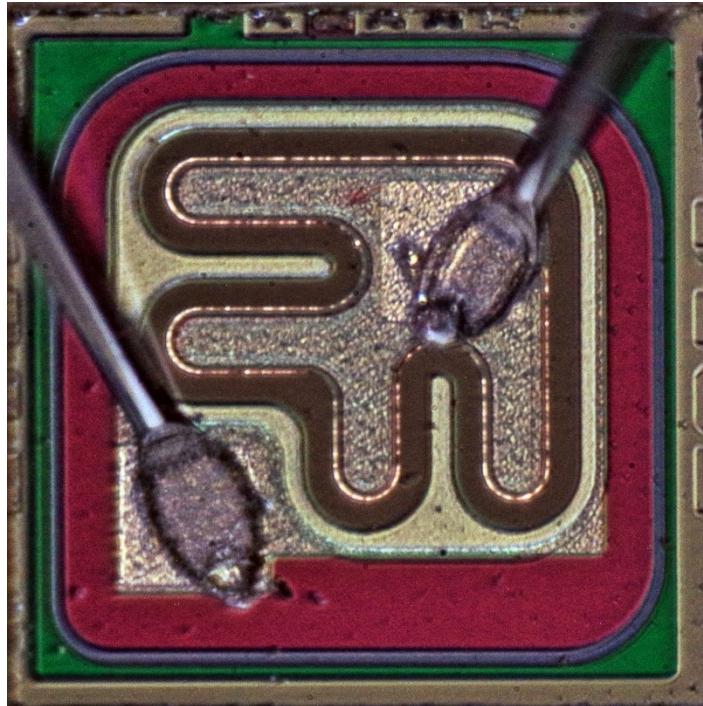


Figure 223 - Visible Glowing of an 2N2222A Transistor in BE Breakdown (1mA)

... and the 2N2857 [7] is here:

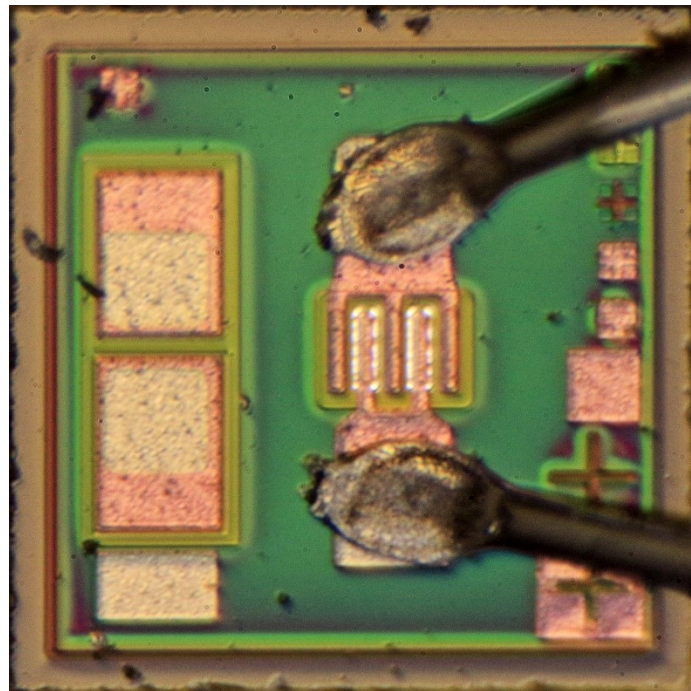


Figure 224 - Visible Glowing of 2N2857 Transistor in BE Breakdown (1mA)

The light comes from discrete spots at the BE boundary. When current is increased, more and more bright spots show up until the whole boundary is lit. The breakdown voltage over current is a step function. Another interesting effect is that the spots at the 2N2222A go out when the transistor warms up, which the 2N2857 does not. The different temperature coefficient of an avalanche (positive) and a tunnel (negative) breakdown process explains this.

## References

- [1] Keysight Inc., “B2900A Series Precision Source/Measure Unit Datasheet.” Accessed: Nov. 29, 2020. [Online]. Available: <https://www.keysight.com/us/en/assets/7018-02794/data-sheets/5990-7009.pdf>.
- [2] Bendix Corporation, “Acceptable Parts List for Space Missions.” Dec. 04, 1966, Accessed: Nov. 26, 2020. [Online]. Available: <https://www.lpi.usra.edu/lunar/ALSEP/pdf/31111000671246.pdf>.
- [3] Microsemi Corp., “2N2222A Technical Data Sheet.” Accessed: Nov. 17, 2020. [Online]. Available: [www.microsemi.com/index.php?option=com\\_docman&task=doc\\_download&gid=8898](http://www.microsemi.com/index.php?option=com_docman&task=doc_download&gid=8898).
- [4] Pulse Microwave, “2N2857 Datasheet Pulse Microwave.” Accessed: Nov. 17, 2020. [Online]. Available: [http://www.mpulsemw.com/Pdf\\_files/2N2857.pdf](http://www.mpulsemw.com/Pdf_files/2N2857.pdf).
- [5] B. A. McDonald, “Three hFE Degradation Mechanisms and their Associated Characteristics,” in *8th Reliability Physics Symposium*, Apr. 1970, pp. 288–297, doi: [10.1109/IRPS.1970.362473](https://doi.org/10.1109/IRPS.1970.362473).
- [6] Richard Kaußler, “Motorola 2N2222A Chip Photographs.” Accessed: Nov. 26, 2020. [Online]. Available: <https://www.richis-lab.de/Bipolar04.htm>.
- [7] Richard Kaußler, “Central Semiconductor 2N2857.” Accessed: Nov. 26, 2020. [Online]. Available: <https://www.richis-lab.de/Bipolar16.htm>.

## 15 Appendix F: The Measurement of Transistor AC Parameters

### 15.1 Introduction

After the DC parameters of a transistor have been established, we want to measure AC characteristics to determine model parameters like time constants, capacitances, and so on. This, by default, happens in a defined RF environment using RF test and measurement instruments.

### 15.2 The Measurement Setup

Is shown below:

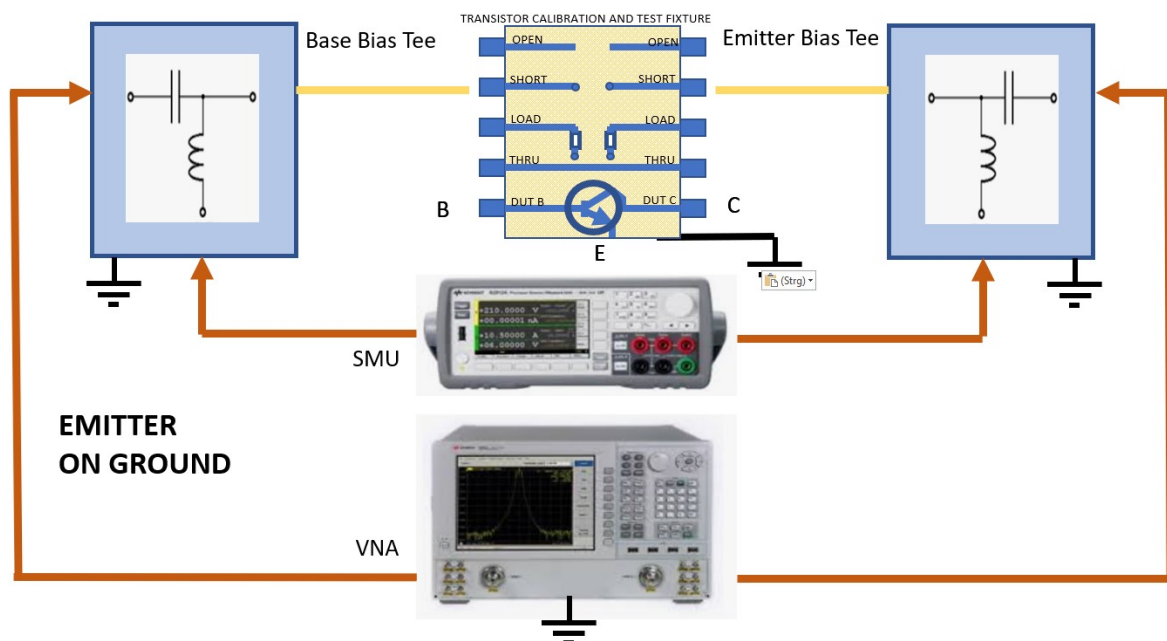


Figure 225 - Transistor AC Parameters Test Environment

The DC is supplied by an SMU (through the bias tees, not shown). For packaged devices we have the difficulty that the test fixture must be calibrated out by a suitable (socket-lookalike) open/short/load calibration. For higher currents, the DC resistances of the complete coaxial path to the DUT must be calibrated out as well. The influence of the bias tees can also not be ignored at very low frequencies, so they must be included in the calibration as well.

The AC parameters are measured using a 50Ohm vector network analyzer (Keysight E5071C used here [1]). The SMU used was a Keysight B2962A [2].

Using the setup above, measurements are performed using the following steps:

1. A grid of DC operating points (Base voltage, Collector Voltage) is defined. The Base Voltage must be very accurate due to the exponential characteristics, and temperature must be measured as well.
2. We run a measurement of DC parameters with the VNA off. These should correspond to the DC measurements done in the test fixture in the previous chapters, except for DC drops along the signal chain.
3. The frequency range to be measured is chosen (here 2MHZ, the bias tee lower limit, to 100MHz). At low bias points we need to exclude self-rectification, so we must run at the



lowest power level possible (here: -40dBm). Without test transistors have  $f_{TS}$  of 200-1300MHz, 2MHz and DC can be expected to behave the same.

4. After automatic calibration, pulsed measurements (1ms, 1s off to mitigate self-heating) are performed for every bias point. For every point, go thru all frequencies of interest and measure all S parameters.
5. The process takes several hours for 200 grid points and 20 frequency values. After the data is collected, fitting procedures are used to determine the time dependent parameters of the SGP spice models.
6. The measurement environment can heat the DUT and measure the (fixture) temperature, both of which are not terribly accurate.

For the TO-18 packaged 2N2222A [3] and the 2N2857 [4] the fitting quality of the parameters were not convincing, especially if higher currents were involved. As far as we found, temperature problems were a reason why, as explained below:

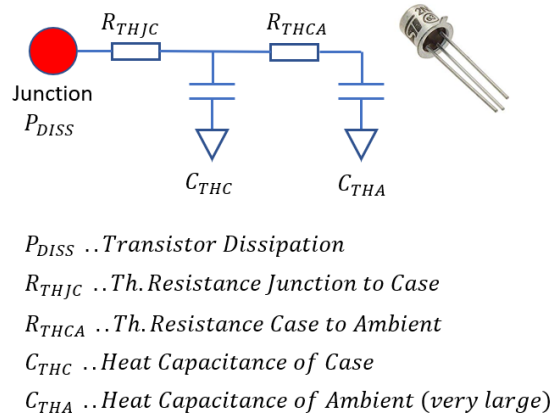
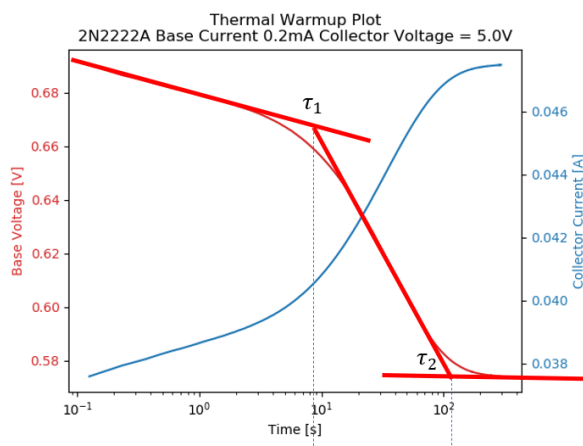
### 15.3 Temperature Effects

Normally, all device parameter extraction activities are carried on directly on a wafer. The thermal parameters are well defined and can be measured accurately in advanced (heated table, sensor pads, ...). For packaged devices, we have no information about the internal construction of our parts, and no information except a global  $R_{TH}$  from the datasheet.

If we look at the thermal conditions inside a packaged transistor, we have the following picture:

#### TEMPERATURE EFFECTS I – THERMAL TIME CONSTANTS

IF WE WANT TO INVESTIGATE HIGH CURRENT EFFECTS IN PACKAGED DEVICES, WE NEED TO INCORPORATE SELF-HEATING



The shorter time constant  $\tau_1$  is in the same range as sweep times. **Conclusion: High Power Sweeps are NOT isothermal. We need to measure  $V_{be}$  and compute the temperature WITHIN measurements.**

Figure 226 - Thermal Conditions in a Packaged Transistor

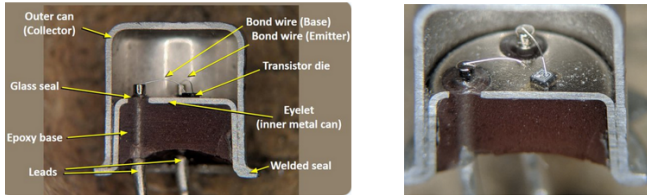
The measurements above were done by dumping power into a transistor and by measuring the BE voltage over time. We clearly see two time constants for a 2N2222A. The settling value defines the sum of the thermal resistances after all thermal reservoirs are charged.

With no documentation about the internal construction available, two specimens were “reverse-engineered” with a grinder and cut the cases open for a 2N2222A and a 2N2857. Their construction is very different, as can be seen here:

### TEMPERATURE EFFECTS I – THERMAL TIME CONSTANTS

#### INTERNAL CONSTRUCTION OF SOME USO OSCILLATOR TRANSISTOR CANDIDATES WITH SPACE QUALIFICATION

##### 2N2222A (TO-18 PLANAR/EPITAXIAL, COLLECTOR ON CASE)

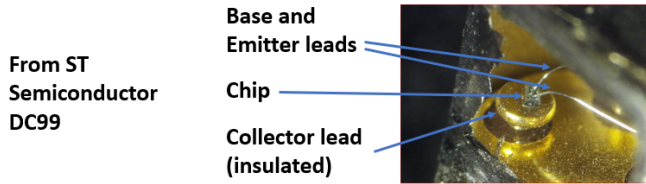


Source: <https://twitter.com/TubeTimeUS/status/1119049413811326976>

2N2222A:  $R_{THJC} = 150^{\circ}\text{C}/\text{W}$ ,  $R_{THJA} = 325^{\circ}\text{C}/\text{W}$

... self heating effect  
10mW gives ca. 1.5°C to 3°C.

##### 2N2857 (TO-72 OVERLAY, ISOLATED CASE)



2N2857 :  $R_{THJC} = 583^{\circ}\text{C}/\text{W}$ ,  $R_{THJA} = 875^{\circ}\text{C}/\text{W}$

... more self heating effects !!  
10mW gives ca. 6°C to 9°C.

... more time constants !! (see later)

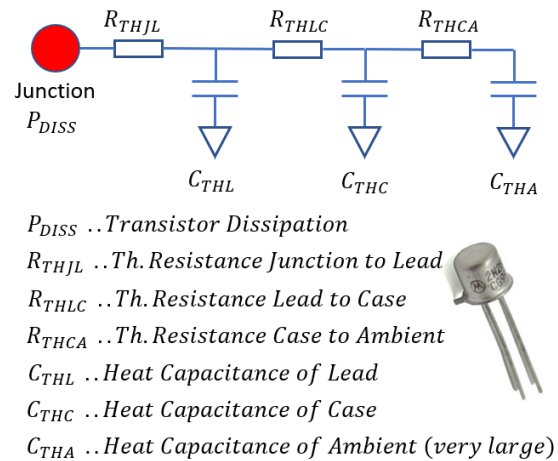
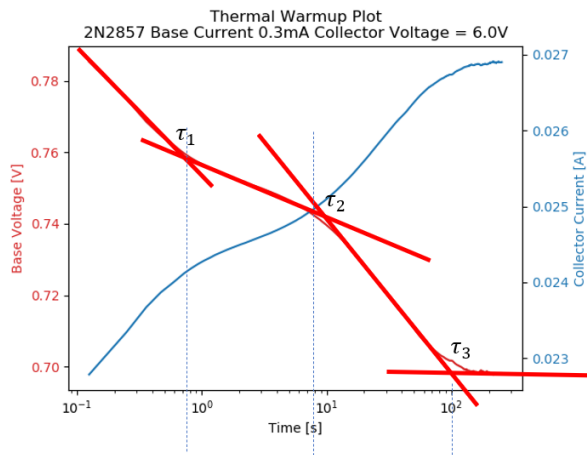
Different packaging results in different thermal capacitances and resistances. RF transistors with insulated case have a higher thermal resistance, and more self-heating.

Figure 227 - Opened Cases for a 2N2222A and a 2N2857

The picture tells it all; Its clear now why the 2N2857 behaves so differently. A view of its time constants confirms that:

### TEMPERATURE EFFECTS III – THERMAL TIME CONSTANTS OF SMALL SIGNAL RF PARTS

#### RF PARTS HAVE A COMPLEX THERMAL TIME BEHAVIOUR



The shorter time constant  $\tau_1$  is in shorter than VNA sweep times. **Conclusion: High Power Sweeps are NOT isothermal. We need to measure Vbe and compute the temperature WITHIN measurements or make a dynamic model.**

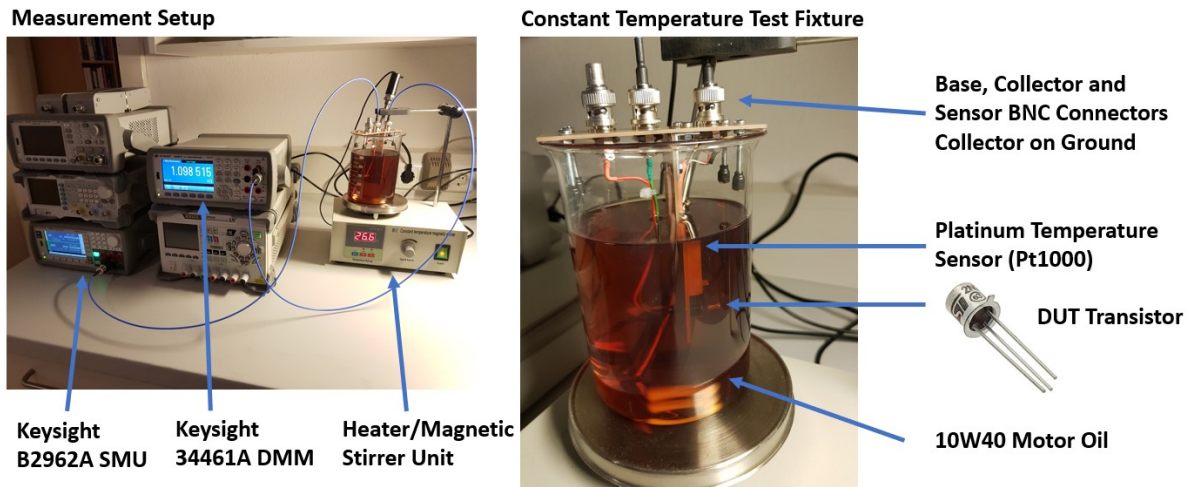
Figure 228 - Thermal time constants of a 2N2857

Because of the different mounting method, a third time constant appears.

As a conclusion of the thermal effects the method of extracting S parameters at different bias points is problematic due to the extreme difficulties to provide a defined thermal environment.



An attempt was made to extract temperature gauging curves in a define long-term measurement, using a thermal bath, looking like this:



We measure  $V_{be}$  at different base currents (10uA, 100uA, 1mA, 10mA) and temperatures (ca. 20-100°C).

Figure 229 - Calibrating Curves for Chip Temperature Made by BE Voltage Measurements

This worked, but does not solve the thermal tail problems during dynamic measurements.

## Conclusions

We made an attempt to extract S-parameters from packaged devices to check simulation models. Due to insufficient data quality caused by self-heating effects only approximate values of dynamic quantities could be obtained, and those were in the approximate range of datasheet and existing SPICE model values (capacitances,  $R_{BB}$ , time constants). Because the time domain simulations gave waveforms that were very close to measured values on the scope, it was concluded that the dynamic model accuracy at 5MHz was good enough, which is plausible if we look at the 200MHz minimum  $f_T$  of the parts used.

The extraction approach could be pursued further, but would need a better thermal management, shorter pulse measurements and other refinements. Shorter pulses, however, collide with the settling time of the bias tees.

## References

- [1] Keysight Inc., "E5071C ENA Vector Network Analyzer Datasheet." Accessed: Nov. 24, 2020. [Online]. Available: <https://www.keysight.com/us/en/assets/7018-01424/data-sheets/5989-5479.pdf>.
- [2] Keysight Inc., "B2962A 6.5 Digit Low Noise Power Source." Accessed: Nov. 20, 2020. [Online]. Available: <https://www.keysight.com/en/pd-2149912-pn-B2962A/65-digit-low-noise-power-source?cc=DE&lc=ger>.
- [3] Microsemi Inc., "2N2222A Datasheet." Accessed: Nov. 21, 2020. [Online]. Available: <https://www.microsemi.com/existing-parts/parts/44797#resources>.
- [4] Pulse Microwave, "2N2857 Datasheet Pulse Microwave." Accessed: Nov. 17, 2020. [Online]. Available: [http://www.mpulsemw.com/Pdf\\_files/2N2857.pdf](http://www.mpulsemw.com/Pdf_files/2N2857.pdf).

## 16 Appendix G: Transistor Noise Measurements

Transistor noise can be measured either directly by amplifying and analyzing it directly, or by evaluation the phase noise created in a sample oscillator. Both methods are discussed and their results presented. What is especially interesting is the flicker noise corner frequency. This frequency, according to the Leeson formula, must be as low as possible to preserve low phase noise close to the carrier. The flicker corner frequency is dependent on bias conditions, but even more on transistor type. It was found that older, low frequency parts have the best values.

### 16.1 The Direct Method Measurement Setup

To measure transistor noise directly, the method described by Berkner [1] was used, as shown below:

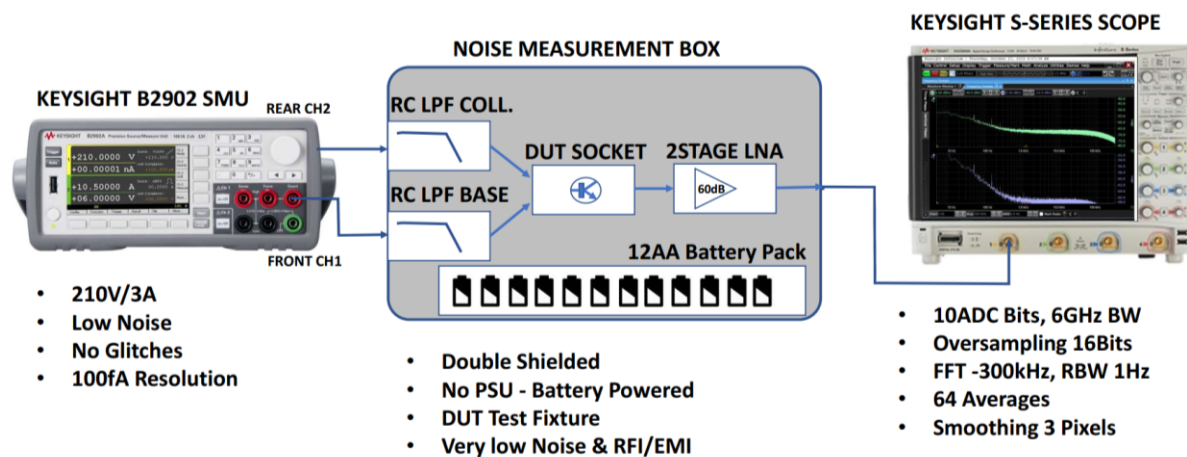


Figure 230 - Transistor Noise Measurement Setup

The filter at the base was an RC lowpass with  $3 \times 100 \mu\text{F} 50\text{V} \parallel 100 \text{nF}$  capacitors and  $4 \times 10\text{K} 1\% 2\text{W}$  metal film resistors, at the collector we had the same with  $4 \times 1\text{K}$  instead of  $10\text{K}$ . The LNAs were battery powered and had a gain of 60dB.

The amplified measurement noise floor is shown below:



Figure 231- Keysight Scope / LNA Instrument Noise Floor (FFT)

-168dBm/1Hz is quite OK, sensitive enough for the transistor measurements intended.

The low range is especially interesting due to  $1/f$  noise, so a zoom in is shown here:



Figure 232 - Keysight Scope / LNA Instrument Noise Floor (FFT) Zoom to LF

At 10Hz we have an increase of just 4dB, and the corner sits at ca. 100Hz. All transistors measured had a corner frequency several times higher than this.

Some line induced peaks are still visible. Even with battery power, double shielding and good high-shield coax cabling internal semi-rigid, external ENVIROFLEX400 (from SUHNER, [2]) it was not possible to eliminate them completely. Probably a fully EMI shielded room would be needed to make this perfect.



A photo of the noise measurement box is shown below:

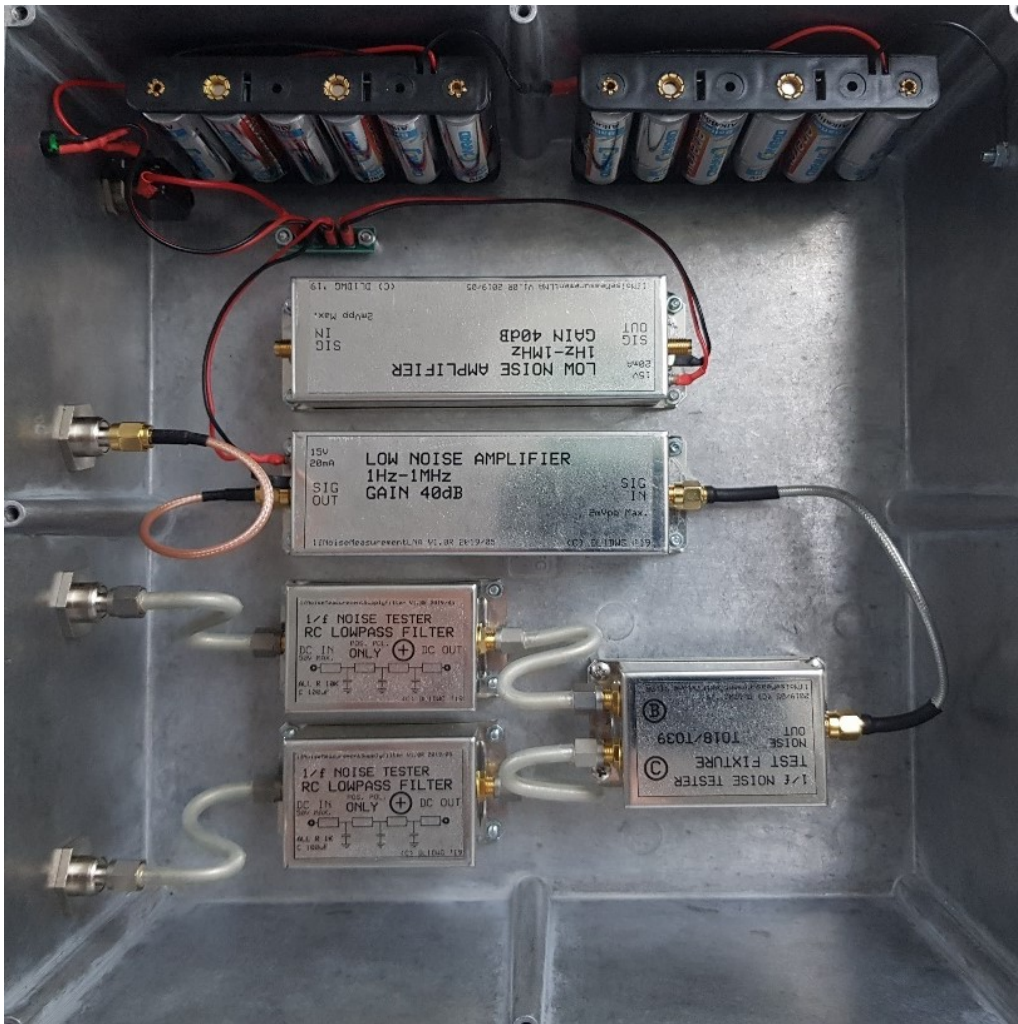


Figure 233 - Noise Measurement Box Internals

At the top we see a 12xAA battery pack, providing an unregulated, but very low noise voltage of 18V. Both LNA stages located below batteries have an internal low-noise LM723 voltage regulator down to 12V.

The test fixture is on the lower right, and the collector and base low pass filters are at the lower left. The setup is housed in a diecast aluminum box with a metal lid.

The amplifiers can be wired to provide either 40 or 60dB of gain, and a battery voltage watchdog circuit was added later.

The schematics of the setup including the first LNA stage is shown below:

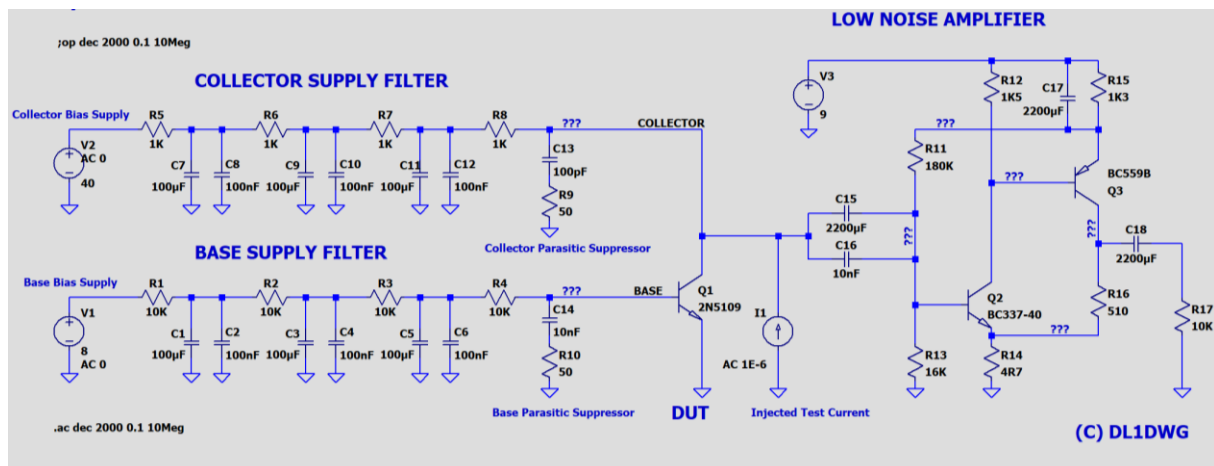


Figure 234 - Schematics of the Base and Collector Filters, the DUT Transistor and the LNA Stage

The collector and base filters are shown at the left, a sample DUT sits in the middle, and the first LNA stage is shown at the right.

The first LNA stage, a common LF LNA front-end [3] uses a BC337-40 LF transistor [4] with 800mA maximum current and a current gain of 400, featuring an exceptionally small base spread resistance and low noise. The PNP type is also a low-noise audio part. The gain of the first stage can be set by the ratio of  $R_{16}/R_{E14}$  (close to the question marks) and finetuned to the factor 100. The second stage is just a x10 op amp stage. The bandwidth of the first LNA stage is 1Hz to ca. 1MHz, stage 2 goes up to ca. 300kHz. The bandwidth must be large enough to accommodate the  $1/f$  corner of the DUT transistors. For the parts we use here  $f_c$  lies between a few 100Hz and ca. 10kHz.

On the scope we need to use all available techniques to enhance resolution:

1. 10Bit ADC at the input
2. Oversampling (The scope has a max. sample rate of 20Gs/second)
3. Boxcar averaging
4. FFT
5. Averaging on the FFT result

All these together create a 16Bit voltage resolution, about a 96dB power dynamic range which is more than sufficient for the measurements intended.

The lower frequency limit necessitates large coupling capacitors, and that in turn has the disadvantage of long settling times (several 10 seconds). During settling, the scope input should be turned off so large voltage swings while charging the caps do not reach the inputs.

A vertical resolution of 50mV/div is sufficient to get useful spectra. Clipping should be avoided by respecting the ca. 1:8 average/peak ratio of a white noise signal (99.6%), so the noisy signal should only fill 12% of the screen.

The detector of the FFT should be set to RMS (power).

Base and collector voltage were provided and measured by Keysight B2902A SMU [5] which provides low-noise power, but also permits high-accuracy current measurements. To adjust the collector voltage wanted, the SMU output must be increased by the voltage drop caused by the filter.

A sample output of a 2N2222A transistor at 500 $\mu$ A collector current and 4V collector voltage is shown below:



Figure 235 - 2N2222A Noise Floor (500 $\mu$ A/4V)

To illustrate all settings, the full scope screenshot of the DSOS604A [6] is shown. Due to all the resolution-enhancement measures we have taken the bandwidth is now down at 111kHz, which is more than enough for the 2N2222A transistor 1/f corner (a few 100Hz). For RF transistors like the 2N2857 the corner frequency would be a few kHz at the same current. Modern HBT, SiGe or PHEMTs would have corner frequencies in the range of several to several ten MHz and are completely unsuitable for our requirements. Furthermore, specialized test fixtures are needed to prevent parasitic oscillations.

## 16.2 The Oscillator Method

To measure transistor noise indirectly, the following approach can be tried:

1. We create an oscillator (design is unimportant) with a resonator bandwidth considerably larger than the suspected flicker noise corner. This is necessary because an extreme Q resonator (like an SC cut crystal with a Q of several Million) will have a filter effect so strong that a corner in the range of 50Hz to several kHz cannot be observed anymore. So, what we need is an LC oscillator, somewhere in the HF range.
2. Then, we plot phase noise. Provided the flicker corner frequency is below the bandwidth of the resonator, there should be a visible change in slope. Applying tangents, the flicker noise corner frequency can be determined.

The approach above has been tried with a 20MHz Colpitts oscillator using a 2N2222A transistor, at different bias conditions. The results are displayed below (base bias from 2V to 6V in 1V steps):

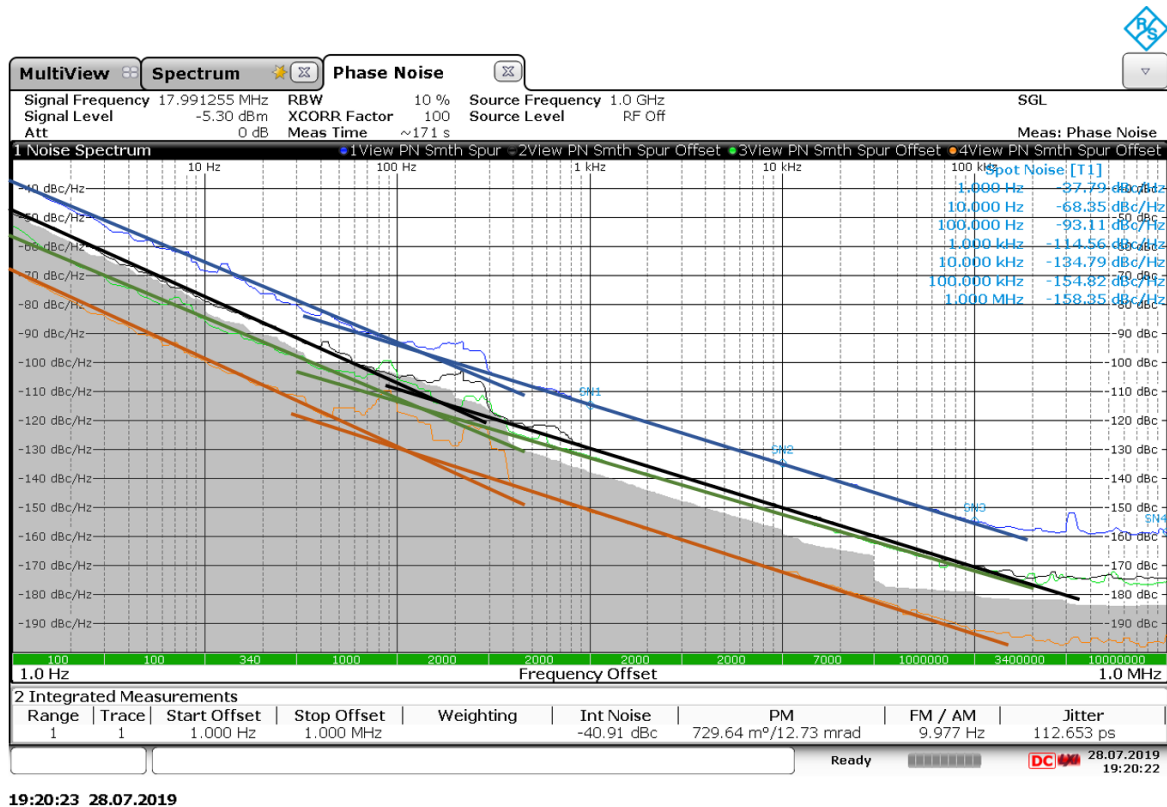


Figure 236 - Measurement of the Flicker Noise Corner in an LC Oscillator

The plot confirms that phase noise off the carrier drops with increasing oscillator power. The corner frequency does not move much (from 200Hz to 100Hz). In all cases, a change from a  $f^3$  law to an  $f^2$  law is clearly visible (check the slope of the tangents). What is remarkable is that the corner frequency is considerable below the value obtained by the DC measurement (ca. 500Hz).

As all Leeson based approaches, this one has to be taken with a grain of salt as well. While the DC approach measures noise power in a spectral interval directly, all quantities like the noise figure  $F$ ,  $AF$  and  $KF$  in the Leeson formula are cyclostationary values, i.e., time averages over an oscillator period. None of these can be directly measured, because they vary widely over the cycle, especially when the transistor experiences cutoff, saturation (and, even worse, BE breakdown).

### 16.3 Noise and Saturation

In the literature [see, e.g., Driscoll 7, p23] it is discouraged to let the oscillator transistor go into saturation. There are some understandable arguments why this is undesirable, among them the drastic increase of capacitances with falling voltages, storage time, reduced gain and so on. On the other hand, the same author suggests that a good oscillator should have a two-sided amplitude limiting mechanism, which is a sort of contradiction.

What is needed is a measurement to determine if the same collector current out of saturation and in saturation is noisier. Using the  $1/f$  noise measurement setup and the 2N2222A, tests were performed at 500uA, with collector voltages of 0.5, 1 and 8V, and the same for 5mA of collector current.

The results were surprising, because in all cases the saturation condition reduced the noise component the collector current significantly.



The 500uA/8V case is shown below:

**MEASURING NOISE FAR FROM SATURATION 2N2222A –  $I_B=3\mu A$ ,  $V_{CX}=10V$ ,  $R_C=4K$ ,  $I_C$  ca. 0.5mA**



**RESULTS:**

1. AMPLE  $V_C = V_{CX} - R_C * I_C = 8V$
2.  $I_C=500\mu A$
3. B ca. 160
4.  $f_c$  ca. 400Hz
5. Ca. -69.5dBm after 60dB Gain

Figure 237 - Noise of an 2N2222A with no Saturation at 500uA  $I_C$

The corner frequency is 400Hz, at a level of -69.5dBm/Hz after a 60dB LNA.

In deep saturation (0.2V at the collector), noise drops by 2dB:

**MEASURING NOISE IN DEEP SATURATION 2N2222A –  $I_B=3\mu A$ ,  $V_{CX}=2.2V$ ,  $R_C=4K$ ,  $I_C$  ca. 0.5mA**



**RESULTS:**

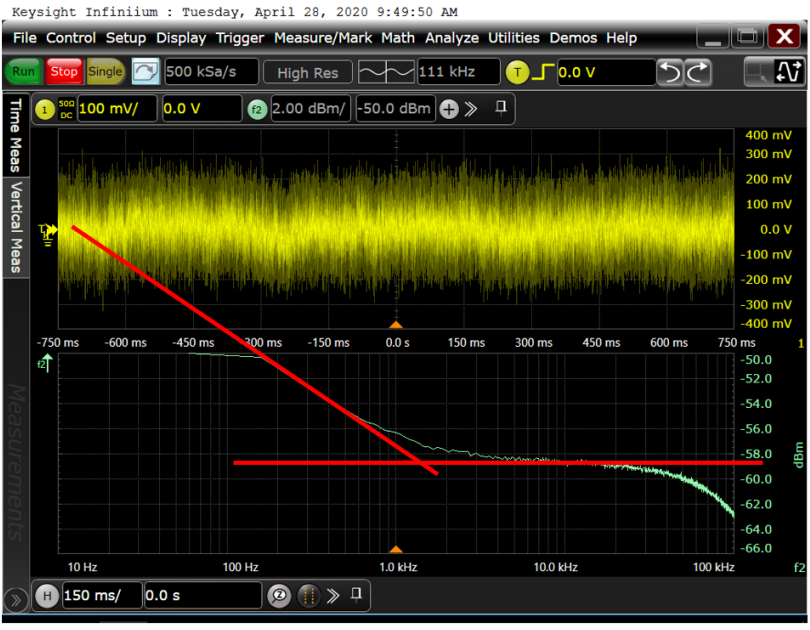
1. VERY LOW  $V_C = V_{CX} - R_C * I_C = 0.2V$
2. DEEP SATURATION,  $V_{BE} < V_{CE}$
3.  $I_C=500\mu A$
1.  $f_c$  ca. 400Hz
2. Ca. -72dBm after 60dB Gain

**- 2dB LESS NOISE -**

Figure 238 - Noise of an 2N2222A Transistor in Deep Saturation at 500uA  $I_C$

Now let us try the same at higher collector currents (5mA):

**MEASURING NOISE OUT OF SATURATION 2N2222A –  $I_B=30\mu A$ ,  $V_{Ck}=25V$ ,  $R_C=4K$ ,  $I_C$  ca. 5mA**



- RESULTS:**
1. HIGH  $V_C = V_{Ck} - R_C \cdot I_C = 3.9V$
  2. NO SATURATION
  3.  $I_C=5.2mA$
- 
1.  $f_c$  ca. 1.5kHz
  2. Ca. -58.5dBm after 60dB Gain

+1.870195 V	Source : AMP#8	Ch 2 Mode
+030.0000 $\mu A$	+030.000 $\mu A$	Ch 2 Source
+05.27730 mA	Source : VOI#8	Ch 2 Limit
+025.0000 V	+025.000 V	Ch 2 Measure
+205.0000 V	Limit (Compliance) : +10.0000 mA	More...

Figure 239 - Noise of an 2N2222A Transistor with no Saturation at 5mA  $I_C$

As was to be expected, noise levels go up and the corner frequency does as well due to the higher collector current noise at 10 times the current. We now have -58.5dBm/Hz and a corner frequency of ca. 1.5kHz with no saturation.

When driving the transistor into saturation at 5mA, we see the following plot:

**MEASURING NOISE IN DEEP SATURATION 2N2222A –  $I_B=30\mu A$ ,  $V_{Ck}=20.3V$ ,  $R_C=4K$ ,  $I_C$  ca. 5mA**



- RESULTS:**
1. LOW  $V_C = V_{Ck} - R_C \cdot I_C = 0.34V$
  2. DEEP SATURATION
  3.  $I_C=4.997mA$
- 
1.  $f_c$  ca. 1.5kHz
  2. Ca. -60.2dBm after 60dB Gain

+1.882801 V	Source : AMP#8	Ch 2 Mode
+030.0000 $\mu A$	+030.000 $\mu A$	Ch 2 Source
+04.99007 mA	Source : VOI#8	Ch 2 Limit
+20.30000 V	+20.3000 V	Ch 2 Measure
+205.0000 V	Limit (Compliance) : +10.0000 mA	More...

Figure 240 - Noise of an 2N2222A Transistor in Deep Saturation at 5mA  $I_C$

Again, noise drops by 1.7dB, and the corner frequency does not move.

A possible explanation from physics could be the following effect. Schottky current occurs when electrons cross a boundary (here: the BC PN junction, a space charge zone). This applies only out of saturation; in deep saturation the BC junction is fully flooded with carriers, current flows from the base to the emitter and collector simultaneously, and the space charge region plus the barrier is gone. What remains is a sort of resistive noise, with the small resistance of the flooded zone.

The bottom line is that the statement that saturation is generally a bad thing for oscillators is not correct. Later measurements will show that the best noise performance of test oscillators was obtained with saturation and not without.

## References

- [1] Jörg Berkner et al., “1/f-Noise BJT Measurements using a Low Noise Current Amplifier.” Accessed: Nov. 24, 2020. [Online]. Available: [https://www.iee.et.tu-dresden.de/iee/eb/forsch/AK-Bipo/2000/AKB\\_2000\\_Berkner\\_1f\\_noise.pdf](https://www.iee.et.tu-dresden.de/iee/eb/forsch/AK-Bipo/2000/AKB_2000_Berkner_1f_noise.pdf).
- [2] Huber und Suhner, “ENVIROFLEX 400 Datasheet.” Accessed: Nov. 20, 2020. [Online]. Available: [https://www.koax24.de/storage/datasheet/de/050118\\_Datenblatt\\_Enviroflex\\_400\\_Enviroflex\\_400.pdf](https://www.koax24.de/storage/datasheet/de/050118_Datenblatt_Enviroflex_400_Enviroflex_400.pdf).
- [3] Vojtěch Janásek, “Design of ultra-low noise amplifiers.” Accessed: Nov. 25, 2020. [Online]. Available: <http://www.janascard.cz/PDF/Design%20of%20ultra%20low%20noise%20amplifiers.pdf>.
- [4] On Semiconductor, “BC337 Amplifier Transistors Datasheet.” Accessed: Nov. 24, 2020. [Online]. Available: <https://www.onsemi.com/pub/Collateral/BC337-D.PDF>.
- [5] Keysight Inc., “B2900A Series Precision Source/Measure Unit Datasheet.” Accessed: Nov. 29, 2020. [Online]. Available: <https://www.keysight.com/us/en/assets/7018-02794/data-sheets/5990-7009.pdf>.
- [6] Keysight, “Infiniium S-Series Oscilloscope Datasheet.” Accessed: Nov. 17, 2020. [Online]. Available: <https://www.keysight.com/us/en/assets/7018-04261/data-sheets/5991-3904.pdf>.
- [7] Michael M. Driscoll, “Low Noise Oscillator Design and Performance,” presented at the 2002 IEEE Frequency Control Symposium, New Orleans, LA, USA, Jun. 2002.

## 17 Appendix H: Chaos and Noise

As we know from theory and experiment (see, e.g., [1] for a chaotic Colpitts with derivation from basic equations or [2] for a Clapp) not only high-quality SC cut crystal oscillators can exhibit chaotic behavior. When a suitable parameter is varied (the series capacitance to the crystal is a good candidate) the usual associated phenomena like period doubling, the creation of subharmonics, squegging and so on can be generated. The ability to create chaotic solution is a native property of the nonlinear differential equation system describing the circuit. For very simple systems the existence of chaotic solutions can be derived by pencil and paper math, for realistic circuits this is not possible, however. Simulations can bridge the gap and show some qualitative effects of chaos, in our case also in the presence of noise sources.

### 17.1 Background Theory

We can describe quite a big class of problems by a generalized nonlinear dynamics approach. The advantage is that no assumptions need to be made about the type of the expected solution, and (in simple cases) predictions about periodicity, stability, limiting and chaos can be made. If we have an oscillator circuit consisting of resistors, capacitors, inductors, voltage and current sources and a transistor we can employ KCL and KVL to formulate a complete set of differential equations describing all voltages and currents in our circuit. In general, these equations will be second order (due to Ls and Cs being present).

By substitution, the second-order equations can be reformulated as a system of first-order equations, so the general shape of the equation system becomes

$$\frac{dX}{dt} = F(X)$$

Where X is the state vector containing all voltages and currents and the substituted variables (which are first order derivatives of voltages and currents over time). F is a vector function that maps all components of the left side to an array of functions of all state vector components on the right side. A general treatment of the general dynamics approach to circuit problems can be found in [3].

The properties of F determine the type of the solution(s) the equation has. For a given phase space point  $X_0$  we could compute the Jacobian matrix J of F, which contains as components all partial derivatives of F by the components of X. The Eigenvalues tell us if the solutions around  $X_0$  grow or decay if they oscillate (i.e., rotate around  $X_0$ ) or if chaos is to be expected (using Lyapunov exponents).

In a simulation approach, we choose a small timestep  $\Delta t$  and compute

$$X_{t+\Delta t} = X_t + \Delta t J X_t$$

The approach is elegant and general but becomes unpractical for even medium sized equation systems. For a realistic multiresonator Clapp oscillator with B Mode suppression the size of J is a matrix larger than 20x20, leaving numeric solution approaches as the only choice.

What is generally missing from our approach is the presence of noise sources. For all systems operating at a nonzero temperature, the components of X contain random variables (i.e., noise currents and voltages) that have either a uniform (white) or weighed (flicker) amplitude spectrum.

If we define a vector  $B$  that contains a set of random (noise) variables we could then try the approach of

$$X_{t+\Delta t} = (X_t + B) + \Delta t J(X_t + B)$$

This looks unspectacular but can change the behavior of the equation drastically. A good example is the stability of fixed points. If we have a fixed point where the first derivative is also vanishing (e.g., for the van der Pol equation the fixed point is the origin), a system without noise would never leave this point even if the Jacobian indicates that it is unstable. With enough noise present, startup is guaranteed.

This effect can be exploited in simulation programs to speed up the startup of extremely high  $Q$  oscillators. During a limited time, a large noise component is injected into the circuit until the simulation has left the “dead zone” around a quadratic fixed point and oscillations can begin. After a while, the noise source can be deactivated.

Another consequence is the reduction of stability of higher order periodic cycles (subharmonics). These cycles only exist in small domains of component values (i.e., the basin of this attractor is very small). With enough noise present, the dwell time of these attractors can be reduced or even eliminated, as will be shown later.

## 17.2 A Simple Example for Noise and Chaos

The probably most famous and simple equation involving chaos is the so-called logistic equation

$$X_{N+1} = RX_N(1 - X_N)$$

This equation emerged from simulation models of a reproducing rabbit population under habitat constraints [4].  $R$  is the reproductive rate, and the bracket term ensures that the normalized population can never go to infinity by limiting growth. When mapping the values of  $X$  over  $R$  for a large number of iterations, we obtain the well-known bifurcation diagram as shown below:

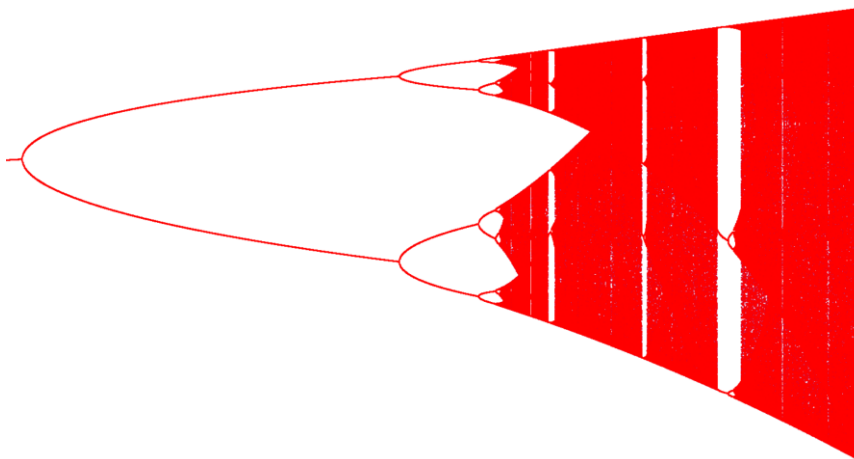


Figure 241 - The Bifurcation Diagram of the Logistic Equation without Noise

The points in the diagram are computed the following way:

1. First, a large number of iterations are performed from a given start value (2000 used here).
2. Next, a sufficiently large number of points after the first phase is computed and plotted (500 used here).

Depending on  $R$ , we get either just a single point after the first phase (settling to a fixed value), or an oscillation between two points, four points, 8 points, and so on (this is the bifurcation area), or chaos

with no recognizable pattern. The chaos, for some values of  $R$ , is interrupted by small gaps of regularities (white stripes on the right).

What makes this equation relevant for our purposes is that (if we now switch to  $X$  as a state vector of the variables of a Clapp oscillator instead of the number of rabbits) it can describe the next point in a simulation based on the last point. We just need to set  $J$  to  $R(1-X)$ . So, the logistic equation is a special case of a dynamic system with a specific Jacobian, and we could study what effect additional noise could have on its behavior.

Let's now introduce a random variable that modifies the result of the next step. A possibility would be to make the reproduction rate  $R$  vary, or by just adding a small random fraction of the population after each step. We would then have:

$$X_{N+1} = \text{abs}(R(X_N + B)(1 - X_N - B))$$

Where  $B$  is our random variable varying between a small  $\epsilon$  around 0. The absolute value is needed to prevent the population becoming negative due to a random undershoot of the second term.

If we look at the equations, we can already see that the noisy equation will start from zero, which the original equation will not. What happens with higher values of  $R$  can be simulated for different values of  $\epsilon$ .

Let us check the startup first, with an  $\epsilon$  value of just 0,01%. The outcome looks like this:

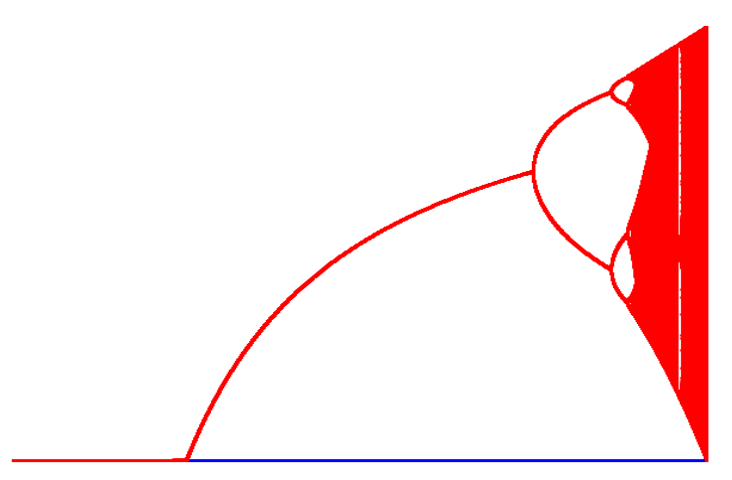
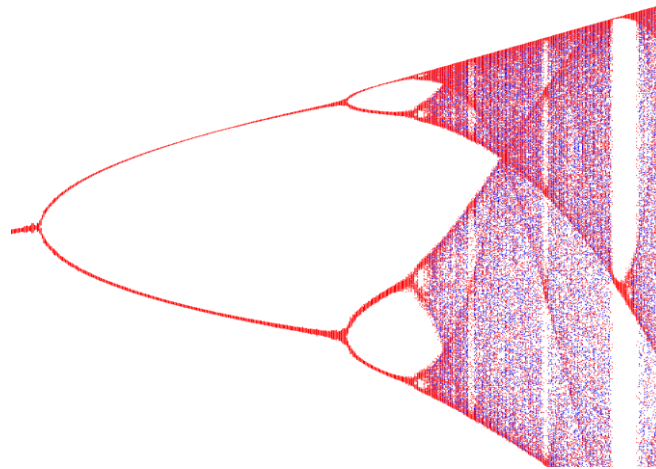


Figure 242 - Startup from Zero with and without Noise (Noise Amplitude 0.0001)

The blue line is the noiseless system, the red curve has a noise amplitude of 0.0001. The bifurcation diagram, in principle but a bit blurred, looks the same as the noiseless curve with a nonzero starting value.

Now let us enable the startup of the noiseless system by setting  $X_0$  to 0.1 and compare the diagrams in more detail.



*Figure 243- Startup from Nonzero Start Value with and without Noise*

We can observe that the noiseless and the noisy curve still coincide on a large scale, with smaller “eyes” appearing a bit smaller when noise is on. Let us use more noise now (1%) and see what happens. The big picture looks like this:

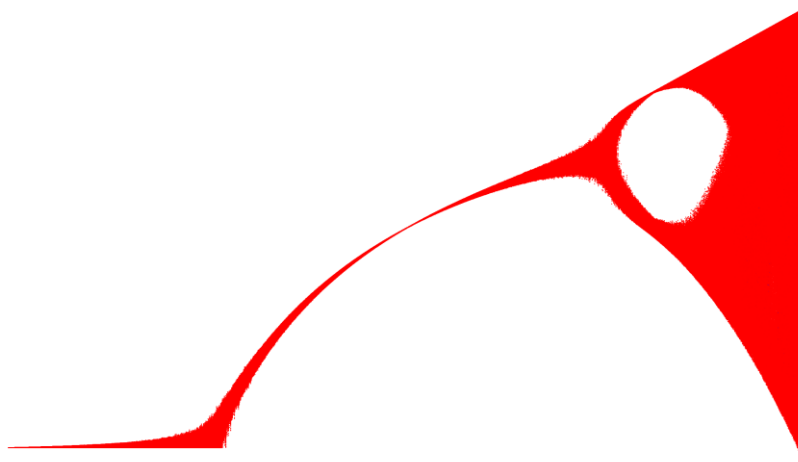


*Figure 244- Startup from Nonzero Start Value with and without Noise (Detail)*

This looks vastly different from the noiseless pattern. All higher order zones without chaos are completely gone, even if the noise amplitude is just 1%.



A zoom in of the second order zone looks like this:

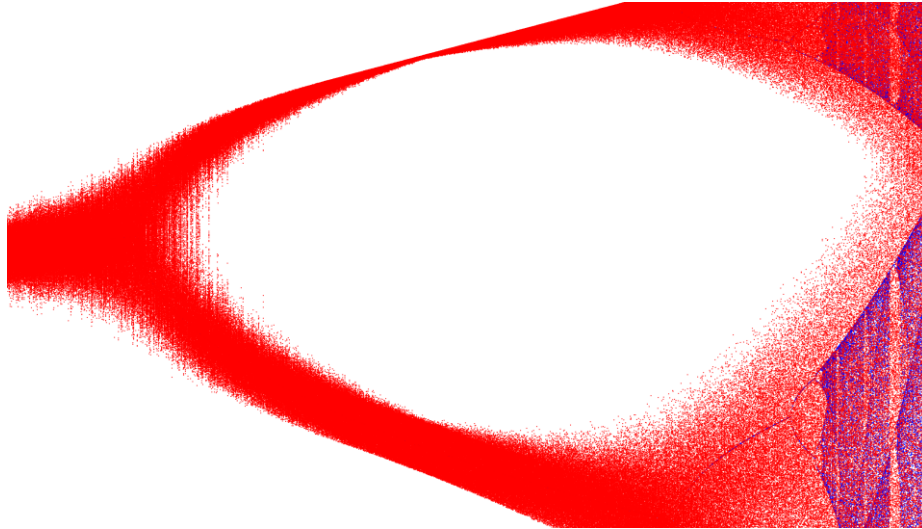


*Figure 245 - Noisy Second Order Zone in Detail*

Showing that all non-chaotic higher order zones are completely flooded except the period doubling zone.

An interesting fact is that there is a spot on the curve where the remaining noise level seems to be extremely low (the thinnest part of the rising curve). The amplitude variation here is about the noise amplitude divided by 100, so this spot of R seems to have a noise cancelling effect. By chance or not, the point coincides with a parameter value where the Lyapunov exponent drops to zero.

## Conclusions

From the simulations above we can adjust our expectations of what noise can change in complex nonlinear dynamic systems like multiresonator oscillators. We have:

1. Even very little noise can make systems start oscillations from square fixed points ( $X=0$ ,  $X'=0$ ). This is in good agreement with the fact that real oscillators also could start with all voltages and currents zero, but thermal noise present.
2. Noise reduces the ability of a system to oscillate in higher order modes by forcing the state vector to leave the (small) basins of higher order attractors. Normally these modes are unwanted, so some noise can be a method avoiding them.
3. In some areas of operation, the noise level present on the state vector components can be much smaller than the noise amplitudes. Identifying these parameter regions and tuning a design to work there could, theoretically, be a way for a real low noise design.
4. Noise destroys scale invariance, or in other words, the self-similarity property of genuine chaotic solution patterns. Scale invariance is limited to structures where the dimensions are significantly larger than the noise component.



## References

- [1] Fadhil Rahma Tahir, "Chaotic Colpitts Oscillator." ResearchGate, Accessed: Nov. 25, 2020. [Online]. Available: [https://www.researchgate.net/publication/319912711\\_Chaotic\\_Colpitts\\_Oscillator/link/59c14dd9a6fdc69b92bbee2/download](https://www.researchgate.net/publication/319912711_Chaotic_Colpitts_Oscillator/link/59c14dd9a6fdc69b92bbee2/download).
- [2] B. Srisuchinwong, B. Munmuangsaen, I. Ahmad, and K. Suibkitwanchai, "On a Simple Single-Transistor-Based Chaotic Snap Circuit: A Maximized Attractor Dimension at Minimized Damping and a Stable Equilibrium," *IEEE Access*, vol. 7, pp. 116643–116660, 2019, doi: [10.1109/ACCESS.2019.2936535](https://doi.org/10.1109/ACCESS.2019.2936535).
- [3] V. I. Nekorkin, *Introduction to Nonlinear Oscillations: Nekorkin/Introduction to Nonlinear Oscillations*. Weinheim, Germany: Wiley-VCH Verlag GmbH & Co. KGaA, 2015.
- [4] Verhulst, P.-F. "Recherches mathématiques sur la loi d'accroissement de la population." *Nouv. mém. de l'Academie Royale des Sci. et Belles-Lettres de Bruxelles* **18**, 1-41, 1845.

## 18 Appendix I: Manufacturer SPICE Models for the 2N2222A

Even for an extremely common transistor like the 2N2222A, there is no common SPICE model for all the many companies that make the part. Some models were collected from various sources on the net. The parameters came directly from the manufacturers and were left as they are.

```
.model 2N2222A MICROSEMI NPN (IS=19.34n XTI=3.0 EG=1.11 VAF=250.3 BF=163.8 ISE=174.3f
+ NE=1.647 IKF=3.0 NK=0.3052 XTB=1.5 BR=11.49 ISC=19.9f
+ NC=1.88 IKR=10.75 RC=0.3567 CJC=11.02p VJC=0.3869 MJC=0.3292
+ FC=0.5 CJE=29.31p VJE=0.9036 MJE=0.4104 TR=38.32n TF=361.8p
+ ITF=5.282 XTF=249.9 VTF=10 mfg=MICROSEMI)
```

```
.model 2N2222A ONSEMI NPN (Is=14.34f Xti=3 Eg=1.11 Vaf=74.03 Bf=255.9 Ne=1.307
+ Ise=14.34f Ikf=.2847 Xtb=1.5 Br=6.092 Nc=2 Isc=0 Ikr=0 Rc=1 Cjc=7.306p Mjc=.3416
+ Vjc=.75 Fc=.5 Cje=22.01p Mje=.377 Vje=.75 Tr=46.91n Tf=411.1p Itf=.6Vtf=1.7 Xtf=3
+ Rb=10 Vceo=40 Icrating=800m mfg=Fairchild)
```

```
.model 2N2222A PHILIPS NPN (IS=1E-14 VAF=100 BF=200 IKF=0.3 XTB=1.5
+ BR=3 CJC=8E-12 CJE=25E-12 TR=100E-9 TF=400E-12 ITF=1 VTF=2 XTF=3
+ RB=10 RC=.3 RE=.2 Vceo=30 Icrating=800m mfg=Philips)
```

```
.MODEL 2N2222A ZETEX NPN (IS =3.0611E-14 NF =1.00124 BF =220 IKF=0.52
+ VAF=104 ISE=7.5E-15 NE =1.41 NR =1.005 BR =4 IKR=0.24
+ VAR=28 ISC=1.06525E-11 NC =1.3728 RB =0.13 RE =0.22
+ RC =0.12 CJC=9.12E-12 MJC=0.3508 VJC=0.4089
+ CJE=27.01E-12 TF =0.325E-9 ITF=1 TR =100E-9 mfg=ZETEX)
```

The spread of important parameters is considerable; The forward current gain BF, e.g., varies from 163.8 to 255.9; The Early voltage VAF runs from 100 to 250, Base resistance RB (important for noise) varies from 0.13 to 10, ...

Device models provided by manufacturers are usually automatically extracted by mass measurements of large production samples. A spread of 20% across parts from different wafers and/or production sites is considered normal, and datasheet values have a safety margin large enough to accommodate variations.

We tried in LTSPICE how the different models would affect simulation results in oscillator circuits. Regarding output power, a spread of ca. 10% was found using the series coupled Clapp circuit.

None of the models provided has AF, KF or BE breakdown parameters specified. In case accurate models are needed it is necessary to perform parameter extraction on individual devices and create individual models per DUT.

This will be discussed in a separate chapter.

## 19 Appendix J: A Modeling Approach to BE Breakdown Noise

As discussed and substantiated by experiments the base-emitter breakdown effect increases oscillator phase noise significantly, contradicting the Leeson formula result that phase noise should decrease with the square of the oscillator output power. By parameter extraction using DC methods and by SPICE model enhancements the measured waveforms could be reproduced in time domain simulators. It is interesting if a similar success would be possible for the phase noise level under breakdown.

### 19.1 Difficulties

The BE breakdown as such does not only limit oscillator output amplitude and increases phase noise, but it also permanently damages the transistor by degrading gain at small to medium currents. BE breakdown is no mode of operation allowed by datasheet limit values<sup>13</sup>, so all guarantees are lost after this “permanent damage”. Tests have shown that about half of 2N2857 RF transistors [2] completely died after a breakdown, so there is definitely a corresponding reliability problem that excludes BE breakdown circuits from any high-reliability or space activity. 2N2222A LF transistors were more robust, but still suffered gain damage (but only 2 out of ca. 50 from different manufacturers died). The breakdown voltage of the specimens analyzed had a considerable spread, but all values were above the worst-case datasheet limits for all types analyzed.

In the light of the facts above the following investigations are of an academic, not a practical nature. No well-designed USO should ever operate even near to BE breakdown conditions.

### 19.2 BE Breakdown Operation

In a running oscillator, BE Breakdown only occurs in a certain combination of bias conditions and output. Raster tests have found which regions are affected, and by simulating using enhanced transistor models the BE voltages as well as the breakdown currents could be accessed and had a very good agreement with waveform and base current measurements. Due to the lack of 2N2857 durability under breakdown conditions tests with this type were abandoned. All further tests only used 2N2222A types, and we waited for some minutes of burn-in until the gain degradation effect has settled in and stabilized. In other words, all tests were made with the permanently damaged parts.

A look at the waveforms of an oscillator under breakdown conditions shows several interesting facts:

1. BE Breakdown occurs at voltages substantially higher than the datasheet limit value (+20..40% with a large spread).
2. BE Breakdown creates large base current spikes but draws no collector current when it happens.
3. The power dissipation inside a transistor during BE breakdown can be in the region of 100mW and more, leading to locally increased chip temperature. The BE breakdown heat occurs at the perimeter of the emitter fingers, not at the collector junction that has better cooling due to the mount method on case. In other words, the dissipating area is extremely small (Ref Kaubler).
4. The conduction angle of the BE breakdown current is rather short, only 10-20°.
5. The rise and fall times of the BE breakdown spikes are short, a few ns in a 5MHz oscillator.
6. The clamping effect of the large BE breakdown current immediately limits the slope of the negative base voltage swing when the BE breakdown voltage is reached. DC curves show as well that the dynamic impedance of a BE junction in breakdown is very low, like a good reference diode.

---

<sup>13</sup> The common caveat phrase in a datasheet runs like: “Stresses exceeding those listed in the Maximum Ratings table may damage the device. If any of these limits are exceeded, device functionality should not be assumed, damage may occur and reliability may be affected” (sample from ON Semiconductor 2N2222A datasheet).

From the theory of semiconductor junctions, it is known that we have two main possible working mechanisms: tunnel and avalanche breakdown. The tunnel mechanism dominates at lower voltages ( $< 5.6$ ), and the avalanche effect is prevalent above 5.6. At the crossing point, both mechanisms occur and their temperature coefficients (tunnel is negative, avalanche positive) cancel, explaining why precision reference Zeners with an extremely low  $T_c$  (down to 5ppm) use 6.2V (explained by a normal forward base diode in addition to the Zener). See [3] for a discussion about the mechanisms.

In all unfortunate 2N2222As used in the test oscillators, the measured breakdown voltages were above ca. 7V (2N2222A datasheets state 6V), so we may assume that the avalanche effect is dominant. This, in a way, is bad news because the avalanche process is extremely complex from a physics perspective.

If we look at the mechanisms in a diode in blocking mode before breakdown occurs, we see a space charge zone with almost no carriers inside<sup>14</sup>. The electric field strength is high, about the terminal voltage divided by the width of the space charge zone, so electrons and holes that emerge from wherever are swiftly accelerated and leave the zone (this constitutes the leakage current of a reverse diode). When terminal voltage is further increased, several new effects appear:

1. Electrons and holes are further accelerated
2. The rate of collision of the accelerated electrons and holes with phonons increases dissipating energy into the Silicon crystal lattice. This causes a decreasing mobility factor with applied voltage.
3. The average temperature of the electrons and holes in the space charge zone increases. Depending on construction, carriers with extreme temperatures could get injected into the planar field oxide of the part. Trapped electrons in the field oxide are responsible to for the breakdown related gain degradation.
4. Some electrons and holes are now so energetic that they can dislocate lattice electrons and holes that are now accelerated as well. If the voltage is high enough to make this a frequent event, a full snowball effect sets in, creating an avalanche of charged particles and making the diode conduct vigorously. The energy used for dislocation is partly transferred to the grid as well, causing local heating.

So far the established theory of the breakdown mechanism. What the theory above suggests is a spectrum that has a strong (exponential) dependency on the applied voltage and a chaotic breakdown triggered by a superposition of carrier avalanches moving thru the space charge zone. It is not clear what kind of spectrum this will create.

Experiments on cut-open 2N2222A test transistors revealed some more interesting facts:

1. The BE breakdown causes electroluminescence in the orange spectrum, even if Silicon is an indirect semiconductor. The interaction with surface states is a possible explanation as well as a process involving two charged carriers instead of just one. The electroluminescence only occurs when the reverse BE current rises above the leakage current, so the glow can be used as an indicator for breakdown.
2. The location where the electroluminescence occurs is made up from tiny spots on the base emitter boundary. No other parts of the electrodes or the chip as a whole emit any (visible) light.
3. If the reverse voltage is gently increased (using a precise SMU) the spots increase in number, but not in brightness. This stepwise behavior also applies to the resulting breakdown current (also measured by a precision SMU). A fully lit boundary happens at current levels that are destructive due to thermal dissipation overload (bear in mind that the BE breakdown appears

---

<sup>14</sup> Almost is important because due to the energy spectrum of grid vibrations at the high-energy tail plus radiation there is always a small but finite creation rate of hole/electron pairs in a space charge zone when the temperature is higher than absolute zero. This rate, along with the corresponding recombination rate, is the cause for the leakage currents of diodes and transistor junctions in reverse mode.

in a very small structure on the surface, unlike the normal large space charge zone between base and collector). Industrial papers about the onset of avalanche diode currents also describe this as a stepwise waveform.

4. There is a thermal hysteresis phenomenon with some lit zones going on and off. This is explainable by the negative temperature coefficient of breakdown current (or the positive coefficient of breakdown voltage). When temperature increases, the phonon scattering increases as well, driving mobility down. Reduced mobility means that the number of avalanche collisions take place in larger distances, reducing the number of freed carriers and consequentially, breakdown current. In other words, the heat created by a breakdown hotspot has a self-quenching effect.
5. The noise current measured at the collector has the shape of superposed left-sided ramps. The increase is very steep, with an almost linear decay, eventually interrupted by other ramp currents. This can be explained by the following heuristic idea: The avalanche electrons or holes form a “triangle” in space moving along the strong drift field. The front of the triangle consists of the “youngest” generation of carriers, while the tail has proportionally fewer numbers until we get back to the carrier that started the whole thing off. It needed a lot of kinetic energy to dislocate the next generation, so the remaining post-collision speed is low and needs time to recover speed. The left-sided ramps are also typical current patterns involved in leakage currents before avalanching. If the source resistance is high and breakdown currents are still small (in the  $\mu\text{A}$  range), the capacitance of the blocked junction creates a similar effect, like an RC relaxation oscillator, but with a chaotic pulse current.
6. Empirical tests with different breakdown currents have shown that the breakdown current becomes less noisy with increased current. This effect is well known from voltage references or “Zener” diodes, where the manufacturers suggest a minimum current. It is also very compatible with the pattern of triangular shaped carrier clouds. The more triangles are superposed, the smaller the resulting fluctuations will be.

### 19.3 Summary of Breakdown Physics, Modeling Approaches

If we confine ourselves to the 2N2222A transistor that degrades but, in most cases, survives an operation using BE breakdown, we must concede that an accurate modeling of the breakdown current apart from a DC curve is extremely complex. The time constants of the participating random processes cover a wide range (seconds for thermal hysteresis, nanoseconds for the formation of the front of an avalanche current pulse), so an elegant yet mathematically and physically correct theory is out of reach. What can be done is a description based on the DC measured noise power density curves, with the added complication that the power densities decrease with DC current and also that the flicker corner depends a bit on the current.

Given the fact that the Leeson formula is using cyclostationary averages for almost all quantities ( $Q_L$ ,  $f_c$ ,  $F$ , ...) we could add another one based on the time averaged value of base breakdown current. This approach is definitively heuristic, but not more or less than the rest of the Leeson formula.

The Rohde approach of deriving the oscillator output noise spectral power densities based on the weighed RMS addition of noise components (base resistor, emitter resistor, current noises, resonator noises) makes use of the fact that an RMS summation of noise components make sense after weighing their spectrum through the transfer functions of the circuit paths of the oscillator. This approach is extremely difficult for avalanche noise due to the complex, time dependent shape of the generated noise spectra.

The clean solution of the problem would be to solve the equations obtained by KCL and KVL for the oscillator circuit but including realistic time-domain random components for noisy quantities. The resulting equation system is a nonlinear set of stochastic differential equations, that, as far we have

researched, was not yet solved for any realistic oscillator case. Another difficulty of this approach that a realistic model for a parametrized time domain random variable model for the BE breakdown current is still outstanding.

#### 19.4 An Experimental Sanity Check for the Breakdown Noise Current

In an IETE paper [5] we conducted measurements relating breakdown current to voltage and found a fitting formula that described the current/voltage dependency for 3 decades of breakdown current. Nothing was said, however, about the noise generated by the process. In the light of the physical mechanisms above more research was done on the current patterns in the time domain, the noise amplitudes and spectra. The measurement setup is as shown below:

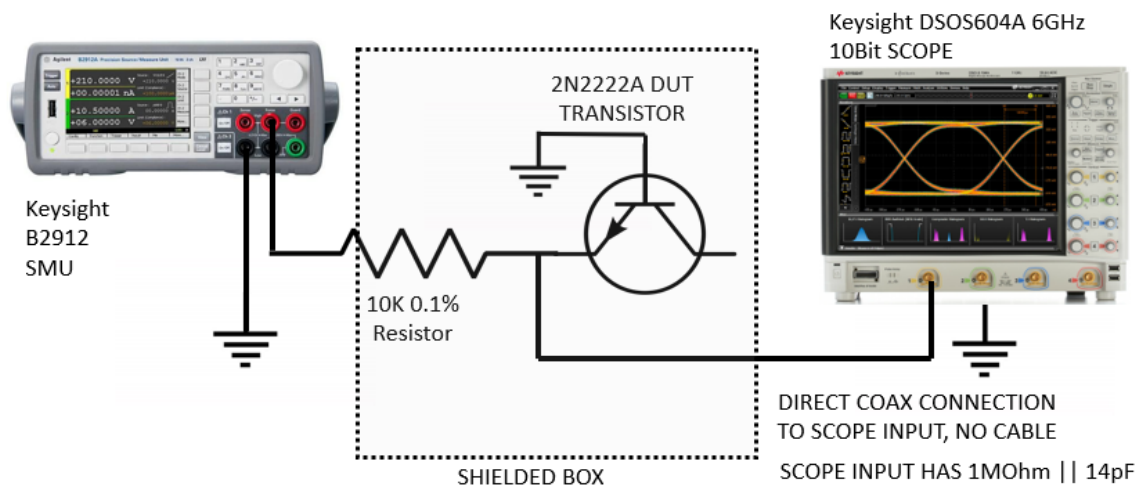


Figure 246 - The Transistor BE Breakdown Noise Measurement Setup

The direct technique using the 50Ohm scope input was not usable because the signal at nanoampere levels would be too small (falling below the noise of the scope itself). Furthermore, the 50Ohm input mode has no AC option and could be damaged in case of a transistor failure. With the AC option shown this cannot happen and the loading is much less, making current fluctuations in the range of several 100nA visible as mV signals. The scope noise was suppressed by using an oversampling high-resolution mode resulting in 15bits of resolution, and by reducing bandwidth to ca. 60MHz.

A computerized measurement process was setup, and for currents ranging from 200nA to 2mA the AC waveform and the peak and RMS noise amplitudes were measured. The curve for the peak and RMS noise voltages is shown below:

**TRANSISTOR BE BREAKDOWN NOISE OVER CURRENT (PEAK AND RMS)**

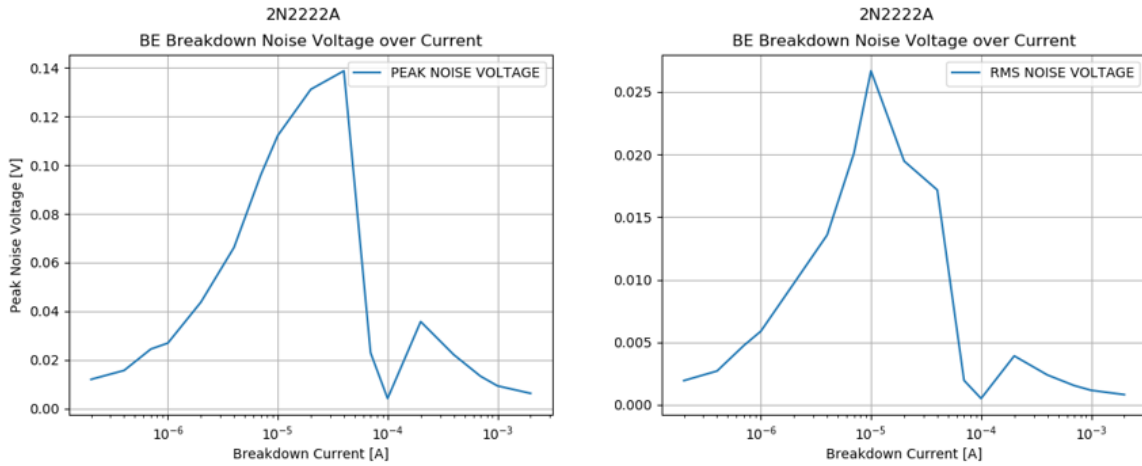
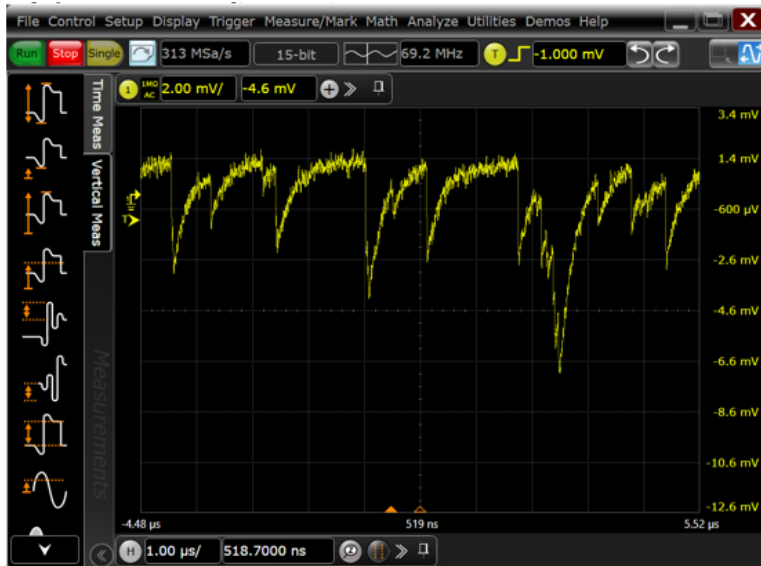


Figure 247 - Peak and RMS Noise Voltages in BE Breakdown over Current (2N2222A)

The curves show a significant peak around 10-40uA of breakdown current. At 10uA, there is a spot with minimal noise, and the peak has an about tenfold increase over the noise generated at very low and very high currents. Let us analyze the waveforms at low (200nA) medium (20uA) and high (2mA) currents. 200nA is first:



- CLASSIC RELAXATION
- RETURN TO A STATIONARY LEVEL
- DISCHARGE VERY FAST, CHARGEUP CURRENT SMALL, TIME CONSTANT 300ns (10K\*30pF)

Figure 248 - Breakdown Voltage Waveforms at 200nA Breakdown Current (2N2222A)

This looks like a waveform well explained by the theory of sporadic avalanche formations above. Similar waveforms were observed by Vishay [4].



The next current level is 20uA (this is around the peak of the generated noise voltage):



- **STILL SOME RELAXATION, BUT ALSO SOME RANDOM NOISE**
- **MUCH LARGER AMPLITUDES**
- **POSITIVE PEAKS INSTEAD OF NEGATIVES**

Figure 249 - Breakdown Voltage Waveforms at 20uA Breakdown Current (2N2222A)

The waveform has changed in many ways; first, the amplitudes are 10 times as large, the peaks occur much more often, and the peaks now point upwards instead of downwards. This could possibly be explained as a mixture of avalanche processes and classic current (Schottky) noise.

At 2mA, things change again, as can be seen below:



- **LOOKS LIKE RANDOM NOISE**
- **SMALL AMPLITUDES**
- **EQUAL PEAKS**

Figure 250 - Breakdown Voltage Waveforms at 2mA Breakdown Current (2N2222A)

This looks like classic white broadband noise.



To check for the spectra involved, FFT measurements were conducted, using the scope's built in spectrum analyzer option. 200nA first:



- FAIRLY FLAT FROM 1kHz TO 500kHz
- FLICKER CORNER AT 500Hz
- -50dBmV

Figure 251 - Breakdown Noise Spectrum at 200nA (2N2222A)

Flicker noise is strong here, up to -30dBmV at 10Hz, typical for relaxation oscillations. At 20uA, the noise level increases significantly as shown below:

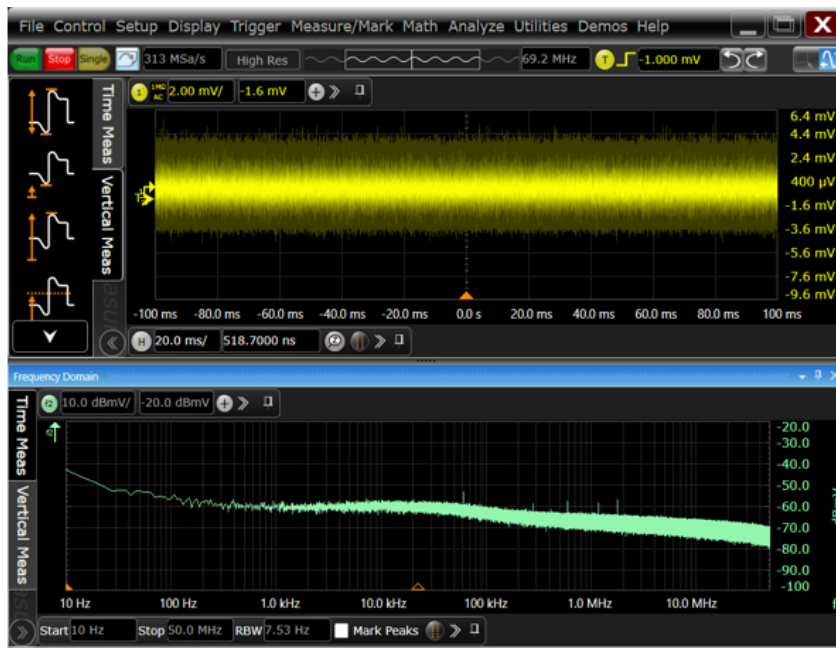


- FAIRLY FLAT FROM 100Hz TO 3MHz
- FLICKER CORNER AT 100Hz
- -30dBmV (!)

Figure 252 - Breakdown Noise Spectrum at 20uA (2N2222A)

Flicker is a lot less pronounced here, but the floor has risen to -30dBmV, and the flat bandwidth has increased further.

Now 2mA:



- FAIRLY FLAT FROM 100Hz TO 100kHz
- FLICKER CORNER AT 100Hz
- -60dBmV

Figure 253 - Breakdown Noise Spectrum at 2mA (2N2222A)

Flicker has now increased (or the white part decreased). Not much variation, and the level has fallen below even the low-current value. This looks like more or less white current noise.

### Conclusions for the Added Phase Noise in Power Oscillators

When looking at the phase space diagrams and the oscillograms of the current pulses of the power oscillator discussed in the IETE paper [5] at 5V/20V, the base breakdown current peak lies at ca. 20mA. This value is far beyond the 2mA we have measured here, so we may safely assume that at 20mA the current noise will be the dominant effect. We did not measure this current in the current setup, because we were afraid a time constant breakdown dissipation of ca. 300mW would kill the transistor (remember that maximum dissipation values are specified with the well-cooled base collector junction in mind, not the delicate emitter finger hotspots).

We could also conclude that the flicker contribution of breakdown alone is not very prominent at higher currents.

If we assume that the breakdown current noise at high DC breakdown currents has a white spectrum with a Schottky magnitude, we may assume that it adds a uniform white noise floor to the whole phase noise, just as other white noise sources like resistances. The magnitude of this increase can be modelled as proportional to the peak (or average) value of the base breakdown current.

What is interesting is what would happen if the oscillator would run just at the onset of breakdown, where the noise generated reaches its maximum.

### 19.5 A Fitted Model for the Measured 2N2222A Clapp Oscillator

Using the IETE paper [5], we can make a Leeson-based extension to the Phase noise formula adding a BE noise term. As for the other terms, the parameters for the breakdown term are cyclostationary values that need to be fitted. The following plots show the phase noise at 15V (no BE breakdown) and 20V (breakdown with 20mA peak reverse base current) of supply voltage, 15V first:

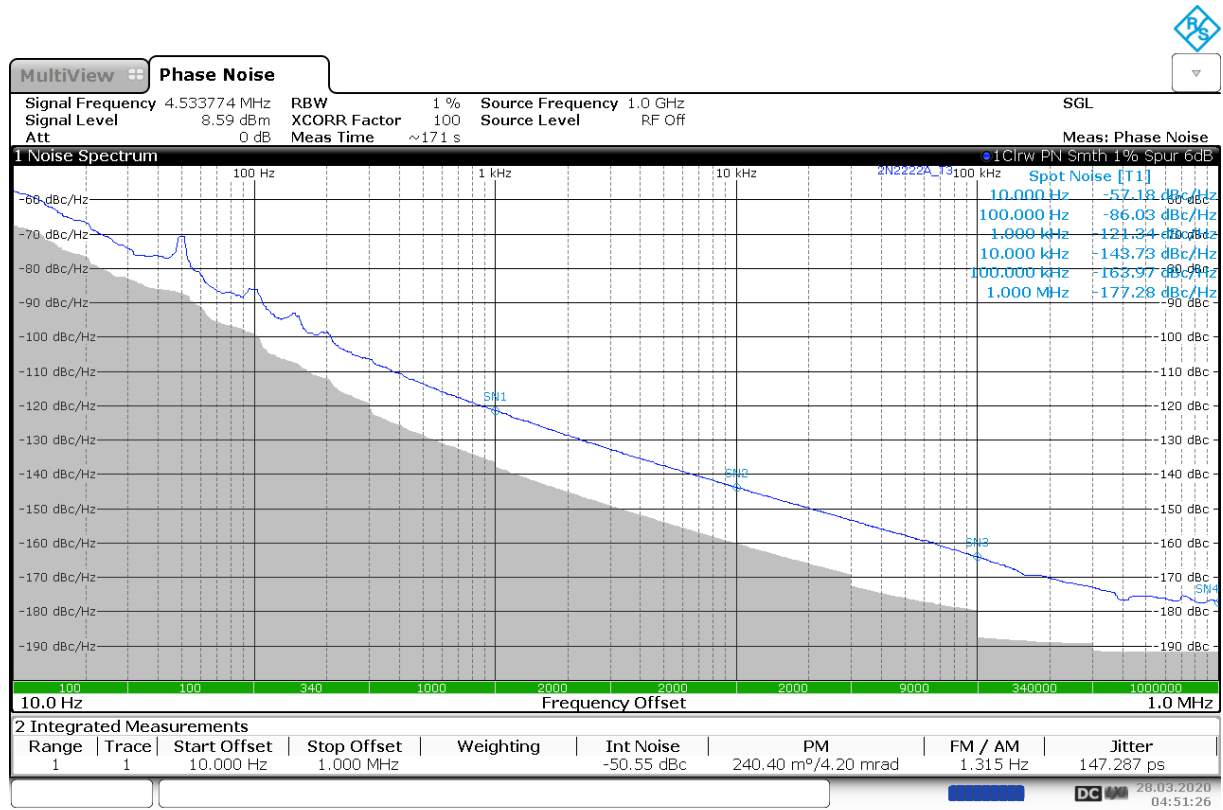


Figure 254 - Clapp Oscillator Phase Noise without BE Breakdown

And then 20V:

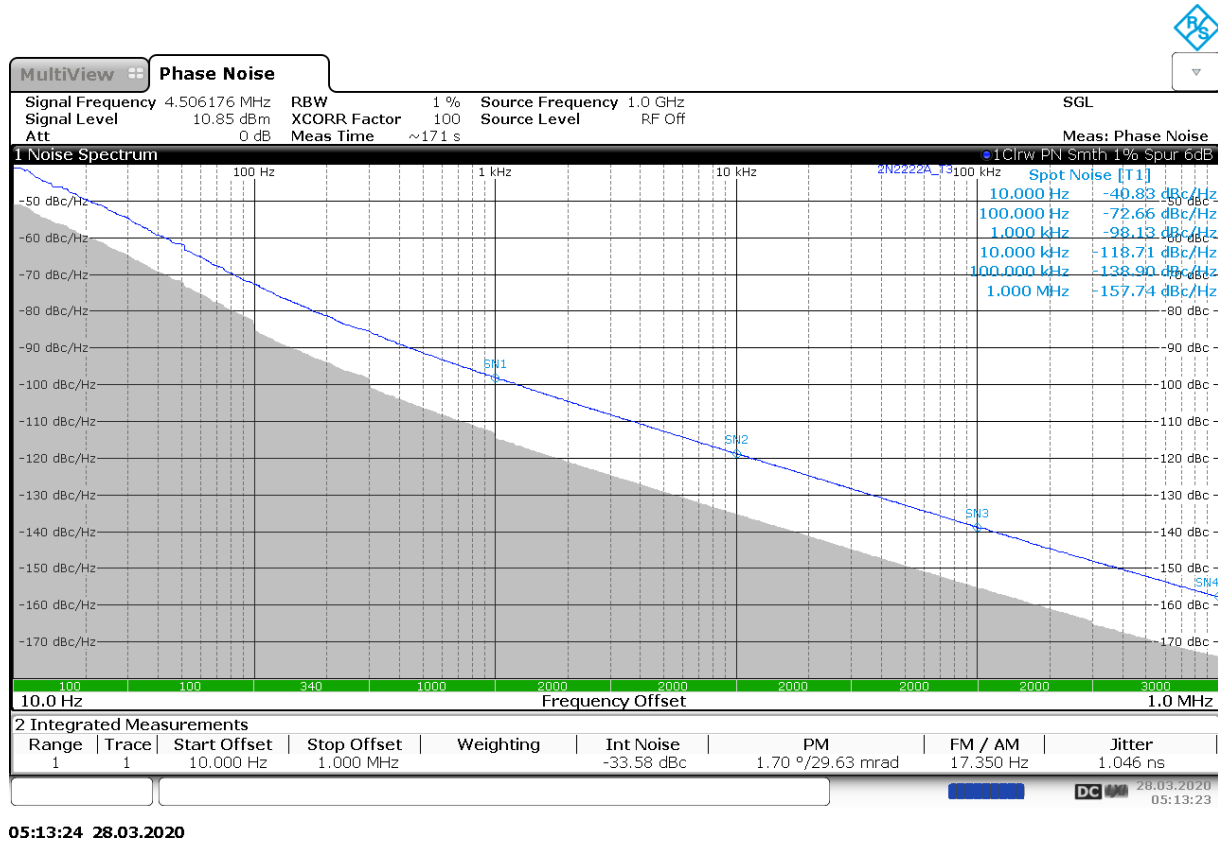


Figure 255 - Clapp Oscillator Phase Noise WITH BE Breakdown

When we look at Leeson’s formula, the 20V case should have delivered less phase noise compared to 15V, in the square of the output power ratio. At 15V we have 8.59dBm, at 20V we have 10.85dBm, so the 20V phase noise floor values should be  $2 \cdot (10.85 - 8.59) = 4.52\text{dB}$  below the 15V values, adjusted by the power difference compared to the measured 20V values is the corrective quantity we need to model to incorporate the influence of the BE breakdown.

Frequency Offset	15V PN	20V PN	Projected 20V	Difference
10	57.18	40.83	61.70	20.87
100	86.03	72.66	90.55	17.89
1K	121.34	98.13	125.86	27.73
10K	143.73	118.71	148.25	29.54
100K	163.79	138.90	168.31	29.41
1M	177.28	157.74	181.10	23.36

Obviously, there are two ranges below and above the flicker corner at about 300Hz. Below the difference is in the range of ca. 19dB, above we have ca. 28dB except for the last value where the 15V curve already flattened out.

We could use the correction term formula proposed in the IETE paper [5].

$$L(f_m) = 10 \log \left\{ \left[ 1 + \frac{f_0^2}{(2f_m Q_L)^2} \right] \left( 1 + \frac{f_c}{f_m} \right) C_{BR} \frac{FkT}{2P_{sav}} + \frac{2kTRK_0^2}{f_m^2} \right\}$$

Where  $C_{BR}$  defines the breakdown term of the form

$$C_{BR} = \left( 1 + k_{BR} \left( \frac{I_{BR}}{I_{AV}} \right)^{a_{BR}} \right) \left( 1 + \frac{f_m}{f_{BR}} \right)$$

but we run into two problems; first, we have the situation that noise *decreases* when approaching the carrier (“inverse flicker”), and, second, at very large offsets the measurement value dips into the noise floor.

The approach taken to correct that works as follows:

For the “Difference” column in the table above we need a fitting formula that covers the low and medium offset range with sufficient precision. To map the difference D, we can use a Lorentzian type formula like

$$D = A0 + \left( 1 + k_{BR} \left( \frac{I_{BR}}{I_{AV}} \right)^{a_{BR}} \right) \frac{\left( \frac{f_m}{f_{BR}} \right)^{a_{fBR}}}{\left( 1 + \left( \frac{f_m}{f_{BR}} \right)^{a_{fBR}} \right)}$$

We can choose A0 as the low-frequency limit of the difference (20.87dBc). Because we have only one measured value with BE breakdown active  $k_{BR}$ ,  $I_{AV}$  and  $a_{BR}$  cannot be derived. If we assume a linear dependency on breakdown current, we have  $a_{BR} = 1$  and we can set  $k_{BR}$  to a factor of 1).  $I_{AV}$  is set to the measured peak breakdown current at 20V, in this case 20mA. For the “negative” flicker term we have a corner frequency of, say 300Hz from the plot. The  $a_{fBR}$  term can only be guessed and was chosen to be 1.5 for a start value. It should be noted that no physical explanation was found for the Lorentzian shape.

The basic data is shown in the plot below:

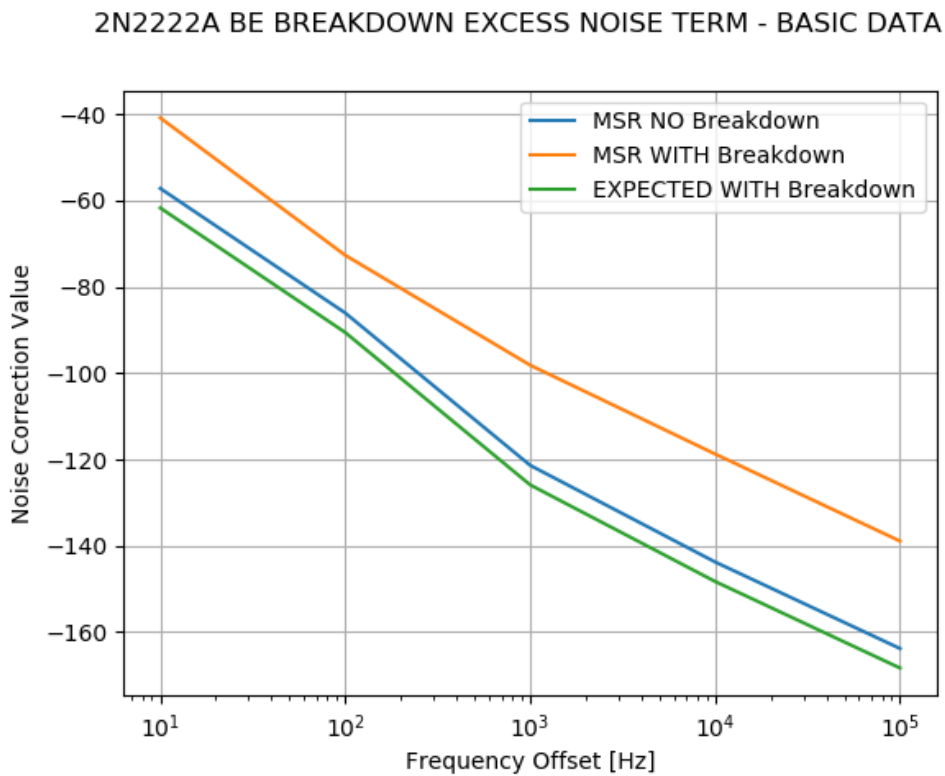


Figure 256 - Measured and Prognosed Data for an Oscillator with and without BE Breakdown (2N2222A)

Using the pragmatic guesses above, a curve fitting algorithm can be employed to compute best least square fits for the parameters. The fitted difference is shown here:

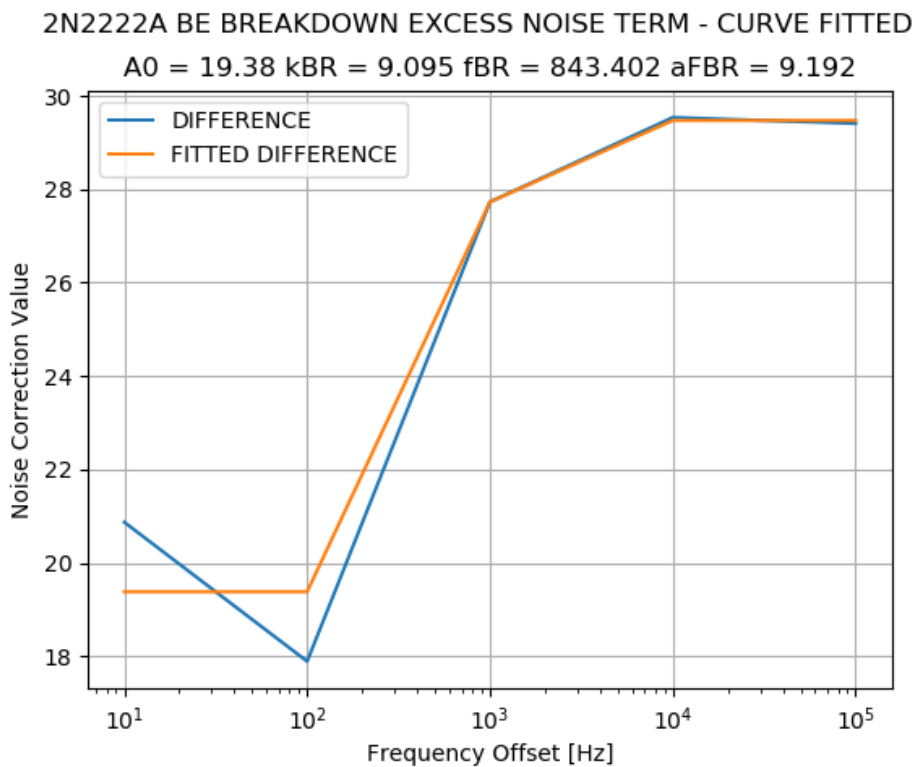


Figure 257 - Measured and Fitted Difference between Leeson Value with and without Breakdown (2N2222A)

The error is below a dB for all measurement points and improves at higher offsets. The 1MHz offset was not treated here due to the dip into the noise floor problem, but could be added later.

If we use the fitted formula to make a final prognosis about the phase noise under breakdown conditions, we obtain a plot like this:

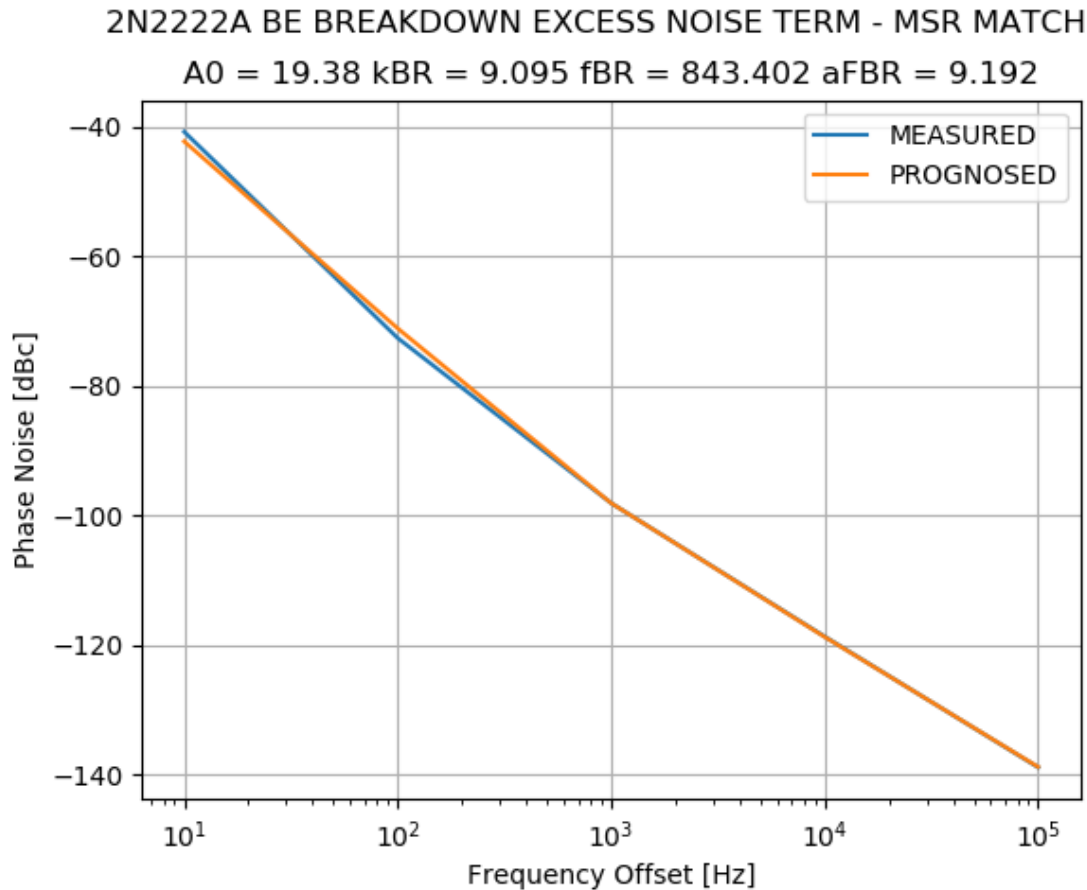


Figure 258 - Measured and Prognosed Phase Noise in Breakdown Conditions (2N2222A)

So, at least for the specific transistor under test, a usable prognosis for the increase in phase noise is possible.

To be on the safe side from a scientific point of view, let us review the restrictions of the approach chosen:

1. We work with transistors where the gain damage has already taken place, the transistor survived the breakdown, showed constant new characteristics and has still enough gain to work in the test oscillator circuit.
2. We have reduced complexity by using averaged breakdown noise values instead of realistic spectra involving the huge variety of physical effects the parts really have.
3. We must again state that operation in BE breakdown leads to a complete loss of validity for all datasheet values from the manufacturers (like gain, leakage currents, transition frequency, saturation voltages, ...). The same applies to simulation models.
4. Breakdown parameter variations between different specimens of the same 2N2222A types are significant between the different manufacturers and generations of chip technology. The modeling approach asks for a transistor device extraction (e.g., for the real  $V_{BE}$  breakdown voltage) before the model can be made.

5. The most important control parameter of the BE breakdown Leeson term is the averaged breakdown base current. This current has either to be modelled in the time domain (after characterization) or measured by a current transformer in a prototype.

## 19.6 Summary

A modeling of the breakdown phase noise is possible, but under severe methodical and pragmatical restrictions. While it is important to understand the mechanism of the creation of added phase noise by the BE breakdown process, it is by far more important to avoid any operation at or close to BE breakdown by a proper circuit design and careful simulation. The negative BE voltage must stay below the datasheet limits **in all phases of oscillator operation** (startup, stabilized state, ...) to avoid permanent transistor damage.

## References

- [1] Microsemi Corp., “2N2222A Technical Data Sheet.” Accessed: Nov. 17, 2020. [Online]. Available: [www.microsemi.com/index.php?option=com\\_docman&task=doc\\_download&gid=8898](http://www.microsemi.com/index.php?option=com_docman&task=doc_download&gid=8898).
- [2] Pulse Microwave, “2N2857 Datasheet Pulse Microwave.” Accessed: Nov. 17, 2020. [Online]. Available: [http://www.mpulsemw.com/Pdf\\_files/2N2857.pdf](http://www.mpulsemw.com/Pdf_files/2N2857.pdf).
- [3] R. B. Fair and H. W. Wivell, “Zener and avalanche breakdown in As-implanted low-voltage Si n-p junctions,” *IEEE Transactions on Electron Devices*, vol. 23, no. 5, pp. 512–518, May 1976, doi: [10.1109/T-ED.1976.18438](https://doi.org/10.1109/T-ED.1976.18438).
- [4] Vishay Inc., “The Noise of Avalanche Breakdown Diodes.” Accessed: Nov. 26, 2020. [Online]. Available: <https://www.vishay.com/docs/85966/thenoiseofavalanchebreakdown.pdf>.
- [5] Wolfgang Griebel, Matthias Rudolph & Ulrich L. Rohde (2020) Added Noise in Oscillators Caused by the Transistor Base Emitter Breakdown Phenomenon, IETE Journal of Research, DOI: [10.1080/03772063.2020.1847702](https://doi.org/10.1080/03772063.2020.1847702)



## 20 Appendix K: Thermal Design

USO crystals are designed for a specific operating temperature that needs to be maintained accurately. For SC cut crystals this operating temperature is at or below the lower turning point where the frequency dependency on temperature is minimal. The manufacturer measures the operating temperature for each individual crystal and includes this information in the datasheet or prints it directly on the crystal (for background info about the SC cut see [1], for a sample datasheet with LTP temperatures see [2]). The compliance to all other specifications (series, resistance, Q, ...) is guaranteed only at this temperature (tolerance is only 0.1°C, normally), making a good oven design a critical part of an USO.

### 20.1 Oven Designs

Commercial, industrial and space OCXOs use one of the following thermal designs:

1. Single oven, OCXO. The crystal temperature is controlled by a regulator, the surrounding circuitry runs at an elevated (but not controlled) temperature. Examples are the HP10811A plus the vast majority of commercial parts (see [3], p46ff for a discussion of the HP10811A heater).
2. Double oven, DOCXO. The crystal is temperature controlled, but the inner core of the oscillator is also controlled to make it even more independent of ambient temperature changes. Examples are Morion MV89, where a reverse engineering documentation is available as well [4]. Size, weight, and power is also increased, however.
3. Dewar flasks OCXOs. The principle of regulation is the same as an DOCXO, but with a significantly better thermal insulation from the environment. The Dewar flasks normally contains the complete oscillator core, so not just the crystal but the complete oscillator circuit runs at a very well-defined elevated temperature, which is good for the crystal but accelerates aging and drift of all other oscillator components. The plug side of the flask is also set to a controlled temperature a few degrees lower than the inside of the flask. Several premium USOs used this design (see [5] for a teardown of an 8601 as no official documentation is available concerning their internals). Energy consumption (after heating up) is very small, but size and weight are not. Mirrored glass Dewar flasks are fragile, too, so not suitable for space designs without special precautions. Titanium flask types work but are not as well insulating.

For the USOs of interest in this paper we will concentrate on a Dewar flask USO using a glass enclosure. This is not a space compliant design but explains the principle and can achieve good thermal stability.

### 20.2 Oven Physics

Independent of the oven type, we have at least the following components:

1. A heating element (usually a power transistor, in some cases resistors or resistive foils were used)
2. A temperature sensor (a precision thermistor or Platinum sensor)
3. The crystal and the surrounding oscillator core.
4. A thermal mass surrounding the crystal and creating an equal temperature environment for the heater, the crystal, and the temperature sensor. This also implies that the thermal mass is made from a material with a high thermal conductivity, e.g., Aluminum or Copper.
5. A large thermal resistance insulation from the crystal and other components to the ambient

An (usually located outside) external regulator circuit then reads the temperature and drives the heater.

The rate of the crystal temperature  $T_X$  change over time is then approximately given by the first order linear differential equation<sup>15</sup>

$$\frac{dT_X}{dt} = \frac{P - \frac{T_X - T_A}{R_{TH}}}{mc_P}$$

Where  $P$  stands for the heater power,  $m$  is the mass of the thermal mass and the oscillator core, and  $R_{TH}$  is the thermal resistance from the inside the oven enclosure to the outside.  $T_A$  stands for the ambient temperature outside the inner oven.  $c_P$  is the specific heat of the thermal mass material. The second enumerator term represents the power loss due to thermal conduction. Only the remaining power will increase the temperature of the thermal mass.

While  $m$  and  $c_P$  are known quantities,  $R_{TH}$  is not. It must be determined by an experiment incorporating a realistic seal (cap) of the Dewar flask, plus some heat losses caused by cables going through the seal cap.

A valid approach is to put the heater, the temperature sensor, and the thermal mass into the Dewar flask (along with some cables used for power supply and signals later) and to apply a known amount of heater power. After thermal equilibrium is established (at  $T_\infty$ ), we have

$$0 = \frac{P - \frac{T_\infty - T_A}{R_{TH}}}{mc_P} \quad \text{and} \quad R_{TH} = \frac{T_\infty - T_A}{P} \quad \text{and} \quad T_\infty = T_A + PR_{TH}$$

With all coefficients known, we can now solve the differential equation by using

$$\frac{dT_X}{dt} = \frac{1}{R_{TH}mc_P} (T_\infty - T_X) = \alpha (T_\infty - T_X), \text{ using}$$

$$\alpha = \frac{1}{R_{TH}mc_P}$$

We could now substitute

$$T_X = T_N + T_\infty \quad \text{and} \quad \frac{dT_X}{dt} = \frac{dT_N}{dt}$$

Resulting in

$$\frac{dT_N}{dt} = -\alpha T_N \quad \text{or} \quad \frac{1}{T_N} \frac{dT_N}{dt} = -\alpha$$

Integration over time results in

$$\ln(T_N) = -\alpha t + C \quad \text{or} \quad T_N = e^{-\alpha t + C} \quad \text{or} \quad T_N = Ke^{-\alpha t}$$

Back substituting to get  $T_X$  gives

$$T_X = Ke^{-\alpha t} + T_\infty$$

At  $t = 0$  we should obtain  $T_X = T_A$ . This defines the integration constant as

$$K = T_A - T_\infty$$

---

<sup>15</sup> In fact, the systems have more than one heat reservoir and more than one thermal resistance. This was ignored here because the heater block is so much more massive than all the other parts together. So strictly speaking, we would have a system of coupled differential equations instead of just one.

The complete formula now reads

$$T_X = (T_A - T_\infty)e^{-\alpha t} + T_\infty$$

Going back to the definitions results in

$$T_X = (-PR_{TH})e^{-\alpha t} + T_A + PR_{TH} = T_A + PR_{TH}(1 - e^{\frac{-t}{R_{TH}mC_P}})$$

And we are done.

The physical design of ovens varies widely, from rather feeble, low mass and thermal inertia parts like the HP10811A or the Morion OCXOs, to the absolutely massive premium USOs using a solid copper block with a mass of 370 grams. Photos and details are from [6]:

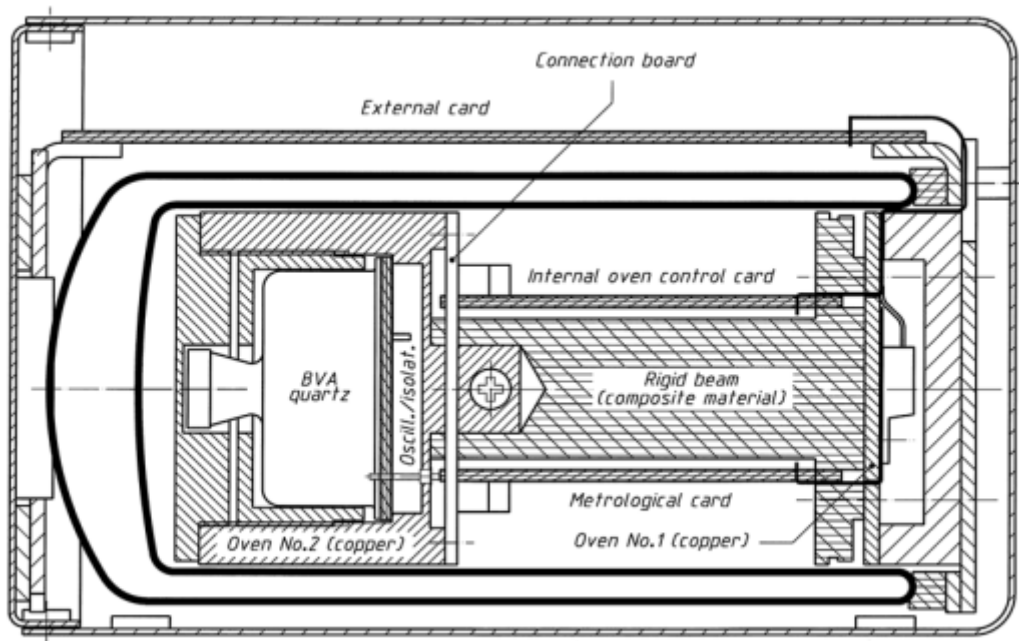


Figure 259 - 8600 Oscillator Mechanical Drawing  
Photo from [6]

This design uses a single Dewar flask with two zones. The core is shown at the left, including the copper block, and the plug heater sits on the right. All parts are machined to leave no thermal gaps. The outside design looks like an 8600 series part [5].

A practical example would run like this:

Suppose we have a thermal mass of 50g of Aluminum ( $C_P$  ca. 900J/kgK), and a thermal resistance of 100°K/W (these are plausible values for a prototype design). Then we have a time constant of

$$\tau = R_{TH}mC_P = 4500s$$

The equilibrium temperature is supposed to be 80°C, so we need ( $T_A$  assumed as 20°C)

$$P = (T_\infty - T_A)/R_{TH} = 0.6W$$

As a continuous power. Heating up can be done a lot faster, say, with about 10 times this power level. The time needed would then be

$$t = -\tau \ln\left(1 - \frac{T_{\infty} - T_A}{PR_{TH}}\right) = 474\text{s}$$

which is around 8 minutes, an acceptable value. If needed, warmup power could be further increased. Fast warmup can create problems due to thermal expansion stress. It should be noted that the thermal conductance from the crystal case to the slab inside is unknown but probably large, because there are no massive attachments, and the interior of an SC premium crystal is a very good vacuum. Even if the thermal mass around has reached equilibrium, the crystal temperature may lag behind a bit.

## References

- [1] TFC Total Frequency Control Ltd., “The SC cut family of quartz crystals.” Accessed: Nov. 23, 2020. [Online]. Available: [https://www.tfc.co.uk/pdfs/SC\\_cut\\_crystals\\_tfc.pdf](https://www.tfc.co.uk/pdfs/SC_cut_crystals_tfc.pdf).
- [2] Conner Winfield Inc., “Precision Low Profile TO-5 SC Crystal Datasheet.” Accessed: Nov. 23, 2020. [Online]. Available: <https://www.datasheet.live/index.php?title=Special:PdfViewer&url=https%3A%2F%2Fpdf.datasheet.live%2Fdatasheets-1%2Fconnor-winfield%2F36420-FRSQ1.pdf>.
- [3] Hewlett Packard Co., “10811A/B Quartz Crystal Oscillator Operating and Service Manual.” Aug. 1980, Accessed: Nov. 23, 2020. [Online]. Available: <http://hparchive.com/Manuals/HP-10811AB-Manual.pdf>.
- [4] Jörn Bartels DK7JB, “Basteltagebuch Morion MV89.” Accessed: Nov. 23, 2020. [Online]. Available: <https://www.bartelsos.de/dk7jb.php/ocxo-morion-mv89a?download=118>.
- [5] Ed Palmer, “Oscilloquartz 8601 BVA Oscillator Teardown.” Accessed: Nov. 23, 2020. [Online]. Available: <http://www.leapsecond.com/museum/osa8601/view.htm>.
- [6] Dr Jacques Chauvin et al., “A NEW GENERATION OF VERY HIGH STABILITY BVA OSCILLATORS,” presented at the International Frequency Control Symposium, 2007, Accessed: Nov. 23, 2020. [Online]. Available: <http://rubiola.org/pdf-articles/conference/2007-ifcs-xtal-osa.pdf>.

## 21 Appendix L: Space Qualified Transistors

### 21.1 Background

A space missions imposes much heavier demands on components than a regular commercial, industrial and even some military environments. The MTBF of space modules like oscillators are normally specified in the range of several 100k to millions of hours (Microchip/Microsemi states 6 to 10 million hours for their USOs [1], p9ff).

In a module the MTBF is dominated by the weakest part(s). Experience from the industry tell us that failure rates of semiconductor components are far higher than passive parts like resistors or capacitors. [2]. This makes the choice of extremely reliable semiconductor components a highly critical issue.

In the course of the space programs numerous standards and test methods were developed to make sure that a space compliant quality level is reached. Please see the “Norms and Standards” chapter for the concepts involved.

### 21.2 Transistor Choices

For commercial or industrial purposes, the transistor market offers several hundred of manufacturers, and tens of thousands of types, at least (depends on how availability is included). Not so for space applications. Here the situation is completely different:

The transistors allowed in space equipment are strictly defined in papers from NASA, ESA and JAXA (the American, European, and Japanese space agencies). All types (bipolar NPN and PNP, JFET, Power, MOSFET, ...) together are in the order of magnitude of just around 100 types. For an example, the “NASA Preferred Parts List” (NPPL). (for low-power NPN Silicon transistors see [3]).

The suppliers that are elected to provide these parts are cut down to a handful of companies only (all having special contracts, security clearances, a clean track record concerning part failures, ...).

For all parts, an impressive catalog of (military and space) standards and procedures must be guaranteed.

All the applicable parts are proven (and old, sometimes > 40 years). Although modern packages are OK (SMD), thru hole parts are still in the lists. [4]

All space transistors come in hermetic packages (metal, glass, ceramic). No plastic is allowed in space, because the chip inside the package could be affected by free ions (e.g., atomic Oxygen) or molecules that may change chip properties.

To guarantee reliability the space agencies may ask for transistor operation with derated parameters (compare, e.g., the space and non-space datasheets, e.g., in [5] for a consumer 2N2222A from ON semiconductor. Minimum gain is significantly higher in the consumer version).

### 21.3 Transistors Suitable for High Stability Space Qualified Oscillators at 5MHz

Basic environmental standards like temperature, temperature and load cycling, vibration and shock, radiation, mechanical stress, ... are left out here because they will be enforced by the procurement standards already discussed. We need to deal with USO circuit relevant properties only.

For a 5MHz oscillator optimized for long term stability in the observation period ( $\tau$ ) range from 0.1 to 10s the following specifications make sense, even without knowing the exact topology or the power level:

**Maximum collector voltage should be above 12-15V.** Why: due to the tank flywheel actions CE voltages can possibly exceed the DC value by a factor of 2 or more. The transistor should not go into breakthrough. Breakthrough effects are treated in a separate chapter.

**Maximum collector current should be a few 10mA minimum,** better more. Why: depending on the design it can make sense to use higher currents for better linearity. Transistor gain drops strongly when approaching the maximum current, this causes distortion and mixing.

**The transition frequency should be 200MHz or higher.** Why: We need sufficient gain to make the circuit start oscillations, even in the presence of a DLD effect. With a gain safety factor of 4 and 5MHz of oscillation frequency, the usual 10x factor gives 200MHz. A transition frequency that is too high can cause parasitic oscillations and more noise [6].

**Gain should be sufficient. 50 or more should be enough.** Why: with more gain, we could make the oscillator more independent of transistor properties by introducing negative feedback and/or lighter tank loading. Warning: the gain constraints must be OK for the whole temperature range if the oscillator is supposed to start from the cold.

**The device should have low "white" noise factor.** Why: We want a low level of far-from carrier noise. Attention: For oscillator operation, the datasheet noise figure is not relevant because it describes a small signal operation only. The large signal noise factor in a non-class A operation is normally 10-100 times larger than this figure.

**The device must have low flicker noise.** Why: flicker noise gets mixed up close to the carrier and downgrades the Allen variance in the range we need it to be as low as possible (0.1-10s). This is more critical than the white noise contribution. Attention: A lot of datasheets do not specify a flicker noise exponent and/or corner frequency. As a rule of thumb, lower frequency transistors have a low flicker noise corner frequency as well [7].

**Maximum dissipation must be within (derated) limits,** even at the elevated oven temperature. This can be a problem for small-packaged SMD parts at, say, 90°C when run at high currents for linearity.

**Simulation models must be available.** If not, a labor-intensive parameter extraction process is necessary. At best, simulation models include pre- and post-radiation data and data for a range of temperatures.

When matching the criteria list above with the list of types allowed for space projects we end up with a rather limited portfolio (extracted from the NPPL, approximate practical values):

Type	Op.Voltage [V]	Ic [mA]	Power [mW]	Gain	Ft [MHz]	NF Spec	Flicker Spec	SPICE Model	Civil Part	Mfg.
2N2222A	40	800	800	200	300	N	N	Y	Y	div.
2N2219A	60	800	1500	200	300	N	N	Y	Y	div.
2N2848	15	30	200	100	200	Y	Y	Y	Y	div.
2N2857	15	30	200	80	1300	Y	Y	Y	Y	div.
2N3866	30	400	1200	80	1000	N	N	Y	Y	div.
2N5109	15	400	1200	60	1000	N	N	Y	Y	div.

*Table of Space Qualified Transistors*

2N2848 has low noise, but  $f_T$  is too, low. 2N3866 has no noise specs.

Another issue is the availability of a “civil” version of a space qualified transistor (sometimes called “engineering model”). The reason for this is that space qualified components (also called “flight model”) do not have “better” data (e.g., more gain or a higher  $f_T$ ), they have data that is guaranteed for a much wider range of environmental conditions plus a higher reliability. Considering the price of JANS parts (can be above 1K€/piece) it is essential for the experimental part of the development process to have civil transistors with the same data (and package) available as their military/space counterparts.

## 21.4 Transistors Selected for the Circuits to be Analyzed and Developed

The following types were selected:

2N2222A. Pros: Still a preferred part in 2019 [3]. Many manufacturers, modern packages available. Civil version extremely cheap. SPICE model available. Cons: Only acceptable  $f_T$ .

2N2857A. Pros: Still a preferred part in 2019 [3]. Several manufacturers, modern packages available. SPICE model available. Cons: higher noise level (white and flicker) at 5MHz. Only used for comparison.

2N5109. Pros: Good  $f_T$ , very linear, high power capabilities, Many manufacturers, civil version available, SPICE model available, good noise figure.

## 21.5 SPICE Models for the Transistors Found on the Web

The models below are examples with some having a flicker exponent and a factor included. Flicker relevant entries are highlighted. AF is 1 by default.

```
.MODEL 2N2222 NPN (IS=19F BF=150 VAF=100 IKF=.18 ISE=50P NE=2.5
BR=7.5 VAR=6.4 IKR=12M ISC=8.7P NC=1.2 RB=50 RE=.4 RC=.3 CJE=26P TF=.5N
CJC=11P TR=7N XTB=1.5 KF=0.032F AF=1)
```

```
.MODEL 2N2219A NPN (IS=14.34F XTI=3 EG=1.11 VAF=74.03 BF=255.9 NE=1.307
ISE=14.34F IKF=.2847 XTB=1.5 BR=6.092 NC=2 ISC=0 IKR=0 RC=1 CJC=7.306P
MJC=.3416 VJC=.75 FC=.5 CJE=22.01P MJE=.377 VJE=.75 TR=46.91N TF=411.1P
ITF=.6 VTF=1.7 XTF=3 RB=10 VCEO=40 ICRATING=800M MFG=PHILIPS)
```

```
*SRC=2N2857; QN2857; BJTs NPN; RF;6V 1.5mA
```

```
*SYM=RFNBJT
```

```
* MOTOROLA 2N2857 6 V 1.5 MA
```

```
.SUBCKT QN2857 1 2 3
```

```
LC 1 4 0.313E-9
```

```
LB 2 6 0.850E-9
```

```
LE 5 3 1.393E-9
```

```
CC 4 5 0.362E-12
```

```
CB 4 6 0.330E-12
```

```
Q1 4 6 5 QR30
```

```
.MODEL QR30 NPN (BF=86 VAF=120 VAR=12.0 RC=12 RB=26
```

```
+RE=4.10 IKF=0.28E-01 ISE=0.36E-14 TF=0.556E-10
```

```
+TR=0.40E-08 ITF=0.11E-01 VTF=0.50E+01 CJC=1.10E-12
```

```
+CJE=1.51E-12 XTI=3.0 NE=1.5 ISC=0.12E-14 EG=1.11
```

```
+XTB=1.5 BR=2.23 VJC=0.75 VJE=0.75 IS=0.40E-15
```

```
+MJC=0.33 MJE=0.33 XTF=4.0 IKR=0.28E-01 KF=0.1E-14
```

```
+NC=1.7 FC=0.50 RBM=18 IRB=0.40E-02 XCJC=0.5)
```

```
.ENDS
```

```
*SRC=MRF3866; MRF3866; BJTs NPN; RF Class C;15V 50mA
```

```
*SYM=RFNBJT
```

```
* 2N3866 CLASS C
```

```
.SUBCKT MRF3866 1 2 3
```

```
LC 1 4 0.169E-9
```

```
LB 2 6 0.790E-9
```

```
LE 5 3 0.279E-9
```

```
CC 4 3 1.490E-12
```

```
CB 4 6 0.463E-12
```

```
Q1 4 6 5 QR89
```

```
.MODEL QR89 NPN (BF=100 VAF=240 VAR=24 RC=4.9 RB=12.2
```

```
+RE=0.132 IKF=0.28 ISE=3.6E-14 TF=7.1E-11
```

```
+TR=8E-09 ITF=0.12 VTF=9.9 CJC=2.24E-12
```

```
+CJE=3.29E-12 XTI=3.0 NE=1.5 ISC=1.2E-14 EG=1.11
```

```
+XTB=1.5 BR=1.5 VJC=0.75 VJE=0.75 IS=4E-15
```

```
+MJC=0.33 MJE=0.33 XTF=4.0 IKR=0.28 KF=1E-15
```

```
+NC=1.7 FC=0.5 RBM=9 IRB=0.04 XCJC=0.5)
```

```
.ENDS
```

```
.MODEL 2N5109 NPN (BF=44 VAF=160 VAR=16 RC=0.69 RB=1.57 RE=2.75 IKF=0.28
```

```
ISE=0.36E-13 TF=0.111N TR=8N ITF=0.82E-01 VTF=0.66E+01 CJC=3P CJE=2P
```

```
XTI=3.0 NE=1.5 ISC=0.12E-13 EG=1.11 XTB=1.5 BR=1.14 VJC=0.75 VJE=0.75
```

```
IS=0.40E-14 MJC=0.33 MJE=0.33 XTF=4 IKR=0.28 KF=1F NC=1.7 FC=0.5 RBM=1.1
```

```
IRB=0.40E-01 XCJC=0.5 MFG=MOTOROLA)
```



Several comments about SPICE models are important:

1. SPICE models for the same part can differ quite strongly between different manufacturers. This is acceptable as long as datasheet values are honored. It shows, however, that SPICE models will not have a pinpoint accuracy.
2. SPICE models are pessimistic in some respects, to keep the manufacturer out of guarantee issues. This definitely applies to breakdown voltages.
3. Some SPICE models are optimized for specified bias conditions (see, e.g., the 2N3866 example above). This implies that large signal behavior might not be exactly modelled.
4. Noise parameters are not always completely specified (KF, AF), and they are correct only for a specific bias situation.
5. Base emitter breakdown is missing from all SPICE models above. A separate chapter will explain how SPICE can be enhanced to include this effect.
6. The same goes for collector breakdown. For our purposes, this is less critical because in the usual oscillator core circuits this limit is not even approached, opposed to BE breakdown.
7. The parameter values usually come from an automatic extraction and curve-fitting process involving a large number of transistor DUTs. In the interest of a good fit of observable quantities like collector, emitter, and base current some parameters can take implausible values (e.g., VAF=240 for the 2N3866). This is normal.

## References

- [1] Microchip Corp., “Microchip Space Forum.” Accessed: Nov. 21, 2020. [Online]. Available: <https://ww1.microchip.com/downloads/en/DeviceDoc/Microchip-Space-Forum-2019-Frequency-and-Timing-09-03-%20Stewart%20Hampton.pdf>.
- [2] RIAC, “Electronic Parts Reliability Data 2014.” Accessed: Nov. 21, 2020. [Online]. Available: <https://www.quanterion.com/wp-content/uploads/2015/09/Front-Material-for-PDF-Viewer-EPRD.pdf>.
- [3] NASA, “NASA Parts Selection List.” Mar. 1998, Accessed: Nov. 21, 2020. [Online]. Available: [https://nepp.nasa.gov/npsl/semicond/transistor/lp\\_npt.htm](https://nepp.nasa.gov/npsl/semicond/transistor/lp_npt.htm).
- [4] Microsemi Inc., “2N2222A Datasheet.” Accessed: Nov. 21, 2020. [Online]. Available: <https://www.microsemi.com/existing-parts/parts/44797#resources>.
- [5] On Semiconductor, “2N2222A Small Signal Switching Transistor Datasheet.” Accessed: Nov. 21, 2020. [Online]. Available: <https://www.onsemi.com/pub/Collateral/2N2222A-D.PDF>.
- [6] Anisha Apte, “A New Analytical Design Method of Ultra-low-noise Voltage Controlled VHF Crystal Oscillators and it’s Validation,” TU Cottbus, Cottbus, 2020.
- [7] Iulian Rosu, “Very Low Phase Noise Vackar VFO for HF Transceivers.” Accessed: Nov. 21, 2020. [Online]. Available: [https://www.qsl.net/va3iul/Very\\_Low\\_Phase\\_Noise\\_VFO/Very\\_Low\\_Phase\\_Noise\\_Vackar\\_VFO.pdf](https://www.qsl.net/va3iul/Very_Low_Phase_Noise_VFO/Very_Low_Phase_Noise_Vackar_VFO.pdf)

## 22 Appendix M: Vibrations

The key element of the setup is the “Buttkicker” at the lower right. It is a powerful electromagnet accelerating a piston with a mass of 1.5kg [2]. Its normal use is to simulate earthquakes in discotheques that are synchronized with heavy metal music. It can take 400W of RMS power (thermally protected) and its frequency range spans from 2Hz to 2kHz. If your workbench is intended to survive power should be limited to below 20W, which is good enough for accelerations of more than 1g.

Buttkicker did not disclose spring constants or other mechanical data. We can nevertheless assume that the vibrator consists of two parts (this was confirmed by a teardown carried out and documented on the web):

1. An inner part (piston) that moves in a magnetic field. It is held in place by an inner spring
2. An outer part (case) that contains a holder and a coil in which the inner part moves

The vibrator unit sits on top of a spring which is needed to isolate the vibrations from the lab surroundings, especially from the extremely sensitive FSWP phase noise analyzer. For practical reasons, this spring is implemented as a balloon made from Silicone (explained later).

### SOME PHYSICS OF THE VIBRATOR

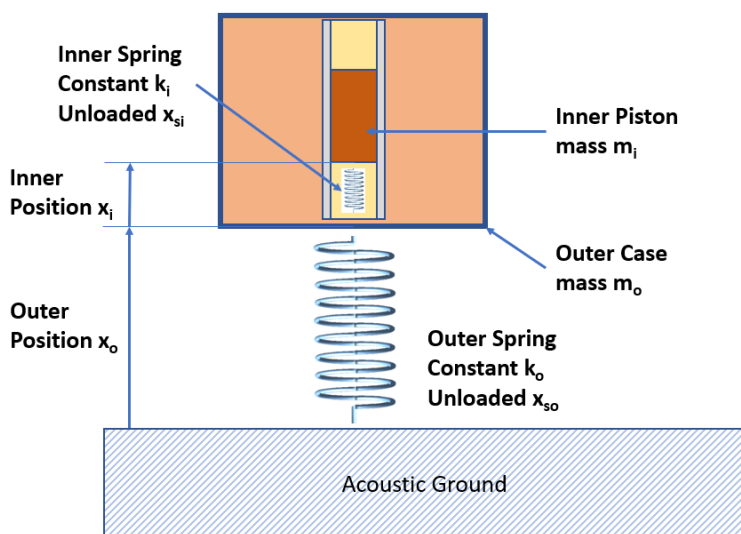


Figure 260 - Buttkicker Vibrator Mechanical Setup

If we describe the system in mathematical terms, we have (for the equilibrium case without any external current)

$$m_i x_i'' = -m_i g - k_i (x_i - x_{si}) = 0$$

Where

$x_i$  is the position of the inner part relative to the outer one

$m_i$  is the mass of the inner part

$g$  is the gravitational constant ( $9.81 \text{ m/s}^2$ )

$k_i$  is the spring constant of the inner spring

$x_{si}$  is the no-force length of the inner spring.

For the outer spring we have

$$m_o x_o'' = -(m_i + m_o)g - k_o(x_o - x_{so}) = 0$$

Where the symbols mean the same as in the last formula, only for the outer part. We have left friction out of consideration for the moment, so there are no single derivatives of  $x$ .

We could solve these equations to obtain the equilibrium positions of the case and the piston.

If we apply current to the vibrator coil, a magnetic force between the case and the piston will move the piston inside the case. This force can be assumed to be proportional to the current applied for a small signal case.<sup>16</sup> The force caused by current flow acts on the piston and case with opposing sign, but it does *not* change the center of gravity of the complete device (case plus piston).

Including the magnetic force, we get

$$m_o x_o'' = -(m_i + m_o)g - k_o(x_o - x_{so}) = pI$$

Where

$p$  is the proportionality factor from force over current and

$I$  is the current in Amps.

Rearranging gives a classic linear 2<sup>nd</sup> order differential equation of the frictionless, linear, driven harmonic oscillator:

$$x_o'' + \frac{k_o}{m_o} x_o + \frac{1}{m_o} (m_i + m_o)g - \frac{k_o}{m_o} x_{so} = \frac{p}{m_o} I$$

The resonance frequency is computed by

$$\omega_0 = \sqrt{\frac{k_o}{m_o}}$$

To make a reality check we can try some vibrator datasheet values and an observation about the spring constant:

$k_o$  is 10<sup>3</sup>N/m, equals ca. 1kp of force for 1cm of compression, and

$m_o$  is 3.5kg (plus the weight of the platform and the OCXO).

So, we end up with a resonance frequency of

$$f_0 = \frac{1}{2\pi} \sqrt{\frac{1000}{3.5}} = ca. 2.7Hz$$

---

<sup>16</sup> This has limits when the piston reaches an endpoint within the case and when the piston moves so far out of the coil that the magnetic field is no longer applying to all of the piston length. This problem is a known source of nonlinearity from loudspeaker design.

Above this frequency our vibrator and spring arrangement has a lowpass characteristic for the external excitation. This is most welcome, because the frequency band of interest for OCXO vibration tests should be free of resonances coming from the measurement apparatus itself. Practical tests have shown that everything is running very smooth starting from ca. 15Hz.

The dependency of the amplitude of  $X_o$  on the frequency  $\omega$  of excitation has the form

$$x_o \sim \frac{pI}{(\omega^2 - \omega_0^2)}$$

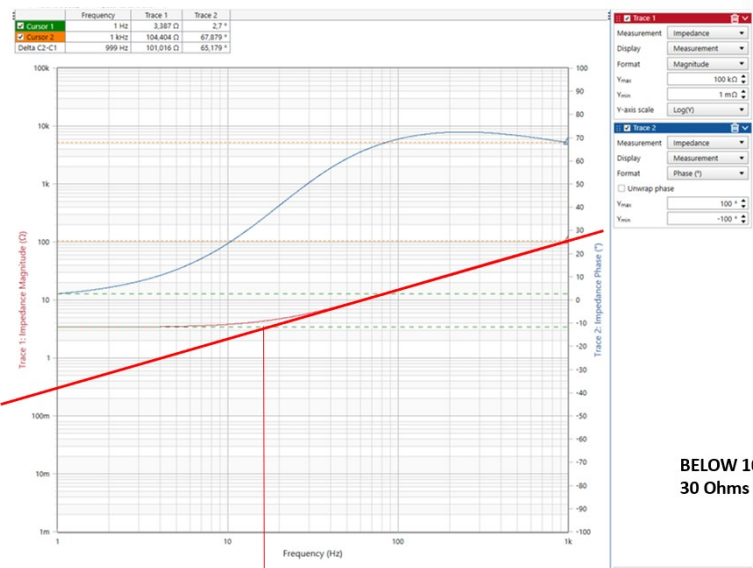
And for the acceleration we have

$$x''_o \sim \frac{\omega^2 pI}{(\omega^2 - \omega_0^2)}$$

For frequencies considerably larger than the resonance, the acceleration becomes a constant.

Impedance measurements using a Bode100 [4] low frequency vector network analyzer (ranges from 1Hz to 50MHz) were performed. The results are shown below:

**FSWP MEASURING MICROPHONIC OSCILLATORS – THE BUTTKICKER IMPEDANCE**



**BELOW 10 Ohms up to 60Hz  
30 Ohms @ 200Hz**

**Equivalent RL Series Circuit:  
R = 3.3Ohms  
L = 16mH**

**CONCLUSION:** Works fine with Audio Amp up to 50-60Hz. Above we need higher drive voltage to generate significant power. Might be still enough to shake OCXOs.

*Figure 261 - Buttkicker Impedance over Frequency*

We see a 3.3Ohms ohmic coil resistance in series with a 16mH inductance.

The next component we need is a power amplifier. An integrated part, the TDA2050A [5] power IC normally used as an audio final amplifier for 50W was used. The schematics is shown below:

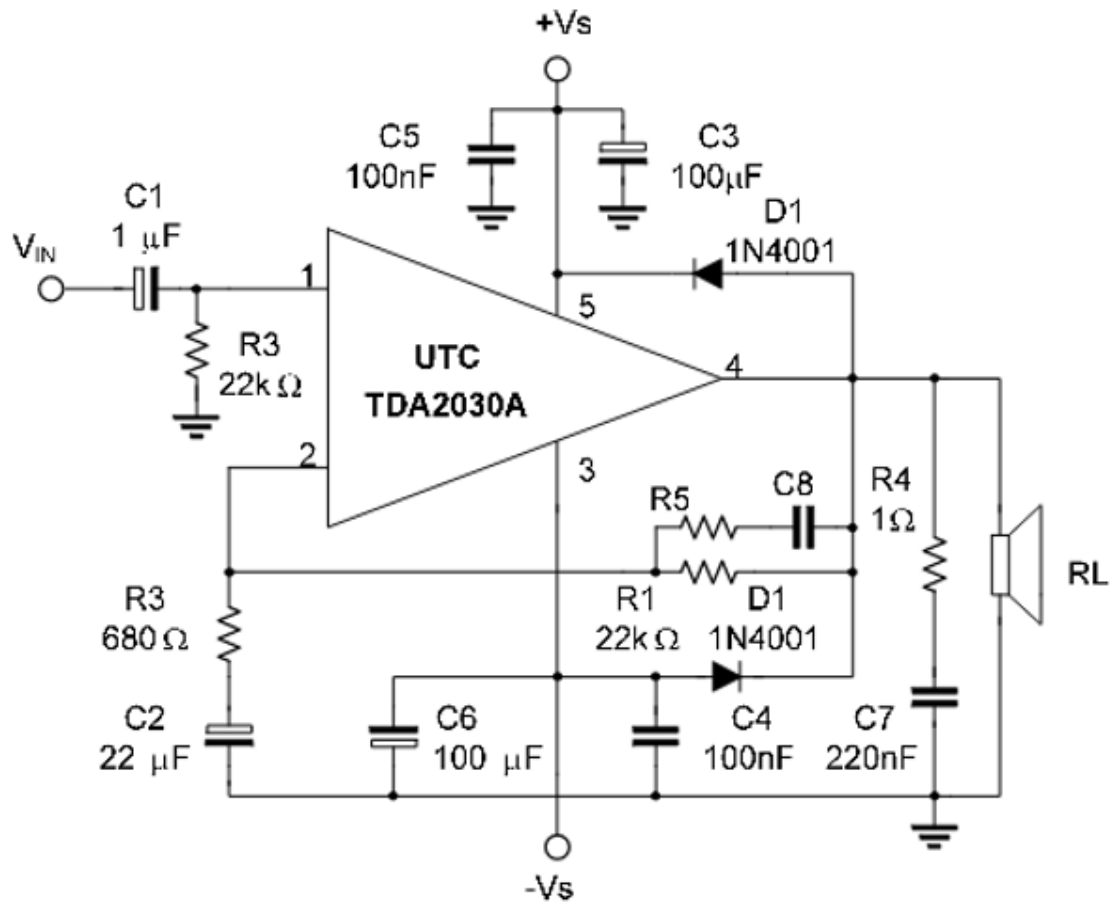


Figure 262 - The Power Amplifier Driving the Buttkicker (TDA2050A was used instead of TDA2030A in Picture)  
Picture from TDA2030 Datasheet [5]

The circuit is a 1:1 implementation of the TDA2050A datasheet, but with a unipolar power supply and substantially increased coupling capacitors to accommodate a 2-3Hz lower frequency limit. The TDA2050A has all kinds of SOAR and thermal protections, but the considerable inductance (and associated stored energy) of the Buttkicker is still a challenge when pulse tests are performed. The D1 diodes in the circuit above try to dump voltage spikes into the supply rails.

After killing its predecessor, the 30W TDA2030A in action, we upgraded to the TDA2050A and built a special power supply that delivers short, high amperage pulses, but limits the average current drain to safe values. The schematics is shown below:

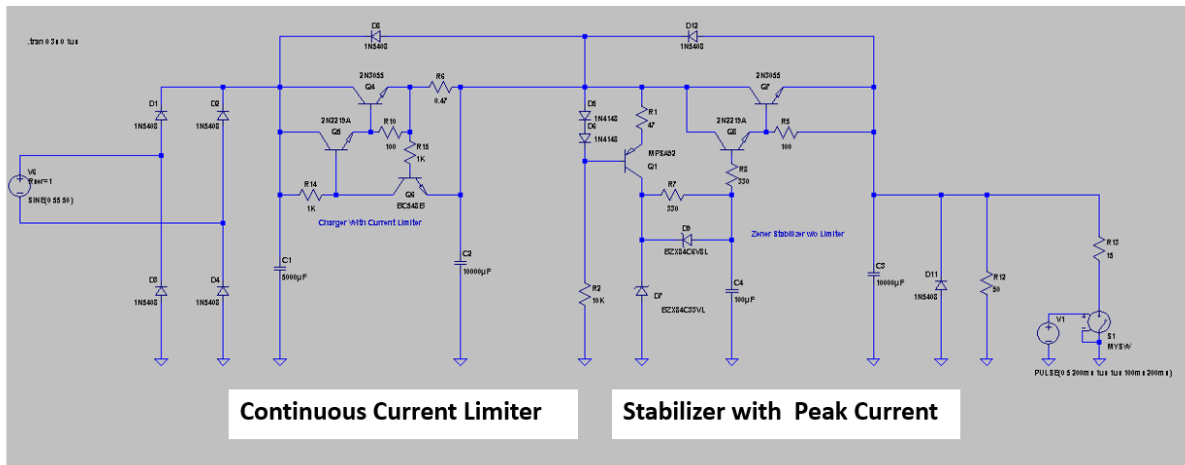


Figure 263 - Pulse Enabled Power Supply to Drive the Buttkicker Amplifier

The continuous limiter can be seen on the left, and the stabilizer with a much higher current limit on the right. The maximum energy this power supply can provide is contained in the capacitor in the middle between the two parts. The upgraded amplifier and power supply have survived all pulse tests so far.

## 22.1 The Acceleration Sensor

We have covered how the vibrations can be generated, now we must also measure them accurately. The method of choice today is to use MEMS (micromechanical systems) technology, like applied in the ADXL203 [6] 2-axis acceleration sensor. The part with key features is shown below:



### ANALOG DEVICES ADXL203 SENSOR 2 AXIS 1.7g

1. 5V OPERATION
2. CENTERED OUTPUTS (2.5V)
3. SENSITIVE – 1V/g
4. LOW NOISE (1mV)
5. ROBUST (3500g)
6. NO LF LIMIT – CAN BE USED AS A POSITION/TILT SENSOR

Figure 264 - ADXL203 MEMS Acceleration Sensor  
Picture from Analog Devices [5]

The physical principle of a MEMS acceleration sensor is the change of capacitances due to a displacement of the capacitor plates, induced by an acceleration force, shown here:

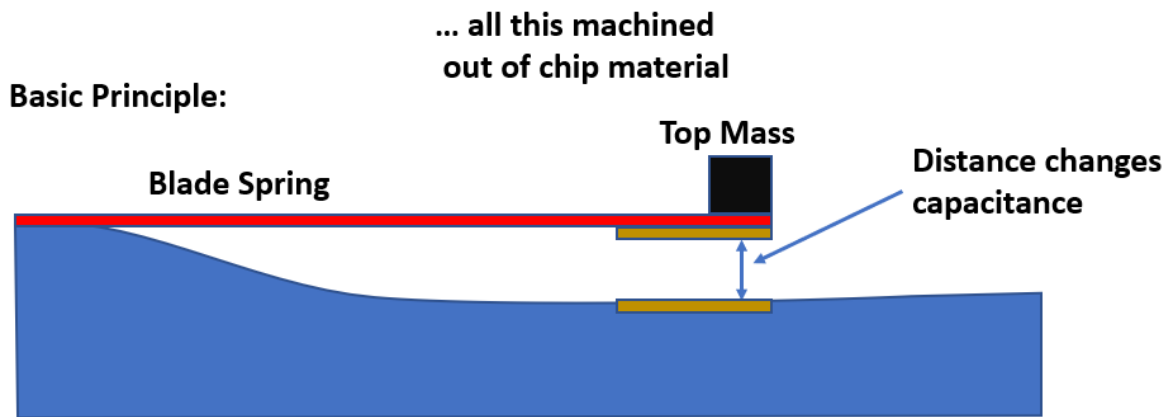


Figure 265 - MEMS Principle of Operation

The capacitance changes inversely proportional to the distance between the two electrodes. The dielectric used is normally air with a relative dielectric constant close to 1.

Modern chip technology can integrate large capacitances even in a small chip area by creating multiple capacitors and springs using etching processes, as this electron microscope photo shows:

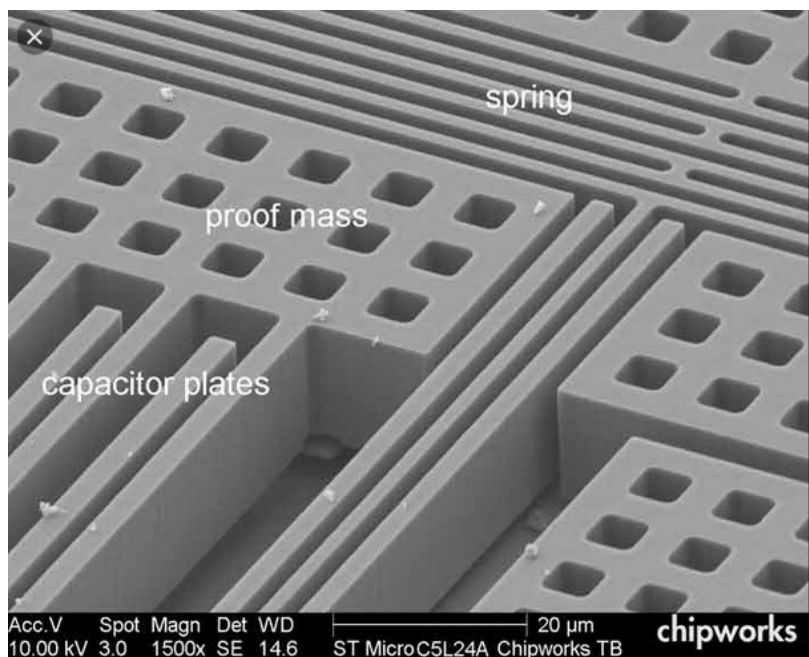


Figure 266 - Detail of the Sensor Area of a MEMS Chip  
Picture from [www.C2MI.com](http://www.C2MI.com)

The ADXL203 has internal oscillators that change their frequency when their controlling capacitances change. These frequency changes are demodulated into amplitude changes that can be processed by external circuits. The ADXL203 prefabricated sensor PCB is optimized for a 50Hz frequency limit. We need about 500Hz, so the default low-pass capacitors were changed to allow 500Hz. The sensor PCB was mounted on a solid Aluminum block securely attached to the base plate of the vibrator:



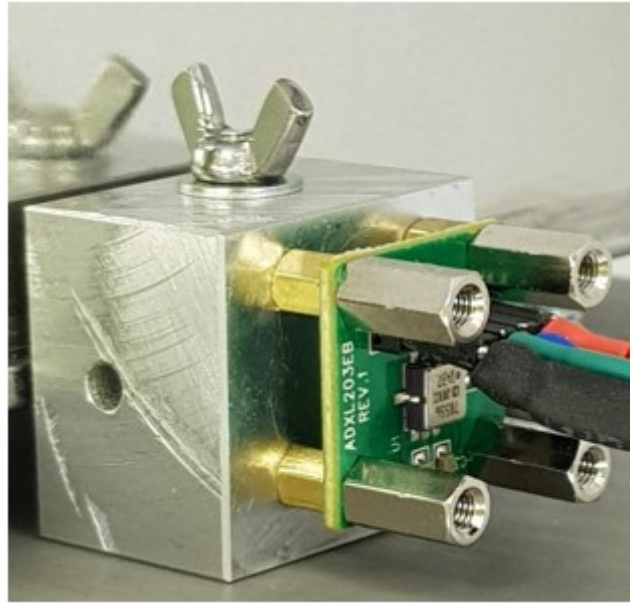


Figure 267 - ADXL203 Sensor Mounted on Aluminum Block

The key issue is that the vibrations from the plate should reach the sensor without further damping or resonances, making a very rigid mounting scheme necessary.

## 22.2 The Acceleration Sensor Postprocessing Amplifier

The output signal of the ADXL203 is centered around half its supply voltage and, due to the higher bandwidth, is still carrying some RF from the ADXL203's internal oscillators. A postprocessing amplifier sets the output level to 0V, using a split power supply. The circuit is shown here:

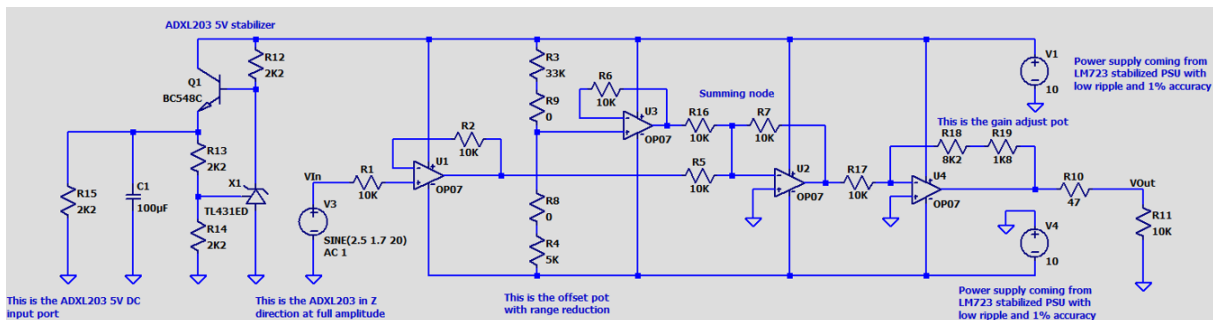


Figure 268 - Acceleration Sensor Postprocessing Amplifier and Filter

The amplifier is made from standard LM324 [7] op amps (due to the high noise level of the ADXL203 no premium op-amp is needed) The mid-supply zero level of the ADXL203 is shifted to a zero-output using a 10-turn pot.

The ADXL is powered from a dedicated regulator to prevent feedback via insufficient PSRR effects.



### 22.3 Damping

It is a critical requirement is that the vibrations should be confined to the test apparatus and not be propagated outside. The FSWP phase noise analyzer itself is quite sensitive to vibrations, so a coupling of the FSWP to the vibration measurement apparatus must be prevented. In the frequency spectrum intended (ca. 10Hz to 200Hz), this is a surprisingly complex requirement. At the very low end, classic damping materials like foam have limited efficiency, and at higher frequencies resonances could be disturbing.

The approach taken was as follows:

Directly following the vibrator, we need a “spring” with the following characteristics:

1. Suitable spring constant
2. Very low mass (so the change of spring COG does not propagate the vibrations)
3. No resonances (high damping)

A Silicone gymnastics ball worked very well here, it was suitably flexible, exceptionally light and absorbed higher frequency sound very well.

The fitting of the ball on a flexible layer over a sand filled tank provided another acoustic lowpass to the bottom of the test container.

Higher frequency resonances of the test container were taken care of by anti-drumming foils placed on all metal surfaces.

The key idea behind the different damping measures taken is a mixture between acoustic dissipation and acoustic impedance mismatch. Acoustic impedance is the product of the density of a material multiplied by the speed of sound in it. The Butt kicker is made of solid Aluminum, the gymnastics ball is made from Silicone rubber. The speed of sound is vastly different in both media (Al: 5km/s, Air 340m/s), plus the density is very different as well, causing a poor transfer of vibrational energy from the Butt kicker into the ball. Similar considerations apply to the rest of the damping methods applied.

A picture of the complete setup is shown below:



*Figure 269 - The Complete Vibration Test Setup - Mechanical Part*

The box on top is the USO under test. All connections (supply, RF out) are made using quality, but flexible coaxial cables fed through foam buffer sleeves, so they do not transfer vibrations to the outer stainless-steel drum. The solid (1cm thick) Aluminum plate below the DUT is attached to the ButtKicker (black part below the plate). Rubber straps keep the plate in place and make sure the plate only vibrates in z direction (up and down). The blue ball supports the Buttkicker and effectively isolates the vibrations and shocks generated from the surroundings. The ball sits on a layer of Styrofoam, which in turn is supported by a canister filled with 10kg of fine sand to suppress resonances. The inside of the stainless-steel drum is covered with car anti-drumming foil.

The device above is working very well. If you create pulses or sinusoidal acceleration does not matter. The residual vibrations are hardly detectable when you put your hand on the desk next to the drum, and, more important, they are not detectable at the desk where the FSWP (which is microphonic itself) is located.

## 22.4 Modeling the Vibration Setup

The complete system is a rather complex electromechanics arrangement that must be modelled in steps. With not all physical parameters available (e.g., from the Buttkicker the manufacturer did not want to disclose magnetic and mechanic internals), it makes sense to measure the components and to extract a reliable model.

We have the following components to take into account:

**The amplifier.** This, electrically, is a high pass with a corner frequency determined by the large electrolytic coupling capacitors (15mF) and the Butt kicker DC resistance of 30hms, giving 3.2Hz. The equation for the frequency response of the amplifier is

$$V_{out} = A V_{in} \frac{\omega RC}{\sqrt{1 + (\omega RC)^2}}$$

The upper frequency limit of the amplifier is so high (10s of kHz) that it can be ignored here (we only measure to 500Hz). A stands for the amplification factor of the amplifier (determined by R<sub>5</sub> and R<sub>4</sub> in the amplifier schematics).

**The Butt kicker** converts current into acceleration. First, we have an RL circuit to take into account, then we have an acceleration proportional to the current, plus a mass to accelerate, so two components. The balloon serves as a spring in this component, and we have a damping component as well. For the RL lowpass we have (L being 16mH and R equals 30hms):

$$I_{BK} = V_{out} \frac{1}{\sqrt{R^2 + (\omega L)^2}}$$

And for the spring/mass system we have:

$$A = \frac{pI}{m} \frac{1}{\sqrt{(\omega_0^2 - \omega^2)^2 + (2\zeta\omega)^2}}$$

Where A stands for the acceleration, p stands for the electromechanics coupling constant, m stands for the mass, and  $\omega_0$  stands for the resonant frequency of the mass/spring system.  $\zeta$  stands for the damping factor.

**The last part is the acceleration sensor.** This converts the acceleration detected into a noisy output voltage, that is low pass filtered with a bandwidth of 500Hz (32K resistance, 10nF capacitance). The transfer function we may expect is a lowpass with a corner frequency of 500Hz. The self-resonance of the ADXL203 is 5kHz, so it can be ignored. For our measurements to just 200Hz, the frequency response of the ADXL203 can be considered to be flat from DC. The maximum measurable g range of the ADXL203 is +/- 1.7g, but this includes static gravity. In the direction where gravity is applied, they just have another 0.7g that can be measured in addition. The 1.7g are no destruction limit (that is 3500g, beyond any practical acceleration that can happen during our measurements).

## 22.5 Determining Physical Parameters

As a next step, we can try to determine the missing quantities in our formulas by using a pulse and then determining the response and its time constants. We do this by using a short current peak and then look at a (probably) exponential decay as a damped mass/spring system should show.

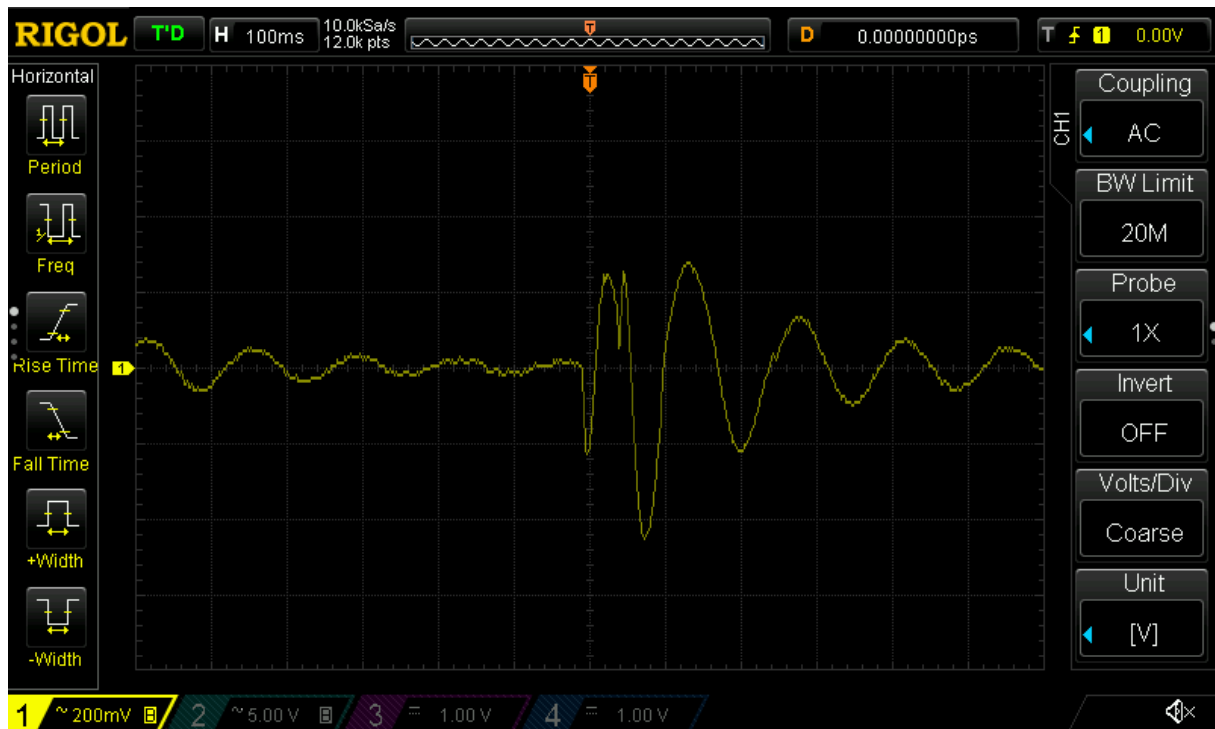


Figure 270 - Acceleration Sensor Output for a Pulse Current

The right part of the screen looks like what we are looking for. Close to the pulse itself, we see some nonlinear behavior (probably the piston moved out of the coil too much). Recording an analyzing the waveform from the 3<sup>rd</sup> zero transition after trigger seems to be linear enough.

We can now use curve fitting to extract the self-resonance frequency and the damping factor:

**HOW TO EXTRACT THE PHYSICAL PROPERTIES OF THE WHOLE SETUP – MATH CURRENT TO ACCELERATION**

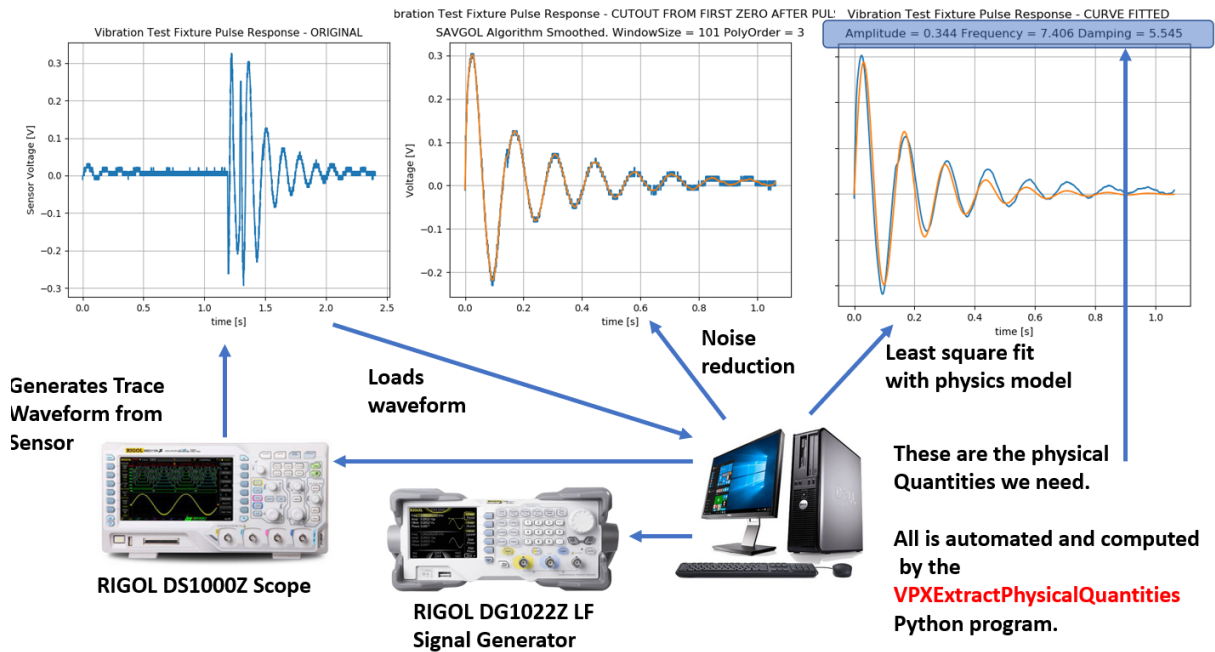


Figure 271 - Vibration Parameter Extraction Method

The instruments used (amplifiers not shown) are a function generator to create the pulse, the measurement setup as discussed, a scope to record the response, and a Python program, doing the math. As shown in the leftmost curve above, the agreement between the simulated waveform using the fitted parameters  $A$ ,  $\omega_0$  and  $\zeta$  is quite good.

The Python program makes use of the Savitzky-Savgol [10] smoothing algorithm to remove the noise and residual RF of the ADXL203. To see why smoothing is needed the picture below shows the raw accelerator signal output (acceleration output signal is in yellow):

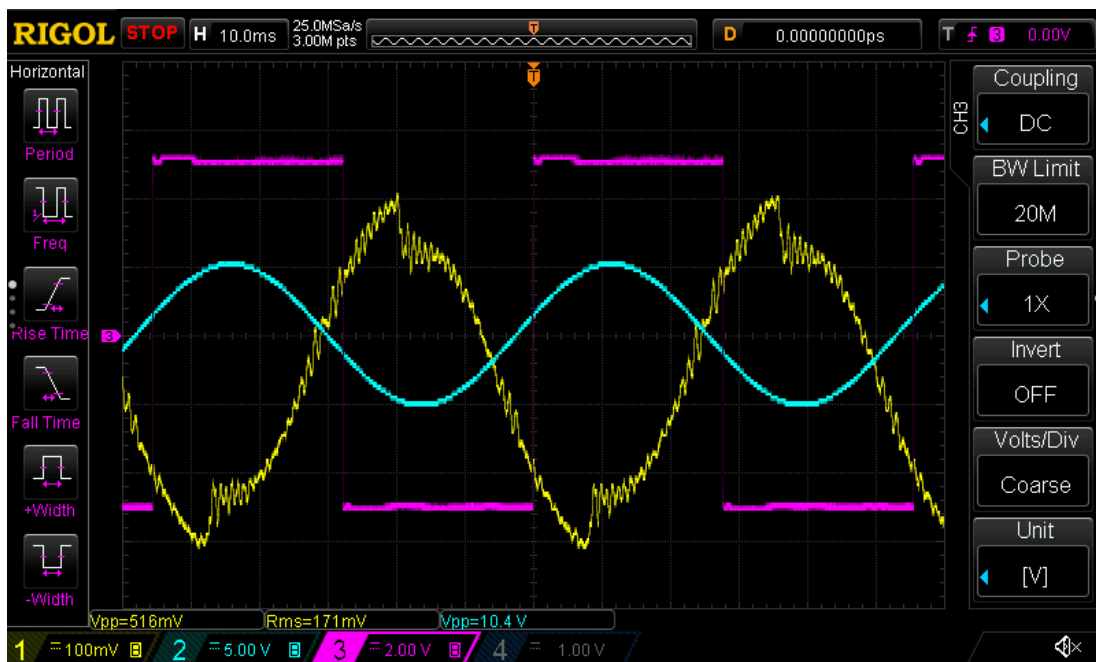


Figure 272 - ADXL203 Output Signal Including RF Leakage and Noise. The pink signal is the driver of the Butt kicker amplifier input, and the cyan trace is an artificial, phase and frequency synchronous trigger signal because triggering on the yellow trace is very unstable due to the noise.

After determining the spring/mass system parameters, we could try to extract the frequency response of the whole setup. This was done using a sweep from 5.5Hz (above self-resonance) to 200Hz at an amplitude of 0.5Vpp at the driver amplifier input. That should guarantee operation in the linear range. The test run output is shown below:

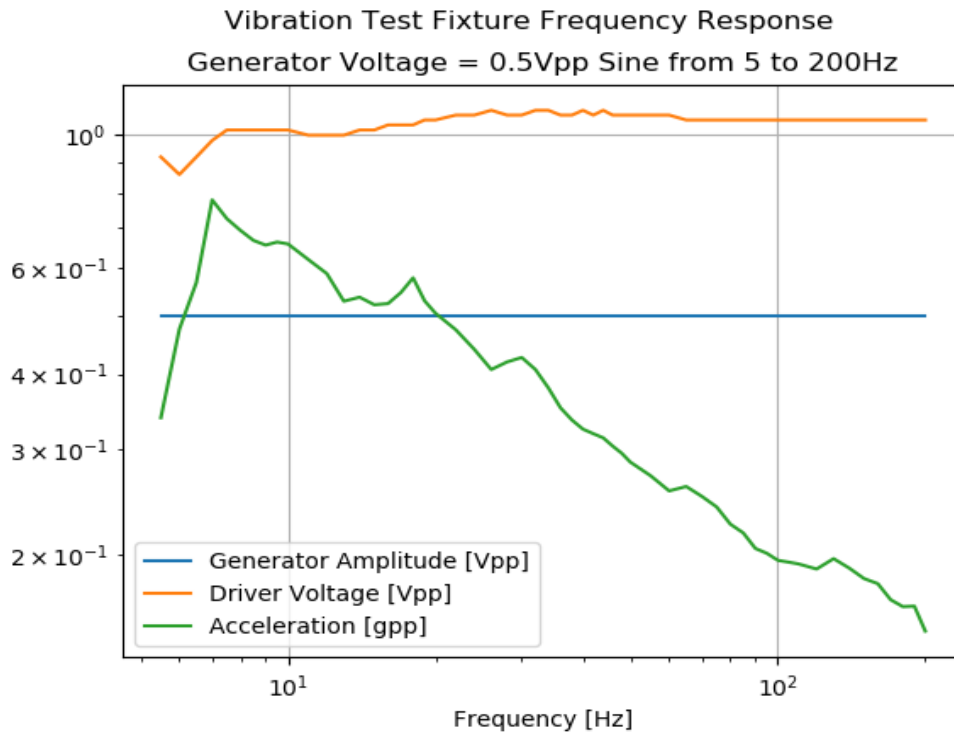


Figure 273 - Generator Amplitude, Driver Voltage and Acceleration over Frequency

The generator amplitude (blue) is kept constant by the signal generators ALC mechanism. The driver output voltage (yellow) increases slightly because of the rising input impedance of the Buttkicker's RL circuit. Acceleration (green) first rises (due to the finite coupling caps), then drops approximately linear as expected.

We could now extract a conversion gain from input to measured acceleration. The plot can be seen here:

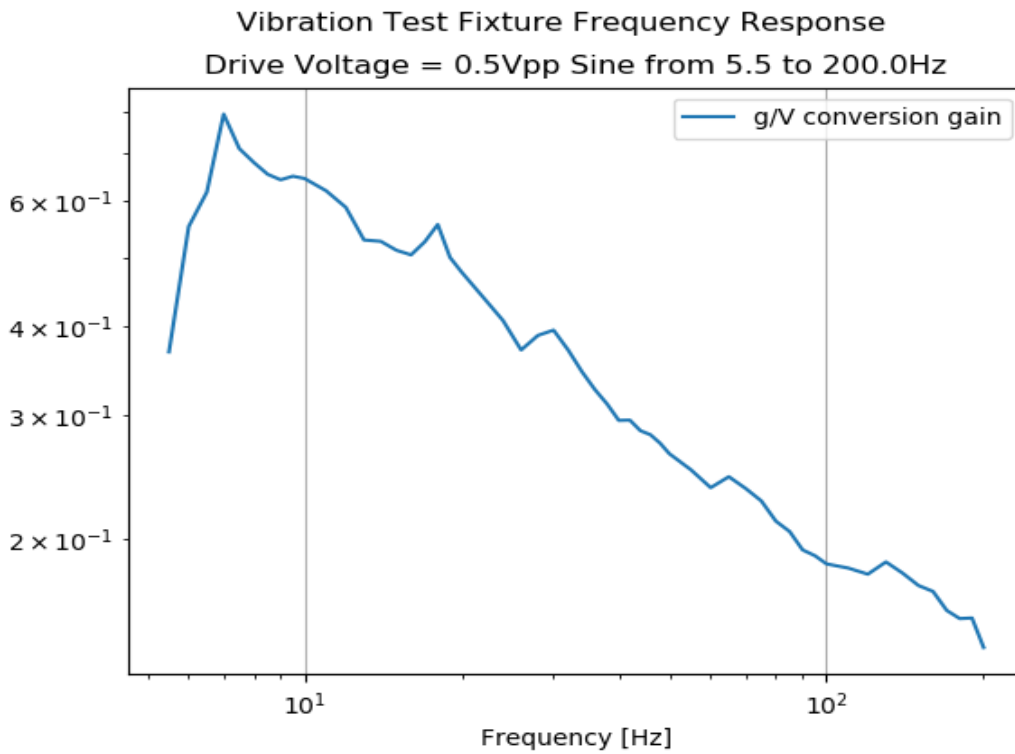


Figure 274 - Measured Conversion Gain in g/V over frequency

As expected, the gain drops with increasing frequency. Curve fitting this with the gain using the extracted parameters shows a usable fit at lower frequencies:

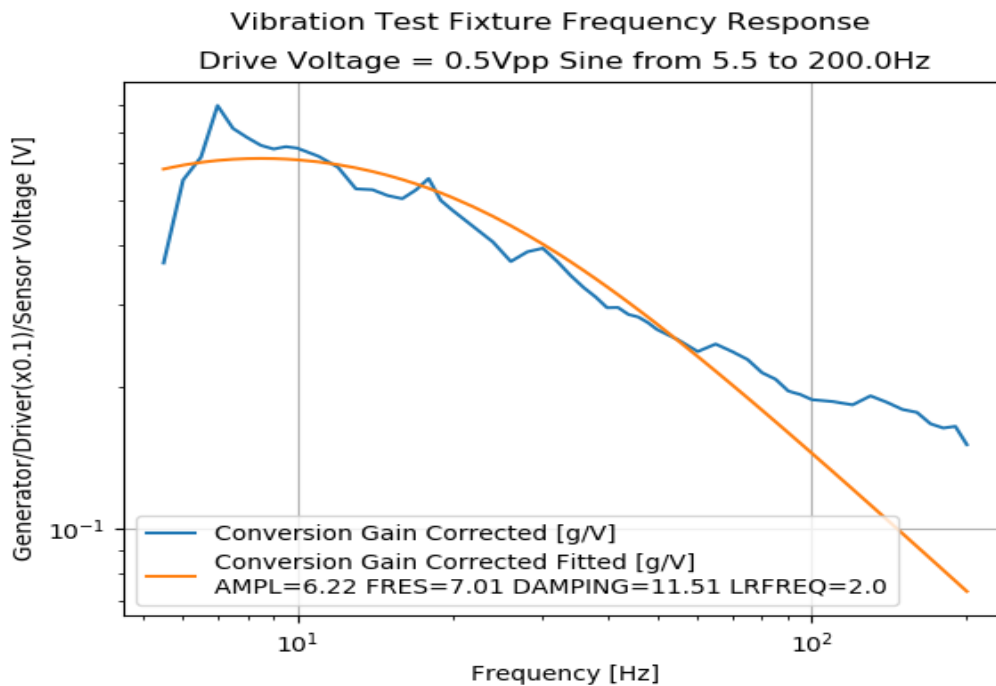


Figure 275 - Curve Fitted Conversion Gain

The fit usable up to ca. 100Hz. The reason for the bad match beyond is the large RF and noise level generated by the ADXL203.

## 22.6 Vibration Measurements of Commercial OCXOs

We can now apply our test environment on well-known commercial oscillators and see how their phase noise changes. First, the Morion MV89 [8] DOCXO at 10MHz, subjected to a 0.8g sinusoidal vibration in vertical direction at 20Hz:

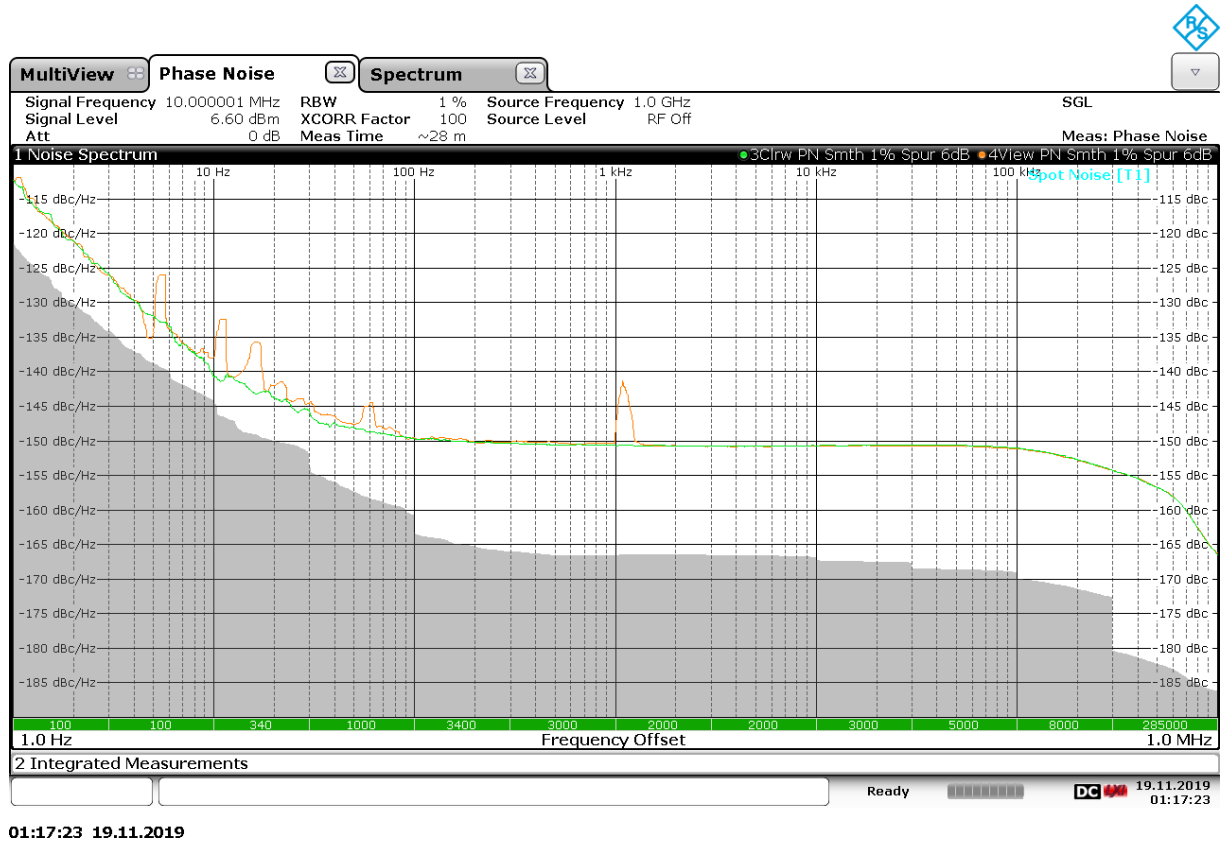


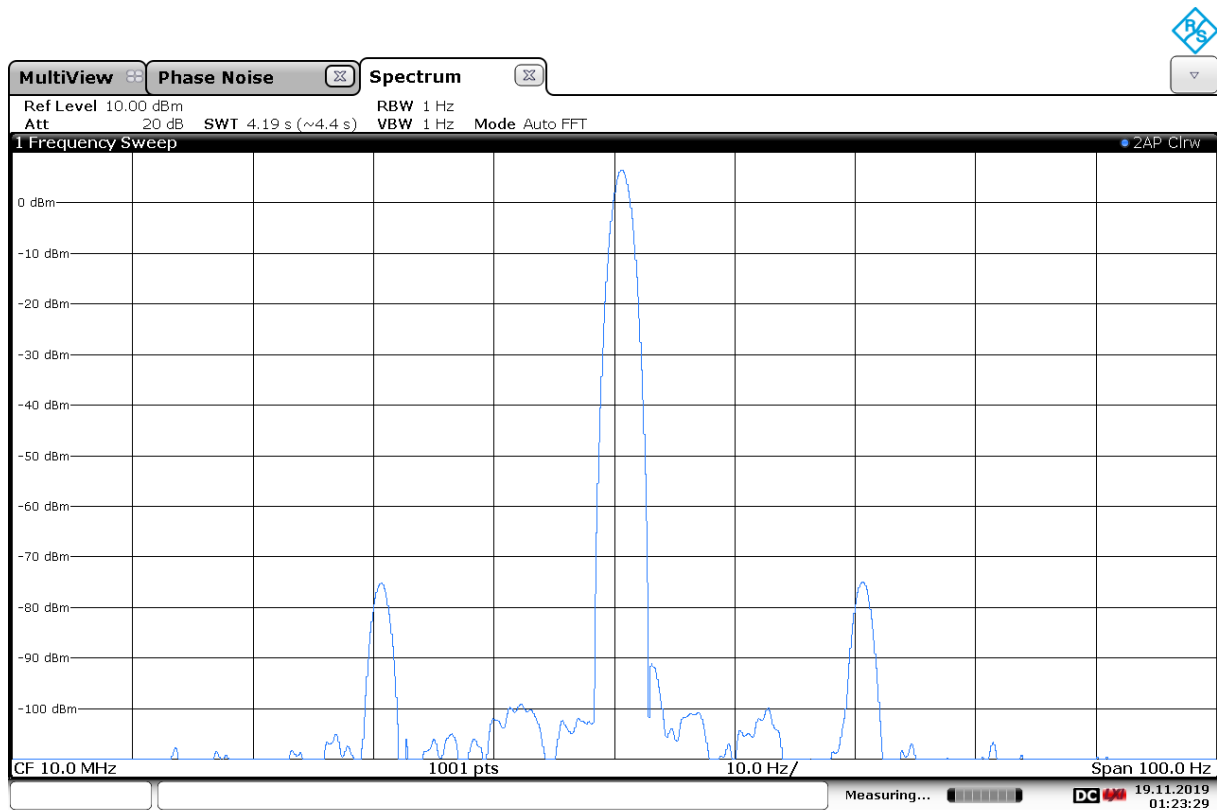
Figure 276 - Morion MV89 Phase Noise Subjected to a 0.8g 20Hz Vertical Sinusoidal Vibration

We see several, 10dB peaks (red) compared to the relatively smooth (green) phase noise curve. The peaks below 100Hz are clearly caused by the acceleration. The 1kHz peak could be an internal mechanical resonance of the MV89 trigger from the vibration, but this is a speculation only.

The MV89 is a lab OCXO with no brilliant phase noise, but an extremely low aging rate.



As a sanity check, we could analyze the output spectrum under vibration loads:



01:23:29 19.11.2019

Figure 277 - Output Spectrum of a MV89 OCXO with Vibration Induced Sidelobes

No surprise here, the 20Hz vibration offset signals are clearly visible at ca. -80dBc.

The phase noise and spectral measurements were repeated for several other commercial OCXOs with similar results (not all shown).

Another important test is the reaction of an OCXO to a shock-like pulse acceleration. To measure that, a pulse from  $-0.8g$  to  $+0.4g$  every second (pulse duration was 10ms) was used. The effect on phase noise was dramatic (MV89 used again):

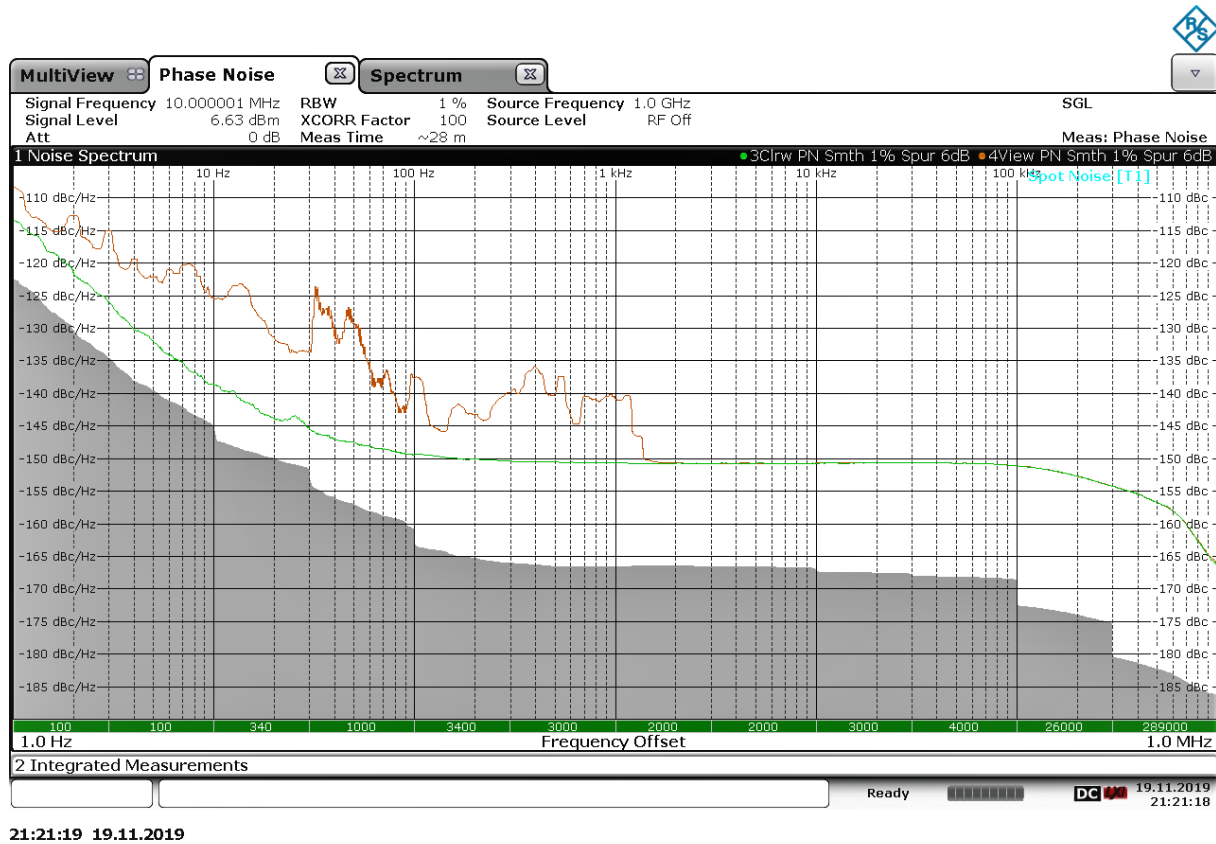


Figure 278 - MV89 Phase Noise under Pulse Acceleration Conditions

The deterioration of phase noise is up to 20dB and not confined to a few spikes. It should be noted that the acceleration applied is below the maximum values in the MV89 datasheet [8]. The conclusion for the MV89 that it is a good and long-term stable lab OCXO, but it needs a quiet place to perform well.

Bernd Neubig from AXTAL was so kind to provide me with crystals that were constructed to be insensitive to vibrations (AXIOM 100MHz, [9]). These 100MHz crystals performed considerably better than classic parts, as the phase noise curve (same conditions as the 20Hz Morion test) shows:

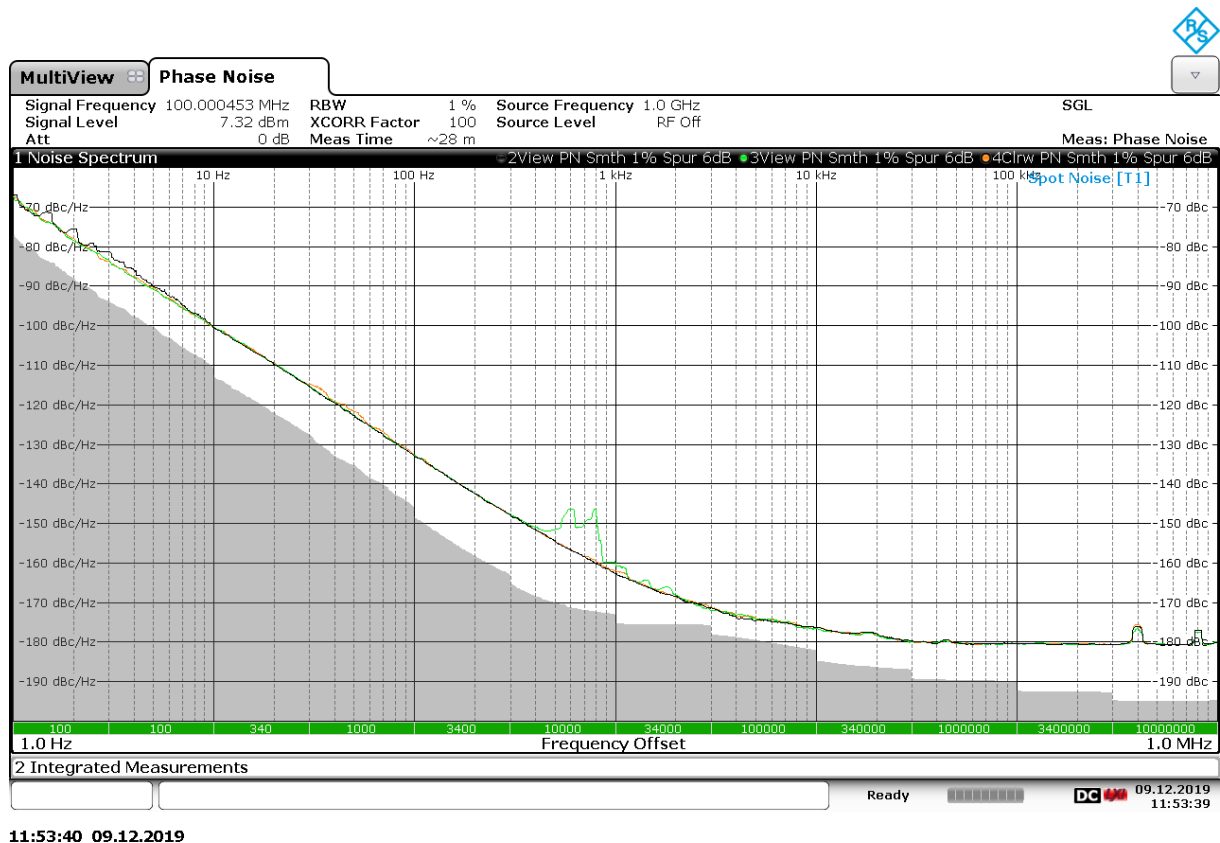


Figure 279 - AXTAL Axiom Vibration-Insensitive Oscillator Phase Noise under Vibration (0.8g/20Hz, Vertical Sinusoidal)

The differences between vibration on and off below 500Hz is very small indeed. There seems to be some resonance between 600Hz and 1kHz where the noise level rises by ca. 10dB. This part could be used for space missions, from a vibration point of view.

## 22.7 Random Vibrations

The assumption of a sinusoidal or strictly repetitive pulse acceleration is practical for measurements but is not very realistic in a space environment. A lot of different acceleration sources like motors, thrusters, valves with fluids flowing through them, positioners (stepper motors) for sun sails and instruments, ...) create an unpredictable and probably broadband background of acceleration amplitudes. What we should therefore measure is the behavior of our oscillators subjected to a random acceleration spectrum.

Just feeding the driver amplifier with a noise signal is no good idea, for the following reasons:

1. We need to level the acceleration, not the input voltage.
2. The acceleration must be bandwidth limited to make useful measurements

The procedure to create a white acceleration spectrum involves the following steps:

1. First, we create a random sequence with a white spectrum for, say, 100s.
2. Next, we create a Fourier transform of this signal creating a more or less flat spectrum.
3. We multiply the spectrum by the inverse transfer gain curve measured before.
4. We limit the bandwidth to the maximum we need and renormalize the amplitude
5. Last, we transform this signal back into the time domain and load it into an arbitrary waveform generator. This signal is then fed into the driver amplifier.

The whole process is illustrated below:

**HOW TO EXTRACT THE PHYSICAL PROPERTIES OF THE WHOLE SETUP – NOISE MEASUREMENTS 2**

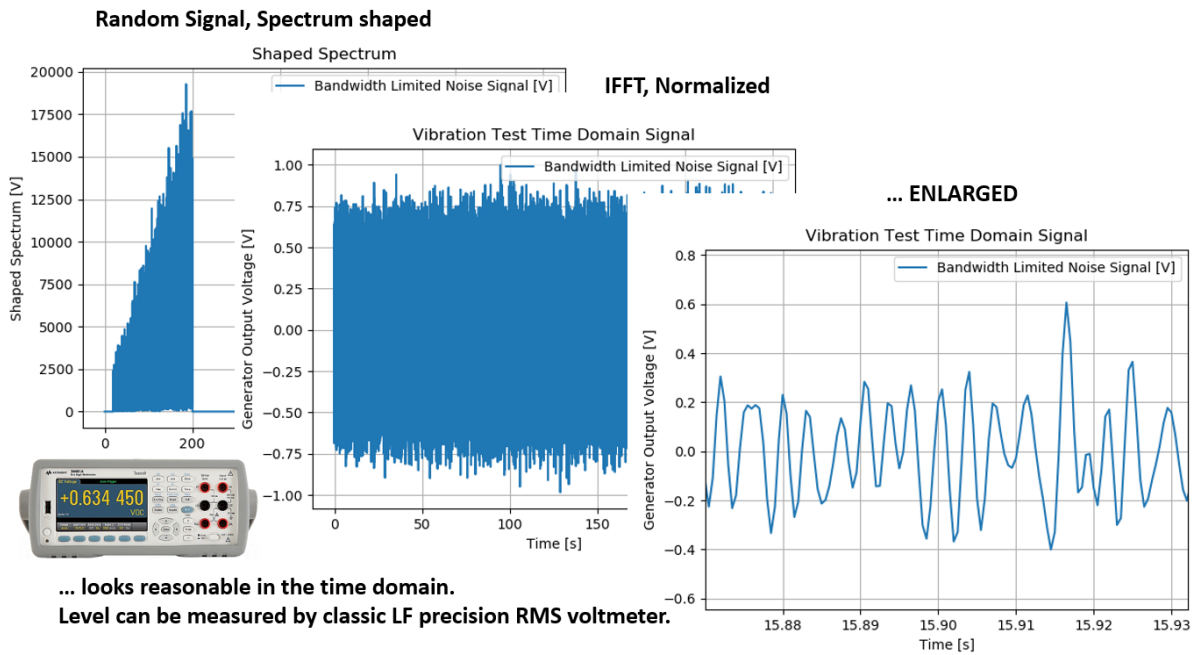
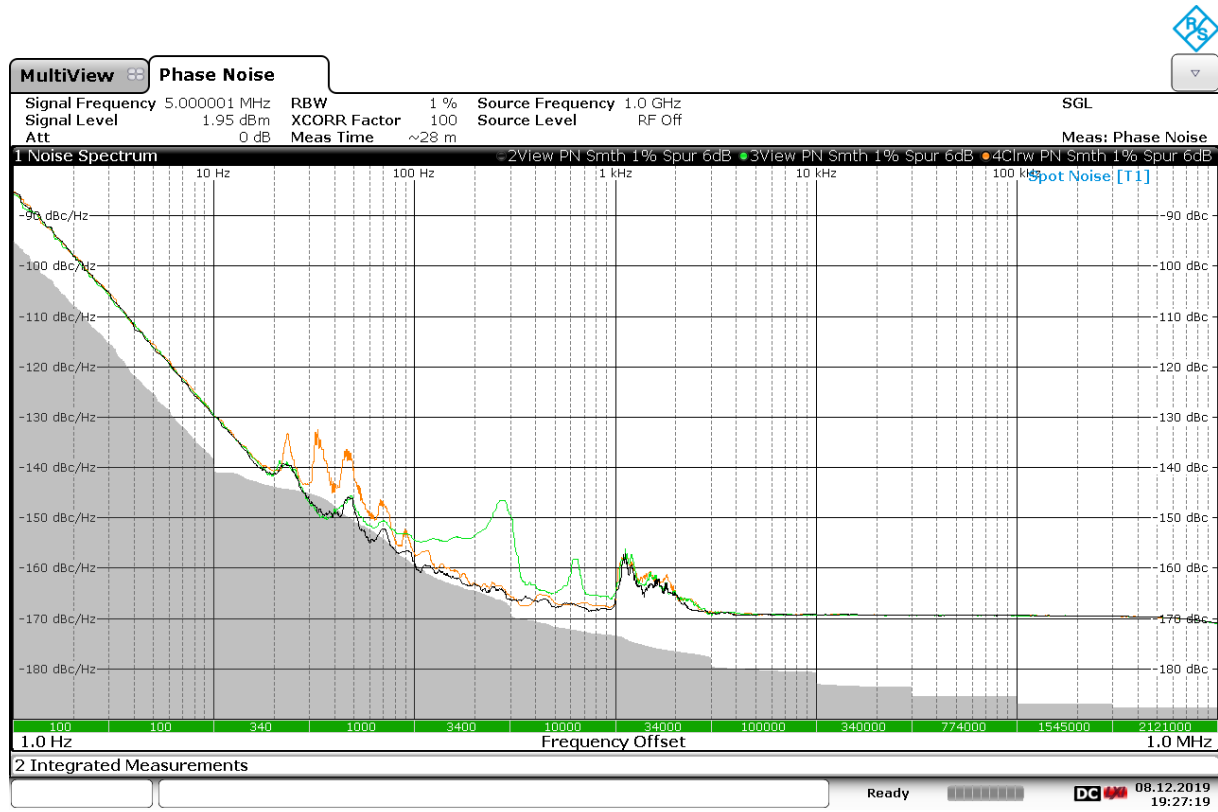


Figure 280 - Random Acceleration Measurement Setup

On the left we see the shaped spectrum, compensating the decreasing transfer gain as frequency rises. The acceleration spectrum obtained is shown in the middle, and a zoom-in of the signal is shown at the right side.

A sample effect of random vibrations on a good 5MHz oscillator (Wenzel 5MHz, unfortunately with no detailed datasheet available) is shown below:



19:27:20 08.12.2019

Figure 281 - OCXO with No, Sinusoidal and Random Vibration Loads

No vibrations are shown in black, the 20Hz 0.8g vertical sinewave acceleration is shown in red, and the random vibration (normalized 0.8g RMS over 200Hz) is shown in green. No surprise, the noise curve covers not only some peaks, but a broader frequency range with a “socket” ending at 200Hz (this was the bandwidth of the noise signal generated).

Even the low vibration sensitivity AXIOM 100MHz crystal above did show an influence of random vibrations:

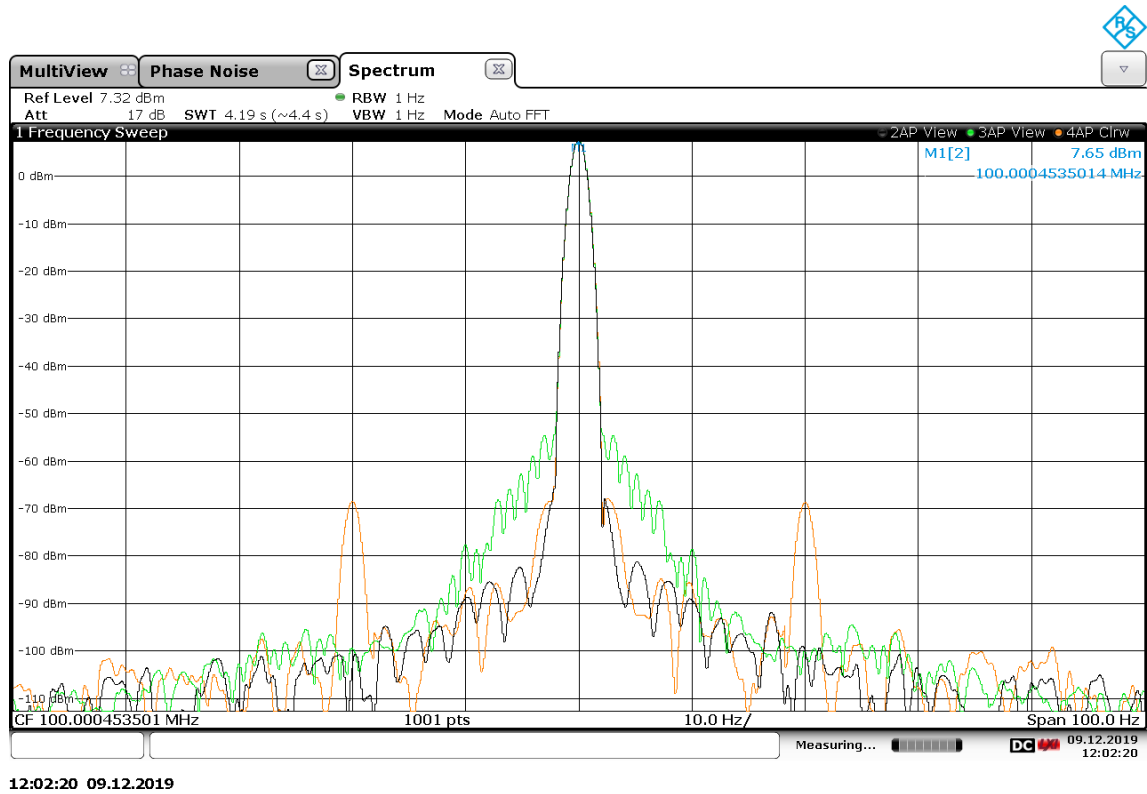


Figure 282 - AXIOM 100MHz Vibration Induced Sidebands

No vibration is black, 20Hz is yellow, random is green. The effect on close to carrier is quite prominent, up to -70dBc around a few Hz.

Last not least, an Allen deviation measurement was made for a Morion MV341 [11] precision oscillator.

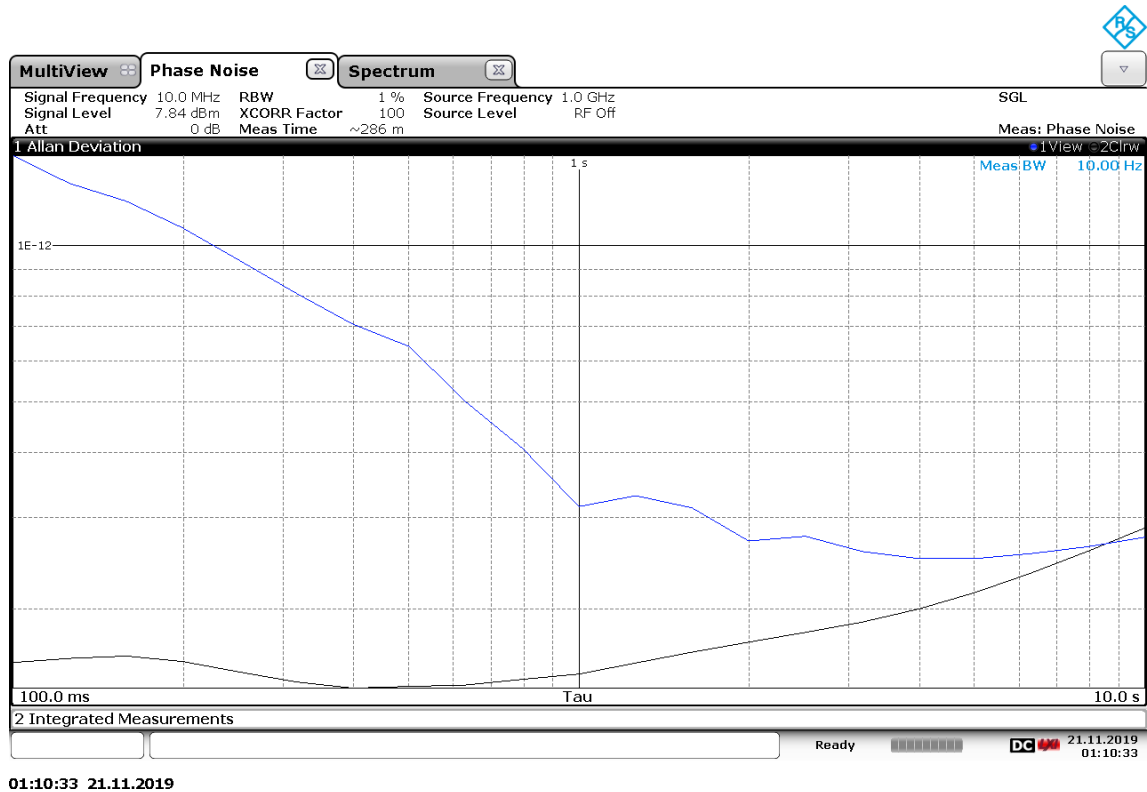


Figure 283 - Morion MV341 Precision Oscillator Allen Deviation under Pulse Acceleration

This very good oscillator loses about a decade of Allen deviation performance at 100ms when vibrated. At larger observation times, the effect almost cancels. Below 100ms the deterioration is even more pronounced, indicating that this oscillator needs a quiet environment.

### 22.8 Crystal Frequency Dependence on Orientation

Gravity as such does not qualify as a vibration source (earthquakes excluded), but it does have an influence on OCXO frequency. This cannot be measured using the FSWP or a similar premium spectrum analyzer because the frequency shifts are too small. A specialized measurement setup is needed, shown here:

#### HOW TO MEASURE CRYSTAL ORIENTATION DEPENDENCE ?

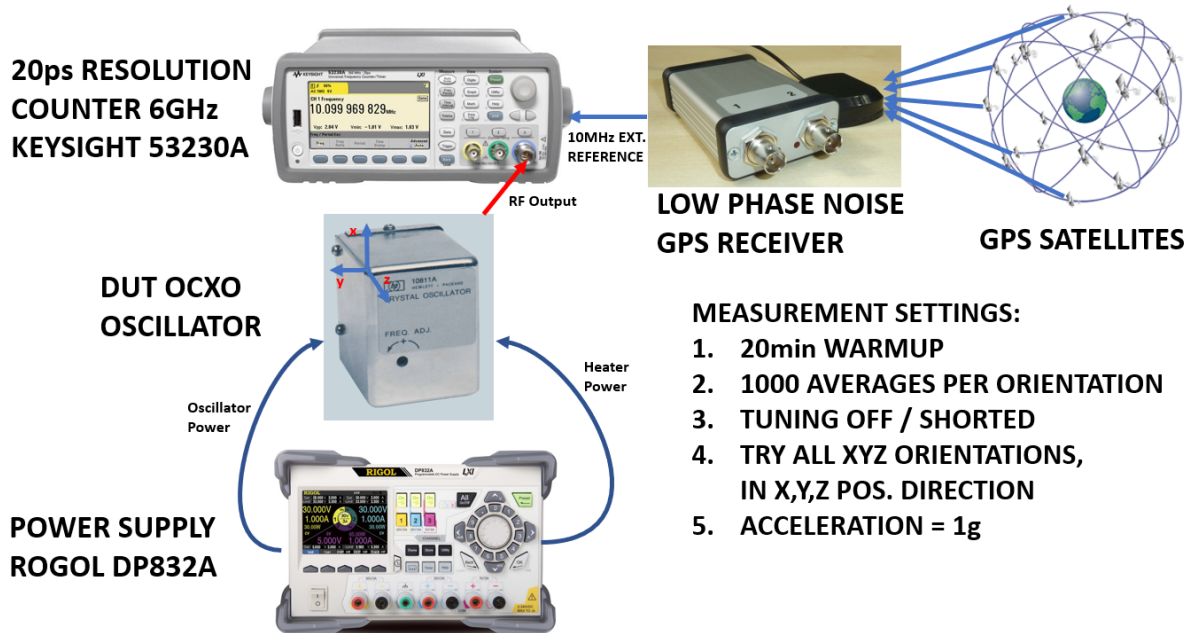


Figure 284 - Frequency over Orientation Measurement Setup

The key instrument here is the Keysight 53230A precision counter [12] with a resolution of 20ps. Using this instrument, synchronized with a low noise GPS-based reference signal, frequency measurements down to the mHz range become possible for our 5 and 10MHz OCXO candidates.

Acceleration is fixed 1g but applied in all 3 directions.

The results for the measured oscillators are shown in the following table:

DUT	f <sub>0</sub> Flat [Hz]	f <sub>0</sub> Side [Hz]	f <sub>0</sub> Top [Hz]	Max. Dev [mHz]	Max. Dev [ppb]	Remarks
Milliren 260-062	4999999.825	4999999.837	4999999.836	12	2.4	
Wenzel 500-03658A	5000000.366	5000000.366	5000000.377	11	2.2	
Wenzel 500-01238A	5000000.155	5000000.159	5000000.152	7	1.4	
Vectron	5000000.943	5000000.941	5000000.958	17	3.4	AT Cut
Morion MV341R1	10000000.171	10000000.166	10000000.193	27	2.4	
Morion MV272/37	10000003.154	00000003.154	10000003.158	4	0.4	Low Vib Sens.
HP 10811A	9999999.975	9999999.979	9999999.988	12	1.2	
Axtal Axiom 75LG-22	100000454.990	100000454.790	100000455.060	270	2.7	Low Vib Sens. (*)

Figure 285 - Table of Frequency Dependence on Orientation

It is no surprise that parts specified for good vibration tolerance are also better regarding orientation sensitivity. The deviations are in the ballpark of the daily aging rates. SC parts, again no surprise, perform better than classis AT cuts.



## 22.9 OCXO Types, Measurement Procedure for Vibration Measurements

OCXOs for ultra-high stability applications fall into two categories when it comes to vibration tolerances:

1. Parts for ground (lab) use. These have extreme accuracy and low phase noise around 1s, but a low (or no) tolerance for vibrations (Example: RAKON HSO-14). Vibration-controlled environments are necessary to achieve datasheet performance (damped, heavy granite lab table, ...).
2. Parts that may be used in aircraft or space applications. Their datasheets do have vibration g specs regarding accuracy and long-term stability, but usually not for phase noise. What is done for practical missions is that the mission owner specifies a spectral and amplitude range for vibrations and a tolerance margin for frequency deviation and phase noise. Unfortunately, these specs are not published (at least none could be found).

We could proceed in the following way to assess the sensitivity of an OCXO with a specified (say, e.g., 0.2g between 10 and 200Hz) maximum acceleration tolerance:

1. First, we run the oscillator after warmup without vibrations and check the close-to carrier signal on a premium (high SFDR) spectrum analyzer (FSWP is fine, SFDR > 90dBc). A span of about 2 x triple the vibration frequency is advisable so that 3<sup>rd</sup> order mixer products can be seen should they occur. Bandwidth must be set low enough (1Hz) so peak frequencies are accurately measurable.
2. Next, we start vibrations and *slowly* sweep the vibration frequency. Then, we note the acceleration from the sensor and the sideband peak generated. The acceleration amplitude will drop at least as much as indicated by the formula in the previous section. If it gets too low, the input amplitude of the vibrator can be increased. The curves obtained (sideband level over acceleration amplitude depending on frequency) show if the OCXO has internal resonances within the swept frequency range. Good OCXOs show no (strong) peaks.
3. We could now measure phase noise at several frequency steps within our range of interest. For good OCXOs this procedure takes quite some time (e.g., 20 minutes), but we can learn about the phase noise degradation at fixed frequencies and amplitudes.

What is probably a smarter method to assess phase noise degradation is the use of a vibration excitation that has a bandwidth limited *white noise acceleration spectrum*. This is not trivial to make, because in order to become white in terms of acceleration (not voltage or current), all frequency dependent effects (by the equations above, but amplitude drop due to inductance, ...) must be normalized out. By inverting the acceleration equation above we get:

$$U \sim x_o'' \frac{(\omega^2 - \omega_0^2)}{\omega^2 p} \sqrt{R^2 + (\omega L)^2}$$

If we are far above the self-resonance, we get

$$U \sim x_o'' \frac{1}{p} \sqrt{R^2 + (\omega L)^2}$$

For our case, this would predict that for 200Hz the voltage would have to be 6 times larger than for low frequencies.

## Conclusions

1. *All* industrial OCXOs are sensitive to vibrations.
2. The better the close to carrier phase noise performance, the more the oscillators degrade when vibrated
3. Low sensitivity types work (AXTAL), but probably also due to generally higher phase noise (100MHz instead of 5 or 10MHz).
4. While sinusoidal or white noise acceleration is detectable and does cause deterioration, the worst case is shock with wideband signals (pikes). This makes the oscillators unusable (within their phase noise specs)
5. Oscillator datasheets do give maximum g values, but no graphs about phase noise deterioration under vibration loads.
6. Vibrations impose a solid performance barrier to what space crystal oscillators can achieve. Premium Allen deviation values around the  $10^{-13}$  and lower range are not possible with vibrations present.
7. Shocks ( $> 0.1-0.2g$ ) must be completely avoided. A suspension against this works but is large and heavy if it should also work against low frequency “bumps”, so not workable for space.
8. It is probably best to power off vibration sources during extreme precision measurements. As the time of the measurements lies in the range of 100s of milliseconds up to a few ten seconds, this should be possible.
9. The scientific community (Driscoll) has proposed multi-crystal arrangements that would cancel out the effects of vibration or shock. They, probably, have never been seen in the wild, probably due to difficulties in synchronizing crystal aging and maintaining a suitable Q.
10. According to B. Neubig vibration insensitive crystal oscillators today are made by using extra stiff crystal holders. This shifts the resonant frequency of the crystal disk / holder (springs) to higher frequencies, and those can be more effectively damped out by mechanical measures.

## References

- [1] John Vig, “Quartz Crystal Resonators and Oscillators.” Accessed: Nov. 19, 2020. [Online]. Available: <http://www.resonal.com/Downloads/John%20R.%20Vig%20-%20tutorial%20on%20Quartz%20Crystals%20and%20Oscillators.pdf>.
- [2] The Guitammer Crop., “ButtKicker LFE Users Guide.” Accessed: Nov. 19, 2020. [Online]. Available: <https://thebuttkicker.com/content/BK-LFE%20Manual.pdf>.
- [3] Tim Weaver, “Has anyone ever opened a Buttkicker.” <https://forums.prosoundweb.com/index.php?topic=120339.0> (accessed Nov. 19, 2020).
- [4] Omicron Labs, “Bode 100 Vector Network Analyzer Datasheet.” Accessed: Nov. 19, 2020. [Online]. Available: <https://www.omicron-lab.com/products/vector-network-analysis/bode-100/>.
- [5] ST Semiconductor, “TDA2050 Datasheet.” Accessed: Nov. 19, 2020. [Online]. Available: <https://www.circuitbasics.com/wp-content/uploads/2016/10/TDA2050-Datasheet.pdf>.
- [6] Analog Devices, “ADXL203 Datasheet.” Accessed: Nov. 19, 2020. [Online]. Available: <https://www.analog.com/en/products/adxl203.html#>.
- [7] On Semiconductor, “LM324 Datasheet.” Accessed: Nov. 19, 2020. [Online]. Available: <https://www.onsemi.com/pub/Collateral/LM324-D.PDF>.
- [8] Morion, Inc., “MV89 Double Oven Ultra Precision OCXO.” Accessed: Nov. 19, 2020. [Online]. Available: [https://morion.com.ru/files/oscillators/84\\_file-en.pdf?1599562603](https://morion.com.ru/files/oscillators/84_file-en.pdf?1599562603).
- [9] AXTAL GmbH., “AXIOM75LG OCXO Datasheet.” Accessed: Nov. 19, 2020. [Online]. Available: <https://www.axtal.com/cms/docs/doc86657.pdf>.
- [10] Abraham. Savitzky and M. J. E. Golay, “Smoothing and Differentiation of Data by Simplified Least Squares Procedures.” *Anal. Chem.*, vol. 36, no. 8, pp. 1627–1639, Jul. 1964, doi: [10.1021/ac60214a047](https://doi.org/10.1021/ac60214a047).
- [11] Morion, Inc., “MV341 Precision Low Phase Noise OCXO.” Accessed: Nov. 19, 2020. [Online]. Available: [http://www.morion-us.com/catalog\\_pdf/mv341.pdf](http://www.morion-us.com/catalog_pdf/mv341.pdf).
- [12] Keysight, “Keysight 53220A/53230A 350 MHz Universal Frequency Counter/Timer.” Accessed: Nov. 19, 2020. [Online]. Available: <https://literature.cdn.keysight.com/litweb/pdf/53220-90001.pdf>.

## 23 Symbols and Abbreviations

Symbol	Description
ACPR	Adjacent Channel Power Ratio
ACPR	Alternating Current
ADS	Advanced Design System (Keysight Simulation Package)
ALC	Automatic Level Control
AM	Amplitude Modulation
B	Bandwidth
BF	Beta forward (SPICE Parameter)
BI	Beta Inverse (Gummel-Poon Parameter)
BN	Beta Forward (Gummel-Poon Parameter)
BR	Beta reverse (SPICE Parameter)
BVA	Improved Crystal Holder
DC	Direct Current
DLD	Drive Level Dependency
DMM	Digital Multimeter
DUT	Device under Test
$e_n(t)$	Noise voltage
F	Noise factor
$f_0$	Center frequency
$f_c$	Flicker corner frequency
FFT	Fast Fourier Transform
$f_m$	Frequency offset
FM	Frequency Modulation
$f_T$	Transition frequency
$G(\omega)$	Gain function
$g_m$	Transistor Transconductance
GPS	Global Positioning System
$H(\omega)$	Transfer function of feedback network
HB	Harmonic Balance
HBT	Heterojunction Bipolar Transistor
HF	High Frequency
HICUM	High Current Model (for Bipolar Transistors)
HP	Hewlett-Packard Corp.
HSO	High Stability Oscillator
$I_B$	Base Current
IETE	Indian Electrotechnical Engineers Association
$I_n$	Modified Bessel functions
$I_s$	Saturation current
J	Jacobian Matrix
JPL	Jet Propulsion Laboratory
k	Boltzmann's Constant
$K_0$	Oscillator voltage gain
KCL	Kirchhoff's Current Law

KVL	Kirchhoff's Voltage Law
$L(f_m)$	Ratio of sideband power in a 1Hz bandwidth at $f_m$
LF	Low Frequency
LO	Local Oscillator
LTI	Linear time independent
LTP	Lower Turning Point (for SC Crystals)
MEMS	Micro electronic-mechanical system
MMIC	Monolithic Microwave Integrated Circuit
NASA	National Aeronautics and Space Agency (USA)
NEPP	NASA Eligible Parts List
NF	Noise figure
NF	Injection Efficiency forward (SPICE Parameter)
NLTD	Nonlinear time dependent
NR	Injection Efficiency Reverse (SPICE Parameter)
ODE	Ordinary Differential Equation
$P_0$	Oscillator output power
PCB	Printed Circuit Board
PHEMT	Pseudomorphic High Electron Mobility Transistor
PI	Proportional-Integral (Regulator)
PLL	Phase Locked Loop
PM	Phase Modulation
PSD	Power spectral density
PSU	Power Supply Unit
$q$	Electron Charge
$Q_0$	Unloaded Q
$Q_L$	Loaded Q
RF	Radio Frequency
RS	Rohde & Schwarz Corp.
SC	Stress Compensated Cut
SMD	Surface Mounted Device
SMU	Source measure unit
SPICE	Simulation program with integrated circuit emphasis
T	Absolute temperature
TLL	Temperature Locked Loop
UHF	Ultra-High Frequency (300MHz-3GHz)
USO	Ultra-Stable Oscillator
$V_A$	Early Voltage
VAF	Early Voltage in Forward Mode (SPICE Parameter)
VAR	Early Voltage in Reverse Mode (SPICE Parameter)
$V_B$	Base Voltage
$V_{BE}$	Emitter Base Voltage
VBIC3	Vertical Bipolar Transistor Simulation Model
VCO	Voltage Controlled Oscillator
VdP	Van der Pol
$V_E$	Emitter Voltage
VHF	Very High Frequency (30-300MHz)
VLBI	Very long Baseline Interferometry

VNA	Vector network analyzer
V <sub>pp</sub>	Voltage peak-peak
V <sub>T</sub>	Temperature Voltage (=kT/q)
$\omega$	Circular frequency
X <sub>C</sub>	Capacitive Impedance
X <sub>L</sub>	Inductive Impedance
Z <sub>IN</sub>	Input Impedance